

Effective Field Theory Approaches to Particle Physics Beyond the Standard Model

by

Zhengkang Zhang

A dissertation submitted in partial fulfillment
of the requirements for the degree of
Doctor of Philosophy
(Physics)
in the University of Michigan
2018

Doctoral Committee:

Professor James D. Wells, Chair
Professor Fred C. Adams
Professor Aaron T. Pierce
Professor Jianming Qian

Zhengkang Zhang

zzkevin@umich.edu

ORCID iD: 0000-0001-8305-5581

© Zhengkang Zhang 2018

Acknowledgements

First of all, I would like to thank my advisor, James Wells. My development as a scientist has been greatly influenced by his invaluable guidance. He has always encouraged me to pursue independent research, to develop new ideas, and to form my own view of the field, while generously sharing his knowledge, experience and insights to guide my thinking — an approach I deeply appreciate.

I would also like to thank Aaron Pierce for teaching me a great deal about the field, especially as my advisor at an early stage of my graduate studies. I am particularly grateful for his patient guidance through my first project, and his continued support and advice later on. Additionally, I would like to thank Christophe Grojean for his support and advice, especially during my stay at DESY Hamburg, where part of this dissertation was completed.

I have greatly benefited from working with my other collaborators as well, including Sebastian Ellis, Alexey Petrov, Stefan Pokorski, Jérémie Quevillon, Bibhushan Shakya, Andrea Wulzer, Tevong You, and Yue Zhao.

My thanks also go to Fred Adams and Jianming Qian for serving on my committee and providing valuable feedback.

I am grateful to Ratindranath Akhoury, Henriette Elvang, Finn Larsen, Roberto Merlin, James Wells, and Kathryn Zurek for their inspiring classes from which I have learned a lot of interesting physics.

I also would like to thank other (past and current) members of the Leinweber Center for Theoretical Physics (formerly Michigan Center for Theoretical Physics), especially Arash Arabi Ardehali, Raymond Co, Josh Foster, Gordy Kane, Jack Kearney, Nick Orlofsky, Sam Roland, Ben Safdi, and Bob Zheng, for many stimulating conversations.

Special thanks go to Mengxing Ye, my brilliant partner in life, for accompanying me through this journey (and teaching me interesting condensed matter physics as well).

The work in this dissertation was funded in part by the U.S. Department of Energy grant DE-SC0007859, the Rackham Summer Award, Rackham Research Grant, and Rackham Dissertation Fellowship.

Table of Contents

Acknowledgements	ii
List of Tables	v
List of Figures	viii
List of Appendices	xii
Chapter 1: Introduction	1
1.1 The Standard Model from an EFT perspective	1
1.2 Precision analyses as indirect probes of new physics	5
1.3 Bottom-up and top-down EFT approaches	6
1.4 What’s new?	9
1.5 Outline of this dissertation	10
Chapter 2: Precision Electroweak Analyses After the Higgs Boson Discovery	13
2.1 Introduction	13
2.2 Standard Model parameters and observables	14
2.3 The formalism	16
2.4 New physics examples	27
2.5 Conclusions	34
Chapter 3: Resolving Charm and Bottom Quark Masses in Precision Higgs Analyses	35
3.1 Introduction	35
3.2 Incorporating low-energy observables into a global precision analysis	38
3.3 Recasting Higgs observables in terms of low-energy observables	39
3.4 Theoretical uncertainties of Higgs partial widths	44
3.5 Conclusions	49

Chapter 4: EFT of Universal Theories and Its RG Evolution	50
4.1 Introduction	50
4.2 Universal theories at LO and beyond	53
4.3 RG effects in the electroweak sector	63
4.4 RG effects in the Yukawa sector	75
4.5 Conclusions	78
Chapter 5: Time to Go Beyond TGC Interpretation of W Pair Production	81
5.1 Introduction	81
5.2 Effective operators and anomalous couplings	83
5.3 Triple gauge coupling measurements: from LEP2 to LHC	85
5.4 Toward a high energy picture of Standard Model deviations	89
5.5 Conclusions	91
Chapter 6: Covariant Diagrams for One-Loop Matching	92
6.1 Introduction	92
6.2 Gauge-covariant functional matching	95
6.3 Covariant diagrams	104
6.4 Examples	116
6.5 Conclusions	143
Chapter 7: EFT Approach to Trans-TeV Supersymmetry	146
7.1 Introduction	146
7.2 Matching the MSSM onto the SMEFT	151
7.3 Bottom-tau Yukawa unification	174
7.4 Higgs couplings in TeV-scale SUSY	183
7.5 Conclusions	190
Chapter 8: Summary and Outlook	192
Appendices	194
Bibliography	213

List of Tables

2.1	(From [131]) The list of observables, their experimental and reference values, and percent relative uncertainties.	17
2.2	(From [131]) Expansion coefficients, as defined in Eq. (2.20), calculated in the basis of input observables containing $\Delta\alpha_{\text{had}}^{(5)}$. These encode the dependence of the output observables on each input observable.	21
2.3	(From [131]) Percent relative uncertainties for the expansion coefficients $c_{ii'}$, with all input observables varied in their 1σ range.	24
2.4	(From [131]) The $r_{ii'}$'s defined in Eq. (2.25), characterizing the ratios of second-order vs. first-order terms in the expansion (in units of percentage).	25
2.5	(From [131]) Expansion coefficients calculated in the basis of input observables containing $\alpha(m_Z)$, which are derived from the numbers in Table 2.2 by a change of basis described in Section 2.3.4.	28
2.6	(From [131]) The b coefficients defined in Eq. (2.68), characterizing the shift in the output observables due to new physics that shifts vector boson self-energies.	32
4.1	(From [111]) Warsaw basis operator combinations that appear in $\mathcal{L}_{\text{universal}}$ in (4.1), in the notation of [3]. In these expressions, repeated generation indices i, j, k, l are summed over, $H^\dagger\sigma^a\overleftrightarrow{D}_\mu H = H^\dagger\sigma^a(D_\mu H) - (D_\mu H)^\dagger\sigma^a H$, $H^\dagger\overleftrightarrow{D}_\mu H = H^\dagger(D_\mu H) - (D_\mu H)^\dagger H$. The Yukawa matrices y_u, y_d, y_e should not be confused with the hypercharges Y_f . The SM vector and scalar currents $J_{G\mu}^A, J_{W\mu}^a, J_{B\mu}, J_y^\alpha$ are defined in (4.2).	54
4.2	(From [111]) Expressions of the 16 universal parameters in terms of the Warsaw basis Wilson coefficients in (4.1). These parameters completely characterize the indirect BSM effects in universal theories at the dimension-6 level. More details of the universal parameters, including their definition from the effective Lagrangian and their expressions in other bases, can be found in [109].	56

4.3	(From [109, 111]) Higgs basis couplings in terms of the universal parameters. $\Delta\epsilon_{1,2,3}$ are independent linear combinations of \hat{S}, \hat{T}, W, Y defined in (4.4). c_{4f} collectively denotes four-fermion effective couplings, and d_{Vf} stands for the dipole-type Vff couplings. Compared with [7], we have written the fractional W mass shift as δ_m instead of δm , and defined $[\delta g_L^{Wq}]_{ij}$ in the gauge-eigenstate rather than mass-eigenstate basis.	57
6.1	(From [60]) Building blocks of covariant diagrams for integrating out heavy bosonic fields (and fermionic fields as well if one follows the approach of Eq. (6.60) to square their quadratic operator), in the absence of mixed heavy-light contributions and open covariant derivatives in the \mathbf{X} matrix, as derived in Section 6.3.1. All previous universal results in the literature [55, 56] can be easily reproduced by computing one-loop covariant diagrams built from these elements; see Section 6.4.1.	112
6.2	(From [60]) Additional building blocks of covariant diagrams in the presence of mixed heavy-light contributions to matching, as derived in Section 6.3.2. Example applications can be found in Sections 6.4.2, 6.4.3 and 6.4.5.	112
6.3	(From [60]) Additional building blocks of covariant diagrams in the presence of open covariant derivatives in the \mathbf{X} matrix, as derived in Section 6.3.3, up to one-open-covariant-derivative terms $P_\mu \mathbf{Z}^\mu + \mathbf{Z}^{\dagger\mu} P_\mu$. Example applications can be found in Section 6.4.3.	113
6.4	(From [60]) Additional building blocks of covariant diagrams when Dirac fermions are involved in matching, as derived in Section 6.3.4. These are used when the quadratic operator for fermionic fields is not squared like in Eq. (6.60). Example applications can be found in Sections 6.4.4 and 6.4.5.	113
6.5	(From [60]) List of universal coefficients in terms of the master integrals defined in Eq. (6.67) (Column 1). The UOLEA master formula for one-loop matching reported in [56] is reproduced by adding up traces of the operators in Column 2 with the corresponding universal coefficients, and multiplying the overall factor $-ic_s$; see Eq. (6.68). The covariant diagrams used to compute each universal coefficient are listed in Column 3. See Appendix B for expressions of the universal coefficients in terms of heavy particle masses.	122
6.6	(From [60]) Summary of the results in Eq. (6.96) for mixed heavy-light contributions to one-loop matching for the scalar triplet model. The SM gauge coupling-independent terms for the three operators $\mathcal{O}_T, \mathcal{O}_H, \mathcal{O}_R$ in Eq. (6.89) are computed (in the $\overline{\text{MS}}$ scheme).	127

7.1	(From [132]) Heavy fields φ_H in the MSSM, their gauge quantum numbers, and conjugate fields (which appear on the left side of \mathcal{Q}_{UV}).	153
7.2	(From [132]) Light fields φ_L in the MSSM, their gauge quantum numbers, and conjugate fields (which appear on the left side of \mathcal{Q}_{UV}). Primed Weyl fermion fields are unphysical auxiliary fields, to be set to zero at the end of the calculation.	154
7.3	(From [132]) Fields contained in the nonzero entries of the MSSM \mathbf{U} matrix, with the heavy fields φ_H to be set to $\varphi_{H,c}$ (which is nonvanishing only for the heavy Higgs Φ). In this table, φ collectively denotes the heavy and light Higgs fields Φ and ϕ , e.g. φ^2 represents $\Phi^2, \Phi\phi, \phi^2$. Also, ψ_f , the Dirac spinors containing SM fermions, are written simply as f for clarity. Detailed expressions of the \mathbf{U} matrix can be found in Appendix C.	155
7.4	(From [132]) Dimension-six operators generated at tree level when matching the MSSM onto the SMEFT. p, r, s, t are generation indices. Tree-level matching alone produces the operator coefficients listed here, but with β' in place of β . As explained in Section 7.2.2, adding the one-loop-generated piece $c_{\Phi\phi}(\Phi_c^*\phi + \phi^*\Phi_c)$ to $\mathcal{L}_{\text{SMEFT}}^{\text{tree}}$ amounts to replacing β' by β in all C_i^{tree}	158
7.5	(From [132]) Covariant diagrams contributing to Higgs potential and Yukawa interactions.	163
7.6	(From [132]) Covariant diagrams contributing to kinetic terms.	164

List of Figures

- 3.1 (From [30]) Contours of $m_c(m_c)$ (top-left), $\Gamma_{H \rightarrow c\bar{c}}$ (top-right), $m_b(m_b)$ (bottom-left), $\Gamma_{H \rightarrow b\bar{b}}$ (bottom-right) in the μ_m - μ_α plane. These plots demonstrate Eqs. (3.18-3.21) with all other inputs fixed. The unlabeled contours represent decreasing values toward the top-left corner in steps of 0.01 GeV, 0.005 GeV, 0.002 MeV, 0.005 MeV, respectively. 45
- 3.2 (From [30]) Percent relative uncertainties in $\Gamma_{H \rightarrow c\bar{c}}$ (left) and $\Gamma_{H \rightarrow b\bar{b}}$ (right) as functions of μ_{\min} from: perturbative uncertainty with $\mu_{\max}^c = 4$ GeV, $\mu_{\max}^b = 15$ GeV (red solid) or alternatively $\mu_{\max}^c = 3, 5$ GeV, $\mu_{\max}^b = 13, 17$ GeV (red dashed), parametric uncertainties from \mathcal{M}_1^c or \mathcal{M}_2^b (orange), $\alpha_s(m_Z)$ (cyan solid), $\mathcal{M}_1^{c,\text{np}}$ (blue, for $\Gamma_{H \rightarrow c\bar{c}}$ only) and m_H (purple). The parametric uncertainty from $\alpha_s(m_Z)$ incorrectly calculated assuming no correlation with m_Q (cyan dotted) is also shown for comparison. The parametric uncertainties are defined as shifts of the central values of $\Gamma_{H \rightarrow c\bar{c}}$ and $\Gamma_{H \rightarrow b\bar{b}}$ for $\mu_{\min} \leq \mu_m, \mu_\alpha \leq \mu_{\max}$ caused by varying the input parameters within the errors quoted in Eqs. (3.24-3.32), with $\mu_{\max}^c = 4$ GeV, $\mu_{\max}^b = 15$ GeV (the kinks are due to the maximum or minimum shifting to a different region in the μ_m - μ_α plane), and are found to be insensitive to μ_{\max} 47

- 4.1 (From [111]) Examples showing how nonuniversal effects can be generated by universal oblique corrections. **Left:** effective Wqq' and $W\ell\nu$ couplings are renormalized differently, due to the different couplings of quarks and leptons to neutral gauge bosons. **Middle:** the $Zb_L\bar{b}_L$ coupling is singled out among all the $Zf\bar{f}$ couplings probed by Z -pole measurements for relatively large running effects proportional to y_t^2 , via loop corrections involving the charged Goldstone boson (or the longitudinal W^\pm if one uses the unitary gauge). **Right:** the Higgs boson couplings to the up- and down-type quarks and leptons are renormalized differently, due to different gauge interactions of the fermions. In each example, the interactions generated for the SM fermions are not in the form of the SM currents, and thus the corresponding operators cannot be eliminated in favor of bosonic operators. These examples, as well as many others, can be more rigorously formulated in terms of $SU(2)_L \times U(1)_Y$ invariant operators, but we prefer to give a more intuitive illustration at this stage. The arguments here will be made concrete in sections 4.3 and 4.4. . . . 52
- 4.2 (From [111]) Theory predictions for $R_\ell = \Gamma_{\text{had}}/\Gamma(Z \rightarrow \ell^+\ell^-)$ and $R_b = \Gamma(Z \rightarrow b\bar{b})/\Gamma_{\text{had}}$ are shifted away from the SM point along the dashed lines, when the universal parameters appearing in (4.40) take the values labeled beside the dots. The anomalous TGC parameters $\Delta\bar{g}_1^Z$, $\Delta\bar{\kappa}_\gamma$ lead to shifts along the same direction as c_{2y} (green dashed line), with the orange stars and triangles indicating the maximum shifts allowed by the LEP2 TGC constraints (95% C.L.) from single-parameter fits (shown in the bottom-right corner) [205]. $\ln \frac{\Lambda}{\mu_{\text{EW}}} = 3$ is assumed, as motivated by TeV-scale new physics. Agreement between the SM predictions as fitted by the Gfitter group [26] and the combined measurements by the LEP and SLD collaborations [139] naively constrains the oblique parameters combination $\Delta\epsilon_3 - c_\theta^2\Delta\epsilon_1$ (blue) defined in (4.41) at the 10^{-3} level. But even when the oblique parameters are interpreted as renormalized at μ_{EW} following our prescriptions, the neglected LL terms in such a LO oblique parameters analysis can actually be significant. The challenge illustrated by this example requires extending the (\hat{S}, \hat{T}, W, Y) parametrization to include additional parameters in a consistent global fit of universal theories beyond LO. 74

5.1	(From [117]) Fractional shift in LEP2 $e^+e^- \rightarrow W^+W^- \rightarrow qq\ell\nu$ differential cross section induced by each of the anomalous couplings in Eq. (5.8), compared with experimental uncertainties (gray dotted) reported in [205]. Assuming lepton flavor universality, effects of the anomalous TGCs being constrained (solid) [214] are seen to dominate over those of Zff vertex and W mass corrections (dashed), even when the latter are set to maximum values allowed by EWPD [45, 92], providing justification for the conventional TGC analysis procedure.	87
5.2	(From [117]) Leading lepton p_T distribution of 8 TeV LHC W^+W^- events in the $e\mu$ channel when each anomalous coupling is turned on individually, compared with experimental data (dots with error bars) and SM predictions (gray dotted). The latter, together with non- WW backgrounds (gray shaded), are taken from [207]. Effects of anomalous TGCs being considered in recent TGC fits (solid) are clearly <i>not</i> dominant over those of δg_R^{Zu} , δg_R^{Zd} (dashed) consistent with EWPD, calling for extension of the conventional TGC analysis procedure.	88
7.1	(From [132]) Points in the MSSM parameter space that allow consistent matching onto the SMEFT and meanwhile realize $b\text{-}\tau$ Yukawa unification, projected onto $(\log M_s, \mu/M_s)$ plane, for several choices of $\tan\beta$. Blue, yellow, green, red points have $x_t \equiv (A_t - \mu \cot\beta)/M_s \in (-4, -\sqrt{6}), (-\sqrt{6}, 0), (0, \sqrt{6}), (\sqrt{6}, 4)$, respectively. Empty circles represent solutions with a gluino lighter than 2 TeV, potentially already in tension with direct LHC searches, depending on decay kinematics.	177
7.2	(From [132]) Same as Figure 7.1, now projected onto $(\log M_s, M_3 /M_s)$ plane.	178
7.3	(From [132]) Same as Figure 7.1, now showing SUSY threshold correction for the Higgs quartic coupling, defined as $\Delta\lambda \equiv \lambda - \lambda_{\text{eff}}$ at the matching scale $\Lambda = M_s$	179
7.4	(From [132]) Same as Figure 7.1, now showing SUSY threshold correction for the bottom Yukawa coupling, defined as $\delta_b \equiv (y_b - y_b^{\text{eff}})/y_b^{\text{eff}}$ at the matching scale $\Lambda = M_s$	180

7.5	(From [132]) Variation of $\delta\kappa_b$ in the region of the $ M_3 -M_s$ plane where a solution exists for exact $b\text{-}\tau$ Yukawa unification, on each x_t branch, with $M_\Phi = 1\text{ TeV}$ and $\tan\beta = 50$. Superimposed are contours of μ/M_s (black) and x_t (red dashed). Light green curves in the $x_t < 0$ plots correspond to the 1 TeV Higgsino dark matter benchmark. Direct superpartner searches probe lower mass regions of the parameter space (with $ M_3 \lesssim 2\text{ TeV}$ potentially already excluded at the LHC depending on decay kinematics), while precision Higgs measurements can be more sensitive to higher mass regions where $\delta\kappa_b$ is enhanced by one-loop corrections.	185
7.6	(From [132]) Same as Figure 7.5, now with $\tan\beta = 20$	186
7.7	(From [132]) Same as Figure 7.5, now with $\tan\beta = 8$	187
7.8	(From [132]) Contours of $ \delta\kappa_b $ in the $M_\Phi\text{-}\tan\beta$ plane, for our benchmark scenario $ M_3 = 5\text{ TeV}$, $M_s = 10\text{ TeV}$, which will evade gluino and stop searches at the LHC. The Higgsino mass is determined by exact $b\text{-}\tau$ Yukawa unification, for which solutions exist for $\tan\beta \gtrsim 5$. Dark solid and dashed curves represent current exclusion limit (95% CL) and projected high-luminosity reach (95% CL with 3 ab^{-1} at 14 TeV) from heavy Higgs searches in the di-tau channel at the LHC, reported assuming the $m_h^{\text{mod}+}$ benchmark scenario. Future Higgs factories, with 0.5-1% projected precision for the $hb\bar{b}$ coupling, will be able to probe much of the parameter space displayed.	188

List of Appendices

Appendix A: Master Integrals in One-Loop Matching	194
Appendix B: Explicit Expressions of Universal Coefficients	199
Appendix C: The MSSM U Matrix	202
C.1 <i>R</i> -parity-even block	202
C.2 <i>R</i> -parity-odd block	204
Appendix D: Cross-Check of SUSY Threshold Corrections Against Feyn- man Diagram Calculation	208

Abstract

This dissertation covers applications of effective field theory (EFT) ideas and techniques to the study of particle physics beyond the Standard Model (SM). The recent discovery of the Higgs boson without other new physics discoveries hints at the possibility that additional exotic states that couple to SM particles, if they exist, are not in the neighborhood of the electroweak scale. In this case, precision measurements of SM processes offer an important indirect probe of heavy new physics that is complementary to direct searches for new particles at high energy colliders, and EFT becomes the tool of choice to bridge a vast range of new physics ideas and experimental observation.

We start with a discussion of the precision analyses program, reviewing the analysis framework and the status of electroweak precision tests. The Higgs boson discovery has added a new module to this program, and we point out new issues related to heavy quark masses that must be taken into account in future precision studies of the Higgs boson.

Various approaches exist in the literature to extract information about new physics from precision analyses. Two examples are oblique parameters and triple gauge couplings (TGCs). We critically examine these conventional approaches in the EFT framework. In particular, we clarify that the applicability of oblique parameters is restricted to universal theories at leading order, and we find that TGCs no longer serve as a general parameterization of new physics effects in W boson pair production with recent LHC data. In both cases, EFT provides a consistent framework to rectify and extend the oversimplified conventional approaches, in order to take full advantage of high energy data to learn about new physics.

We next turn to the subject of EFT matching, i.e. deriving a low energy EFT by integrating out heavy degrees of freedom from an ultraviolet theory. We develop a diagrammatic framework to carry out covariant functional matching calculations in a systematic manner. In contrast to conventional Feynman diagram methods, our approach avoids the detour of computing correlation functions, and meanwhile preserves gauge covariance and simplifies calculations. Finally, we apply this new technique to trans-TeV supersymmetry, and show that future precision Higgs measurements can probe scenarios of Yukawa unification featuring heavy superpartners beyond direct LHC reach.

Chapter 1

Introduction

1.1 The Standard Model from an EFT perspective

Our current understanding of elementary particles and their interactions is encoded in what is known as the Standard Model (SM) of particle physics. It is a quantum field theory (QFT) based on $SU(3)_c \times SU(2)_L \times U(1)_Y$ gauge invariance, that describes strong and electroweak interactions among a set of matter fields, including quarks, leptons, and the Higgs.

The Lagrangian of the SM can be written as

$$\begin{aligned} \mathcal{L}_{\text{SM}} = & -\frac{1}{4}G_{\mu\nu}^A G^{A\mu\nu} - \frac{1}{4}W_{\mu\nu}^a W^{a\mu\nu} - \frac{1}{4}B_{\mu\nu}B^{\mu\nu} + |D_\mu H|^2 - m_H^2 |H|^2 - \lambda |H|^4 \\ & + \sum_{f \in \{q, l, u, d, e\}} i \bar{f} \gamma^\mu D_\mu f - [(\bar{u} y_u^\dagger q_\beta \epsilon^{\beta\alpha} + \bar{q}^\alpha V_{\text{CKM}} y_d d + \bar{l}^\alpha y_e e) H_\alpha + \text{h.c.}]. \end{aligned} \quad (1.1)$$

The field content of the SM is as follows.

- G, W, B are the spin-1 gauge bosons of $SU(3)_c, SU(2)_L, U(1)_Y$, respectively, with field strengths defined by $G_{\mu\nu}^A = \partial_{[\mu} G_{\nu]}^A + g_s f^{ABC} G_\mu^B G_\nu^C$, $W_{\mu\nu}^a = \partial_{[\mu} W_{\nu]}^a + g \epsilon^{abc} W_\mu^b W_\nu^c$, $B_{\mu\nu} = \partial_{[\mu} B_{\nu]}$, where $(\dots)_{[\mu, \nu]} \equiv (\dots)_{\mu\nu} - (\dots)_{\nu\mu}$.
- H is the spin-0 Higgs field. It is an $SU(3)_c$ singlet, $SU(2)_L$ doublet, and has $U(1)_Y$ hypercharge $Y_H = \frac{1}{2}$.
- There are three generations of spin- $\frac{1}{2}$ fermion fields; each of q, l, u, d, e carries a generation index that we have suppressed in Eq. (1.1) for simplicity. Among them, q, u, d are quarks in the fundamental representation of $SU(3)_c$, while l, e are $SU(3)_c$ singlet leptons. The left-handed fields $q = (u_L, d_L)$, $l = (\nu, e_L)$ are $SU(2)_L$ doublets, while the right-handed fields $u = u_R, d = d_R, e = e_R$ are $SU(2)_L$ singlets. The $U(1)_Y$ hypercharge assignments are $\{Y_q, Y_l, Y_u, Y_d, Y_e\} = \{\frac{1}{6}, -\frac{1}{2}, \frac{2}{3}, -\frac{1}{3}, -1\}$.

There are three types of interactions among these fields:

- Gauge interactions, dictated by minimal coupling. For example, for $f = q$, $D_\mu = \partial_\mu - ig_s T^A G_\mu^A - ig t^a W_\mu^a - ig' Y_f B_\mu$, with $[T^A, T^B] = [\frac{\lambda^A}{2}, \frac{\lambda^B}{2}] = if^{ABC} \frac{\lambda^C}{2}$, $[t^a, t^b] = [\frac{\sigma^a}{2}, \frac{\sigma^b}{2}] = i\epsilon^{abc} \frac{\sigma^c}{2}$ (λ and σ are the Gell-Mann and Pauli matrices, respectively); the $SU(3)_c$ and/or $SU(2)_L$ pieces are absent for other fermion fields neutral under these gauge groups.
- Yukawa interactions, which couple the fermions to the Higgs. The flavor structure of SM Yukawa interactions is such that all the gauge-eigenstate fermion fields are also mass eigenstates except $d_L = V_{\text{CKM}} d'_L$ where d'_L is a mass eigenstate. In Eq. (1.1), α and β are $SU(2)_L$ indices of the doublet fields, while generation indices are implicitly summed over; the 3×3 Yukawa matrices in generation space y_u, y_d, y_e are diagonal and real.
- Higgs self interaction, with a Mexican hat-shaped potential that spontaneously breaks the electroweak symmetry $SU(2)_L \times U(1)_Y$ down to $U(1)_Q$, with $Q = t^3 + Y$ being the unbroken generator identified with electric charge. In unitary gauge, $H = \frac{1}{\sqrt{2}}(0, v + h)$ where $v = \sqrt{-m_H^2/\lambda} \simeq 246$ GeV at tree level, and h is the physical Higgs boson.

Electroweak symmetry breaking mixes W^3 and B to form mass eigenstates, the Z boson and the photon, and generates masses for the W^\pm, Z bosons as well as fermions. Explicitly, we have

$$W_\mu^\pm = \frac{1}{\sqrt{2}}(W_\mu^1 \mp iW_\mu^2), \quad Z_\mu = c_\theta W_\mu^3 - s_\theta B_\mu, \quad A_\mu = s_\theta W_\mu^3 + c_\theta B_\mu, \quad (1.2)$$

where

$$c_\theta = \frac{g}{\sqrt{g^2 + g'^2}} = \frac{e}{g'}, \quad s_\theta = \frac{g'}{\sqrt{g^2 + g'^2}} = \frac{e}{g}. \quad (1.3)$$

At tree level, the masses are given by

$$m_W = m_Z c_\theta = \frac{1}{2} g v, \quad m_f = \frac{1}{\sqrt{2}} y_f v \quad (f = u, d, e), \quad (1.4)$$

with fermion masses m_f understood as 3×3 diagonal matrices in generation space.

The SM, in the form of Eq. (1.1), has been established over the past several decades via the observation of all the particles – most recently a 125 GeV Higgs boson h in 2012 [1, 2] – and extensive tests of most of their interactions. However, from the modern effective field theory (EFT) point of view, Eq. (1.1) is really just a leading order approximation to an EFT that is valid at the energy scales that have been probed so far.

This can be seen as follows. When constructing a QFT, we are supposed to write down all terms consistent with postulated symmetries, e.g. Lorentz and gauge invariance, in a local Lagrangian. Eq. (1.1) indeed contains almost all operators consistent with Lorentz symmetry and $SU(3)_c \times SU(2)_L \times U(1)_Y$ gauge invariance up to dimension four (with the exceptions of a cosmological constant and a QCD θ term, which will not be discussed here). However, there is no reason to stop at dimension four. There is one legitimate operator $(LH)^2$ at dimension five, and many more at dimension six, seven, etc. [3, 4]. All of them are in principle present in our effective Lagrangian, commonly known as the SMEFT:

$$\mathcal{L}_{\text{SMEFT}} = \mathcal{L}_{\text{SM}} + \left[\frac{1}{\Lambda^{(5)}} (LH)^2 + \text{h.c.} \right] + \sum_i \frac{1}{(\Lambda_i^{(6)})^2} \mathcal{O}_i^{(d=6)} + \sum_i \frac{1}{(\Lambda_i^{(7)})^3} \mathcal{O}_i^{(d=7)} + \dots \quad (1.5)$$

For recent reviews on the SMEFT, see [5–7]. Note that a Lagrangian has dimension four, so an operator of dimension d has a coefficient with mass dimension $4 - d$, which we write as a scale (of dimension one) Λ raised to the appropriate power. If all these Λ 's are much higher than the energy scales probed experimentally, we would expect our theory prediction for any observable to be unaffected by the higher dimensional operators. In this case, it would be a good approximation to just write $\mathcal{L}_{\text{SMEFT}} \simeq \mathcal{L}_{\text{SM}}$, with \mathcal{L}_{SM} given in Eq. (1.1).

There is one exception, though, namely the observation of neutrino oscillations (see e.g. [8] for a review), which Eq. (1.1) is not able to explain. Up to dimension four level, neutrinos are massless, and no oscillations can occur. Nonzero neutrino masses are however generated in the presence of the dimension-five operator $(LH)^2$, and they scale as $m_\nu \sim v^2/\Lambda^{(5)}$. To get a neutrino mass of order 0.1 eV from this operator, we need $\Lambda^{(5)} \sim 10^{14-15}$ GeV.

If all higher dimensional operators are suppressed by the same scale Λ , we see that the observation of neutrino oscillations, which point to such high Λ 's as 10^{14-15} GeV, actually *explains* the tremendous success of Eq. (1.1) in all other experimental tests. Another well-known hint that $\mathcal{L}_{\text{SMEFT}}$ may be well approximated by \mathcal{L}_{SM} is the nonobservation of proton decay, which constrains some dimension-six operators to be suppressed by a similar scale [9].

At present, it is indeed a viable possibility that the Λ 's in Eq. (1.5) are all much higher than the weak scale. If this were true, the search for new physics would be hopeless. Technically, this is because Eq. (1.5) makes predictions for observables as series expansions in E/Λ . Thus, it would be impossible to distinguish $\mathcal{L}_{\text{SMEFT}}$ from \mathcal{L}_{SM} at energies too much lower than Λ , e.g. $\mathcal{O}(\text{TeV})$ or less. Also, non-SM exotic states are not required to exist within experimentally probed energies, as such series expansions lead to well-defined and physical predictions as long as $E \ll \Lambda$. This latter aspect should be contrasted with the situation before the Higgs boson discovery — it was known from perturbative unitarity considerations that the then-established EFT cannot have an arbitrarily high cutoff, and then-unknown

degrees of freedom must be present below a few hundred GeV [10] (and indeed we found the 125 GeV Higgs boson).

Nevertheless, there is a major flaw of this possibility, namely

$$|m_H^2| \lll \Lambda^2. \quad (1.6)$$

We know that the SMEFT has to be ultraviolet (UV) completed around some cutoff scale Λ , by a new theory valid above that scale which involves new degrees of freedom inactive at low energy¹. When the UV theory, whatever it is, is matched onto the SMEFT, the coefficient of the $|H|^2$ operator, with mass dimension two, generically receives a threshold correction of order Λ^2 (possibly slightly suppressed by loop factors and/or small couplings), as we can see simply by dimensional analysis. To arrive at Eq. (1.6), significant fine-tuning would be needed so that various $\mathcal{O}(\Lambda^2)$ contributions cancel to precisely produce a much lower m_H^2 .² This is the well-known naturalness or hierarchy problem, cast in the EFT language. To alleviate this fine tuning, we therefore prefer Λ (and hence new physics) to be not too far above the weak scale, e.g. (a few) TeV.

Now we seem to have a conundrum: neutrino oscillations and proton stability apparently suggest a very high cutoff Λ for our SMEFT, while naturalness concerns motivate a cutoff close to the weak scale. However, both neutrino oscillations and proton decay are special phenomena because they violate accidental global symmetries of \mathcal{L}_{SM} , lepton number (L) and baryon number (B) in particular. Thus, it is reasonable to expect that new physics that cures the hierarchy problem may lie at a scale $\Lambda \sim \mathcal{O}(\text{TeV})$ and preserves B and L , and allows for a consistent EFT description up to a much higher, new cutoff scale, where B and L are violated by the next layer of UV completion. An example of this possibility is supersymmetry (SUSY) with R parity, which screens quantum corrections to the Higgs mass above the SUSY breaking scale, while preserving B and L to avoid proton decay. Similar considerations apply when reconciling $\Lambda \sim \mathcal{O}(\text{TeV})$ with flavor physics constraints, which requires a nontrivial flavor structure of new physics [12], such as minimal flavor violation [13].

The upshot is that there are good reasons to believe that Nature is described by the SMEFT of Eq. (1.5) (rather than Eq. (1.1)) at the weak scale, with some of the higher-dimensional operators suppressed by a scale Λ that is not too far above, where new physics

¹One may argue that $\Lambda^{(5)} \sim 10^{14}$ GeV is not really necessary if neutrino masses are purely Dirac. However, there is a fundamental limit on how high Λ can be, as we know a quantum gravity UV completion is needed at the Planck scale $M_{\text{pl}} \sim 10^{19}$ GeV. Thus, one cannot deny the hierarchy problem of Eq. (1.6) unless our basic EFT concepts, well-established up to the weak scale, were to be radically compromised in the (unknown) theory of quantum gravity. See [11] for further discussion.

²Note that m_H^2 is renormalized multiplicatively in the SMEFT in a mass-independent scheme such as the commonly used $\overline{\text{MS}}$. Thus it has to be small not only at the weak scale, but also at Λ .

would appear that alleviates fine-tuning. An important task of current particle physics research is to search for such new physics in all possible ways.

To close this section, we remark that there are several additional hints of new physics beyond the SM, including dark matter, the baryon asymmetry of the universe, cosmic inflation, the strong CP problem, etc. (see e.g. [14,15]). However, we would like to emphasize the unique role of the hierarchy problem, in that while all the other problems can in principle be solved with new physics at much higher energies, the fine-tuning of Eq. (1.6) cries out for a solution in the vicinity of the weak scale. In this respect, the naturalness belief (despite having been slightly relaxed quantitatively by recent LHC results) is perhaps the best reason to be optimistic about new discoveries in the foreseeable future.

1.2 Precision analyses as indirect probes of new physics

The search for new physics beyond the SM is an extensive program, and efforts must be made at all frontiers. As far as TeV-scale new physics relevant for naturalness is concerned, the best case scenario would be to observe their direct production at high energy colliders, such as the LHC. As a typical example, the scalar top partner (stop), in SUSY can be searched for via pair production at the LHC in various decay channels of the stops, e.g. jets + missing transverse energy when both stops decay hadronically. Recent LHC data have excluded stop masses up to as high as ~ 850 GeV, depending on the lightest neutralino mass [16–21].

A limitation of direct searches, however, is that they have to be carried out on a case-by-case basis, by looking for signatures that would be produced by each well-motivated new physics scenario. For example, if the new states responsible for solving the hierarchy problem are vectorlike top partners, which generically appear in composite Higgs models, rather than stops in SUSY, they would decay into e.g. Zt , ht or Wb , and thus have to be searched for in these channels [22,23].

Moreover, in many scenarios, the existence of new particles can be hidden from direct searches, if it decays into final states that have large backgrounds. One extreme example is a new particle with a large exotic decay branching ratio into several jets within the acceptance of the detector, which would be buried under huge QCD background at the LHC. Thus, one cannot always fully rely on direct production to look for new physics.

On the other hand, it has been realized for quite some time now that precision measurements of SM processes can provide indirect probes of new physics, complementary to direct searches. The idea is that even if new particles evade direct searches – either because they are too heavy to be produced with the available collider energy, or because their signatures cannot be discerned from SM backgrounds – they can contribute to SM processes as inter-

mediate states, and so can be searched for via deviations of measured observables from SM predictions.

Over the past few decades, high-precision measurements of electroweak and flavor observables have found remarkable agreement with the SM, leading to stringent constraints on BSM effects in these sectors; see e.g. [24–28]. The Higgs sector of the SM will be put under similar scrutiny once more data are collected, and even global analyses combining data from all sectors may become possible [29, 30].

As in direct searches, one can of course examine each new physics model individually against precision data and see what regions of parameter space are allowed (see e.g. [31–36]). However, for precision analyses, it is possible, and often desirable to perform more general analyses whose results can be translated into broad classes of BSM scenarios. As we will discuss in more detail below, EFT provides a consistent and useful framework to do so, provided experimental measurements are made at energies below new particle thresholds.

To gain some intuition on the power of precision measurements, let us make some simple estimates. Suppose the observable new physics effect is encoded in some dimension-six operator (which is the most common case). This would generically result in fractional deviations from SM predictions of $\mathcal{O}(v^2/\Lambda^2)$ for some observables, and $\mathcal{O}(E^2/\Lambda^2)$ for others. Thus, if our experiment is sensitive to these deviations at the 10% (1%, 0.1%) level, we would be able to probe

$$\Lambda \sim 0.8 (2.5, 8) \text{ TeV} \quad \text{for } \mathcal{O}(v^2/\Lambda^2) \text{ deviation,} \quad (1.7a)$$

$$\Lambda \sim 3 (10, 30) \text{ TeV} \quad \text{for } \mathcal{O}(E^2/\Lambda^2) \text{ deviation at } E = 1 \text{ TeV.} \quad (1.7b)$$

Of course, one should keep in mind that Λ is not to be directly identified with masses of new particles — it is generally a ratio of mass and powers of couplings, possibly multiplied by powers of $16\pi^2$ if the operator is loop generated. Nevertheless, the numbers in Eq. (1.7) are encouraging, and suggest at least in some scenarios, precision measurements can offer a powerful indirect probe of TeV-scale new physics.

1.3 Bottom-up and top-down EFT approaches

EFT offers a bridge between heavy new physics models and lower energy experimental observations, which can be crossed in both ways.

From the bottom-up point of view, the idea is to use power counting arguments to keep only the terms in $\mathcal{L}_{\text{SMEFT}}$ that are expected to give the dominant deviations from the SM, while remaining agnostic about concrete UV models giving rise to these operators.

Experimental data are translated into constraints on the parameter space spanned by a finite set of operator coefficients, without reference to any UV theory.

For such a bottom-up EFT approach to be useful, we need a well-motivated power counting scheme, so that our truncated EFT accommodates low energy limits of interesting UV theories, and thus, knowledge we gain from experimental data on the EFT parameter space can be meaningfully interpreted in these UV theories when needed.

One motivation is generality — we want our EFT to accommodate as many interesting UV scenarios as possible. In this regard, a scheme that is perhaps the most often used is Λ power counting. With the general expectation that observable effects of higher dimensional operators are suppressed by higher powers of Λ , it is common practice to truncate the SMEFT Lagrangian at dimension six level,

$$\mathcal{L}_{\text{SMEFT}} \simeq \mathcal{L}_{\text{SM}} + \sum_i \frac{1}{(\Lambda_i^{(6)})^2} \mathcal{O}_i^{(d=6)} \equiv \mathcal{L}_{\text{SM}} + \sum_i c_i \mathcal{O}_i^{(d=6)}. \quad (1.8)$$

Here we have dropped the single dimension-five operator, which is presumably suppressed by a much higher scale $\Lambda^{(5)} \gg \Lambda_i^{(6)}$. In this case, our SMEFT parameter space is spanned by $\{c_i\}$ (in addition to SM parameters).

There are different bases in which $\{c_i\}$ can be defined, and it must be clearly stated which basis is used when quoting bounds on a specific operator coefficient. More precisely, a complete, nonredundant basis is needed to make $\{c_i\}$ unambiguous. In particular, redundancies can arise because different operators can be transformed into each other by integration by parts, group theoretic identities, or field redefinitions, and all of them should not be kept in a valid, nonredundant basis. The freedom of choosing different operators to be kept results in the multitude of operator bases commonly used in the literature, including the Warsaw basis [3], the EGGM basis [37], the SILH basis [38], and the Higgs basis [7]. All of them are equivalent parameterizations of the SMEFT truncated at dimension six level, and are convenient for different phenomenological and theoretical applications.

There exist other power counting schemes, motivated by broad features of UV theories. The finite set of operators kept in the EFT Lagrangian would differ from Eq. (1.8), but the EFT parameter space is similarly spanned by a finite set of operator coefficients like $\{c_i\}$. For example, chiral power counting [39–44] is suitable for strongly-coupled new physics scenarios where electroweak symmetry breaking is nonlinearly realized. Such alternative schemes will not be discussed further in this dissertation.

The central question in bottom-up EFT studies is: *what can we learn about the SMEFT, i.e. values of $\{c_i\}$ in Eq. (1.8), from experimental data, and what does that imply for new physics?* Up to now, a first-order answer to this question is, unfortunately, that all c_i 's are

consistent with zero, and we have no clue what new physics UV-completes the SMEFT.

There is, however, more detailed information we have learned. Some directions in the $\{c_i\}$ space are more constrained than others, most importantly due to better experimental precisions achieved for some observables than others. Thus, when building a new physics model, we should better make sure that the well-constrained (combinations of) c_i 's are not generated with unacceptable sizes.

In fact, many of the SMEFT studies in recent years take advantage of this *precision hierarchy* to organize the otherwise complicated and unilluminating analyses. As far as electroweak and Higgs physics are concerned, this has resulted in the following standard picture [29, 38, 45, 46].

- Pole observables, such as the W boson mass, the Z boson width, etc., have been measured at electron-positron colliders, LEP and SLC in particular, some of which reaching the per-mil level.
- Diboson production processes, such as $e^+e^- \rightarrow W^+W^-$ and $pp \rightarrow W^+W^-$, have been measured to the 1-10% level.
- Higgs observables, such as Higgs boson production cross sections and decay branching fractions, have only been measured recently, with even worse precision.

With this information, we can classify dimension-six operators according to which set of observables they affect. Then it becomes clear which operator is constrained at what level.

It is worth emphasizing that a key advantage of the bottom-up EFT approach is that information about the SMEFT can be learned in a UV model-independent way. The focus is usually a broad-brush picture of new physics that is sufficient to capture generic features. It is a separate step to make the UV-EFT connection concrete, if one wishes to learn about precision constraints on a specific UV theory.

The top-down EFT approach has a different starting point. Here we would like to study some specified UV theory for new physics, say some realization of SUSY. Because states much heavier than experimental energies decouple from observation, the appropriate way to do calculations is to first match the full theory onto an EFT by integrating out the heavy states, then renormalization group (RG) evolve the EFT from the heavy particle thresholds down to lower energies where experiments are performed, and finally use the EFT at these lower energies to calculate observables. If multiple heavy particles are present at disparate scales, they should be integrated out in sequence, with several layers of EFTs RG evolved in the respective energy regimes. In this way, large logarithms of mass ratios can be resummed, so that our theory predictions for observables become more accurate and reliable.

The central question in top-down EFT studies is: *given a UV theory, what is the low-energy EFT, and what are its observable consequences?* The answer to this question is of course UV theory specific.

As new particles are excluded up to higher masses by LHC data, this top-down EFT approach becomes more useful in the study of beyond SM physics. As an example, as weak-scale SUSY has become less favored, there has been growing interest recently in EFT calculations of SUSY corrections to the Higgs potential, greatly improving upon previous full theory calculations [47–53].

A key ingredient of top-down EFT studies is matching a given UV theory onto its low-energy EFT. EFT matching calculations are typically performed using Feynman diagram methods. This involves calculating correlation functions among the light fields in the UV theory, expanding them in inverse powers of a heavy mass scale, then extracting the relevant parts for the operator coefficients by comparing with the same correlation functions computed in the EFT (see e.g. [54]). This traditional Feynman diagram approach, albeit familiar and well-developed, is a rather roundabout route from the UV theory to the EFT. In contrast, there are more elegant alternative methods for obtaining operator coefficients, which avoid the need for computing correlation functions. They are based on direct evaluation of the functional path integral, and have gone through significant development recently [55–61]. The key technique involved is developed in Chapter 6 of this dissertation, which is based on [60].

Both bottom-up and top-down EFT approaches reviewed above are complementary, as we continue to dig for hints of new physics from precision data. Top-down studies tell us which effective operators may be more interesting to search for, and guide our choice of power counting schemes to make bottom-up studies more useful. Meanwhile, bottom-up studies tell us what kinds of SM deformations are still allowed by data (in terms of model-independent constraints on the EFT parameter space), and guide our model building to make top-down studies better oriented. It is by combining both approaches that the EFT framework offers a valuable tool in our quest for new physics.

1.4 What’s new?

While the basic concepts of EFT have been standard knowledge for decades, there have been new developments on the subject in recent years. We would like to highlight a few in the following.

- The LHC has discovered the Higgs boson and begun to measure its properties, making

it possible for the first time to perform global precision analyses incorporating Higgs data. (Bottom-up) EFT provides the natural framework to do so, and has thus received renewed interest [29, 37–46, 62–120].

- The importance of a better understanding and treatment of theory uncertainties in precision analyses has attracted more attention. For example, new issues have been pointed out regarding SM parametric uncertainties in precision Higgs calculations [30, 121], and regarding EFT calculation uncertainties in precision electroweak fits [91, 104, 114].
- The high energy data acquired at the LHC are challenging the precision hierarchy paradigm reviewed in the previous section. This is because in the presence of operators causing $\mathcal{O}(E^2/\Lambda^2)$ deviations from the SM, the name of the game is no longer precision alone, as going to higher energy is sometimes easier than achieving better experimental precision. Ideas have been explored on how to take advantage of high energy data to better constrain the SMEFT parameter space, and to possibly reorganize bottom-up EFT analyses [116, 117, 119].
- The LHC high energy data have also brought up the issue of EFT validity in some cases, where the Λ scales probed may not be much higher than experimental energies. Care is needed to derive and interpret results of bottom-up EFT studies [113, 115].
- New knowledge about QFT has been learned from EFT-motivated studies. In addition to functional matching techniques mentioned in the previous section, we have learned, for example, an intriguing holomorphic structure of the dimension-six operator anomalous dimensions [122–124], an algorithm to count the number of independent operators at a certain dimensionality based on Hilbert series [4, 125–127], helicity selection rules for SMEFT amplitudes at high energy [128–130], to name just a few.

Our hope is that, as new data keep coming, new ideas will develop, and EFT will continue to be a fertile ground for making progress in our understanding of fundamental physics.

1.5 Outline of this dissertation

The body of this dissertation consists of three parts. We first discuss aspects of precision analyses, with Chapters 2 and 3 devoted to electroweak and Higgs physics, respectively. Next, Chapters 4 and 5 cover bottom-up EFT applications, in describing universal theories and interpreting W pair production, respectively. Finally, in Chapters 6 and 7 we take a

top-down EFT approach, developing the covariant diagrams technique for one-loop matching and then applying it to trans-TeV supersymmetry. An outline of each chapter is given in the following.

Chapter 2: Precision Electroweak Analyses after the Higgs Boson Discovery

The discovery of the Higgs boson and measurement of its mass allow, for the first time, precision electroweak analysis to be formulated in an expansion formalism. In this chapter, which is based on [131], written in collaboration with James D. Wells, we present expansion formulas for many electroweak observables, which consistently incorporate parametric dependence, and facilitate calculations within and beyond the SM.

Chapter 3: Resolving Charm and Bottom Quark Masses in Precision Higgs Analyses

Higgs observables, e.g. partial widths and branching ratios, are conventionally calculated with charm and bottom quark masses treated as input parameters. In this chapter, which is based on [30], written in collaboration with Alexey A. Petrov, Stefan Pokorski and James D. Wells, we point out that this procedure hides important uncertainties and correlations in quark mass extractions from low-energy observables, which must be taken into account in future precision studies.

Chapter 4: EFT of Universal Theories and its RG Evolution

Constraints on oblique parameters, e.g. S , T parameters, from precision electroweak data are, generally speaking, only applicable to universal theories at leading order. In this chapter, which is based on [109, 111], written in collaboration with James D. Wells, we present an EFT description of universal theories, clarifying restrictions on the EFT parameter space necessary for the use of oblique parameters. Moreover, theories that are universal at high scales can flow to EFTs at the electroweak scale that are non-universal. With a detailed renormalization group analysis, we point out, in particular, that a consistent fit to precision electroweak data should go beyond the oblique parameters framework even for universal UV theories.

Chapter 5: Time to Go Beyond TGC Interpretation of W Pair Production

The conventional interpretation of W boson pair production at lepton and hadron colliders as triple gauge coupling (TGC) measurements is based on the “TGC dominance assumption.” In this chapter, which is based on [117], we find that, contrary to conventional knowledge, this

assumption is challenged by high-energy data, calling for re-organization of EFT analyses to better search for new physics effects.

Chapter 6: Covariant Diagrams for One-Loop Matching

Matching a UV theory onto a low-energy EFT by integrating out heavy states can be accomplished with more elegant and simpler methods than Feynman diagrams. In this chapter, which is based on [60], we introduce a diagrammatic framework that preserves gauge covariance, dubbed “covariant diagrams,” which is based on functional matching ideas and greatly facilitates one-loop matching calculations.

Chapter 7: EFT Approach to Trans-TeV Supersymmetry

Lack of superpartner discoveries, together with Higgs boson mass measurements, points to SUSY scales somewhat decoupled from the weak scale. In this chapter, which is based on [132], written in collaboration with James D. Wells, we present a detailed EFT analysis of this scenario, taking advantage of the covariant diagrams technique. We explore implications of bottom-tau Yukawa unification on SUSY spectra and Higgs coupling modifications.

Chapter 2

Precision Electroweak Analyses After the Higgs Boson Discovery

Until recently precision electroweak computations were fundamentally uncertain due to lack of knowledge about the existence of the Standard Model Higgs boson and its mass. For this reason substantial calculational machinery had to be carried along for each calculation that changed the Higgs boson mass and other parameters of the Standard Model. Now that the Higgs boson is discovered and its mass is known to within a percent, we are able to compute reliable semi-analytic expansions of electroweak observables. In this section, we present results of those computations in the form of expansion formulae. In addition to the convenience of having these expressions, we show how the approach makes investigating new physics contributions to precision electroweak observables much easier.

2.1 Introduction

Precision electroweak analyses have played an important role in testing the Standard Model (SM) and constraining new physics. Now this program has entered a new era with the discovery of the Higgs boson [1,2]. The sub-percentage-level determination of the Higgs boson mass [1,2,133] constitutes the last piece of a complete set of input observables. Electroweak observables can now be calculated to unprecedented accuracy, leading to unprecedented sensitivity to new physics beyond the SM.

The standard approach of precision electroweak analysis is to perform a χ^2 analysis, which involves varying the model parameters, or equivalently, a set of input observables to minimize the χ^2 function. In practice, this can be facilitated by an expansion about some reference values of the input, since we have a set of well-measured input observables that allows little variation. We present such an expansion formalism, and apply it to deriving

constraints on new physics models. Most of the numerical results in what follows reflect state-of-the-art calculations of the electroweak observables, as implemented in the ZFITTER package [134, 135].

This chapter is organized as follows. We first review the definition of the electroweak observables under consideration in Section 2.2. Then in Section 2.3 we present the expansion formalism for calculating the SM and new physics contributions to the observables. The result will be that given the values of 6 input observables, and the new physics model, all observables can be easily calculated. The tools needed in this calculation, including the reference values of all observables, and the expansion coefficients, are presented. Next, we illustrate how to use the formalism by working out some new physics examples in Section 2.4. Finally, in Section 2.5 we summarize.

2.2 Standard Model parameters and observables

The parameters of the SM include the gauge couplings g_3, g_2, g_1 , the Yukawa couplings y_f , flavor angles, the Higgs vacuum expectation value v and self-coupling λ . For the purpose of precision electroweak analysis, with inconsequential errors we can treat all Yukawa couplings except that for the top quark as constants, and correspondingly set the lepton and light quark masses to their default values in ZFITTER (see [134]). Then there are six parameters¹ in the theory:

$$\{g_3, g_2, g_1, y_t, v, \lambda\}. \quad (2.1)$$

There are an infinite number of SM observables that can be defined. They correspond to well-defined quantities that are measured in experiments. The SM predicts each observable as a function of the parameters in Eq. (2.1). The success of the SM relies on the fact that the prediction for all observables agree with precision measurements, with suitable choices of the parameters. If some new physics beyond the SM were to exist, it could potentially destroy the agreement. Thus, precision analysis enables us to put stringent constraints on new physics models. In this study we focus on the following list of observables, mostly relevant to precision tests of the electroweak theory.

- Pole mass of the particles: m_Z, m_W, m_t, m_H .
- Observables associated with the strengths of the strong, weak, and electromagnetic interactions: $\alpha_s(m_Z), G_F$, and $\alpha(m_Z)$. The Fermi constant G_F is defined via the

¹We do not include flavor CKM angles in our calculations since all standard precision electroweak observables do not substantively depend on these angles.

muon lifetime [136]. $\alpha(m_Z)$ is related to the fine structure constant α_0 defined in the Thomson limit via

$$\alpha(m_Z) = \frac{\alpha_0}{1 - \Delta\alpha_\ell - \Delta\alpha_t - \Delta\alpha_{\text{had}}^{(5)}}. \quad (2.2)$$

We treat $\alpha_0 = 1/137.035999074(44)$ [136, 137] as a constant, since it is extraordinarily well measured. The contribution from leptons $\Delta\alpha_\ell$ and the top quark $\Delta\alpha_t$ are perturbatively calculable and known very accurately, so the uncertainty in $\alpha(m_Z)$ essentially comes from the incalculable light hadron contribution $\Delta\alpha_{\text{had}}^{(5)}$, which is extracted from low energy $e^+e^- \rightarrow \text{hadrons}$ data via dispersion relations [136]. For simplicity, we will occasionally (especially in subscripts) drop the scale “ (m_Z) ” in $\alpha_s(m_Z)$ and $\alpha(m_Z)$, and write $\Delta\alpha_{\text{had}}^{(5)}$ as $\Delta\alpha$ in the following.

- Z boson decay observables: total width Γ_Z , and partial widths into fermions $\Gamma_f \equiv \Gamma(Z \rightarrow f\bar{f})$. Also we define and use the invisible and hadronic partial widths²:

$$\Gamma_{\text{inv}} \equiv 3\Gamma_\nu, \quad \Gamma_{\text{had}} \equiv \Gamma(Z \rightarrow \text{hadrons}) \simeq \Gamma_u + \Gamma_d + \Gamma_c + \Gamma_s + \Gamma_b. \quad (2.3)$$

The ratios of partial widths are defined and also included in our observables list:

$$R_\ell \equiv \frac{\Gamma_{\text{had}}}{\Gamma_\ell}, \quad R_q \equiv \frac{\Gamma_q}{\Gamma_{\text{had}}}, \quad (2.4)$$

where ℓ and q denote any one of the lepton and quark species, respectively.

- $e^+e^- \rightarrow \text{hadrons}$ cross section at the Z pole:

$$\sigma_{\text{had}} = 12\pi \frac{\Gamma_e \Gamma_{\text{had}}}{m_Z^2 \Gamma_Z^2}. \quad (2.5)$$

- Forward-backward asymmetries for $e^+e^- \rightarrow f\bar{f}$ at the Z pole:

$$A_{\text{FB}}^{0,b} f = \frac{\sigma_F - \sigma_B}{\sigma_F + \sigma_B} = \frac{3}{4} \mathcal{A}_e \mathcal{A}_f. \quad (2.6)$$

The asymmetry parameters \mathcal{A}_f are related to the definition of the effective electroweak mixing angle $\sin^2 \theta_{\text{eff}}^f$ by

$$\mathcal{A}_f = \frac{2(1 - 4|Q_f| \sin^2 \theta_{\text{eff}}^f)}{1 + (1 - 4|Q_f| \sin^2 \theta_{\text{eff}}^f)^2}, \quad (2.7)$$

² Γ_{had} is not quite the sum of all Γ_q , as there are $\mathcal{O}(\alpha_s^3)$ corrections that cannot be attributed to any Γ_q [138]. However, these corrections are small, and are neglected in ZFITTER.

where Q_f is the electric charge of fermion f .

The experimental results for these observables are listed in Table 2.1. For all the Z pole observables, we use the numbers presented in [139], which are combinations of various experimental results at LEP and SLC. Among these observables, lepton universality is assumed only for $\sin^2 \theta_{\text{eff}}^e$. For $\sin^2 \theta_{\text{eff}}^e$, we also list the PDG combination [136] of D0 [140] and CDF [141] results (the second number). m_W from [142] is the average of LEP2 [143] and Tevatron [142] results. m_H is the PDG average [136] of ATLAS [1] and CMS [133] results.

Table 2.1 also contains the reference theory values around which we expand, and their percent relative uncertainties. These theory quantities will be introduced and discussed in detail in Section 2.3.2.

2.3 The formalism

2.3.1 Expansion about reference point

Let us denote the set of SM parameters in Eq. (2.1) by $\{p_{k'}\}$, and the set of SM observables by $\{\widehat{O}_i\}$. The theoretical prediction for each observable can be calculated in the SM as a function of all parameters:

$$\widehat{O}_i^{\text{th}} = \widehat{O}_i^{\text{SM}}(\{p_{k'}\}). \quad (2.8)$$

The notation here is that primed roman indices run from 1 to N_p , the number of SM parameters, while unprimed ones run from 1 to N_O , the number of observables under consideration. Note that N_p is finite, while N_O can presumably be infinite (we must at least have $N_O > N_p$ in order to test any theory). The analysis in this section is done with $N_p = 6$ and $N_O = 31$, with $\{p_{k'}\}$ given in Eq. (2.1) and $\{\widehat{O}_i\}$ listed in Table 2.1.

Next, suppose we want to study some new physics model beyond the SM, which contains a set of new parameters collectively denoted as p^{NP} (“NP” for “new physics”). Then at least some $\widehat{O}_i^{\text{th}}$ will receive new contribution. We expect such new contribution to be small, in the light of apparently good agreement between SM predictions and precision electroweak data. We can thus write

$$\widehat{O}_i^{\text{th}} = \widehat{O}_i^{\text{SM}}(\{p_{k'}\}) + \delta^{\text{NP}} \widehat{O}_i(\{p_{k'}\}, p^{\text{NP}}). \quad (2.9)$$

We wish to decide whether the new physics model is compatible with precision electroweak data, i.e. whether the $\widehat{O}_i^{\text{th}}$ predicted by Eq. (2.9) are compatible with the experimentally measured values $\widehat{O}_i^{\text{expt}}$.

One common misconception in such analysis is that a new physics model would be ruled out if, for some very precisely measured observables, e.g. $G_F^{\text{expt}} = 1.1663787(6) \times 10^{-5} \text{ GeV}^{-2}$,

\widehat{O}_i	$\widehat{O}_i^{\text{expt}}$	$\widehat{O}_i^{\text{ref}}$	$P[\widehat{O}_i^{\text{ref}}]$
m_Z [GeV]	91.1876(21) [139]	91.1876	
G_F [GeV ⁻²]	1.1663787(6)e-5 [136]	1.1663787e-5	
$\Delta\alpha_{\text{had}}^{(5)}$	0.02772(10) [136]	0.02772	
m_t [GeV]	173.20(87) [144]	173.20	
$\alpha_s(m_Z)$	0.1185(6) [136]	0.1185	
m_H [GeV]	125.9(4) [136]	125.9	
$\alpha(m_Z)$	7.81592(86)e-3 [136]	7.75611e-3	0.01
m_W [GeV]	80.385(15) [142]	80.3614	0.01
Γ_e [MeV]	83.92(12) [139]	83.9818	0.02
Γ_μ [MeV]	83.99(18) [139]	83.9812	0.02
Γ_τ [MeV]	84.08(22) [139]	83.7916	0.02
Γ_b [MeV]	377.6(1.3) [139]	375.918	0.04
Γ_c [MeV]	300.5(5.3) [139]	299.969	0.06
Γ_{inv} [GeV]	0.4974(25) [139]	0.501627	0.02
Γ_{had} [GeV]	1.7458(27) [139]	1.74169	0.04
Γ_Z [GeV]	2.4952(23) [139]	2.49507	0.03
σ_{had} [nb]	41.541(37) [139]	41.4784	0.01
R_e	20.804(50) [139]	20.7389	0.03
R_μ	20.785(33) [139]	20.7391	0.03
R_τ	20.764(45) [139]	20.7860	0.03
R_b	0.21629(66) [139]	0.215835	0.02
R_c	0.1721(30) [139]	0.172229	0.01
$\sin^2 \theta_{\text{eff}}^e$	0.23153(16) [139]	0.231620	0.04
	0.23200(76) [136]		
$\sin^2 \theta_{\text{eff}}^b$	0.281(16) [139]	0.232958	0.03
$\sin^2 \theta_{\text{eff}}^c$	0.2355(59) [139]	0.231514	0.04
\mathcal{A}_e	0.1514(19) [139]	0.146249	0.44
\mathcal{A}_b	0.923(20) [139]	0.934602	0.00
\mathcal{A}_c	0.670(27) [139]	0.667530	0.04
$A_{\text{FB}}^{0,b}e$	0.0145(25) [139]	0.0160415	0.88
$A_{\text{FB}}^{0,b}b$	0.0992(16) [139]	0.102513	0.44
$A_{\text{FB}}^{0,b}c$	0.0707(35) [139]	0.0732191	0.48

Table 2.1: (From [131]) The list of observables, their experimental and reference values, and percent relative uncertainties.

the new physics contribution $\delta^{\text{NP}}\widehat{O}_i$ exceeds the experimental error. The point is that the SM parameters $\{p_{k'}\}$ are not directly measured experimentally. Rather, in testing the SM, we adjust $\{p_{k'}\}$ and see that for some choice of all parameters $\{p_{k'}^{\text{ref}}\}$, all $\widehat{O}_i^{\text{SM}}$ agree well with $\widehat{O}_i^{\text{expt}}$. In the presence of new physics, we should do the same thing, and will typically arrive at a different choice of $\{p_{k'}^{\text{ref}}\}$, and hence different $\widehat{O}_i^{\text{SM}}$, which may allow the new physics model to survive (in some regions of parameter space spanned by p^{NP}) despite a large $\delta^{\text{NP}}\widehat{O}_i$.

The statements above are made more precise by the χ^2 analysis, which is the standard way of doing precision electroweak analysis. With correlations among the observables ignored, and experimental errors assumed larger than theoretical errors, the χ^2 function is defined by

$$\chi^2(\{p_{k'}\}, p^{\text{NP}}) = \sum_i \left[\frac{\widehat{O}_i^{\text{th}}(\{p_{k'}\}, p^{\text{NP}}) - \widehat{O}_i^{\text{expt}}}{\Delta\widehat{O}_i^{\text{expt}}} \right]^2, \quad (2.10)$$

where $\Delta\widehat{O}_i^{\text{expt}}$ are the experimental uncertainties of the observables. To decide whether some p^{NP} in the new physics model parameter space survives precision tests, we vary $\{p_{k'}\}$ to minimize the χ^2 function to find the best fit to experimental data, and see if this minimum χ^2 is small enough. A good discussion of how to interpret the statistics of the χ^2 distribution can be found in [136].

In principle, one can calculate $\widehat{O}_i^{\text{th}}$ each time a different $\{p_{k'}\}$ is chosen in this minimization procedure. But in practice, we can do it once and for all by carrying out an expansion about some reference point in the SM parameter space $\{p_{k'}^{\text{ref}}\}$. Such an expansion is useful because precision data does not allow much variation in each parameter. Thus, let's choose some $\{p_{k'}^{\text{ref}}\}$ that lead to good agreement between $\widehat{O}_i^{\text{SM}}$ and $\widehat{O}_i^{\text{expt}}$, and write

$$\widehat{O}_i^{\text{SM}}(\{p_{k'}\}) = \widehat{O}_i^{\text{ref}} + \sum_{k'} \frac{\partial\widehat{O}_i^{\text{SM}}}{\partial p_{k'}}(p_{k'} - p_{k'}^{\text{ref}}) + \dots \quad (2.11)$$

where $\widehat{O}_i^{\text{ref}} \equiv \widehat{O}_i^{\text{SM}}(\{p_{k'}^{\text{ref}}\})$, and the partial derivatives are taken at $p_{k'} = p_{k'}^{\text{ref}}$ (this will be implicitly assumed in the following). Alternatively, define

$$\bar{\delta}^{\text{SM}}\widehat{O}_i(\{p_{k'}\}) \equiv \frac{\widehat{O}_i^{\text{SM}}(\{p_{k'}\}) - \widehat{O}_i^{\text{ref}}}{\widehat{O}_i^{\text{ref}}}, \quad \bar{\delta}p_{k'} \equiv \frac{p_{k'} - p_{k'}^{\text{ref}}}{p_{k'}^{\text{ref}}}, \quad G_{ik'} \equiv \frac{p_{k'}^{\text{ref}}}{\widehat{O}_i^{\text{ref}}} \frac{\partial\widehat{O}_i^{\text{SM}}}{\partial p_{k'}}. \quad (2.12)$$

Then we have a more concise expression for Eq. (2.11):

$$\bar{\delta}^{\text{SM}}\widehat{O}_i = \sum_{k'} G_{ik'} \bar{\delta}p_{k'} + \dots \quad (2.13)$$

Here $\bar{\delta}$ means “fractional shift from the reference value”, and the superscript on $\bar{\delta}^{\text{SM}}\widehat{O}_i$ indicates the shift comes from shifts in SM parameters. Ignoring higher order terms in the expansion, the constant $G_{ik'}$ is the fractional change in $\widehat{O}_i^{\text{SM}}$ caused by the fractional change in $p_{k'}$, and hence characterizes the sensitivity of the i th SM observable (as calculated in the SM) to the k' th SM parameter.

In the presence of perturbative new physics contributions, let’s define

$$\bar{\delta}\widehat{O}_i^{\text{th}}(\{p_{k'}\}, p^{\text{NP}}) \equiv \frac{\widehat{O}_i^{\text{th}}(\{p_{k'}\}, p^{\text{NP}}) - \widehat{O}_i^{\text{ref}}}{\widehat{O}_i^{\text{ref}}}, \quad \xi_i(\{p_{k'}\}, p^{\text{NP}}) \equiv \frac{\delta^{\text{NP}}\widehat{O}_i(\{p_{k'}\}, p^{\text{NP}})}{\widehat{O}_i^{\text{ref}}}. \quad (2.14)$$

Then Eq. (2.9) can be expanded as, to first order,

$$\bar{\delta}\widehat{O}_i^{\text{th}} = \bar{\delta}^{\text{SM}}\widehat{O}_i + \xi_i = \sum_{k'} G_{ik'}\bar{\delta}p_{k'} + \xi_i. \quad (2.15)$$

The calculation of $\widehat{O}_i^{\text{th}}$ and hence χ^2 is then facilitated if we have at hand the constants $p_{k'}^{\text{ref}}$, $\widehat{O}_i^{\text{ref}}$ and $G_{ik'}$.

2.3.2 Recasting observables in terms of observables

The approach above is indirect, in the sense that the input of the analysis, the parameters $\{p_{k'}\}$, are not directly measurable – only $\{\widehat{O}_i\}$ are well-defined observables. We can do better if we use N_p very well measured observables $\{\widehat{O}_{i'}\}$ as input. Note that primed indices, which run from 1 to N_p , are used for input observables. Inverting the functions $\widehat{O}_i^{\text{SM}}(\{p_{k'}\})$, we can express other observables as functions of these input observables. Then it is immediately clear from $\widehat{O}_{i'}^{\text{expt}}$ and $\Delta\widehat{O}_{i'}^{\text{expt}}$ what reference values for the input we should use, and by how much they are allowed to vary. In our analysis, $N_p = 6$, and a convenient choice for the 6 input observables is

$$\{\widehat{O}_{i'}\} = \{m_Z, G_F, \Delta\alpha_{\text{had}}^{(5)}, m_t, \alpha_s(m_Z), m_H\}. \quad (2.16)$$

The reference values for these input observables are taken to be the central values experimentally measured; see Table 2.1. All other observables are output observables, and their reference values $\widehat{O}_i^{\text{ref}}$ are evaluated at $\widehat{O}_{i'} = \widehat{O}_{i'}^{\text{ref}}$ with the help of ZFITTER. See [131] for technical details.

We also show in Table 2.1 the “percent relative uncertainties” $P[\widehat{O}_i^{\text{ref}}]$, defined as the maximum value of

$$100 \left| \frac{\widehat{O}_i^{\text{SM}}(\{\widehat{O}_{i'}\}) - \widehat{O}_i^{\text{ref}}}{\widehat{O}_i^{\text{ref}}} \right| \quad (2.17)$$

when all $\{\widehat{O}_{i'}\}$ are varied in their 1σ range around $\{\widehat{O}_{i'}^{\text{expt}}\}$. We do not distinguish between positive and negative relative uncertainties because, as we have checked, the asymmetry in the uncertainties for all observables considered here are very small.

To work out the expansion about the reference point, we assume the input observables $\{\widehat{O}_{i'}\}$ are the first N_p observables in the list $\{\widehat{O}_i\}$. Then we can simply invert the first N_p equations in Eq. (2.13). To first order,

$$\bar{\delta}^{\text{SM}}\widehat{O}_{i'} = \sum_{k'} G_{i'k'}\bar{\delta}p_{k'} = \sum_{k'} \widetilde{G}_{i'k'}\bar{\delta}p_{k'} \quad \Rightarrow \quad \bar{\delta}p_{k'} = \sum_{i'} (\widetilde{G}^{-1})_{k'i'}\bar{\delta}^{\text{SM}}\widehat{O}_{i'}. \quad (2.18)$$

Note that G is a $N_O \times N_p$ matrix, while \widetilde{G} is the upper $N_p \times N_p$ block of G . Then Eq. (2.13) suggests

$$\bar{\delta}^{\text{SM}}\widehat{O}_i = \sum_{k',i'} G_{ik'}(\widetilde{G}^{-1})_{k'i'}\bar{\delta}^{\text{SM}}\widehat{O}_{i'} \equiv \sum_{i'} c_{ii'}\bar{\delta}^{\text{SM}}\widehat{O}_{i'}, \quad (2.19)$$

where we have defined

$$c_{ii'} \equiv \sum_{k'} G_{ik'}(\widetilde{G}^{-1})_{k'i'} = \frac{\widehat{O}_{i'}^{\text{ref}}}{\widehat{O}_i^{\text{ref}}} \frac{\partial \widehat{O}_i^{\text{SM}}}{\partial \widehat{O}_{i'}^{\text{SM}}}. \quad (2.20)$$

Eq. (2.19) expresses the shift in any observable in terms of shifts in the input observables, as calculated in the SM. Notably, the upper $N_p \times N_p$ block of the $N_O \times N_p$ matrix c is the identity matrix, i.e. $c_{j'i'} = \delta_{j'i'}$. For $i > N_p$, i.e. the output observables, the calculation of $c_{ii'}$ is nontrivial. We present in Table 2.2 the results for these expansion coefficients for the observables discussed in Section 2.2, which we calculate using ZFITTER. These coefficients are useful not only because they facilitate the calculation of SM observables. They also give us information on the sensitivity of the calculated observables to each input observable.

In the presence of new physics, Eq. (2.15) becomes

$$\bar{\delta}\widehat{O}_i^{\text{th}} = \sum_{i'} c_{ii'}\bar{\delta}^{\text{SM}}\widehat{O}_{i'} + \xi_i = \sum_{i'} c_{ii'}(\bar{\delta}\widehat{O}_{i'}^{\text{th}} - \xi_{i'}) + \xi_i = \sum_{i'} c_{ii'}\bar{\delta}\widehat{O}_{i'}^{\text{th}} + \bar{\delta}^{\text{NP}}\widehat{O}_i, \quad (2.21)$$

where

$$\begin{aligned} \bar{\delta}^{\text{NP}}\widehat{O}_i &\equiv \xi_i - \sum_{i'} c_{ii'}\xi_{i'} \\ &= \xi_i - c_{i,m_Z}\xi_{m_Z} - c_{i,G_F}\xi_{G_F} - c_{i,\Delta\alpha}\xi_{\Delta\alpha} - c_{i,m_t}\xi_{m_t} - c_{i,\alpha_s}\xi_{\alpha_s} - c_{i,m_H}\xi_{m_H}. \end{aligned} \quad (2.22)$$

Eq. (2.21) expresses the shift in any observable in terms of shifts in the input observables and new physics effects. Note that for the input observables, since $c_{j'i'} = \delta_{j'i'}$, Eq. (2.22) indicates $\bar{\delta}^{\text{NP}}\widehat{O}_{i'} = 0$, and Eq. (2.21) trivially becomes $\bar{\delta}\widehat{O}_{i'}^{\text{th}} = \bar{\delta}\widehat{O}_{i'}^{\text{th}}$. This is forced to be true in our formalism, where $\widehat{O}_{i'}^{\text{th}}$ are inputs of the analysis, independent of new physics. Of

\widehat{O}_i	c_{i,m_Z}	c_{i,G_F}	$c_{i,\Delta\alpha}$	c_{i,m_t}	c_{i,α_s}	c_{i,m_H}
m_Z	1	0	0	0	0	0
G_F	0	1	0	0	0	0
$\Delta\alpha_{\text{had}}^{(5)}$	0	0	1	0	0	0
m_t	0	0	0	1	0	0
$\alpha_s(m_Z)$	0	0	0	0	1	0
m_H	0	0	0	0	0	1
$\alpha(m_Z)$	4.796e-3	0	0.02946	1.541e-4	-1.007e-5	0
m_W	1.427	0.2201	-6.345e-3	0.01322	-9.599e-4	-7.704e-4
Γ_e	3.377	1.198	-5.655e-3	0.01883	-1.253e-3	-7.924e-4
Γ_μ	3.377	1.198	-5.655e-3	0.01883	-1.253e-3	-7.924e-4
Γ_τ	3.383	1.198	-5.668e-3	0.01884	-1.254e-3	-7.931e-4
Γ_b	3.844	1.411	-0.01227	-0.01267	0.03672	-1.057e-3
Γ_c	4.151	1.590	-0.01721	0.02751	0.05046	-1.394e-3
Γ_{inv}	2.996	1.006	5.635e-5	0.01567	-9.967e-4	-4.873e-4
Γ_{had}	3.938	1.476	-0.01393	0.01578	0.03690	-1.204e-3
Γ_Z	3.692	1.353	-0.01028	0.01607	0.02543	-1.019e-3
σ_{had}	-2.069	-0.03281	9.806e-4	2.476e-3	-0.01522	4.057e-5
R_e	0.5608	0.2780	-8.272e-3	-3.045e-3	0.03815	-4.120e-4
R_μ	0.5608	0.2780	-8.272e-3	-3.045e-3	0.03815	-4.120e-4
R_τ	0.5554	0.2776	-8.259e-3	-3.053e-3	0.03816	-4.113e-4
R_b	-0.09434	-0.06530	1.652e-3	-0.02845	-1.782e-4	1.477e-4
R_c	0.2133	0.1135	-3.284e-3	0.01173	0.01356	-1.898e-4
$\sin^2 \theta_{\text{eff}}^e$	-2.818	-1.423	0.04203	-0.02330	1.796e-3	2.195e-3
$\sin^2 \theta_{\text{eff}}^b$	-2.823	-1.417	0.04204	-6.914e-3	1.201e-3	2.116e-3
$\sin^2 \theta_{\text{eff}}^c$	-2.819	-1.423	0.04202	-0.02331	1.795e-3	2.194e-3
\mathcal{A}_e	35.13	17.74	-0.5239	0.2905	-0.02239	-0.02737
\mathcal{A}_b	0.4525	0.2271	-6.737e-3	1.108e-3	-1.924e-4	-3.390e-4
\mathcal{A}_c	3.386	1.710	-0.05048	0.02800	-2.156e-3	-2.636e-3
$A_{\text{FB}}^{0,b}e$	70.27	35.48	-1.048	0.5810	-0.04479	-0.05473
$A_{\text{FB}}^{0,b}b$	35.59	17.97	-0.5306	0.2916	-0.02259	-0.02771
$A_{\text{FB}}^{0,b}c$	38.52	19.45	-0.5744	0.3185	-0.02455	-0.03000

Table 2.2: (From [131]) Expansion coefficients, as defined in Eq. (2.20), calculated in the basis of input observables containing $\Delta\alpha_{\text{had}}^{(5)}$. These encode the dependence of the output observables on each input observable.

course, new physics does contribute $\xi_{i'}$ to the calculation of $\widehat{O}_{i'}^{\text{th}}$, but as we decide to use some particular values for the input $\widehat{O}_{i'}^{\text{th}}$ to be consistent with $\widehat{O}_{i'}^{\text{expt}}$ (which are extraordinarily well measured), we find ourselves adjusting the SM parameters to compensate for $\xi_{i'}$. This adjustment gets propagated into the shift in $\widehat{O}_i^{\text{th}}$ due to new physics for $i > N_p$. As a result, Eq. (2.22) shows that for the output observables, $\bar{\delta}^{\text{NP}}\widehat{O}_i$ is not simply ξ_i , but is related to $\xi_{i'}$ for all input observables.

To close this subsection we remark on the calculation of ξ_i . In practice this is done at tree-level or one-loop-level, if we are only interested in constraining a new physics model at percentage level accuracy. Also, the definition of ξ_i , Eq. (2.14), instructs us to calculate them in terms of Lagrangian parameters, which can then be eliminated in favor of input observables using the tree-level relations between the two. This does not conflict with the ‘‘precision’’ part of the analysis, since we are doing two different perturbative expansions in the calculation: the expansion in SM couplings, and the expansion in new physics effects. Since new physics makes tiny contributions to $\widehat{O}_i^{\text{th}}$, to discern them we have to calculate the SM part as precisely as possible, carrying out the expansion in SM couplings to as high order as possible. On the other hand, in most cases the new physics contributions ξ_i need not be calculated beyond leading order, since they are already very small.

2.3.3 Beyond first order

The above perturbative expansion carried out to first order is expected to be sufficient for the purpose of precision electroweak analysis, since we have chosen a very well-measured set of input observables, so that the expansion parameters $\bar{\delta}\widehat{O}_{i'}^{\text{th}}$ are tiny. The impact of higher order terms in the expansion can be seen from the sensitivity of the expansion coefficients $c_{ii'}$ to the choice of reference values for the input observables $\widehat{O}_{i'}^{\text{ref}}$. In Table 2.3 we show the percent relative uncertainties for $c_{ii'}$, defined similarly to Eq. (2.17).

Alternatively, without varying $\widehat{O}_{i'}^{\text{ref}}$, we can explicitly write down the next order terms in the expansion:

$$\bar{\delta}^{\text{SM}}\widehat{O}_i = \sum_{i'} c_{ii'} \bar{\delta}^{\text{SM}}\widehat{O}_{i'} + \frac{1}{2!} \sum_{i'j'} c_{ii'j'} \bar{\delta}^{\text{SM}}\widehat{O}_{i'} \bar{\delta}^{\text{SM}}\widehat{O}_{j'} + \dots \equiv \sum_{i'} (c_{ii'} + \Delta c_{ii'}) \bar{\delta}^{\text{SM}}\widehat{O}_{i'} + \dots \quad (2.23)$$

where

$$c_{ii'j'} \equiv \frac{\widehat{O}_{i'}^{\text{ref}} \widehat{O}_{j'}^{\text{ref}}}{\widehat{O}_i^{\text{ref}}} \frac{\partial^2 \widehat{O}_i^{\text{SM}}}{\partial \widehat{O}_{i'}^{\text{SM}} \partial \widehat{O}_{j'}^{\text{SM}}}. \quad (2.24)$$

Then the size of second order terms in Eq. (2.23) compared with the first order term is

characterized by the ratio

$$\left| \frac{\Delta c_{ii'}}{c_{ii'}} \right| = \left| \frac{\sum_{j'} c_{ii'j'} \bar{\delta}^{\text{SM}} \widehat{O}_{j'}}{2c_{ii'}} \right| \leq \frac{\sum_{j'} |c_{ii'j'}| |\bar{\delta}^{\text{SM}} \widehat{O}_{j'}|}{2|c_{ii'}|} \equiv 0.01 r_{ii'}. \quad (2.25)$$

We show in Table 2.4 the $r_{ii'}$ calculated with $\bar{\delta}^{\text{SM}} \widehat{O}_{j'} = \Delta \widehat{O}_{j'}^{\text{expt}} / \widehat{O}_{j'}^{\text{ref}}$. The results follow a similar pattern as in Table 2.3.

Tables 2.3 and 2.4 both show that the uncertainties on the observables calculations are negligible due to uncertainty in the first-order expansion coefficient $c_{ii'}$'s. Most entries manifestly demonstrate this with values of less than 1% corrections to the first-order coefficients that are already governing less than 1% shifts in the observables due to the small uncertainties of the input observables to the calculation (see Table 2.1). Only in a couple of places does the uncertainty reach more than 1%, but the final uncertainty on the observables themselves is of course significantly lower than that. To illustrate this, let us consider the largest $P[c_{ii'}]$ in Table 2.3, $P[c_{R_b, \alpha_s}]$, which is the uncertainty in the expansion coefficient of $\alpha_s - \alpha_s^{\text{ref}}$ in the computation for R_b . It yields an uncertainty on R_b of

$$\begin{aligned} \Delta R_b &\simeq R_b^{\text{ref}} |22\% \times c_{R_b, \alpha_s} \times \bar{\delta} \alpha_s| \\ &\simeq 0.216 (0.22 \times 0.0002 \times 0.005) \simeq 5 \times 10^{-8}, \end{aligned} \quad (2.26)$$

which is much smaller than the experimental uncertainty of 7×10^{-4} . Therefore, in practice this 22% uncertainty does not concern us, and we can be confident that the first-order expansion expressions are sufficient for any precision electroweak analysis given the current uncertainties in observables.

2.3.4 Change of basis

Our choice of input observables as in Eq. (2.16) is convenient for the calculation of expansion coefficients in ZFITTER. In principle, any set of $N_p = 6$ independent observables can serve as input, though we should better choose those most precisely measured observables to minimize the uncertainty due to higher order terms in the expansion. In this respect, an equally good choice as Eq. (2.16) could be

$$\{\widehat{O}_i\} = \{m_Z, G_F, \alpha(m_Z), m_t, \alpha_s(m_Z), m_H\}, \quad (2.27)$$

since essentially all the uncertainty in $\alpha(m_Z)$ comes from $\Delta \alpha_{\text{had}}^{(5)}$. This basis may be preferable in practice, since it is often more convenient to do calculations with $\alpha(m_Z)$, rather than

\widehat{O}_i	$P[c_{i,m_Z}]$	$P[c_{i,G_F}]$	$P[c_{i,\Delta\alpha}]$	$P[c_{i,m_t}]$	$P[c_{i,\alpha_s}]$	$P[c_{i,m_H}]$
$\alpha(m_Z)$	0.05	-	0.37	1.19	1.64	-
m_W	0.02	0.05	0.44	0.87	1.20	0.23
Γ_e	0.04	0.07	0.42	1.09	1.53	0.60
Γ_μ	0.04	0.07	0.42	1.09	1.53	0.60
Γ_τ	0.04	0.07	0.42	1.09	1.53	0.60
Γ_b	0.01	0.02	0.43	0.96	0.41	0.27
Γ_c	0.01	0.01	0.39	0.88	0.64	0.33
Γ_{inv}	0.00	0.01	0.63	1.04	1.51	0.74
Γ_{had}	0.01	0.01	0.41	1.10	0.50	0.35
Γ_Z	0.00	0.01	0.39	1.07	0.52	0.39
σ_{had}	0.06	2.08	2.41	1.31	0.50	2.81
R_e	0.31	0.32	0.69	1.40	0.47	0.36
R_μ	0.31	0.32	0.69	1.40	0.47	0.36
R_τ	0.32	0.33	0.69	1.40	0.47	0.36
R_b	0.13	0.28	0.41	0.92	22.06	0.88
R_c	0.12	0.14	0.41	0.87	1.26	0.35
$\sin^2 \theta_{\text{eff}}^e$	0.02	0.01	0.39	0.97	1.26	0.12
$\sin^2 \theta_{\text{eff}}^b$	0.02	0.02	0.39	0.75	1.16	0.05
$\sin^2 \theta_{\text{eff}}^c$	0.02	0.01	0.39	0.97	1.26	0.12
\mathcal{A}_e	0.51	0.50	0.88	1.10	1.42	0.46
\mathcal{A}_b	0.09	0.09	0.46	0.80	1.21	0.11
\mathcal{A}_c	0.14	0.14	0.52	1.00	1.30	0.16
$A_{\text{FB}}^{0,b}e$	0.51	0.50	0.88	1.10	1.42	0.46
$A_{\text{FB}}^{0,b}b$	0.50	0.49	0.88	1.10	1.42	0.46
$A_{\text{FB}}^{0,b}c$	0.48	0.47	0.85	1.09	1.41	0.43

Table 2.3: (From [131]) Percent relative uncertainties for the expansion coefficients $c_{ii'}$, with all input observables varied in their 1σ range.

$\widehat{\mathcal{O}}_i$	r_{i,m_Z}	r_{i,G_F}	$r_{i,\Delta\alpha}$	r_{i,m_t}	r_{i,α_s}	r_{i,m_H}
$\alpha(m_Z)$	0.03	-	0.01	0.85	0.66	-
m_W	0.01	0.03	0.03	0.18	0.35	0.18
Γ_e	0.03	0.04	0.20	0.30	0.52	0.18
Γ_μ	0.03	0.04	0.20	0.30	0.52	0.18
Γ_τ	0.03	0.04	0.20	0.30	0.52	0.18
Γ_b	0.02	0.02	0.04	0.24	0.10	0.07
Γ_c	0.02	0.03	0.02	0.21	0.09	0.16
Γ_{inv}	0.01	0.01	0.12	0.27	0.51	0.21
Γ_{had}	0.02	0.02	0.02	0.29	0.04	0.14
Γ_Z	0.02	0.02	0.02	0.29	0.05	0.13
σ_{had}	0.03	1.04	1.02	0.39	0.02	1.49
R_e	0.17	0.17	0.17	0.46	0.02	0.31
R_μ	0.17	0.17	0.17	0.46	0.02	0.31
R_τ	0.17	0.17	0.17	0.46	0.02	0.31
R_b	0.05	0.13	0.05	0.20	10.69	0.59
R_c	0.06	0.07	0.05	0.19	0.38	0.31
$\sin^2 \theta_{\text{eff}}^e$	0.03	0.02	0.03	0.24	0.38	0.19
$\sin^2 \theta_{\text{eff}}^b$	0.03	0.02	0.03	0.13	0.34	0.17
$\sin^2 \theta_{\text{eff}}^c$	0.03	0.02	0.03	0.24	0.38	0.19
\mathcal{A}_e	0.04	0.03	0.04	0.24	0.38	0.20
\mathcal{A}_b	0.04	0.04	0.05	0.14	0.35	0.18
\mathcal{A}_c	0.05	0.05	0.06	0.24	0.39	0.20
$A_{\text{FB}}^{0,b}e$	0.18	0.19	0.18	0.42	0.55	0.37
$A_{\text{FB}}^{0,b}b$	0.03	0.03	0.04	0.24	0.38	0.19
$A_{\text{FB}}^{0,b}c$	0.00	0.01	0.01	0.23	0.37	0.19

Table 2.4: (From [131]) The $r_{i'}$'s defined in Eq. (2.25), characterizing the ratios of second-order vs. first-order terms in the expansion (in units of percentage).

$\Delta\alpha_{\text{had}}^{(5)}$, as input. In this subsection we derive the rules for translating the expansion coefficients $c_{ii'}$, which are calculated in the basis Eq. (2.16), into those for the basis Eq. (2.27). To avoid confusion, denote the latter by $d_{ii'}$. Also, superscripts ‘‘SM’’ will be dropped for simplicity in this subsection.

First, consider $d_{i,\alpha}$. We need to determine the shift in \widehat{O}_i caused by $\bar{\delta}\alpha(m_Z)$, with the other 5 input observables held fixed. If we work in the basis Eq. (2.16), this shift in $\alpha(m_Z)$ is an outcome of the following shift in $\Delta\alpha_{\text{had}}^{(5)}$ (with other input observables fixed):

$$\bar{\delta}\Delta\alpha_{\text{had}}^{(5)} = [c_{\alpha,\Delta\alpha}]^{-1} \bar{\delta}\alpha(m_Z). \quad (2.28)$$

And the shift in \widehat{O}_i is

$$\bar{\delta}\widehat{O}_i = c_{i,\Delta\alpha} \bar{\delta}\Delta\alpha_{\text{had}}^{(5)} = c_{i,\Delta\alpha} [c_{\alpha,\Delta\alpha}]^{-1} \bar{\delta}\alpha(m_Z). \quad (2.29)$$

Thus,

$$d_{i,\alpha} = \frac{\bar{\delta}\widehat{O}_i}{\bar{\delta}\alpha(m_Z)} = c_{i,\Delta\alpha} [c_{\alpha,\Delta\alpha}]^{-1}. \quad (2.30)$$

Next, consider $d_{ii'}$ for $i' \neq \alpha(m_Z)$. Take d_{i,m_Z} as an example. We need to shift m_Z while keeping other observables in Eq. (2.27), including $\alpha(m_Z)$, fixed, and find the resulting shift in \widehat{O}_i . Working in the basis Eq. (2.16), we can do this in two steps. First, shift m_Z by $\bar{\delta}m_Z$. As a result,

$$\bar{\delta}\widehat{O}_i = c_{i,m_Z} \bar{\delta}m_Z, \quad \bar{\delta}\alpha(m_Z) = c_{\alpha,m_Z} \bar{\delta}m_Z. \quad (2.31)$$

Second, shift $\Delta\alpha_{\text{had}}^{(5)}$ by

$$\bar{\delta}\Delta\alpha_{\text{had}}^{(5)} = -[c_{\alpha,\Delta\alpha}]^{-1} c_{\alpha,m_Z} \bar{\delta}m_Z. \quad (2.32)$$

As a result,

$$\bar{\delta}\widehat{O}_i = c_{i,\Delta\alpha} \bar{\delta}\Delta\alpha_{\text{had}}^{(5)} = -c_{i,\Delta\alpha} [c_{\alpha,\Delta\alpha}]^{-1} c_{\alpha,m_Z} \bar{\delta}m_Z, \quad (2.33)$$

$$\bar{\delta}\alpha(m_Z) = c_{\alpha,\Delta\alpha} \bar{\delta}\Delta\alpha_{\text{had}}^{(5)} = -c_{\alpha,m_Z} \bar{\delta}m_Z. \quad (2.34)$$

The effect of both steps is to hold all observables in Eq. (2.27) other than m_Z , in particular $\alpha(m_Z)$, fixed. And we get the desired result

$$d_{i,m_Z} = \frac{\bar{\delta}\widehat{O}_i}{\bar{\delta}m_Z} = c_{i,m_Z} - c_{i,\Delta\alpha} [c_{\alpha,\Delta\alpha}]^{-1} c_{\alpha,m_Z}. \quad (2.35)$$

As a special case, Eqs. (2.30) and (2.35) also hold for $i = \Delta\alpha_{\text{had}}^{(5)}$:

$$d_{\Delta\alpha,\alpha} = [c_{\alpha,\Delta\alpha}]^{-1}, \quad (2.36)$$

$$d_{\Delta\alpha,m_Z} = -[c_{\alpha,\Delta\alpha}]^{-1} c_{\alpha,m_Z}, \quad (2.37)$$

where we have used $c_{\Delta\alpha,\Delta\alpha} = 1$, $c_{\Delta\alpha,m_Z} = 0$.

In the basis Eq. (2.27), the theory predictions for the observables (with respect to the reference values) are calculated from

$$\bar{\delta}\widehat{O}_i^{\text{th}} = \sum_{i'} d_{ii'} \bar{\delta}\widehat{O}_{i'}^{\text{th}} + \bar{\delta}^{\text{NP}} \widehat{O}_i, \quad (2.38)$$

where

$$\begin{aligned} \bar{\delta}^{\text{NP}} \widehat{O}_i &\equiv \xi_i - \sum_{i'} d_{ii'} \xi_{i'} \\ &= \xi_i - d_{i,m_Z} \xi_{m_Z} - d_{i,G_F} \xi_{G_F} - d_{i,\alpha} \xi_\alpha - d_{i,m_t} \xi_{m_t} - d_{i,\alpha_s} \xi_{\alpha_s} - d_{i,m_H} \xi_{m_H}. \end{aligned} \quad (2.39)$$

We list the expansion coefficients $d_{ii'}$, as calculated from Eqs. (2.30) and (2.35), in Table 2.5.

2.4 New physics examples

In this section we present some examples of calculating new physics contributions to electroweak observables, using the formalism developed in Section 2.3. We work in the basis Eq. (2.27), with $\alpha(m_Z)$ as an input observable.

2.4.1 Shifts in $Zb\bar{b}$ couplings

Suppose some new physics model shifts the Z boson couplings to left- and right-handed b quarks [145]

$$c_L^b \rightarrow c_L^b(1 + \varepsilon_L), \quad c_R^b \rightarrow c_R^b(1 + \varepsilon_R). \quad (2.40)$$

None of the input observables is affected at tree level. Thus, the impact of the shifts of these couplings can be calculated straightforwardly from observables that directly depend on c_L^b and c_R^b . The set of observables directly affected include Γ_b , Γ_{had} , $R_{e,\mu,\tau}$, $R_{c,b}$, Γ_Z , σ_{had} , \mathcal{A}_b , $A_{\text{FB}}^{0,b}$, and $\sin^2 \theta_{\text{eff}}^b$. Their shifts from this new physics contribution can be expressed as

$$\bar{\delta}^{\text{NP}} \widehat{O}_i = \xi_i. \quad (2.41)$$

\widehat{O}_i	d_{i,m_Z}	d_{i,G_F}	$d_{i,\alpha}$	d_{i,m_t}	d_{i,α_s}	d_{i,m_H}
m_Z	1	0	0	0	0	0
G_F	0	1	0	0	0	0
$\alpha(m_Z)$	0	0	1	0	0	0
m_t	0	0	0	1	0	0
$\alpha_s(m_Z)$	0	0	0	0	1	0
m_H	0	0	0	0	0	1
$\Delta\alpha_{\text{had}}^{(5)}$	-0.1628	0	33.94	-5.232e-3	3.417e-4	0
m_W	1.428	0.2201	-0.2154	0.01325	-9.621e-4	-7.704e-4
Γ_e	3.378	1.198	-0.1920	0.01886	-1.255e-3	-7.924e-4
Γ_μ	3.378	1.198	-0.1920	0.01886	-1.255e-3	-7.924e-4
Γ_τ	3.384	1.198	-0.1924	0.01887	-1.256e-3	-7.931e-4
Γ_b	3.846	1.411	-0.4166	-0.01260	0.03672	-1.057e-3
Γ_c	4.154	1.590	-0.5842	0.02760	0.05045	-1.394e-3
Γ_{inv}	2.996	1.006	1.913e-3	0.01567	-9.967e-4	-4.873e-4
Γ_{had}	3.940	1.476	-0.4727	0.01586	0.03690	-1.204e-3
Γ_Z	3.694	1.353	-0.3490	0.01612	0.02543	-1.019e-3
σ_{had}	-2.070	-0.03281	0.03328	2.471e-3	-0.01522	4.057e-5
R_e	0.5622	0.2780	-0.2807	-3.002e-3	0.03815	-4.120e-4
R_μ	0.5622	0.2780	-0.2807	-3.002e-3	0.03815	-4.120e-4
R_τ	0.5568	0.2776	-0.2803	-3.009e-3	0.03815	-4.113e-4
R_b	-0.09461	-0.06530	0.05608	-0.02846	-1.777e-4	1.477e-4
R_c	0.2138	0.1135	-0.1115	0.01174	0.01356	-1.898e-4
$\sin^2\theta_{\text{eff}}^e$	-2.825	-1.423	1.426	-0.02352	1.811e-3	2.195e-3
$\sin^2\theta_{\text{eff}}^b$	-2.830	-1.417	1.427	-7.134e-3	1.215e-3	2.116e-3
$\sin^2\theta_{\text{eff}}^c$	-2.826	-1.423	1.426	-0.02353	1.809e-3	2.194e-3
\mathcal{A}_e	35.22	17.74	-17.78	0.2932	-0.02257	-0.02737
\mathcal{A}_b	0.4536	0.2271	-0.2287	1.143e-3	-1.947e-4	-3.390e-4
\mathcal{A}_c	3.395	1.710	-1.713	0.02827	-2.174e-3	-2.636e-3
$A_{\text{FB}}^{0,b}e$	70.44	35.48	-35.56	0.5865	-0.04515	-0.05473
$A_{\text{FB}}^{0,b}b$	35.67	17.97	-18.01	0.2944	-0.02277	-0.02771
$A_{\text{FB}}^{0,b}c$	38.61	19.45	-19.50	0.3215	-0.02475	-0.03000

Table 2.5: (From [131]) Expansion coefficients calculated in the basis of input observables containing $\alpha(m_Z)$, which are derived from the numbers in Table 2.2 by a change of basis described in Section 2.3.4.

Let's begin by computing the shift in Γ_b . At tree level, $\Gamma_b \propto [(c_L^b)^2 + (c_R^b)^2]$, which when expanded leads to the shift $\bar{\delta}^{\text{NP}}\Gamma_b = \xi_{\Gamma_b}$, where

$$\xi_{\Gamma_b} = \frac{2(c_L^b)^2}{(c_L^b)^2 + (c_R^b)^2}\varepsilon_L + \frac{2(c_R^b)^2}{(c_L^b)^2 + (c_R^b)^2}\varepsilon_R \simeq 1.94\varepsilon_L + 0.0645\varepsilon_R. \quad (2.42)$$

Knowing this shift in Γ_b enables us to simply compute the shift of other observables that depend on Γ_b in terms of ξ_{Γ_b} :

$$\bar{\delta}^{\text{NP}}\Gamma_{\text{had}} = \bar{\delta}^{\text{NP}}R_e = \bar{\delta}^{\text{NP}}R_\mu = \bar{\delta}^{\text{NP}}R_\tau = -\bar{\delta}^{\text{NP}}R_c = R_b\xi_{\Gamma_b} \simeq 0.216\xi_{\Gamma_b}, \quad (2.43)$$

$$\bar{\delta}^{\text{NP}}R_b = \bar{\delta}^{\text{NP}}\Gamma_b - \bar{\delta}^{\text{NP}}\Gamma_{\text{had}} = (1 - R_b)\xi_{\Gamma_b} \simeq 0.784\xi_{\Gamma_b}, \quad (2.44)$$

$$\bar{\delta}^{\text{NP}}\Gamma_Z = B_b\xi_{\Gamma_b} \simeq 0.151\xi_{\Gamma_b}, \quad (2.45)$$

$$\bar{\delta}^{\text{NP}}\sigma_{\text{had}} = \bar{\delta}^{\text{NP}}\Gamma_{\text{had}} - 2\bar{\delta}^{\text{NP}}\Gamma_Z = (R_b - 2B_b)\xi_{\Gamma_b} \simeq -0.0855\xi_{\Gamma_b}, \quad (2.46)$$

where $B_b = \Gamma_b/\Gamma_Z$ is the branching ratio of $Z \rightarrow b\bar{b}$.

The asymmetry observables are also affected due to the shift in \mathcal{A}_b . At tree level,

$$\mathcal{A}_b = \frac{(c_L^b)^2 - (c_R^b)^2}{(c_L^b)^2 + (c_R^b)^2}, \quad (2.47)$$

which leads to a shift $\bar{\delta}^{\text{NP}}\mathcal{A}_b = \xi_{\mathcal{A}_b}$, where

$$\xi_{\mathcal{A}_b} = \frac{4(c_L^b)^2(c_R^b)^2}{(c_L^b)^4 - (c_R^b)^4}(\varepsilon_L - \varepsilon_R) \simeq 0.134(\varepsilon_L - \varepsilon_R). \quad (2.48)$$

We can then straightforwardly compute $\bar{\delta}^{\text{NP}}A_{\text{FB}}^{0,b}$ and $\bar{\delta}^{\text{NP}}\sin^2\theta_{\text{eff}}^b$ in terms of $\xi_{\mathcal{A}_b}$:

$$\bar{\delta}^{\text{NP}}A_{\text{FB}}^{0,b} = \xi_{\mathcal{A}_b}, \quad (2.49)$$

and

$$\bar{\delta}^{\text{NP}}\sin^2\theta_{\text{eff}}^b = \left[\frac{\sin^2\theta_{\text{eff}}^b}{\mathcal{A}_b} \frac{\partial\mathcal{A}_b}{\partial\sin^2\theta_{\text{eff}}^b} \right]^{-1} \xi_{\mathcal{A}_b} = \frac{(1 - \frac{4}{3}\sin^2\theta_{\text{eff}}^b)[1 + (1 - \frac{4}{3}\sin^2\theta_{\text{eff}}^b)^2]}{-\frac{4}{3}\sin^2\theta_{\text{eff}}^b[1 - (1 - \frac{4}{3}\sin^2\theta_{\text{eff}}^b)^2]} \xi_{\mathcal{A}_b} \simeq -6.24\xi_{\mathcal{A}_b}. \quad (2.50)$$

Thus, $\bar{\delta}^{\text{NP}}\widehat{O}_i$ for all observables are expressed in terms of ξ_{Γ_b} or $\xi_{\mathcal{A}_b}$, which are simply related to $\varepsilon_L, \varepsilon_R$ via Eqs. (2.42) and (2.48).

2.4.2 Shifts in vector boson self-energies

In many new physics scenarios, there exist exotic states that do not couple directly to SM fermions but have charges under the SM gauge groups. These states affect electroweak observables via shifts in vector boson self-energies [146]. At one-loop level, the dependence of various observables on vector boson self-energies is as follows [147]:

$$m_Z^2 = [m_Z^2]^{(0)}(1 + \pi_{zz}), \quad (2.51)$$

$$m_W^2 = [m_W^2]^{(0)}(1 + \pi_{ww}), \quad (2.52)$$

$$G_F = [G_F]^{(0)}(1 - \pi_{ww}^0), \quad (2.53)$$

$$\alpha(m_Z) = [\alpha(m_Z)]^{(0)}(1 + \pi'_{\gamma\gamma}), \quad (2.54)$$

$$\sin^2 \theta_{\text{eff}}^f = s^2 \left(1 - \frac{c}{s} \pi_{\gamma z} \right), \quad (2.55)$$

$$\Gamma_f = [\Gamma_f]^{(0)} \left(1 + \pi'_{zz} + \frac{1}{2} \pi_{zz} + a_f \pi_{\gamma z} \right), \quad (2.56)$$

where superscripts “(0)” denote tree-level values, and $s = \frac{g_1}{\sqrt{g_1^2 + g_2^2}}$, $c = \frac{g_2}{\sqrt{g_1^2 + g_2^2}}$. We have also defined

$$\pi_{zz} \equiv \frac{\Pi_{ZZ}(m_Z^2)}{m_Z^2}, \quad (2.57)$$

$$\pi'_{zz} \equiv \lim_{q^2 \rightarrow m_Z^2} \frac{\Pi_{ZZ}(q^2) - \Pi_{ZZ}(m_Z^2)}{q^2 - m_Z^2}, \quad (2.58)$$

$$\pi_{\gamma z} \equiv \frac{\Pi_{\gamma Z}(m_Z^2)}{m_Z^2}, \quad (2.59)$$

$$\pi'_{\gamma\gamma} \equiv \lim_{q^2 \rightarrow 0} \frac{\Pi_{\gamma\gamma}(q^2) - \Pi_{\gamma\gamma}(0)}{q^2}, \quad (2.60)$$

$$\pi_{ww} \equiv \frac{\Pi_{WW}(m_W^2)}{m_W^2}, \quad (2.61)$$

$$\pi_{ww}^0 \equiv \frac{\Pi_{WW}(0)}{m_W^2}. \quad (2.62)$$

The a_f in Eq. (2.56) can be derived from

$$\Gamma_f = [\Gamma_f]^{(0)} (1 + \pi'_{zz} + \pi_{zz}) \frac{1 + (1 - 4|Q_f| \sin^2 \theta_{\text{eff}}^f)^2}{1 + (1 - 4|Q_f| s^2)^2} \quad (2.63)$$

and Eq. (2.55). The result is

$$a_f = \frac{8sc|Q_f|(1 - 4|Q_f|s^2)}{1 + (1 - 4|Q_f|s^2)^2} = 4sc|Q_f|[\mathcal{A}_f]^{(0)}. \quad (2.64)$$

With $s^2 \simeq \sin^2 \theta_{\text{eff}}^e = 0.231620$, which is good at tree level, we have

$$a_\nu = 0, \quad a_\ell = 0.2468, \quad a_u = 0.7505, \quad a_d = 0.5262. \quad (2.65)$$

With Eqs. (2.51-2.56), it is straightforward to calculate contributions from new physics. Denote the shifts in vector boson self-energies by $\delta^{\text{NP}} \pi_{zz}$, etc.; i.e.

$$\pi_{zz} \rightarrow \pi_{zz} + \delta^{\text{NP}} \pi_{zz}, \quad \text{etc.} \quad (2.66)$$

Note the absence of “bar” on δ , since this is the absolute shift, not the fractional shift. Then for the input observables,

$$\xi_{m_Z} = \frac{1}{2} \delta^{\text{NP}} \pi_{zz}, \quad \xi_{G_F} = -\delta^{\text{NP}} \pi_{ww}^0, \quad \xi_\alpha = \delta^{\text{NP}} \pi'_{\gamma\gamma}, \quad \xi_{m_t} = \xi_{\alpha_s} = \xi_{m_H} = 0. \quad (2.67)$$

These shifts propagate into shifts in the output observables, while leaving the input observables unchanged due to new physics (i.e. $\bar{\delta}^{\text{NP}} \widehat{O}_{i'} = 0$). The new physics contribution to the output observables can be conveniently expressed as:

$$\begin{aligned} \bar{\delta}^{\text{NP}} \widehat{O}_i &= \xi_i - \sum_{i'} d_{ii'} \xi_{i'} \\ &\equiv b_{i,zz} \delta^{\text{NP}} \pi_{zz} + b'_{i,zz} \delta^{\text{NP}} \pi'_{zz} + b_{i,\gamma\gamma} \delta^{\text{NP}} \pi_{\gamma\gamma} + b'_{i,\gamma\gamma} \delta^{\text{NP}} \pi'_{\gamma\gamma} + b_{i,ww} \delta^{\text{NP}} \pi_{ww} + b^0_{i,ww} \delta^{\text{NP}} \pi_{ww}^0 \end{aligned} \quad (2.68)$$

In the following we discuss the calculation of these b coefficients.

- $b'_{i,zz}$, $b_{i,ww}$ are the simplest, since they vanish for most of the observables. In particular, $b'_{i,zz}$, which comes from wavefunction renormalization, is nonzero only for Z boson decay widths:

$$b'_{\Gamma_f,zz} = b'_{\Gamma_{\text{inv}},zz} = b'_{\Gamma_{\text{had}},zz} = b'_{\Gamma_Z,zz} = 1. \quad (2.69)$$

Note that wavefunction renormalization cancels out in σ_{had} , and ratios of decay widths. $b_{i,ww}$ is related to the shift in the W boson mass, so is nonzero only for:

$$b_{m_W,ww} = \frac{1}{2}. \quad (2.70)$$

- $b_{i,zz}$, $b'_{i,\gamma\gamma}$, $b^0_{i,ww}$ are simply related to d_{i,m_Z} , $d_{i,\alpha}$, d_{i,G_F} , respectively. Since $\pi'_{\gamma\gamma}$, π_{ww}^0 only enter $\alpha(m_Z)$, G_F , respectively, we have

$$b'_{i,\gamma\gamma} = -d_{i,\alpha}, \quad b^0_{i,ww} = d_{i,G_F} \quad (2.71)$$

\widehat{O}_i	$b_{i,zz}$	$b'_{i,zz}$	$b_{i,\gamma z}$	$b'_{i,\gamma\gamma}$	$b_{i,ww}$	$b_{i,ww}^0$
m_W	-0.7140	0	0	0.2154	0.5	0.2201
Γ_e	-1.189	1	0.2468	0.1920	0	1.198
Γ_μ	-1.189	1	0.2468	0.1920	0	1.198
Γ_τ	-1.192	1	0.2468	0.1924	0	1.198
Γ_b	-1.423	1	0.5262	0.4166	0	1.411
Γ_c	-1.577	1	0.7505	0.5842	0	1.590
Γ_{inv}	-0.9982	1	0	-1.913e-3	0	1.006
Γ_{had}	-1.470	1	0.6027	0.4727	0	1.476
Γ_Z	-1.347	1	0.4420	0.3490	0	1.353
σ_{had}	0.03475	0	-0.03460	-0.03328	0	-0.03281
R_e	-0.2811	0	0.3559	0.2807	0	0.2780
R_μ	-0.2811	0	0.3559	0.2807	0	0.2780
R_τ	-0.2784	0	0.3559	0.2803	0	0.2776
R_b	0.04731	0	-0.07647	-0.05608	0	-0.06530
R_c	-0.1069	0	0.1479	0.1115	0	0.1135
$\sin^2 \theta_{\text{eff}}^e$	1.413	0	-1.821	-1.426	0	-1.423
$\sin^2 \theta_{\text{eff}}^b$	1.415	0	-1.821	-1.427	0	-1.417
$\sin^2 \theta_{\text{eff}}^c$	1.413	0	-1.821	-1.426	0	-1.423
\mathcal{A}_e	-17.61	0	22.71	17.78	0	17.74
\mathcal{A}_b	-0.2268	0	0.2876	0.2287	0	0.2271
\mathcal{A}_c	-1.697	0	2.192	1.713	0	1.710
$A_{\text{FB}}^{0,b}e$	-35.22	0	45.41	35.56	0	35.48
$A_{\text{FB}}^{0,b}b$	-17.84	0	22.99	18.01	0	17.97
$A_{\text{FB}}^{0,b}c$	-19.31	0	24.90	19.50	0	19.45

Table 2.6: (From [131]) The b coefficients defined in Eq. (2.68), characterizing the shift in the output observables due to new physics that shifts vector boson self-energies.

for all \widehat{O}_i . Similarly,

$$b_{i,zz} = -\frac{1}{2}d_{i,m_Z} \quad (2.72)$$

except for those observables having direct dependence on the Z boson mass:

$$b_{i,zz} = \frac{1}{2}(1 - d_{i,m_Z}) \quad \text{for } i = \Gamma_f, \Gamma_{\text{inv}}, \Gamma_{\text{had}}, \Gamma_Z, \quad (2.73)$$

$$b_{\sigma_{\text{had}},zz} = -\frac{1}{2}(2 + d_{i,m_Z}). \quad (2.74)$$

- Finally, $b_{i,\gamma z}$ should be derived from the dependence on $\sin^2 \theta_{\text{eff}}^f$. For the Z partial widths, it can be read off from Eq. (2.56):

$$b_{\Gamma_f,\gamma z} = a_f, \quad b_{\Gamma_{\text{inv}},\gamma z} = 3a_\nu = 0, \quad (2.75)$$

with a_f given in Eqs. (2.64) and (2.65). For $i = \Gamma_{\text{had}}, \Gamma_Z$, $b_{i,\gamma z}$ is a weighted sum. At leading order:

$$b_{\Gamma_{\text{had}},\gamma z} = \sum_{f \in \text{had}} \frac{\Gamma_f}{\Gamma_{\text{had}}} b_{\Gamma_f,\gamma z} = \frac{\sum_{f \in \text{had}} [1 + (1 - 4|Q_f|s^2)^2] b_{\Gamma_f,\gamma z}}{\sum_{f \in \text{had}} [1 + (1 - 4|Q_f|s^2)^2]}, \quad (2.76)$$

$$b_{\Gamma_Z,\gamma z} = \sum_f \frac{\Gamma_f}{\Gamma_Z} b_{\Gamma_f,\gamma z} = \frac{\sum_f [1 + (1 - 4|Q_f|s^2)^2] b_{\Gamma_f,\gamma z}}{\sum_f [1 + (1 - 4|Q_f|s^2)^2]}. \quad (2.77)$$

For the ratios of partial widths, and the Z -pole cross section:

$$b_{R_\ell,\gamma z} = b_{\Gamma_{\text{had}},\gamma z} - b_{\Gamma_\ell,\gamma z}, \quad b_{R_q,\gamma z} = b_{\Gamma_q,\gamma z} - b_{\Gamma_{\text{had}},\gamma z}, \quad b_{\sigma_{\text{had}},\gamma z} = b_{\Gamma_e,\gamma z} + b_{\Gamma_{\text{had}},\gamma z} - 2b_{\Gamma_Z,\gamma z} \quad (2.78)$$

For the asymmetry observables, we can read off from Eq. (2.55):

$$b_{\sin^2 \theta_{\text{eff}}^f,\gamma z} = -\frac{c}{s}. \quad (2.79)$$

And hence, at leading order,

$$b_{\mathcal{A}_f,\gamma z} = \frac{s^2}{[\mathcal{A}_f]^{(0)}} \frac{\partial[\mathcal{A}_f]^{(0)}}{\partial(s^2)} b_{\sin^2 \theta_{\text{eff}}^f,\gamma z} = \frac{4|Q_f|sc[1 - (1 - 4|Q_f|s^2)^2]}{(1 - 4|Q_f|s^2)[1 - (1 + 4|Q_f|s^2)^2]}, \quad (2.80)$$

$$b_{A_{\text{FB}}^{0,b},\gamma z} = b_{\mathcal{A}_e,\gamma z} + b_{\mathcal{A}_f,\gamma z}. \quad (2.81)$$

The numerical values for these b coefficients are listed in Table 2.6. The calculation is done with $s^2 = 0.231620$, and the sign conventions for the gauge couplings are $g_1 > 0$, $g_2 > 0$ (hence $s > 0$).

2.5 Conclusions

In this section we presented an expansion formalism that facilitates precision electroweak analyses. By recasting all observables in terms of six very well measured input observables, we can calculate each of them easily by expanding about the reference values of the input observables, chosen in accord with experimental measurements. Also, the formalism developed here can be applied in a simple manner to calculate new physics corrections to electroweak observables and derive constraints on new physics models. Some examples were worked out for illustration.

For numerical results we calculated the reference values and expansion coefficients using the ZFITTER package. Most, though not all, of these results reflect state-of-the-art calculations in the literature. Various higher order calculations of electroweak observables have been done since the release of ZFITTER 6.42 in 2005, but their impact on precision analysis is not significant at present because the power of the precision program is limited by experimental errors. However, improvements of our results to better accuracy with the inclusion of these and future calculations may be necessary in the future, if experimental priorities of next-generation facilities involve Giga-Z or Tera-Z options [148, 149]. With 10^9 or 10^{12} Z bosons produced at a future collider, unprecedented levels of reliable theoretical calculations will be needed to meet the unprecedented levels of experimental accuracy. We hope that the formalism presented here, with improving numerical results, will continue to be helpful for efficient and reliable calculations of SM results and beyond the SM corrections in the precision electroweak program.

Chapter 3

Resolving Charm and Bottom Quark Masses in Precision Higgs Analyses

A conventional approach to precision calculations of Higgs boson observables uses quark masses m_c and m_b as inputs. However, quark masses are single numbers that hide a variety of low-energy data from which they are extracted, and also hide the various sources of theoretical uncertainties and correlations with additional input parameters such as α_s . Higher-precision calculations, which are needed to give meaning to future measurements, require more direct engagement with the low-energy data in a global analysis. We present an initial calculation in this direction, which illustrates the procedure and reveals some of the theory uncertainties that challenge subpercent determinations of Higgs boson partial widths.

3.1 Introduction

The discovery of the Higgs boson [1,2] marks the beginning of a new era for precision studies. Not only is unprecedented precision achieved in Standard Model (SM) calculations [24–26, 131] with the knowledge of the Higgs boson mass [133,150], but experimental data on a large number of Higgs observables [151] allows us for the first time to scrutinize the Higgs sector of the SM [121] and beyond [70,152,153]. Any discrepancy between precision data and SM predictions would be an indication of new physics.

Though not explicitly stated in the context of precision Higgs analysis, an important role in this program is played by low-energy observables, such as moments of e^+e^- annihilation cross section and moments of semileptonic B decay distributions. In fact, our knowledge of the charm and bottom quark masses m_Q ($Q = c, b$), which are important inputs of precision Higgs calculations, largely comes from analyzing these low-energy data. This can be seen from the fact that the Particle Data Group (PDG) [154] average of the scale-invariant masses

in the $\overline{\text{MS}}$ scheme [i.e. solutions to $m_Q(\mu) = \mu$],

$$m_c(m_c) = 1.275(25) \text{ GeV}, \quad (3.1)$$

$$m_b(m_b) = 4.18(3) \text{ GeV}, \quad (3.2)$$

is dominated by m_Q extractions from low-energy data. These $\overline{\text{MS}}$ masses, as well as pole masses, have been used in the literature to estimate the theoretical precision achievable in precision Higgs calculations [121, 155].

However, looking into the future, such indirect engagement of low-energy observables in precision Higgs analysis might be ultimately unsatisfactory. A large amount of low-energy data has been highly processed to yield just two numbers, as in Eqs. (3.1) and (3.2). It is not even clear whether these numbers accurately reflect our knowledge of m_Q , because the averaging involves m_Q extractions some of which are apparently correlated due to similar data and/or methods used. The error bars assigned to them contain experimental uncertainties from many different measurements, as well as theoretical uncertainties from calculating many different quantities. In addition, a self-described inflation of uncertainties by the PDG [156] is introduced to account for underestimated systematic errors in some m_Q extractions [157]. Finally, Eqs. (3.1) and (3.2) do not retain possible correlations between $\alpha_s(m_Z)$ and the extracted m_Q . They are thus treated as independent inputs in precision Higgs analysis, which is strictly speaking not correct.

As we strive for the highest-precision calculation possible in order to match percent (or even perhaps parts-per-mil) level of experimental precision achievable in the foreseeable future¹, the rich information hidden in Eqs. (3.1) and (3.2) should be revealed, and the role of individual low-energy observables emphasized. Conceivably, a global χ^2 fit would become more powerful in testing the SM when low-energy observables sensitive to m_Q as well as Higgs observables are incorporated. The scale-invariant masses $m_Q(m_Q)$ would be then only inputs of the *calculation*. They are not considered as *observables* with experimental values and uncertainties, but are parameters to be tuned to minimize the χ^2 function, where only true *observables* are included.

In this section we propose the idea of directly working with low-energy observables in precision Higgs analysis. In addition to the global fit perspective mentioned above, low-energy observables can also play a role in identifying individual sources of theoretical uncertainties

¹Though precision measurements of Higgs observables, especially the partial widths into $c\bar{c}$ and $b\bar{b}$ discussed in this section, are difficult at the LHC, such high precision is generally believed to be achievable at the International Linear Collider, the Future Circular Collider, and the Circular Electron Positron Collider. For recent analyses, see e.g. [158–161]. We also note that for the $b\bar{b}$ channel, the importance of a higher theory precision is further emphasized by its relevance to the calculation of the total widths and all branching ratios of the Higgs boson.

in precision Higgs calculations. This is conveniently done by eliminating $m_Q(m_Q)$ from our input in favor of two low-energy observables, and recasting Higgs observables in terms of these and other input observables. For this procedure to be meaningful, the two observables chosen should be representative of the large amount of low-energy data contributing to Eqs. (3.1) and (3.2), in the sense that m_Q extracted from them alone should be precise enough. In the language of a global χ^2 fit, the ideal choices would be two observables that dominate the low-energy observables contribution to χ^2 . In this regard, a reasonable, though by no means exclusive, option would be to use the moments \mathcal{M}_1^c and \mathcal{M}_2^b of $e^+e^- \rightarrow Q\bar{Q}$ inclusive cross section, defined by

$$\mathcal{M}_n^Q \equiv \int \frac{ds}{s^{n+1}} R_Q(s), \quad \text{where } R_Q \equiv \frac{\sigma(e^+e^- \rightarrow Q\bar{Q}X)}{\sigma(e^+e^- \rightarrow \mu^+\mu^-)}, \quad (3.3)$$

with the precise definition of R_Q from experimental data discussed in [162]. $m_c(m_c)$ and $m_b(m_b)$ reported in the literature from analyzing these moments typically have $\mathcal{O}(10 \text{ MeV})$ uncertainties quoted [157, 162–164]. For the Higgs observables we will focus on the partial widths $\Gamma_{H \rightarrow c\bar{c}}$ and $\Gamma_{H \rightarrow b\bar{b}}$, and assess the level of precision we can achieve in SM predictions for them. We will see that with direct contact made between these partial widths and the low-energy moments, the vague notion of “uncertainties from m_Q ” is decomposed into concrete sources of uncertainties. In particular, parametric uncertainties from input observables \mathcal{M}_1^c , \mathcal{M}_2^b and $\alpha_s(m_Z)$ ², and perturbative uncertainties due to missing higher-order corrections to the moments can be exposed separately. We note that while the parametric uncertainties are currently expected to be at the percent level, and are in principle reducible with future data and more careful experimental extraction of the moments, the perturbative uncertainties may represent a bigger challenge due to lack of knowledge of the appropriate renormalization scales in the low-energy regime. It is therefore worthwhile to further investigate theoretical as well as experimental aspects of the low-energy observables for the precision Higgs program to succeed.

²It should be noted that we will treat $\alpha_s(m_Z)$ as both a calculational input and an observable with a central value and uncertainty. In principle one could treat $\alpha_s(m_Z)$ as merely a calculational parameter and let the observables that are highly sensitive to the $\alpha_s(m_Z)$ value be part of the global fit, analogous to what we have done with $m_Q(m_Q)$. However, $\alpha_s(m_Z)$ is one step further removed from direct determination of $H \rightarrow b\bar{b}, c\bar{c}$ partial widths compared to $m_Q(m_Q)$, and so treating $\alpha_s(m_Z)$ as both an input parameter and (highly processed) observable is numerically justified.

3.2 Incorporating low-energy observables into a global precision analysis

The strongest tests of the SM rely on comparing its predictions across all accessible energy scales. By disentangling the information contained in the charm and bottom quark masses in the context of precision Higgs analysis, we expose an interesting interplay between Higgs observables and low-energy observables. The sensitivity to m_Q that they share in common suggests the inclusion of both in the precision program.

An incomplete list of candidates for low-energy observables can be inferred from the m_Q extraction literature, and includes low [157, 162–164] and high [165–168] moments of R_Q mentioned above, and their variants [169, 170], moments of lepton energy and hadron mass distributions of semileptonic B decay [171–173], etc. We denote them collectively as $\{\widehat{O}_i^{\text{low}}\}$, with i running from 1 to the number of low-energy observables we wish to incorporate into the analysis. All these candidates should be carefully examined, and correlations among them should be understood, so that the best choices can be made for $\{\widehat{O}_i^{\text{low}}\}$.

In the high-energy regime, the observables include, for example, various partial widths, branching ratios, and production cross sections of the Higgs boson. Let us call them $\{\widehat{O}_i^{\text{high}}\}$. If not restricted to precision Higgs analysis, one may even include in $\{\widehat{O}_i^{\text{high}}\}$ the electroweak observables, such as the effective weak mixing angle, Z boson partial widths, and forward-backward asymmetries in e^+e^- annihilation at the Z pole. This will make the global analysis even more powerful, because the Higgs observables are sensitive to the same set of input observables as the electroweak observables:

$$\{\widehat{O}_k^{\text{in}}\} \equiv \{m_Z, G_F, \alpha(m_Z), m_t, \alpha_s(m_Z), m_H\}. \quad (3.4)$$

Parenthetically we remark that the common practice of treating the top quark mass m_t as an input observable is justified for present purposes. A more careful treatment of m_t , like what we do here with m_c and m_b , may be needed in the future when precision measurements on the $t\bar{t}$ threshold are carried out at an e^+e^- collider.

Additional calculational inputs, which are not necessarily of the observable type, include the charm and bottom quark masses $\{m_Q(m_Q)\} \equiv \{m_c(m_c), m_b(m_b)\}$. There may be other input parameters, which we denote collectively by $\{p_k^{\text{other}}\}$. Examples are the τ lepton mass, flavor angles, and nonperturbative parameters (e.g. gluon condensate) involved in some low-energy observables.

Assuming the potentially complicated correlations among all the high- and low-energy observables will be understood in time, we may ultimately subject all the observables to a

global fit, by minimizing the χ^2 function with respect to the inputs:

$$\text{Calculation inputs:} \quad \{\mathcal{I}_k\} \equiv \{\widehat{O}_k^{\text{in}}\} \cup \{m_Q(m_Q)\} \cup \{p_k^{\text{other}}\}, \quad (3.5)$$

$$\text{Fit observables:} \quad \{\widehat{O}_i\} \equiv \{\widehat{O}_i^{\text{in}}\} \cup \{\widehat{O}_i^{\text{high}}\} \cup \{\widehat{O}_i^{\text{low}}\}, \quad (3.6)$$

$$\text{To minimize:} \quad \chi^2 = \sum_{ij} \left[\widehat{O}_i^{\text{th}}(\{\mathcal{I}_k\}) - \widehat{O}_i^{\text{expt}} \right] V_{ij}^{-1} \left[\widehat{O}_j^{\text{th}}(\{\mathcal{I}_k\}) - \widehat{O}_j^{\text{expt}} \right]. \quad (3.7)$$

Here “th” and “expt” denote theoretical and experimental values, respectively, and V is the covariance matrix containing uncertainties and correlations among observables. The calculational inputs could just as well be chosen to be a minimal set of Lagrangian parameters; however, it is most convenient for our purposes to choose a combination of observables and Lagrangian parameters as the minimal set of calculational inputs.

Compared with the conventional approach where low-energy data contribute indirectly via the averaged $\{m_Q(m_Q)\}$, our proposal of directly working with low-energy observables allows appropriate treatment of all the correlations and uncertainties. In particular, there is no averaging over correlated m_Q extractions, and the calculational inputs $\{m_Q(m_Q)\}$ and $\alpha_s(m_Z)$ are no longer correlated. Challenging as it is, such a global analysis is worth further investigation. As a long-term goal for the precision program, it will test our understanding of elementary particle physics at an unprecedented level.

As a final remark in this section, the techniques described above are to be employed in a rigorous test of the SM. The resulting statistical test from the χ^2 analysis is for determining the likelihood of the compatibility of the data with the SM hypothesis. It is straightforward to apply these techniques to a slightly different model, which we call the κ SM, defined to be exactly the SM theory except that each coupling of the Higgs boson to SM states has a free parameter κ_i in front that is varied to fit the data (see e.g. [69, 152, 174]). In that case, the χ^2 analysis must include these κ_i as *extra* input variables and the resulting fit tests the compatibility of the κ SM theory with the data and, if compatible, gives confidence intervals for the κ_i values. Just as with the SM, at the next level of precision analysis of the κ SM it is important to address the role of low-energy observables that we study here.

3.3 Recasting Higgs observables in terms of low-energy observables

In order to investigate sources of theoretical uncertainties in calculating the Higgs observables, it is helpful to recast them in terms of a set of input observables without invoking a global fit. In the simplest case, suppose all the observables under consideration are in-

sensitive to $\{p_k^{\text{other}}\}$. We choose two low-energy observables $\widehat{O}_1^{\text{low}}, \widehat{O}_2^{\text{low}}$. By inverting the functions

$$\widehat{O}_1^{\text{low}} = \widehat{O}_1^{\text{low}} \left[\{\widehat{O}_k^{\text{in}}\}, \{m_Q(m_Q)\} \right], \quad \widehat{O}_2^{\text{low}} = \widehat{O}_2^{\text{low}} \left[\{\widehat{O}_k^{\text{in}}\}, \{m_Q(m_Q)\} \right], \quad (3.8)$$

we express the quark masses in terms of $\widehat{O}_1^{\text{low}}, \widehat{O}_2^{\text{low}}$:

$$m_c(m_c) = m_c(m_c) \left[\{\widehat{O}_k^{\text{in}}\}, \widehat{O}_1^{\text{low}}, \widehat{O}_2^{\text{low}} \right], \quad m_b(m_b) = m_b(m_b) \left[\{\widehat{O}_k^{\text{in}}\}, \widehat{O}_1^{\text{low}}, \widehat{O}_2^{\text{low}} \right]. \quad (3.9)$$

$\{m_Q(m_Q)\}$ can then be eliminated from the calculation of the Higgs observables:

$$\widehat{O}_i^{\text{high}} = \widehat{O}_i^{\text{high}} \left[\{\widehat{O}_k^{\text{in}}\}, \{m_Q(m_Q)\} \right] = \widehat{O}_i^{\text{high}} \left[\{\widehat{O}_k^{\text{in}}\}, \widehat{O}_1^{\text{low}}, \widehat{O}_2^{\text{low}} \right], \quad (3.10)$$

and we have achieved the goal of recasting Higgs observables in terms of low-energy input observables $\widehat{O}_1^{\text{low}}, \widehat{O}_2^{\text{low}}$. From Eq. (3.10) it is clear that the precision in the SM prediction for the Higgs observables will benefit from improved knowledge of m_Q , which ultimately comes from better measurements of the low-energy observables.

Our choices for the low-energy input observables,

$$\widehat{O}_1^{\text{low}}, \widehat{O}_2^{\text{low}} = \mathcal{M}_1^c, \mathcal{M}_2^b, \quad (3.11)$$

require only a slight generalization of the simple formalism above. We will take into account an additional input, the gluon condensate, as $\{p_k^{\text{other}}\}$ in the case of \mathcal{M}_1^c , but its contribution allows for a simplified treatment. In fact, the simplicity of the analysis is our main motivation for choosing these moments as inputs rather than other low-energy observables which lead to similar level of precision in the extracted m_Q . For example, if we were to use semileptonic B meson decay observables (see e.g. [171–173]), more input parameters in $\{p_k^{\text{other}}\}$ will show up, including flavor angles and four nonperturbative parameters. Also, the low moments (\mathcal{M}_n^Q with $n \leq 4$) chosen here are computationally more straightforward than the high moments ($n \geq 10$; see e.g. [165–168]). The former can be calculated conveniently in the relativistic theory, while a nonrelativistic effective theory treatment is needed for the latter. In addition, since the calculation involves $\overline{\text{MS}}$ quark masses, there is no need for introducing other mass schemes. Potentially large uncertainties associated with mass scheme conversion (e.g. from pole or kinetic masses to $\overline{\text{MS}}$ masses), which is needed for some other methods, can thus be avoided. We also note that the approach of extracting m_Q from the low moments was recently recast by the lattice QCD community [175–177], and future development in this direction may shed light on the precision Higgs program [178].

To calculate \mathcal{M}_n^Q , one applies quark-hadron duality [179] to relate the moments \mathcal{M}_n^Q to vector current correlators,

$$\mathcal{M}_n^Q = \frac{12\pi^2}{n!} \left(\frac{d}{dq^2} \right)^n \Pi_Q(q^2) \Big|_{q^2=0}, \quad \text{where} \quad (3.12)$$

$$(q^2 g_{\mu\nu} - q_\mu q_\nu) \Pi_Q(q^2) = -i \int d^4x e^{iq \cdot x} \langle 0 | T j_\mu(x) j_\nu^\dagger(0) | 0 \rangle, \quad (3.13)$$

with j_μ being the electromagnetic current of Q . Π_Q can be calculated as an operator product expansion:

$$\mathcal{M}_n^Q = \frac{(Q_Q/(2/3))^2}{(2m_Q(\mu))^{2n}} \sum_{i,j} \bar{C}_{n,i}^{(j)}(n_f) \left(\frac{\alpha_s(\mu)}{\pi} \right)^i \ln^j \frac{m_Q(\mu)^2}{\mu^2} + \mathcal{M}_n^{Q,\text{np}}, \quad (3.14)$$

where Q_Q is the electric charge of quark Q . As one can see, the values of these moments depend on the quark masses, a fact that QCD sum rules practitioners use to extract quark masses (for reviews see [180, 181]). The two terms in Eq. (3.14) come from perturbation theory and nonperturbative condensates, respectively. The perturbative part is known up to $\mathcal{O}(\alpha_s^3)$ [182], while the gluon condensate contribution, which dominates $\mathcal{M}_n^{Q,\text{np}}$, has been calculated to next-to-leading order [183]. Note that the coefficients $\bar{C}_{n,i}^{(j)}$ are functions of n_f , the number of active quark flavors. The common choices are $n_f = 4$ for $Q = c$ and $n_f = 5$ for $Q = b$. These are also the numbers of active quark flavors assumed for $\alpha_s(\mu)$ and $m_Q(\mu)$ in Eq. (3.14). $\alpha_s(m_Z)$ is defined for $n_f = 5$, and should be matched to the 4-flavor effective coupling at the bottom quark threshold before being used in Eq. (3.14) for \mathcal{M}_n^c . In our calculations the matching is done assuming 4.2 GeV for both the threshold scale and $m_b(m_b)$, but all the results are found to be insensitive to the details of threshold matching.

$m_Q(\mu)$ are usually extracted by comparing the theoretical calculation with experimental data for \mathcal{M}_n^Q (see [157, 162] for technical details). Normally the lowest moment \mathcal{M}_1^c is taken for the charm quark so as to suppress the nonperturbative contribution to the subpercent level [157, 162, 184]. For the bottom quark the gluon condensate can be safely neglected at the present level of precision [162], and the second moment \mathcal{M}_2^b is preferred due to large experimental uncertainty in \mathcal{M}_1^b . We also neglect $\mathcal{O}(m_c^2/m_b^2)$ terms in \mathcal{M}_2^b , not explicitly written out in Eq. (3.14), which constitute a tiny contribution [162].

It is pointed out in [157] that the scales at which m_Q and α_s are renormalized should be considered independently to avoid bias in the uncertainty estimate. Eq. (3.14) then should

be generalized to

$$\mathcal{M}_n^Q = \frac{(Q_Q/(2/3))^2}{(2m_Q(\mu_m))^{2n}} \sum_{i,a,b} C_{n,i}^{(a,b)}(n_f) \left(\frac{\alpha_s(\mu_\alpha)}{\pi} \right)^i \ln^a \frac{m_Q(\mu_m)^2}{\mu_m^2} \ln^b \frac{m_Q(\mu_m)^2}{\mu_\alpha^2} + \mathcal{M}_n^{Q,\text{np}}. \quad (3.15)$$

The coefficients in this equation $C_{n,i}^{(a,b)}$ can be readily derived from $\bar{C}_{n,i}^{(j)}$ via renormalization group (RG) equations, and numerical results for $n_f = 4$ can be found in [157]. Due to unknown $\mathcal{O}(\alpha_s^4)$ terms, the calculated \mathcal{M}_n^Q exhibit dependence on both μ_m and μ_α . Scale dependence is a general feature of finite-order perturbative calculations, and should be considered with care in estimating theoretical uncertainties. We have more to say on this below.

With $m_Q(\mu_m)$, $\alpha_s(\mu_\alpha)$ related to $m_Q(m_Q)$, $\alpha_s(m_Z)$ via RG equations, Eq. (3.15) matches the general form of Eq. (3.8), with $\alpha_s(m_Z)$ being the only relevant element in $\{\widehat{O}_k^{\text{in}}\}$. There are additional inputs μ_m , μ_α and $\mathcal{M}_n^{Q,\text{np}}$. So in our case, Eq. (3.8) is modified as:

$$\mathcal{M}_1^c = \mathcal{M}_1^c \left[\alpha_s(m_Z), m_c(m_c), \mu_m^c, \mu_\alpha^c, \mathcal{M}_1^{c,\text{np}} \right], \quad (3.16)$$

$$\mathcal{M}_2^b = \mathcal{M}_2^b \left[\alpha_s(m_Z), m_b(m_b), \mu_m^b, \mu_\alpha^b \right], \quad (3.17)$$

where we have neglected $\mathcal{M}_2^{b,\text{np}}$. As mentioned above, the nonperturbative contribution has been claimed to be negligible for the bottom quark. We have checked this in the case of \mathcal{M}_2^b , where the contribution from $\mathcal{M}_2^{b,\text{np}}$ is below 0.1%, which should be compared to the experimental uncertainty of \mathcal{M}_2^b of about 1%. Treating $\mathcal{M}_1^{c,\text{np}}$ and $m_c(m_c)$ as independent inputs, which we will justify later, and focusing on the Higgs boson partial widths to $c\bar{c}$ and $b\bar{b}$ as examples of $\{\widehat{O}_i^{\text{high}}\}$, we have, in place of Eqs. (3.9) and (3.10),

$$m_c(m_c) = m_c(m_c) \left[\alpha_s(m_Z), \mathcal{M}_1^c, \mu_m^c, \mu_\alpha^c, \mathcal{M}_1^{c,\text{np}} \right], \quad (3.18)$$

$$m_b(m_b) = m_b(m_b) \left[\alpha_s(m_Z), \mathcal{M}_2^b, \mu_m^b, \mu_\alpha^b \right], \quad (3.19)$$

$$\begin{aligned} \Gamma_{H \rightarrow c\bar{c}} &= \Gamma_{H \rightarrow c\bar{c}} \left[\{\widehat{O}_k^{\text{in}}\}, m_c(m_c), \mu_H^c \right] \\ &= \Gamma_{H \rightarrow c\bar{c}} \left[\{\widehat{O}_k^{\text{in}}\}, \mathcal{M}_1^c, \mu_m^c, \mu_\alpha^c, \mu_H^c, \mathcal{M}_1^{c,\text{np}} \right], \end{aligned} \quad (3.20)$$

$$\begin{aligned} \Gamma_{H \rightarrow b\bar{b}} &= \Gamma_{H \rightarrow b\bar{b}} \left[\{\widehat{O}_k^{\text{in}}\}, m_b(m_b), \mu_H^b \right] \\ &= \Gamma_{H \rightarrow b\bar{b}} \left[\{\widehat{O}_k^{\text{in}}\}, \mathcal{M}_2^b, \mu_m^b, \mu_\alpha^b, \mu_H^b \right], \end{aligned} \quad (3.21)$$

where μ_H^c , μ_H^b collectively denote other renormalization scales involved in the calculation of the partial widths. These are nevertheless not the only scale dependences for the partial widths in such an analysis. The residual scale dependences of the low-energy observables

are seen to propagate into the extracted quark masses, and constitute part of the uncertainties in $m_Q(m_Q)$. These uncertainties eventually propagate into the calculations of Higgs observables, and are reflected in the μ_m, μ_α dependences in Eqs. (3.20) and (3.21). Note also that in the second equalities in Eqs. (3.20) and (3.21), the $\alpha_s(m_Z)$ dependence in the partial widths has been changed to account for the correlation with $m_Q(m_Q)$ reflected in Eqs. (3.18) and (3.19).

Eqs. (3.20) and (3.21) represent the final results of the exercise of recasting Higgs observables in terms of low-energy observables, with the information contained in $m_Q(m_Q)$ fully resolved. They will be used in the next section to investigate the theoretical uncertainties in these partial widths.

To close this section we remark on the treatment of $\mathcal{M}_1^{c,\text{np}}$. The known terms read [183]

$$\mathcal{M}_1^{c,\text{np}} = \frac{\langle \frac{\alpha_s}{\pi} G^2 \rangle}{(2m_c^{\text{pole}})^6} \left[-16.042 - 168.07 \frac{\alpha_s(\mu)}{\pi} + \mathcal{O}(\alpha_s^2) \right], \quad (3.22)$$

where $\langle \frac{\alpha_s}{\pi} G^2 \rangle$ is the gluon condensate. The commonly used value in the context of charm quark mass extraction is derived from τ decay data [185]:

$$\left\langle \frac{\alpha_s}{\pi} G^2 \right\rangle = 0.006 \pm 0.012 \text{ GeV}^4. \quad (3.23)$$

In addition to the imprecise knowledge of $\langle \frac{\alpha_s}{\pi} G^2 \rangle$, we note two other sources of uncertainties in $\mathcal{M}_1^{c,\text{np}}$. First, it is argued in [157, 184] that $\mathcal{M}_1^{c,\text{np}}$ should be expressed in terms of the pole mass rather than the $\overline{\text{MS}}$ mass in order to have a stable α_s expansion. We agree with this argument, but note that the use of the pole mass may introduce further ambiguities. For example, if one tries to calculate the pole mass from the $\overline{\text{MS}}$ mass, the result will be very sensitive to the loop order. Second, considerable uncertainty is introduced by the μ dependence of the bracket in Eq. (3.22), since the $\mathcal{O}(\alpha_s^2)$ terms are not known. This renormalization scale is not necessarily related to μ_α or μ_m in the perturbation theory contributions [the first term in Eq. (3.15)]. All these uncertainties and ambiguities will dilute any conceivable correlation between $\mathcal{M}_1^{c,\text{np}}$ and $m_c(m_c)$, justifying our treatment of them as independent inputs. In our analysis the following value for $\mathcal{M}_1^{c,\text{np}}$ will be assumed:

$$\mathcal{M}_1^{c,\text{np}} = -0.0001_{-0.0014}^{+0.0006} \text{ GeV}^{-2}. \quad (3.24)$$

The central value corresponds to $\langle \frac{\alpha_s}{\pi} G^2 \rangle = 0.006 \text{ GeV}^4$, $m_c^{\text{pole}} = 1.7 \text{ GeV}$ and $\mu = 3 \text{ GeV}$ in Eq. (3.22). The errors are very conservatively estimated by taking the extreme values $m_c^{\text{pole}} = 1.4 \text{ GeV}$, $\mu = 1 \text{ GeV}$, and varying $\langle \frac{\alpha_s}{\pi} G^2 \rangle$ in the range in Eq. (3.23). Even with the

extreme values considered, $\mathcal{M}_1^{c,\text{np}}$ is still a subpercent-level contribution to $\mathcal{M}_1^c \sim 0.2 \text{ GeV}^{-2}$.

3.4 Theoretical uncertainties of Higgs partial widths

It is clear from Eqs. (3.20) and (3.21) that there are two types of uncertainties in the calculation of the Higgs partial widths. Parametric uncertainty results from imprecise knowledge of the input parameters, including the input observables (\mathcal{M}_1^c , \mathcal{M}_2^b and those in $\{\widehat{O}_k^{\text{in}}\}$) and the nonperturbative parameter $\mathcal{M}_1^{c,\text{np}}$. The experimental values and errors of the input observables are:

$$\mathcal{M}_1^c = 0.2121(20)(30) \text{ GeV}^{-2} \quad [157], \quad (3.25)$$

$$\mathcal{M}_2^b = 2.819(27) \times 10^{-5} \text{ GeV}^{-4} \quad [184], \quad (3.26)$$

$$\alpha_s(m_Z) = 0.1185(6) \quad [154], \quad (3.27)$$

$$m_H = 125.7(4) \text{ GeV} \quad [154], \quad (3.28)$$

$$m_t = 173.21(51)(71) \text{ GeV} \quad [154], \quad (3.29)$$

$$m_Z = 91.1876(21) \text{ GeV} \quad [154], \quad (3.30)$$

$$\alpha(m_Z) = 1/127.940(14) \quad [154], \quad (3.31)$$

$$G_F = 1.1663787(6) \times 10^{-5} \text{ GeV}^{-2} \quad [154]. \quad (3.32)$$

For \mathcal{M}_1^c and m_t the two experimental uncertainties are statistical and systematic, respectively. There is an additional systematic uncertainty in \mathcal{M}_2^b associated with the prescriptions used in extracting moments from data. This is discussed in [184], and we adopt ‘‘Option A’’ in that paper because among the three options considered there it appears to yield the most consistent results for $m_Q(m_Q)$ across different moments.

Perturbative uncertainty, on the other hand, is associated with unknown higher-order terms in perturbation theory calculations, and leads to residual dependence of calculated observables on the renormalization scales. When the partial widths are recast in terms of \mathcal{M}_1^c and \mathcal{M}_2^b as in Eqs. (3.20) and (3.21), multiple scales enter. μ_H comes from the calculation of the Higgs boson decay. The associated perturbative uncertainty has been studied in the literature; see e.g. [121] where it is found to be small compared with parametric uncertainty. Here we focus on μ_m , μ_α , which originate from the calculation of the low-energy observables \mathcal{M}_1^c , \mathcal{M}_2^b [see Eqs. (3.15-3.17)]. Their contribution to the total theoretical uncertainty will be singled out below by setting all input parameters to their central values in Eqs. (3.24-3.32), and setting $\mu_H = m_H$.

We study the perturbative uncertainty from μ_m , μ_α in two steps. First, $m_Q(\mu_m)$ are

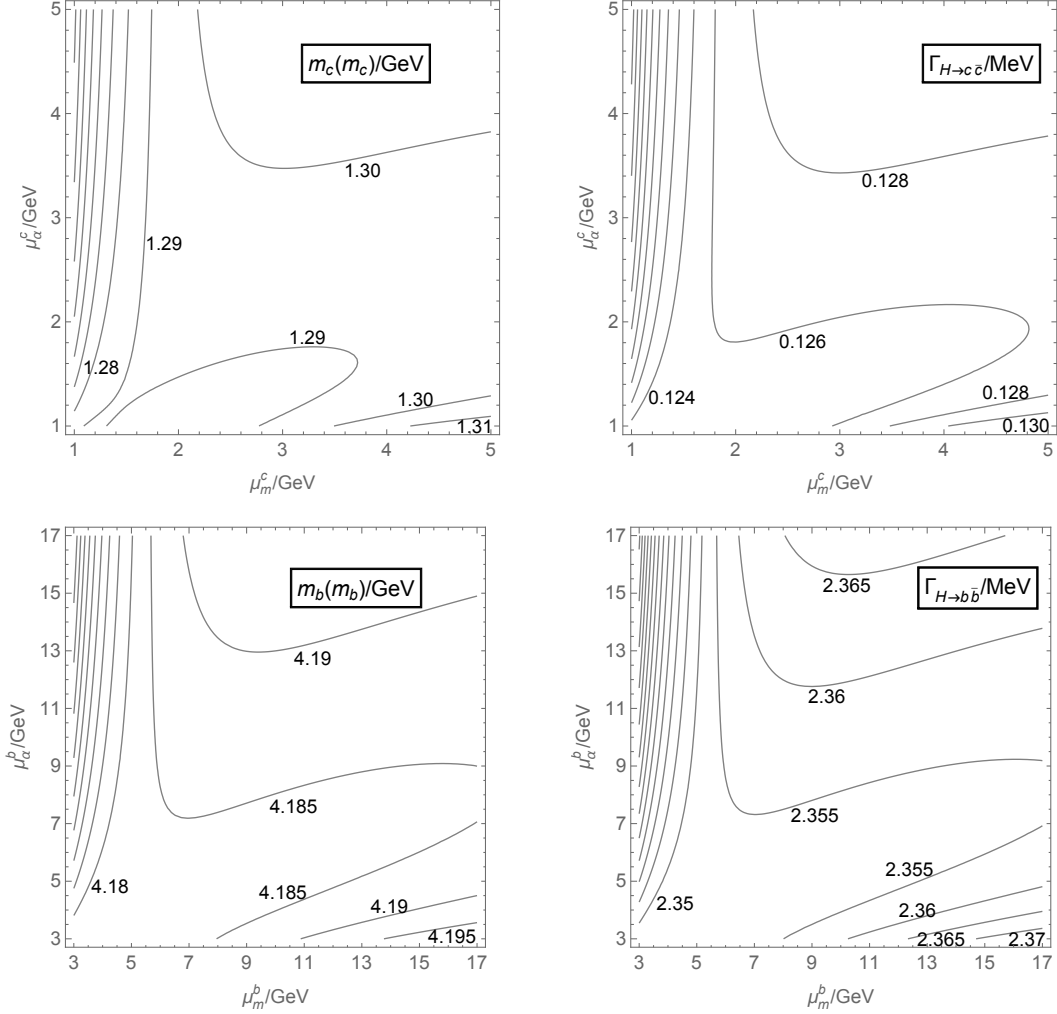


Figure 3.1: (From [30]) Contours of $m_c(m_c)$ (top-left), $\Gamma_{H \rightarrow c\bar{c}}$ (top-right), $m_b(m_b)$ (bottom-left), $\Gamma_{H \rightarrow b\bar{b}}$ (bottom-right) in the μ_m - μ_α plane. These plots demonstrate Eqs. (3.18-3.21) with all other inputs fixed. The unlabeled contours represent decreasing values toward the top-left corner in steps of 0.01 GeV, 0.005 GeV, 0.002 MeV, 0.005 MeV, respectively.

calculated by iteratively solving Eq. (3.15) following the procedure explained in [157], from which $m_Q(m_Q)$ are derived. We use the RunDec package [186] for RG running and threshold matching to the highest loop order implemented in the package. Second, the partial widths $\Gamma_{H \rightarrow c\bar{c}}$, $\Gamma_{H \rightarrow b\bar{b}}$ are calculated using the expansion formulas in [121]. The results of both steps are shown in Fig. 3.1 as contour plots in the μ_m - μ_α plane³. They correspond to Eqs. (3.18-3.21) with other inputs fixed. These plots illustrate the propagation of μ_m , μ_α dependence from low-energy moments calculations to Higgs partial widths.

To estimate the perturbative uncertainty, a common practice is to identify a characteristic

³The numerical difference between our $m_c(m_c)$ contour plot and Fig. 6(c) in [157] is due to the input \mathcal{M}_1^c and $\alpha_s(m_Z)$ used, and to a lesser extent the treatment of $\mathcal{M}_1^{c,\text{np}}$.

scale of the process of interest, and vary the renormalization scale within a factor of two around that scale. For example, μ_H has been varied from $m_H/2$ to $2m_H$ in [121]. However, this method is not directly applicable to μ_m and μ_α , since \mathcal{M}_n^Q receive contributions from all energy scales as evident in Eq. (3.3). One might guess from qualitative features of $R_Q(s)$ that the characteristic scale should be $\mathcal{O}(2m_Q)$, the masses of quarkonium resonances. But due to the relatively large value of α_s in the low-energy regime, the exact number, and hence the range in which we choose to vary μ_m, μ_α can greatly affect the result of our uncertainty estimates. This is already clear from Fig. 3.1, where $\Gamma_{H \rightarrow c\bar{c}}$ and $\Gamma_{H \rightarrow b\bar{b}}$ are seen to exhibit rapid variation in the low- μ_m regime.

Lacking an optimal method to estimate the perturbative uncertainty, we refrain from giving exact numbers, but instead aim to illustrate the ambiguity in the estimate of perturbative uncertainty by varying μ_m and μ_α independently within an adjustable range $[\mu_{\min}, \mu_{\max}]$. We will focus on the uncertainties in the partial widths, and remark that they are related to the uncertainties in $m_Q(m_Q)$ by [121]

$$\frac{\Delta\Gamma_{H \rightarrow c\bar{c}}}{\Gamma_{H \rightarrow c\bar{c}}} \simeq \frac{\Delta m_c(m_c)}{10 \text{ MeV}} \times 2.1\%, \quad \frac{\Delta\Gamma_{H \rightarrow b\bar{b}}}{\Gamma_{H \rightarrow b\bar{b}}} \simeq \frac{\Delta m_b(m_b)}{10 \text{ MeV}} \times 0.56\%. \quad (3.33)$$

The perturbative uncertainty, defined as half the difference between the maximum and minimum values of $\Gamma_{H \rightarrow c\bar{c}}, \Gamma_{H \rightarrow b\bar{b}}$, depends on μ_{\min} and μ_{\max} . We present the results in Fig. 3.2 in terms of “percent relative uncertainties,” defined to be $100\Delta\Gamma/\Gamma$. The red solid curves show the estimated perturbative uncertainties as functions of μ_{\min} , with μ_{\max}^c (μ_{\max}^b) fixed at 4 (15) GeV. Alternative choices for μ_{\max}^c (μ_{\max}^b), 3 and 5 (13 and 17) GeV, give rise to the red dashed curves. These can be compared with the dominant parametric uncertainties shown by the other curves in Fig. 3.2 (see figure caption for details). The popular choices in the literature $(\mu_{\min}^c, \mu_{\max}^c) = (2, 4)$ GeV and $(\mu_{\min}^b, \mu_{\max}^b) = (5, 15)$ GeV yield perturbative uncertainties of 1.2% and 0.33% for $\Gamma_{H \rightarrow c\bar{c}}$ and $\Gamma_{H \rightarrow b\bar{b}}$, respectively, comparable with parametric uncertainties. However, the perturbative uncertainties increase rapidly and dominate the total theoretical uncertainties if lower renormalization scales are considered. The result of the theoretical uncertainty estimate is then strongly dependent on the artificial choice of μ_{\min} . This poses a serious ambiguity in precision analysis, and calls for more enlightened prescriptions for the uncertainty estimate. We note two possible directions in this regard.

The first direction was suggested very recently in [187] in the context of m_Q extraction. There it is argued that the large perturbative uncertainty from completely uncorrelated variation of μ_m and μ_α is probably an overestimate. To get the perturbative uncertainty under control, a “convergence test” is performed to identify regions in the μ_m - μ_α plane where the perturbative series converges too slowly (characterized by a large convergence

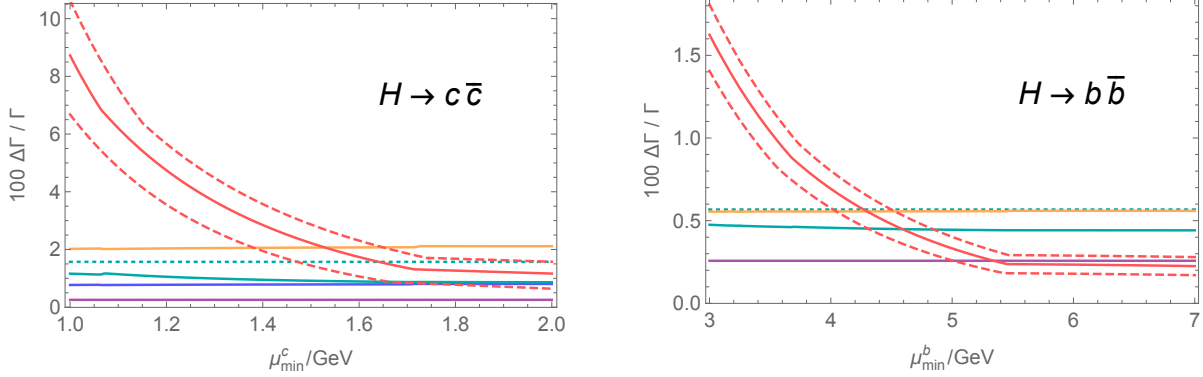


Figure 3.2: (From [30]) Percent relative uncertainties in $\Gamma_{H \rightarrow c\bar{c}}$ (left) and $\Gamma_{H \rightarrow b\bar{b}}$ (right) as functions of μ_{\min} from: perturbative uncertainty with $\mu_{\max}^c = 4$ GeV, $\mu_{\max}^b = 15$ GeV (red solid) or alternatively $\mu_{\max}^c = 3, 5$ GeV, $\mu_{\max}^b = 13, 17$ GeV (red dashed), parametric uncertainties from \mathcal{M}_1^c or \mathcal{M}_2^b (orange), $\alpha_s(m_Z)$ (cyan solid), $\mathcal{M}_1^{c,np}$ (blue, for $\Gamma_{H \rightarrow c\bar{c}}$ only) and m_H (purple). The parametric uncertainty from $\alpha_s(m_Z)$ incorrectly calculated assuming no correlation with m_Q (cyan dotted) is also shown for comparison. The parametric uncertainties are defined as shifts of the central values of $\Gamma_{H \rightarrow c\bar{c}}$ and $\Gamma_{H \rightarrow b\bar{b}}$ for $\mu_{\min} \leq \mu_m, \mu_\alpha \leq \mu_{\max}$ caused by varying the input parameters within the errors quoted in Eqs. (3.24-3.32), with $\mu_{\max}^c = 4$ GeV, $\mu_{\max}^b = 15$ GeV (the kinks are due to the maximum or minimum shifting to a different region in the μ_m - μ_α plane), and are found to be insensitive to μ_{\max} .

parameter). These regions are then discarded in the uncertainty estimate. Following the approach outlined in [187], we find that the discarded regions correspond to the upper-left and bottom-right corners in each plot in Fig. 3.1, where $m_Q(m_Q)$ and the partial widths exhibit rapid variation. The final result in [187] is a reduced perturbative uncertainty: 14 MeV and 10 MeV for $m_c(m_c)$ and $m_b(m_b)$, respectively, corresponding to 2.9% and 0.56% relative uncertainties in $\Gamma_{H \rightarrow c\bar{c}}$ and $\Gamma_{H \rightarrow b\bar{b}}$, respectively.

The convergence test is a well-motivated idea, reflecting the intuition that a proper scale choice should not lead to very slow convergence. However, further study is necessary to examine various details of the approach. For instance, one may consider loosening the constraints $m_c(m_c) \leq \mu_m^c, \mu_\alpha^c \leq 4$ GeV, $m_b(m_b) \leq \mu_m^b, \mu_\alpha^b \leq 15$ GeV imposed in [187]. In particular, μ_m, μ_α slightly lower than $m_Q(m_Q)$ should be allowed as long as one retains 4-flavor (5-flavor) effective strong coupling for the charm (bottom) quark. Also, the convergence criterion may be refined. The definition of the convergence parameter in [187] assumes an approximate geometric series behavior of the α_s series, but we find the latter falls off more slowly than a geometric series in most cases. Furthermore, it remains to seek a less arbitrary prescription for the fraction of (μ_m, μ_α) to be discarded, and to investigate whether the convergence parameter is a good indicator of the size of higher-order corrections. In any case, to be conservative the reduced perturbative uncertainties mentioned above should be

interpreted with caution before the approach is developed further.

As an alternative direction, one may consider the possibility of finding an optimal scale via a defensible scale-setting procedure, such as the one advocated by Brodsky-Lepage-Mackenzie (BLM) [188]. The BLM scale for an observable is obtained by absorbing the n_f terms in the perturbation series, which come from the QCD beta function, into the running coupling α_s . This is arguably the physical scale of the process, with higher-order corrections associated with RG running appropriately resummed. We also note that the BLM procedure extended to all orders based on the principle of maximum conformality [189] has been demonstrated to be self-consistent [190]. In the case of \mathcal{M}_n^Q , however, there are two renormalized parameters α_s and m_Q , and naive application of the BLM procedure might be problematic. This is because even when the n_f terms are absorbed into running α_s and/or m_Q , the leading-order mass renormalization, which is independent of n_f , may lead to large loop corrections which are difficult to identify. Indeed, we find that naive application of BLM, namely absorbing the $n_f\alpha_s^2$ terms, sets scales for μ_m and μ_α which are strongly disfavored by the convergence test. In light of the importance of a more precise m_Q determination, it might be worthwhile to investigate the nontrivial possibility of generalizing the BLM method and its extensions [189,191] to include running quark masses.

The parametric uncertainties, on the other hand, are seen from Fig. 3.2 to be dominated by experimental measurement uncertainties of \mathcal{M}_1^c and \mathcal{M}_2^b (orange). Reduction of these will rely on more precise measurements of $R_Q(s)$ and more careful treatment of experimental data. At present the major problem is the lack of data above $\sqrt{s} = 11.2$ GeV, resulting in large uncertainties in the bottom quark moments [184]. Also, the quarkonium resonances are currently treated in the narrow width approximation, the quality of which should be examined in light of higher precision requirements in the future. $\alpha_s(m_Z)$ (cyan solid) constitutes a subdominant source of parametric uncertainties. Its contribution is seen to be smaller than the incorrect estimate assuming no correlation between $\alpha_s(m_Z)$ and m_Q (cyan dashed), due to partial cancelation between direct $\alpha_s(m_Z)$ dependence and indirect dependence through m_Q . With our conservative estimate (i.e. erring on the large side) in Eq. (3.24), $\mathcal{M}_1^{c,mp}$ leads to an uncertainty in $\Gamma_{H \rightarrow c\bar{c}}$ (blue) at a similar level as $\alpha_s(m_Z)$. This may represent a challenge in the future, and calls for further investigation of the gluon condensate contribution. The uncertainty due to m_H (purple) is less important, while other input observables listed at the beginning of this section have a negligible effect on the parametric uncertainty.

3.5 Conclusions

For the precision Higgs program to succeed in the future, additional effort is required to improve the precision of SM calculations in order to match the proposed experimental accuracy. A better understanding of theoretical uncertainties is critical. Toward this aim, we emphasize the role of low-energy observables, and further propose the idea of a global analysis incorporating relevant observables across all energy regimes. Rather than contributing indirectly via the charm and bottom quark masses, low-energy observables explicitly participate in such a precision analysis. Future studies in this direction should examine all candidates of low-energy observables, and determine an efficient set of observables for the global fit.

In the context of precision Higgs calculations, we focused on the Higgs boson partial widths to charm and bottom quarks, and investigated the theoretical uncertainties in these observables. By eliminating charm and bottom quark masses in favor of low-energy observables \mathcal{M}_1^c and \mathcal{M}_2^b , we recast the partial widths in terms of these and other input observables. Much information originally hidden in uncertainties in the highly processed quark masses becomes transparent. Experimental uncertainties in the low-energy observables are directly propagated into the Higgs partial widths, and the uncertainty due to $\alpha_s(m_Z)$ is treated properly. Perturbative uncertainties are difficult to assess due to the ambiguity in the choice of renormalization scales in the low-energy regime, and can dominate the total theoretical uncertainty of the Higgs partial widths if lower values of the renormalization scales are considered than is usually the case in the literature.

Such analysis points to future directions in the precision program. For the partial widths considered here, we note that while future experimental progress could potentially reduce parametric uncertainties significantly, our ability to make precise predictions on the Higgs partial widths will not improve unless better understanding of the perturbative uncertainty is achieved. As for \mathcal{M}_1^c and \mathcal{M}_2^b studied here, this might require the calculation of $\mathcal{O}(\alpha_s^4)$ corrections to $\Pi_Q(q^2)$ (in the low- q^2 limit) and/or more enlightened scale setting. Though the actual situation may be better in a global fit where \mathcal{M}_1^c and \mathcal{M}_2^b are not the only low-energy observables involved, it remains crucial to carefully investigate whether the scale-setting problem is also present for other low-energy observables sensitive to m_Q . If the perturbative uncertainty gets under control, the precision program, where both low-energy observables and Higgs observables play an important role, will be promising in studying properties of the Higgs boson, and even more generally testing the SM across a wide range of energy scales and probing new physics ideas.

Chapter 4

EFT of Universal Theories and Its RG Evolution

The conventional oblique parameters analyses of precision electroweak data can be consistently cast in the modern framework of the Standard Model effective field theory (SMEFT) when restrictions are imposed on the SMEFT parameter space so that it describes universal theories. However, the usefulness of such analyses is challenged by the fact that universal theories at the scale of new physics, where they are matched onto the SMEFT, can flow to nonuniversal theories with renormalization group (RG) evolution down to the electroweak scale, where precision observables are measured. The departure from universal theories at the electroweak scale is not arbitrary, but dictated by the universal parameters at the matching scale. But to define oblique parameters, and more generally universal parameters at the electroweak scale that directly map onto observables, additional prescriptions are needed for the treatment of RG-induced nonuniversal effects. We perform a RG analysis of the SMEFT description of universal theories, and discuss the impact of RG on simplified, universal-theories-motivated approaches to fitting precision electroweak and Higgs data.

4.1 Introduction

The quest for new physics beyond the Standard Model (BSM) has been, and will continue to be proceeding through both direct and indirect searches for their effects. While direct searches for BSM signatures have to be carried out with particular models (often simplified ones) in mind, indirect searches through precision measurements of Standard Model (SM) processes often admit more general approaches that are model-independent to some extent. A classic example is the oblique parameters formalism [192], the widely-adopted version of which was proposed by Peskin and Takeuchi [146], and further developed by others [193,194].

Here, just a few parameters, most notably S and T (or their rescaled versions \hat{S} and \hat{T}), capture the new physics modifications of the vector boson self-energies, which are assumed to be the dominant BSM effects (hence the name “oblique”). Modern studies in this direction are migrating to the Standard Model effective field theory (SMEFT) approach; see e.g. [5, 6, 62] for recent reviews. In this case, the SM Lagrangian, supplemented by the complete set of dimension-6 operators built from the SM field content, provides a most general and consistent framework for calculating the leading BSM effects on precision observables, assuming there are no new light states and the new physics scale Λ is much higher than the electroweak scale μ_{EW} .

Reconciliation of the oblique parameters formalism and the more general SMEFT is based on the realization that the former is generally speaking only applicable to universal theories, a restricted class of BSM theories whose SMEFT representation can be cast in a form that involves bosonic operators only [109] (see also [87] for an earlier study with similar motivations). By bosonic operators, we mean dimension-6 operators built from the SM bosons. There are 16 of them one can possibly write down that are independent and CP-even, as we have shown in [109], so the effective theory of universal theories has a 16-dimensional parameter space, independent of the SMEFT basis choice. In turn, they can be mapped onto 16 independent phenomenological parameters, called “*universal parameters*” in [109], 5 of which coincide with the familiar oblique parameters. At leading order (LO) in $\frac{v^2}{\Lambda^2}$, they lead to a universal pattern of deviations from the SM. In the recently-proposed Higgs basis framework [7], this pattern is encoded in a set of relations among the otherwise independent effective couplings.

Beyond LO, however, complications can arise. In particular, the 16-dimensional parameter space of universal theories, being a subspace of the full SMEFT parameter space, is not guaranteed to be closed under renormalization group (RG) evolution. In fact, it is intuitively clear that nonuniversal effects can indeed be generated by RG, because even if one starts with a bosonic basis (consisting of 16 independent bosonic operators) [109], fermionic operators, i.e. operators containing SM fermions, can be generated that are not organized into the SM currents and hence cannot be eliminated in favor of bosonic operators. Three examples involving oblique corrections are illustrated in figure 4.1. This qualitative argument can be made concrete by a detailed RG analysis of universal theories, which we perform in this chapter,¹ aided by the recently-calculated full anomalous dimension matrix for the

¹It should be noted that in the SMEFT framework, observables at the electroweak scale are calculated as a double series expansion, in powers of both $\frac{E^2}{\Lambda^2} \sim \frac{v^2}{\Lambda^2}$ and the loop factor $\frac{1}{16\pi^2}$. Terms of order $(\frac{v^2}{\Lambda^2})^0 (\frac{1}{16\pi^2})^n$ can be taken into account by incorporating higher-order SM calculations independently of new physics contributions [131]. The LO new physics effects, like those discussed in [109], are of order $(\frac{v^2}{\Lambda^2})^1 (\frac{1}{16\pi^2})^0$. The RG effects analyzed in the present chapter correspond to order $(\frac{v^2}{\Lambda^2})^1 (\frac{1}{16\pi^2})^1$ terms in the double expansion

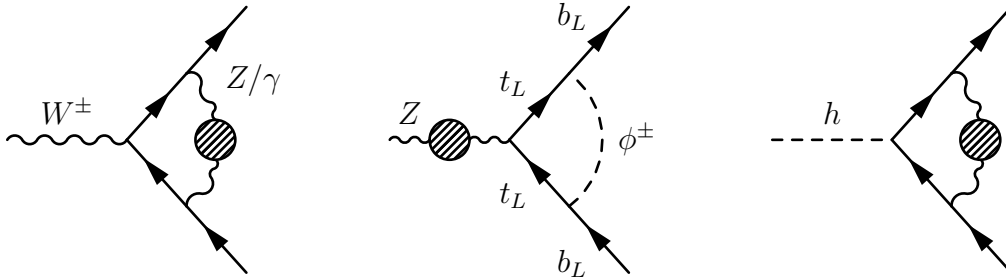


Figure 4.1: (From [111]) Examples showing how nonuniversal effects can be generated by universal oblique corrections. **Left:** effective Wqq' and $Wl\nu$ couplings are renormalized differently, due to the different couplings of quarks and leptons to neutral gauge bosons. **Middle:** the $Zb_L\bar{b}_L$ coupling is singled out among all the $Zf\bar{f}$ couplings probed by Z -pole measurements for relatively large running effects proportional to y_t^2 , via loop corrections involving the charged Goldstone boson (or the longitudinal W^\pm if one uses the unitary gauge). **Right:** the Higgs boson couplings to the up- and down-type quarks and leptons are renormalized differently, due to different gauge interactions of the fermions. In each example, the interactions generated for the SM fermions are not in the form of the SM currents, and thus the corresponding operators cannot be eliminated in favor of bosonic operators. These examples, as well as many others, can be more rigorously formulated in terms of $SU(2)_L \times U(1)_Y$ invariant operators, but we prefer to give a more intuitive illustration at this stage. The arguments here will be made concrete in sections 4.3 and 4.4.

dimension-6 operators [76, 77, 80] (see also [83]).

As a consequence of the RG-induced nonuniversal effects, an effective theory that is universal at the new physics scale Λ can become nonuniversal at the electroweak scale μ_{EW} . This means that, without introducing further prescriptions, the universal parameters \hat{S} , \hat{T} , etc. are not unambiguously defined beyond LO at the electroweak scale. However, the usefulness of these parameters is not plagued, since after all, their values at the high scale Λ are what we really need to know to infer the shape of BSM physics. The latter are well-defined in universal theories, and the 16 of them are sufficient to describe phenomenology also at μ_{EW} , despite the theory becoming nonuniversal after RG evolution. Departures from universal BSM effects are not arbitrary as in generic nonuniversal theories, but can be calculated in terms of these parameters.

An important motivation for the recent trend to push the SMEFT analyses beyond LO [29, 37, 38, 55, 56, 64–67, 69, 70, 72, 73, 76, 77, 79, 80, 82, 83, 86, 91, 95, 96, 99, 102, 104, 106, 195–200] (see also [39–44, 78, 89, 90, 101, 201]) is the observation that for some very well-measured observables, it is possible to derive additional constraints on the effective operators contribut-

that are enhanced by $\ln \frac{\Lambda}{\mu_{EW}}$. Terms of order $(\frac{v^2}{\Lambda^2})^2 (\frac{1}{16\pi^2})^0$ may also have an impact, but the effective Lagrangian has to be extended beyond the dimension-6 level to account for them. The latter [125, 126] is beyond the scope of the present work. See also [90, 91, 104] for related discussions.

ing at higher loop order, which are otherwise less constrained.² In the full SMEFT, this can be done at the leading logarithmic (LL) level by first constraining the Wilson coefficients at μ_{EW} via LO expressions of the observables at the electroweak scale, and then RG-evolving these constraints to Λ . The same is not true for the universal parameters \hat{S} , \hat{T} , etc. As we will see, with additional prescriptions, it is possible to define these parameters at μ_{EW} , but they do not capture all the LL corrections to all observables no matter what prescriptions are adopted. This implies, in particular, that the conventional oblique parameters analysis incorporating only LO effects of the oblique parameters is not a priori justified at the LL level, where additional parameters that should have been included in the fit may have a numerical impact. Also, a simplified global fit to Higgs data where a single rescaling parameter $\Delta\bar{\kappa}_F$ is assumed for all the $hf\bar{f}$ couplings may not be appropriate, since it may not even accurately capture the phenomenology of universal theories.

4.2 Universal theories at LO and beyond

4.2.1 The universal theories EFT at LO

In this subsection, we briefly review the results in [109]. The SMEFT description of universal theories at LO can be formulated in three equivalent ways, in terms of effective operators, universal parameters, or Higgs basis couplings.

As mentioned in the introduction, the effective Lagrangian of universal theories consists of \mathcal{L}_{SM} plus 16 independent CP-even bosonic operators. In the Warsaw basis [3], only 9 of them are kept, while the remaining bosonic operators are eliminated by field redefinitions, or equivalently, by applying the SM equations of motion, in favor of combinations of fermionic operators. Despite the appearance of a proliferation of fermionic operators, the number of independent parameters (Wilson coefficients) is still 16. To be specific, using the notation of [3] for the Warsaw basis operators Q_i , we have

$$\begin{aligned} \mathcal{L}_{\text{universal}} = & \mathcal{L}_{\text{SM}} + \frac{1}{v^2}(C_{HW}Q_{HW} + C_{HB}Q_{HB} + C_{HG}Q_{HG} + C_{HWB}Q_{HWB} + C_WQ_W \\ & + C_GQ_G + C_{HD}Q_{HD} + C_{H\Box}Q_{H\Box} + C_HQ_H + C_{HJW}Q_{HJW} + C_{HJB}Q_{HJB} \\ & + C_{2JW}Q_{2JW} + C_{2JB}Q_{2JB} + C_{2JG}Q_{2JG} + C_yQ_y + C_{2y}Q_{2y}), \end{aligned} \quad (4.1)$$

where C_i are $\mathcal{O}(\frac{v^2}{\Lambda^2})$ Wilson coefficients, and Q_{HJW} , Q_{HJB} , Q_{2JW} , Q_{2JB} , Q_{2JG} , Q_y , Q_{2y} are combinations of fermionic operators listed in table 4.1. Note that the SM fermion fields

²Note, however, that in some of these references, bounds on the oblique parameters are used to constrain the SMEFT parameter space possibly beyond the universal theories subspace, which can lead to inconsistencies as argued in [109] (see also [87]). The results should therefore be interpreted with caution.

Definition	Warsaw basis operator combination
$Q_{HJW} \equiv \frac{ig}{2}(H^\dagger \sigma^a \overleftrightarrow{D}_\mu H) J_W^{a\mu}$	$\frac{1}{4}g^2([Q_{Hq}^{(3)}]_{ii} + [Q_{Hl}^{(3)}]_{ii})$
$Q_{HJB} \equiv \frac{ig'}{2}(H^\dagger \overleftrightarrow{D}_\mu H) J_B^\mu$	$\frac{1}{2}g'^2(Y_q[Q_{Hq}^{(1)}]_{ii} + Y_l[Q_{Hl}^{(1)}]_{ii} + Y_u[Q_{Hu}]_{ii} + Y_d[Q_{Hd}]_{ii} + Y_e[Q_{He}]_{ii})$
$Q_{2JW} \equiv J_{W\mu}^a J_W^{a\mu}$	$g^2(\frac{1}{4}[Q_{qq}^{(3)}]_{iiij} - \frac{1}{4}[Q_{ul}]_{iiij} + \frac{1}{2}[Q_{ul}]_{ijji} + \frac{1}{2}[Q_{lq}^{(3)}]_{iiij})$
$Q_{2JB} \equiv J_{B\mu} J_B^\mu$	$g'^2(Y_q^2[Q_{qq}^{(1)}]_{iiij} + Y_l^2[Q_{ll}]_{iiij} + 2Y_q Y_l [Q_{lq}^{(1)}]_{iiij} + Y_u^2[Q_{uu}]_{iiij} + Y_d^2[Q_{dd}]_{iiij} + Y_e^2[Q_{ee}]_{iiij} + 2Y_q Y_u [Q_{qu}^{(1)}]_{iiij} + 2Y_q Y_d [Q_{qd}^{(1)}]_{iiij} + 2Y_q Y_e [Q_{qe}]_{iiij} + 2Y_l Y_u [Q_{lu}]_{iiij} + 2Y_l Y_d [Q_{ld}]_{iiij} + 2Y_l Y_e [Q_{le}]_{iiij} + 2Y_u Y_d [Q_{ud}^{(1)}]_{iiij} + 2Y_u Y_e [Q_{eu}]_{iiij} + 2Y_d Y_e [Q_{ed}]_{iiij})$
$Q_{2JG} \equiv J_{G\mu}^A J_G^{A\mu}$	$g_s^2(-\frac{1}{6}[Q_{qq}^{(1)}]_{iiij} + \frac{1}{4}[Q_{qq}^{(1)}]_{ijji} + \frac{1}{4}[Q_{qq}^{(3)}]_{ijji} - \frac{1}{6}[Q_{uu}]_{iiij} + \frac{1}{2}[Q_{uu}]_{ijji} - \frac{1}{6}[Q_{dd}]_{iiij} + \frac{1}{2}[Q_{dd}]_{ijji} + 2[Q_{qu}^{(8)}]_{iiij} + 2[Q_{qd}^{(8)}]_{iiij} + 2[Q_{ud}^{(8)}]_{iiij})$
$Q_y \equiv H ^2(H_\alpha J_y^\alpha + \text{h.c.})$	$[y_u]_{ij}[Q_{uH}]_{ij} + [V_{\text{CKM}} y_d]_{ij}[Q_{dH}]_{ij} + [y_e]_{ij}[Q_{eH}]_{ij} + \text{h.c.}$
$Q_{2y} \equiv J_{y\alpha}^\dagger J_y^\alpha$	$-[y_u]_{il}[y_u^\dagger]_{kj}(\frac{1}{6}[Q_{qu}^{(1)}]_{ijkl} + [Q_{qu}^{(8)}]_{ijkl}) - \frac{1}{2}[y_e]_{il}[y_e^\dagger]_{kj}[Q_{le}]_{ijkl} - [V_{\text{CKM}} y_d]_{il}[y_d^\dagger V_{\text{CKM}}^\dagger]_{kj}(\frac{1}{6}[Q_{qd}^{(1)}]_{ijkl} + [Q_{qd}^{(8)}]_{ijkl}) + ([y_u]_{ij}[V_{\text{CKM}} y_d]_{kl}[Q_{quqd}^{(1)}]_{ijkl} - [y_e]_{ij}[y_u]_{kl}[Q_{lequ}^{(1)}]_{ijkl} + [y_e]_{ij}[y_d^\dagger V_{\text{CKM}}^\dagger]_{kl}[Q_{ledq}]_{ijkl} + \text{h.c.})$

Table 4.1: (From [111]) Warsaw basis operator combinations that appear in $\mathcal{L}_{\text{universal}}$ in (4.1), in the notation of [3]. In these expressions, repeated generation indices i, j, k, l are summed over, $H^\dagger \sigma^a \overleftrightarrow{D}_\mu H = H^\dagger \sigma^a (D_\mu H) - (D_\mu H)^\dagger \sigma^a H$, $H^\dagger \overleftrightarrow{D}_\mu H = H^\dagger (D_\mu H) - (D_\mu H)^\dagger H$. The Yukawa matrices y_u, y_d, y_e should not be confused with the hypercharges Y_f . The SM vector and scalar currents $J_{G\mu}^A, J_{W\mu}^a, J_{B\mu}, J_y^\alpha$ are defined in (4.2).

appear in these combinations via the vector and scalar currents in the SM,

$$J_{G\mu}^A \equiv g_s \sum_{f \in \{q,u,d\}} \bar{f} \gamma_\mu T^A f, \quad (4.2a)$$

$$J_{W\mu}^a \equiv g \sum_{f \in \{q,l\}} \bar{f} \gamma_\mu \frac{\sigma^a}{2} f, \quad (4.2b)$$

$$J_{B\mu} \equiv g' \sum_{f \in \{q,l,u,d,e\}} Y_f \bar{f} \gamma_\mu f, \quad (4.2c)$$

$$J_y^\alpha \equiv \bar{u} y_u^\dagger q_\beta \epsilon^{\beta\alpha} + \bar{q}^\alpha V_{CKM} y_d d + \bar{l}^\alpha y_e e. \quad (4.2d)$$

Our notation is such that

$$\mathcal{L}_{\text{SM}} \supset G^{A\mu} J_{G\mu}^A + W^{a\mu} J_{W\mu}^a + B^\mu J_{B\mu} - (H_\alpha J_y^\alpha + \text{h.c.}). \quad (4.3)$$

We will stick to the Warsaw basis for the calculations in this chapter, in order to conveniently use the results in [76, 77, 80]. The forms of $\mathcal{L}_{\text{universal}}$ in other SMEFT bases, as well as the dictionaries for translating between the bases for universal theories, can be found in [109].

If we restrict ourselves to the 16-dimensional parameter space of universal theories, a subspace of the full SMEFT parameter space, there is a unique well-motivated procedure to define the oblique parameters at LO. The field-redefinition ambiguity associated with the vector boson self-energies is eliminated by ensuring the oblique parameters defining conditions are satisfied [109, 194]. At the dimension-6 level, there are 5 nonvanishing oblique parameters \hat{S} , \hat{T} , W , Y , Z , which constitute a subset of the 16 independent *universal parameters*. By our choice in [109], the latter also include: 4 anomalous triple-gauge couplings (TGCs) $\Delta \bar{g}_1^Z$, $\Delta \bar{\kappa}_\gamma$, $\bar{\lambda}_\gamma$, $\bar{\lambda}_g$; 3 rescaling factors for the h^3 , hff , hVV vertices $\Delta \bar{\kappa}_3$, $\Delta \bar{\kappa}_F$, $\Delta \bar{\kappa}_V$; 3 parameters for $hV_{\mu\nu} V'^{\mu\nu}$ -type interactions absent in the SM f_{gg} , $f_{z\gamma}$, $f_{\gamma\gamma}$; 1 four-fermion coupling $c_{2y} \sim \mathcal{O}(y_f^2)$. Each of these universal parameters can be identified as the coefficient of a term in $\mathcal{L}_{\text{universal}}$ in the electroweak symmetry broken phase in the unitary gauge, after the field and parameter redefinitions detailed in [109]. The 16 universal parameters are just a phenomenologically convenient linear mapping from the 16 independent Wilson coefficients in (4.1); see table 4.2. As such, they constitute a complete characterization of universal theories in the SMEFT framework at the dimension-6 level.

As yet another equivalent description of the universal theories EFT, the Higgs basis couplings, defined in [7] at LO in $\frac{v^2}{\Lambda^2}$, make the leading BSM effects on precision observables manifest. As ensured by the Higgs basis defining conditions [7, 109], they capture vertex corrections involving the physical particles. Furthermore, since the input observables are not shifted at tree level, simple LO relations can be written down between some precision

Universal parameter	Warsaw basis expression
\hat{S}	$g^2 \left(\frac{1}{gg'} C_{HWB} + \frac{1}{4} C_{HJW} + \frac{1}{4} C_{HJB} - \frac{1}{2} C_{2JW} - \frac{1}{2} C_{2JB} \right)$
\hat{T}	$-\frac{1}{2} C_{HD} + \frac{g'^2}{2} (C_{HJB} - C_{2JB})$
W	$-\frac{g^2}{2} C_{2JW}$
Y	$-\frac{g^2}{2} C_{2JB}$
Z	$-\frac{g^2}{2} C_{2JG}$
$\Delta \bar{g}_1^Z$	$-\frac{g^2}{4c_\theta^2} (C_{HJW} - 2C_{2JW})$
$\Delta \bar{\kappa}_\gamma$	$\frac{c_\theta}{s_\theta} C_{HWB}$
$\bar{\lambda}_\gamma$	$-\frac{3g}{2} C_W$
$\bar{\lambda}_g$	$-\frac{3g^2}{2g_s} C_G$
$\Delta \kappa_3$	$-\frac{1}{\lambda} C_H + 3C_{H\Box} - \frac{3}{4} C_{HD} - \frac{g^2}{4} (C_{HJW} - C_{2JW})$
$\Delta \bar{\kappa}_F$	$-C_y + C_{H\Box} - \frac{1}{4} C_{HD} - \frac{g^2}{4} (C_{HJW} - C_{2JW})$
$\Delta \bar{\kappa}_V$	$C_{H\Box} - \frac{1}{4} C_{HD} - \frac{3g^2}{4} (C_{HJW} - C_{2JW})$
f_{gg}	$\frac{4}{g_s^2} C_{HG}$
$f_{z\gamma}$	$\frac{2}{gg'} [2c_\theta s_\theta (C_{HW} - C_{HB}) - (c_\theta^2 - s_\theta^2) C_{HWB}]$
$f_{\gamma\gamma}$	$4 \left(\frac{1}{g^2} C_{HW} + \frac{1}{g'^2} C_{HB} - \frac{1}{gg'} C_{HWB} \right)$
c_{2y}	C_{2y}

Table 4.2: (From [111]) Expressions of the 16 universal parameters in terms of the Warsaw basis Wilson coefficients in (4.1). These parameters completely characterize the indirect BSM effects in universal theories at the dimension-6 level. More details of the universal parameters, including their definition from the effective Lagrangian and their expressions in other bases, can be found in [109].

Higgs basis coupling	Universal parameters expression
δ_m	$\frac{c_\theta^2}{c_\theta^2 - s_\theta^2} \frac{\Delta\epsilon_1}{2} - \frac{\Delta\epsilon_2}{2} - \frac{s_\theta^2}{c_\theta^2 - s_\theta^2} \Delta\epsilon_3$
$[\delta g_L^{Wf}]_{ij} (f = q, l)$	$\delta_{ij} \left(\frac{c_\theta^2}{c_\theta^2 - s_\theta^2} \frac{\Delta\epsilon_1}{2} - \frac{s_\theta^2}{c_\theta^2 - s_\theta^2} \Delta\epsilon_3 \right)$
$[\delta g_L^{Zf}]_{ij} (f = u_L, d_L, e_L, \nu)$	$\delta_{ij} \left[T_f^3 \frac{\Delta\epsilon_1}{2} + Q_f \frac{s_\theta^2}{c_\theta^2 - s_\theta^2} \left(\frac{\Delta\epsilon_1}{2} - \Delta\epsilon_3 \right) \right]$
$[\delta g_R^{Zf}]_{ij} (f = u_R, d_R, e_R)$	$\delta_{ij} Q_f \frac{s_\theta^2}{c_\theta^2 - s_\theta^2} \left(\frac{\Delta\epsilon_1}{2} - \Delta\epsilon_3 \right)$
δg_{1z}	$\Delta \bar{g}_1^Z - \frac{\Delta\epsilon_2}{c_\theta^2} + \frac{s_\theta^2}{c_\theta^2 - s_\theta^2} \left(\frac{\Delta\epsilon_1}{2s_\theta^2} - \frac{\Delta\epsilon_3}{c_\theta^2} \right)$
$\delta \kappa_\gamma$	$\Delta \bar{\kappa}_\gamma$
λ_γ	$\bar{\lambda}_\gamma$
c_{3G}	$-\frac{2}{3g_s^2 g^2} \bar{\lambda}_g$
$\delta \lambda_3$	$\lambda \Delta \kappa_3$
$[\delta y_{f'}]_{ij} (f' = u, d, e)$	$\delta_{ij} \Delta \bar{\kappa}_F$
δc_z	$\Delta \bar{\kappa}_V$
$c_{gg}, c_{z\gamma}, c_{\gamma\gamma}$	$f_{gg}, f_{z\gamma}, f_{\gamma\gamma}$, respectively
c_{4f}	combinations of W, Y, Z, c_{2y}
$[\delta g_L^{Wq}]_{ij}, [d_{Vf}]_{ij}$	0

Table 4.3: (From [109, 111]) Higgs basis couplings in terms of the universal parameters. $\Delta\epsilon_{1,2,3}$ are independent linear combinations of \hat{S}, \hat{T}, W, Y defined in (4.4). c_{4f} collectively denotes four-fermion effective couplings, and d_{Vf} stands for the dipole-type Vff couplings. Compared with [7], we have written the fractional W mass shift as δ_m instead of δm , and defined $[\delta g_L^{Wq}]_{ij}$ in the gauge-eigenstate rather than mass-eigenstate basis.

observables and the Higgs basis couplings. For example, the fractional shifts in $\Gamma(Z \rightarrow b_L \bar{b}_L)$ and $\Gamma(Z \rightarrow b_R \bar{b}_R)$ are proportional to $[\delta g_L^{Zd}]_{33}$ and $[\delta g_R^{Zd}]_{33}$, respectively. In general, the Higgs basis couplings are linear combinations of Wilson coefficients in the Warsaw basis (or any other complete nonredundant basis). In the special case of universal theories, we have worked out in [109] the Higgs basis couplings in terms of the universal parameters. They are reproduced here in table 4.3, where the $\Delta\epsilon$ parameters [194, 202, 203] are 3 independent linear combinations of \hat{S} , \hat{T} , W , Y ,

$$\Delta\epsilon_1 \equiv \hat{T} - W - \frac{s_\theta^2}{c_\theta^2} Y, \quad \Delta\epsilon_2 \equiv -W, \quad \Delta\epsilon_3 \equiv \hat{S} - W - Y. \quad (4.4)$$

A universal pattern of fermion couplings can be seen from table 4.3. In particular, all the Vff vertex corrections depend on just 2 parameters $\Delta\epsilon_1$, $\Delta\epsilon_3$, and all the hff vertices are rescaled by a common factor $(1 + \Delta\bar{\kappa}_F)$. This is not the case for generic nonuniversal theories, where the number of independent couplings is equal to the number of independent dimension-6 operators in the full SMEFT. For universal theories, on the other hand, the generically independent couplings are related as follows,

$$\delta g_L^{Wq} = \delta g_L^{Wl}, \quad \frac{\delta g_R^{Zu}}{Y_u} = \frac{\delta g_R^{Zd}}{Y_d} = \frac{\delta g_R^{Ze}}{Y_e},$$

$$\delta g_L^{Ze} + \delta g_L^{Z\nu} = \delta g_R^{Ze}, \quad \delta g_L^{Zu} + \delta g_L^{Zd} = \delta g_R^{Zu} + \delta g_R^{Zd}, \quad (4.5a)$$

$$\delta y_u = \delta y_d = \delta y_e = \Delta\bar{\kappa}_F. \quad (4.5b)$$

We will call (4.5) “*universal relations*” from here on. Compared with [109], we have replaced Q_u , Q_d , Q_e by the equivalent Y_u , Y_d , Y_e for later convenience. Each Higgs basis coupling appearing in (4.5) represents the diagonal elements of a 3×3 matrix in generation space that is proportional to δ_{ij} for universal theories. Additional universal relations among 4-fermion couplings can be written down, which do not concern us here. Essentially, the universal relations among the generically independent Higgs basis couplings are in exact correspondence with the correlations among the otherwise independent fermionic operator Wilson coefficients shown in table 4.1, e.g.

$$\delta g_L^{Wq} = \delta g_L^{Wl} \quad \Leftrightarrow \quad [C_{Hq}^{(3)}]_{ij} = [C_{Hl}^{(3)}]_{ij} \left(= \delta_{ij} \frac{g^2}{4} C_{HJW} \right). \quad (4.6)$$

4.2.2 Overview of RG-induced nonuniversal effects

Beyond LO, renormalization is needed, and the Wilson coefficients as renormalized Lagrangian parameters should have renormalization scales μ associated with them. The scale

dependence of the Wilson coefficients is captured by the RG equations, which at leading order are governed by the anomalous dimensions γ_{ij} ,

$$\dot{C}_i \equiv 16\pi^2 \frac{d}{d \ln \mu} C_i(\mu) = \sum_j \gamma_{ij} C_j(\mu). \quad (4.7)$$

It should be emphasized that γ_{ij} are unambiguous only when a complete nonredundant basis of effective operators is specified. The Warsaw basis adopted here is the same basis used in [76, 77, 80] to calculate the full γ_{ij} matrix for the dimension-6 operators.

The renormalization scale μ should be properly chosen to avoid large radiative corrections beyond a fixed-order calculation. If we are interested in the deviations of precision observables at the electroweak scale, $\mu \sim \mu_{\text{EW}}$ is desired, because large logarithms in the perturbative expansion can be avoided when the observables are expressed in terms of $C_i(\mu_{\text{EW}})$. But on the other hand, to infer the shape of the UV theory at a higher scale $\Lambda \gg \mu_{\text{EW}}$, which is the ultimate goal of SMEFT analyses, $C_i(\Lambda)$ are needed, because we should better set $\mu \sim \Lambda$ when the SMEFT is matched onto a specific new physics model in the UV. Solving (4.7) to leading order, which is sufficient for most practical purposes, we obtain

$$C_i(\mu_{\text{EW}}) = C_i(\Lambda) - \frac{1}{16\pi^2} \ln \frac{\Lambda}{\mu_{\text{EW}}} \sum_j \gamma_{ij} C_j(\Lambda). \quad (4.8)$$

The second term in this equation contributes to the LL corrections of the observables which are affected by $C_i Q_i$ at LO, when they are calculated in terms of the Wilson coefficients at $\mu = \Lambda$. To be specific, up to higher-order terms, the fractional shift of an observable $\hat{\mathcal{O}}$ is

$$\delta^{\text{NP}} \hat{\mathcal{O}} \equiv \frac{\hat{\mathcal{O}} - \hat{\mathcal{O}}^{\text{SM}}}{\hat{\mathcal{O}}^{\text{SM}}} = \sum_i a_i C_i(\mu_{\text{EW}}) = \sum_i a_i C_i(\Lambda) - \frac{1}{16\pi^2} \ln \frac{\Lambda}{\mu_{\text{EW}}} \sum_{i,j} a_i \gamma_{ij} C_j(\Lambda), \quad (4.9)$$

where a_i are functions of properly-renormalized SM parameters, which can be recast in terms of the input observables [131]. It is based on (4.9) that constraints on $C_i(\mu_{\text{EW}})$ derived from precision data can be translated into constraints on (combinations of) $C_j(\Lambda)$'s, some of which are less accessible otherwise; see e.g. [37, 38, 73, 99].

For universal theories, a key observation is that the correlations among the fermionic operator Wilson coefficients at the matching scale Λ , represented by a set of linear equations

$$\sum_i b_i C_i(\Lambda) = 0, \quad (4.10)$$

are not necessarily preserved by RG evolution, because it is possible that

$$\sum_{i,j} b_i \gamma_{ij} C_j(\Lambda) \neq 0. \quad (4.11)$$

As a consequence, at the electroweak scale μ_{EW} where precision observables are measured, we may have

$$\sum_i b_i C_i(\mu_{\text{EW}}) \neq 0. \quad (4.12)$$

For example, while $[C_{Hq}^{(3)}]_{ij} - [C_{Hl}^{(3)}]_{ij} = 0$ at $\mu = \Lambda$ for universal theories, the same is in general not true at $\mu = \mu_{\text{EW}}$, as we will show in section 4.3. When (4.12) happens, the universal theory at Λ flows to a nonuniversal theory at μ_{EW} . We say that nonuniversal effects are induced by RG evolution.

The observation above poses a challenge for defining oblique parameters, and more generally universal parameters, at the electroweak scale. In general, the oblique parameters defining conditions, which require the absence of fermionic operators, cannot be satisfied no matter how the fields and parameters are redefined due to the theory being nonuniversal. Additional prescriptions are needed if one wishes to define and use these parameters, which can be somewhat arbitrary. This also means that without additional prescriptions, it is in general not meaningful to talk about RG evolution of the universal parameters.

Nevertheless, as far as observables are concerned, there are no ambiguities, since (4.9), which relates $\bar{\delta}^{\text{NP}} \hat{\mathcal{O}}$ to $C_i(\Lambda)$ at LL accuracy, always holds. With the linear mapping in table 4.2, we can recast $\bar{\delta}^{\text{NP}} \hat{\mathcal{O}}$ in terms of the 16 universal parameters defined at the matching scale, $\hat{S}(\Lambda)$, $\hat{T}(\Lambda)$, etc., as long as the theory is universal at Λ . The RG-induced nonuniversal effects then manifest themselves in the fact that all the LL corrections in (4.9) cannot be absorbed into the running of the parameters appearing in the LO expression for $\bar{\delta}^{\text{NP}} \hat{\mathcal{O}}$, namely the 16 universal parameters. In the following sections, we will define $\hat{S}(\mu_{\text{EW}})$, $\hat{T}(\mu_{\text{EW}})$, etc. to absorb part of the LL corrections, following some well-motivated additional prescriptions. The prediction for $\bar{\delta}^{\text{NP}} \hat{\mathcal{O}}$ then involves the LO expression in terms of these universal parameters at μ_{EW} , plus additional LL terms. The presence of the latter may potentially affect the interpretation and usefulness of global fits to observables at μ_{EW} assuming the theory is universal at this scale, including the conventional oblique parameters fits. But when they are taken into account, consistent constraints on $\hat{S}(\Lambda)$, $\hat{T}(\Lambda)$, etc. at the LL level can in principle be derived from precision data, which can be used to infer the BSM new physics at Λ if it is universal.³

³The accuracy of the LL-level constraints on the universal parameters is a separate issue that deserves further investigation. If the LL corrections are important for some observables, the NLO finite terms not

The close connection between the Higgs basis couplings and precision observables at LO offers an equivalent and convenient way to formulate the analysis. While it is still a matter of debate how to extend the Higgs basis framework beyond LO, at least at the LL level there is a straightforward procedure. In the full SMEFT at the dimension-6 level, we can think of the Higgs basis couplings as *defined by* the linear combinations of Wilson coefficients in the Warsaw basis (or any other complete nonredundant basis) worked out in [7], *with the renormalization scale dependence included*. For example, in our notation,

$$[\delta g_L^{Wl}(\mu)]_{ij} \equiv [C_{Hl}^{(3)}(\mu)]_{ij} - \frac{c_\theta s_\theta}{c_\theta^2 - s_\theta^2} C_{HWB}(\mu) - \frac{c_\theta^2}{c_\theta^2 - s_\theta^2} C_0(\mu), \quad (4.13a)$$

$$[\delta g_L^{Wq}(\mu)]_{ij} \equiv [C_{Hq}^{(3)}(\mu)]_{ij} - \frac{c_\theta s_\theta}{c_\theta^2 - s_\theta^2} C_{HWB}(\mu) - \frac{c_\theta^2}{c_\theta^2 - s_\theta^2} C_0(\mu), \quad (4.13b)$$

where

$$C_0(\mu) \equiv \frac{1}{4} \left\{ C_{HD}(\mu) + 2([C_{Hl}^{(3)}(\mu)]_{11} + [C_{Hl}^{(3)}(\mu)]_{22}) - ([C_{ll}(\mu)]_{1221} + [C_{ll}(\mu)]_{2112}) \right\} \quad (4.14)$$

is a combination of Wilson coefficients coming from undoing the shifts in the input observables m_Z and G_F , as required by the Higgs basis defining conditions. Note that $c_\theta = \frac{g}{\sqrt{g^2 + g'^2}}$, $s_\theta = \frac{g'}{\sqrt{g^2 + g'^2}}$ are also μ -dependent. The running of the Higgs basis couplings with μ follows from the RG equations for the Warsaw basis Wilson coefficients and the SM parameters. For universal theories at Λ , the universal relations in (4.5) should actually read $\delta g_L^{Wq}(\Lambda) = \delta g_L^{Wl}(\Lambda)$, etc. After RG evolution down to the electroweak scale, these relations are violated in the sense that $\delta g_L^{Wq}(\mu_{EW}) \neq \delta g_L^{Wl}(\mu_{EW})$, etc., due to $[C_{Hq}^{(3)}(\mu_{EW})]_{ij} \neq [C_{Hl}^{(3)}(\mu_{EW})]_{ij}$, etc., as mentioned below (4.12). This was already alluded to in figure 4.1, and will be demonstrated in detail in the next section. Defined in this way, the Higgs basis couplings renormalized at μ_{EW} directly map onto $\bar{\delta}^{\text{NP}} \hat{\mathcal{O}}$. Two example observables we will discuss later are $R_\ell \equiv \Gamma_{\text{had}}/\Gamma(Z \rightarrow \ell^+ \ell^-)$ (assuming lepton flavor universality) and $R_b \equiv \Gamma(Z \rightarrow b\bar{b})/\Gamma_{\text{had}}$, where Γ_{had} is the hadronic Z decay partial width. From their LO expressions,

$$R_\ell = \frac{3 \left\{ \sum_{i=1}^2 \left[([g_L^{Zu}]_{ii})^2 + ([g_R^{Zu}]_{ii})^2 \right] + \sum_{i=1}^3 \left[([g_L^{Zd}]_{ii})^2 + ([g_R^{Zd}]_{ii})^2 \right] \right\}}{([g_L^{Ze}]_{jj})^2 + ([g_R^{Ze}]_{jj})^2} \quad (j = 1, 2, \text{ or } 3), \quad (4.15a)$$

enhanced by $\ln \frac{\Lambda}{\mu_{EW}}$ may also be [95, 102]. In any case, the effect of the neglected terms in a finite-order perturbative calculation may be accounted for by introducing SMEFT theory uncertainties, as advocated recently in [91, 104] in the more general context of fitting the full SMEFT.

$$R_b = \frac{([g_L^{Zd}]_{33})^2 + ([g_R^{Zd}]_{33})^2}{\sum_{i=1}^2 \left[([g_L^{Zu}]_{ii})^2 + ([g_R^{Zu}]_{ii})^2 \right] + \sum_{i=1}^3 \left[([g_L^{Zd}]_{ii})^2 + ([g_R^{Zd}]_{ii})^2 \right]}, \quad (4.15b)$$

where $[g_{L,R}^{Zf}]_{ij} = \delta_{ij}g_{L,R}^{Zf} + [\delta g_{L,R}^{Zf}(\mu_{\text{EW}})]_{ij}$ with $g_L^{Zf} \equiv T_f^3 - Q_f s_\theta^2(\mu_{\text{EW}})$, $g_R^{Zf} \equiv -Q_f s_\theta^2(\mu_{\text{EW}})$, it follows that the fractional corrections with respect to the SM are given by

$$\bar{\delta}^{\text{NP}} R_\ell = \bar{\delta}^{\text{NP}} \Gamma_{\text{had}} - \frac{2}{(g_L^{Ze})^2 + (g_R^{Ze})^2} (g_L^{Ze} [\delta g_L^{Ze}(\mu_{\text{EW}})]_{jj} + g_R^{Ze} [\delta g_R^{Ze}(\mu_{\text{EW}})]_{jj}), \quad (4.16a)$$

$$\bar{\delta}^{\text{NP}} R_b = \frac{2}{(g_L^{Zd})^2 + (g_R^{Zd})^2} (g_L^{Zd} [\delta g_L^{Zd}(\mu_{\text{EW}})]_{33} + g_R^{Zd} [\delta g_R^{Zd}(\mu_{\text{EW}})]_{33}) - \bar{\delta}^{\text{NP}} \Gamma_{\text{had}}, \quad (4.16b)$$

where

$$\begin{aligned} \bar{\delta}^{\text{NP}} \Gamma_{\text{had}} = & \frac{2}{2 \left[(g_L^{Zu})^2 + (g_R^{Zu})^2 \right] + 3 \left[(g_L^{Zd})^2 + (g_R^{Zd})^2 \right]} \times \\ & \left\{ \sum_{i=1}^2 \left(g_L^{Zu} [\delta g_L^{Zu}(\mu_{\text{EW}})]_{ii} + g_R^{Zu} [\delta g_R^{Zu}(\mu_{\text{EW}})]_{ii} \right) \right. \\ & \left. + \sum_{i=1}^3 \left(g_L^{Zd} [\delta g_L^{Zd}(\mu_{\text{EW}})]_{ii} + g_R^{Zd} [\delta g_R^{Zd}(\mu_{\text{EW}})]_{ii} \right) \right\}. \end{aligned} \quad (4.17)$$

To end this subsection, we comment on a subtlety associated with defining phenomenological parameters in the electroweak symmetry broken phase. The renormalized vacuum expectation value of the Higgs field is a scheme-dependent quantity. To avoid introducing unnecessary scheme dependence into the running of the Wilson coefficients, we take the v appearing in (4.1) to be simply a constant, say 246.2 GeV. As a consequence, when the universal parameters and Higgs basis couplings, defined from the effective Lagrangian in the broken phase, are calculated in terms of the Wilson coefficients, factors of $\frac{2|\langle H \rangle|^2}{v^2} = 1 + \dots$ appear. We treat the \dots pieces as part of the one-loop counterterms, not to be included in the renormalized Higgs basis couplings, or renormalized universal parameters when they are properly defined. These terms are relevant for a full NLO calculation, but do not affect the LL corrections proportional to $\ln \frac{\Lambda}{\mu_{\text{EW}}}$ that are the focus of the present chapter.

4.3 RG effects in the electroweak sector

4.3.1 The universal limit

We first look at the electroweak sector, and begin with the limit $y_f \rightarrow 0$. The Lagrangian at the new physics scale Λ is (4.1) with $C_y = C_{2y} = 0$. We see from table 4.1 that the $\psi^2 H^2 D$ -class operators, which affect the Vff effective couplings, are related in universal theories at LO as follows,

$$[C_{Hq}^{(3)}]_{ij} = [C_{Hl}^{(3)}]_{ij} = \delta_{ij} \frac{g^2}{4} C_{HJW}, \quad (4.18a)$$

$$[\{C_{Hq}^{(1)}, C_{Hl}^{(1)}, C_{Hu}, C_{Hd}, C_{He}\}]_{ij} = \{Y_q, Y_l, Y_u, Y_d, Y_e\} \delta_{ij} \frac{g'^2}{2} C_{HJB}. \quad (4.18b)$$

These relations are equivalent to the universal relations in (4.5a). Using the formulas in [80], we find the one-loop running of these Wilson coefficients,

$$[\dot{C}_{Hq}^{(3)}]_{ij} = \delta_{ij} g^2 \left(\frac{1}{6} C_{H\Box} + \frac{7}{12} g^2 C_{HJW} + \frac{23}{6} g^2 C_{2JW} + \frac{1}{54} g'^2 C_{2JB} + \frac{8}{9} g_s^2 C_{2JG} \right), \quad (4.19a)$$

$$[\dot{C}_{Hl}^{(3)}]_{ij} = \delta_{ij} g^2 \left(\frac{1}{6} C_{H\Box} + \frac{7}{12} g^2 C_{HJW} + \frac{23}{6} g^2 C_{2JW} + \frac{1}{6} g'^2 C_{2JB} \right), \quad (4.19b)$$

$$[\dot{C}_{Hq}^{(1)}]_{ij} = Y_q \delta_{ij} g'^2 \left[\frac{1}{3} (C_{H\Box} + C_{HD}) + \frac{41}{6} g'^2 C_{HJB} + g^2 C_{2JW} + \frac{361}{27} g'^2 C_{2JB} + \frac{16}{9} g_s^2 C_{2JG} \right], \quad (4.19c)$$

$$[\dot{C}_{Hl}^{(1)}]_{ij} = Y_l \delta_{ij} g'^2 \left[\frac{1}{3} (C_{H\Box} + C_{HD}) + \frac{41}{6} g'^2 C_{HJB} + g^2 C_{2JW} + \frac{41}{3} g'^2 C_{2JB} \right], \quad (4.19d)$$

$$[\dot{C}_{Hu}]_{ij} = Y_u \delta_{ij} g'^2 \left[\frac{1}{3} (C_{H\Box} + C_{HD}) + \frac{41}{6} g'^2 C_{HJB} + \frac{376}{27} g'^2 C_{2JB} + \frac{16}{9} g_s^2 C_{2JG} \right], \quad (4.19e)$$

$$[\dot{C}_{Hd}]_{ij} = Y_d \delta_{ij} g'^2 \left[\frac{1}{3} (C_{H\Box} + C_{HD}) + \frac{41}{6} g'^2 C_{HJB} + \frac{364}{27} g'^2 C_{2JB} + \frac{16}{9} g_s^2 C_{2JG} \right], \quad (4.19f)$$

$$[\dot{C}_{He}]_{ij} = Y_e \delta_{ij} g'^2 \left[\frac{1}{3} (C_{H\Box} + C_{HD}) + \frac{41}{6} g'^2 C_{HJB} + \frac{44}{3} g'^2 C_{2JB} \right]. \quad (4.19g)$$

Note that only the Wilson coefficients that are nonzero at LO (i.e. at $\mu = \Lambda$) need to be kept on the RHS of these equations. We have used table 4.1, or equivalently (4.18) and (4.23) below, to rewrite them in terms of the coefficients of the operator combinations in (4.1) for universal theories.

From the discussion in section 4.2.2, it is clear that the relations in (4.18) are preserved by RG evolution only in the limit $C_{2JW} = C_{2JB} = C_{2JG} = 0$, namely $W = Y = Z = 0$ at LO (i.e. at $\mu = \Lambda$). We call this limit, together with $y_f \rightarrow 0$, the “universal limit.”

In the universal limit, fermionic operators in the electroweak sector are generated by RG evolution, but they are organized into the combinations Q_{HJW} , Q_{HJB} that appear in the LO

Lagrangian for universal theories. Thus, without any further prescriptions, it is unambiguous to define C_{HJW}, C_{HJB} at the electroweak scale, and write down their RG equations,

$$\dot{C}_{HJW} = \frac{2}{3}C_{H\Box} + \frac{26}{3}g^2C_{HJW}, \quad (4.20a)$$

$$\dot{C}_{HJB} = \frac{2}{3}(C_{H\Box} + C_{HD}). \quad (4.20b)$$

These are derived from

$$16\pi^2 \frac{d}{d \ln \mu} (g^2 C_{HJW}) = g^2 \left(\frac{2}{3} C_{H\Box} + \frac{7}{3} g^2 C_{HJW} \right), \quad (4.21a)$$

$$16\pi^2 \frac{d}{d \ln \mu} (g'^2 C_{HJB}) = g'^2 \left[\frac{2}{3} (C_{H\Box} + C_{HD}) + \frac{41}{3} g'^2 C_{HJB} \right], \quad (4.21b)$$

which follow from (4.18), (4.19), and the well-known one-loop running of the SM gauge couplings

$$\dot{g} = -\frac{19}{6}g^3, \quad \dot{g}' = \frac{41}{6}g'^3. \quad (4.22)$$

We can extend this analysis to the 4-fermion interactions. The correlations among the Wilson coefficients, i.e. the counterparts of (4.18), can be read off from table 4.1 (see also [110]), with contributions from Q_{2y} neglected for the moment,

$$[C_{ul}]_{ijkl} = \left(\frac{1}{2} \delta_{il} \delta_{jk} - \frac{1}{4} \delta_{ij} \delta_{kl} \right) g^2 C_{2JW} + Y_l^2 \delta_{ij} \delta_{kl} g'^2 C_{2JB}, \quad (4.23a)$$

$$[C_{qq}^{(3)}]_{ijkl} = \frac{1}{4} \delta_{ij} \delta_{kl} g^2 C_{2JW} + \frac{1}{4} \delta_{il} \delta_{jk} g_s^2 C_{2JG}, \quad (4.23b)$$

$$[C_{lq}^{(3)}]_{ijkl} = \frac{1}{2} \delta_{ij} \delta_{kl} g^2 C_{2JW}, \quad (4.23c)$$

$$\begin{aligned} & [\{C_{lq}^{(1)}, C_{ee}, C_{ud}^{(1)}, C_{eu}, C_{ed}, C_{qu}^{(1)}, C_{qd}^{(1)}, C_{qe}, C_{lu}, C_{ld}, C_{le}\}]_{ijkl} = \\ & \{2Y_l Y_q, Y_e^2, 2Y_u Y_d, 2Y_u Y_e, 2Y_d Y_e, 2Y_q Y_u, 2Y_q Y_d, 2Y_q Y_e, 2Y_l Y_u, 2Y_l Y_d, 2Y_l Y_e\} \\ & \delta_{ij} \delta_{kl} g'^2 C_{2JB}, \end{aligned} \quad (4.23d)$$

$$[C_{qq}^{(1)}]_{ijkl} = Y_q^2 \delta_{ij} \delta_{kl} g'^2 C_{2JB} + \left(\frac{1}{4} \delta_{il} \delta_{jk} - \frac{1}{6} \delta_{ij} \delta_{kl} \right) g_s^2 C_{2JG}, \quad (4.23e)$$

$$[\{C_{uu}, C_{dd}\}]_{ijkl} = \{Y_u^2, Y_d^2\} \delta_{ij} \delta_{kl} g'^2 C_{2JB} + \left(\frac{1}{2} \delta_{il} \delta_{jk} - \frac{1}{6} \delta_{ij} \delta_{kl} \right) g_s^2 C_{2JG}, \quad (4.23f)$$

$$[C_{ud}^{(8)}]_{ijkl} = [C_{qu}^{(8)}]_{ijkl} = [C_{qd}^{(8)}]_{ijkl} = 2\delta_{ij} \delta_{kl} g_s^2 C_{2JG}. \quad (4.23g)$$

For $C_{2JW} = C_{2JB} = C_{2JG} = 0$ at LO, we find, from [80],

$$[\dot{C}_{ul}]_{ijkl} = \left(\frac{1}{2} \delta_{il} \delta_{jk} - \frac{1}{4} \delta_{ij} \delta_{kl} \right) g^2 \left(\frac{g^2}{3} C_{HJW} \right) + Y_l^2 \delta_{ij} \delta_{kl} g'^2 \left(\frac{g'^2}{3} C_{HJB} \right), \quad (4.24a)$$

$$[\{\dot{C}_{qq}^{(3)}, \dot{C}_{lq}^{(3)}\}]_{ijkl} = \left\{\frac{1}{4}, \frac{1}{2}\right\} \delta_{ij} \delta_{kl} g^2 \left(\frac{g^2}{3} C_{HJW}\right), \quad (4.24b)$$

$$\begin{aligned} & [\{\dot{C}_{qq}^{(1)}, \dot{C}_{lq}^{(1)}, \dot{C}_{uu}, \dot{C}_{dd}, \dot{C}_{ee}, \dot{C}_{ud}^{(1)}, \dot{C}_{eu}, \dot{C}_{ed}, \dot{C}_{qu}^{(1)}, \dot{C}_{qd}^{(1)}, \dot{C}_{qe}, \dot{C}_{lu}, \dot{C}_{ld}, \dot{C}_{le}\}]_{ijkl} = \\ & \{Y_q^2, 2Y_l Y_q, Y_u^2, Y_d^2, Y_e^2, 2Y_u Y_d, 2Y_u Y_e, 2Y_d Y_e, 2Y_q Y_u, 2Y_q Y_d, 2Y_q Y_e, 2Y_l Y_u, 2Y_l Y_d, 2Y_l Y_e\} \\ & \delta_{ij} \delta_{kl} g'^2 \left(\frac{g'^2}{3} C_{HJB}\right), \end{aligned} \quad (4.24c)$$

$$[\dot{C}_{ud}^{(8)}]_{ijkl} = [\dot{C}_{qu}^{(8)}]_{ijkl} = [\dot{C}_{qd}^{(8)}]_{ijkl} = 0. \quad (4.24d)$$

The pattern in these equations, when compared with (4.23), indicates that in the universal limit defined above, the 4-fermion interactions are also universal after RG evolution. Thus, as in (4.20), we can unambiguously define

$$C_{2JW}(\mu_{EW}) = -\frac{1}{16\pi^2} \ln \frac{\Lambda}{\mu_{EW}} \dot{C}_{2JW}, \quad (4.25a)$$

$$C_{2JB}(\mu_{EW}) = -\frac{1}{16\pi^2} \ln \frac{\Lambda}{\mu_{EW}} \dot{C}_{2JB}, \quad (4.25b)$$

where

$$\dot{C}_{2JW} = \frac{g^2}{3} C_{HJW}, \quad (4.26a)$$

$$\dot{C}_{2JB} = \frac{g'^2}{3} C_{HJB}. \quad (4.26b)$$

Here the running of g and g' is not relevant, since \dot{g}, \dot{g}' are multiplied by the values of C_{2JW}, C_{2JB} at LO which vanish. We see that, if the operators Q_{2JW}, Q_{2JB} are not generated by the universal new physics at $\mu = \Lambda$, they will be generated at one-loop level by RG evolution down to $\mu = \mu_{EW}$, and result in a universal pattern in the 4-fermion interactions at the electroweak scale. The operator Q_{2JG} , on the other hand, is not generated by RG evolution at this order if it is absent at the new physics scale.

Eqs. (4.20) and (4.26) allow us to write down meaningful RG equations for the oblique parameters in the universal limit, namely $y_f = 0$, and $C_{2JW} = C_{2JB} = C_{2JG} = 0$, or equivalently $W = Y = Z = 0$, at $\mu = \Lambda$. To do so, we further need table 4.2, the RG equations for the bosonic Wilson coefficients from [76, 80],

$$\dot{C}_{HWB} = \left(\frac{4}{3}g^2 + \frac{19}{3}g'^2 + 4\lambda\right) C_{HWB} - 3g^2 g' C_W + 2gg'(C_{HW} + C_{HB}), \quad (4.27a)$$

$$\dot{C}_{HD} = \left(\frac{9}{2}g^2 - \frac{5}{6}g'^2 + 12\lambda\right) C_{HD} + \frac{20}{3}g'^2 C_{H\Box} + \frac{40}{3}g'^4 C_{HJB}, \quad (4.27b)$$

and the running of the SM gauge couplings (4.22). The results are

$$\begin{aligned}\dot{\hat{S}} &= -\frac{1}{3}(19g^2 - g'^2)\hat{S} - \frac{1}{2}g^2\hat{T} - \frac{1}{3}(27g^2 - g'^2)c_\theta^2\Delta\bar{g}_1^Z + \frac{1}{6}(33g^2 + g'^2 + 24\lambda)\Delta\bar{\kappa}_\gamma + 2g^2\bar{\lambda}_\gamma \\ &\quad + \frac{1}{3}g^2\Delta\bar{\kappa}_V + \frac{1}{2}g^2(g^2 - g'^2)f_{z\gamma} + e^2g^2f_{\gamma\gamma}\end{aligned}\quad (4.28a)$$

$$\dot{\hat{T}} = \frac{3}{2}(3g^2 + 8\lambda)\left[\hat{T} - 2\frac{s_\theta^2}{c_\theta^2}(\hat{S} - \Delta\bar{\kappa}_\gamma)\right] - 24\lambda s_\theta^2\Delta\bar{g}_1^Z - 3g'^2\Delta\bar{\kappa}_V, \quad (4.28b)$$

$$\dot{W} = \frac{2}{3}g^2c_\theta^2\Delta\bar{g}_1^Z, \quad (4.28c)$$

$$\dot{Y} = -\frac{2}{3}g'^2(\hat{S} + c_\theta^2\Delta\bar{g}_1^Z - \Delta\bar{\kappa}_\gamma). \quad (4.28d)$$

Similarly, $\dot{Z} = 0$. In (4.28) we have recast the Wilson coefficients on the RHS in terms of universal parameters. Following these evolution equations from Λ to μ_{EW} , we obtain the oblique parameters at the electroweak scale,

$$\hat{S}(\mu_{\text{EW}}) = \hat{S}(\Lambda) - \frac{1}{16\pi^2} \ln \frac{\Lambda}{\mu_{\text{EW}}} \dot{\hat{S}}, \quad (4.29a)$$

$$\hat{T}(\mu_{\text{EW}}) = \hat{T}(\Lambda) - \frac{1}{16\pi^2} \ln \frac{\Lambda}{\mu_{\text{EW}}} \dot{\hat{T}}, \quad (4.29b)$$

$$W(\mu_{\text{EW}}) = W(\Lambda) - \frac{1}{16\pi^2} \ln \frac{\Lambda}{\mu_{\text{EW}}} \dot{W}, \quad (4.29c)$$

$$Y(\mu_{\text{EW}}) = Y(\Lambda) - \frac{1}{16\pi^2} \ln \frac{\Lambda}{\mu_{\text{EW}}} \dot{Y}, \quad (4.29d)$$

which are to be used to calculate the observables, or alternatively, the Higgs basis couplings at $\mu = \mu_{\text{EW}}$, in the electroweak sector. For example,

$$\begin{aligned}[\delta g_L^{Wl}(\mu_{\text{EW}})]_{ij} &= [\delta g_L^{Wq}(\mu_{\text{EW}})]_{ij} = \delta_{ij} \left[\frac{c_\theta^2}{c_\theta^2 - s_\theta^2} \frac{\Delta\epsilon_1(\mu_{\text{EW}})}{2} - \frac{s_\theta^2}{c_\theta^2 - s_\theta^2} \Delta\epsilon_3(\mu_{\text{EW}}) \right] \\ &= \frac{\delta_{ij}}{2(c_\theta^2 - s_\theta^2)} \left[-2s_\theta^2\hat{S}(\mu_{\text{EW}}) + c_\theta^2\hat{T}(\mu_{\text{EW}}) - (c_\theta^2 - 2s_\theta^2)W(\mu_{\text{EW}}) + s_\theta^2Y(\mu_{\text{EW}}) \right],\end{aligned}\quad (4.30)$$

where the SM parameters c_θ , s_θ are also renormalized at $\mu = \mu_{\text{EW}}$. We stress again that (4.28), (4.29), (4.30) are unambiguous only in the universal limit $W(\Lambda) = Y(\Lambda) = Z(\Lambda) = 0$, $y_f = 0$ [we have kept $W(\Lambda)$, $Y(\Lambda)$ in (4.29) for later convenience]; otherwise the theory becomes nonuniversal after RG evolution and it is not even clear how to define the oblique parameters at μ_{EW} . We will go beyond this limit in the next subsection.

One interesting observation from (4.28) is that, with our definition of universal parameters, and in the special universal limit discussed above where these equations are meaningful, the \hat{S} and \hat{T} parameters mix under RG evolution. This is true despite the fact that C_{HWB}

and C_{HD} , which *contribute to* \hat{S} and \hat{T} , respectively, do not mix in the Warsaw basis, even when the full SMEFT is considered [80]. The reason is that, as is clear from table 4.2, \hat{S} and \hat{T} *should not be identified with* C_{HWB} and C_{HD} . The additional contributions to these oblique parameters lead to the mixing observed here.

4.3.2 Nonuniversal effects beyond the universal limit

Now we are ready to turn back on the LO $C_{2JW}, C_{2JB}, C_{2JG}$ (while still assuming $y_f \rightarrow 0$), and study the nonuniversal effects due to their contributions to the RG evolution. These effects are conveniently represented by violations of the universal relations (4.5a). Using (4.19), together with the relations between the Higgs basis couplings and the Warsaw basis Wilson coefficients [7], we find

$$\delta\dot{g}_L^{Wq} - \delta\dot{g}_L^{Wl} = \dot{C}_{Hq}^{(3)} - \dot{C}_{Hl}^{(3)} = g^2 \left(-\frac{4}{27}g'^2 C_{2JB} + \frac{8}{9}g_s^2 C_{2JG} \right) = \frac{8}{27}(g'^2 Y - 6g_s^2 Z), \quad (4.31a)$$

$$\frac{\delta\dot{g}_R^{Zu}}{Y_u} - \frac{\delta\dot{g}_R^{Zd}}{Y_d} = -\frac{1}{2} \left(\frac{\dot{C}_{Hu}}{Y_u} - \frac{\dot{C}_{Hd}}{Y_d} \right) = -\frac{g'^2}{2} \frac{4}{9} C_{2JB} = \frac{4}{9} \frac{s_\theta^2}{c_\theta^2} g'^2 Y, \quad (4.31b)$$

$$\begin{aligned} \frac{\delta\dot{g}_R^{Zd}}{Y_d} - \frac{\delta\dot{g}_R^{Ze}}{Y_e} &= -\frac{1}{2} \left(\frac{\dot{C}_{Hd}}{Y_d} - \frac{\dot{C}_{He}}{Y_e} \right) \\ &= -\frac{g'^2}{2} \left(-\frac{32}{27}g'^2 C_{2JB} + \frac{16}{9}g_s^2 C_{2JG} \right) = \frac{16}{27} \frac{s_\theta^2}{c_\theta^2} (-2g'^2 Y + 3g_s^2 Z), \end{aligned} \quad (4.31c)$$

$$\begin{aligned} \delta\dot{g}_L^{Ze} + \delta\dot{g}_L^{Z\nu} - \delta\dot{g}_R^{Ze} &= -\frac{1}{2} (2\dot{C}_{Hl}^{(1)} - \dot{C}_{He}) \\ &= -\frac{g'^2}{2} (-g^2 C_{2JW} + g'^2 C_{2JB}) = \frac{s_\theta^2}{c_\theta^2} (-g^2 W + g'^2 Y), \end{aligned} \quad (4.31d)$$

$$\begin{aligned} \delta\dot{g}_L^{Zu} + \delta\dot{g}_L^{Zd} - \delta\dot{g}_R^{Zu} - \delta\dot{g}_R^{Zd} &= -\frac{1}{2} (2\dot{C}_{Hq}^{(1)} - \dot{C}_{Hu} - \dot{C}_{Hd}) \\ &= -\frac{g'^2}{2} \left(\frac{1}{3}g^2 C_{2JW} - \frac{1}{3}g'^2 C_{2JB} \right) = \frac{1}{3} \frac{s_\theta^2}{c_\theta^2} (g^2 W - g'^2 Y), \end{aligned} \quad (4.31e)$$

where diagonal elements have been assumed for the matrices in generation space. It follows that at the electroweak scale,

$$\delta g_L^{Wq}(\mu_{EW}) - \delta g_L^{Wl}(\mu_{EW}) = -\frac{1}{16\pi^2} \ln \frac{\Lambda}{\mu_{EW}} \cdot \frac{8}{27} (g'^2 Y - 6g_s^2 Z), \quad (4.32a)$$

$$\frac{\delta g_R^{Zu}(\mu_{EW})}{Y_u} - \frac{\delta g_R^{Zd}(\mu_{EW})}{Y_d} = -\frac{1}{16\pi^2} \ln \frac{\Lambda}{\mu_{EW}} \cdot \frac{4}{9} \frac{s_\theta^2}{c_\theta^2} g'^2 Y, \quad (4.32b)$$

$$\frac{\delta g_R^{Zd}(\mu_{EW})}{Y_d} - \frac{\delta g_R^{Ze}(\mu_{EW})}{Y_e} = -\frac{1}{16\pi^2} \ln \frac{\Lambda}{\mu_{EW}} \cdot \frac{16}{27} \frac{s_\theta^2}{c_\theta^2} (-2g'^2 Y + 3g_s^2 Z), \quad (4.32c)$$

$$\delta g_L^{Ze}(\mu_{\text{EW}}) + \delta g_L^{Z\nu}(\mu_{\text{EW}}) - \delta g_R^{Ze}(\mu_{\text{EW}}) = -\frac{1}{16\pi^2} \ln \frac{\Lambda}{\mu_{\text{EW}}} \cdot \frac{s_\theta^2}{c_\theta^2} (-g^2 W + g'^2 Y), \quad (4.32d)$$

$$\begin{aligned} & \delta g_L^{Zu}(\mu_{\text{EW}}) + \delta g_L^{Zd}(\mu_{\text{EW}}) - \delta g_R^{Zu}(\mu_{\text{EW}}) - \delta g_R^{Zd}(\mu_{\text{EW}}) \\ &= -\frac{1}{16\pi^2} \ln \frac{\Lambda}{\mu_{\text{EW}}} \cdot \frac{1}{3} \frac{s_\theta^2}{c_\theta^2} (g^2 W - g'^2 Y), \end{aligned} \quad (4.32e)$$

where W, Y, Z are the well-defined oblique parameters at the new physics scale (where the theory is universal). Eq. (4.32) shows that the universal relations (4.5a) that hold at LO in universal theories are violated. But unlike generic nonuniversal theories, they are violated in a universal (rather than arbitrary) way. Despite the RG-induced nonuniversal effects, the theory and its phenomenology is still completely characterized by the 16 independent universal parameters at $\mu = \Lambda$ (14 in the limit $y_f \rightarrow 0$), and no further parameters are needed unlike in generic nonuniversal theories.

As far as observables, or Higgs basis couplings at $\mu = \mu_{\text{EW}}$, are concerned, our discussion in section 4.2.2 indicates that it is not possible to absorb all the LL terms into the running of the oblique parameters that contribute at LO, if W, Y, Z are nonzero at the new physics scale. However, from this perspective, it is convenient to still define $\hat{S}(\mu_{\text{EW}}), \hat{T}(\mu_{\text{EW}}), W(\mu_{\text{EW}}), Y(\mu_{\text{EW}})$ to be their values in the universal limit as in (4.29), with $\hat{S}, \hat{T}, \hat{W}, \hat{Y}$ given by (4.28), even beyond this limit when $W(\Lambda), Y(\Lambda), Z(\Lambda)$ are nonzero, so that they can at least absorb a significant part of the LL corrections. The remaining LL corrections are proportional to W, Y, Z , and can be taken into account as additional contributions. Following this strategy, we find, for example,

$$\begin{aligned} & [\delta g_L^{Wl}(\mu_{\text{EW}})]_{ij} = \\ & \frac{\delta_{ij}}{2(c_\theta^2 - s_\theta^2)} \left\{ -2s_\theta^2 \hat{S}(\mu_{\text{EW}}) + c_\theta^2 \hat{T}(\mu_{\text{EW}}) - (c_\theta^2 - 2s_\theta^2) W(\mu_{\text{EW}}) + s_\theta^2 Y(\mu_{\text{EW}}) \right. \\ & \left. + \frac{1}{16\pi^2} \ln \frac{\Lambda}{\mu_{\text{EW}}} \left[\left(10g^2 - \frac{45}{2} g'^2 \right) c_\theta^2 W + \left(\frac{11}{2} g^2 - \frac{44}{3} g'^2 - 12\lambda \right) s_\theta^2 Y \right] \right\}, \end{aligned} \quad (4.33a)$$

$$\begin{aligned} & [\delta g_L^{Wq}(\mu_{\text{EW}})]_{ij} = \\ & \frac{\delta_{ij}}{2(c_\theta^2 - s_\theta^2)} \left\{ -2s_\theta^2 \hat{S}(\mu_{\text{EW}}) + c_\theta^2 \hat{T}(\mu_{\text{EW}}) - (c_\theta^2 - 2s_\theta^2) W(\mu_{\text{EW}}) + s_\theta^2 Y(\mu_{\text{EW}}) \right. \\ & \left. + \frac{1}{16\pi^2} \ln \frac{\Lambda}{\mu_{\text{EW}}} \left[\left(10g^2 - \frac{45}{2} g'^2 \right) c_\theta^2 W + \left(\frac{265}{54} g^2 - \frac{380}{27} g'^2 - 12\lambda \right) s_\theta^2 Y + \frac{32}{9} (c_\theta^2 - s_\theta^2) g_s^2 Z \right] \right\}, \end{aligned} \quad (4.33b)$$

as a generalization of (4.30), with the SM parameters still renormalized at μ_{EW} . These equations quantitatively explain the first example in figure 4.1. They are obtained by applying the RG equations presented in [76, 80] to the full expressions (4.13), and later identifying

the various Wilson coefficients involved as combinations of universal parameters, and absorbing part of the LL terms into the running of the oblique parameters according to (4.28), (4.29). Alternatively, (4.33) can be more easily derived by realizing that the additional terms compared to (4.30) can be obtained by turning on W, Y, Z only (i.e. adjusting the Wilson coefficients according to table 4.2 to make sure they are the only nonzero universal parameters) when following the steps explained above, and keeping the LL terms. We emphasize that $\hat{S}(\mu_{EW}), \hat{T}(\mu_{EW}), W(\mu_{EW}), Y(\mu_{EW})$ in (4.33) do not have an obvious and unambiguous interpretation in terms of vector boson self-energy corrections, but are simply defined for convenience to absorb *part* of the LL corrections. Our prescriptions are by no means the only choice for defining them, but are well-motivated since they leads to relatively simple expressions for the observables and Higgs basis couplings at $\mu = \mu_{EW}$, such as (4.33).

Finally, we lift the restriction $y_f \rightarrow 0$ (and meanwhile allowing for nonzero $C_{2JW}, C_{2JB}, C_{2JG}$). The additional effects come from either the 2 additional operators Q_y, Q_{2y} , or the y_f -dependent contributions to the anomalous dimensions calculated in [77], or both. Keeping only the leading terms in y_t , we find,

$$[\dot{C}_{Hq}^{(3)}]_{ij} = \delta_{ij} \frac{3}{2} y_t^2 g^2 (C_{HJW} - 2C_{2JW}) + \delta_{i3} \delta_{j3} y_t^2 \left(-\frac{1}{2} C_{H\Box} + \frac{1}{2} g^2 C_{HJW} - \frac{1}{4} g'^2 C_{HJB} + \frac{1}{2} g^2 C_{2JW} - \frac{1}{18} g'^2 C_{2JB} - \frac{8}{3} g_s^2 C_{2JG} \right), \quad (4.34a)$$

$$[\dot{C}_{Hl}^{(3)}]_{ij} = \delta_{ij} \frac{3}{2} y_t^2 g^2 (C_{HJW} - 2C_{2JW}), \quad (4.34b)$$

$$[\dot{C}_{Hq}^{(1)}]_{ij} = Y_q \delta_{ij} 3y_t^2 g'^2 (C_{HJB} - 2C_{2JB}) + \delta_{i3} \delta_{j3} y_t^2 \left[\frac{1}{2} (C_{H\Box} + C_{HD}) - \frac{9}{4} g^2 C_{HJW} + \frac{3}{2} g^2 C_{2JW} + \frac{1}{18} g'^2 C_{2JB} + \frac{8}{3} g_s^2 C_{2JG} + \left(y_t^2 - \frac{2}{9} g'^2 \right) C_{2y} \right], \quad (4.34c)$$

$$[\dot{C}_{Hl}^{(1)}]_{ij} = Y_l \delta_{ij} 3y_t^2 g'^2 (C_{HJB} - 2C_{2JB}), \quad (4.34d)$$

$$[\dot{C}_{Hu}^{(1)}]_{ij} = Y_u \delta_{ij} 3y_t^2 g'^2 (C_{HJB} - 2C_{2JB}) + \delta_{i3} \delta_{j3} y_t^2 \left[-(C_{H\Box} + C_{HD}) + \frac{5}{2} g^2 C_{HJB} - \frac{16}{9} g'^2 C_{2JB} - \frac{16}{3} g_s^2 C_{2JG} - \left(y_t^2 + \frac{1}{9} g'^2 \right) C_{2y} \right], \quad (4.34e)$$

$$[\dot{C}_{Hd}^{(1)}]_{ij} = Y_d \delta_{ij} 3y_t^2 g'^2 (C_{HJB} - 2C_{2JB}), \quad (4.34f)$$

$$[\dot{C}_{He}^{(1)}]_{ij} = Y_e \delta_{ij} 3y_t^2 g'^2 (C_{HJB} - 2C_{2JB}). \quad (4.34g)$$

These should be added to (4.19). Comparing with (4.18), we see that the additional nonuniversal effects are significant only for the third-generation q and u , i.e. t_L, b_L and t_R . They can be represented by the following additional breaking of the universal relations, supplementing

(4.32),

$$[\delta g_L^{Wq}]_{33} - \delta g_L^{Wl} = -\frac{y_t^2}{16\pi^2} \ln \frac{\Lambda}{\mu_{\text{EW}}} \left[-\frac{3s_\theta^2}{2c_\theta^2} \hat{S} + \frac{1}{4} \hat{T} - \frac{9}{4} W + \frac{49s_\theta^2}{36c_\theta^2} Y + \frac{16g_s^2}{3g^2} Z \right. \\ \left. - \frac{1}{2} (c_\theta^2 + 3s_\theta^2) \Delta \bar{g}_1^Z + \frac{3s_\theta^2}{2c_\theta^2} \Delta \bar{\kappa}_\gamma - \frac{1}{2} \Delta \bar{\kappa}_V \right] \quad (4.35a)$$

$$\frac{[\delta g_R^{Zu}]_{33}}{Y_u} - \frac{\delta g_R^{Zd}}{Y_d} = -\frac{y_t^2}{16\pi^2} \ln \frac{\Lambda}{\mu_{\text{EW}}} \left[-\frac{15s_\theta^2}{4c_\theta^2} \hat{S} - \frac{15}{8} \hat{T} - \frac{9}{8} W + \frac{71s_\theta^2}{24c_\theta^2} Y - 8 \frac{g_s^2}{g^2} Z \right. \\ \left. - \frac{3}{4} (3c_\theta^2 + 5s_\theta^2) \Delta \bar{g}_1^Z + \frac{15s_\theta^2}{4c_\theta^2} \Delta \bar{\kappa}_\gamma + \frac{3}{4} \Delta \bar{\kappa}_V + \frac{1}{12} (9y_t^2 + g'^2) c_{2y} \right], \quad (4.35b)$$

$$[\delta g_L^{Zu}]_{33} + [\delta g_L^{Zd}]_{33} - [\delta g_R^{Zu}]_{33} - \delta g_R^{Zd} = -\frac{y_t^2}{16\pi^2} \ln \frac{\Lambda}{\mu_{\text{EW}}} \left[\frac{5}{2} \hat{T} - \frac{9}{2} W - \frac{11s_\theta^2}{18c_\theta^2} Y + \frac{32g_s^2}{3g^2} Z \right. \\ \left. - 6c_\theta^2 \Delta \bar{g}_1^Z - \Delta \bar{\kappa}_V - \frac{1}{6} (9y_t^2 - g'^2) c_{2y} \right]. \quad (4.35c)$$

The other universal relations are not violated up to $y_f^2/y_t^2 (f \neq t)$ suppressed terms. Note also that, as indicated above, $[\delta g_R^{Zd}]_{33}$ is not modified by terms proportional to y_t^2 , so $[\delta g_R^{Zd}]_{ij} \propto \delta_{ij}$ still holds approximately.

The universal pieces in (4.34), on the other hand, can be conveniently attributed to the running of C_{HJW} , C_{HJB} in addition to (4.20),

$$\dot{C}_{HJW} = 6y_t^2 (C_{HJW} - 2C_{2JW}), \quad (4.36a)$$

$$\dot{C}_{HJB} = 6y_t^2 (C_{HJB} - 2C_{2JB}). \quad (4.36b)$$

Note that the one-loop beta functions of g , g' do not depend on y_t . Regarding the 4-fermion interactions related to the W, Y, Z parameters, the additional contributions to the anomalous dimensions are significant only for the third-generation quarks t_L, b_L, t_R , and there is no universal part to be added to \dot{C}_{2JW} , \dot{C}_{2JB} , \dot{C}_{2JG} . Further, the running of C_{HWB} , C_{HD} in (4.27) should be supplemented by the following additional terms, taken from [77],

$$\dot{C}_{HWB} = 6y_t^2 C_{HWB}, \quad (4.37a)$$

$$\dot{C}_{HD} = 6y_t^2 (2C_{HD} - g'^2 C_{HJB}), \quad (4.37b)$$

The discussion above implies that up to nonuniversal effects that are important for the third-generation quarks t_L, b_L, t_R only, the y_f -dependent RG effects in the electroweak sector are universal and can be conveniently attributed to the running of the oblique parameters. Referring to table 4.2 for the translation between the universal parameters and the Warsaw

basis Wilson coefficients, we find

$$\dot{\hat{S}} = 6y_t^2 \hat{S}, \quad \dot{\hat{T}} = 12y_t^2 \hat{T}, \quad \dot{W} = \dot{Y} = 0. \quad (4.38)$$

These equations are to be added to (4.28). Similarly, we still have $\dot{Z} = 0$. We remark in passing that (4.28) and (4.38) can also be derived from the results in [37], where the submatrix of γ_{ij} involving the bosonic operators in the EGM basis is calculated. Referring to [109] for the expressions of the universal parameters in this basis, we have explicitly checked that the results are the same as we presented above.

Defined in this way, the oblique parameters that appear in the LO expressions of electroweak observables, when renormalized at $\mu = \mu_{\text{EW}}$, absorb all the $\mathcal{O}(\frac{y_t^2}{16\pi^2} \ln \frac{\Lambda}{\mu_{\text{EW}}})$ corrections, except for observables involving the Z boson couplings to t_L , b_L and t_R . Among them, only the $Z b_L \bar{b}_L$ coupling is directly probed by precision Z -pole data, for which we obtain (suppressing the gauge-coupling-dependent LL corrections proportional to W , Y , Z discussed in the previous subsection),

$$\begin{aligned} & [\delta g_L^{Zd}(\mu_{\text{EW}})]_{33} \\ &= \frac{1}{12(c_\theta^2 - s_\theta^2)} \left[4s_\theta^2 \hat{S}(\mu_{\text{EW}}) - (3 - 4s_\theta^2) \hat{T}(\mu_{\text{EW}}) + (3 - 8s_\theta^2) W(\mu_{\text{EW}}) - \frac{s_\theta^2}{c_\theta^2} Y(\mu_{\text{EW}}) \right] \\ &+ \frac{y_t^2}{32\pi^2} \ln \frac{\Lambda}{\mu_{\text{EW}}} \left[\frac{s_\theta^2}{c_\theta^2} (\hat{S} - \Delta \bar{\kappa}_\gamma) - \hat{T} + 3W + (7 - 6s_\theta^2) \Delta \bar{g}_1^Z + \left(y_t^2 - \frac{2}{9} g^2 \right) c_{2y} \right]. \quad (4.39) \end{aligned}$$

The physical picture of this effect was already discussed in the second example in figure 4.1.

4.3.3 Implications for the oblique parameters fit

So far, we have found that while universal theories at the new physics scale do not in general remain universal after RG evolution down to the electroweak scale, precision observables in the electroweak sector allow for a separation of universal and nonuniversal effects induced by RG evolution. With our prescriptions for the separation, the universal effects are conveniently attributed to the running of the oblique parameters, given by the sum of (4.28) and (4.38). This serves as a definition of the oblique parameters at the electroweak scale; see (4.29). Corrections to the electroweak observables not involving the third-generation quarks t_L , b_L , t_R can be represented, to LL and leading y_t accuracy, by the LO expressions with \hat{S} , \hat{T} , W , Y renormalized at μ_{EW} , plus additional (nonuniversal) terms proportional to $\frac{1}{16\pi^2} \ln \frac{\Lambda}{\mu_{\text{EW}}} \cdot \{W, Y, Z\}$; see e.g. (4.33). For the electroweak observables involving t_L , b_L , or t_R , on the other hand, additional terms of order $\frac{y_t^2}{16\pi^2} \ln \frac{\Lambda}{\mu_{\text{EW}}}$ should be added, which also involve some less-constrained nonoblique universal parameters; see e.g. (4.39).

If these additional LL terms were absent (or negligible), the conventional oblique parameters fit, where theory predictions of observables incorporating LO contributions from the oblique parameters are confronted with precision electroweak data, would be a consistent procedure to derive constraints on universal theories. Bounds on the oblique parameters obtained in this way could be interpreted as bounds on $\hat{S}(\mu_{\text{EW}})$, $\hat{T}(\mu_{\text{EW}})$, $W(\mu_{\text{EW}})$, $Y(\mu_{\text{EW}})$ defined in (4.29). The latter could then be mapped onto constraints on the universal parameters at the new physics scale Λ , following the sum of (4.28) and (4.38).

In reality, however, the additional LL terms due to RG-induced nonuniversal effects, which involve some less-constrained universal parameters, may not be negligible compared with LO contributions from \hat{S} , \hat{T} , W , Y , as well as experimental and SM theoretical uncertainties. If this is the case, one should go beyond LO for a consistent fit of universal theories to precision electroweak data. But as far as universal theories are concerned, the underlying number of free parameters is still much smaller than that in the full SMEFT. At the LL order, only a few additional parameters, defined by linear combinations of the universal parameters at Λ , are sufficient. While a full-fledged global analysis is beyond the scope of the present chapter, we will illustrate this point with an example in the next subsection.

4.3.4 Example: R_ℓ and R_b in universal theories

We consider the two observables R_ℓ and R_b introduced at the end of section 4.2.2, and see how their SMEFT predictions are affected by the additional nonuniversal LL terms. Similar to the examples shown in the previous subsections, namely (4.33) and (4.39), the Higgs basis couplings renormalized at μ_{EW} that appear in (4.16) can be worked out. Eq. (4.16) then becomes, numerically,

$$\begin{aligned} \bar{\delta}^{\text{NP}} R_\ell &= -0.36 [\Delta\epsilon_3(\mu_{\text{EW}}) - c_\theta^2 \Delta\epsilon_1(\mu_{\text{EW}})] \\ &\quad + \frac{\ln(\Lambda/\mu_{\text{EW}})}{3} (0.13Z - 0.053\Delta\bar{g}_1^Z + 0.0028\Delta\bar{\kappa}_\gamma - 0.0091c_{2y}), \end{aligned} \quad (4.40a)$$

$$\begin{aligned} \bar{\delta}^{\text{NP}} R_b &= 0.079 [\Delta\epsilon_3(\mu_{\text{EW}}) - c_\theta^2 \Delta\epsilon_1(\mu_{\text{EW}})] \\ &\quad + \frac{\ln(\Lambda/\mu_{\text{EW}})}{3} (-0.19\Delta\bar{g}_1^Z + 0.010\Delta\bar{\kappa}_\gamma - 0.032c_{2y}), \end{aligned} \quad (4.40b)$$

where

$$\Delta\epsilon_3(\mu_{\text{EW}}) - c_\theta^2 \Delta\epsilon_1(\mu_{\text{EW}}) = \hat{S}(\mu_{\text{EW}}) - 0.77\hat{T}(\mu_{\text{EW}}) - 0.23W(\mu_{\text{EW}}) - 0.77Y(\mu_{\text{EW}}) \quad (4.41)$$

is a common oblique parameters combination entering the two observables at LO, expressed in terms of the $\Delta\epsilon$ parameters defined in (4.4).⁴ We have neglected the additional LL terms proportional to \hat{S} , \hat{T} , W , Y , since these parameters already appear in the LO expressions. The numerical impact of these neglected terms is to correct the coefficients of $\Delta\epsilon_3(\mu_{\text{EW}}) - c_\theta^2\Delta\epsilon_1(\mu_{\text{EW}})$ by order $\frac{1}{16\pi^2} \ln \frac{\Lambda}{\mu_{\text{EW}}}$ numbers, and is expected to be less important than the invasion of additional, possibly less-constrained parameters Z , $\Delta\bar{g}_1^Z$, $\Delta\bar{\kappa}_\gamma$, c_{2y} through RG evolution from Λ to μ_{EW} .

The various terms in (4.40) shift the theory predictions for R_ℓ and R_b in different directions in the R_ℓ - R_b plane. This is shown by the dashed lines in figure 4.2, assuming $\ln \frac{\Lambda}{\mu_{\text{EW}}} = 3$ as expected from $\Lambda \sim \mathcal{O}(\text{TeV})$. The new physics corrections can be compared with the SM predictions from the Gfitter fit [26],

$$R_\ell = 20.743 \pm 0.017, \quad R_b = 0.21578 \pm 0.00011, \quad (\text{SM}) \quad (4.42)$$

which is based on the Z -pole measurements from the LEP and SLD collaborations [139],

$$R_\ell = 20.767 \pm 0.025, \quad R_b = 0.21629 \pm 0.00066. \quad (\text{LEP+SLD}) \quad (4.43)$$

As we can see from figure 4.2, a LO oblique parameters fit would naively constrain the linear combination $\Delta\epsilon_3 - c_\theta^2\Delta\epsilon_1$ (blue), properly renormalized at μ_{EW} , to be $\mathcal{O}(10^{-3})$. However, reasonable values of other universal parameters, namely $\mathcal{O}(\frac{v^2}{\Lambda^2})$, which enter the LL corrections, can significantly change the picture. In particular, values of $\mathcal{O}(10^{-2})$ and $\mathcal{O}(10^{-1})$ for the Z (red) and c_{2y} (green) parameters, respectively, which may be generated by heavy QCD-charged states and scalar states, lead to corrections larger than the experimental and SM theoretical uncertainties. It would be interesting to compare these numbers with direct constraints on the parameters Z (see e.g. [204]) and c_{2y} , and obtain a fuller understanding of allowed parameter ranges through a global SMEFT analysis. The anomalous TGC parameters $\Delta\bar{g}_1^Z$ and $\Delta\bar{\kappa}_\gamma$ shift the theory predictions along the same direction as c_{2y} , since all three parameters contribute via $[\delta g_L^{Zd}]_{33}$ only. They are directly constrained by measurements at LEP2, and more recently also at the LHC.⁵ The green line segment between the orange stars (triangles) represents the 95% C.L. interval allowed by the combined LEP2 constraint on

⁴With only observables involving ratios of Zff couplings such as R_ℓ and R_b , one cannot break this degeneracy, because $g_i^{Zf} + \delta g_i^{Zf} = (1 + \frac{\Delta\epsilon_1}{2})g_i^{Zf} - Q_f \frac{s_\theta^2}{c_\theta^2 - s_\theta^2}(\Delta\epsilon_3 - c_\theta^2\Delta\epsilon_1)$, for both $i = L, R$. When $\Delta\epsilon_3 - c_\theta^2\Delta\epsilon_1 = 0$, all Zff couplings are rescaled by a common factor, and ratios of couplings are unchanged. This flat direction can be lifted by considering other observables such as the Z boson total width.

⁵Though experimental constraints are on δg_{1z} , $\delta\kappa_\gamma$ defined with respect to the physical particles, the difference between δg_{1z} and $\Delta\bar{g}_1^Z$, which involve $\Delta\epsilon_{1,2,3}$ (see table 4.3), is not relevant, since when interpreted in universal theories, oblique corrections are always assumed to vanish in experimental TGC analyses. See [109] for more discussion.

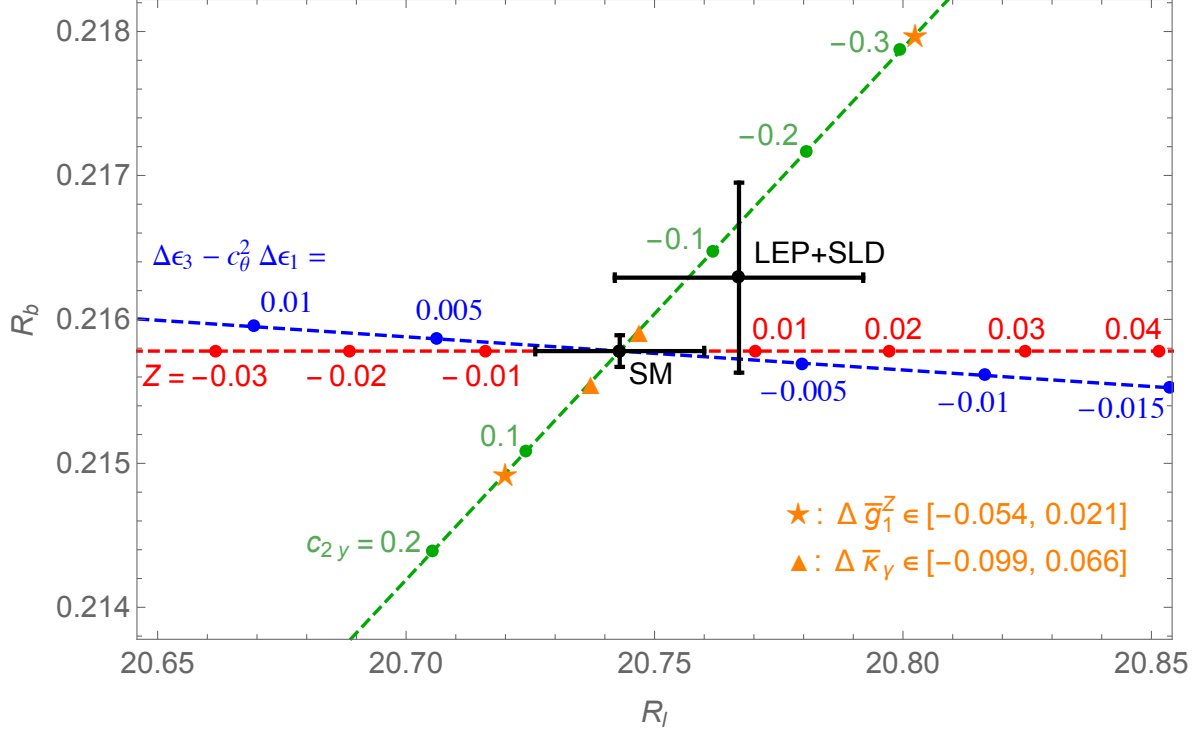


Figure 4.2: (From [111]) Theory predictions for $R_\ell = \Gamma_{\text{had}}/\Gamma(Z \rightarrow \ell^+\ell^-)$ and $R_b = \Gamma(Z \rightarrow b\bar{b})/\Gamma_{\text{had}}$ are shifted away from the SM point along the dashed lines, when the universal parameters appearing in (4.40) take the values labeled beside the dots. The anomalous TGC parameters $\Delta\bar{g}_1^Z$, $\Delta\bar{\kappa}_\gamma$ lead to shifts along the same direction as c_{2y} (green dashed line), with the orange stars and triangles indicating the maximum shifts allowed by the LEP2 TGC constraints (95% C.L.) from single-parameter fits (shown in the bottom-right corner) [205]. $\ln \frac{\Lambda}{\mu_{\text{EW}}} = 3$ is assumed, as motivated by TeV-scale new physics. Agreement between the SM predictions as fitted by the Gfitter group [26] and the combined measurements by the LEP and SLD collaborations [139] naively constrains the oblique parameters combination $\Delta\epsilon_3 - c_\theta^2\Delta\epsilon_1$ (blue) defined in (4.41) at the 10^{-3} level. But even when the oblique parameters are interpreted as renormalized at μ_{EW} following our prescriptions, the neglected LL terms in such a LO oblique parameters analysis can actually be significant. The challenge illustrated by this example requires extending the (\hat{S}, \hat{T}, W, Y) parametrization to include additional parameters in a consistent global fit of universal theories beyond LO.

$\Delta\bar{g}_1^Z$ ($\Delta\bar{\kappa}_\gamma$) taken from the LEP electroweak working group final report [205]. These constraints are derived allowing one anomalous TGC parameter to be nonzero at a time, and are shown here for illustration purpose only. We see that values of $\Delta\bar{g}_1^Z$ as allowed by the above constraint can contribute significant corrections to R_ℓ and R_b .

Our example shows that the RG-induced nonuniversal effects that are usually neglected can indeed challenge the interpretation and usefulness of the LO oblique parameters analysis. In practice, this means that for a consistent global fit of universal theories to precision electroweak data, one should go beyond the conventional approach with the (\hat{S}, \hat{T}, W, Y) parametrization. An extension to LL order should at least involve two additional parameters,

$$\tilde{Z} \equiv Z \ln \frac{\Lambda}{\mu_{\text{EW}}}, \quad \delta\tilde{g}_L^{Zb} \equiv \left[(7 - 6s_\theta^2)\Delta\bar{g}_1^Z - \frac{s_\theta^2}{c_\theta^2}\Delta\bar{\kappa}_\gamma + \left(y_t^2 - \frac{2}{9}g'^2 \right) c_{2y} \right] \ln \frac{\Lambda}{\mu_{\text{EW}}}, \quad (4.44)$$

where $\delta\tilde{g}_L^{Zb}$ is proportional to the linear combination of the less-constrained universal parameters appearing in the LL term in (4.39). For the two observables R_ℓ and R_b discussed in this subsection, \tilde{Z} and $\delta\tilde{g}_L^{Zb}$ capture shifts in the directions of the red and green dashed lines in figure 4.2, respectively. Further extending the analysis to include NLO finite corrections may introduce more parameters, but the total number of free parameters is no more than 16, the number of universal parameters defined at Λ .⁶ Extended in this way, the oblique parameters analysis can be consistent and useful, and yet simpler than the full SMEFT if one is interested only in universal theories (see [91, 104] for discussions on consistent analyses of the full SMEFT).

4.4 RG effects in the Yukawa sector

We next turn to the Yukawa sector, and show how the universal relation (4.5b) can be violated by RG evolution. The observation that RG evolution in universal theories can induce nonuniversal rescaling of all SM fermion Yukawa couplings was previously made in [38], based on partial results on the anomalous dimensions γ_{ij} for one fermion generation, and assuming a limited set of nonzero Wilson coefficients. Our analysis in this section takes into account the full γ_{ij} that became available after [38], and all the parameters characterizing universal theories classified in [109].

⁶A further challenge can potentially arise at this order, if constraints on the universal parameters are to be interpreted in specific UV models. Since a NLO calculation of observables requires one-loop matching [55, 56, 195–198] of the Wilson coefficients contributing at LO, we need to assume that the UV model does not generate operators beyond those in (4.1) even at one-loop matching. This assumption is implicit in our EFT definition of universal theories, but may not be satisfied by all UV theories that would otherwise be regarded as universal.

The dimension-6 operators relevant for Yukawa coupling corrections are those in the $\psi^2 H^3$ class. At LO, their Wilson coefficients are related in universal theories as follows,

$$[\{C_{uH}, C_{dH}, C_{eH}\}]_{ij} = [\{y_u, V_{\text{CKM}} y_d, y_e\}]_{ij} C_y. \quad (4.45)$$

The running of these Wilson coefficients is in general complicated by the nontrivial flavor structure in the quark sector. For example, $[\dot{C}_{dH}]_{ij}$ contains terms proportional to $[y_u y_u^\dagger V_{\text{CKM}} y_d]_{ij}$, which, unlike $[V_{\text{CKM}} y_d]_{ij}$ that $[C_{dH}]_{ij}$ is proportional to at LO, cannot be diagonalized by applying V_{CKM}^\dagger on the left. Thus, a redefinition of the CKM matrix is needed after RG evolution. However, the third-generation quarks are hardly affected by this complication, since we can approximate V_{CKM} by a block-diagonal matrix,

$$V_{\text{CKM}} \simeq \begin{pmatrix} 1 & \lambda_W & 0 \\ -\lambda_W & 1 & 0 \\ 0 & 0 & 1 \end{pmatrix}, \quad (4.46)$$

where a subscript ‘‘W’’ has been added to the Wolfenstein parameter $\lambda_W \simeq 0.23$ to avoid confusion with the Higgs self-coupling λ . With $\mathcal{O}(\lambda_W^2)$ terms neglected, RG evolution in universal theories does not mix the third-generation quarks with the first- and second-generation ones. We will focus on the experimentally most accessible third-generation Yukawa coupling corrections in the following, adopting the approximation (4.46) and neglecting terms suppressed by y_f^2/y_t^2 ($f \neq t$). Using the results in [76, 77, 80] and table 4.1, we find

$$\begin{aligned} [\dot{C}_{uH}]_{33} &= y_t \left[\left(\frac{51}{2} y_t^2 + 24\lambda - 8g_s^2 - \frac{27}{4} g^2 - \frac{35}{12} g'^2 \right) C_y - 12y_t^2 (y_t^2 - \lambda) C_{2y} \right. \\ &\quad - (3y_t^2 - 3\lambda - 4g^2 + g'^2) g^2 C_{HJW} + \left(\frac{1}{2} y_t^2 + \lambda - g^2 + \frac{2}{3} g'^2 \right) g'^2 C_{HJB} \\ &\quad + \frac{16}{9} (y_t^2 - \lambda) g'^2 C_{2JB} + \frac{64}{3} (y_t^2 - \lambda) g_s^2 C_{2JG} \\ &\quad - \left(6y_t^2 + 4\lambda - \frac{10}{3} g^2 \right) C_{H\Box} + \left(y_t^2 + 2\lambda - \frac{3}{2} g^2 + \frac{3}{2} g'^2 \right) C_{HD} \\ &\quad \left. - gg' C_{HWB} + 32g_s^2 C_{HG} + 9g^2 C_{HW} + \frac{17}{3} g'^2 C_{HB} \right], \quad (4.47a) \end{aligned}$$

$$\begin{aligned} [\dot{C}_{dH}]_{33} &= y_b \left[\left(\frac{21}{2} y_t^2 + 24\lambda - 8g_s^2 - \frac{27}{4} g^2 - \frac{23}{12} g'^2 \right) C_y - 14y_t^2 (y_t^2 - \lambda) C_{2y} \right. \\ &\quad - \left(\frac{3}{2} y_t^2 - 3\lambda - 4g^2 + \frac{1}{2} g'^2 \right) g^2 C_{HJW} + \left(\lambda - \frac{1}{2} g^2 - \frac{1}{3} g'^2 \right) g'^2 C_{HJB} \\ &\quad + \frac{8}{9} \lambda g'^2 C_{2JB} - \frac{64}{3} \lambda g_s^2 C_{2JG} - \left(4\lambda - \frac{10}{3} g^2 \right) C_{H\Box} + \left(2\lambda - \frac{3}{2} g^2 + \frac{3}{2} g'^2 \right) C_{HD} \end{aligned}$$

$$+gg'C_{HWB} + 32g_s^2C_{HG} + 9g^2C_{HW} + \frac{5}{3}g'^2C_{HB} \Big], \quad (4.47b)$$

$$\begin{aligned} [\dot{C}_{eH}]_{33} = & y_\tau \left[\left(15y_t^2 + 24\lambda - \frac{27}{4}g^2 - \frac{21}{4}g'^2 \right) C_y - 12y_t^2(y_t^2 - \lambda)C_{2y} \right. \\ & - \left(3y_t^2 - 3\lambda - 4g^2 + \frac{3}{2}g'^2 \right) g^2 C_{HJW} + \left(\lambda - \frac{3}{2}g^2 + 3g'^2 \right) g'^2 C_{HJB} \\ & - 8\lambda g'^2 C_{2JB} - \left(4\lambda - \frac{10}{3}g^2 \right) C_{H\Box} + \left(2\lambda - \frac{3}{2}g^2 + \frac{3}{2}g'^2 \right) C_{HD} \\ & \left. - 3gg'C_{HWB} + 9g^2C_{HW} + 15g'^2C_{HB} \right]. \end{aligned} \quad (4.47c)$$

While there are overlapping terms in these equations, there is no obvious well-motivated way to make the separation between universal vs. nonuniversal effects. We thus refrain from defining the running of $\Delta\bar{\kappa}_F$ as we did for the oblique parameters in the previous section, but simply present the violation of the universal relation (4.5b) at the electroweak scale. To do so, we note that, in our notation,

$$\delta y_t - \delta y_b = - \left(\frac{[C_{uH}]_{33}}{y_t} - \frac{[C_{dH}]_{33}}{y_b} \right), \quad \delta y_b - \delta y_\tau = - \left(\frac{[C_{dH}]_{33}}{y_b} - \frac{[C_{eH}]_{33}}{y_\tau} \right), \quad (4.48)$$

where $\delta y_t, \delta y_b, \delta y_\tau$ represent $[\delta y_u]_{33}, [\delta y_d]_{33}, [\delta y_e]_{33}$, respectively. Combining (4.19) and the one-loop running of the SM Yukawa couplings,

$$\dot{y}_t = y_t \left(\frac{9}{2}y_t^2 - 8g_s^2 - \frac{9}{4}g^2 - \frac{17}{12}g'^2 \right), \quad (4.49a)$$

$$\dot{y}_b = y_b \left(\frac{3}{2}y_t^2 - 8g_s^2 - \frac{9}{4}g^2 - \frac{5}{12}g'^2 \right), \quad (4.49b)$$

$$\dot{y}_\tau = y_\tau \left(3y_t^2 - \frac{9}{4}g^2 - \frac{15}{4}g'^2 \right), \quad (4.49c)$$

we obtain

$$\begin{aligned} \delta y_t(\mu_{EW}) - \delta y_b(\mu_{EW}) &= -\frac{1}{16\pi^2} \ln \frac{\Lambda}{\mu_{EW}} (\delta \dot{y}_t - \delta \dot{y}_b) \\ &= \frac{1}{16\pi^2} \ln \frac{\Lambda}{\mu_{EW}} \left[-6y_t^2(2\Delta\bar{\kappa}_F - \Delta\bar{\kappa}_V) + 4g'^2 s_\theta^2 \Delta\bar{g}_1^Z - 2g'^2 \frac{s_\theta^2}{c_\theta^2} \Delta\bar{\kappa}_\gamma \right. \\ &\quad - 2(g^2 - 2g'^2) \frac{s_\theta^2}{c_\theta^2} \hat{S} + y_t^2 \hat{T} + (3y_t^2 + 2g'^2)W - \left(\frac{41}{9}y_t^2 - \frac{16}{3}\lambda - 2g^2 + 4g'^2 \right) \frac{s_\theta^2}{c_\theta^2} Y \\ &\quad \left. - \frac{128}{3}y_t^2 \frac{g_s^2}{g^2} Z + 2(y_t^2 - \lambda)y_t^2 c_{2y} + g'^2(e^2 f_{\gamma\gamma} - g'^2 f_{z\gamma}) \right] \\ &\simeq \frac{\ln(\Lambda/\mu_{EW})}{3} (-0.23\Delta\bar{\kappa}_F + 0.11\Delta\bar{\kappa}_V + 0.0022\Delta\bar{g}_1^Z - 0.0014\Delta\bar{\kappa}_\gamma - 0.0019\hat{S} + 0.019\hat{T} \\ &\quad + 0.061W - 0.020Y - 2.8Z + 0.032c_{2y} + 0.00023f_{\gamma\gamma} - 0.00031f_{z\gamma}), \end{aligned} \quad (4.50a)$$

$$\begin{aligned}
\delta y_b(\mu_{\text{EW}}) - \delta y_\tau(\mu_{\text{EW}}) &= -\frac{1}{16\pi^2} \ln \frac{\Lambda}{\mu_{\text{EW}}} (\delta \dot{y}_b - \delta \dot{y}_\tau) \\
&= \frac{1}{16\pi^2} \ln \frac{\Lambda}{\mu_{\text{EW}}} \left[3y_t^2 (\Delta \bar{\kappa}_F - \Delta \bar{\kappa}_V) - \frac{40}{3} g'^2 s_\theta^2 \Delta \bar{g}_1^Z + \frac{20}{3} g'^2 \frac{s_\theta^2}{c_\theta^2} \Delta \bar{\kappa}_\gamma \right. \\
&\quad + 4 \left(g^2 - \frac{10}{3} g'^2 \right) \frac{s_\theta^2}{c_\theta^2} \hat{S} - \left(3y_t^2 + 4g'^2 \right) W - 4 \left(\frac{40}{9} \lambda + g^2 - \frac{10}{3} g'^2 \right) \frac{s_\theta^2}{c_\theta^2} Y \\
&\quad \left. + \frac{128}{3} \lambda \frac{g_s^2}{g^2} Z - 2(y_t^2 - \lambda) y_t^2 c_{2y} + 8g_s^4 f_{gg} - \frac{10}{3} g'^2 (e^2 f_{\gamma\gamma} - g'^2 f_{z\gamma}) \right] \\
&\simeq \frac{\ln(\Lambda/\mu_{\text{EW}})}{3} (0.056 \Delta \bar{\kappa}_F - 0.056 \Delta \bar{\kappa}_V - 0.0074 \Delta \bar{g}_1^Z + 0.0048 \Delta \bar{\kappa}_\gamma - 0.000014 \hat{S} \\
&\quad - 0.066 W - 0.013 Y + 0.37 Z - 0.032 c_{2y} + 0.34 f_{gg} - 0.00078 f_{\gamma\gamma} + 0.0010 f_{z\gamma}) (4.50b)
\end{aligned}$$

The terms in these equations involving the oblique parameters correspond to the effect illustrated by the third example in figure 4.1.

The numerical results in (4.50) show that significant deviations from the universal relation (4.5b) are possible. For example, in the simplest scenario where $\Delta \bar{\kappa}_F$ is the only nonnegligible universal parameter at the new physics scale Λ , we have $\delta y_t(\Lambda) = \delta y_b(\Lambda) = \delta y_\tau(\Lambda) = \Delta \bar{\kappa}_F$, but $\delta y_t(\mu_{\text{EW}}) \simeq 0.77 \delta y_b(\mu_{\text{EW}})$, $\delta y_b(\mu_{\text{EW}}) \simeq 1.056 \delta y_\tau(\mu_{\text{EW}})$ after RG evolution, if $\ln \frac{\Lambda}{\mu_{\text{EW}}} \simeq 3$. Further deviations can be induced by other universal parameters, such as $\Delta \bar{\kappa}_V$, Z , c_{2y} , f_{gg} , if they are generated at Λ . Therefore, the sometimes adopted simplified approach to precision Higgs fit where a common rescaling factor is assumed for all the SM fermion Yukawa couplings does not find its justification in universal theories. This assumption applies to the the effective hff couplings at $\mu \sim m_h \sim \mu_{\text{EW}}$, and appears fine-tuned in light of the RG-induced nonuniversal effects illustrated above. Thus, even for universal theories, it is desirable to keep these parameters separate when fitting them to data.

4.5 Conclusions

The usefulness of simplified frameworks for precision analyses lies in the fact that they are much more tractable than the full SMEFT with a vast parameter space, and yet capture broad classes of BSM scenarios. The oblique parameters framework, which characterizes effects of universal theories on precision electroweak observables, has been widely-used for more than two decades now, and finds its justification at LO in the modern SMEFT approach with a consistent description of universal theories in the SMEFT [109]. In many cases, however, it is desirable to go beyond LO in the new physics effects, and simplified frameworks should be properly extended to incorporate RG evolution.

In this chapter, we have performed a RG analysis of universal theories in the SMEFT

framework. The key observation is that under RG evolution, universal theories at the new physics scale Λ , which reside in a 16-dimensional subspace of the full SMEFT parameter space, can flow out of this subspace, and become nonuniversal at the electroweak scale μ_{EW} where their effects on precision observables are measured. But the departure from universal theories at μ_{EW} is not arbitrary, as the theory is still usefully described by the 16 universal parameters defined at Λ . The main consequences of this observation are the following.

- The universal pattern of deviations from SM predictions seen at LO in the universal theories EFT is distorted after RG evolution from Λ to μ_{EW} . The RG-induced nonuniversal effects lead to well-defined departures (dictated by the 16 universal parameters at Λ) from the LO universal relations (4.5) among some generically independent Higgs basis couplings (in the sense explained at the end of section 4.2.2); see (4.32), (4.35), (4.50).
- Since there is in general no unique procedure to define the oblique parameters (and more generally universal parameters) for nonuniversal theories, additional prescriptions are needed for $\hat{S}(\mu_{\text{EW}})$, $\hat{T}(\mu_{\text{EW}})$, etc. to be meaningful. Our prescriptions are shown in (4.29), where the running of the oblique parameters is given by the sum of (4.28) and (4.38).
- With our prescriptions, LO expressions for the new physics corrections to electroweak observables $\bar{\delta}^{\text{NP}}\hat{\mathcal{O}}$ can be used with \hat{S} , \hat{T} , W , Y renormalized at μ_{EW} , supplemented by additional LL terms that cannot be absorbed into the running of the oblique parameters. An example calculation of two well-measured observables R_ℓ and R_b shows that the additional LL terms can be numerically important; see (4.40) and figure 4.2. This implies that, even for universal theories, a consistent precision electroweak fit should go beyond the $\{\hat{S}, \hat{T}, W, Y\}$ parametrization. But unlike generic nonuniversal theories, the additional parameters to be incorporated are a small number of linear combinations of other universal parameters invading through RG evolution from Λ to μ_{EW} ; see (4.44).
- The Yukawa couplings of all SM fermions are in general not modified in the same way even in universal theories. In particular, (4.50) shows the potentially sizable RG-induced deviations from a universal rescaling for the top, bottom and tau Yukawa couplings (as parameters in the Higgs basis framework). Thus, fitting a common Yukawa coupling rescaling factor to Higgs data as based on LO intuitions from universal theories is of limited use.

Two additional aspects of RG-induced nonuniversal effects not discussed in this chapter are the generation of the dipole-type couplings d_{Vf} (which vanish at LO in universal theories; see table 4.3), and a nonuniversal pattern of 4-fermion interactions. They correspond to violations of the two other features of universal theories at LO listed in section 4.2 of [109] that are not captured by the universal relations (4.5).⁷ Following the discussion in [80], we see the former affects the muon anomalous magnetic moment, but not $\mu \rightarrow e\gamma$ or electric dipole moments, if the theory is universal (and CP-conserving) at Λ . The latter aspect may have an impact on precision analyses of LEP2 data in the oblique parameters framework, and can also be relevant for future precision measurements on a higher-energy e^+e^- collider where also the top quark can be pair-produced. In any case, to make maximal use of existing and upcoming precision data for indirect searches of physics beyond the SM, simplified parameterizations of new physics effects, as motivated by specific classes of BSM scenarios like universal theories, should be consistently cast in the SMEFT framework (if the absence of new light states is assumed), and checked for robustness against RG evolution.

⁷There it is also mentioned that $\delta g_R^{Wq} = 0$ at LO in universal theories; see table 4.3 of this chapter. A nonzero δg_R^{Wq} is generated by RG evolution at $\mathcal{O}(y_u y_d)$.

Chapter 5

Time to Go Beyond TGC

Interpretation of W Pair Production

W boson pair production processes at e^+e^- and pp colliders have been conventionally interpreted as measurements of WWZ and $WW\gamma$ triple gauge couplings (TGCs). Such interpretation is based on the assumption that new physics effects other than anomalous TGCs are negligible. While this “TGC dominance assumption” was well-motivated and useful at LEP2 thanks to precision electroweak constraints, it is already challenged by recent LHC data. In fact, contributions from anomalous Z boson couplings that are allowed by electroweak precision data but neglected in LHC analyses, being enhanced at high energy, can even dominate over those from the anomalous TGCs considered. This limits the generality of the anomalous TGC constraints derived in current analyses, and necessitates extension of the analysis framework and change of physics interpretation. The issue will persist as we continue to explore the high energy frontier. We clarify and analyze the situation in the effective field theory framework, which provides a useful organizing principle for understanding Standard Model deviations in the high energy regime.

5.1 Introduction

The nonabelian nature of the Standard Model (SM) gauge groups has the crucial consequence of gauge boson self-interactions. In the electroweak sector, the structure of WWZ and $WW\gamma$ triple gauge couplings (TGCs) follows from $SU(2)_L \times U(1)_Y$ gauge invariance and the pattern of its spontaneous breaking. Heavy new physics beyond the SM may leave footprints on the low-energy effective theory in the form of anomalous TGCs. Conventionally, these effects

are parameterized by the following Lagrangian [206],

$$\begin{aligned} \mathcal{L}_{\text{TGC}} = ig \left\{ (W_{\mu\nu}^+ W^{-\mu} - W_{\mu\nu}^- W^{+\mu}) [(1 + \delta g_{1z}) c_\theta Z^\nu + s_\theta A^\nu] \right. \\ \left. + \frac{1}{2} W_{[\mu}^+ W_{\nu]}^- [(1 + \delta \kappa_z) c_\theta Z^{\mu\nu} + (1 + \delta \kappa_\gamma) s_\theta A^{\mu\nu}] \right. \\ \left. + \frac{1}{m_W^2} W_\mu^{+\nu} W_\nu^{-\rho} (\lambda_z c_\theta Z_\rho^\mu + \lambda_\gamma s_\theta A_\rho^\mu) \right\}, \end{aligned} \quad (5.1)$$

assuming CP conservation. Here $W_{\mu\nu}^\pm = \partial_\mu W_\nu^\pm - \partial_\nu W_\mu^\pm$, $W_{[\mu}^+ W_{\nu]}^- = W_\mu^+ W_\nu^- - W_\nu^+ W_\mu^-$, g is the $SU(2)_L$ gauge coupling, and s_θ (c_θ) denotes the sine (cosine) of the weak mixing angle. The anomalous TGC parameters δg_{1z} , $\delta \kappa_z$, $\delta \kappa_\gamma$, λ_z , λ_γ , which vanish in the SM, have been intensively studied in search of evidence for new physics. LEP2 measurements of W pair (and to a lesser extent also single W) production were able to confirm SM predictions and constrain the anomalous TGCs at the $\lesssim 10\%$ level [45, 205]. Recent years have seen renewed interest in TGC studies, motivated by progress on LHC electroweak measurements as well as connection with Higgs physics [6, 71, 103]. Impressively, with several diboson measurements at 7 and 8 TeV combined, LHC has already exceeded LEP2 in setting limits on anomalous TGCs [112]. The WW [207, 208] and WZ [209, 210] channels played a dominant role in this achievement. Prospects of future facilities have also been discussed, with numbers as small as 10^{-4} – 10^{-3} quoted for anomalous TGC sensitivities [211, 212], showing great potential of uncovering new physics beyond the SM in electroweak interactions.

In previous TGC analyses, it is often assumed that Eq. (5.1) encodes *all* the relevant beyond-SM effects on the observables under study. This assumption, which we shall call the “TGC dominance assumption,” is obviously not satisfied for arbitrary new physics scenarios. Nevertheless, it is well-motivated and useful if other possible deformations of the SM are experimentally constrained to be small. Whether the latter is the case should be carefully assessed to give meaning to TGC studies.

To do so, we consider the most general SM deformations due to decoupled new physics at a high scale Λ , which can be captured by the SM effective field theory (EFT) at experimentally accessible energies, assumed to be much below Λ . Generically, assuming lepton number conservation up to Λ , leading corrections to the SM Lagrangian arise from dimension-six effective operators,

$$\mathcal{L}_{\text{SMEFT}} = \mathcal{L}_{\text{SM}} + \sum_i \frac{C_i}{v^2} \mathcal{O}_i + \dots, \quad (5.2)$$

with $C_i \sim \mathcal{O}(\frac{v^2}{\Lambda^2})$ up to model-dependent coupling or loop factors. In this framework, search of SM deviations becomes a global analysis program, with experimental input on different processes probing various directions of the $\{C_i\}$ parameter space [29, 46, 114]. Conventional

TGC analyses via e.g. W pair production are usually interpreted as constraining the linear combinations of C_i giving rise to anomalous TGCs. This is based on the TGC dominance assumption, which asserts that other combinations of C_i affecting the observables under study can be effectively set to zero. It is commonly believed that the latter combinations are well constrained by electroweak precision data (EWPD) and can hardly have any impact.

It is the purpose of this study to revisit the TGC dominance assumption and assess its validity in light of recent improvements on TGC constraints from LHC data. We focus on the WW channel given its relevance at both e^+e^- and pp colliders. There have been claims in the previous literature that the TGC dominance assumption is valid in the case of $e^+e^- \rightarrow W^+W^-$ at LEP2 [29,45], and we will verify them explicitly. On the other hand, as we will see, this assumption is no longer supported by EWPD when analyzing recent LHC results. A key observation is that some of the neglected effects, even though constrained by Z pole data, are enhanced at higher energies and become nonnegligible compared with the anomalous TGC effects under study. The situation calls for extension of the TGC analysis framework to allow for more general interpretations of experimental results. Further, from the SMEFT point of view, as we continue to explore the high energy frontier, it will be perhaps more useful to organize our knowledge of effective operators in terms of their high energy behaviors, rather than the anomalous couplings they induce as is conventionally done.

5.2 Effective operators and anomalous couplings

We start by reviewing the theoretical framework in order to precisely formulate the TGC dominance assumption. We shall be guided by the SMEFT at dimension-six level to identify potentially important beyond-SM effects in addition to anomalous TGCs. In the Warsaw basis [3], which we adopt here for concreteness, the following operators contribute to $f\bar{f} \rightarrow W^+W^-$ at tree level:

$$\begin{aligned}
\mathcal{O}_{HWB} &= H^\dagger \sigma^a H W_{\mu\nu}^a B^{\mu\nu}, & \mathcal{O}_{HD} &= |H^\dagger (D_\mu H)|^2, \\
\mathcal{O}_{3W} &= \epsilon^{abc} W_\mu^{a\nu} W_\nu^{b\rho} W_\rho^{c\mu}, & [\mathcal{O}_l]_{ijkn} &= (\bar{l}_i \gamma_\mu l_j) (\bar{l}_k \gamma^\mu l_n), \\
[\mathcal{O}_{HF}^{(3)}]_{ij} &= i(H^\dagger \sigma^a (D_\mu H) - (D_\mu H^\dagger) \sigma^a H) (\bar{F}_i \gamma^\mu \sigma^a F_j), \\
[\mathcal{O}_{HF}^{(1)}]_{ij} &= i(H^\dagger (D_\mu H) - (D_\mu H^\dagger) H) (\bar{F}_i \gamma^\mu F_j), \\
[\mathcal{O}_{Hf}]_{ij} &= i(H^\dagger (D_\mu H) - (D_\mu H^\dagger) H) (\bar{f}_i \gamma^\mu f_j),
\end{aligned} \tag{5.3}$$

where F, f denote $SU(2)_L$ doublet and singlet fields, respectively, and i, j are generation indices. We assume minimal flavor violation [13] for simplicity, and neglect operators whose

coefficients are suppressed by SM Yukawa couplings.

One can work out the anomalous couplings induced by the dimension-six operators in Eq. (5.3). To avoid ambiguities associated with field and parameter redefinitions, we follow [7, 213] and define anomalous couplings with respect to mass eigenstate fields in unitary gauge with canonically normalized kinetic terms, after SM parameters have been properly redefined such that the conventional input observables m_Z , G_F , α , etc. are not shifted (see [109] for connection with the oblique parameters formalism [146, 193, 194]). In this framework, $f\bar{f} \rightarrow W^+W^-$ can receive new physics contributions from: *i*) anomalous TGCs defined in Eq. (5.1); *ii*) W boson mass shift

$$\mathcal{L}_{m_W} = (1 + \delta_m)^2 \frac{g^2 v^2}{4} W_\mu^+ W^{-\mu}; \quad (5.4)$$

and *iii*) Zff and Wff' vertex corrections (with f' being the $SU(2)_L$ partner of f)

$$\begin{aligned} \mathcal{L}_{\text{vertex}} = & \sum_f \frac{g}{c_\theta} ((T_f^3 - Q_f s_\theta^2) \delta_{ij} + [\delta g_{L/R}^{Zf}]_{ij}) Z_\mu \bar{f}_i \gamma^\mu f_j \\ & + \frac{g}{\sqrt{2}} [(\delta_{ij} + [\delta g_L^{Wq}]_{ij}) W_\mu^+ \bar{u}_{Li} \gamma^\mu (V_{\text{CKM}} d_L)_j \\ & + (\delta_{ij} + [\delta g_L^{Wl}]_{ij}) W_\mu^+ \bar{\nu}_i \gamma^\mu e_{Lj} + \text{h.c.}], \end{aligned} \quad (5.5)$$

where f now runs over mass eigenstates ν_L , $e_{L,R}$, $u_{L,R}$, $d_{L,R}$, and generation indices i, j are summed over. These anomalous couplings are not all independent. In particular, anomalous TGCs satisfy the well-known relations,

$$\delta\kappa_z = \delta g_{1z} - \frac{s_\theta^2}{c_\theta^2} \delta\kappa_\gamma, \quad \lambda_z = \lambda_\gamma, \quad (5.6)$$

while Zff and Wff' vertex corrections are also related,

$$\delta g_L^{Wq} = \delta g_L^{Zu} - \delta g_L^{Zd}, \quad \delta g_L^{Wl} = \delta g_L^{Z\nu} - \delta g_L^{Ze}. \quad (5.7)$$

Therefore, there are 5(6) independent anomalous couplings contributing to $f\bar{f} \rightarrow W^+W^-$ with right-handed (left-handed) incoming fermion: δg_{1z} , $\delta\kappa_\gamma$, λ_γ , δ_m , plus δg_R^{Zf} (δg_L^{Zf} and $\delta g_L^{Zf'}$). In particular, $e^+e^- \rightarrow W^+W^-$ at LEP2 involves 7 independent anomalous couplings

$$\{\delta g_{1z}, \delta\kappa_\gamma, \lambda_\gamma, \delta g_L^{Ze}, \delta g_L^{Z\nu}, \delta g_R^{Ze}, \delta_m\}, \quad (5.8)$$

while $pp \rightarrow W^+W^-$ at the LHC involves 8 when only first-generation quarks are considered

in the initial state

$$\{\delta g_{1z}, \delta \kappa_\gamma, \lambda_\gamma, \delta g_L^{Zu}, \delta g_R^{Zu}, \delta g_L^{Zd}, \delta g_R^{Zd}, \delta_m\}, \quad (5.9)$$

with generation indices $i, j = 1$ implicit.

The dictionary between effective operator coefficients and the anomalous couplings listed above reads

$$\begin{aligned} \delta g_{1z} &= \frac{1}{c_\theta^2 - s_\theta^2} \left(-\frac{s_\theta}{c_\theta} C_{HWB} - \frac{1}{4} C_{HD} - \delta v \right), \\ \delta \kappa_\gamma &= \frac{c_\theta}{s_\theta} C_{HWB}, \quad \lambda_\gamma = -\frac{3}{2} g C_{3W}, \\ [\delta g_L^{Zf}]_{ij} &= T_f^3 [C_{HF}^{(3)}]_{ij} - \frac{1}{2} [C_{HF}^{(1)}]_{ij} \\ &\quad - \left[Q_f \frac{c_\theta s_\theta}{c_\theta^2 - s_\theta^2} C_{HWB} + \left(T_f^3 + Q_f \frac{s_\theta^2}{c_\theta^2 - s_\theta^2} \right) \left(\frac{1}{4} C_{HD} + \delta v \right) \right] \delta_{ij}, \\ [\delta g_R^{Zf}]_{ij} &= -\frac{1}{2} [C_{Hf}]_{ij} - Q_f \left[\frac{c_\theta s_\theta}{c_\theta^2 - s_\theta^2} C_{HWB} + \frac{s_\theta^2}{c_\theta^2 - s_\theta^2} \left(\frac{1}{4} C_{HD} + \delta v \right) \right] \delta_{ij}, \\ \delta_m &= -\frac{1}{c_\theta^2 - s_\theta^2} \left(c_\theta s_\theta C_{HWB} + \frac{1}{4} c_\theta^2 C_{HD} + s_\theta^2 \delta v \right), \end{aligned} \quad (5.10)$$

where F denotes the $SU(2)_L$ doublet containing f_L , and $\delta v \equiv \frac{1}{2}([C_{Hl}^{(3)}]_{11} + [C_{Hl}^{(3)}]_{22}) - \frac{1}{4}([C_{U}]_{1221} + [C_{U}]_{2112})$.

With the discussion above, it should be clear that, as far as the dimension-six SMEFT is concerned, the TGC dominance assumption corresponds to keeping only the subset $\{\delta g_{1z}, \delta \kappa_\gamma, \lambda_\gamma\}$ of anomalous couplings in Eqs. (5.8) and (5.9). We see from Eq. (5.10) that, once the operators inducing $\delta g_{1z}, \delta \kappa_\gamma$ are turned on, one then has to adjust $C_{HF}^{(3,1)}, C_{Hf}$ to ensure that vertex corrections vanish.

5.3 Triple gauge coupling measurements: from LEP2 to LHC

Now we make a first attempt to assess the validity of the TGC dominance assumption in W pair production processes. For illustration, we will allow each of the additional anomalous couplings,

$$\{\delta g_L^{Ze}, \delta g_L^{Z\nu}, \delta g_R^{Ze}, \delta g_L^{Zu}, \delta g_R^{Zu}, \delta g_L^{Zd}, \delta g_R^{Zd}, \delta_m\} \quad (5.11)$$

to be maximal within the 2σ intervals in Eq. (40) of [45] and Eq. (4.4) of [92], which are derived from EWPD assuming flavor universality, and see how much correction they can induce on some representative observables. This is to be compared with contributions from

anomalous TGCs being considered in conventional TGC analyses, as well as experimental uncertainties.

TGC analyses at LEP2 made use of $e^+e^- \rightarrow W^+W^-$ measurements with unpolarized e^+e^- beams at center-of-mass energies up to 209 GeV. We consider as an example observable $\frac{d\sigma}{d\cos\theta}(e^+e^- \rightarrow W^+W^- \rightarrow qq\ell\nu)$ with θ being the angle between W^- and e^- momenta and $\ell = e, \mu$ (either sign), at $\sqrt{s} = 198.38$ GeV. This is reported for 10 bins of $\cos\theta$ in Table 5.6 of [205] based on data from 194 to 204 GeV, with a luminosity-weighted average of 198.38 GeV. Fig. 5.1 shows the fractional shift in $\frac{d\sigma}{d\cos\theta}$ with respect to the SM, calculated at tree level, when each of the anomalous couplings in Eq. (5.8) is turned on individually, along with experimental uncertainties (gray dotted). Contributions from $\delta g_L^{Zu}, \delta g_L^{Zd}$ via W branching ratio modifications are within ± 0.005 and not shown. Numerical values chosen for the anomalous TGCs reflect the level of LEP2 constraints — they correspond to maximal deviations from zero allowed by the LEP2 three-parameter fit (95% C.L. intervals in Table 11.7 of [214]). It is seen that possible contributions from vertex and W mass corrections as allowed by EWPD are indeed well beyond experimental sensitivity, thus providing justification for the conventional TGC analysis procedure (though the situation may be more subtle when theoretical errors from EFT calculations are considered [114]).

At the LHC, anomalous TGC constraints greatly benefit from the $W^+W^- \rightarrow e^\pm\mu^\mp\nu\nu$ channel. For illustration, we follow the ATLAS 8 TeV analysis [207], and numerically calculate the leading lepton p_T distribution. Our results are shown in Fig. 5.2, with values of anomalous TGCs chosen at the 95% C.L. upper limits from the recent TGC fit [112], which are comparable to those reported by the experimental collaborations. We see that, unlike the situation at LEP2, contributions from $\delta g_R^{Zu}, \delta g_R^{Zd}$ as allowed by EWPD can be at a similar level as, and even dominant over those from anomalous TGCs being considered (effects of other anomalous couplings are very small and not shown). The issue becomes more severe if the flavor universality assumption is relaxed, as vertex corrections are even less constrained in that case [92]. Therefore, interpreting LHC WW data as a measurement of TGCs while neglecting these additional, potentially more important effects limits the generality of the results. A consistent global fit should include effects of $\delta g_R^{Zu}, \delta g_R^{Zd}$ along with those of $\delta g_{1z}, \delta\kappa_\gamma, \lambda_\gamma$ when considering such data, and interpret the latter as constraining this extended parameter space.

As a side remark, we note that large contributions from $\delta g_R^{Zu}, \delta g_R^{Zd}$ are dominated by new physics amplitude squared terms rather than interference with the SM. The same is true for anomalous TGCs [115]. Generically, it is difficult for LHC data to be sensitive to interference terms due to limited precision. Yet, consistent interpretation of dimension-six SMEFT constraints can be made in some restricted contexts, in particular strongly-coupled

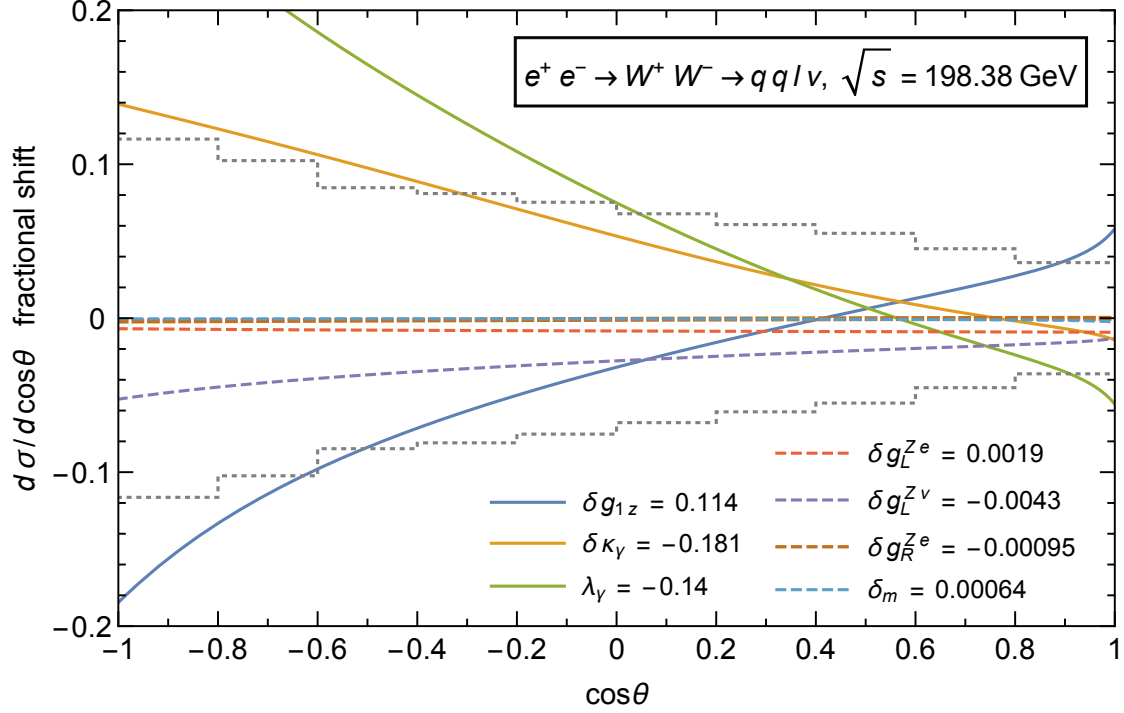


Figure 5.1: (From [117]) Fractional shift in LEP2 $e^+e^- \rightarrow W^+W^- \rightarrow qq\ell\nu$ differential cross section induced by each of the anomalous couplings in Eq. (5.8), compared with experimental uncertainties (gray dotted) reported in [205]. Assuming lepton flavor universality, effects of the anomalous TGCs being constrained (solid) [214] are seen to dominate over those of Zff vertex and W mass corrections (dashed), even when the latter are set to maximum values allowed by EWPD [45,92], providing justification for the conventional TGC analysis procedure.

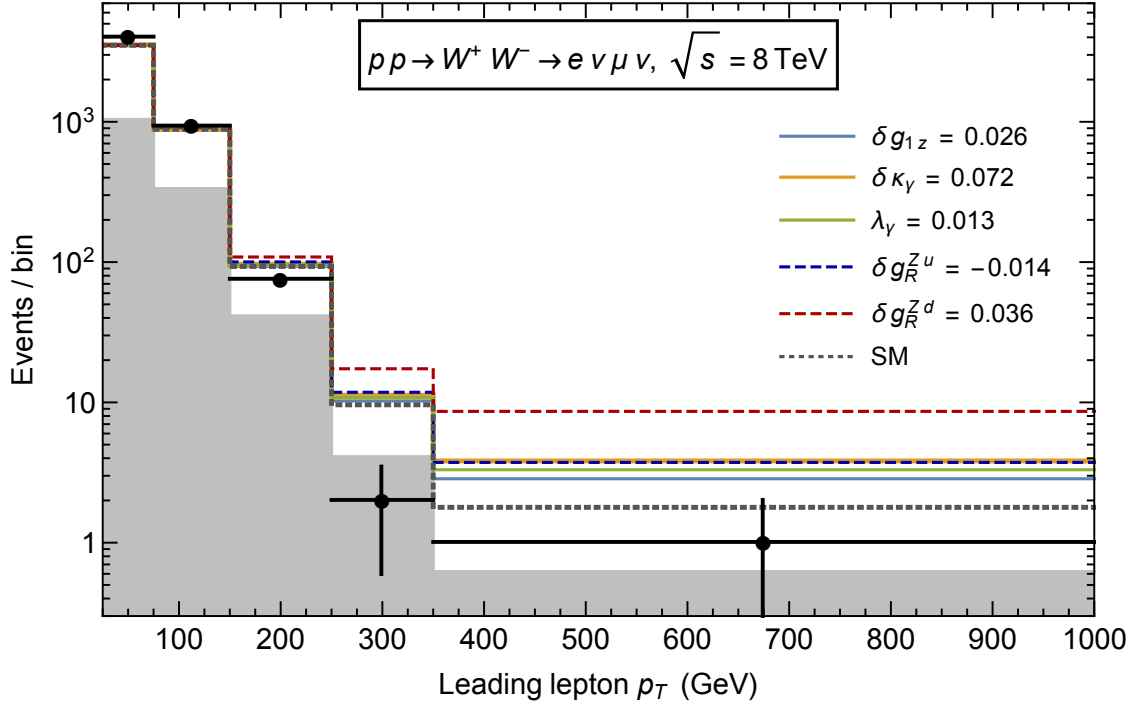


Figure 5.2: (From [117]) Leading lepton p_T distribution of 8 TeV LHC W^+W^- events in the $e\mu$ channel when each anomalous coupling is turned on individually, compared with experimental data (dots with error bars) and SM predictions (gray dotted). The latter, together with non- WW backgrounds (gray shaded), are taken from [207]. Effects of anomalous TGCs being considered in recent TGC fits (solid) are clearly *not* dominant over those of δg_R^{Zu} , δg_R^{Zd} (dashed) consistent with EWPD, calling for extension of the conventional TGC analysis procedure.

scenarios, where dimension-eight operators' contributions are expected to be subdominant by power counting [113].

5.4 Toward a high energy picture of Standard Model deviations

The reason for the different conclusions regarding LEP2 and LHC is twofold. First, Z couplings to quarks are less constrained than those to leptons; even a nonzero δg_R^{Zd} is favored due to the $Z \rightarrow b\bar{b}$ forward-backward asymmetry anomaly [139]. Second, as we will discuss below, some vertex corrections, even though constrained by Z -pole data, lead to cross section corrections relative to the SM that grow with \hat{s} . Their effects are thus amplified at higher energies. This latter aspect will persist in the future. In particular, it has been proposed to measure $e^+e^- \rightarrow W^+W^-$ at much higher energies and precisions than LEP2 to search for deviations from the SM. But whether such deviations, if established, should be interpreted as indicating anomalous TGCs will crucially depend on our knowledge of the additional effects, which in turn depends on availability of precision data of other observables. We leave a detailed study to future work, but simply comment here that in the scenario where improved Z -pole measurements will not occur before the next $e^+e^- \rightarrow W^+W^-$ measurements (as envisioned for the ILC [215]), TGC interpretations will indeed be challenged by possibly large effects of $\delta g_L^{Z\nu}$, δg_R^{Ze} .

In fact, searches of SM deviations at the LHC and future colliders share a common theme of going to higher energy and taking advantage of the anomalous growth of cross sections. In the case of $f\bar{f} \rightarrow W^+W^-$, consider the high energy limit $v \ll \sqrt{\hat{s}} \ll \Lambda$, where

$$\begin{aligned} \frac{d\sigma_{f_L\bar{f}_R}}{d\cos\theta} &= \frac{\pi\alpha^2(1-\cos^2\theta)}{4N_c m_Z^2 c_\theta^4 s_\theta^4} [T_f^3(c_\theta^2 - s_\theta^2) + Q_f s_\theta^2] \cdot \\ &\quad \left[-\delta g_L^{Zf'} - (T_f^3 - Q_f s_\theta^2) \delta g_{1z} + (T_f^3 - Q_f) \frac{s_\theta^2}{c_\theta^2} \delta\kappa_\gamma \right] + \mathcal{O}(\hat{s}^{-1}) \\ &= \frac{\pi\alpha^2(1-\cos^2\theta)}{8N_c m_Z^2 c_\theta^4 s_\theta^4} [T_f^3(c_\theta^2 - s_\theta^2) + Q_f s_\theta^2] [C_{HF}^{(1)} + 2T_f^3 C_{HF}^{(3)}] + \mathcal{O}(\hat{s}^{-1}), \end{aligned} \quad (5.12)$$

$$\begin{aligned} \frac{d\sigma_{f_R\bar{f}_L}}{d\cos\theta} &= \frac{\pi\alpha^2(1-\cos^2\theta)}{4N_c m_Z^2 c_\theta^4 s_\theta^2} Q_f \left(-\delta g_R^{Zf} + Q_f s_\theta^2 \delta g_{1z} - Q_f \frac{s_\theta^2}{c_\theta^2} \delta\kappa_\gamma \right) + \mathcal{O}(\hat{s}^{-1}) \\ &= \frac{\pi\alpha^2(1-\cos^2\theta)}{8N_c m_Z^2 c_\theta^4 s_\theta^2} Q_f C_{Hf} + \mathcal{O}(\hat{s}^{-1}). \end{aligned} \quad (5.13)$$

Here θ is the angle between the W^- and f momenta. Only terms linear in anomalous couplings or operator coefficients have been shown, which are sufficient for making our point

in the following discussion. We comment in passing that unlike the case of LHC, quadratic terms are subdominant for $e^+e^- \rightarrow W^+W^-$ up to $\sqrt{s} \sim 1$ TeV, when values of vertex corrections consistent with EWPD and per-mil-level δg_{1z} , $\delta\kappa_\gamma$ are considered (contributions from λ_γ do not grow with energy at linear level [115,128], and can be dominated by quadratic terms).

The high energy behavior shown in Eqs. (5.12) and (5.13) can be easily understood and reproduced using the Goldstone boson equivalence theorem [68], which states that scattering amplitudes involving longitudinal gauge bosons coincide with those involving the corresponding Goldstone bosons in the high energy limit. For example, $\mathcal{O}_{Hf} \supset i(\phi^-\partial_\mu\phi^+ - \phi^+\partial_\mu\phi^-)(\bar{f}\gamma^\mu f)$, with ϕ^\pm being the Goldstone bosons eaten by W^\pm , mediates $f_R\bar{f}_L \rightarrow \phi^+\phi^-$ via a contact interaction vertex, with an amplitude proportional to $\frac{\hat{s}}{\Lambda^2}$ by dimensional analysis. The corresponding amplitude $f_R\bar{f}_L \rightarrow W_L^+W_L^-$ (“ L ” in W_L^\pm for “longitudinal”) thus also grows with \hat{s} , in contrast to the SM amplitude which $\sim \hat{s}^0$. On the other hand, \mathcal{O}_{HWB} , \mathcal{O}_{HD} and \mathcal{O}_U do not mediate $f\bar{f} \rightarrow \phi^+\phi^-$ at tree level, while their contributions to $f\bar{f} \rightarrow W_T^+W_T^-$, either direct or via shifting input observables, necessarily involve factors of the Higgs vev and hence $\sim \frac{v^2}{\Lambda^2}$. Another interesting feature of Eq. (5.12) is that δg_L^{WF} and δg_L^{Zf} contribute via the combination $2T_f^3\delta g_L^{WF} - \delta g_L^{Zf} = -\delta g_L^{Zf'}$ in the high energy limit. This can be seen from $SU(2)_L$ -conjugating, schematically, $\frac{v^2}{\Lambda^2}(gZ_\mu)(\bar{f}'_L\gamma^\mu f'_L) \rightarrow \frac{\phi^+\phi^-}{\Lambda^2}(i\partial_\mu)(\bar{f}_L\gamma^\mu f_L)$.

The discussion above suggests that as precision studies are pushed to higher energies, it is useful to reorganize our thinking about SM deviations. Conventionally, the experimental precision hierarchy between pole observables and $f\bar{f} \rightarrow W^+W^-$ has motivated the use of anomalous couplings and the procedure of constraining first the parameters in Eq. (5.11), and then anomalous TGCs with the former set to zero. As higher energies $\sqrt{\hat{s}} \gtrsim v$ are reached, we are probing the electroweak symmetric phase where fully $SU(2) \times U(1)$ -invariant effective operators are more useful to guide our thinking than anomalous couplings defined in the broken phase. In this regard, a better-motivated separation is between operators that lead to anomalous growth with energy for the cross sections under consideration vs. those that do not. This separation can be made also when quadratic terms, not shown in Eqs. (5.12) and (5.13), are included. For $f\bar{f} \rightarrow W^+W^-$, the first set consists of $\mathcal{O}_{HF}^{(1,3)}$, \mathcal{O}_{Hf} , and also \mathcal{O}_{3W} when quadratic terms are considered. Interestingly, $\mathcal{O}_{HF}^{(1,3)}$, \mathcal{O}_{Hf} do not by themselves induce anomalous TGCs, but are turned on only to adjust $\delta g_{L,R}^{Zf}$ to zero in conventional TGC analyses; see Eq. (5.10). Within the range of validity of the SMEFT ($\sqrt{\hat{s}} \ll \Lambda$), this set of operators is likely to be more accessible experimentally, leading to a different precision hierarchy than before.

5.5 Conclusions

As precision measurements continue to explore higher energies in order to resolve SM deviations enhanced in this regime, our understanding of existing constraints also evolves; and so does the overall picture of the SMEFT parameter space. In particular, it should be kept in mind that EWPD will not always render Zff vertex corrections completely irrelevant for other observables. Meanwhile, accessibility to various directions of the SMEFT parameter space will rely more heavily on high energy behaviors of effective operators, rather than the anomalous couplings they induce. We have illustrated this point in the case of W pair production. The TGC three-parameter fit framework has been useful and convenient in past studies of SM deviations in such processes. But now it is time to go beyond this simplified parameterization, as the key assumption that additional new physics effects are well-constrained and negligible is already – and will continue to be – challenged by experimental progress at the high energy frontier. A consistent global SMEFT analysis should include not only anomalous TGCs, but all parameters whose effects are enhanced at high energy when fitting W pair data, so that the results can be interpreted more generally.

Chapter 6

Covariant Diagrams for One-Loop Matching

In this chapter, we present a diagrammatic formulation of recently-revived covariant functional approaches to one-loop matching from an ultraviolet (UV) theory to a low-energy effective field theory. Various terms following from a covariant derivative expansion (CDE) are represented by diagrams which, unlike conventional Feynman diagrams, involve gauge-covariant quantities and are thus dubbed “covariant diagrams.” The use of covariant diagrams helps organize and simplify one-loop matching calculations, which we illustrate with examples. Of particular interest is the derivation of UV model-independent universal results, which reduce matching calculations of specific UV models to applications of master formulas. We show how such derivation can be done in a more concise manner than the previous literature, and discuss how additional structures that are not directly captured by existing universal results, including mixed heavy-light loops, open covariant derivatives, and mixed statistics, can be easily accounted for.

6.1 Introduction

Matching from an ultraviolet (UV) theory to a low-energy effective field theory (EFT) beyond tree level has gained renewed interest in recent years. On the phenomenological side, one-loop matching is in many cases necessary for accurate translation of experimental constraints on the Standard Model (SM) EFT parameter space into those on specific new physics models. On the theoretical side, it is interesting to realize that matching calculations can be accomplished in more elegant and oftentimes simpler ways than using Feynman diagrams. For the latter aspect, the idea is to directly tackle the path integral, and identify and expand heavy fields’ contributions to the functional determinant arising at one-loop level to obtain

effective operators involving the light fields. Such functional approaches to matching have at least two important virtues:

- By performing a *covariant* derivative expansion (CDE), one can work with gauge-covariant quantities in all steps of the calculation, and thus automatically arrive at gauge-invariant effective operators in the end. This is unlike conventional Feynman diagram methods, where gauge-invariant final results are obtained only after putting together individual pieces which may not be separately gauge-invariant.
- The generality of such approaches has brought up the possibility of obtaining *universal* results. With general assumptions on the form of the UV theory, evaluation of the functional determinants involved proceeds in a model-independent way, which can thus be done once and for all. The result will be widely-applicable master formulas, from which matching calculations for specific models are reduced to matrix algebra.

The development and use of covariant functional approaches to matching dates back to the 1980s; see e.g. [216–218]. The subject was revived recently, thanks to the work [55] by Henning, Lu and Murayama (HLM). Following the CDE approach of Gaillard [216] and Cheyette [218], HLM presented in [55] a universal master formula for one-loop matching, assuming degenerate mass spectrum for the heavy particles. Applications of this master formula to various examples have been illustrated by HLM in [55], and also by others in [196–198]. The HLM master formula was generalized by Drozd, Ellis, Quevillon and You [56] to the case of nondegenerate heavy particle masses. The same Gaillard-Cheyette CDE approach is followed in [56], and the resulting master formula is dubbed the “Universal One-Loop Effective Action” (UOLEA), to emphasize the universality of the approach, as discussed in the second bullet point above. The UOLEA was applied to the example of integrating out nondegenerate stops in [56].

It was later pointed out, however, that the HLM/UOLEA master formulas, in their original forms at least, do not capture possible contributions from mixed heavy-light loops [219] (see also [220]). The reason can be most easily understood by noting that light fields are treated as background fields in [55, 56] and are thus not allowed to run in loops. Fixes to this problem were soon proposed, following different CDEs [57], or alternatively still within the UOLEA framework [58]. Although technically quite different, both approaches in [57] and [58] share a similar spirit, namely to include quantum fluctuations of light fields also, and then identify and subtract off nonlocal pieces from the functional determinant to obtain local effective operators. These studies provide, at the very least, a proof of principle that mixed heavy-light loops can be accounted for in covariant functional approaches to matching. This latter point was further corroborated recently in [59], following an alternative

CDE approach that builds upon [221, 222]. Compared with [57, 58], matching calculations are simplified in [59] partly due to the use of expansion by regions techniques [223–225], which allow local pieces of the functional determinant to be directly identified, so that no subtraction procedure is needed.

These recent developments of functional matching techniques are, unfortunately, also accompanied by different levels of technical complication compared with [55, 56]. It should be emphasized that the motivation for studying functional matching lies not only in theoretical curiosity, but also, at least equally importantly, in practical usefulness. In this latter respect, the goal is to develop a set of tools for matching that is easy to use even for those not necessarily familiar with all the technical subtleties of functional methods. There are at least two possibilities for achieving this goal:

- Ideally we wish to obtain a truly *universal* master formula, as an extension of the results presented in [55, 56]. Such an extension requires incorporation of not only mixed heavy-light contributions mentioned above [61], but also e.g. open covariant derivatives (covariant derivatives acting openly to the right as opposed to appearing in commutators) and mixed statistics (both bosonic and fermionic fields in the loop).
- Even if deriving such extended universal results turns out to be too involved to be completed very soon, we may still take advantage of the *covariant* feature of functional approaches, and consider alternatives to Feynman diagram methods that simplify calculations and offer useful intuition, even though on a case-by-case basis. This will also bring new options for more efficient automation of matching calculations¹.

It is the purpose of this chapter to present a tool that will be useful for making progress along both these lines. The idea is to have a diagrammatic formulation of one-loop functional matching which is as systematic as the conventional Feynman diagram approach, but differs crucially from the latter by preserving gauge covariance in intermediate steps. It is perhaps not surprising that this is possible, since recent studies of functional matching [57–59] all follow diagrammatic intuitions to some extent. We will show explicitly how to establish such a gauge-covariant diagrammatic formulation, building upon the approach of [59] (which we provide a more rigorous derivation of)², and how to use it in one-loop matching calculations. The diagrams introduced are dubbed “covariant diagrams” — they are in a sense gauge-covariant versions of Feynman diagrams. Just like Feynman diagrams, which keep track of terms in an expansion of correlation functions, covariant diagrams keep track of terms in

¹See e.g. [226] for recent progress on automation of Feynman diagrammatic matching.

²The approach of [55, 56] also allows for a diagrammatic formulation, which is however more complicated technically and will not be discussed further.

a CDE in functional matching. Let us clarify that enumerating and computing covariant diagrams is equivalent to selecting and evaluating various terms of interest that result from a CDE. But as we will see, it is both technically simpler and conceptually more intuitive than the latter, and meanwhile preserves the universality feature of functional matching procedures.

6.2 Gauge-covariant functional matching

The problem of matching can be formulated as follows: given an UV Lagrangian $\mathcal{L}_{\text{UV}}[\Phi, \phi]$ for a set of heavy fields Φ of masses $\{M_i\}$ and a set of light fields ϕ of masses $\{m_{i'}\} \ll \{M_i\}$,

$$\mathcal{L}_{\text{EFT}}[\phi] = ? \quad \text{s.t.} \quad \Gamma_{\text{L,UV}}[\phi_{\text{b}}] = \Gamma_{\text{EFT}}[\phi_{\text{b}}]. \quad (6.1)$$

Here $\Gamma_{\text{L,UV}}$ is the one-light-particle-irreducible (1LPI) effective action calculated in the UV theory, while Γ_{EFT} is the one-particle-irreducible (1PI) effective action (a.k.a. quantum action) calculated in the low-energy EFT. They will be computed as functionals of background fields ϕ_{b} by the standard procedures of the background field method (see e.g. [227, 228]). Eq. (6.1) ensures that the UV theory and the EFT give identical physical predictions regarding the light fields.

In this section, we shall focus on the simplest case of real scalar fields for illustration. The results derived below can be easily generalized to other types of fields.

6.2.1 Calculating $\Gamma_{\text{L,UV}}[\phi_{\text{b}}]$

To compute $\Gamma_{\text{L,UV}}[\phi_{\text{b}}]$, we start from the path integral,

$$Z_{\text{UV}}[J_{\Phi}, J_{\phi}] = \int [D\Phi][D\phi] e^{i \int d^d x (\mathcal{L}_{\text{UV}}[\Phi, \phi] + J_{\Phi} \Phi + J_{\phi} \phi)}, \quad (6.2)$$

and separate all fields contained in the heavy and light field multiplets into classical backgrounds (labeled by subscripts “b”) and quantum fluctuations (labeled by primes),

$$\Phi = \Phi_{\text{b}} + \Phi', \quad \phi = \phi_{\text{b}} + \phi'. \quad (6.3)$$

The background fields and sources are related by

$$0 = \frac{\delta \mathcal{L}_{\text{UV}}}{\delta \Phi}[\Phi_{\text{b}}, \phi_{\text{b}}] + J_{\Phi} = \frac{\delta \mathcal{L}_{\text{UV}}}{\delta \phi}[\Phi_{\text{b}}, \phi_{\text{b}}] + J_{\phi}. \quad (6.4)$$

The 1LPI effective action $\Gamma_{\text{L,UV}}[\phi_{\text{b}}]$ is obtained as the Legendre transform of the path integral with respect to the light fields,

$$\Gamma_{\text{L,UV}}[\phi_{\text{b}}] = -i \log Z_{\text{UV}}[J_{\Phi} = 0, J_{\phi}] - \int d^d x J_{\phi} \phi_{\text{b}}. \quad (6.5)$$

Note that J_{Φ} is set to zero because we are interested in correlation functions with no external sources of the heavy fields.

With the separation in Eq. (6.3), the UV theory Lagrangian plus source terms can be written as

$$\mathcal{L}_{\text{UV}}[\Phi, \phi] + J_{\Phi} \Phi + J_{\phi} \phi = \mathcal{L}_{\text{UV}}[\Phi_{\text{b}}, \phi_{\text{b}}] + J_{\Phi} \Phi_{\text{b}} + J_{\phi} \phi_{\text{b}} - \frac{1}{2} (\Phi'^T \phi'^T) \mathcal{Q}_{\text{UV}}[\Phi_{\text{b}}, \phi_{\text{b}}] \begin{pmatrix} \Phi' \\ \phi' \end{pmatrix} + \dots \quad (6.6)$$

where the quadratic operator

$$\mathcal{Q}_{\text{UV}}[\Phi_{\text{b}}, \phi_{\text{b}}] \equiv \begin{pmatrix} -\frac{\delta^2 \mathcal{L}_{\text{UV}}}{\delta \Phi^2}[\Phi_{\text{b}}, \phi_{\text{b}}] & -\frac{\delta^2 \mathcal{L}_{\text{UV}}}{\delta \Phi \delta \phi}[\Phi_{\text{b}}, \phi_{\text{b}}] \\ -\frac{\delta^2 \mathcal{L}_{\text{UV}}}{\delta \phi \delta \Phi}[\Phi_{\text{b}}, \phi_{\text{b}}] & -\frac{\delta^2 \mathcal{L}_{\text{UV}}}{\delta \phi^2}[\Phi_{\text{b}}, \phi_{\text{b}}] \end{pmatrix}. \quad (6.7)$$

Note that in Eq. (6.6), terms linear in ϕ' or Φ' vanish due to Eq. (6.4). We therefore obtain the tree-level result as the stationary point approximation,

$$\begin{aligned} Z_{\text{UV}}^{\text{tree}}[J_{\Phi}, J_{\phi}] &= \int [D\Phi][D\phi] e^{i \int d^d x (\mathcal{L}_{\text{UV}}[\Phi_{\text{b}}, \phi_{\text{b}}] + J_{\Phi} \Phi_{\text{b}} + J_{\phi} \phi_{\text{b}})} \propto e^{i \int d^d x (\mathcal{L}_{\text{UV}}[\Phi_{\text{c}}, \phi_{\text{c}}] + J_{\Phi} \Phi_{\text{c}} + J_{\phi} \phi_{\text{c}})} \\ \Rightarrow \Gamma_{\text{L,UV}}^{\text{tree}}[\phi_{\text{b}}] &= \int d^d x \mathcal{L}_{\text{UV}}[\Phi_{\text{c}}[\phi_{\text{b}}], \phi_{\text{b}}], \end{aligned} \quad (6.8)$$

up to an irrelevant constant term, where $\Phi_{\text{c}}[\phi_{\text{b}}]$ (subscript ‘‘c’’ for ‘‘classical’’) is defined by

$$\Phi_{\text{c}}[\phi_{\text{b}}] \equiv \Phi_{\text{b}}[J_{\Phi} = 0] \quad \text{i.e.} \quad \frac{\delta \mathcal{L}_{\text{UV}}}{\delta \Phi}[\Phi_{\text{c}}[\phi_{\text{b}}], \phi_{\text{b}}] \equiv \left. \frac{\delta \mathcal{L}_{\text{UV}}[\Phi, \phi]}{\delta \Phi} \right|_{\Phi = \Phi_{\text{c}}[\phi_{\text{b}}], \phi = \phi_{\text{b}}} = 0. \quad (6.9)$$

In other words, $\Phi_{\text{c}}[\phi_{\text{b}}]$ solves the classical equations of motion for the heavy fields when the light fields are treated as backgrounds.

Up to one-loop level, we have

$$\begin{aligned} Z_{\text{UV}}[J_{\Phi}, J_{\phi}] &\simeq Z_{\text{UV}}^{\text{tree}} \int [D\Phi'][D\phi'] \exp \left\{ -\frac{i}{2} \int d^d x (\Phi'^T \phi'^T) \mathcal{Q}_{\text{UV}}[\Phi_{\text{b}}, \phi_{\text{b}}] \begin{pmatrix} \Phi' \\ \phi' \end{pmatrix} \right\} \\ &\propto Z_{\text{UV}}^{\text{tree}} (\det \mathcal{Q}_{\text{UV}}[\Phi_{\text{b}}, \phi_{\text{b}}])^{-\frac{1}{2}} \end{aligned}$$

$$\Rightarrow \Gamma_{L,UV}^{1\text{-loop}}[\phi_b] = \frac{i}{2} \log \det \mathcal{Q}_{UV}[\Phi_c[\phi_b], \phi_b], \quad (6.10)$$

which is familiar from standard calculations of 1PI effective actions.

6.2.2 Calculating $\Gamma_{\text{EFT}}[\phi_b]$

On the EFT side, suppose

$$\mathcal{L}_{\text{EFT}}[\phi] = \mathcal{L}_{\text{EFT}}^{\text{tree}}[\phi] + \mathcal{L}_{\text{EFT}}^{1\text{-loop}}[\phi] + \dots \quad (6.11)$$

where $\mathcal{L}_{\text{EFT}}^{\text{tree}}$ and $\mathcal{L}_{\text{EFT}}^{1\text{-loop}}$ contain effective operators generated at tree and one-loop level, respectively. The path integral can be evaluated up to one-loop level,

$$\begin{aligned} Z_{\text{EFT}}[J_\phi] &= \int [D\phi] e^{i \int d^d x (\mathcal{L}_{\text{EFT}}[\phi] + J_\phi \phi)} \\ &\simeq e^{i \int d^d x (\mathcal{L}_{\text{EFT}}[\phi_b] + J_\phi \phi_b)} \int [D\phi'] e^{-\frac{i}{2} \int d^d x \phi'^T \mathcal{Q}_{\text{EFT}}^{\text{tree}}[\phi_b] \phi'} \\ &\propto e^{i \int d^d x (\mathcal{L}_{\text{EFT}}^{\text{tree}}[\phi_b] + \mathcal{L}_{\text{EFT}}^{1\text{-loop}}[\phi_b] + J_\phi \phi_b)} (\det \mathcal{Q}_{\text{EFT}}^{\text{tree}}[\phi_b])^{-\frac{1}{2}}, \end{aligned} \quad (6.12)$$

where the quadratic operator

$$\mathcal{Q}_{\text{EFT}}[\phi_b] \equiv -\frac{\delta^2 \mathcal{L}_{\text{EFT}}}{\delta \phi^2}[\phi_b]. \quad (6.13)$$

Again, in the exponent, terms linear in ϕ' vanish due to the relation

$$\frac{\delta \mathcal{L}_{\text{EFT}}}{\delta \phi}[\phi_b] + J_\phi = 0. \quad (6.14)$$

We therefore obtain the 1PI effective action in the EFT up to one-loop level,

$$\begin{aligned} \Gamma_{\text{EFT}}[\phi_b] &= -i \log Z_{\text{EFT}}[J_\phi] - \int d^d x J_\phi \phi_b \\ &\simeq \int d^d x \left(\mathcal{L}_{\text{EFT}}^{\text{tree}}[\phi_b] + \mathcal{L}_{\text{EFT}}^{1\text{-loop}}[\phi_b] \right) + \frac{i}{2} \log \det \mathcal{Q}_{\text{EFT}}^{\text{tree}}[\phi_b], \end{aligned} \quad (6.15)$$

$$\Rightarrow \Gamma_{\text{EFT}}^{\text{tree}}[\phi_b] = \int d^d x \mathcal{L}_{\text{EFT}}^{\text{tree}}[\phi_b], \quad (6.16)$$

$$\Gamma_{\text{EFT}}^{1\text{-loop}}[\phi_b] = \int d^d x \mathcal{L}_{\text{EFT}}^{1\text{-loop}}[\phi_b] + \frac{i}{2} \log \det \mathcal{Q}_{\text{EFT}}^{\text{tree}}[\phi_b]. \quad (6.17)$$

The meaning of the above equations is clear. The tree-level quantum action is given by the tree-level terms in the classical action, while at one-loop level, the quantum action contains

two pieces — one-loop-size effective operators used at tree level, and tree-level-size effective operators used at one-loop level.

6.2.3 Matching $\Gamma_{\text{L,UV}}[\phi_{\mathbf{b}}]$ and $\Gamma_{\text{EFT}}[\phi_{\mathbf{b}}]$

Equating Eqs. (6.8), (6.10) and Eqs. (6.16), (6.17), we obtain the EFT Lagrangian that satisfies the matching condition (6.1). At tree level,

$$\mathcal{L}_{\text{EFT}}^{\text{tree}}[\phi] = \mathcal{L}_{\text{UV}}[\Phi_{\mathbf{c}}[\phi], \phi] \rightarrow \mathcal{L}_{\text{UV}}[\hat{\Phi}_{\mathbf{c}}[\phi], \phi], \quad (6.18)$$

where $\hat{\Phi}_{\mathbf{c}}[\phi]$ is the local operator expansion of the nonlocal object $\Phi_{\mathbf{c}}[\phi]$. The extra step from $\Phi_{\mathbf{c}}[\phi]$ to $\hat{\Phi}_{\mathbf{c}}[\phi]$ is necessary so that $\mathcal{L}_{\text{EFT}}[\phi]$ consists of local operators. As a trivial example, suppose

$$\mathcal{L}_{\text{UV}}[\Phi, \phi] = \mathcal{L}_0[\phi] + \Phi^T F[\phi] - \frac{1}{2} \Phi^T (-P^2 + M^2) \Phi, \quad (6.19)$$

where $P_\mu \equiv iD_\mu$. The advantage of introducing this notation is that P_μ is a hermitian operator. $\Phi_{\mathbf{c}}[\phi]$ is obtained by solving the classical equation of motion [see Eq. (6.9)],

$$\frac{\delta \mathcal{L}_{\text{UV}}}{\delta \Phi} = F[\phi] - (-P^2 + M^2) \Phi = 0 \quad \Rightarrow \quad \Phi_{\mathbf{c}}[\phi] = \frac{1}{-P^2 + M^2} F[\phi]. \quad (6.20)$$

This is a nonlocal quantity due to the appearance of P^2 in the denominator. The corresponding local operator expansion, which should appear in the EFT, reads

$$\hat{\Phi}_{\mathbf{c}}[\phi] = \frac{1}{M^2} F[\phi] + \frac{1}{M^2} P^2 \frac{1}{M^2} F[\phi] + \dots \quad (6.21)$$

Moving on to one-loop level, we have

$$\int d^d x \mathcal{L}_{\text{EFT}}^{1\text{-loop}}[\phi] = \frac{i}{2} \log \det \mathcal{Q}_{\text{UV}}[\Phi_{\mathbf{c}}[\phi], \phi] - \frac{i}{2} \log \det \mathcal{Q}_{\text{EFT}}^{\text{tree}}[\phi]. \quad (6.22)$$

To proceed, we follow [59] and block-diagonalize \mathcal{Q}_{UV} . With the following short-hand notation for the elements of \mathcal{Q}_{UV} ,

$$\mathcal{Q}_{\text{UV}}[\Phi, \phi] = \begin{pmatrix} -\frac{\delta^2 \mathcal{L}_{\text{UV}}}{\delta \Phi^2}[\Phi, \phi] & -\frac{\delta^2 \mathcal{L}_{\text{UV}}}{\delta \Phi \delta \phi}[\Phi, \phi] \\ -\frac{\delta^2 \mathcal{L}_{\text{UV}}}{\delta \phi \delta \Phi}[\Phi, \phi] & -\frac{\delta^2 \mathcal{L}_{\text{UV}}}{\delta \phi^2}[\Phi, \phi] \end{pmatrix} \equiv \begin{pmatrix} \Delta_H[\Phi, \phi] & X_{HL}[\Phi, \phi] \\ X_{LH}[\Phi, \phi] & \Delta_L[\Phi, \phi] \end{pmatrix}, \quad (6.23)$$

it is easy to show that

$$V^\dagger \mathcal{Q}_{\text{UV}} V = \begin{pmatrix} \Delta_H - X_{HL} \Delta_L^{-1} X_{LH} & 0 \\ 0 & \Delta_L \end{pmatrix} \quad \text{with} \quad V = \begin{pmatrix} \mathbf{1} & 0 \\ -\Delta_L^{-1} X_{LH} & \mathbf{1} \end{pmatrix}. \quad (6.24)$$

Note that for real scalar fields, $X_{HL} = X_{LH}$ and both are hermitian. When generalized to complex fields, $X_{HL} = X_{LH}^\dagger$. With Eq. (6.24), the first term on the RHS of Eq. (6.22) becomes

$$\frac{i}{2} \log \det \mathcal{Q}_{\text{UV}}[\Phi_c[\phi], \phi] = \frac{i}{2} \log \det (\Delta_H - X_{HL} \Delta_L^{-1} X_{LH}) + \frac{i}{2} \log \det \Delta_L, \quad (6.25)$$

where the arguments $[\Phi_c[\phi], \phi] \rightarrow [\hat{\Phi}_c[\phi], \phi]$ have been dropped on the RHS for simplicity. Note that $\Phi_c[\phi]$ should be replaced by $\hat{\Phi}_c[\phi]$ to form local operators of the EFT.

Let us now look at the second term on the RHS of Eq. (6.22). With Eqs. (6.13) and (6.18), we have

$$\begin{aligned} \mathcal{Q}_{\text{EFT}}^{\text{tree}}[\phi] &= -\frac{\delta^2 \mathcal{L}_{\text{UV}}[\hat{\Phi}_c[\phi], \phi]}{\delta \phi^2} = -\frac{\delta}{\delta \phi} \left(\frac{\delta \mathcal{L}_{\text{UV}}}{\delta \phi} [\hat{\Phi}_c[\phi], \phi] + \frac{\delta \hat{\Phi}_c[\phi]}{\delta \phi} \frac{\delta \mathcal{L}_{\text{UV}}}{\delta \Phi} [\hat{\Phi}_c[\phi], \phi] \right) \\ &= -\frac{\delta}{\delta \phi} \left(\frac{\delta \mathcal{L}_{\text{UV}}}{\delta \phi} [\hat{\Phi}_c[\phi], \phi] \right) = -\frac{\delta^2 \mathcal{L}_{\text{UV}}}{\delta \phi^2} [\hat{\Phi}_c[\phi], \phi] - \frac{\delta \hat{\Phi}_c[\phi]}{\delta \phi} \frac{\delta^2 \mathcal{L}_{\text{UV}}}{\delta \Phi \delta \phi} [\hat{\Phi}_c[\phi], \phi] \\ &= \Delta_L [\hat{\Phi}_c[\phi], \phi] - X_{LH} \hat{\Delta}_H^{-1} X_{HL} [\hat{\Phi}_c[\phi], \phi]. \end{aligned} \quad (6.26)$$

When going from the first line to the second, we have used $\frac{\delta \mathcal{L}_{\text{UV}}}{\delta \Phi} [\hat{\Phi}_c[\phi], \phi] = \frac{\delta \mathcal{L}_{\text{UV}}}{\delta \Phi} [\Phi_c[\phi], \phi] = 0$ — this is true because the EoM can be solved order by order in $\frac{1}{M}$ to obtain a local operator expansion $\hat{\Phi}_c[\phi]$. To arrive at the last line of Eq. (6.26), note that

$$\begin{aligned} 0 &= \frac{\delta}{\delta \phi} \left(\frac{\delta \mathcal{L}_{\text{UV}}}{\delta \Phi} [\hat{\Phi}_c[\phi], \phi] \right) = \frac{\delta^2 \mathcal{L}_{\text{UV}}}{\delta \phi \delta \Phi} [\hat{\Phi}_c[\phi], \phi] + \frac{\delta \hat{\Phi}_c[\phi]}{\delta \phi} \frac{\delta^2 \mathcal{L}_{\text{UV}}}{\delta \Phi^2} [\hat{\Phi}_c[\phi], \phi] \\ &= -X_{LH} [\hat{\Phi}_c[\phi], \phi] - \frac{\delta \hat{\Phi}_c[\phi]}{\delta \phi} \Delta_H [\hat{\Phi}_c[\phi], \phi] \\ &\Rightarrow \frac{\delta \hat{\Phi}_c[\phi]}{\delta \phi} = -X_{LH} \Delta_H^{-1} [\hat{\Phi}_c[\phi], \phi] \rightarrow -X_{LH} \hat{\Delta}_H^{-1} [\hat{\Phi}_c[\phi], \phi], \end{aligned} \quad (6.27)$$

where $\hat{\Delta}_H^{-1}$ is the local operator expansion of Δ_H^{-1} . We therefore obtain

$$\begin{aligned} -\frac{i}{2} \log \det \mathcal{Q}_{\text{EFT}}^{\text{tree}}[\phi] &= -\frac{i}{2} \log \det (\Delta_L - X_{LH} \hat{\Delta}_H^{-1} X_{HL}) \\ &= -\frac{i}{2} \log \det \Delta_L - \frac{i}{2} \log \det (\mathbf{1} - \Delta_L^{-1} X_{LH} \hat{\Delta}_H^{-1} X_{HL}) \end{aligned}$$

$$\begin{aligned}
&= -\frac{i}{2} \log \det \Delta_L - \frac{i}{2} \log \det \left(\mathbf{1} - \hat{\Delta}_H^{-1} X_{HL} \Delta_L^{-1} X_{LH} \right) \\
&= -\frac{i}{2} \log \det \Delta_L + \frac{i}{2} \log \det \hat{\Delta}_H - \frac{i}{2} \log \det \left(\hat{\Delta}_H - X_{HL} \Delta_L^{-1} X_{LH} \right),
\end{aligned} \tag{6.28}$$

with the arguments $[\hat{\Phi}_c[\phi], \phi]$ implicit. Adding this equation to Eq. (6.25), we finally obtain, according to Eq. (6.22),

$$\begin{aligned}
\int d^d x \mathcal{L}_{\text{EFT}}^{\text{1-loop}}[\phi] &= \frac{i}{2} \left(\log \det (\Delta_H - X_{HL} \Delta_L^{-1} X_{LH}) - \log \det (\hat{\Delta}_H - X_{HL} \Delta_L^{-1} X_{LH}) \right) \\
&\quad + \frac{i}{2} \log \det \hat{\Delta}_H,
\end{aligned} \tag{6.29}$$

where again, the arguments $[\hat{\Phi}_c[\phi], \phi]$ are implicit. As expected, $\log \det \Delta_L$ which comes from pure light loops cancels between the two terms.

6.2.4 Hard vs. soft

The formula obtained above for one-loop matching using functional methods, Eq. (6.29), is quite abstract. To make use of it, a key observation, as emphasized in [59], is that with dimensional regularization (which we adopt, together with the $\overline{\text{MS}}$ scheme, throughout this chapter), each “log det” can be separated into “hard” and “soft” region contributions, namely

$$\log \det X = \log \det X|_{\text{hard}} + \log \det X|_{\text{soft}}. \tag{6.30}$$

What “hard” and “soft” mean is the following: for the “loop integrals” that appear in the computation of $\log \det X$, which involve heavy and light particle masses $\{M_i\}$, $\{m_{i'}\}$, and a “loop momentum” (i.e. integration variable) q ,

- the hard region contribution is obtained by first expanding the integrand for $|q^2| \sim M_i^2 \gg |m_{i'}^2|$, and then performing the integration over the *full* momentum space;
- the soft region contribution is obtained by first expanding the integrand for $|q^2| \sim |m_{i'}^2| \ll M_i^2$, and then performing the integration over the *full* momentum space.

The nontrivial identity (6.30) is known as the method of expansion by regions, which has been well-known in Feynman diagrammatic multi-loop calculations; see e.g. [223–225]. As a simple one-loop example, consider the following *IR- and UV-finite* integral (in $d = 4 - \epsilon$

dimensions):

$$\begin{aligned} \int \frac{d^d q}{(2\pi)^d} \frac{1}{(q^2 - M^2)(q^2 - m^2)^2} &= \frac{i}{16\pi^2} \left[\frac{1}{M^2 - m^2} \left(1 - \log \frac{M^2}{m^2} \right) - \frac{m^2}{(M^2 - m^2)^2} \log \frac{M^2}{m^2} \right] \\ &= \frac{i}{16\pi^2} \frac{1}{M^2} \left(1 - \log \frac{M^2}{m^2} \right) + \mathcal{O}(M^{-4}). \end{aligned} \quad (6.31)$$

The hard and soft regions yield *IR- and UV-divergent* integrals, respectively:

$$\begin{aligned} \int \frac{d^d q}{(2\pi)^d} \frac{1}{(q^2 - M^2)(q^2 - m^2)^2} \Big|_{\text{hard}} &= \int \frac{d^d q}{(2\pi)^d} \frac{1}{(q^2 - M^2)q^4} (1 + \dots) \\ &= \frac{i}{16\pi^2} \frac{1}{M^2} \left(\frac{2}{\epsilon} + 1 - \log \frac{M^2}{\mu^2} \right) + \mathcal{O}(M^{-4}), \end{aligned} \quad (6.32a)$$

$$\begin{aligned} \int \frac{d^d q}{(2\pi)^d} \frac{1}{(q^2 - M^2)(q^2 - m^2)^2} \Big|_{\text{soft}} &= \int \frac{d^d q}{(2\pi)^d} \left[-\frac{1}{M^2} \frac{1}{(q^2 - m^2)^2} + \dots \right] \\ &= \frac{i}{16\pi^2} \frac{1}{M^2} \left(-\frac{2}{\epsilon} + \log \frac{m^2}{\mu^2} \right) + \mathcal{O}(M^{-4}), \end{aligned} \quad (6.32b)$$

where $\frac{2}{\epsilon} \equiv \frac{2}{\epsilon} - \gamma + \log 4\pi$ with $\epsilon = 4 - d$. However, the $\frac{1}{\epsilon}$ singularities cancel when the two equations are added, and the finite result of the original integral is reproduced.

Now we can simplify Eq. (6.29). The crucial statements are

$$\log \det(\hat{\Delta}_H - X_{HL}\Delta_L^{-1}X_{LH}) = \log \det(\Delta_H - X_{HL}\Delta_L^{-1}X_{LH}) \Big|_{\text{soft}}, \quad (6.33a)$$

$$\log \det \hat{\Delta}_H = \log \det \Delta_H \Big|_{\text{soft}} = 0. \quad (6.33b)$$

It is not hard to understand that replacing Δ_H by $\hat{\Delta}_H$ singles out the soft part, because M_i dependence comes only from Δ_H , and a local operator expansion corresponds to the limit $M_i \rightarrow \infty$. On the other hand, $\log \det \Delta_H \Big|_{\text{soft}}$ vanishes because for pure heavy loops, expanding in the soft region gives rise to scaleless integrals. Combining Eqs. (6.29), (6.30) and (6.33), we finally arrive at the following formula,

$$\begin{aligned} \int d^d x \mathcal{L}_{\text{EFT}}^{1\text{-loop}}[\phi] &= \frac{i}{2} \log \det(\Delta_H - X_{HL}\Delta_L^{-1}X_{LH}) \Big|_{\text{hard}} \\ &= \frac{i}{2} \text{Tr} \log(\Delta_H - X_{HL}\Delta_L^{-1}X_{LH}) \Big|_{\text{hard}}. \end{aligned} \quad (6.34)$$

6.2.5 Evaluating the functional trace

The initial steps of evaluating the functional trace (6.34) are standard, which we reproduce here for the sake of completeness. Recall that entries of the infinite-dimensional matrix

$\Delta_H - X_{HL}\Delta_L^{-1}X_{LH}$, which we shall call Δ to simplify notation, are labeled by spacetime indices x (momentum indices q) when the UV theory Lagrangian is written in position (momentum) space, i.e. in terms of $\Phi(x)$, $\phi(x)$ ($\tilde{\Phi}(q)$, $\tilde{\phi}(q)$), plus possible internal indices. Δ contains x and $i\partial_x$ in position space, which become operators \hat{x} and \hat{p} in general. We evaluate its trace using the momentum eigenstate basis, and follow standard manipulations familiar from quantum mechanics,

$$\begin{aligned}
\text{Tr } \Delta(\hat{x}, \hat{p}) &= \int \frac{d^d q}{(2\pi)^d} \langle q | \text{tr } \Delta(\hat{x}, \hat{p}) | q \rangle = \int d^d x \int \frac{d^d q}{(2\pi)^d} \langle q | x \rangle \langle x | \text{tr } \Delta(\hat{x}, \hat{p}) | q \rangle \\
&= \int d^d x \int \frac{d^d q}{(2\pi)^d} e^{iq \cdot x} \text{tr } \Delta(x, i\partial_x) e^{-iq \cdot x} = \int d^d x \int \frac{d^d q}{(2\pi)^d} \text{tr } \Delta(x, i\partial_x + q) \\
&= \int d^d x \int \frac{d^d q}{(2\pi)^d} \text{tr } \Delta(x, i\partial_x - q), \tag{6.35}
\end{aligned}$$

where “tr” is over internal indices only, and we have used $\langle x | q \rangle = e^{-iq \cdot x}$. The last equality follows from a conventional change of integration variable $q \rightarrow -q$. As a result,

$$\mathcal{L}_{\text{EFT}}^{\text{1-loop}}[\phi] = \frac{i}{2} \int \frac{d^d q}{(2\pi)^d} \text{tr} \log(\Delta_H - X_{HL}\Delta_L^{-1}X_{LH})_{P \rightarrow P-q} \Big|_{\text{hard}}. \tag{6.36}$$

At this point, there is one additional transformation that can be made [55, 56, 216, 218], but is optional. The idea is to put all covariant derivatives P_μ into commutators, e.g. $[P_\mu, P_\nu]$, $[P_\mu, X(x)]$, by sandwiching the $\text{tr} \log$ between $e^{P \cdot \partial_q}$ and $e^{-P \cdot \partial_q}$ (which trivially become 1’s when acting on identities on both sides) and using the Baker-Campbell-Hausdorff (BCH) formula. This transformation is convenient in the sense that all intermediate steps from here on will involve P_μ ’s only through commutators, as does the final result³. But meanwhile, it makes the computation more tedious because of a plethora of terms resulting from applying the BCH formula. This is especially true when the quadratic operator \mathcal{Q}_{UV} contains open covariant derivatives, namely P_μ ’s acting openly to the right as opposed to appearing in commutators, in addition to those from kinetic terms. Another disadvantage is that with the introduction of ∂_q which does not commute with q , the logarithm cannot be expanded in a simple way due to the fact that $\log(AB) \neq \log A + \log B$ when $[A, B] \neq 0$ ⁴. As a way out, an auxiliary integral is introduced in [55, 56], which nevertheless complicates the integrations to be done. Therefore, we choose to follow [57, 59] and proceed without making this additional transformation.

³Recall that P_μ as an operator acts on everything to its right, so e.g. $iD_\mu \phi$ ’s in the final result for \mathcal{L}_{EFT} really mean $[P_\mu, \phi]$. On the other hand, gauge field strengths can be written as $[P_\mu, P_\nu]$ up to normalization.

⁴Recall that “tr” is over internal indices only, so $\text{tr} [\partial_q, f(q)] \neq 0$. Also, $\int \frac{d^d q}{(2\pi)^d} [\partial_q, f(q)] = \int \frac{d^d q}{(2\pi)^d} f'(q)$ may not vanish due to UV divergences.

6.2.6 Covariant derivative expansion (CDE)

The next step is to perform a CDE, i.e. to make an expansion in power series of P_μ while keeping P_μ intact (as opposed to separating it into $i\partial_\mu$ and gA_μ). Suppose, quite generally,

$$\Delta_H = -P^2 + M^2 + X_H, \quad (6.37)$$

where

$$M = \text{diag}(M_1, M_2, \dots) \quad (6.38)$$

is the mass matrix of the heavy field multiplet Φ ⁵. In general, X_H may take the form

$$X_H[\Phi, \phi, P_\mu] = U_H[\Phi, \phi] + P_\mu Z_H^\mu[\Phi, \phi] + Z_H^{\dagger\mu}[\Phi, \phi] P_\mu + P_\mu P_\nu Z_H^{\mu\nu}[\Phi, \phi] + Z_H^{\dagger\mu\nu}[\Phi, \phi] P_\nu P^\mu + \dots \quad (6.39)$$

In the hard region, the logarithm in Eq. (6.36) can be expanded as follows:

$$\begin{aligned} \log(\Delta_H - X_{HL}\Delta_L^{-1}X_{LH})_{P \rightarrow P-q} &= \log(-q^2 + M^2 + 2q \cdot P - P^2 + X_H - X_{HL}\Delta_L^{-1}X_{LH}) \\ &= \log(-q^2 + M^2) + \log\left[1 - (q^2 - M^2)^{-1}(2q \cdot P - P^2 + X_H - X_{HL}\Delta_L^{-1}X_{LH})\right] \\ &= \log(-q^2 + M^2) - \sum_{n=1}^{\infty} \frac{1}{n} \left[(q^2 - M^2)^{-1}(2q \cdot P - P^2 + X_H - X_{HL}\Delta_L^{-1}X_{LH})\right]^n, \end{aligned} \quad (6.40)$$

where the substitution $P \rightarrow P - q$ is assumed in X_H and $X_{HL}\Delta_L^{-1}X_{LH}$. Therefore, up to an additive constant,

$$\begin{aligned} \mathcal{L}_{\text{EFT}}^{\text{1-loop}}[\phi] &= -\frac{i}{2} \text{tr} \sum_{n=1}^{\infty} \frac{1}{n} \int \frac{d^d q}{(2\pi)^d} \left[(q^2 - M^2)^{-1} \right. \\ &\quad \left. (2q \cdot P - P^2 + X_H|_{P \rightarrow P-q} - X_{HL}\Delta_L^{-1}X_{LH}|_{P \rightarrow P-q}) \right]^n \Big|_{\text{hard}}. \end{aligned} \quad (6.41)$$

As before, $X_{H,HL,LH}$ and Δ_L have arguments $[\hat{\Phi}_c[\phi], \phi]$. Eq. (6.41) holds for the special case of real scalars but can be straightforwardly generalized. It will be our starting point for deriving a covariant diagrammatic formulation of one-loop matching in the next section.

⁵It is always possible to simultaneously diagonalize the P_μ and M matrices, since mass mixing can only happen among fields with identical gauge quantum numbers, as far as unbroken gauge symmetries are concerned. On the other hand, if the UV theory is written in the broken phase of a spontaneously broken gauge symmetry, there could also be mass mixing induced by spontaneous symmetry breaking. In that case, gauge fields associated with the broken symmetries would not appear in P_μ in the first place, so the diagonalization is still possible.

6.3 Covariant diagrams

6.3.1 Pure heavy loops

We first look at the simplest case, where the following three restrictions are satisfied:

- $X_{HL} = X_{LH} = 0$, i.e. no mixed heavy-light contributions to one-loop matching. This already covers a broad class of UV models where heavy fields do not couple linearly to light degrees of freedom and $\Phi_c = 0$.
- X_H does not contain open covariant derivatives, i.e. $X_H = U_H$; see Eq. (6.39).
- The field multiplet Φ contains only bosonic fields.

After developing the basics of covariant diagrams for this simplest case, we will lift the above restrictions one by one in the next three subsections.

For real scalars, we can directly use Eq. (6.41), which becomes, under the above restrictions,

$$\mathcal{L}_{\text{EFT}}^{1\text{-loop}}[\phi] = -\frac{i}{2} \text{tr} \sum_{n=1}^{\infty} \frac{1}{n} \int \frac{d^d q}{(2\pi)^d} \left[(q^2 - M^2)^{-1} (2q \cdot P - P^2 + U_H) \right]^n. \quad (6.42)$$

Note that, with no light masses involved, the hard part of the integral is trivially equal to the original integral. A key observation is that each term in the sum in Eq. (6.42) factorizes into a loop integral over q and a trace involving P_μ and U_H that gives rise to effective operators. The nonvanishing loop integrals involved have the generic form

$$\int \frac{d^d q}{(2\pi)^d} \frac{q^{\mu_1} \dots q^{\mu_{2n_c}}}{(q^2 - M_i^2)^{n_i} (q^2 - M_j^2)^{n_j} \dots} \equiv g^{\mu_1 \dots \mu_{2n_c}} \mathcal{I}[q^{2n_c}]_{ij\dots}^{n_i n_j \dots}, \quad (6.43)$$

where $g^{\mu_1 \dots \mu_{2n_c}}$ is the completely symmetric tensor, e.g. $g^{\mu\nu\rho\sigma} = g^{\mu\nu}g^{\rho\sigma} + g^{\mu\rho}g^{\nu\sigma} + g^{\mu\sigma}g^{\nu\rho}$. Eq. (6.43) defines the *master integrals* $\mathcal{I}[q^{2n_c}]_{ij\dots}^{n_i n_j \dots}$. We use the symbol “ \mathcal{I} ” to distinguish from the master integrals in [56] which are denoted by “ I ” and involve an extra auxiliary integral. Some useful master integrals are summarized in Appendix A.

Eq. (6.42) has a straightforward diagrammatic representation as a sum of one-loop diagrams with propagators $\frac{1}{q^2 - M^2}$ and vertex insertions $2q \cdot P$, $-P^2$ and U_H . The loop integral can be read off from a diagram simply by counting the numbers of propagators (for each species) and $2q \cdot P$ vertices. As a result of evaluating the loop integral as in Eq. (6.43), various terms in $g^{\mu_1 \dots \mu_{2n_c}}$ Lorentz-contract the P_μ 's from $2q \cdot P$ insertions in different ways, and all possibilities are summed over. We can keep track of such contractions by connecting

two $2q \cdot P$ vertices by a dotted line. The above procedure can be easily understood with an example,

$$\begin{array}{c} i \\ \circ \\ \vdots \\ \bullet \cdots \bullet \\ \vdots \\ \circ \\ j \end{array} = -\frac{i}{2} \frac{1}{2} \mathcal{I}[q^2]_{ij}^{22} \text{tr}((2P^\mu) U_{Hij} (2P_\mu) U_{Hji}), \quad (6.44)$$

where the diagram is read clockwise, and filled and empty circles represent $2q \cdot P$ and U_H insertions, respectively (recall that P_μ is diagonal in the field multiplet space and hence does not change the propagator label). Eq. (6.44) represents a term in the expansion (6.42). The only element in Eq. (6.44) which we have not discussed is the symmetry factor $\frac{1}{2}$, coming from $\frac{1}{n} = \frac{1}{4}$ (four propagators) multiplied by 2 (two identical contributions $\text{tr}((2P^\mu) U_{Hij} (2P_\mu) U_{Hji})$ and $\text{tr}(U_{Hij} (2P_\mu) U_{Hji} (2P^\mu))$). An easy way to find this symmetry factor is to note the \mathbb{Z}_2 symmetry of the diagram under rotation. It is not hard to show that in general, the presence of a \mathbb{Z}_S symmetry of a diagram under rotation indicates a symmetry factor $\frac{1}{S}$. We see that our diagrammatic formulation automatically collects terms from the CDE containing equivalent operator traces, and thus makes finding such factors a trivial task.

One can draw all possible diagrams like the one in Eq. (6.44) to keep track of all terms in the expansion (6.42) up to a certain order. These terms, which contain operator structures with open covariant derivatives, would eventually organize into independent operators with covariant derivatives appearing only in commutators (recall that the final result can always be written in a form that involves P_μ 's only via commutators). For example, we could enumerate all diagrams containing two P_μ 's and two U_H 's, which include the one in Eq. (6.44), a second diagram with adjacent P_μ contractions, and a third diagram with a $-P^2$ insertion. The latter two diagrams represent

$$-\frac{i}{2} \mathcal{I}[q^2]_{ij}^{31} \text{tr}((2P^\mu) (2P_\mu) U_{Hij} U_{Hji}) - \frac{i}{2} \mathcal{I}_{ij}^{21} \text{tr}((-P^2) U_{Hij} U_{Hji}), \quad (6.45)$$

with no symmetry factors. Here and in the following, we abbreviate $\mathcal{I}[q^0]_{ij\dots}^{n_i n_j \dots}$ as $\mathcal{I}_{ij\dots}^{n_i n_j \dots}$. Adding up the three terms in Eqs. (6.44) and (6.45), and making use of the identity $\mathcal{I}_{ij}^{21} = 2\mathcal{I}[q^2]_{ij}^{22} + 4\mathcal{I}[q^2]_{ij}^{31}$,⁶ we arrive at one single operator of the desired form (without open covariant derivatives),

$$\begin{aligned}
 & -i \left\{ \mathcal{I}[q^2]_{ij}^{22} \text{tr}(P^\mu U_{Hij} P_\mu U_{Hji}) + \left(2\mathcal{I}[q^2]_{ij}^{31} - \frac{1}{2} \mathcal{I}_{ij}^{21} \right) \text{tr}(P^2 U_{Hij} U_{Hji}) \right\} \\
 & = -i \mathcal{I}[q^2]_{ij}^{22} \text{tr}(P^\mu U_{Hij} P_\mu U_{Hji} - P^2 U_{Hij} U_{Hji})
 \end{aligned}$$

⁶This identity can be easily proved by writing $\mathcal{I}[q^2]_{ij}^{22} = \frac{1}{4}(\mathcal{I}_{ij}^{21} + M_j^2 \mathcal{I}_{ij}^{22})$, $\mathcal{I}[q^2]_{ij}^{31} = \frac{1}{4}(\mathcal{I}_{ij}^{21} + M_i^2 \mathcal{I}_{ij}^{31})$ and using the formulas in Appendix A.

$$\begin{aligned}
&= -\frac{i}{2} \mathcal{I}[q^2]_{ij}^{22} \text{tr}(2 P^\mu U_{H ij} P_\mu U_{H ji} - P^2 U_{H ij} U_{H ji} - P^2 U_{H ji} U_{H ij}) \\
&= -\frac{i}{2} \mathcal{I}[q^2]_{ij}^{22} \text{tr}([P^\mu, U_{H ij}][P_\mu, U_{H ji}]). \tag{6.46}
\end{aligned}$$

Alternatively, we could have anticipated the form of the final result before enumerating the diagrams — there is only one independent operator involving two P_μ 's and two U_H 's, namely $\text{tr}([P^\mu, U_H][P_\mu, U_H])$, so we know all relevant terms in the CDE must add up to

$$\begin{aligned}
&c_{ij} \text{tr}([P^\mu, U_{H ij}][P_\mu, U_{H ji}]) \\
&= 2c_{ij} \text{tr}(P^\mu U_{H ij} P_\mu U_{H ji}) - (c_{ij} + c_{ji}) \text{tr}(P^2 U_{H ij} U_{H ji}). \tag{6.47}
\end{aligned}$$

To determine the coefficient c_{ij} , it is actually not necessary to compute all three diagrams as we did above. Since the last two diagrams only contribute to the second term of Eq. (6.47), we could have obtained c_{ij} without computing them, simply by comparing Eq. (6.44) to the first term of Eq. (6.47). The result would be $c_{ij} = -\frac{i}{2} \mathcal{I}[q^2]_{ij}^{22}$, in agreement with Eq. (6.46).

In fact, it is generally true that to determine the coefficients of all independent effective operators in the final result, it is sufficient to compute just a subset of all possible diagrams. This is simply because when P_μ 's are involved, the number of independent structures one can write down with open covariant derivatives (two for the example above, $\text{tr}(P^\mu U_{H ij} P_\mu U_{H ji})$ and $\text{tr}(P^2 U_{H ij} U_{H ji})$) is greater than the number of independent operators with P_μ 's appearing only in commutators (only one, $\text{tr}([P^\mu, U_{H ij}][P_\mu, U_{H ji}])$). While we do not have an algorithm to determine, in full generality, the minimal set of diagrams to be computed, we have discovered a useful prescription that greatly reduces the workload: all diagrams with either $-P^2$ insertions or *adjacent* P_μ contractions, namely those that yield $\text{tr}(\dots P^2 \dots)$, can be dropped. In the example above, this prescription corresponds to not explicitly writing down and computing Eq. (6.45) which, as we have seen, only provides redundant information on c_{ij} . In fact, in many of the examples in Section 6.4, this prescription will reduce the diagrams to be computed to a minimal set, in the sense that we will have just enough information to determine all the operator coefficients in the final results.

The above discussion can also be applied to other types of bosonic fields. A complex scalar is equivalent to a multiplet of two real scalars, e.g. its real and imaginary parts. In practice it is often more convenient to use a multiplet consisting of the complex scalar itself and an appropriately-defined complex conjugate field. We will see explicitly how this is done in the next section. For vector bosons, with the addition of the R_ξ gauge fixing term, the

UV Lagrangian contains the following terms quadratic in the quantum fluctuations,

$$-\frac{1}{2} V_\alpha^{t a} \left\{ (-g^{\alpha\beta}) (-(P^2)_{ab} + M_V^2 \delta_{ab}) - \left(1 - \frac{1}{\xi}\right) (P^\alpha P^\beta)_{ab} + U_{H ab}^{\alpha\beta} \right\} V_\beta^{t b} \quad (6.48)$$

It is convenient to use the Feynman gauge $\xi = 1$, where Δ_H takes the form of Eq. (6.37) as in the scalar case, so that the same procedure of using covariant diagrams can be followed⁷. The only nontrivial extension is that vector boson fields carry Lorentz indices, which are regarded as additional internal indices and should be contracted with $-g_{\alpha\beta}$ (note minus sign!) when computing traces. This can be seen as follows,

$$\begin{aligned} \log\{(-g^{\alpha\beta})(-P^2 + M_V^2) + U_H^{\alpha\beta}\}_{P \rightarrow P-q} &= \log\{(-g^{\alpha\beta})(-q^2 + M_V^2 + 2q \cdot P - P^2) + U_H^{\alpha\beta}\} \\ &= \log\{(-g^{\alpha\gamma})(-q^2 + M_V^2)\} \\ &\quad + \log\{\delta_\gamma^\beta - (-g_{\gamma\delta})(q^2 - M_V^2)^{-1}((-g^{\delta\beta})(2q \cdot P - P^2) + U_H^{\delta\beta})\}, \end{aligned} \quad (6.49)$$

with internal indices a, b dropped for simplicity. As an example, when only vector fields are considered, the trace in Eq. (6.44) should be understood as

$$\begin{aligned} \text{tr}(P^\mu U_{H ij} P_\mu U_{H ji}) &= \\ &(-g_{\alpha_1 \beta_1})(-g_{\alpha_2 \beta_2})(-g_{\alpha_3 \beta_3})(-g_{\alpha_4 \beta_4}) \text{tr}((-g^{\beta_4 \alpha_1} P^\mu)(U_{H ij}^{\beta_1 \alpha_2})(-g^{\beta_2 \alpha_3} P_\mu)(U_{H ji}^{\beta_3 \alpha_4})), \end{aligned} \quad (6.50)$$

with all Lorentz indices written out explicitly. The “tr” in the second line of Eq. (6.50) then indicates a trace over the remaining internal indices.

A summary of the building blocks of covariant diagrams and the operator structures they represent in the restricted case discussed in this subsection can be found in Table 6.1 of Section 6.3.5.

6.3.2 Mixed heavy-light loops

Next, we allow $X_{HL, LH}$ to be nonzero, while still assuming the absence of open covariant derivatives. Specifically, we consider

$$X_{HL} = U_{HL}, \quad X_{LH} = U_{LH}, \quad (6.51a)$$

$$\Delta_L = -P^2 + m^2 + X_L = -P^2 + m^2 + U_L. \quad (6.51b)$$

⁷The associated Goldstone boson and ghost fields can also be treated in the same way as scalars, except that ghost loops come with a factor of (-1) due to the Grassmannian Gaussian integral.

where

$$m = \text{diag}(m_1, m_2, \dots) \quad (6.52)$$

is the mass matrix of the light field multiplet ϕ . The additional piece in Eq. (6.41) becomes

$$\begin{aligned} -X_{HL}\Delta_L^{-1}X_{LH}|_{P \rightarrow P-q} &= U_{HL}(q^2 - m^2 - 2q \cdot P + P^2 - U_L)^{-1}U_{LH} \\ &\rightarrow U_{HL} \sum_{n=0}^{\infty} \left[\frac{1}{q^2} (m^2 + 2q \cdot P - P^2 + U_L) \right]^n \frac{1}{q^2} U_{LH}. \end{aligned} \quad (6.53)$$

The expansion above is suitable in the hard region where $|q^2| \gg |m^2|$. Eq. (6.53) as a whole can be thought of as a new type of insertion in the heavy loop, in addition to $2q \cdot P$, $-P^2$, U_H considered in the previous subsection. Equivalently, the expansion of Eq. (6.53) instructs us to draw one-loop diagrams involving both heavy and light propagators which represent $\frac{1}{q^2 - M^2}$ and $\frac{1}{q^2}$, respectively. $2q \cdot P$, $-P^2$ and U_H can be inserted in heavy propagators as before, while $2q \cdot P$, $-P^2$, U_L and m^2 can be inserted in light propagators. U_{HL} (U_{LH}) connects an incoming heavy (light) propagator and an outgoing light (heavy) propagator, when the diagrams are read clockwise. Loop integrals now have the form

$$\int \frac{d^d q}{(2\pi)^d} \frac{q^{\mu_1} \dots q^{\mu_{2n_c}}}{(q^2 - M_i^2)^{n_i} (q^2 - M_j^2)^{n_j} \dots (q^2)^{n_L}} \equiv g^{\mu_1 \dots \mu_{2n_c}} \mathcal{I}[q^{2n_c}]_{ij \dots 0}^{n_i n_j \dots n_L}. \quad (6.54)$$

Eq. (6.54) defines an extended set of master integrals $\mathcal{I}[q^{2n_c}]_{ij \dots 0}^{n_i n_j \dots n_L}$, some of which are summarized in Appendix A. Note that these loop integrals do not depend on light particle masses because the latter are treated as vertex insertions. This implies, in particular, that in the case of massless particles, there is no need to keep m^2 nonzero as an IR regulator.

As a simple example, we show a mixed heavy-light version of Eq. (6.44),

$$\begin{aligned} \begin{array}{c} i \quad \circ \quad i' \\ \curvearrowright \quad \curvearrowleft \\ \bullet \quad \dots \quad \bullet \\ \curvearrowleft \quad \curvearrowright \\ i \quad \circ \quad i' \end{array} &= -\frac{i}{2} \mathcal{I}[q^2]_{i0}^{22} \text{tr}((2P^\mu) U_{HL}{}_{i\bar{i}'} (2P_\mu) U_{LH}{}_{\bar{i}'i}), \end{aligned} \quad (6.55)$$

where light propagators are represented by dashed lines, and labeled by primed indices. Note the absence of a nontrivial symmetry factor in this case. The additional building blocks of covariant diagrams discussed in this subsection are summarized in Table 6.2 of Section 6.3.5.

6.3.3 Open covariant derivatives

In addition to $U_{H,HL,LH,L}$ considered above, the $X_{H,HL,LH,L}$ matrices may also contain terms involving open covariant derivatives; see Eq. (6.39). These terms are slightly different from

the U terms because they are modified by the substitution $P \rightarrow P - q$. For example, terms in Eq. (6.39) with one open covariant derivative become

$$P_\mu Z_H^\mu + Z_H^{\dagger\mu} P_\mu \rightarrow P_\mu Z_H^\mu + Z_H^{\dagger\mu} P_\mu - q_\mu Z_H^\mu - Z_H^{\dagger\mu} q_\mu, \quad (6.56)$$

resulting in two types of vertex insertions: $P_\mu Z_H^\mu$ and $Z_H^{\dagger\mu} P_\mu$ are just like U insertions, while $-q_\mu Z_H^\mu$ and $-Z_H^{\dagger\mu} q_\mu$ are similar to $2q \cdot P$ insertions. In the latter case, the q_μ 's involved are part of the loop integral, which gives rise to $g^{\mu_1 \dots \mu_{2n_c}}$. Lorentz contractions are thus possible not only between P_μ 's from $2q \cdot P$ insertions, but also $Z_H^{(\dagger)\mu}$'s from $-q_\mu Z_H^\mu$, $-Z_H^{\dagger\mu} q_\mu$ insertions. We shall use the same symbol for the two types of $Z^{(\dagger)}$ insertions — they are distinguished by whether or not a contraction is indicated (by a dotted line as before). As a simple example,

$$\begin{array}{c} j \\ \circlearrowleft \\ \text{■} \quad \text{■} \\ \circlearrowright \\ i \end{array} = -\frac{i}{2} \mathcal{I}_{ij}^{11} \text{tr}(P_\mu Z_{Hij}^\mu Z_{Hji}^{\dagger\nu} P_\nu), \quad (6.57a)$$

$$\begin{array}{c} j \\ \circlearrowleft \\ \text{■} \cdots \text{■} \\ \circlearrowright \\ i \end{array} = -\frac{i}{2} \mathcal{I}[q^2]_{ij}^{11} \text{tr}(Z_{Hij}^\mu Z_{H\mu ji}^\dagger), \quad (6.57b)$$

where light and dark gray squares represent $(P_\mu)Z_H^\mu$ and $Z_H^{\dagger\mu}(P_\mu)$ insertions, respectively. Here and in the following, “[q^{2n_c}]” is dropped when writing master integrals with $n_c = 0$.

We have focused on pure heavy loops in the discussion above for concreteness, but there is no essential difference for mixed heavy-light loops, which may involve $Z_{HL,LH,L}^{(\dagger)}$. A summary of possible $Z^{(\dagger)}$ insertions (up to one-open-covariant-derivative terms) can be found in Table 6.3 of Section 6.3.5. Also, it is straightforward to extend the procedure to terms in the X matrices with more than one open covariant derivatives, though more complex notation may be needed to keep track of Lorentz contractions.

6.3.4 Loops with fermions

Up to now we have considered loops with bosonic fields only. Fermionic fields have a different form of quadratic operator \mathcal{Q}_{UV} , with e.g. $-\not{P} + M$ in the case of Dirac fermions in place of $-P^2 + M^2$. There are at least two approaches one can follow. One is to square the quadratic operator to match the general form in the bosonic case. To give an example for illustration, suppose

$$\mathcal{L}_{UV}[\Psi, \phi] = \mathcal{L}_0[\phi] + \bar{\Psi}(\not{P} - M - X_H[\phi])\Psi, \quad (6.58)$$

where ϕ denotes collectively light fields, and Ψ is a heavy Dirac fermion. We assume $X_H = X_{H,e} + X_{H,o}$ with $X_{H,e}$ ($X_{H,o}$) containing terms with even (odd) numbers of gamma matrices. There is no mixed heavy-light contribution to matching in this case, so

$$S_{\text{EFT}}^{1\text{-loop}} = -i \text{Tr} \log(\not{P} - M - X_H). \quad (6.59)$$

Note the different overall sign compared with bosonic case, due to the Grassmannian nature of the Ψ field. Using the fact that traces of gamma matrices are invariant under changing signs of all gamma matrices, we have

$$\begin{aligned} S_{\text{EFT}}^{1\text{-loop}} &= -\frac{i}{2} [\text{Tr} \log(\not{P} - M - X_{H,e} - X_{H,o}) + \text{Tr} \log(-\not{P} - M - X_{H,e} + X_{H,o})] \\ &= -\frac{i}{2} \text{Tr} \log(-\not{P}^2 + M^2 + 2MX_{H,e} + X_H(X_{H,e} - X_{H,o}) - [\not{P}, X_{H,e}] + \{\not{P}, X_{H,o}\}) \\ &= -\frac{i}{2} \text{Tr} \log(-P^2 + M^2 - \frac{i}{2}\sigma^{\mu\nu}G'_{\mu\nu} + 2MX_{H,e} \\ &\quad + X_H(X_{H,e} - X_{H,o}) - [\not{P}, X_{H,e}] + \{\not{P}, X_{H,o}\}), \end{aligned} \quad (6.60)$$

where $G'_{\mu\nu} = [D_\mu, D_\nu] = -igG_{\mu\nu}$ and $\sigma^{\mu\nu} = \frac{i}{2}[\gamma^\mu, \gamma^\nu]$. The calculation then proceeds as in the bosonic case, with $-\frac{i}{2}\sigma^{\mu\nu}G'_{\mu\nu} + 2MX_{H,e} + X_H(X_{H,e} - X_{H,o}) - [\not{P}, X_{H,e}] + \{\not{P}, X_{H,o}\}$ playing the role of X_H .

In this study, however, we follow an alternative strategy so as to derive a more straightforward diagrammatic formulation of one-loop functional matching. Still using the example above and, for the moment, further assuming $X_H = U_H$ does not contain open covariant derivatives for simplicity, we repeat the steps in Sections 6.2.5 and 6.2.6 *without* squaring the quadratic operator,

$$\begin{aligned} \mathcal{L}_{\text{EFT}}^{1\text{-loop}} &= -i \int \frac{d^d q}{(2\pi)^d} \text{tr} \log(\not{P} - \not{q} - M - U_H) \\ &= -i \int \frac{d^d q}{(2\pi)^d} \text{tr} \log(-\not{q} - M) - i \int \frac{d^d q}{(2\pi)^d} \text{tr} \log[1 - (-\not{q} - M)^{-1}(-\not{P} + U_H)] \\ &= \text{const.} + i \text{tr} \sum_{n=1}^{\infty} \frac{1}{n} \int \frac{d^d q}{(2\pi)^d} [(-\not{q} - M)^{-1}(-\not{P} + U_H)]^n. \end{aligned} \quad (6.61)$$

This is a fermionic version of Eq. (6.42), after the irrelevant constant term is dropped. The diagrammatic representation in this case involves fermionic propagators $(-\not{q} - M)^{-1}$ and vertex insertions $-\not{P}$ and U_H . The rules of drawing covariant diagrams and reading off their expressions are similar to the bosonic case, but we note the following three major differences:

- The prefactor has a different sign due to the fermionic Gaussian integral. It is conve-

nient to denote the prefactor by $-ic_s$, as is common in the literature. We have seen that for real bosonic degrees of freedom, $c_s = \frac{1}{2}$, while for Dirac fermions, $c_s = -1$. In any case, c_s can be easily seen from the Gaussian integral involved. For example, $c_s = -1$ for ghost fields, and $c_s = -\frac{1}{2}$ for Weyl fermions.

- Each fermionic propagator contains two terms,

$$(-\not{q} - M)^{-1} = \frac{-\not{q} + M}{q^2 - M^2} = \frac{M}{q^2 - M^2} + \frac{-q_\mu \gamma^\mu}{q^2 - M^2}. \quad (6.62)$$

The first term is just the bosonic propagator multiplied by M , while the second term involves q_μ in the numerator which modifies the loop integral compared with the bosonic case. The situation is the same as that of Eq. (6.56) in the previous subsection. We shall continue to use dotted lines to indicate contractions among Lorentz vectors associated with q_μ (in this case γ^μ). Our rule is to take the first or second term in Eq. (6.62) depending on whether the fermionic propagator is connected to a dotted line. To give an example,

$$\begin{array}{c} \text{Diagram: A circle with two empty circles at the top and bottom vertices.} \end{array} = i \frac{1}{2} \mathcal{I}_i^2 M^2 \text{tr} U_H^2, \quad (6.63a)$$

$$\begin{array}{c} \text{Diagram: A circle with two empty circles at the top and bottom vertices, and a horizontal dotted line across the middle.} \end{array} = i \frac{1}{2} \mathcal{I}[q^2]_i^2 \text{tr}((-\gamma^\mu)U_H(-\gamma_\mu)U_H), \quad (6.63b)$$

where $\frac{1}{2}$ is a symmetry factor, and it is understood that $M_i = M$ in the master integrals. As before, we have used empty circles for U_H insertions.

- Covariant derivative insertions are in the form of $-\not{P}$ which, unlike $2q \cdot P$, is q -independent and thus decouples from the loop integral. We shall continue to use filled circles to denote covariant derivative insertions in fermion propagators, but they should not be contracted (i.e. connected by dotted lines) with each other in this case.

With the new features discussed above taken into account, it is straightforward to generalize the procedures of the previous two subsections to incorporate mixed heavy-light loops and additional structures in the X matrices in the fermionic case. Mixed bosonic-fermionic loops can also be handled — the derivation in this case is actually very similar to that of mixed heavy-light loops. The sign of c_s is determined by the propagator from which one starts reading a diagram, with no ambiguity. For example, one may have $\text{tr}(\dots U_{BF} \dots U_{FB} \dots)$ or $\text{tr}(\dots U_{FB} \dots U_{BF} \dots)$, depending on whether one starts reading the diagram from a bosonic

Element of diagram	Symbol	Expression
heavy propagator (bosonic)	$\frac{i}{-}$	1
P insertion (bosonic, heavy)	$\frac{i}{-} \bullet \frac{j}{-}$ \vdots	$2P_\mu \delta_{ij}$
U insertion (heavy-heavy)	$\frac{i}{-} \circ \frac{j}{-}$	U_{Hij}

Table 6.1: (From [60]) Building blocks of covariant diagrams for integrating out heavy bosonic fields (and fermionic fields as well if one follows the approach of Eq. (6.60) to square their quadratic operator), in the absence of mixed heavy-light contributions and open covariant derivatives in the \mathbf{X} matrix, as derived in Section 6.3.1. All previous universal results in the literature [55, 56] can be easily reproduced by computing one-loop covariant diagrams built from these elements; see Section 6.4.1.

Element of diagram	Symbol	Expression
light propagator (bosonic)	$\frac{i'}{-}$	1
light mass insertion (bosonic)	$\frac{i'}{-} \times \frac{j'}{-}$	$m_{i'}^2 \delta_{i'j'}$
P insertion (bosonic, light)	$\frac{i'}{-} \bullet \frac{j'}{-}$ \vdots	$2P_\mu \delta_{i'j'}$
U insertion (heavy-light)	$\frac{i}{-} \circ \frac{j'}{-}$	$U_{HLij'}$
U insertion (light-heavy)	$\frac{i'}{-} \circ \frac{j}{-}$	$U_{LH i'j}$
U insertion (light-light)	$\frac{i'}{-} \circ \frac{j'}{-}$	$U_{L i'j'}$

Table 6.2: (From [60]) Additional building blocks of covariant diagrams in the presence of mixed heavy-light contributions to matching, as derived in Section 6.3.2. Example applications can be found in Sections 6.4.2, 6.4.3 and 6.4.5.

(B) or fermionic (F) propagator. The values of the two traces are opposite to each other, since U_{BF} and U_{FB} are fermionic and anticommuting (while all \dots 's are bosonic), so they give the same result when multiplied by opposite spin factors.

The new ingredients for building covariant diagrams involving Dirac fermions are summarized in Table 6.4 of Section 6.3.5. We further note that, as in the bosonic case discussed in Section 6.3.1, the prescription of dropping terms involving $\text{tr}(\dots P^\mu P_\mu \dots)$ can be adopted. These terms can arise, for example, when two fermionic propagators are contracted which are separated by two \not{P} insertions and one uncontracted fermionic propagator, provided that the loop integral is convergent — this is because $\gamma^\mu \not{P} \not{P} \gamma_\mu = 4P^2 + \mathcal{O}(\epsilon)$ where $\epsilon = 4 - d$.

6.3.5 Summary: recipe for one-loop matching

All derivations from Section 6.2 to Section 6.3.4 are done *once and for all*. Now we summarize the results obtained into a recipe that can be easily followed without repeating the derivations.

Element of diagram	Symbol	Expression
Z insertion (uncontracted, heavy-heavy)	$\frac{i \text{---} \square \text{---} j}{\text{---}}$	$P_\mu Z_H^\mu ij$
Z insertion (uncontracted, heavy-light)	$\frac{i \text{---} \square \text{---} j'}{\text{---}}$	$P_\mu Z_{HL}^\mu ij'$
Z insertion (uncontracted, light-heavy)	$\frac{i' \text{---} \square \text{---} j}{\text{---}}$	$P_\mu Z_{LH}^\mu i'j$
Z insertion (uncontracted, light-light)	$\frac{i' \text{---} \square \text{---} j'}{\text{---}}$	$P_\mu Z_L^\mu i'j'$
Z insertion (contracted, heavy-heavy)	$\frac{i \text{---} \square \text{---} j}{\vdots}$	$-Z_H^\mu ij$
Z insertion (contracted, heavy-light)	$\frac{i \text{---} \square \text{---} j'}{\vdots}$	$-Z_{HL}^\mu ij'$
Z insertion (contracted, light-heavy)	$\frac{i' \text{---} \square \text{---} j}{\vdots}$	$-Z_{LH}^\mu i'j$
Z insertion (contracted, light-light)	$\frac{i' \text{---} \square \text{---} j'}{\vdots}$	$-Z_L^\mu i'j'$
Z^\dagger insertion (uncontracted, heavy-heavy)	$\frac{i \text{---} \blacksquare \text{---} j}{\text{---}}$	$Z_H^{\dagger\mu} P_\mu ij$
Z^\dagger insertion (uncontracted, heavy-light)	$\frac{i \text{---} \blacksquare \text{---} j'}{\text{---}}$	$Z_{LH}^{\dagger\mu} P_\mu ij'$
Z^\dagger insertion (uncontracted, light-heavy)	$\frac{i' \text{---} \blacksquare \text{---} j}{\text{---}}$	$Z_{HL}^{\dagger\mu} P_\mu i'j$
Z^\dagger insertion (uncontracted, light-light)	$\frac{i' \text{---} \blacksquare \text{---} j'}{\text{---}}$	$Z_L^{\dagger\mu} P_\mu i'j'$
Z^\dagger insertion (contracted, heavy-heavy)	$\frac{i \text{---} \blacksquare \text{---} j}{\vdots}$	$-Z_H^{\dagger\mu} ij$
Z^\dagger insertion (contracted, heavy-light)	$\frac{i \text{---} \blacksquare \text{---} j'}{\vdots}$	$-Z_{LH}^{\dagger\mu} ij'$
Z^\dagger insertion (contracted, light-heavy)	$\frac{i' \text{---} \blacksquare \text{---} j}{\vdots}$	$-Z_{HL}^{\dagger\mu} i'j$
Z^\dagger insertion (contracted, light-light)	$\frac{i' \text{---} \blacksquare \text{---} j'}{\vdots}$	$-Z_L^{\dagger\mu} i'j'$

Table 6.3: (From [60]) Additional building blocks of covariant diagrams in the presence of open covariant derivatives in the \mathbf{X} matrix, as derived in Section 6.3.3, up to one-open-covariant-derivative terms $P_\mu \mathbf{Z}^\mu + \mathbf{Z}^{\dagger\mu} P_\mu$. Example applications can be found in Section 6.4.3.

Element of diagram	Symbol	Expression
heavy propagator (fermionic, uncontracted)	$\frac{i}{\text{---}}$	M_i
heavy propagator (fermionic, contracted)	$\frac{i}{\vdots}$	$-\gamma^\mu$
light propagator (fermionic)	$\frac{i'}{\text{---}}$	$-\gamma^\mu$
light mass insertion (fermionic)	$\frac{i' \text{---} \mathbf{x} \text{---} j'}{\text{---}}$	$m_{i'} \delta_{i'j'}$
P insertion (fermionic, heavy)	$\frac{i \text{---} \bullet \text{---} j}{\text{---}}$	$-\not{P} \delta_{ij}$
P insertion (fermionic, light)	$\frac{i' \text{---} \bullet \text{---} j'}{\text{---}}$	$-\not{P} \delta_{i'j'}$

Table 6.4: (From [60]) Additional building blocks of covariant diagrams when Dirac fermions are involved in matching, as derived in Section 6.3.4. These are used when the quadratic operator for fermionic fields is not squared like in Eq. (6.60). Example applications can be found in Sections 6.4.4 and 6.4.5.

Starting from an UV Lagrangian $\mathcal{L}_{\text{UV}}[\Phi, \phi]$ involving heavy fields Φ of masses $\{M_i\}$ and light fields ϕ of masses $\{m_{i'}\} \ll \{M_i\}$, the low-energy EFT can be obtained up to one loop level with the following procedure:

1. Solve the classical equation of motion $\frac{\delta \mathcal{L}_{\text{UV}}}{\delta \Phi} [\Phi_c[\phi], \phi] = 0$ for $\Phi_c[\phi]$ as an expansion of local operators⁸. The tree-level effective Lagrangian is given by $\mathcal{L}_{\text{EFT}}^{\text{tree}}[\phi] = \mathcal{L}_{\text{UV}}[\Phi_c[\phi], \phi]$.
2. Expand all fields about classical backgrounds, $\Phi = \Phi_b + \Phi'$, $\phi = \phi_b + \phi'$, and *extract the \mathbf{X} matrix* from terms in \mathcal{L}_{UV} that are quadratic in the quantum fluctuations,

$$\mathcal{L}_{\text{UV, quad.}} = -\frac{1}{2}(\Phi'^{\dagger}, \phi'^{\dagger}) (\mathbf{K} + \mathbf{X}[\Phi_b, \phi_b]) \begin{pmatrix} \Phi' \\ \phi' \end{pmatrix} \quad \text{with} \quad \mathbf{X} = \begin{pmatrix} X_H & X_{HL} \\ X_{LH} & X_L \end{pmatrix}, \quad (6.64)$$

where \mathbf{K} is the diagonal kinetic operator with elements $-P^2 + M_i^2$ ($-P^2 + m_{i'}^2$) for heavy (light) bosons and $-\not{P} + M_i$ ($-\not{P} + m_{i'}$) for heavy (light) fermions. Note that the notation $P_\mu \equiv iD_\mu$ is introduced, which is a hermitian operator. A field whose kinetic term has prefactor -1 rather than $-\frac{1}{2}$, such as a complex scalar or a Dirac fermion, is usually represented by two fields in the field multiplet (e.g. itself and its appropriately-defined conjugate), so that Eq. (6.64) still holds. For gauge boson fields, add gauge-fixing terms and use the Feynman gauge ($\xi = 1$). If the (hermitian) \mathbf{X} matrix contains open covariant derivatives (P_μ 's acting openly to the right instead of appearing in commutators), cast it in the following form,

$$\mathbf{X} = \mathbf{U} + P_\mu \mathbf{Z}^\mu + \mathbf{Z}^{\dagger\mu} P_\mu + \dots \quad (6.65)$$

with \mathbf{U} and \mathbf{Z} matrices containing no open covariant derivatives.

3. Draw one-loop diagrams consisting of *propagators* and *vertex insertions*. In the simplest case of pure heavy bosonic loops with no open covariant derivatives in \mathbf{X} (Section 6.3.1), only those listed in Table 6.1 are needed. Additional elements needed for mixed heavy-light loops (Section 6.3.2), open covariant derivatives (up to $P_\mu \mathbf{Z}^\mu + \mathbf{Z}^{\dagger\mu} P_\mu$ terms, Section 6.3.3), and loops with Dirac fermions (Section 6.3.4) are listed in Tables 6.2, 6.3 and 6.4, respectively. These will be sufficient for the example calculations that we show in the next section. In each diagram, at least one heavy propagator must be present, and dotted lines emanating from all “contracted” propagators and vertex insertions must be connected in pairs.

⁸From here on we omit the hat in $\hat{\Phi}_c[\phi]$ and simply write $\Phi_c[\phi]$. The distinction between the two was important in our derivation in Section 6.2, but will not be relevant in the rest of this chapter.

4. The value of a diagram is given by

$$-ic_s \frac{1}{S} \mathcal{I}[q^{2n_c}]_{ij\dots 0}^{n_i n_j \dots n_L} \text{tr } \mathcal{O}. \quad (6.66)$$

- $\frac{1}{S}$ is a *symmetry factor* that is present if the diagram has a \mathbb{Z}_S symmetry under rotation.
- n_i, n_j , etc., n_L and n_c are the numbers of heavy propagators of type i, j , etc., light propagators and (dotted) contraction lines, respectively. The *master integrals* are defined by

$$\int \frac{d^d q}{(2\pi)^d} \frac{q^{\mu_1} \dots q^{\mu_{2n_c}}}{(q^2 - M_i^2)^{n_i} (q^2 - M_j^2)^{n_j} \dots (q^2)^{n_L}} \equiv g^{\mu_1 \dots \mu_{2n_c}} \mathcal{I}[q^{2n_c}]_{ij\dots 0}^{n_i n_j \dots n_L}. \quad (6.67)$$

where $g^{\mu_1 \dots \mu_{2n_c}}$ is the completely symmetric tensor, e.g. $g^{\mu\nu\rho\sigma} = g^{\mu\nu}g^{\rho\sigma} + g^{\mu\rho}g^{\nu\sigma} + g^{\mu\sigma}g^{\nu\rho}$. These master integrals can be worked out and tabulated as in Appendix A. For simplicity, we will omit the argument “[q^{2n_c}]” when $n_c = 0$.

- The *operator structure* \mathcal{O} is obtained by starting from any propagator on the loop and reading off expressions of propagators and vertex insertions (see Tables 6.1-6.4) clockwise, with Lorentz indices contracted between elements connected by a dotted line.
- The *spin factor* c_s , discussed in the first bullet point below Eq. (6.61), is determined by the propagator one starts from when reading the diagram. There are no extra tricky minus signs as in conventional Feynman diagrams.

Note that in our formalism, no functional manipulations nor loop integrations are needed — one simply reads off the elements of a diagram and look up the tabulated master integrals.

5. Add up all diagrams with operator structures up to desired dimensionality (e.g. up to dimension six). For specific applications one may wish to study just a few effective operators rather than the entire effective Lagrangian. To determine which diagrams should be computed, write out the field content of various vertex insertions, and enumerate combinations of them that may give rise to the effective operators of interest (we will illustrate this procedure below, in Eqs. (6.94), (6.95), and Eqs. (6.102), (6.103)). Also, as discussed in Sections 6.3.1 and 6.3.4, diagrams giving rise to $\text{tr } \mathcal{O} = \text{tr}(\dots P^2 \dots)$ can be omitted. These include, e.g. those with contractions between adjacent bosonic P insertions, or (when the loop integral is convergent) between fermionic propagators

separated by two fermionic P insertions and one uncontracted fermionic heavy propagator. Also note that diagrams which are mirror images of each other are related by hermitian conjugation, so only one in such a pair needs to be explicitly computed.

6. The $\text{tr}(\dots P^2 \dots)$ terms omitted in the previous step can be recovered by requiring the operator structures obtained organize into gauge-invariant operator traces where P_μ 's only appear in commutators. However, instead of working out these extra terms explicitly, it is often easier in practice to first write down all independent operator traces expected in the final result, and then expand the commutators and match the result of the previous step to solve for their coefficients.
7. Finally, to obtain $\mathcal{L}_{\text{EFT}}^{1\text{-loop}}[\phi]$ for a specific $\mathcal{L}_{\text{UV}}[\Phi, \phi]$, evaluate the operator traces by plugging in specific forms of the \mathbf{U} and \mathbf{Z} matrices, with Φ set to $\Phi_c[\phi]$. The traces are over internal indices of the fields, including Lorentz indices carried by vector bosons which should be contracted using $-g_{\alpha\beta}$ as discussed in Section 6.3.1.

It should be emphasized that while the procedure above has been stated in the context of matching a specific UV theory to an EFT, Steps 3-6 are actually universal and independent of UV model details. The only assumption made about the UV Lagrangian is the (quite general) form of its quadratic terms (see Step 2). Therefore, *Steps 3-6 above also constitute a recipe for deriving universal results of one-loop matching.*

6.4 Examples

6.4.1 Universal One-Loop Effective Action (UOLEA) simplified

As a first application of the covariant diagrams techniques introduced in the previous section, we reproduce the Universal One-Loop Effective Action (UOLEA) reported in [56] (and [55] for the degenerate limit) with a simpler derivation. Recall that the UOLEA is a universal master formula for one-loop matching up to dimension six level in the absence of mixed heavy-light contributions and open covariant derivatives in the \mathbf{X} matrix. We will show that this master formula can be obtained as a *sum of covariant diagrams* easily built from the ingredients in Table 6.1.

We begin by writing down all independent operator traces involving P_μ and U_H which may contain terms with operator dimensions up to six,

$$\begin{aligned} \mathcal{L}_{\text{UOLEA}} = & -ic_s \text{tr} \left\{ f_2^i U_{ii} + f_3^i G_i^{\prime\mu\nu} G'_{\mu\nu,i} + f_4^{ij} U_{ij} U_{ji} \right. \\ & \left. + f_5^i [P^\mu, G'_{\mu\nu,i}] [P_\rho, G_i^{\prime\rho\nu}] + f_6^i G'^\mu_{\nu,i} G'^\nu_{\rho,i} G'^\rho_{\mu,i} \right\} \end{aligned}$$

$$\begin{aligned}
& + f_7^{ij} [P^\mu, U_{ij}][P_\mu, U_{ji}] + f_8^{ijk} U_{ij}U_{jk}U_{ki} + f_9^i U_{ii}G_i^{\prime\mu\nu}G'_{\mu\nu,i} \\
& + f_{10}^{ijkl} U_{ij}U_{jk}U_{kl}U_{li} + f_{11}^{ijk} U_{ij}[P^\mu, U_{jk}][P_\mu, U_{ki}] \\
& + f_{12}^{ij} [P^\mu, [P_\mu, U_{ij}]] [P^\nu, [P_\nu, U_{ji}]] + f_{13}^{ij} U_{ij}U_{ji}G_i^{\prime\mu\nu}G'_{\mu\nu,i} \\
& + f_{14}^{ij} [P^\mu, U_{ij}][P^\nu, U_{ji}]G'_{\nu\mu,i} + f_{15}^{ij} (U_{ij}[P^\mu, U_{ji}] - [P^\mu, U_{ij}]U_{ji})[P^\nu, G'_{\nu\mu,i}] \\
& + f_{16}^{ijklm} U_{ij}U_{jk}U_{kl}U_{lm}U_{mi} \\
& + f_{17}^{ijkl} U_{ij}U_{jk}[P^\mu, U_{kl}][P_\mu, U_{li}] + f_{18}^{ijkl} U_{ij}[P^\mu, U_{jk}]U_{kl}[P_\mu, U_{li}] \\
& + f_{19}^{ijklmn} U_{ij}U_{jk}U_{kl}U_{lm}U_{mn}U_{ni} \Big\}, \tag{6.68}
\end{aligned}$$

where $U \equiv U_H$ has operator dimension ≥ 1 , and $G'_{\mu\nu} \equiv -[P_\mu, P_\nu] = -igG_{\mu\nu}$. Note that $G'_{\mu\nu}$, like P_μ , is a diagonal matrix in the field multiplet space, and we use $G'_{\mu\nu,i}$ to denote its diagonal elements. We have adopted the notation in [56] for the *universal coefficients* f_N ($N = 2, \dots, 19$)⁹. In the following, we compute in turn terms in Eq. (6.68) with 0, 2, 4, 6 covariant derivatives, from which the universal coefficients can be extracted.

$\mathcal{O}(P^0)$ terms ($f_{2,4,8,10,16,19}$). Diagrams with no P insertions all share a similar structure, from which six universal coefficients can be derived, each in terms of a single master integral:

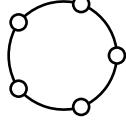
$$\begin{aligned}
\text{Diagram 1} & = -ic_s \mathcal{I}_i^1 \text{tr} U_{ii} \quad \Rightarrow \quad f_2^i = \mathcal{I}_i^1, \tag{6.69a}
\end{aligned}$$

$$\begin{aligned}
\text{Diagram 2} & = -ic_s \frac{1}{2} \mathcal{I}_{ij}^{11} \text{tr}(U_{ij}U_{ji}) \quad \Rightarrow \quad f_4^{ij} = \frac{1}{2} \mathcal{I}_{ij}^{11}, \tag{6.69b}
\end{aligned}$$

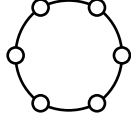
$$\begin{aligned}
\text{Diagram 3} & = -ic_s \frac{1}{3} \mathcal{I}_{ijk}^{111} \text{tr}(U_{ij}U_{jk}U_{ki}) \quad \Rightarrow \quad f_8^{ijk} = \frac{1}{3} \mathcal{I}_{ijk}^{111}, \tag{6.69c}
\end{aligned}$$

$$\begin{aligned}
\text{Diagram 4} & = -ic_s \frac{1}{4} \mathcal{I}_{ijkl}^{1111} \text{tr}(U_{ij}U_{jk}U_{kl}U_{li}) \quad \Rightarrow \quad f_{10}^{ijkl} = \frac{1}{4} \mathcal{I}_{ijkl}^{1111}, \tag{6.69d}
\end{aligned}$$

⁹Some redundancies in the parameterization in [56] have been removed here. In particular, the terms $f_{12,a}^{ij} [P^\mu, [P^\nu, U_{ij}]] [P_\mu, [P_\nu, U_{ji}]] + f_{12,b}^{ij} [P^\mu, [P^\nu, U_{ij}]] [P_\nu, [P_\mu, U_{ji}]]$ written out in [56] can be set to zero because $f_{12,a/b}^{ij} = -f_{12,a/b}^{ji}$ while the operator traces are symmetric in i, j . Also, $f_{15,a}^{ijk}$ and $f_{15,b}^{ijk}$ introduced in [56], which are associated with $U_{ij}[P^\mu, U_{jk}][P^\nu, G'_{\nu\mu,ki}]$ and $-[P^\mu, U_{ij}]U_{jk}[P^\nu, G'_{\nu\mu,ki}]$, respectively, are equal when $k = i$ (as dictated by $G'_{\mu\nu}$ being diagonal).



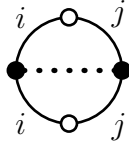
$$= -ic_s \frac{1}{5} \mathcal{I}_{ijklm}^{11111} \text{tr}(U_{ij}U_{jk}U_{kl}U_{lm}U_{mi}) \Rightarrow f_{16}^{ijklm} = \frac{1}{5} \mathcal{I}_{ijklm}^{11111}, \quad (6.69e)$$



$$= -ic_s \frac{1}{6} \mathcal{I}_{ijklmn}^{111111} \text{tr}(U_{ij}U_{jk}U_{kl}U_{lm}U_{mn}U_{ni}) \Rightarrow f_{19}^{ijklmn} = \frac{1}{6} \mathcal{I}_{ijklmn}^{111111}. \quad (6.69f)$$

We have omitted propagator labels i, j, \dots in the diagrams above for simplicity, which can be trivially restored. Note the symmetry factor $\frac{1}{S}$ with S being the number of U insertions.

$\mathcal{O}(P^2)$ terms ($f_{7,11,17,18}$). The two P insertions must be contracted with each other. To avoid adjacent contraction, at least two U insertions are needed:

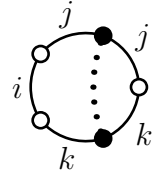


$$= -ic_s \frac{2^2}{2} \mathcal{I}[q^2]_{ij}^{22} \text{tr}(P^\mu U_{ij} P_\mu U_{ji}) \subset -ic_s \mathcal{I}[q^2]_{ij}^{22} \text{tr}([P^\mu, U_{ij}][P_\mu, U_{ji}])$$

$$\Rightarrow f_7^{ij} = \mathcal{I}[q^2]_{ij}^{22}. \quad (6.70)$$

This diagram was in fact already worked out in Eq. (6.44). The meaning of “ \subset ” is that with the addition of terms involving $\text{tr}(\dots P^2 \dots)$, the RHS can be obtained from the LHS; in other words, the RHS is the only independent gauge-invariant operator (or operator combination) with all P_μ 's appearing in commutators which can contain the structure on the LHS.

With three U insertions, still only a single diagram contributes:



$$= -ic_s 2^2 \mathcal{I}[q^2]_{ijk}^{122} \text{tr}(U_{ij} P^\mu U_{jk} P_\mu U_{ki}). \quad (6.71)$$

To derive the corresponding universal coefficient f_{11} in the UOLEA, note that

$$f_{11}^{ijk} \text{tr}(U_{ij}[P^\mu, U_{jk}][P_\mu, U_{ki}]) \supset f_{11}^{ijk} \text{tr}(U_{ij} P^\mu U_{jk} P_\mu U_{ki} + U_{jk} P^\mu U_{ki} P_\mu U_{ij} - U_{ki} P^\mu U_{ij} P_\mu U_{jk})$$

$$= (f_{11}^{ijk} + f_{11}^{kij} - f_{11}^{jki}) \text{tr}(U_{ij} P^\mu U_{jk} P_\mu U_{ki})$$

$$\Rightarrow f_{11}^{ijk} + f_{11}^{kij} - f_{11}^{jki} = 4 \mathcal{I}[q^2]_{ijk}^{122}, \quad (6.72)$$

which can be solved simply by permuting the indices $i \rightarrow j \rightarrow k$ and adding to the original equation. We thus obtain f_{11} in terms of two master integrals,

$$f_{11}^{ijk} = 2(\mathcal{I}[q^2]_{ijk}^{122} + \mathcal{I}[q^2]_{ijk}^{212}). \quad (6.73)$$

Finally, with four U insertions, there are two possible diagrams:

$$\begin{array}{c}
\begin{array}{c} j \\ \circ \\ i \circ \dots \circ k \\ \circ \\ l \end{array} \\
= -ic_s \frac{2^2}{2} \mathcal{I}[q^2]_{ijkl}^{2121} \text{tr}(P^\mu U_{ij} U_{jk} P_\mu U_{kl} U_{li}), \quad (6.74a)
\end{array}$$

$$\begin{array}{c}
\begin{array}{c} i \\ \circ \\ l \circ \dots \circ i \\ \circ \\ k \circ \dots \circ j \end{array} \\
= -ic_s 2^2 \mathcal{I}[q^2]_{ijkl}^{2211} \text{tr}(P^\mu U_{ij} P_\mu U_{jk} U_{kl} U_{li}). \quad (6.74b)
\end{array}$$

They organize into two independent operator traces, which we have chosen to be

$$\begin{aligned}
& f_{17}^{ijkl} \text{tr}(U_{ij} U_{jk} [P^\mu, U_{kl}] [P_\mu, U_{li}]) + f_{18}^{ijkl} \text{tr}(U_{ij} [P^\mu, U_{jk}] U_{kl} [P_\mu, U_{li}]) \\
\supset & (-f_{17}^{ijkl} + f_{18}^{ijkl} + f_{18}^{jkli}) \text{tr}(P^\mu U_{ij} U_{jk} P_\mu U_{kl} U_{li}) \\
& + (f_{17}^{klij} + f_{17}^{jkli} - f_{18}^{ijkl} - f_{18}^{klij}) \text{tr}(P^\mu U_{ij} P_\mu U_{jk} U_{kl} U_{li}). \quad (6.75)
\end{aligned}$$

We therefore obtain the following two equations,

$$-f_{17}^{ijkl} + f_{18}^{ijkl} + f_{18}^{jkli} = 2\mathcal{I}[q^2]_{ijkl}^{2121}, \quad f_{17}^{klij} + f_{17}^{jkli} - f_{18}^{ijkl} - f_{18}^{klij} = 4\mathcal{I}[q^2]_{ijkl}^{2211}. \quad (6.76)$$

which are solved by

$$f_{17}^{ijkl} = 2(\mathcal{I}[q^2]_{ijkl}^{2112} + \mathcal{I}[q^2]_{ijkl}^{1212} + \mathcal{I}[q^2]_{ijkl}^{1122}), \quad (6.77a)$$

$$\begin{aligned}
f_{18}^{ijkl} &= \mathcal{I}[q^2]_{ijkl}^{2121} + \mathcal{I}[q^2]_{ijkl}^{2112} + \mathcal{I}[q^2]_{ijkl}^{1221} + \mathcal{I}[q^2]_{ijkl}^{1212} + \mathcal{I}[q^2]_{ijkl}^{1122} - \mathcal{I}[q^2]_{ijkl}^{2211} \\
&\rightarrow \mathcal{I}[q^2]_{ijkl}^{2121} + \mathcal{I}[q^2]_{ijkl}^{2112} + \mathcal{I}[q^2]_{ijkl}^{1221} + \mathcal{I}[q^2]_{ijkl}^{1212}. \quad (6.77b)
\end{aligned}$$

We have dropped terms in f_{18}^{ijkl} that are antisymmetric under $ij \leftrightarrow kl$, since the associated operator trace is symmetric. We see that f_{17} and f_{18} together depend on only five master integrals.

$\mathcal{O}(P^4)$ terms ($f_{3,9,12,13,14,15}$). The four P insertions can be contracted among themselves without U insertions:

$$\begin{array}{c}
\begin{array}{c} \circ \\ \circ \\ \circ \\ \circ \end{array} \\
= -ic_s \frac{2^4}{4} \mathcal{I}[q^4]_i^4 \text{tr}(P^\mu P^\nu P_\mu P_\nu) \subset -ic_s 2 \mathcal{I}[q^4]_i^4 \text{tr}([P^\mu, P^\nu][P_\mu, P_\nu]) \\
\Rightarrow f_3^i = 2\mathcal{I}[q^4]_i^4. \quad (6.78)
\end{array}$$

Similarly, with one U insertion,

$$\begin{aligned}
\begin{array}{c} \bullet \\ \bullet \\ \bullet \\ \bullet \\ \bullet \\ \bullet \\ \bullet \\ \bullet \\ \bullet \\ \bullet \end{array} &= -ic_s 2^4 \mathcal{I}[q^4]_i^5 \text{tr}(U_{ii} P^\mu P^\nu P_\mu P_\nu) \subset -ic_s 8 \mathcal{I}[q^4]_i^5 \text{tr}(U_{ii} [P^\mu, P^\nu] [P_\mu, P_\nu]) \\
\Rightarrow f_9^i &= 8 \mathcal{I}[q^4]_i^5.
\end{aligned} \tag{6.79}$$

With two U insertions, four diagrams can be drawn:

$$\begin{array}{c} j \\ \bullet \\ \bullet \\ \bullet \\ \bullet \\ \bullet \\ \bullet \\ \bullet \\ \bullet \\ \bullet \\ i \end{array} = -ic_s 2^4 \mathcal{I}[q^4]_{ij}^{51} \text{tr}(P^\mu P^\nu P_\mu P_\nu U_{ij} U_{ji}), \tag{6.80a}$$

$$\begin{array}{c} i \\ \bullet \\ \bullet \\ \bullet \\ \bullet \\ \bullet \\ \bullet \\ \bullet \\ \bullet \\ \bullet \\ j \end{array} = -ic_s 2^4 \mathcal{I}[q^4]_{ij}^{42} \text{tr}(P^\mu P^\nu P_\mu U_{ij} P_\nu U_{ji}), \tag{6.80b}$$

$$\begin{array}{c} i \\ \bullet \\ \bullet \\ \bullet \\ \bullet \\ \bullet \\ \bullet \\ \bullet \\ \bullet \\ \bullet \\ j \end{array} = -ic_s \frac{2^4}{2} \mathcal{I}[q^4]_{ij}^{33} \text{tr}(P^\mu P^\nu U_{ij} P_\mu P_\nu U_{ji}), \tag{6.80c}$$

$$\begin{array}{c} i \\ \bullet \\ \bullet \\ \bullet \\ \bullet \\ \bullet \\ \bullet \\ \bullet \\ \bullet \\ \bullet \\ j \end{array} = -ic_s \frac{2^4}{2} \mathcal{I}[q^4]_{ij}^{33} \text{tr}(P^\mu P^\nu U_{ij} P_\nu P_\mu U_{ji}). \tag{6.80d}$$

These terms are contained in four independent operator traces, which we have chosen to be

$$\begin{aligned}
& f_{12}^{ij} \text{tr}([P^\mu, [P_\mu, U_{ij}]] [P^\nu, [P_\nu, U_{ji}]]) + f_{13}^{ij} \text{tr}(U_{ij} U_{ji} [P^\mu, P^\nu] [P_\mu, P_\nu]) \\
& + f_{14}^{ij} \text{tr}([P^\mu, U_{ij}] [P^\nu, U_{ji}] [P_\mu, P_\nu]) + f_{15}^{ij} \text{tr}((U_{ij} [P^\mu, U_{ji}] - [P^\mu, U_{ij}] U_{ji}) [P^\nu, [P_\mu, P_\nu]]) \\
\supset & (2f_{13}^{ij} - f_{14}^{ij} - 4f_{15}^{ij}) \text{tr}(P^\mu P^\nu P_\mu P_\nu U_{ij} U_{ji}) + (2f_{14}^{ij} + 4f_{15}^{ij}) \text{tr}(P^\mu P^\nu P_\mu U_{ij} P_\nu U_{ji}) \\
& - f_{14}^{ij} \text{tr}(P^\mu P^\nu U_{ij} P_\mu P_\nu U_{ji}) + (4f_{12}^{ij} + f_{14}^{ij}) \text{tr}(P^\mu P^\nu U_{ij} P_\nu P_\mu U_{ji}).
\end{aligned} \tag{6.81}$$

Solving the set of four equations,

$$\begin{aligned}
2f_{13}^{ij} - f_{14}^{ij} - 4f_{15}^{ij} &= 16 \mathcal{I}[q^4]_{ij}^{51}, & 2f_{14}^{ij} + 4f_{15}^{ij} &= 16 \mathcal{I}[q^4]_{ij}^{42}, \\
-f_{14}^{ij} &= 8 \mathcal{I}[q^4]_{ij}^{33}, & 4f_{12}^{ij} + f_{14}^{ij} &= 8 \mathcal{I}[q^4]_{ij}^{33},
\end{aligned} \tag{6.82}$$

we obtain the four universal coefficients $f_{12,13,14,15}$ in terms of just three master integrals:

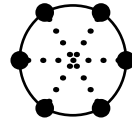
$$f_{12}^{ij} = 4\mathcal{I}[q^4]_{ij}^{33}, \quad (6.83a)$$

$$f_{13}^{ij} = 4(\mathcal{I}[q^4]_{ij}^{33} + 2\mathcal{I}[q^4]_{ij}^{42} + 2\mathcal{I}[q^4]_{ij}^{51}), \quad (6.83b)$$

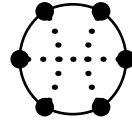
$$f_{14}^{ij} = -8\mathcal{I}[q^4]_{ij}^{33}, \quad (6.83c)$$

$$f_{15}^{ij} = 4(\mathcal{I}[q^4]_{ij}^{33} + \mathcal{I}[q^4]_{ij}^{42}). \quad (6.83d)$$

$\mathcal{O}(P^6)$ terms ($f_{5,6}$). Only pure gauge pieces are of interest here, since P^6 already has operator dimension six. There are two diagrams contributing, which differ by Lorentz contraction:



$$= -ic_s \frac{2^6}{6} \mathcal{I}[q^6]_i^6 \text{tr}(P^\mu P^\nu P^\rho P_\mu P_\nu P_\rho), \quad (6.84a)$$



$$= -ic_s \frac{2^6}{2} \mathcal{I}[q^6]_i^6 \text{tr}(P^\mu P^\nu P^\rho P_\nu P_\mu P_\rho). \quad (6.84b)$$

They follow from two independent operators, which are chosen as

$$\begin{aligned} & f_5^i \text{tr}([P^\mu, [P_\mu, P_\nu]] [P_\rho, [P^\rho, P^\nu]]) - f_6^i \text{tr}([P_\mu, P^\nu][P_\nu, P^\rho][P_\rho, P^\mu]) \\ \supset & f_6^i \text{tr}(P^\mu P^\nu P^\rho P_\mu P_\nu P_\rho) + (4f_5^i - 3f_6^i) \text{tr}(P^\mu P^\nu P^\rho P_\nu P_\mu P_\rho). \end{aligned} \quad (6.85)$$

As a result, we have

$$f_6^i = \frac{32}{3} \mathcal{I}[q^6]_i^6, \quad 4f_5^i - 3f_6^i = 32 \mathcal{I}[q^6]_i^6, \quad (6.86)$$

which yield

$$f_5^i = 16 \mathcal{I}[q^6]_i^6, \quad f_6^i = \frac{32}{3} \mathcal{I}[q^6]_i^6. \quad (6.87)$$

We summarize the results of the four paragraphs above in Table 6.5. Complete agreement is found between our explicit expressions of the universal coefficients in terms of heavy particle masses (listed in Appendix B) and those reported in [56], upon proper symmetrizations allowed by symmetries of operator traces under exchanging particle labels (e.g. our f_8^{ijk} is equal to $\frac{1}{3}(f_8^{ijk} + f_8^{jki} + f_8^{kij})$ in [56]). Note, however, that we have obtained the universal coefficients in terms of much fewer master integrals, and many of their explicit expressions are also simpler than those in [56].

Universal coefficient	Operator	Diagram(s)
$f_2^i = \mathcal{I}_i^1$	U_{ii}	Eq. (6.69a)
$f_3^i = 2 \mathcal{I}[q^4]_i^4$	$G_i^{\prime\mu\nu} G'_{\mu\nu,i}$	Eq. (6.78)
$f_4^{ij} = \frac{1}{2} \mathcal{I}_{ij}^{11}$	$U_{ij} U_{ji}$	Eq. (6.69b)
$f_5^i = 16 \mathcal{I}[q^6]_i^6$	$[P^\mu, G'_{\mu\nu,i}][P_\rho, G_i^{\prime\rho\nu}]$	Eq. (6.84)
$f_6^i = \frac{32}{3} \mathcal{I}[q^6]_i^6$	$G_{\nu,i}^{\prime\mu} G'_{\rho,i}{}^{\nu} G_{\mu,i}^{\prime\rho}$	
$f_7^{ij} = \mathcal{I}[q^2]_{ij}^{22}$	$[P^\mu, U_{ij}][P_\mu, U_{ji}]$	Eq. (6.70)
$f_8^{ijk} = \frac{1}{3} \mathcal{I}_{ijk}^{111}$	$U_{ij} U_{jk} U_{ki}$	Eq. (6.69c)
$f_9^i = 8 \mathcal{I}[q^4]_i^5$	$U_{ii} G_i^{\prime\mu\nu} G'_{\mu\nu,i}$	Eq. (6.79)
$f_{10}^{ijkl} = \frac{1}{4} \mathcal{I}_{ijkl}^{1111}$	$U_{ij} U_{jk} U_{kl} U_{li}$	Eq. (6.69d)
$f_{11}^{ijk} = 2(\mathcal{I}[q^2]_{ijk}^{122} + \mathcal{I}[q^2]_{ijk}^{212})$	$U_{ij}[P^\mu, U_{jk}][P_\mu, U_{ki}]$	Eq. (6.71)
$f_{12}^{ij} = 4 \mathcal{I}[q^4]_{ij}^{33}$	$[P^\mu, [P_\mu, U_{ij}]] [P^\nu, [P_\nu, U_{ji}]]$	Eq. (6.80)
$f_{13}^{ij} = 4(\mathcal{I}[q^4]_{ij}^{33} + 2 \mathcal{I}[q^4]_{ij}^{42} + 2 \mathcal{I}[q^4]_{ij}^{51})$	$U_{ij} U_{ji} G_i^{\prime\mu\nu} G'_{\mu\nu,i}$	
$f_{14}^{ij} = -8 \mathcal{I}[q^4]_{ij}^{33}$	$[P^\mu, U_{ij}][P^\nu, U_{ji}] G'_{\nu\mu,i}$	
$f_{15}^{ij} = 4(\mathcal{I}[q^4]_{ij}^{33} + \mathcal{I}[q^4]_{ij}^{42})$	$(U_{ij}[P^\mu, U_{ji}] - [P^\mu, U_{ij}]U_{ji}) [P^\nu, G'_{\nu\mu,i}]$	
$f_{16}^{ijklm} = \frac{1}{5} \mathcal{I}_{ijklm}^{11111}$	$U_{ij} U_{jk} U_{kl} U_{lm} U_{mi}$	
$f_{17}^{ijkl} = 2(\mathcal{I}[q^2]_{ijkl}^{2112} + \mathcal{I}[q^2]_{ijkl}^{1212} + \mathcal{I}[q^2]_{ijkl}^{1122})$	$U_{ij} U_{jk} [P^\mu, U_{kl}][P_\mu, U_{li}]$	Eq. (6.74)
$f_{18}^{ijkl} = \mathcal{I}[q^2]_{ijkl}^{2121} + \mathcal{I}[q^2]_{ijkl}^{2112} + \mathcal{I}[q^2]_{ijkl}^{1221} + \mathcal{I}[q^2]_{ijkl}^{1212}$	$U_{ij}[P^\mu, U_{jk}]U_{kl}[P_\mu, U_{li}]$	
$f_{19}^{ijklmn} = \frac{1}{6} \mathcal{I}_{ijklmn}^{111111}$	$U_{ij} U_{jk} U_{kl} U_{lm} U_{mn} U_{ni}$	Eq. (6.69f)

Table 6.5: (From [60]) List of universal coefficients in terms of the master integrals defined in Eq. (6.67) (Column 1). The UOLEA master formula for one-loop matching reported in [56] is reproduced by adding up traces of the operators in Column 2 with the corresponding universal coefficients, and multiplying the overall factor $-ic_s$; see Eq. (6.68). The covariant diagrams used to compute each universal coefficient are listed in Column 3. See Appendix B for expressions of the universal coefficients in terms of heavy particle masses.

6.4.2 Integrating out a scalar triplet: the scalar sector

We next consider more specific examples where additional ingredients in Tables 6.2, 6.3 and 6.4 are involved in covariant diagrams. Our goal is to demonstrate the techniques, instead of deriving complete universal master formulas. The latter task has been initiated in [61], and will be completed in future publications.

As a standard test case, a simple extension of the SM by a heavy electroweak scalar triplet was used in several recent papers [57–59] to illustrate various functional approaches to mixed heavy-light matching at work. The scalar sector of the model is given by

$$\begin{aligned} \mathcal{L}_{\text{UV}} \supset & |D_\mu \phi|^2 - m^2 |\phi|^2 - \lambda |\phi|^4 + \frac{1}{2} (D_\mu \Phi^a)^2 - \frac{1}{2} M^2 \Phi^a \Phi^a - \frac{1}{4} \lambda_\Phi (\Phi^a \Phi^a)^2 \\ & + \kappa \phi^\dagger \sigma^a \phi \Phi^a - \eta |\phi|^2 \Phi^a \Phi^a, \end{aligned} \quad (6.88)$$

where Φ is a heavy $SU(2)_L$ triplet with zero hypercharge, and ϕ is the light SM Higgs doublet with mass squared $m^2 < 0$. We shall focus on the following subset of dimension-six effective operators¹⁰ generated by integrating out Φ ,

$$\mathcal{O}_T = \frac{1}{2} (\phi^\dagger \overleftrightarrow{D}_\mu \phi)^2, \quad \mathcal{O}_H = \frac{1}{2} (\partial_\mu |\phi|^2)^2, \quad \mathcal{O}_R = |\phi|^2 |D_\mu \phi|^2, \quad (6.89)$$

where $\phi^\dagger \overleftrightarrow{D}_\mu \phi = \phi^\dagger (D_\mu \phi) - (D_\mu \phi^\dagger) \phi$. Pure heavy contributions to the operator coefficients can be easily obtained by applying the degenerate limit of the UOLEA, which is illustrated in [55]. We will thus be interested in computing mixed heavy-light contributions. We first reproduce, in the present subsection, the results in [57, 58] for terms independent of the SM gauge couplings. Terms that depend on the SM gauge couplings, which involve treatment of open covariant derivatives and were not obtained in [57, 58], will be computed in the next subsection.

To begin with, we solve for $\Phi_c[\phi]$ up to the order needed [counting κ as $\mathcal{O}(M)$],

$$\Phi_c^a[\phi] = \frac{\kappa}{M^2} \phi^\dagger \sigma^a \phi - \frac{\kappa}{M^4} \left[2\eta |\phi|^2 (\phi^\dagger \sigma^a \phi) + D^2 (\phi^\dagger \sigma^a \phi) \right] + \mathcal{O}(M^{-5}), \quad (6.90)$$

and extract the \mathbf{U} matrix from the quadratic terms of Eq. (6.88),

$$\mathcal{L}_{\text{UV, quad.}} \supset -\frac{1}{2} (\Phi'^a \ \phi'^\dagger \ \tilde{\phi}'^\dagger) (-P^2 + \mathbf{M}^2 + \mathbf{U}[\Phi_b, \phi_b, \tilde{\phi}_b]) \begin{pmatrix} \Phi'^b \\ \phi' \\ \tilde{\phi}' \end{pmatrix}, \quad (6.91)$$

¹⁰We will not make any field or parameter redefinitions unless otherwise specified, so that the operator coefficients are unambiguous.

where

$$\mathbf{M}^2 = \text{diag}(M^2 \delta^{ab}, m^2, m^2), \quad (6.92)$$

$$\mathbf{U} = \begin{pmatrix} U_H & (U_{HL})_{1 \times 2} \\ (U_{LH})_{2 \times 1} & (U_L)_{2 \times 2} \end{pmatrix} = \begin{pmatrix} U_{\Phi}^{ab} & (U_{\phi\Phi}^{\dagger a})_{1 \times 2} \\ (U_{\phi\Phi}^b)_{2 \times 1} & (U_{\phi})_{2 \times 2} \end{pmatrix}. \quad (6.93)$$

The internal index “*b*” (italicized) should not be confused with the subscript label “b” (for background). The components of the \mathbf{U} matrix, with Φ set to $\Phi_c[\phi]$, read

$$U_{\Phi}^{ab} = 2\eta |\phi|^2 \delta^{ab} + \lambda_{\Phi} (\Phi_c^d \Phi_c^d \delta^{ab} + 2 \Phi_c^a \Phi_c^b) \sim \mathcal{O}(\phi^2, \phi^4, P^2 \phi^4, \dots), \quad (6.94a)$$

$$U_{\phi\Phi}^b = \begin{pmatrix} -\kappa \sigma^b \phi + 2\eta \phi \Phi_c^b \\ \kappa \sigma^b \tilde{\phi} + 2\eta \tilde{\phi} \Phi_c^b \end{pmatrix} \sim \mathcal{O}(\phi, \phi^3, P^2 \phi^3, \dots), \quad (6.94b)$$

$$U_{\phi} = \begin{pmatrix} 2\lambda (|\phi|^2 \mathbf{1}_2 + \phi \phi^{\dagger}) - \kappa \Phi_c^d \sigma^d + \eta \Phi_c^d \Phi_c^d \mathbf{1}_2 & 2\lambda \phi \tilde{\phi}^{\dagger} \\ 2\lambda \tilde{\phi} \phi^{\dagger} & 2\lambda (|\phi|^2 \mathbf{1}_2 + \tilde{\phi} \tilde{\phi}^{\dagger}) + \kappa \Phi_c^d \sigma^d + \eta \Phi_c^d \Phi_c^d \mathbf{1}_2 \end{pmatrix} \\ \sim \mathcal{O}(\phi^2, \phi^4, P^2 \phi^2, P^2 \phi^4, \dots). \quad (6.94c)$$

Note that the two real components of the complex scalar ϕ should be written out separately in the field multiplet. In practice, it is convenient to use ϕ and $\tilde{\phi} \equiv i\sigma^2 \phi^*$, since $\tilde{\phi}$ transforms in the same way as ϕ under $SU(2)_L$.

From Eq. (6.94) it is clear that to obtain mixed heavy-light contributions to the operators $\mathcal{O}_T, \mathcal{O}_H, \mathcal{O}_R$ in Eq. (6.89), all of which contain four ϕ 's and two covariant derivatives, we need to compute one-loop covariant diagrams that are proportional to

$$U_{HL}U_{LH}, U_{HL}U_LU_{LH}, P^2U_{HL}U_{LH}, P^2U_{HL}U_{LH}U_H, P^2U_{HL}U_LU_{LH}, P^2(U_{HL}U_{LH})^2. \quad (6.95)$$

Using the rules in Tables 6.1 and 6.2, we have (with $M_i = M$ in the master integrals from here on)

$$\begin{array}{c} \text{---} \circ \text{---} \text{---} \circ \text{---} \\ \text{---} \text{---} \text{---} \end{array} = -ic_s \mathcal{I}_{i0}^{11} \text{tr}(U_{HL}U_{LH}), \quad (6.96a)$$

$$\begin{array}{c} \text{---} \circ \text{---} \text{---} \circ \text{---} \\ \text{---} \text{---} \text{---} \end{array} = -ic_s \mathcal{I}_{i0}^{12} \text{tr}(U_{HL}U_LU_{LH}), \quad (6.96b)$$

$$= -ic_s 2^2 \mathcal{I}[q^2]_{i0}^{22} \text{tr}(P^\mu U_{HL} P_\mu U_{LH}) \subset -ic_s 2 \mathcal{I}[q^2]_{i0}^{22} \text{tr}([P^\mu, U_{HL}][P_\mu, U_{LH}]),$$

(6.96c)

$$= -ic_s 2^2 \{ \mathcal{I}[q^2]_{i0}^{41} \text{tr}(P_\mu U_{HL} U_{LH} P^\mu U_H) \\ + \mathcal{I}[q^2]_{i0}^{32} \text{tr}(P^\mu U_H U_{HL} P_\mu U_{LH} + P^\mu U_{HL} P_\mu U_{LH} U_H) \}$$

$$\subset -ic_s \{ 4 \mathcal{I}[q^2]_{i0}^{32} \text{tr}([P^\mu, U_{HL}][P_\mu, U_{LH}] U_H) \\ + 2 (\mathcal{I}[q^2]_{i0}^{41} + \mathcal{I}[q^2]_{i0}^{32}) \text{tr}([P^\mu, U_{HL} U_{LH}][P_\mu, U_H]) \},$$

(6.96d)

$$= -ic_s 2^2 \{ \mathcal{I}[q^2]_{i0}^{14} \text{tr}(P_\mu U_{LH} U_{HL} P^\mu U_L) \\ + \mathcal{I}[q^2]_{i0}^{23} \text{tr}(P^\mu U_L U_{LH} P_\mu U_{HL} + P^\mu U_{LH} P_\mu U_{HL} U_L) \}$$

$$\subset -ic_s \{ 4 \mathcal{I}[q^2]_{i0}^{23} \text{tr}([P^\mu, U_{LH}][P_\mu, U_{HL}] U_L) \\ + 2 (\mathcal{I}[q^2]_{i0}^{14} + \mathcal{I}[q^2]_{i0}^{23}) \text{tr}([P^\mu, U_{LH} U_{HL}][P_\mu, U_L]) \},$$

(6.96e)

$$= -ic_s 2^2 \left\{ \frac{1}{2} \mathcal{I}[q^2]_{i0}^{42} \text{tr}(P^\mu U_{HL} U_{LH} P_\mu U_{HL} U_{LH}) + \frac{1}{2} \mathcal{I}[q^2]_{i0}^{24} \text{tr}(P^\mu U_{LH} U_{HL} P_\mu U_{LH} U_{HL}) \right. \\ \left. + \mathcal{I}[q^2]_{i0}^{33} \text{tr}(P^\mu U_{HL} P_\mu U_{LH} U_{HL} U_{LH} + P^\mu U_{LH} P_\mu U_{HL} U_{LH} U_{HL}) \right\}$$

$$\subset -ic_s \{ (2 \mathcal{I}[q^2]_{i0}^{24} + 4 \mathcal{I}[q^2]_{i0}^{33}) \text{tr}([P^\mu, U_{HL}][P_\mu, U_{LH}] U_{HL} U_{LH}) \\ + (2 \mathcal{I}[q^2]_{i0}^{42} + 4 \mathcal{I}[q^2]_{i0}^{33}) \text{tr}([P^\mu, U_{LH}][P_\mu, U_{HL}] U_{LH} U_{HL}) \\ + (\mathcal{I}[q^2]_{i0}^{42} + \mathcal{I}[q^2]_{i0}^{24} + 2 \mathcal{I}[q^2]_{i0}^{33}) \\ \text{tr}([P^\mu, U_{HL}] U_{LH} [P_\mu, U_{HL}] U_{LH} + U_{HL} [P^\mu, U_{LH}] U_{HL} [P_\mu, U_{LH}]) \}.$$

(6.96f)

Note that diagrams with m^2 insertions are of higher order and therefore not considered. The results in the equations above are summarized in Table 6.6, where explicit expressions for the coefficients and operators are also worked out. Summing up all terms in the table, we

obtain (with $c_s = \frac{1}{2}$ and μ set to M)

$$\begin{aligned} \mathcal{L}_{\text{EFT}}^{\text{1-loop}}[\phi] \supset & \frac{1}{16\pi^2} \frac{3\kappa^2}{2M^2} |D_\mu \phi|^2 + \frac{1}{16\pi^2} \frac{\kappa^2}{M^4} \left[\left(\frac{\kappa^2}{2M^2} - 8\eta + 3\lambda \right) \mathcal{O}_T \right. \\ & \left. + \left(-\frac{9\kappa^2}{2M^2} - 6\eta + 10\lambda \right) \mathcal{O}_H + \left(-\frac{21\kappa^2}{2M^2} - 21\eta + 25\lambda \right) \mathcal{O}_R \right], \end{aligned} \quad (6.97)$$

in agreement with [57, 58, 219]¹¹.

Two comments are in order:

- The calculation above parallels that in [58]. In particular, it is the same calculation in the “Operator” column of Table 6.6 that is done in [58]; the coefficients part, however, follows from a more straightforward computation here than in [58].
- While the calculation in this subsection was done in the context of the scalar triplet model, most of the results obtained are universal. In fact, the only model-dependent part is the expression after each “ \rightarrow ” in the “Operator” column of Table 6.6. In this respect, Eq. (6.96) constitutes part of the derivation of a master formula for mixed heavy-light matching (with degenerate heavy particle masses), which we plan to complete in future work.

6.4.3 Integrating out a scalar triplet: the gauge sector

Now we move on to the gauge sector of the scalar triplet model. To account for mixed heavy-light contributions to one-loop matching that involve SM gauge interactions, we need to extend the field multiplet to include the electroweak gauge bosons. The relevant quadratic pieces of the UV theory Lagrangian then read

$$\mathcal{L}_{\text{UV, quad.}} \supset -\frac{1}{2} (\Phi'^a \ \phi'^\dagger \ \tilde{\phi}'^\dagger \ W'_\alpha{}^a \ B'_\alpha) (-P^2 + \mathbf{M}^2 + \mathbf{U} + P_\mu \mathbf{Z}^\mu + \mathbf{Z}^{\dagger\mu} P_\mu) \begin{pmatrix} \Phi'^b \\ \phi' \\ \tilde{\phi}' \\ W'_\beta{}^b \\ B'_\beta \end{pmatrix}, \quad (6.98)$$

¹¹There is an additional contribution to $\mathcal{L}_{\text{EFT}}^{\text{1-loop}}[\phi]$ from $\mathcal{L}_{\text{EFT}}^{\text{tree}}[\phi] \supset \frac{\kappa^2}{M^4} (\mathcal{O}_T + 2\mathcal{O}_R) \rightarrow (1 - \frac{1}{16\pi^2} \frac{3\kappa^2}{M^2}) \frac{\kappa^2}{M^4} (\mathcal{O}_T + 2\mathcal{O}_R)$ if one rescales the SM Higgs field $\phi \rightarrow (1 - \frac{1}{16\pi^2} \frac{3\kappa^2}{4M^2}) \phi$ to render its kinetic term canonically normalized.

Coefficient	Operator
$-ic_s \mathcal{I}_{i0}^{11} = \frac{c_s}{16\pi^2} (1 - \log \frac{M^2}{\mu^2})$	$\text{tr}(U_{HL}U_{LH})$ $\rightarrow U_{\phi\Phi}^{\dagger a} U_{\phi\Phi}^a \supset -\frac{16\kappa^2\eta}{M^4} (\mathcal{O}_T + 2\mathcal{O}_R)$
$-ic_s \mathcal{I}_{i0}^{12} = \frac{c_s}{16\pi^2} \frac{1}{M^2} (1 - \log \frac{M^2}{\mu^2})$	$\text{tr}(U_{HL}U_LU_{LH})$ $\rightarrow U_{\phi\Phi}^{\dagger a} U_{\phi} U_{\phi\Phi}^a \supset \frac{4\kappa^4}{M^4} (\mathcal{O}_T + 2\mathcal{O}_R)$
$-ic_s 2 \mathcal{I}[q^2]_{i0}^{22} = \frac{c_s}{16\pi^2} (-\frac{1}{2M^2})$	$\text{tr}([P^\mu, U_{HL}][P_\mu, U_{LH}])$ $\rightarrow [P^\mu, U_{\phi\Phi}^{\dagger a}][P_\mu, U_{\phi\Phi}^a]$ $\supset -6\kappa^2 D_\mu\phi ^2 + \frac{8\kappa^2\eta}{M^2} (\mathcal{O}_H + \mathcal{O}_R)$
$-ic_s 4 \mathcal{I}[q^2]_{i0}^{32} = \frac{c_s}{16\pi^2} \frac{1}{2M^4}$	$\text{tr}([P^\mu, U_{HL}][P_\mu, U_{LH}]U_H)$ $\rightarrow [P^\mu, U_{\phi\Phi}^{\dagger a}][P_\mu, U_{\phi\Phi}^b]U_{\Phi}^{ba} \supset -12\kappa^2\eta\mathcal{O}_R$
$-ic_s 2 (\mathcal{I}[q^2]_{i0}^{41} + \mathcal{I}[q^2]_{i0}^{32}) = \frac{c_s}{16\pi^2} \frac{1}{3M^4}$	$\text{tr}([P^\mu, U_{HL}U_{LH}][P_\mu, U_H])$ $\rightarrow [P^\mu, U_{\phi\Phi}^{\dagger a}U_{\phi\Phi}^b][P_\mu, U_{\Phi}^{ba}] \supset -24\kappa^2\eta\mathcal{O}_H$
$-ic_s 4 \mathcal{I}[q^2]_{i0}^{23} = \frac{c_s}{16\pi^2} \frac{1}{M^4} (-\frac{5}{2} + \log \frac{M^2}{\mu^2})$	$\text{tr}([P^\mu, U_{LH}][P_\mu, U_{HL}]U_L)$ $\rightarrow [P^\mu, U_{\phi\Phi}^a][P_\mu, U_{\phi\Phi}^{\dagger a}]U_{\phi}$ $\supset 2\kappa^2 [(\frac{\kappa^2}{M^2} - 2\lambda)\mathcal{O}_T - \frac{\kappa^2}{M^2}\mathcal{O}_H$ $\quad + (\frac{\kappa^2}{M^2} - 10\lambda)\mathcal{O}_R]$
$-ic_s 2 (\mathcal{I}[q^2]_{i0}^{14} + \mathcal{I}[q^2]_{i0}^{23}) = \frac{c_s}{16\pi^2} (-\frac{1}{2M^4})$	$\text{tr}([P^\mu, U_{LH}U_{HL}][P_\mu, U_L])$ $\rightarrow [P^\mu, U_{\phi\Phi}^a U_{\phi\Phi}^{\dagger a}][P_\mu, U_{\phi}]$ $\supset 4\kappa^2 [(-\frac{\kappa^2}{M^2} + 2\lambda)\mathcal{O}_T$ $\quad - 10\lambda\mathcal{O}_H - \frac{2\kappa^2}{M^2}\mathcal{O}_R]$
$-ic_s (2 \mathcal{I}[q^2]_{i0}^{24} + 4 \mathcal{I}[q^2]_{i0}^{33}) = \frac{c_s}{16\pi^2} \frac{1}{M^6}$	$\text{tr}([P^\mu, U_{HL}][P_\mu, U_{LH}]U_{HL}U_{LH})$ $\rightarrow [P^\mu, U_{\phi\Phi}^{\dagger a}][P_\mu, U_{\phi\Phi}^b]U_{\phi\Phi}^{\dagger b}U_{\phi\Phi}^a \supset -12\kappa^4\mathcal{O}_R$
$-ic_s (2 \mathcal{I}[q^2]_{i0}^{42} + 4 \mathcal{I}[q^2]_{i0}^{33}) = \frac{c_s}{16\pi^2} \frac{1}{M^6} (\frac{17}{6} - \log \frac{M^2}{\mu^2})$	$\text{tr}([P^\mu, U_{LH}][P_\mu, U_{HL}]U_{LH}U_{HL})$ $\rightarrow [P^\mu, U_{\phi\Phi}^a][P_\mu, U_{\phi\Phi}^{\dagger a}]U_{\phi\Phi}^b U_{\phi\Phi}^{\dagger b}$ $\supset -2\kappa^4 (\mathcal{O}_H + 4\mathcal{O}_R)$
$-ic_s (\mathcal{I}[q^2]_{i0}^{42} + \mathcal{I}[q^2]_{i0}^{24} + 2 \mathcal{I}[q^2]_{i0}^{33}) = \frac{c_s}{16\pi^2} \frac{5}{12M^6}$	$\text{tr}([P^\mu, U_{HL}]U_{LH}[P_\mu, U_{HL}]U_{LH}$ $\quad + U_{HL}[P^\mu, U_{LH}]U_{HL}[P_\mu, U_{LH}])$ $\rightarrow [P^\mu, U_{\phi\Phi}^{\dagger a}]U_{\phi\Phi}^b [P_\mu, U_{\phi\Phi}^{\dagger b}]U_{\phi\Phi}^a$ $\quad + U_{\phi\Phi}^{\dagger a} [P^\mu, U_{\phi\Phi}^b]U_{\phi\Phi}^{\dagger b} [P_\mu, U_{\phi\Phi}^a]$ $\supset 4\kappa^4 (-5\mathcal{O}_H + 4\mathcal{O}_R)$

Table 6.6: (From [60]) Summary of the results in Eq. (6.96) for mixed heavy-light contributions to one-loop matching for the scalar triplet model. The SM gauge coupling-independent terms for the three operators $\mathcal{O}_T, \mathcal{O}_H, \mathcal{O}_R$ in Eq. (6.89) are computed (in the $\overline{\text{MS}}$ scheme).

where the arguments $[\Phi_b, \phi_b, \tilde{\phi}_b, W_b, B_b]$ of the \mathbf{U} and \mathbf{Z} matrices have been dropped for simplicity, and

$$\mathbf{M}^2 = \text{diag}(M^2, m^2, m^2, 0, 0), \quad (6.99)$$

$$\mathbf{U} = \begin{pmatrix} U_H & (U_{HL})_{1 \times 4} \\ (U_{LH})_{4 \times 1} & (U_L)_{4 \times 4} \end{pmatrix} = \begin{pmatrix} U_\Phi^{ab} & (U_{\phi\Phi}^\dagger)^a & U_{\Phi W}^{ab\beta} & 0 \\ (U_{\phi\Phi}^b)_{2 \times 1} & (U_\phi)_{2 \times 2} & (U_{\phi W}^{b\beta})_{2 \times 1} & (U_{\phi B}^\beta)_{2 \times 1} \\ U_{\Phi W}^{\dagger ab\alpha} & (U_{\phi W}^\dagger)^{\alpha\alpha} & U_W^{ab\alpha\beta} & U_{BW}^{\alpha\beta} \\ 0 & (U_{\phi B}^\dagger)_{1 \times 2} & U_{BW}^{b\alpha\beta} & U_B^{\alpha\beta} \end{pmatrix} \quad (6.100)$$

$$\mathbf{Z}^\mu = \begin{pmatrix} Z_H^\mu & (Z_{HL}^\mu)_{1 \times 4} \\ (Z_{LH}^\mu)_{4 \times 1} & (Z_L^\mu)_{4 \times 4} \end{pmatrix} = \begin{pmatrix} 0 & \mathbf{0}_{1 \times 2} & Z_{\Phi W}^{\mu ab\beta} & 0 \\ \mathbf{0}_{2 \times 1} & \mathbf{0}_{2 \times 2} & (Z_{\phi W}^{\mu b\beta})_{2 \times 1} & (Z_{\phi B}^{\mu\beta})_{2 \times 1} \\ 0 & \mathbf{0}_{1 \times 2} & 0 & 0 \\ 0 & \mathbf{0}_{1 \times 2} & 0 & 0 \end{pmatrix}. \quad (6.101)$$

Note that W and B vector bosons are massless in the $SU(2)_L \times U(1)_Y$ symmetric phase and, as discussed in Section 6.3.2, there is no need to retain their masses in the calculation as IR regulators. Also, Lorentz indices α, β of the vector bosons are treated on the same footing as internal indices. With Φ set to $\Phi_c[\phi]$, the relevant components of the \mathbf{U} and \mathbf{Z} matrices are, in addition to those in Eq. (6.94),

$$Z_{\Phi W}^{\mu ab\beta} = g^{\mu\beta} i g \epsilon^{adb} \Phi_c^d \sim \mathcal{O}(g\phi^2, gP^2\phi^2, g\phi^4, \dots), \quad U_{\Phi W} = [P_\mu, Z_{\Phi W}^\mu], \quad (6.102a)$$

$$Z_{\phi W}^{\mu b\beta} = -g^{\mu\beta} \frac{g}{2} \begin{pmatrix} \sigma^b \phi \\ \sigma^b \tilde{\phi} \end{pmatrix} \sim \mathcal{O}(g\phi), \quad U_{\phi W} = [P_\mu, Z_{\phi W}^\mu], \quad (6.102b)$$

$$Z_{\phi B}^{\mu\beta} = -g^{\mu\beta} \frac{g'}{2} \begin{pmatrix} \phi \\ -\tilde{\phi} \end{pmatrix} \sim \mathcal{O}(g'\phi), \quad U_{\phi B} = [P_\mu, Z_{\phi B}^\mu]. \quad (6.102c)$$

We are interested in terms in $\mathcal{L}_{\text{EFT}}^{1\text{-loop}}$ from mixed heavy-light matching that are $\mathcal{O}(g^2 P^2 \phi^4)$ or $\mathcal{O}(g'^2 P^2 \phi^4)$ ¹², which can come from, schematically,

$$\begin{aligned} Z_{\Phi W} Z_{\Phi W}^\dagger &\subset Z_{HL} Z_{HL}^\dagger, & P^2 Z_{\Phi W} Z_{\Phi W}^\dagger &\subset P^2 Z_{HL} Z_{HL}^\dagger, \\ P Z_{\Phi W} U_{\Phi W}^\dagger + \text{h.c.} &\subset P Z_{HL} U_{LH} + \text{h.c.}, & U_{\Phi W} U_{\Phi W}^\dagger &\subset U_{HL} U_{LH}; \\ Z_{\Phi W} Z_{\phi W}^\dagger U_{\phi\Phi} + \text{h.c.} &\subset Z_{HL} Z_L^\dagger U_{LH} + \text{h.c.}, \\ P^2 U_{\phi\Phi}^\dagger Z_{\phi W} Z_{\Phi W}^\dagger + \text{h.c.} &\subset P^2 U_{HL} Z_L Z_{HL}^\dagger + \text{h.c.}, \end{aligned} \quad (6.103a)$$

¹²Higher powers of g or g' are not possible at one loop, which can be easily seen by \hbar dimension counting.

$$\begin{aligned}
P Z_{\Phi W} U_{\phi W}^\dagger U_{\phi\Phi} + \text{h.c.} &\subset P Z_{HL} U_L U_{LH} + \text{h.c.}, \\
P U_{\phi\Phi}^\dagger Z_{\phi W} U_{\Phi W}^\dagger + \text{h.c.} &\subset P U_{HL} Z_L U_{LH} + \text{h.c.}, \\
U_{\Phi W} U_{\phi W}^\dagger U_{\phi\Phi} + \text{h.c.} &\subset U_{HL} U_L U_{LH}; \tag{6.103b}
\end{aligned}$$

$$\begin{aligned}
P^2 U_{\phi\Phi}^\dagger Z_{\phi V} Z_{\phi V}^\dagger U_{\phi\Phi} &\subset P^2 U_{HL} Z_L Z_L^\dagger U_{LH}, \\
P U_{\phi\Phi}^\dagger Z_{\phi V} U_{\phi V}^\dagger U_{\phi\Phi} + \text{h.c.} &\subset P U_{HL} Z_L U_L U_{LH} + \text{h.c.}, \\
U_{\phi\Phi}^\dagger U_{\phi V} U_{\phi V}^\dagger U_{\phi\Phi} &\subset U_{HL} U_L^2 U_{LH}, \tag{6.103c}
\end{aligned}$$

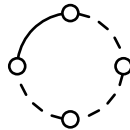
where $V = W, B$. Note that the vector boson block of the \mathbf{U} matrix (not explicitly written out above) does not contribute, since each of $U_{W,WB,BW,B}$ already contains two powers of SM gauge couplings, and additional insertions of U or Z , which are necessary in order to have at least one heavy propagator in the loop, will bring in more powers of g or g' .

In Eq. (6.103), we have organized the operator structures by the total number of Z and U insertions, which makes the enumeration straightforward. To proceed, however, it is more convenient to group the terms in Eq. (6.103) by the powers of P and $Z^{(\dagger)}$. We will do so in the following paragraphs, and compute each group in turn using the rules in Tables 6.1, 6.2, and 6.3. We will derive universal results before working out explicit forms of effective operators for the scalar triplet model.

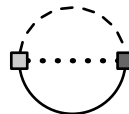
$\mathcal{O}(P^0 Z^0)$ **terms.** Two of the three terms are readily available from the first two rows of Table 6.6,

$$\mathcal{L}_{\text{EFT}}^{1\text{-loop}} \supset \frac{c_s}{16\pi^2} \left(1 - \log \frac{M^2}{\mu^2}\right) \left\{ \text{tr}(U_{HL} U_{LH}) + \frac{1}{M^2} \text{tr}(U_{HL} U_L U_{LH}) \right\}. \tag{6.104}$$

The remaining term in this group easily follows from a single diagram,

$$
= $-i c_s \mathcal{I}_{i0}^{13} \text{tr}(U_{HL} U_L^2 U_{LH}) = \frac{c_s}{16\pi^2} \left(1 - \log \frac{M^2}{\mu^2}\right) \frac{1}{M^4} \text{tr}(U_{HL} U_L^2 U_{LH}). \tag{6.105}$$$

$\mathcal{O}(P^0 Z^2)$ **terms.** Both terms in this group are also straightforward to compute, with the Z^μ and $Z^{\dagger\mu}$ contracted so that no P_μ 's are picked up from vertex insertions:

$$
= $-i c_s \mathcal{I}[q^2]_{i0}^{11} \text{tr}(Z_{HL}^\mu Z_{HL\mu}^\dagger) = \frac{c_s}{16\pi^2} \left(\frac{3}{8} - \frac{1}{4} \log \frac{M^2}{\mu^2}\right) M^2 \text{tr}(Z_{HL}^\mu Z_{HL\mu}^\dagger), \tag{6.106a}$$$

$$\begin{aligned}
& + \text{h.c.} = -ic_s \mathcal{I}[q^2]_{i0}^{12} \text{tr}(Z_{HL}^\mu Z_{L\mu}^\dagger U_{LH}) + \text{h.c.} \\
& = \frac{c_s}{16\pi^2} \left(\frac{3}{8} - \frac{1}{4} \log \frac{M^2}{\mu^2} \right) \text{tr}(Z_{HL}^\mu Z_{L\mu}^\dagger U_{LH} + \text{h.c.}). \tag{6.106b}
\end{aligned}$$

$\mathcal{O}(P^1 Z^1)$ **terms.** More diagrams contribute in this case, since the covariant derivative can either come from an uncontracted $Z^{(\dagger)}$ insertion, or be directly inserted. In the latter case, the P and $Z^{(\dagger)}$ insertions should be contracted. The four terms in this group are calculated as follows:

$$\begin{aligned}
& = -ic_s \{ (\mathcal{I}_{i0}^{11} - 2\mathcal{I}[q^2]_{i0}^{21}) \text{tr}(P_\mu Z_{HL}^\mu U_{LH}) - 2\mathcal{I}[q^2]_{i0}^{12} \text{tr}(Z_{HL}^\mu P_\mu U_{LH}) \} + \text{h.c.} \\
& = \frac{c_s}{16\pi^2} \left(\frac{3}{4} - \frac{1}{2} \log \frac{M^2}{\mu^2} \right) \text{tr}(P_\mu Z_{HL}^\mu U_{LH} - Z_{HL}^\mu P_\mu U_{LH}) + \text{h.c.} \\
& = \frac{c_s}{16\pi^2} \left(\frac{3}{4} - \frac{1}{2} \log \frac{M^2}{\mu^2} \right) \text{tr}([P_\mu, Z_{HL}^\mu] U_{LH} + \text{h.c.}), \tag{6.107a}
\end{aligned}$$

$$\begin{aligned}
& = -ic_s \{ (\mathcal{I}_{i0}^{12} - 2\mathcal{I}[q^2]_{i0}^{22}) \text{tr}(P_\mu Z_{HL}^\mu U_L U_{LH}) \\
& \quad - 2\mathcal{I}[q^2]_{i0}^{13} \text{tr}(Z_{HL}^\mu P_\mu U_L U_{LH} + Z_{HL}^\mu U_L P_\mu U_{LH}) \} + \text{h.c.} \\
& = \frac{c_s}{16\pi^2} \frac{1}{M^2} \left(\frac{3}{4} - \frac{1}{2} \log \frac{M^2}{\mu^2} \right) \\
& \quad \text{tr}(2P_\mu Z_{HL}^\mu U_L U_{LH} - Z_{HL}^\mu P_\mu U_L U_{LH} - Z_{HL}^\mu U_L P_\mu U_{LH}) + \text{h.c.} \\
& = \frac{c_s}{16\pi^2} \frac{1}{M^2} \left(\frac{3}{4} - \frac{1}{2} \log \frac{M^2}{\mu^2} \right) \text{tr}([P_\mu, Z_{HL}^\mu] U_L U_{LH} - Z_{HL}^\mu U_L [P_\mu, U_{LH}] + \text{h.c.}), \tag{6.107b}
\end{aligned}$$

$$\begin{aligned}
& = -ic_s \{ (\mathcal{I}_{i0}^{12} - 2\mathcal{I}[q^2]_{i0}^{13}) \text{tr}(U_{HL} P_\mu Z_L^\mu U_{LH}) - 2\mathcal{I}[q^2]_{i0}^{13} \text{tr}(U_{HL} Z_L^\mu P_\mu U_{LH}) \\
& \quad - 2\mathcal{I}[q^2]_{i0}^{22} \text{tr}(U_{HL} Z_L^\mu U_{LH} P_\mu) \} + \text{h.c.} \\
& = \frac{c_s}{16\pi^2} \frac{1}{M^2} \left\{ \left(\frac{1}{4} - \frac{1}{2} \log \frac{M^2}{\mu^2} \right) \text{tr}(U_{HL} P_\mu Z_L^\mu U_{LH}) + \left(-\frac{3}{4} + \frac{1}{2} \log \frac{M^2}{\mu^2} \right) \text{tr}(U_{HL} Z_L^\mu P_\mu U_{LH}) \right.
\end{aligned}$$

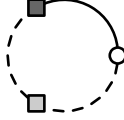
$$\begin{aligned}
& + \frac{1}{2} \text{tr}(U_{HL} Z_L^\mu U_{LH} P_\mu) + \text{h.c.} \} \\
= & \frac{c_s}{16\pi^2} \frac{1}{M^2} \left\{ \left(\frac{3}{4} - \frac{1}{2} \log \frac{M^2}{\mu^2} \right) \text{tr}(U_{HL} [P_\mu, Z_L^\mu] U_{LH}) + \frac{1}{2} \text{tr}([P_\mu, U_{HL}] Z_L^\mu U_{LH}) + \text{h.c.} \right\}, \\
& \hspace{15em} (6.107c)
\end{aligned}$$

$$\begin{aligned}
& \text{Diagram 1} + \text{Diagram 2} + \text{Diagram 3} + \text{Diagram 4} + \text{Diagram 5} + \text{h.c.} \\
& \text{Diagram 1: A dashed circle with two white circles at the top and bottom, and a square on the right.} \\
& \text{Diagram 2: A dashed circle with two white circles at the top and bottom, a square on the right, and a black dot on the upper arc.} \\
& \text{Diagram 3: A dashed circle with two white circles at the top and bottom, a square on the right, and a black dot on the lower arc.} \\
& \text{Diagram 4: A dashed circle with two white circles at the top and bottom, a square on the right, and a black dot on the left arc.} \\
& \text{Diagram 5: A dashed circle with two white circles at the top and bottom, a square on the right, and a black dot on the upper arc.}
\end{aligned}$$

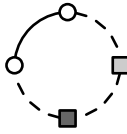
$$\begin{aligned}
= & -i c_s \left\{ (\mathcal{I}_{i0}^{13} - 2 \mathcal{I}[q^2]_{i0}^{14}) \text{tr}(U_{HL} P_\mu Z_L^\mu U_L U_{LH}) \right. \\
& - 2 \mathcal{I}[q^2]_{i0}^{14} \text{tr}(U_{HL} Z_L^\mu P_\mu U_L U_{LH} + U_{HL} Z_L^\mu U_L P_\mu U_{LH}) \\
& \left. - 2 \mathcal{I}[q^2]_{i0}^{23} \text{tr}(U_{HL} Z_L^\mu U_L U_{LH} P_\mu) \right\} + \text{h.c.} \\
= & \frac{c_s}{16\pi^2} \frac{1}{M^4} \left\{ \left(\frac{1}{4} - \frac{1}{2} \log \frac{M^2}{\mu^2} \right) \text{tr}(U_{HL} P_\mu Z_L^\mu U_L U_{LH}) \right. \\
& + \left(-\frac{3}{4} + \frac{1}{2} \log \frac{M^2}{\mu^2} \right) \text{tr}(U_{HL} Z_L^\mu P_\mu U_L U_{LH} + U_{HL} Z_L^\mu U_L P_\mu U_{LH}) \\
& \left. + \left(\frac{5}{4} - \frac{1}{2} \log \frac{M^2}{\mu^2} \right) \text{tr}(U_{HL} Z_L^\mu U_L U_{LH} P_\mu) + \text{h.c.} \right\} \\
= & \frac{c_s}{16\pi^2} \frac{1}{M^4} \left\{ \left(\frac{3}{4} - \frac{1}{2} \log \frac{M^2}{\mu^2} \right) \text{tr}(U_{HL} [P_\mu, Z_L^\mu] U_L U_{LH} - U_{HL} Z_L^\mu U_L [P_\mu, U_{LH}]) \right. \\
& \left. + \frac{1}{2} \text{tr}([P_\mu, U_{HL}] Z_L^\mu U_L U_{LH}) + \text{h.c.} \right\}. \\
& \hspace{15em} (6.107d)
\end{aligned}$$

$\mathcal{O}(P^2 Z^2)$ terms. The number of diagrams increases further, but the calculation is still quite manageable even if done by hand. Since the procedure should be clear by now, we refrain from enumerating all the diagrams for the three terms in this group, but simply report the final results:

$$\begin{aligned}
& \text{Diagram 1} + (2 + 6) \text{ more} \\
& \text{Diagram 1: A dashed circle with two white circles at the top and bottom, and two squares on the left and right.} \\
\subset & \frac{c_s}{16\pi^2} \left\{ \left(\frac{5}{72} - \frac{1}{12} \log \frac{M^2}{\mu^2} \right) \text{tr}([P^\mu, Z_{HL}^\nu] [P_\mu, Z_{HL}^\dagger \nu]) \right. \\
& + \left(-\frac{11}{18} + \frac{1}{3} \log \frac{M^2}{\mu^2} \right) \text{tr}([P_\mu, Z_{HL}^\mu] [P_\nu, Z_{HL}^\dagger \nu]) \\
& \left. + \left(\frac{1}{18} - \frac{1}{6} \log \frac{M^2}{\mu^2} \right) \text{tr}(Z_{HL}^\mu Z_{HL}^\dagger \nu [P_\mu, P_\nu]) + \left(-\frac{11}{36} + \frac{1}{6} \log \frac{M^2}{\mu^2} \right) \text{tr}(Z_{HL}^\mu [P_\mu, P_\nu] Z_{HL}^\dagger \nu) \right\}, \\
& \hspace{15em} (6.108a)
\end{aligned}$$


 $+ \text{h.c.} + (6 + 15) \text{ more}$

$$\begin{aligned}
&\subset \frac{c_s}{16\pi^2} \frac{1}{M^2} \\
&\left\{ \left(-\frac{5}{72} + \frac{1}{12} \log \frac{M^2}{\mu^2} \right) \text{tr}(U_{HL}[P^\mu, [P_\mu, Z_L^\nu]] Z_{HL\nu}^\dagger) - \frac{1}{6} \text{tr}([P^\mu, U_{HL}] Z_L^\nu [P_\mu, Z_{HL\nu}^\dagger]) \right. \\
&+ \left(-\frac{7}{9} + \frac{1}{3} \log \frac{M^2}{\mu^2} \right) \text{tr}(U_{HL}[P_\mu, Z_L^\mu] [P_\nu, Z_{HL}^{\dagger\nu}]) + \frac{1}{6} \text{tr}(U_{HL}[P_\nu, Z_L^\mu] [P_\mu, Z_{HL}^{\dagger\nu}]) \\
&+ \left(\frac{5}{36} - \frac{1}{6} \log \frac{M^2}{\mu^2} \right) \text{tr}([P_\nu, U_{HL}] [P_\mu, Z_L^\mu] Z_{HL}^{\dagger\nu}) - \frac{1}{3} \text{tr}([P_\mu, U_{HL}] Z_L^\mu [P_\nu, Z_{HL}^{\dagger\nu}]) \\
&- \frac{1}{12} \text{tr}(U_{HL} Z_L^\mu Z_{HL}^{\dagger\nu} [P_\mu, P_\nu]) + \left(-\frac{17}{36} + \frac{1}{6} \log \frac{M^2}{\mu^2} \right) \text{tr}(U_{HL} Z_L^\mu [P_\mu, P_\nu] Z_{HL}^{\dagger\nu}) \\
&\left. + \left(\frac{11}{36} - \frac{1}{6} \log \frac{M^2}{\mu^2} \right) \text{tr}(U_{HL}[P_\mu, P_\nu] Z_L^\mu Z_{HL}^{\dagger\nu}) + \text{h.c.} \right\}, \tag{6.108b}
\end{aligned}$$


 $+ (4 + 17) \text{ more}$

$$\begin{aligned}
&\subset \frac{c_s}{16\pi^2} \frac{1}{M^4} \left\{ \left(\frac{5}{72} - \frac{1}{12} \log \frac{M^2}{\mu^2} \right) \cdot \right. \\
&\quad \text{tr}(U_{HL}[P^\mu, Z_L^\nu] [P_\mu, Z_{L\nu}^\dagger] U_{LH} + ([P^\mu, U_{HL}] [P_\mu, Z_L^\nu] Z_{L\nu}^\dagger U_{LH} + \text{h.c.})) \\
&\quad - \frac{1}{6} \text{tr}(U_{HL}[P^\mu, Z_L^\nu] Z_{L\nu}^\dagger [P_\mu, U_{LH}] + \text{h.c.}) \\
&\quad + \left(-\frac{17}{24} + \frac{1}{4} \log \frac{M^2}{\mu^2} \right) \text{tr}([P^\mu, U_{HL}] Z_L^\nu Z_{L\nu}^\dagger [P_\mu, U_{LH}]) \\
&\quad + \left(-\frac{11}{36} + \frac{1}{6} \log \frac{M^2}{\mu^2} \right) \text{tr}(U_{HL}[P_\mu, Z_L^\mu] [P_\nu, Z_L^{\dagger\nu}] U_{LH} + U_{HL}[P_\nu, Z_L^\mu] [P_\mu, Z_L^{\dagger\nu}] U_{LH}) \\
&\quad + \left(\frac{11}{18} - \frac{1}{3} \log \frac{M^2}{\mu^2} \right) \text{tr}([P_\nu, U_{HL}] [P_\mu, Z_L^\mu] Z_L^{\dagger\nu} U_{LH} + \text{h.c.}) \\
&\quad + \left(-\frac{17}{36} + \frac{1}{6} \log \frac{M^2}{\mu^2} \right) \text{tr}([P_\mu, U_{HL}] [P_\nu, Z_L^\mu] Z_L^{\dagger\nu} U_{LH} + \text{h.c.}) \\
&\quad - \frac{1}{3} \text{tr}(U_{HL}[P_\mu, Z_L^\mu] Z_L^{\dagger\nu} [P_\nu, U_{LH}] + \text{h.c.}) - \frac{1}{6} \text{tr}([P_\mu, U_{HL}] Z_L^\mu Z_L^{\dagger\nu} [P_\nu, U_{LH}]) \\
&\quad \left. + \frac{1}{12} \text{tr}(U_{HL} Z_L^\mu Z_L^{\dagger\nu} U_{LH} [P_\mu, P_\nu]) - \frac{1}{6} \text{tr}(U_{HL} Z_L^\mu Z_L^{\dagger\nu} [P_\mu, P_\nu] U_{LH} + \text{h.c.}) \right\}. \tag{6.108c}
\end{aligned}$$

In the equations above, we have shown, for each term, the one diagram with zero P insertions, and the number of diagrams with one and two P insertions (e.g. 2 and 6, respectively, for the $P^2 Z_{HL} Z_{HL}^\dagger$ term). The counting excludes hermitian conjugation and adjacent P_μ contractions. Following the rules in Section 6.3.5, the reader should be able to easily draw

all the diagrams, and fill in the intermediate steps (which are straightforward though perhaps a bit lengthy) that lead to the final results in Eq. (6.108).

All results presented in the four paragraphs above, namely Eqs. (6.104), (6.105), (6.106), (6.107) and (6.108), are universal and model-independent. Now we focus on the scalar triplet model, and work out the traces involved in these equations that yield the three effective operators in Eq. (6.89):

$$\begin{aligned} & \text{tr}(U_{HL}U_{LH}), \text{tr}([P_\mu, Z_{HL}^\mu]U_{LH}) \text{ and h.c.}, -\text{tr}([P_\mu, Z_{HL}^\mu][P_\nu, Z_{HL}^{\dagger\nu}]) \\ & \rightarrow -g_{\alpha\beta}U_{\Phi W}^{ab\alpha}U_{\Phi W}^{\dagger b\alpha\beta} \supset -\frac{4\kappa^2}{M^4}g^2(\mathcal{O}_T + 2\mathcal{O}_R); \end{aligned} \quad (6.109a)$$

$$\begin{aligned} & \text{tr}(U_{HL}U_LU_{LH}), \text{tr}([P_\mu, Z_{HL}^\mu]U_LU_{LH} + \text{h.c.}), \\ & \text{tr}(U_{HL}[P_\mu, Z_L^\mu]U_{LH} + \text{h.c.}), -\text{tr}(U_{HL}[P_\mu, Z_L^\mu][P_\nu, Z_{HL}^{\dagger\nu}] + \text{h.c.}) \\ & \rightarrow -g_{\alpha\beta}U_{\Phi W}^{ab\alpha}U_{\Phi W}^{\dagger b\beta}U_{\phi\Phi}^a + \text{h.c.} \supset \frac{4\kappa^2}{M^2}g^2(\mathcal{O}_T + 2\mathcal{O}_R); \end{aligned} \quad (6.109b)$$

$$\begin{aligned} & \text{tr}(U_{HL}U_L^2U_{LH}), \text{tr}(U_{HL}[P_\mu, Z_L^\mu]U_LU_{LH}) \text{ and h.c.}, -\text{tr}(U_{HL}[P_\mu, Z_L^\mu][P_\nu, Z_L^{\dagger\nu}]U_{LH}) \\ & \rightarrow -g_{\alpha\beta}(U_{\phi\Phi}^{\dagger a}U_{\phi W}^{b\alpha}U_{\phi W}^{\dagger b\beta}U_{\phi\Phi}^a + U_{\phi\Phi}^{\dagger a}U_{\phi B}^\alpha U_{\phi B}^{\dagger\beta}U_{\phi\Phi}^a) \\ & \supset \frac{\kappa^2}{2}[g^2(\mathcal{O}_T - 4\mathcal{O}_R) + g'^2(\mathcal{O}_H - 2\mathcal{O}_R)]; \end{aligned} \quad (6.109c)$$

$$\begin{aligned} & \text{tr}(Z_{HL}^\mu Z_{HL\mu}^\dagger) \\ & \rightarrow -g_{\alpha\beta}Z_{\Phi W}^{\mu ab\alpha}Z_{\Phi W\mu}^{\dagger b\alpha\beta} \supset -\left(1 - \frac{\epsilon}{4}\right)\frac{32\kappa^2}{M^6}g^2(\mathcal{O}_T + 2\mathcal{O}_R); \end{aligned} \quad (6.109d)$$

$$\begin{aligned} & \text{tr}(Z_{HL}^\mu Z_{L\mu}^\dagger U_{LH} + \text{h.c.}) \\ & \rightarrow -g_{\alpha\beta}Z_{\Phi W}^{\mu ab\alpha}Z_{\phi W\mu}^{\dagger b\beta}U_{\phi\Phi}^a + \text{h.c.} \supset \left(1 - \frac{\epsilon}{4}\right)\frac{32\kappa^2}{M^4}g^2(\mathcal{O}_T + 2\mathcal{O}_R); \end{aligned} \quad (6.109e)$$

$$\begin{aligned} & \text{tr}(Z_{HL}^\mu U_L[P_\mu, U_{LH}] + \text{h.c.}), -\text{tr}([P_\nu, U_{HL}][P_\mu, Z_L^\mu]Z_{HL}^{\dagger\nu} + \text{h.c.}) \\ & \rightarrow -g_{\alpha\beta}Z_{\Phi W}^{\mu ab\alpha}U_{\phi W}^{\dagger b\beta}[P_\mu, U_{\phi\Phi}^a] + \text{h.c.} \supset -\frac{4\kappa^2}{M^2}g^2(\mathcal{O}_T - \mathcal{O}_H + \mathcal{O}_R); \end{aligned} \quad (6.109f)$$

$$\begin{aligned} & \text{tr}([P_\mu, U_{HL}]Z_L^\mu U_{LH} + \text{h.c.}), -\text{tr}([P_\mu, U_{HL}]Z_L^\mu[P_\nu, Z_{HL}^{\dagger\nu}] + \text{h.c.}) \\ & \rightarrow -g_{\alpha\beta}[P_\mu, U_{\phi\Phi}^{\dagger a}]Z_{\phi W}^{\mu b\alpha}U_{\Phi W}^{\dagger b\alpha\beta} + \text{h.c.} \supset \frac{4\kappa^2}{M^2}g^2(\mathcal{O}_T + 2\mathcal{O}_R); \end{aligned} \quad (6.109g)$$

$$\begin{aligned} & \text{tr}(U_{HL}Z_L^\mu U_L[P_\mu, U_{LH}] + \text{h.c.}), -\text{tr}([P_\nu, U_{HL}][P_\mu, Z_L^\mu]Z_L^{\dagger\nu}U_{LH} + \text{h.c.}) \\ & \rightarrow -g_{\alpha\beta}(U_{\phi\Phi}^{\dagger a}Z_{\phi W}^{\mu b\alpha}U_{\phi W}^{\dagger b\beta}[P_\mu, U_{\phi\Phi}^a] + U_{\phi\Phi}^{\dagger a}Z_{\phi B}^{\mu\alpha}U_{\phi B}^{\dagger\beta}[P_\mu, U_{\phi\Phi}^a]) + \text{h.c.} \\ & \supset 4\kappa^2g^2(\mathcal{O}_T - \mathcal{O}_H + \mathcal{O}_R); \end{aligned} \quad (6.109h)$$

$$\begin{aligned} & \text{tr}([P_\mu, U_{HL}]Z_L^\mu U_LU_{LH} + \text{h.c.}), -\text{tr}(U_{HL}[P_\mu, Z_L^\mu]Z_L^{\dagger\nu}[P_\nu, U_{LH}] + \text{h.c.}) \\ & \rightarrow -g_{\alpha\beta}([P_\mu, U_{\phi\Phi}^{\dagger a}]Z_{\phi W}^{\mu b\alpha}U_{\phi W}^{\dagger b\beta}U_{\phi\Phi}^a + [P_\mu, U_{\phi\Phi}^{\dagger a}]Z_{\phi B}^{\mu\alpha}U_{\phi B}^{\dagger\beta}U_{\phi\Phi}^a) + \text{h.c.} \end{aligned}$$

$$\supset -\kappa^2[g^2(5\mathcal{O}_T + 4\mathcal{O}_R) + g'^2(\mathcal{O}_H - 2\mathcal{O}_R)]; \quad (6.109i)$$

$$\begin{aligned} & \text{tr}([P^\mu, Z_{HL}^\nu][P_\mu, Z_{HL\nu}^\dagger]) \\ & \rightarrow -g_{\alpha\beta}[P^\mu, Z_{\Phi W}^{\nu ab\alpha}][P_\mu, Z_{\Phi W\nu}^{\dagger ba\beta}] \supset \left(1 - \frac{\epsilon}{4}\right) \frac{16\kappa^2}{M^4} g^2(\mathcal{O}_T + 2\mathcal{O}_R); \end{aligned} \quad (6.109j)$$

$$\begin{aligned} & \text{tr}(U_{HL}[P^\mu, [P_\mu, Z_L^\nu]]Z_{HL\nu}^\dagger + \text{h.c.}) \\ & \rightarrow -g_{\alpha\beta}U_{\phi\Phi}^{\dagger a}[P^\mu, [P_\mu, Z_{\phi W}^{\nu b\alpha}]]Z_{\phi W\nu}^{\dagger ba\beta} + \text{h.c.} \supset \left(1 - \frac{\epsilon}{4}\right) \frac{16\kappa^2}{M^2} g^2(\mathcal{O}_H + \mathcal{O}_R); \end{aligned} \quad (6.109k)$$

$$\begin{aligned} & \text{tr}([P^\mu, U_{HL}]Z_L^\nu[P_\mu, Z_{HL\nu}^\dagger] + \text{h.c.}) \\ & \rightarrow -g_{\alpha\beta}[P^\mu, U_{\phi\Phi}^{\dagger a}]Z_{\phi W}^{\nu b\alpha}[P_\mu, Z_{\phi W\nu}^{\dagger ba\beta}] + \text{h.c.} \supset -\left(1 - \frac{\epsilon}{4}\right) \frac{16\kappa^2}{M^2} g^2(\mathcal{O}_T + 2\mathcal{O}_R); \end{aligned} \quad (6.109l)$$

$$\begin{aligned} & \text{tr}(U_{HL}[P_\nu, Z_L^\mu][P_\mu, Z_{HL}^{\nu\dagger}] + \text{h.c.}) \\ & \rightarrow -g_{\alpha\beta}U_{\phi\Phi}^{\dagger a}[P^\mu, Z_{\phi W}^{\nu b\alpha}][P_\mu, Z_{\phi W\nu}^{\dagger ba\beta}] + \text{h.c.} \supset -\frac{4\kappa^2}{M^2} g^2(\mathcal{O}_T + 2\mathcal{O}_R); \end{aligned} \quad (6.109m)$$

$$\begin{aligned} & \text{tr}(U_{HL}[P^\mu, Z_L^\nu][P_\mu, Z_{L\nu}^\dagger]U_{LH}) \\ & \rightarrow -g_{\alpha\beta}(U_{\phi\Phi}^{\dagger a}[P^\mu, Z_{\phi W}^{\nu b\alpha}][P_\mu, Z_{\phi W\nu}^{\dagger b\beta}]U_{\phi\Phi}^a + U_{\phi\Phi}^{\dagger a}[P^\mu, Z_{\phi B}^{\nu\alpha}][P_\mu, Z_{\phi B\nu}^{\dagger\beta}]U_{\phi\Phi}^a) \\ & \supset -\left(1 - \frac{\epsilon}{4}\right) 2\kappa^2[g^2(\mathcal{O}_T - 4\mathcal{O}_R) + g'^2(\mathcal{O}_H - 2\mathcal{O}_R)]; \end{aligned} \quad (6.109n)$$

$$\begin{aligned} & \text{tr}([P^\mu, U_{HL}][P_\mu, Z_L^\nu]Z_{L\nu}^\dagger U_{LH} + \text{h.c.}) \\ & \rightarrow -g_{\alpha\beta}([P^\mu, U_{\phi\Phi}^{\dagger a}][P_\mu, Z_{\phi W}^{\nu b\alpha}]Z_{\phi W\nu}^{\dagger b\beta}U_{\phi\Phi}^a + [P^\mu, U_{\phi\Phi}^{\dagger a}][P_\mu, Z_{\phi B}^{\nu\alpha}]Z_{\phi B\nu}^{\dagger\beta}U_{\phi\Phi}^a) + \text{h.c.} \\ & \supset -\left(1 - \frac{\epsilon}{4}\right) 16\kappa^2 g^2(\mathcal{O}_T - \mathcal{O}_H + \mathcal{O}_R); \end{aligned} \quad (6.109o)$$

$$\begin{aligned} & \text{tr}(U_{HL}[P^\mu, Z_L^\nu]Z_{L\nu}^\dagger[P_\mu, U_{LH}] + \text{h.c.}) \\ & \rightarrow -g_{\alpha\beta}(U_{\phi\Phi}^{\dagger a}[P^\mu, Z_{\phi W}^{\nu b\alpha}]Z_{\phi W\nu}^{\dagger b\beta}[P_\mu, U_{\phi\Phi}^a] + U_{\phi\Phi}^{\dagger a}[P^\mu, Z_{\phi B}^{\nu\alpha}]Z_{\phi B\nu}^{\dagger\beta}[P_\mu, U_{\phi\Phi}^a]) + \text{h.c.} \\ & \supset \left(1 - \frac{\epsilon}{4}\right) 4\kappa^2[g^2(5\mathcal{O}_T + 4\mathcal{O}_R) + g'^2(\mathcal{O}_H - 2\mathcal{O}_R)]; \end{aligned} \quad (6.109p)$$

$$\begin{aligned} & \text{tr}([P^\mu, U_{HL}]Z_L^\nu Z_{L\nu}^\dagger[P_\mu, U_{LH}]) \\ & \rightarrow -g_{\alpha\beta}([P^\mu, U_{\phi\Phi}^{\dagger a}]Z_{\phi W}^{\nu b\alpha}Z_{\phi W\nu}^{\dagger b\beta}[P_\mu, U_{\phi\Phi}^a] + [P^\mu, U_{\phi\Phi}^{\dagger a}]Z_{\phi B}^{\nu\alpha}Z_{\phi B\nu}^{\dagger\beta}[P_\mu, U_{\phi\Phi}^a]) \\ & \supset -\left(1 - \frac{\epsilon}{4}\right) 2\kappa^2[g^2(\mathcal{O}_T - 4\mathcal{O}_R) + g'^2(\mathcal{O}_H - 2\mathcal{O}_R)]; \end{aligned} \quad (6.109q)$$

$$\begin{aligned} & \text{tr}(U_{HL}[P_\nu, Z_L^\mu][P_\mu, Z_L^{\nu\dagger}]U_{LH}) \\ & \rightarrow -g_{\alpha\beta}(U_{\phi\Phi}^{\dagger a}[P_\nu, Z_{\phi W}^{\mu b\alpha}][P_\mu, Z_{\phi W}^{\nu b\beta}]U_{\phi\Phi}^a + U_{\phi\Phi}^{\dagger a}[P_\nu, Z_{\phi B}^{\mu\alpha}][P_\mu, Z_{\phi B}^{\nu\beta}]U_{\phi\Phi}^a) \\ & \supset -\frac{\kappa^2}{2}[g^2(\mathcal{O}_T - 4\mathcal{O}_R) + g'^2(\mathcal{O}_H - 2\mathcal{O}_R)]; \end{aligned} \quad (6.109r)$$

$$\begin{aligned} & \text{tr}([P_\mu, U_{HL}][P_\nu, Z_L^\mu]Z_L^{\nu\dagger}U_{LH} + \text{h.c.}) \\ & \rightarrow -g_{\alpha\beta}([P_\mu, U_{\phi\Phi}^{\dagger a}][P_\nu, Z_{\phi W}^{\mu b\alpha}]Z_{\phi W}^{\nu b\beta}U_{\phi\Phi}^a + [P_\mu, U_{\phi\Phi}^{\dagger a}][P_\nu, Z_{\phi B}^{\mu\alpha}]Z_{\phi B}^{\nu\beta}U_{\phi\Phi}^a) + \text{h.c.} \end{aligned}$$

$$\supset -4\kappa^2 g^2 (\mathcal{O}_T - \mathcal{O}_H + \mathcal{O}_R); \quad (6.109s)$$

$$\begin{aligned} & \text{tr}([P_\mu, U_{HL}] Z_L^\mu Z_L^{\dagger\nu} [P_\nu, U_{LH}]) \\ & \rightarrow -g_{\alpha\beta} ([P_\mu, U_{\phi\Phi}^{\dagger a}] Z_{\phi W}^{\mu b\alpha} Z_{\phi W}^{\dagger\nu b\beta} [P_\nu, U_{\phi\Phi}^a] + [P_\mu, U_{\phi\Phi}^{\dagger a}] Z_{\phi B}^{\mu\alpha} Z_{\phi B}^{\dagger\nu\beta} [P_\nu, U_{\phi\Phi}^a]) \\ & \supset -\frac{\kappa^2}{2} [g^2 (\mathcal{O}_T - 4\mathcal{O}_R) + g'^2 (\mathcal{O}_H - 2\mathcal{O}_R)]. \end{aligned} \quad (6.109t)$$

Note that Lorentz indices of the gauge boson fields α, β should be contracted with $-g_{\alpha\beta}$, as discussed in Section 6.3.1. Also, $\mathcal{O}(\epsilon)$ terms from $g_{\alpha\beta} g^{\alpha\beta} = d = 4 - \epsilon$ must be kept in cases where the master integrals have $\frac{1}{\epsilon}$ poles. The latter were not written out explicitly above, but can be easily recovered by

$$-\log \frac{M^2}{\mu^2} \rightarrow \frac{2}{\epsilon} - \log \frac{M^2}{\mu^2}. \quad (6.110)$$

Adding up all terms in Eqs. (6.104), (6.105), (6.106), (6.107) and (6.108) with the replacement Eq. (6.110), plugging in Eq. (6.109), and finally dropping $\frac{1}{\epsilon}$ poles, we obtain the final result (with $c_s = \frac{1}{2}$ and μ set to M in the $\overline{\text{MS}}$ scheme),

$$\mathcal{L}_{\text{EFT}}^{\text{1-loop}}[\phi] \supset \frac{1}{16\pi^2} \frac{5\kappa^2}{8M^4} [g^2 \mathcal{O}_T + g'^2 \mathcal{O}_H - (4g^2 + 2g'^2) \mathcal{O}_R]. \quad (6.111)$$

This agrees with the result in [219] obtained by Feynman diagram calculations.

6.4.4 Integrating out a vectorlike fermion: pure gauge operators

Our final two examples demonstrate treatment of fermions in our covariant diagram approach. In the present subsection, we consider a simple but quite general setup of a vectorlike fermion of mass M charged under some gauge symmetry. We will compute pure gauge effective operators up to dimension six which are generated by integrating out the heavy vectorlike fermion, independent of possible presence of light matter fields. The results are familiar in various contexts, including integrating out a heavy quark flavor in QCD, and integrating out a heavy vectorlike fermion that may arise in many beyond-SM scenarios. We also note that the same results are obtained in [55] following the alternative approach to integrating out heavy fermions discussed at the beginning of Section 6.3.4.

$\mathcal{O}(P^4)$ terms. We first consider diagrams with four (fermionic) P insertions. Five diagrams can be drawn which differ by whether and how the heavy fermionic propagators are contracted with each other. One of them can be dropped where fermionic propagators separated by two P insertions are contracted (while the loop integral $\mathcal{I}[q^2]_i^4$ is finite), because it

only gives rise to $\text{tr}(\dots P^2 \dots)$. The remaining four diagrams are, by the rules in Table 6.4,

$$\begin{aligned}
&= -ic_s \left\{ \frac{1}{4} M^4 \mathcal{I}_i^4 \text{tr}(\not{P}^4) + M^2 \mathcal{I}[q^2]_i^4 \text{tr}(\gamma^\alpha \not{P} \gamma_\alpha \not{P}^3) \right. \\
&\quad \left. + \mathcal{I}[q^4]_i^4 \left(\frac{1}{2} \text{tr}(\gamma^\alpha \not{P} \gamma_\alpha \not{P} \gamma^\beta \not{P} \gamma_\beta \not{P}) + \frac{1}{4} \text{tr}(\gamma^\alpha \not{P} \gamma^\beta \not{P} \gamma_\alpha \not{P} \gamma_\beta \not{P}) \right) \right\}. \quad (6.112)
\end{aligned}$$

Evaluation of the gamma matrix traces is standard and straightforward,

$$\text{tr}(\not{P}^4) = \text{tr}(\gamma^\mu \gamma^\nu \gamma^\rho \gamma^\sigma) \text{tr}(P_\mu P_\nu P_\rho P_\sigma) \supset -4 \text{tr}(P^\mu P^\nu P_\mu P_\nu), \quad (6.113a)$$

$$\text{tr}(\gamma^\alpha \not{P} \gamma_\alpha \not{P}^3) = -2 \text{tr}(\not{P}^4) + \mathcal{O}(\epsilon) \supset 8 \text{tr}(P^\mu P^\nu P_\mu P_\nu) + \mathcal{O}(\epsilon), \quad (6.113b)$$

$$\text{tr}(\gamma^\alpha \not{P} \gamma_\alpha \not{P} \gamma^\beta \not{P} \gamma_\beta \not{P}) = 4(1 - \epsilon) \text{tr}(\not{P}^4) \supset -16(1 - \epsilon) \text{tr}(P^\mu P^\nu P_\mu P_\nu), \quad (6.113c)$$

$$\begin{aligned}
\text{tr}(\gamma^\alpha \not{P} \gamma^\beta \not{P} \gamma_\alpha \not{P} \gamma_\beta \not{P}) &= \text{tr}(\gamma^\alpha \gamma^\mu \gamma^\beta \gamma^\nu \gamma_\alpha \gamma^\rho \gamma_\beta \gamma^\sigma) \text{tr}(P_\mu P_\nu P_\rho P_\sigma) \\
&= \{-2 \text{tr}(\gamma^\nu \gamma^\beta \gamma^\mu \gamma^\rho \gamma_\beta \gamma^\sigma) + \epsilon \text{tr}(\gamma^\mu \gamma^\beta \gamma^\nu \gamma^\rho \gamma_\beta \gamma^\sigma)\} \text{tr}(P_\mu P_\nu P_\rho P_\sigma) \\
&= \{-8g^{\mu\rho} \text{tr}(\gamma^\nu \gamma^\sigma) + 2\epsilon \text{tr}(\gamma^\nu \gamma^\mu \gamma^\rho \gamma^\sigma) + 4\epsilon g^{\nu\rho} \text{tr}(\gamma^\mu \gamma^\sigma)\} \text{tr}(P_\mu P_\nu P_\rho P_\sigma) \\
&= \{8\epsilon g^{\mu\nu} g^{\rho\sigma} - (32 - 8\epsilon)g^{\mu\rho} g^{\nu\sigma} + 8\epsilon g^{\mu\sigma} g^{\nu\rho}\} \text{tr}(P_\mu P_\nu P_\rho P_\sigma) \\
&\supset -32 \left(1 - \frac{\epsilon}{4}\right) \text{tr}(P^\mu P^\nu P_\mu P_\nu), \quad (6.113d)
\end{aligned}$$

where terms involving $\text{tr}(\dots P^2 \dots)$ have been dropped. Note that $\mathcal{O}(\epsilon)$ terms must be kept for the last two traces, since they are multiplied by $\mathcal{I}[q^4]_i^4$ which contains a $\frac{1}{\epsilon}$ pole. Plugging Eq. (6.113) into (6.112), we have

$$\begin{aligned}
\mathcal{L}_{\text{EFT}}^{1\text{-loop}} &\supset -ic_s \left\{ -M^4 \mathcal{I}_i^4 + 8M^2 \mathcal{I}[q^2]_i^4 + (-16 + 10\epsilon) \mathcal{I}[q^4]_i^4 \right\} \text{tr}(P^\mu P^\nu P_\mu P_\nu) \\
&= \frac{c_s}{16\pi^2} \frac{2}{3} \log \frac{M^2}{\mu^2} \text{tr}(P^\mu P^\nu P_\mu P_\nu) \subset -\frac{1}{16\pi^2} \frac{1}{3} \log \frac{M^2}{\mu^2} \text{tr}([P^\mu, P^\nu][P_\mu, P_\nu]) \\
&= -\frac{1}{16\pi^2} \frac{1}{3} \log \frac{M^2}{\mu^2} \text{tr}(G'^{\mu\nu} G'_{\mu\nu}) = \frac{g^2}{16\pi^2} T(R) \left(-\frac{4}{3} \log \frac{M^2}{\mu^2} \right) \left(-\frac{1}{4} G^{a\mu\nu} G_{\mu\nu}^a \right) \quad (6.114)
\end{aligned}$$

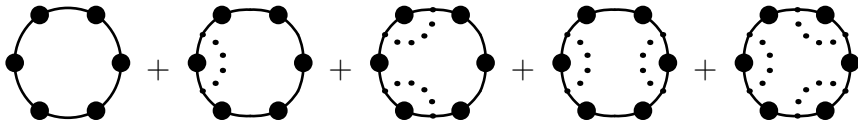
where $T(R)$ is the Dynkin index for the representation R of the heavy vectorlike fermion, defined by $\text{tr}(t_R^a t_R^b) = T(R) \delta^{ab}$ with t_R^a being the generators in representation R ; for example, $T(R) = \frac{1}{2}$ and N for the fundamental and adjoint representations of $SU(N)$, respectively. Also, recall $c_s = -1$ for Dirac fermions¹³, and $G'_{\mu\nu} = -[P_\mu, P_\nu] = -igG_{\mu\nu} = -igG_{\mu\nu}^a t_R^a$. One

¹³Unlike in Eq. (6.64), here $\mathcal{L}_{\text{UV,quad}}$ can be written with prefactor -1 , with only the vectorlike fermion field in the field multiplet of interest, and it is not necessary to represent this single Dirac fermion field by two fields as mentioned below Eq. (6.64). Of course the latter is OK to do, in which case the two fields

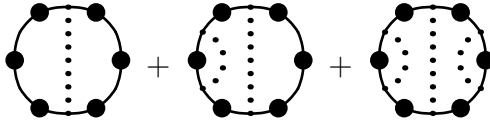
can rescale the gauge fields to canonically normalize the kinetic terms while keeping $gG_{\mu\nu}$ unchanged. The result is the familiar one-loop matching formula for the gauge coupling across a heavy vectorlike fermion mass threshold (see e.g. [229]),

$$\frac{g_{\text{eff}}^2(\mu)}{g^2(\mu)} = 1 + \frac{g^2}{16\pi^2} T(R) \left(\frac{4}{3} \log \frac{M^2}{\mu^2} \right). \quad (6.115)$$

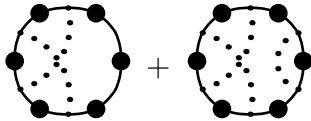
$\mathcal{O}(P^6)$ terms. Diagrams with six P insertions can be computed similarly. We enumerate them in the following, using $\gamma^\alpha \gamma^\mu \gamma_\alpha = -2\gamma^\mu$ to simplify the operator trace. Again, diagrams only giving rise to $\text{tr}(\dots P^2 \dots)$ are dropped.



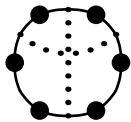
$$= -ic_s \left\{ \frac{1}{6} M^6 \mathcal{I}_i^6 + (-2) M^4 \mathcal{I}[q^2]_i^6 + (-2)^2 \left(1 + \frac{1}{2} \right) M^2 \mathcal{I}[q^4]_i^6 + (-2)^3 \frac{1}{3} \mathcal{I}[q^6]_i^6 \right\} \text{tr}(\not{P}^6), \quad (6.116a)$$



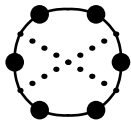
$$= -ic_s \left\{ \frac{1}{2} M^4 \mathcal{I}[q^2]_i^6 + (-2) M^2 \mathcal{I}[q^4]_i^6 + (-2)^2 \frac{1}{2} \mathcal{I}[q^6]_i^6 \right\} \text{tr}(\gamma^\alpha \not{P}^3 \gamma_\alpha \not{P}^3), \quad (6.116b)$$



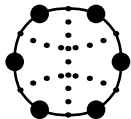
$$= -ic_s \left\{ M^2 \mathcal{I}[q^4]_i^6 + (-2) \mathcal{I}[q^6]_i^6 \right\} \text{tr}(\gamma^\alpha \not{P} \gamma^\beta \not{P} \gamma_\alpha \not{P} \gamma_\beta \not{P}^3), \quad (6.116c)$$



$$= -ic_s M^2 \mathcal{I}[q^4]_i^6 \text{tr}(\gamma^\alpha \not{P} \gamma^\beta \not{P} \gamma_\alpha \not{P}^2 \gamma_\beta \not{P}^2), \quad (6.116d)$$

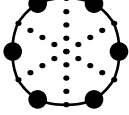


$$= -ic_s \frac{1}{2} M^2 \mathcal{I}[q^4]_i^6 \text{tr}(\gamma^\alpha \not{P} \gamma^\beta \not{P}^2 \gamma_\alpha \not{P} \gamma_\beta \not{P}^2), \quad (6.116e)$$



$$= -ic_s \frac{1}{2} \mathcal{I}[q^6]_i^6 \text{tr}(\gamma^\alpha \not{P} \gamma^\beta \not{P} \gamma^\delta \not{P} \gamma_\alpha \not{P} \gamma_\delta \not{P} \gamma_\beta \not{P}), \quad (6.116f)$$

would effectively have $c_s = -\frac{1}{2}$ each and contribute equally to $\mathcal{L}_{\text{EFT}}^{1\text{-loop}}$, leading to the same final result as Eq. (6.114).



$$= -ic_s \frac{1}{6} \mathcal{I}[q^6]_i \text{tr}(\gamma^\alpha \not{P} \gamma^\beta \not{P} \gamma^\delta \not{P} \gamma_\alpha \not{P} \gamma_\beta \not{P} \gamma_\delta \not{P}). \quad (6.116g)$$

All loop integrals appearing in the equations above are finite, so $\mathcal{O}(\epsilon)$ terms can always be dropped when evaluating the traces:

$$\text{tr}(\not{P}^6) \supset -4 \text{tr}(P^\mu P^\nu P^\rho P_\mu P_\nu P_\rho) + 12 \text{tr}(P^\mu P^\nu P^\rho P_\mu P_\rho P_\nu), \quad (6.117a)$$

$$\text{tr}(\gamma^\alpha \not{P}^3 \gamma_\alpha \not{P}^3) \supset -8 \text{tr}(P^\mu P^\nu P^\rho P_\mu P_\nu P_\rho) + 8 \text{tr}(P^\mu P^\nu P^\rho P_\mu P_\rho P_\nu), \quad (6.117b)$$

$$\text{tr}(\gamma^\alpha \not{P} \gamma^\beta \not{P} \gamma_\alpha \not{P} \gamma_\beta \not{P}^3) \supset 32 \text{tr}(P^\mu P^\nu P^\rho P_\mu P_\rho P_\nu), \quad (6.117c)$$

$$\text{tr}(\gamma^\alpha \not{P} \gamma^\beta \not{P} \gamma_\alpha \not{P}^2 \gamma_\beta \not{P}^2) \supset 16 \text{tr}(P^\mu P^\nu P^\rho P_\mu P_\nu P_\rho) - 16 \text{tr}(P^\mu P^\nu P^\rho P_\mu P_\rho P_\nu), \quad (6.117d)$$

$$\text{tr}(\gamma^\alpha \not{P} \gamma^\beta \not{P}^2 \gamma_\alpha \not{P} \gamma_\beta \not{P}^2) \supset -16 \text{tr}(P^\mu P^\nu P^\rho P_\mu P_\nu P_\rho) + 48 \text{tr}(P^\mu P^\nu P^\rho P_\mu P_\rho P_\nu), \quad (6.117e)$$

$$\text{tr}(\gamma^\alpha \not{P} \gamma^\beta \not{P} \gamma^\delta \not{P} \gamma_\alpha \not{P} \gamma_\beta \not{P} \gamma_\delta \not{P}) \supset -32 \text{tr}(P^\mu P^\nu P^\rho P_\mu P_\nu P_\rho) - 96 \text{tr}(P^\mu P^\nu P^\rho P_\mu P_\rho P_\nu), \quad (6.117f)$$

$$\text{tr}(\gamma^\alpha \not{P} \gamma^\beta \not{P} \gamma^\delta \not{P} \gamma_\alpha \not{P} \gamma_\beta \not{P} \gamma_\delta \not{P}) \supset -128 \text{tr}(P^\mu P^\nu P^\rho P_\mu P_\nu P_\rho), \quad (6.117g)$$

where terms involving $\text{tr}(\dots P^2 \dots)$ have been dropped as before. Plugging Eq. (6.117) into (6.116), we can organize the two operator traces into two independent dimension-six pure gauge operators,

$$\begin{aligned} \mathcal{L}_{\text{EFT}}^{1\text{-loop}} &\supset -ic_s \left\{ -\frac{2}{3} M^6 \mathcal{I}_i^6 + 4M^4 \mathcal{I}[q^2]_i^6 - \frac{128}{3} \mathcal{I}[q^6]_i^6 \right\} \text{tr}(P^\mu P^\nu P^\rho P_\mu P_\nu P_\rho) \\ &\quad - ic_s \left\{ 2M^6 \mathcal{I}_i^6 - 20M^4 \mathcal{I}[q^2]_i^6 + 96M^2 \mathcal{I}[q^4]_i^6 - 128 \mathcal{I}[q^6]_i^6 \right\} \text{tr}(P^\mu P^\nu P^\rho P_\mu P_\rho P_\nu) \\ &= \frac{c_s}{16\pi^2} \frac{1}{M^2} \left\{ -\frac{1}{45} \text{tr}(P^\mu P^\nu P^\rho P_\mu P_\nu P_\rho) + \frac{3}{5} \text{tr}(P^\mu P^\nu P^\rho P_\mu P_\rho P_\nu) \right\} \\ &\subset \frac{c_s}{16\pi^2} \frac{1}{M^2} \left\{ \frac{2}{15} \text{tr}([P^\mu, G'_{\mu\nu}][P_\rho, G'^{\rho\nu}]) - \frac{1}{45} \text{tr}(G'^{\mu\nu} G'_{\nu\rho} G'^{\rho\mu}) \right\} \\ &= \frac{1}{16\pi^2} \frac{1}{M^2} \frac{g^2}{60} T(R) (16\mathcal{O}_{2G} - 4\mathcal{O}_{3G}), \end{aligned} \quad (6.118)$$

where

$$\mathcal{O}_{2G} = -\frac{1}{2} (D^\mu G_{\mu\nu}^a)^2, \quad \mathcal{O}_{3G} = \frac{g}{6} f^{abc} G^{a\mu}{}_\nu G^{b\nu}{}_\rho G^{c\rho}{}_\mu. \quad (6.119)$$

6.4.5 Integrating out a charged scalar singlet: penguin operators

We finally consider an example for one-loop matching involving mixed statistics. The UV theory is the SM extended by a heavy $SU(2)_L$ singlet scalar h with hypercharge -1 , which

couples to the SM Higgs and lepton doublets ϕ and l . The Lagrangian reads

$$\mathcal{L}_{\text{UV}} = \mathcal{L}_{\text{SM}} + |D_\mu h|^2 - M^2|h|^2 - \alpha|h|^4 - \beta|\phi|^2|h|^2 + \bar{l}f^\dagger\tilde{l}h + h^\dagger\tilde{l}fl, \quad (6.120)$$

where $\tilde{l} \equiv i\sigma^2 l^c$, with charge conjugation defined as $l^c \equiv -i\gamma^2 l^*$. f is a 3×3 antisymmetric matrix in generation space; e.g. $\tilde{l}fl$ is short for $\tilde{l}_a f_{ab} l_b$ with generation indices a, b summed over. One-loop matching of this model onto the SMEFT is discussed in [219, 230], with mixed heavy-light contributions obtained by computing Feynman diagrams. Here, we focus on a subset of dimension-6 operators generated in this model – the penguin operators – as an example to demonstrate the use of covariant diagrams involving heavy bosonic and light fermionic loop propagators.

We shall continue to use the four-component notation, treating l as a Dirac fermion field whose right-handed component should be set to zero in the end — this is legitimate since the unphysical component l_R cannot appear only in the loop. The quadratic terms in \mathcal{L}_{UV} needed for our calculation read

$$\mathcal{L}_{\text{UV, quad}} \supset -\frac{1}{2} \begin{pmatrix} h'^\dagger & h'^T & \bar{l}' & \tilde{l}' \end{pmatrix} \begin{pmatrix} (-P^2 + M^2 + U_h)_{2 \times 2} & (U_{hl})_{2 \times 2} \\ (U_{lh})_{2 \times 2} & (-\not{P} + U_l)_{2 \times 2} \end{pmatrix} \begin{pmatrix} h' \\ h'^* \\ l' \\ \tilde{l}' \end{pmatrix}, \quad (6.121)$$

where

$$U_h = \begin{pmatrix} 2\alpha(|h_c|^2 + h_c h_c^\dagger) + \beta|\phi|^2 & 2\alpha h_c h_c^T \\ 2\alpha h_c^* h_c^\dagger & 2\alpha(|h_c|^2 + h_c^* h_c^T) + \beta|\phi|^2 \end{pmatrix},$$

$$U_l = \begin{pmatrix} 0 & -2f^\dagger h_c \\ -2h_c^\dagger f & 0 \end{pmatrix}, \quad U_{lh} = \begin{pmatrix} -2f^\dagger \tilde{l} & 0 \\ 0 & -2fl \end{pmatrix}, \quad U_{hl} = \begin{pmatrix} -2\tilde{l}f & 0 \\ 0 & -2\bar{l}f^\dagger \end{pmatrix} \quad (6.122)$$

The light fields ϕ, l, \tilde{l} are understood as background fields ϕ_b, l_b, \tilde{l}_b . Parametrically, $h_c[\phi, l] \sim \mathcal{O}(f l^2)$ at leading order, whose explicit form will not be relevant for our calculation. The separations of the complex scalar h into (h, h^*) (with $h^* = h^\dagger$ for a scalar singlet) and the Dirac fermion l into (l, \tilde{l}) are necessary due to the presence of off-diagonal terms in U_h and U_l . As a result, each bosonic (fermionic) field in the field multiplet of Eq. (6.121) effectively has $c_s = \frac{1}{2}$ ($c_s = -\frac{1}{2}$). This is similar to the separation of the SM Higgs field ϕ into $(\phi, \tilde{\phi})$ in the scalar triplet example in Sections 6.4.2 and 6.4.3.

The penguin operators we wish to compute are $\sim \mathcal{O}(P^3 l^2)$. At one-loop level, they can only arise from covariant diagrams with one U_{hl} , one U_{lh} and three P insertions. There are nine such diagrams, two of which are hermitian conjugates of each other. They can be easily enumerated by distributing three P insertions on the h and l propagators and contracting the bosonic P insertions and fermionic light propagators (which, unlike the fermionic heavy propagators, cannot be left uncontracted). We will always start reading a covariant diagram from a bosonic propagator, and thus $c_s = \frac{1}{2}$. Dropping $\text{tr}(\dots P^2 \dots)$ terms as before, we have

$$\begin{aligned}
 \text{Diagram 1} &= -i c_s (-2^3) \mathcal{I}[q^4]_{i0}^{41} \text{tr}(U_{hl} \gamma^\mu U_{lh} P^\nu P_\mu P_\nu) = \frac{c_s}{16\pi^2} \frac{1}{M^2} \frac{1}{9} \text{tr}(U_{hl} \gamma^\mu U_{lh} P^\nu P_\mu P_\nu), \\
 &\hspace{15em} (6.123a)
 \end{aligned}$$

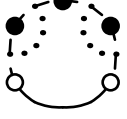
$$\begin{aligned}
 \text{Diagram 2} &= -i c_s (-2^2) \mathcal{I}[q^4]_{i0}^{32} \text{tr}(U_{hl} \gamma^\mu \gamma^\rho \gamma^\nu P_\rho U_{lh} P_\mu P_\nu) \\
 &= \frac{c_s}{16\pi^2} \frac{1}{M^2} \frac{1}{12} \text{tr}(U_{hl} \gamma^\mu \gamma^\rho \gamma^\nu P_\rho U_{lh} P_\mu P_\nu) \\
 &\supset \frac{c_s}{16\pi^2} \frac{1}{M^2} \left\{ \frac{1}{12} \text{tr}(U_{hl} \gamma^\mu P^\nu U_{lh} (P_\mu P_\nu + P_\nu P_\mu)) \right. \\
 &\quad \left. + \frac{1}{48} \text{tr}(i U_{hl} (\sigma^{\mu\nu} \gamma^\rho + \gamma^\rho \sigma^{\mu\nu}) P_\rho U_{lh} [P_\mu, P_\nu]) \right\}, \\
 &\hspace{15em} (6.123b)
 \end{aligned}$$

$$\begin{aligned}
 \text{Diagram 3} &= -i c_s (-2^2) \mathcal{I}[q^4]_{i0}^{32} \text{tr}(U_{hl} \gamma^\mu \gamma^\rho \gamma^\nu P_\rho U_{lh} P_\nu P_\mu) \\
 &= \frac{c_s}{16\pi^2} \frac{1}{M^2} \frac{1}{12} \text{tr}(U_{hl} \gamma^\mu \gamma^\rho \gamma^\nu P_\rho U_{lh} P_\nu P_\mu) \\
 &\supset \frac{c_s}{16\pi^2} \frac{1}{M^2} \left\{ \frac{1}{12} \text{tr}(U_{hl} \gamma^\mu P^\nu U_{lh} (P_\mu P_\nu + P_\nu P_\mu)) \right. \\
 &\quad \left. - \frac{1}{48} \text{tr}(i U_{hl} (\sigma^{\mu\nu} \gamma^\rho + \gamma^\rho \sigma^{\mu\nu}) P_\rho U_{lh} [P_\mu, P_\nu]) \right\}, \\
 &\hspace{15em} (6.123c)
 \end{aligned}$$

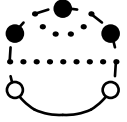
$$\begin{aligned}
 \text{Diagram 4} &= -i c_s (-2) \mathcal{I}[q^4]_{i0}^{23} \text{tr}(U_{hl} \gamma^\alpha \gamma^\mu \gamma^\rho \gamma^\nu \gamma_\alpha P_\mu P_\nu U_{lh} P_\rho) \\
 &= \frac{c_s}{16\pi^2} \frac{1}{M^2} \left(-\frac{1}{6} \right) \text{tr}(U_{hl} \gamma^\nu \gamma^\rho \gamma^\mu P_\mu P_\nu U_{lh} P_\rho) \\
 &\supset \frac{c_s}{16\pi^2} \frac{1}{M^2} \left\{ -\frac{1}{6} \text{tr}(U_{hl} \gamma^\mu (P_\mu P_\nu + P_\nu P_\mu) U_{lh} P^\nu) \right. \\
 &\quad \left. + \frac{1}{24} \text{tr}(i U_{hl} (\sigma^{\mu\nu} \gamma^\rho + \gamma^\rho \sigma^{\mu\nu}) [P_\mu, P_\nu] U_{lh} P_\rho) \right\}, \\
 &\hspace{15em} (6.123d)
 \end{aligned}$$

$$\text{Diagram 5} + \text{Diagram 6}$$

$$\begin{aligned}
&= -ic_s(-2) \mathcal{I}[q^4]_{i0}^{23} \text{tr}(U_{hl}\gamma^\alpha\gamma^\mu\gamma_\alpha\gamma^\nu\gamma^\rho P_\mu P_\nu U_{lh}P_\rho + U_{hl}\gamma^\rho\gamma^\mu\gamma^\alpha\gamma^\nu\gamma_\alpha P_\mu P_\nu U_{lh}P_\rho) \\
&= \frac{c_s}{16\pi^2} \frac{1}{M^2} \left(-\frac{1}{6}\right) \text{tr}(U_{hl}\gamma^\mu\gamma^\nu\gamma^\rho P_\mu P_\nu U_{lh}P_\rho + U_{hl}\gamma^\rho\gamma^\mu\gamma^\nu P_\mu P_\nu U_{lh}P_\rho) \\
&\supset \frac{c_s}{16\pi^2} \frac{1}{M^2} \frac{1}{12} \text{tr}(iU_{hl}(\sigma^{\mu\nu}\gamma^\rho + \gamma^\rho\sigma^{\mu\nu})[P_\mu, P_\nu]U_{lh}P_\rho), \tag{6.123e}
\end{aligned}$$



$$\begin{aligned}
&= -ic_s(-1) \mathcal{I}[q^4]_{i0}^{14} \text{tr}(U_{hl}\gamma^\alpha\gamma^\mu\gamma_\alpha\gamma^\nu\gamma^\beta\gamma^\rho\gamma_\beta P_\mu P_\nu P_\rho U_{lh}) \\
&= -ic_s(-4 + 4\epsilon) \mathcal{I}[q^4]_{i0}^{14} \text{tr}(U_{hl}\gamma^\mu\gamma^\nu\gamma^\rho P_\mu P_\nu P_\rho U_{lh}) \\
&= \frac{c_s}{16\pi^2} \left(\frac{1}{36} + \frac{1}{6} \log \frac{M^2}{\mu^2}\right) \text{tr}(U_{hl}\gamma^\mu\gamma^\nu\gamma^\rho P_\mu P_\nu P_\rho U_{lh}) \\
&\supset \frac{c_s}{16\pi^2} \left(-\frac{1}{144} - \frac{1}{24} \log \frac{M^2}{\mu^2}\right) \text{tr}(iU_{hl}(\sigma^{\mu\nu}\gamma^\rho[P_\mu, P_\nu]P_\rho + \gamma^\rho\sigma^{\mu\nu}P_\rho[P_\mu, P_\nu])U_{lh}), \tag{6.123f}
\end{aligned}$$



$$\begin{aligned}
&= -ic_s(-1) \mathcal{I}[q^4]_{i0}^{14} \text{tr}(U_{hl}\gamma^\alpha\gamma^\mu\gamma^\beta\gamma^\nu\gamma_\beta\gamma^\rho\gamma_\alpha P_\mu P_\nu P_\rho U_{lh}) \\
&= -ic_s \mathcal{I}[q^4]_{i0}^{14} \left\{ (-4 + 2\epsilon) \text{tr}(U_{hl}\gamma^\rho\gamma^\nu\gamma^\mu P_\mu P_\nu P_\rho U_{lh}) \right. \\
&\quad \left. + 2\epsilon \text{tr}(U_{hl}\gamma^\mu\gamma^\nu\gamma^\rho P_\mu P_\nu P_\rho U_{lh}) \right\} \\
&= \frac{c_s}{16\pi^2} \frac{1}{M^2} \left\{ \left(-\frac{5}{36} + \frac{1}{6} \log \frac{M^2}{\mu^2}\right) \text{tr}(U_{hl}\gamma^\rho\gamma^\nu\gamma^\mu P_\mu P_\nu P_\rho U_{lh}) \right. \\
&\quad \left. + \frac{1}{6} \text{tr}(U_{hl}\gamma^\mu\gamma^\nu\gamma^\rho P_\mu P_\nu P_\rho U_{lh}) \right\} \\
&\supset \frac{c_s}{16\pi^2} \frac{1}{M^2} \left\{ \left(\frac{5}{18} - \frac{1}{3} \log \frac{M^2}{\mu^2}\right) \text{tr}(U_{hl}\gamma^\mu P^\nu P_\mu P_\nu U_{lh}) \right. \\
&\quad \left. + \left(-\frac{11}{144} + \frac{1}{24} \log \frac{M^2}{\mu^2}\right) \text{tr}(iU_{hl}(\sigma^{\mu\nu}\gamma^\rho[P_\mu, P_\nu]P_\rho + \gamma^\rho\sigma^{\mu\nu}P_\rho[P_\mu, P_\nu])U_{lh}) \right\}, \tag{6.123g}
\end{aligned}$$



$$\begin{aligned}
&= -ic_s(-1) \mathcal{I}[q^4]_{i0}^{14} \text{tr}(U_{hl}\gamma^\alpha\gamma^\mu\gamma^\beta\gamma^\nu\gamma_\alpha\gamma^\rho\gamma_\beta P_\mu P_\nu P_\rho U_{lh}) \\
&\supset -ic_s \mathcal{I}[q^4]_{i0}^{14} \left\{ 8 \text{tr}(U_{hl}\gamma^\mu P^\nu P_\mu P_\nu U_{lh}) \right. \\
&\quad \left. - \frac{\epsilon}{2} \text{tr}(iU_{hl}(\sigma^{\mu\nu}\gamma^\rho[P_\mu, P_\nu]P_\rho + \gamma^\rho\sigma^{\mu\nu}P_\rho[P_\mu, P_\nu])U_{lh}) \right\} \\
&= \frac{c_s}{16\pi^2} \frac{1}{M^2} \left\{ \left(\frac{11}{18} - \frac{1}{3} \log \frac{M^2}{\mu^2}\right) \text{tr}(U_{hl}\gamma^\mu P^\nu P_\mu P_\nu U_{lh}) \right. \\
&\quad \left. - \frac{1}{24} \text{tr}(iU_{hl}(\sigma^{\mu\nu}\gamma^\rho[P_\mu, P_\nu]P_\rho + \gamma^\rho\sigma^{\mu\nu}P_\rho[P_\mu, P_\nu])U_{lh}) \right\}, \tag{6.123h}
\end{aligned}$$

where $\sigma^{\mu\nu} = \frac{1}{2}[\gamma^\mu, \gamma^\nu]$. The $\mathcal{O}(\epsilon)$ terms coming from gamma matrix algebra must be

kept when computing the last three diagrams, which involve the divergent master integral $\mathcal{I}[q^4]_{i0}^{14} = \frac{1}{24M_i^2}(\frac{11}{6} - \log \frac{M_i^2}{\mu^2})$, understood as $\frac{1}{24M_i^2}(\frac{2}{\epsilon} + \frac{11}{6} - \log \frac{M_i^2}{\mu^2})$. The following identities, together with the standard gamma matrix formulas, are useful in deriving Eq. (6.123),

$$\gamma^\mu \gamma^\nu = g^{\mu\nu} - i\sigma^{\mu\nu}, \quad (6.124a)$$

$$\begin{aligned} \gamma^\mu \gamma^\rho \gamma^\nu &= \frac{1}{2}(\{\gamma^\mu, \gamma^\rho\}\gamma^\nu + \gamma^\mu\{\gamma^\rho, \gamma^\nu\} - \gamma^\rho\gamma^\mu\gamma^\nu - \gamma^\mu\gamma^\nu\gamma^\rho) \\ &= g^{\mu\rho}\gamma^\nu + g^{\nu\rho}\gamma^\mu - g^{\mu\nu}\gamma^\rho + \frac{i}{2}(\sigma^{\mu\nu}\gamma^\rho + \gamma^\rho\sigma^{\mu\nu}) \end{aligned} \quad (6.124b)$$

$$\begin{aligned} &= g^{\mu\rho}\gamma^\nu + g^{\nu\rho}\gamma^\mu - \frac{1}{2}(\gamma^\rho\{\gamma^\mu, \gamma^\nu\} + \{\gamma^\mu, \gamma^\nu\}\gamma^\rho - \gamma^\rho\gamma^\nu\gamma^\mu - \gamma^\nu\gamma^\mu\gamma^\rho) \\ &= \frac{3}{2}(g^{\mu\rho}\gamma^\nu + g^{\nu\rho}\gamma^\mu) - 2g^{\mu\nu}\gamma^\rho - \frac{i}{2}(\sigma^{\rho\nu}\gamma^\mu + \gamma^\nu\sigma^{\mu\rho}), \end{aligned} \quad (6.124c)$$

$$\begin{aligned} \gamma^\alpha\gamma^\mu\gamma^\beta\gamma^\nu\gamma_\alpha\gamma^\rho\gamma_\beta &= \frac{1}{2}\{-2(\gamma^\nu\gamma^\beta\gamma^\mu\gamma^\rho\gamma_\beta + \gamma^\alpha\gamma^\mu\gamma^\rho\gamma_\alpha\gamma^\nu) + \epsilon(\gamma^\mu\gamma^\beta\gamma^\nu\gamma^\rho\gamma_\beta + \gamma^\alpha\gamma^\mu\gamma^\nu\gamma_\alpha\gamma^\rho)\} \\ &= -8g^{\mu\rho}\gamma^\nu + 2\epsilon(g^{\nu\rho}\gamma^\mu + g^{\mu\nu}\gamma^\rho) + \epsilon(\gamma^\nu\gamma^\mu\gamma^\rho + \gamma^\mu\gamma^\rho\gamma^\nu) \\ &= -8g^{\mu\rho}\gamma^\nu + 3\epsilon(g^{\nu\rho}\gamma^\mu + g^{\mu\nu}\gamma^\rho) + i\epsilon(\sigma^{\mu\nu}\gamma^\rho + \gamma^\mu\sigma^{\nu\rho}). \end{aligned} \quad (6.124d)$$

Note that we have been careful to keep all expressions in the intermediate steps of the calculation manifestly hermitian, in order to easily obtain manifestly hermitian final results. This is why we have applied gamma matrix formulas in a symmetric manner in Eq. (6.124). Adding up all diagrams computed in Eq. (6.123), we have

$$\begin{aligned} \mathcal{L}_{\text{EFT}}^{\text{1-loop}} &\supset \frac{c_s}{16\pi^2} \frac{1}{M^2} \text{tr} \left\{ \frac{1}{9} U_{hl} \gamma^\mu U_{lh} P^\nu P_\mu P_\nu + \frac{1}{6} U_{hl} \gamma^\mu P^\nu U_{lh} (P_\mu P_\nu + P_\nu P_\mu) \right. \\ &\quad - \frac{1}{6} U_{hl} \gamma^\mu (P_\mu P_\nu + P_\nu P_\mu) U_{lh} P^\nu + \left(\frac{8}{9} - \frac{2}{3} \log \frac{M^2}{\mu^2} \right) U_{hl} \gamma^\mu P^\nu P_\mu P_\nu U_{lh} \\ &\quad + \frac{1}{8} i U_{hl} (\sigma^{\mu\nu} \gamma^\rho + \gamma^\rho \sigma^{\mu\nu}) [P_\mu, P_\nu] U_{lh} P_\rho \\ &\quad \left. - \frac{1}{8} i U_{hl} (\sigma^{\mu\nu} \gamma^\rho [P_\mu, P_\nu] P_\rho + \gamma^\rho \sigma^{\mu\nu} P_\rho [P_\mu, P_\nu]) U_{lh} \right\} \\ &\subset \frac{c_s}{16\pi^2} \frac{1}{M^2} \text{tr} \left\{ \frac{1}{12} (U_{hl} \gamma^\mu [P_\nu, [P^\nu, [P_\mu, U_{lh}]]] + U_{hl} \gamma^\mu [P_\mu, [P^\nu, [P_\nu, U_{lh}]]]) \right. \\ &\quad - \frac{1}{18} U_{hl} \gamma^\nu U_{lh} [P^\mu, [P_\mu, P_\nu]] + \left(-\frac{4}{9} + \frac{1}{3} \log \frac{M^2}{\mu^2} \right) U_{hl} \gamma^\nu [P^\mu, [P_\mu, P_\nu]] U_{lh} \\ &\quad \left. - \frac{1}{8} (i U_{hl} \sigma^{\mu\nu} \gamma^\rho [P_\mu, P_\nu] [P_\rho, U_{lh}] - i [P_\rho, U_{hl}] \sigma^{\mu\nu} \gamma^\rho [P_\mu, P_\nu] U_{lh}) \right\} \\ &= \frac{c_s}{16\pi^2} \frac{1}{M^2} \left\{ -\frac{1}{3} [i \bar{l} f^\dagger f (D^2 \not{D} + \not{D} D^2) l + i \bar{\tilde{l}} f f^\dagger (D^2 \not{D} + \not{D} D^2) \tilde{l}] \right. \\ &\quad + \frac{2}{9} [(\bar{l} f^\dagger f \gamma^\nu l) D^\mu (g' B_{\mu\nu} Y_{h^*}) + (\bar{\tilde{l}} f f^\dagger \gamma^\nu \tilde{l}) D^\mu (g' B_{\mu\nu} Y_h)] \\ &\quad \left. + \left(\frac{16}{9} - \frac{4}{3} \log \frac{M^2}{\mu^2} \right) \right\} \end{aligned}$$

$$\begin{aligned}
& \left[\bar{l} f^\dagger f \gamma^\nu D^\mu \left(g W_{\mu\nu}^a \frac{\tau^a}{2} + g' B_{\mu\nu} Y_l \right) l + \bar{\tilde{l}} f f^\dagger \gamma^\nu D^\mu \left(g W_{\mu\nu}^a \frac{\tau^a}{2} + g' B_{\mu\nu} Y_l \right) \tilde{l} \right] \\
& + \frac{1}{2} \left[i \bar{l} f^\dagger f \sigma^{\mu\nu} \left(g W_{\mu\nu}^a \frac{\tau^a}{2} + g' B_{\mu\nu} Y_l \right) \not{D} l \right. \\
& \quad \left. + i \bar{\tilde{l}} f f^\dagger \sigma^{\mu\nu} \left(g W_{\mu\nu}^a \frac{\tau^a}{2} + g' B_{\mu\nu} Y_l \right) \not{D} \tilde{l} + \text{h.c.} \right] \Big\} \\
= & \frac{1}{16\pi^2} \frac{1}{M^2} \left\{ -\frac{1}{3} i \bar{l} f^\dagger f (D^2 \not{D} + \not{D} D^2) l \right. \\
& + \frac{2}{3} \left(\frac{5}{3} - \log \frac{M^2}{\mu^2} \right) g' (\bar{l} f^\dagger f \gamma^\nu l) (D^\mu B_{\mu\nu}) + \frac{2}{3} \left(\frac{4}{3} - \log \frac{M^2}{\mu^2} \right) g (\bar{l} f^\dagger f \gamma^\nu \tau^a l) (D^\mu W_{\mu\nu}^a) \\
& \left. + \frac{1}{4} [i g' (\bar{l} f^\dagger f \sigma^{\mu\nu} \not{D} l) B_{\mu\nu} + \text{h.c.}] + \frac{1}{4} [i g' (\bar{\tilde{l}} f f^\dagger \sigma^{\mu\nu} \tau^a \not{D} \tilde{l}) W_{\mu\nu}^a + \text{h.c.}] \right\}, \quad (6.125)
\end{aligned}$$

where we have denoted the sigma matrices by τ^a to avoid clash of notation. Note that the form of $[P_\mu, P_\nu] = igG_{\mu\nu}$ depends on the propagator on which it is inserted, e.g. $[P_\mu, P_\nu] = igW_{\mu\nu}^a \frac{\tau^a}{2} + ig'B_{\mu\nu}Y$ and $ig'B_{\mu\nu}Y$ for $SU(2)_L$ doublets and singlets, respectively. Also, we see that terms involving l and \tilde{l} contribute equally, yielding a factor of 2 which cancels against $c_s = \frac{1}{2}$ in the last line of Eq. (6.125). Our results agree with those obtained in [230] by Feynman diagram calculations.

6.5 Conclusions

Matching from an UV theory to a low-energy EFT via gauge-covariant functional methods, as an alternative to Feynman diagrams, will continue to be both theoretically interesting and practically useful. We are now at a stage where one-loop universal master formulas are available [55, 56] and have proven useful in the simplest cases (namely in the absence of mixed heavy-light contributions, open covariant derivatives, etc.), while various proposals exist [57–59] to deal with such additional structures that arise in practical applications. An interesting question to explore at this point is whether ideas from these (or other similar) proposals can be implemented as easily as existing universal master formulas, without the need for additional functional manipulations which might make functional matching methods less accessible.

To this end, we have introduced covariant diagrams as a tool to keep track of functional matching calculations. They are easy to use, and provide physical intuition. Specifically, we carried out a functional matching procedure that builds upon and extends the approach of [59], from which a set of rules for associating terms in a CDE with one-loop diagrams was derived — this was done, *once and for all*, in Sections 6.2 through 6.3.4. The rules are reminiscent of conventional Feynman rules, but with a crucial difference that only gauge-covariant quantities are involved. The recipe summarized in Section 6.3.5 can be easily followed in

one-loop matching calculations, including those involving mixed heavy-light contributions, open covariant derivatives and mixed statistics, which are not directly captured by existing universal results. We presented many example calculations in Section 6.4, showing technical details for the sake of pedagogy. They provide nontrivial tests of our covariant diagrams formalism. As a byproduct, some universal results incorporating the additional structures were obtained in the intermediate steps, which are also useful beyond the specific UV models considered in this chapter.

Compared with Feynman diagrammatic matching, our formalism inherits some key advantages of functional matching, namely gauge covariance in intermediate steps and the possibility of obtaining universal results as discussed in the Introduction. In addition, compared with recently-proposed functional matching approaches, our covariant diagrammatic formulation has the following highlights:

- No additional functional manipulations (nor subtraction procedures) are needed. One simply draws diagrams and reads off associated master integrals and operator structures, which is more intuitive conceptually.
- The step of collecting identical terms in a CDE is automatically achieved by associating a symmetry factor to each covariant diagram, which trivially follows from rotation symmetry of the diagram.
- Loops with fermions are easily handled. As in the pure bosonic case, vertex insertion rules are directly obtained from the quadratic pieces of the UV Lagrangian without explicitly block-diagonalizing the quadratic operator.

An attractive direction to move forward in, as far as functional matching methods are concerned, is trying to fully exploit their universality feature and derive more general universal master formulas for one-loop matching. It is an intriguing possibility that as many interesting UV theories as possible can be matched onto low-energy EFTs simply by applying a few master formulas. In this regard, covariant diagrams provide a useful tool to organize and simplify the calculations involved — we already saw in Section 6.4.1 that they allow for a simpler derivation of existing universal results. Meanwhile, even in the absence of complete universal results, one can already take advantage of covariant diagram techniques to facilitate one-loop matching calculations for specific UV models of phenomenological interest, as we did in Sections 6.4.2 through 6.4.5. We also comment that the algorithm of enumerating and computing covariant diagrams can in principle be automated, providing a useful and efficient alternative to automated Feynman diagrammatic matching calculations. Besides, it is interesting to consider the possibility of extending covariant diagram techniques beyond

one loop for EFT matching, and more generally for extracting UV information of a quantum field theory (including e.g. renormalization group evolution [57]).

Chapter 7

EFT Approach to Trans-TeV Supersymmetry

Dismissing traditional naturalness concerns while embracing the Higgs boson mass measurement and unification motivates careful analysis of trans-TeV supersymmetric theories. We take an effective field theory (EFT) approach, matching the Minimal Supersymmetric Standard Model (MSSM) onto the Standard Model (SM) EFT by integrating out heavy superpartners, and evolving MSSM and SMEFT parameters according to renormalization group equations in each regime. Our matching calculation is facilitated by the covariant diagrams formulation of functional matching techniques, with the full one-loop SUSY threshold corrections encoded in just 30 diagrams. Requiring consistent matching onto the SMEFT with its parameters (those in the Higgs potential in particular) measured at low energies, and in addition requiring unification of bottom and tau Yukawa couplings at the scale of gauge coupling unification, we detail the solution space of superpartner masses from the TeV scale to well above. We also provide detailed views of parameter space where Higgs coupling measurements have probing capability at future colliders beyond the reach of direct superpartner searches at the LHC.

7.1 Introduction

The lack of new physics discoveries at the LHC has led us to consider the possibility that beyond Standard Model (BSM) states responsible for solving the outstanding problems in particle physics, e.g. unification and dark matter, are much heavier than the weak scale. In this scenario, weak-scale phenomenology can be conveniently described by an effective field theory (EFT). With heavy new particles integrated out, their virtual effects are encoded in higher-dimensional effective operators involving the light Standard Model (SM) fields.

Recent years have seen a growing EFT literature, many of which aim to carefully examine phenomenological impact of higher-dimensional operators; see e.g. [5–7] for reviews. Experimental data have put constraints on many of these operators, which can be translated into constraints on, e.g. masses and couplings of heavy new particles, once the BSM theory is specified.

On the other hand, the usefulness of EFT approaches to BSM physics extends beyond bottom-up studies. From a top-down perspective, we may be interested to ask whether some attractive speculative ideas – supersymmetry (SUSY), unification, etc. – can be realized in specific BSM setups, while being consistent with the SMEFT we have established at low energy. To address such questions requires careful matching between the full theory and EFT parameters across heavy particle thresholds. In particular, in addition to higher-dimensional operators being generated, changes in renormalizable operator coefficients across thresholds are often important to account for. These “threshold corrections” are invisible to low-energy experiment, but may be crucial for answering questions regarding high-scale physics, like the one on SUSY and unification posed above.

For example, in the context of the Minimal Supersymmetric Standard Model (MSSM), we would like to know what regions of parameter space can realize unification of not only the three gauge couplings, but also the bottom and tau Yukawa couplings, and meanwhile allow consistent matching onto the SMEFT with its parameters (those in the Higgs potential in particular) measured at low energy. Further, we would like to know what phenomenological implications, if any, such parameter choices may have.

These are questions we would like to investigate in this chapter, taking a top-down EFT approach. We will compute the full one-loop contributions to the SM renormalizable operators when heavy BSM states in the MSSM are integrated out, from which SUSY threshold corrections to all SM parameters can be easily obtained. As we will see, threshold corrections to the bottom Yukawa and Higgs quartic couplings are of particular importance for achieving both b - τ Yukawa unification and consistent matching onto the SMEFT.

In this calculation, we find solutions for SUSY scales from TeV up to 10^{10} GeV. However, only the lower edge of this broad trans-TeV window can be within experimental reach. Given the further motivation of a dark matter candidate, we will take a closer look at the 1-10 TeV regime. In particular, we will extend our one-loop matching calculation to the dimension-six level, and obtain parametrically enhanced contributions to the operators affecting $hb\bar{b}$ and $h\tau^+\tau^-$ couplings, which can dominate over tree-level effects. We will show how precision Higgs measurements constitute a powerful indirect probe of TeV-scale SUSY with b - τ Yukawa unification that is complementary to direct superpartner searches.

We note that while the full one-loop SUSY threshold corrections (as well as sparticle

mass corrections) in the MSSM have been known for some time [231], growing interest in EFT formulations of the calculation is quite recent (see e.g. [47–53]). This is of course largely due to higher-scale SUSY having been less attractive from the fine-tuning point of view. Here we shall adopt the perspective that the weak scale may indeed be fine-tuned to some degree, with new particles in the trans-TeV regime, justifying an EFT treatment. In this case, the MSSM still exhibits several attractive features, including gauge and Yukawa coupling unification as mentioned above, and may also provide a dark matter candidate. Our philosophy here is in line with earlier studies in [232, 233] on Yukawa unification with heavy superpartners. In particular, the capability of unification and dark matter requirements to severely constrain the SUSY parameter space has been recently emphasized in [233].

A new ingredient of our work is that, instead of computing low-energy observables such as SM particle masses and the Fermi constant, we obtain SUSY threshold corrections directly from the path integral by taking advantage of functional matching techniques, which have attracted much attention and undergone interesting developments recently [55–61, 216–218] (see also [196–198, 219, 220]). Such techniques can greatly simplify EFT matching calculations, thanks to preservation of gauge covariance and exhibition of a universal structure [56, 58, 61]. In [60], a concise diagrammatic formulation of functional matching at one-loop level was obtained: the low-energy effective Lagrangian directly derives from a sum of “covariant diagrams,” following a set of simple rules. This approach is general enough to overcome several limitations of previous formulations, and so will be used here.

From the technical point of view, our calculation also serves as a nontrivial test case for the covariant diagrams technique. It also further demonstrates the simplicity of the approach. In particular, with just 30 covariant diagrams, we are able to obtain full one-loop SUSY threshold corrections in agreement with existing results in the literature.

7.1.1 EFT matching, threshold corrections and observables

Consider a general BSM theory whose Lagrangian has the following form,

$$\mathcal{L}[\varphi_{\text{BSM}}, \varphi_{\text{SM}}] = \mathcal{L}_{\text{SM}}[\varphi_{\text{SM}}] + \mathcal{L}_{\text{BSM}}[\varphi_{\text{BSM}}, \varphi_{\text{SM}}]. \quad (7.1)$$

Here φ_{SM} , φ_{BSM} collectively denote fields within and beyond the SM, respectively. The SM part of the Lagrangian reads

$$\begin{aligned} \mathcal{L}_{\text{SM}} = & |D_\mu \phi|^2 + \sum_{f=q,u,d,l,e} \bar{f} i \not{D} f - \frac{1}{4} G_{\mu\nu}^A G^{A\mu\nu} - \frac{1}{4} W_{\mu\nu}^I W^{I\mu\nu} - \frac{1}{4} B_{\mu\nu} B^{\mu\nu} \\ & - m^2 |\phi|^2 - \lambda |\phi|^4 - (\bar{\psi}_u \mathbf{y}_u \psi_q \cdot \epsilon \cdot \phi + \bar{\psi}_d \mathbf{y}_d \psi_q \cdot \phi^* + \bar{\psi}_e \mathbf{y}_e \psi_l \cdot \phi^* + \text{h.c.}), \end{aligned} \quad (7.2)$$

where $\epsilon = i\sigma^2$, and dots denote $SU(2)_L$ index contractions. ψ_f are four-component spinors containing the SM chiral fermions f , e.g. $\psi_q = (q_a, 0)$, $\psi_u = (0, u^{\dagger a})$, etc. Here and in the following, we use boldface, e.g. $\mathbf{y}_u, \mathbf{y}_d, \mathbf{y}_e$, for 3×3 matrices in generation space.

The EFT approach applies when the BSM fields φ_{BSM} are much heavier than the SM weak scale. In this case, integrating out φ_{BSM} from the path integral results in a local effective Lagrangian for φ_{SM} ,

$$\begin{aligned} \int [D\varphi_{\text{BSM}}][D\varphi_{\text{SM}}] e^{i \int d^d x (\mathcal{L}_{\text{SM}} + \mathcal{L}_{\text{BSM}})} &= \int [D\varphi_{\text{SM}}] e^{i \int d^d x (\mathcal{L}_{\text{SM}} + \mathcal{L}_{(d \leq 4)} + \mathcal{L}_{(d=5)} + \mathcal{L}_{(d=6)} + \dots)} \\ &\equiv \int [D\varphi_{\text{SM}}] e^{i \int d^d x \mathcal{L}_{\text{SMEFT}}}. \end{aligned} \quad (7.3)$$

As implied in the equation above, this procedure of matching \mathcal{L} onto $\mathcal{L}_{\text{SMEFT}}$ generally produces extra renormalizable ($d \leq 4$) pieces in the EFT Lagrangian, in addition to \mathcal{L}_{SM} that already exists in the full theory. However, they can be absorbed into \mathcal{L}_{SM} via proper redefinitions of fields and couplings and thus do not have observable consequences at low energy. To be explicit, let us write

$$\begin{aligned} \mathcal{L}_{(d \leq 4)} &= \delta Z_\phi |D_\mu \phi|^2 + \sum_{f=q,u,d,l,e} \bar{\psi}_f \delta \mathbf{Z}_f i \not{D} \psi_f \\ &\quad - \frac{1}{4} \delta Z_G G_{\mu\nu}^A G^{A\mu\nu} - \frac{1}{4} \delta Z_W W_{\mu\nu}^I W^{I\mu\nu} - \frac{1}{4} \delta Z_B B_{\mu\nu} B^{\mu\nu} \\ &\quad + \delta m^2 |\phi|^2 + \delta \lambda |\phi|^4 \\ &\quad + (\bar{\psi}_u \delta \mathbf{y}_u \psi_q \cdot \epsilon \cdot \phi + \bar{\psi}_d \delta \mathbf{y}_d \psi_q \cdot \phi^* + \bar{\psi}_e \delta \mathbf{y}_e \psi_l \cdot \phi^* + \text{h.c.}). \end{aligned} \quad (7.4)$$

Rescaling the SM fields to retain canonical normalization of their kinetic terms (up to terms of second order or higher in the δZ 's¹),

$$\hat{\varphi}_{\text{SM}} = \left(1 + \frac{1}{2} \delta Z_{\varphi_{\text{SM}}}\right) \varphi_{\text{SM}}, \quad (7.5)$$

and defining effective parameters as follows,

$$\begin{aligned} g_3^{\text{eff}} &= g_3 \left(1 - \frac{1}{2} \delta Z_G\right), & g^{\text{eff}} &= g \left(1 - \frac{1}{2} \delta Z_W\right), & g'^{\text{eff}} &= g' \left(1 - \frac{1}{2} \delta Z_B\right), \\ m_{\text{eff}}^2 &= m^2 (1 - \delta Z_\phi) - \delta m^2, & \lambda_{\text{eff}} &= \lambda (1 - 2 \delta Z_\phi) - \delta \lambda, \\ \mathbf{y}_u^{\text{eff}} &= \mathbf{y}_u - \delta \mathbf{y}_u - \frac{1}{2} (\mathbf{y}_u \delta \mathbf{Z}_q + \delta \mathbf{Z}_u \mathbf{y}_u + \mathbf{y}_u \delta Z_\phi), \\ \mathbf{y}_d^{\text{eff}} &= \mathbf{y}_d - \delta \mathbf{y}_d - \frac{1}{2} (\mathbf{y}_d \delta \mathbf{Z}_q + \delta \mathbf{Z}_d \mathbf{y}_d + \mathbf{y}_d \delta Z_\phi), \end{aligned}$$

¹Here $\delta Z_{\varphi_{\text{SM}}}$ is understood as the matrix $\delta \mathbf{Z}_f$ for $\varphi_{\text{SM}} = f$, which is symmetric in generation space as required by hermiticity of the Lagrangian.

$$\mathbf{y}_e^{\text{eff}} = \mathbf{y}_e - \delta \mathbf{y}_e - \frac{1}{2}(\mathbf{y}_e \delta \mathbf{Z}_l + \delta \mathbf{Z}_e \mathbf{y}_e + \mathbf{y}_e \delta Z_\phi), \quad (7.6)$$

we obtain

$$\begin{aligned} \mathcal{L}_{\text{SMEFT}} &= |D_\mu \hat{\phi}|^2 + \sum_{f=q,u,d,l,e} \bar{f} i \not{D} f - \frac{1}{4} \hat{G}_{\mu\nu}^A \hat{G}^{A\mu\nu} - \frac{1}{4} \hat{W}_{\mu\nu}^I \hat{W}^{I\mu\nu} - \frac{1}{4} \hat{B}_{\mu\nu} \hat{B}^{\mu\nu} \\ &\quad - m_{\text{eff}}^2 |\hat{\phi}|^2 - \lambda_{\text{eff}} |\hat{\phi}|^4 - (\bar{\psi}_u \mathbf{y}_u^{\text{eff}} \hat{\psi}_q \cdot \epsilon \cdot \hat{\phi} + \bar{\psi}_d \mathbf{y}_d^{\text{eff}} \hat{\psi}_q \cdot \hat{\phi}^* + \bar{\psi}_e \mathbf{y}_e^{\text{eff}} \hat{\psi}_l \cdot \hat{\phi}^* + \text{h.c.}) \\ &\quad + \mathcal{L}_{(d=5)} + \mathcal{L}_{(d=6)} + \dots, \end{aligned} \quad (7.7)$$

where

$$D_\mu = \partial_\mu - i g_3^{\text{eff}} t^A \hat{G}_\mu^A - i g^{\text{eff}} t^I \hat{W}_\mu^I - i g'^{\text{eff}} Y \hat{B}_\mu, \quad (7.8)$$

with t^A , t^I being the $SU(3)_c$ and $SU(2)_L$ generators in the corresponding representation.

We see that while the renormalizable part of $\mathcal{L}_{\text{SMEFT}}$ contains the same operators as the \mathcal{L}_{SM} part of the full theory Lagrangian, their coefficients, i.e. the parameters labeled by “eff” whose values we can extract from experiment, are generally different from their counterparts in the full theory. These differences are usually referred to as “threshold corrections,” and are important to take into account when studying higher-energy phenomena of the full theory, such as unification in the MSSM. It is clear from Eq. (7.6) that threshold corrections are directly related to operator coefficients in the $\mathcal{L}_{(d \leq 4)}$ piece generated from the matching procedure of Eq. (7.3).

On the other hand, the non-renormalizable part of $\mathcal{L}_{\text{SMEFT}}$, i.e. $\mathcal{L}_{(d=5)} + \mathcal{L}_{(d=6)} + \dots$, can cause low-energy observations to deviate from expectations of the renormalizable SM: $\mathcal{L}_{(d=5)}$ contains just one operator which is responsible for non-zero neutrino masses, while $\mathcal{L}_{(d=6)}$ contains a large number of operators which contribute to e.g. electroweak, Higgs, and flavor observables. For example, consider the following dimension-six operators (neglecting differences between φ_{SM} and $\hat{\varphi}_{\text{SM}}$),

$$\mathcal{L}_{(d=6)} \supset |\phi|^2 (\bar{\psi}_q \mathbf{C}_{d\phi} \psi_d) \cdot \phi + |\phi|^2 (\bar{\psi}_l \mathbf{C}_{e\phi} \psi_e) \cdot \phi + \text{h.c.} \quad (7.9)$$

After RG evolved down to the weak scale, they affect couplings of the SM Higgs boson to down-type quarks and leptons, and hence observables like the Higgs boson partial widths. When fermion masses are used as inputs of the calculation, we have

$$\Gamma(h \rightarrow f\bar{f}) = (1 + \delta\kappa_f)^2 \Gamma(h \rightarrow f\bar{f})_{\text{SM}}, \quad (7.10)$$

with

$$\delta\kappa_b = -\frac{C_{b\phi}v^2}{y_b^{\text{eff}}}, \quad \delta\kappa_\tau = -\frac{C_{\tau\phi}v^2}{y_\tau^{\text{eff}}}, \quad (7.11)$$

etc. at tree level, where $y_{b,\tau}^{\text{eff}}$, $C_{b\phi,\tau\phi}$ are 33 elements of $\mathbf{y}_{d,e}^{\text{eff}}$, $\mathbf{C}_{d\phi,e\phi}$, respectively.

Note that $C_{b\phi,\tau\phi} \sim \Lambda^{-2}$ with Λ being the scale of new physics being integrated out, and therefore, the observable BSM effects $\delta\kappa_{b,\tau}$ decouple as $\frac{v^2}{\Lambda^2}$ as Λ increases. This is in contrast to the (unobservable) threshold corrections discussed above, which originate from $d \leq 4$ operators and thus do not decouple. We will see in Section 7.3 that in the specific case of the MSSM with b - τ Yukawa unification, threshold corrections to λ and y_b are actually larger for higher SUSY scales.

Meanwhile, in addition to the Λ power counting, the low-energy EFT is also organized by a loop counting. Take the calculation of $\Gamma(h \rightarrow b\bar{b})$ for example. Higher order corrections come from both EFT matching for $d > 4$ operators ($C_{b\phi} = C_{b\phi}^{\text{tree}} + C_{b\phi}^{\text{1-loop}} + \dots$ in the present case) and loop level Feynman diagrams in the EFT. Generally speaking, when Λ is much higher than the weak scale, the only such corrections that are essential to take into account are the non-decoupling ones from the renormalizable SM loops, namely corrections to $\Gamma(h \rightarrow b\bar{b})_{\text{SM}}$ (see [234–236] for state-of-the-art calculations). An exception is when $\mathcal{O}(\frac{1}{16\pi^2\Lambda^2})$ corrections are parametrically enhanced, e.g. by $\tan\beta \gg 1$ in the case of the MSSM. We will see in Section 7.4 that such enhanced contributions to $C_{b\phi}^{\text{1-loop}}$ can dominate over $C_{b\phi}^{\text{tree}}$ in some regions of the MSSM parameter space, and are therefore also essential to take into account when making predictions for $\Gamma(h \rightarrow b\bar{b})$ in the EFT. The results can of course be further refined by computing non-enhanced contributions, and even higher order terms in both the Λ^{-1} and loop expansions (see e.g. [200, 237–239]). See also [41, 90, 240, 241] for related discussions on EFT power counting.

7.2 Matching the MSSM onto the SMEFT

7.2.1 MSSM fields and interactions

We now use the covariant diagrams technique to match the MSSM onto the SMEFT. To begin with, we need to extract the field content (including gauge quantum numbers of each field which determine the form of P_μ) and the interaction matrix $\mathbf{U}[\varphi]$ of the MSSM.

The complete MSSM field multiplet $(\varphi_H, \varphi_L)^T$ is given in Tables 7.1 and 7.2. We have explicitly written out the internal indices carried by each field for clarity. In particular, we use i, A, α, I, a and \dot{a} for $SU(3)_c$ fundamental and adjoint, $SU(2)_L$ fundamental and adjoint, and spinor indices on the conjugate fields on the left side of the quadratic operator \mathcal{Q}_{UV} ,

and j, B, β, J, b and \dot{b} for those on the fields on the right side.

The scalar sector of the MSSM consists of sfermions and two Higgs doublets. For the latter, we choose a basis (Φ, ϕ) where the mass matrix in the electroweak-symmetric phase is diagonal,

$$\begin{aligned} \mathcal{L}_{\text{MSSM}} &\supset -(\mu^2 + m_{H_u}^2)|H_u|^2 - (\mu^2 + m_{H_d}^2)|H_d|^2 - b(H_u \cdot \epsilon \cdot H_d + \text{h.c.}) \\ &= -m^2|\phi|^2 - M_\Phi^2|\Phi|^2. \end{aligned} \quad (7.12)$$

The (Φ, ϕ) and (H_u, H_d) bases are related by

$$\Phi = c_{\beta'} H_u + s_{\beta'} \epsilon \cdot H_d^*, \quad \phi = s_{\beta'} H_u - c_{\beta'} \epsilon \cdot H_d^*. \quad (7.13)$$

where we have abbreviated $\sin \beta' \equiv s_{\beta'}$, $\cos \beta' \equiv c_{\beta'}$, with β' defined by

$$\tan 2\beta' = \frac{2b}{m_{H_u}^2 - m_{H_d}^2}. \quad (7.14)$$

Note that β' is different from what is usually referred to as β as in $\tan \beta = \frac{v_u}{v_d}$, the ratio of vacuum expectation values (vevs) of H_u and H_d . In fact, at one-loop level, minimizing the effective potential, we can see that the two are related by²

$$\beta = \beta' + \frac{1}{M_\Phi^2} s_{\beta'} c_{\beta'} \left(\frac{t_u}{v_u} - \frac{t_d}{v_d} \right) \mathcal{O}\left(\frac{\Lambda^2}{16\pi^2}\right) + \mathcal{O}(\Lambda^{-2}), \quad (7.15)$$

in the decoupling limit $|m^2| \ll M_{\Phi, \tilde{f}, \tilde{\chi}, \tilde{V}}^2 \sim \mathcal{O}(\Lambda^2)$ that we are interested in. Here t_u, t_d are one-loop tadpoles, whose analytical expressions can be found in e.g. [231].

As for fermions, we choose to work with four-component spinor fields. In particular, we write the Higgsinos as a Dirac spinor, and the gauginos as Majorana spinors. The SM chiral fermions f are embedded into Dirac spinors ψ_f , in which we also retain unphysical wrong-chirality Weyl fermions f' , and set them to zero only at the end of the calculation³.

Interactions among the MSSM fields in Tables 7.1 and 7.2 are encoded in the covariant derivative P_μ and interaction matrices $\mathbf{U}[\varphi]$, $\mathbf{Z}[\varphi]$ in our functional matching formalism. They are extracted from the terms in the MSSM Lagrangian that are quadratic in quantum

²Here we are defining β in a tadpole-free scheme, where v_u, v_d denote the location of the minimum of the loop-corrected effective potential (and are gauge dependent). An alternative scheme that is also commonly used defines v_u, v_d by the location of the minimum of the tree-level Higgs potential, independent of gauge choice; in that scheme, $\tan \beta$ differs from $\tan \beta'$ only by $\mathcal{O}(\Lambda^{-2})$ terms.

³Generally, such embedding would require additionally writing projection operators in interaction terms to pick up the physical fermion fields. However, this is not necessary in the special case of R -parity-conserving MSSM considered here.

MSSM field	$SU(3)_c \times SU(2)_L \times U(1)_Y$	Conjugate field
Heavy spin-0 ($c_s = \frac{1}{2}$)		
Φ_β	$(1, 2, \frac{1}{2})$	$\Phi^{*\alpha}$
$\Phi^{*\beta}$	$(1, \bar{2}, -\frac{1}{2})$	Φ_α
$\tilde{q}_{j\beta} = (u_{Lj}, d_{Lj})$	$(3, 2, \frac{1}{6})$	$\tilde{q}^{*i\alpha}$
$\tilde{q}^{*j\beta} = (u_L^{*j}, d_L^{*j})$	$(\bar{3}, \bar{2}, -\frac{1}{6})$	$\tilde{q}_{i\alpha}$
$\tilde{u}_j = \tilde{u}_{Rj}$	$(3, 1, \frac{2}{3})$	\tilde{u}^{*i}
$\tilde{u}^{*j} = \tilde{u}_R^{*j}$	$(\bar{3}, 1, -\frac{2}{3})$	\tilde{u}_i
$\tilde{d}_j = \tilde{d}_{Rj}$	$(3, 1, -\frac{1}{3})$	\tilde{d}^{*i}
$\tilde{d}^{*j} = \tilde{d}_R^{*j}$	$(\bar{3}, 1, \frac{1}{3})$	\tilde{d}_i
$\tilde{l}_\beta = (\nu_L, e_L)$	$(1, 2, -\frac{1}{2})$	$\tilde{l}^{*\alpha}$
$\tilde{l}^{*\beta} = (\nu_L^*, e_L^*)$	$(1, \bar{2}, \frac{1}{2})$	\tilde{l}_α
$\tilde{e} = \tilde{e}_R$	$(1, 1, -1)$	\tilde{e}^*
$\tilde{e}^* = \tilde{e}_R^*$	$(1, 1, 1)$	\tilde{e}
Heavy spin-1/2 ($c_s = -\frac{1}{2}$)		
$\tilde{\chi}_\beta = \begin{pmatrix} \tilde{\chi}_{ub\beta} \\ \epsilon_{\beta\delta} \tilde{\chi}_d^{\dagger b\delta} \end{pmatrix}$	$(1, 2, \frac{1}{2})$	$\overline{\tilde{\chi}}^\alpha = (\epsilon^{\alpha\gamma} \tilde{\chi}_{d\gamma}^a, \chi_{u\dot{a}}^\dagger{}^\alpha)$
$\tilde{\chi}^{c\beta} = \begin{pmatrix} \epsilon^{\beta\delta} \tilde{\chi}_{db\delta} \\ \tilde{\chi}_u^{\dagger b\beta} \end{pmatrix}$	$(1, \bar{2}, -\frac{1}{2})$	$\overline{\tilde{\chi}}_\alpha^c = (\tilde{\chi}_{u\alpha}^a, \epsilon_{\alpha\gamma} \chi_{d\dot{a}}^\dagger{}^\gamma)$
$\tilde{g}^B = \begin{pmatrix} \lambda_{gb}^B \\ \lambda_g^{\dagger bB} \end{pmatrix}$	$(8, 1, 0)$	$\overline{\tilde{g}}^A = (\lambda_g^{aA}, \lambda_{g\dot{a}}^{\dagger A})$
$\tilde{W}^J = \begin{pmatrix} \lambda_{Wb}^J \\ \lambda_W^{\dagger bJ} \end{pmatrix}$	$(1, 3, 0)$	$\overline{\tilde{W}}^I = (\lambda_W^{aI}, \lambda_{W\dot{a}}^{\dagger I})$
$\tilde{B} = \begin{pmatrix} \lambda_{Bb} \\ \lambda_B^{\dagger b} \end{pmatrix}$	$(1, 1, 0)$	$\overline{\tilde{B}} = (\lambda_B^a, \lambda_{B\dot{a}}^\dagger)$

Table 7.1: (From [132]) Heavy fields φ_H in the MSSM, their gauge quantum numbers, and conjugate fields (which appear on the left side of \mathcal{Q}_{UV}).

MSSM field	$SU(3)_c \times SU(2)_L \times U(1)_Y$	Conjugate field
Light spin-0 ($c_s = \frac{1}{2}$)		
ϕ_β	$(1, 2, \frac{1}{2})$	$\phi^{*\alpha}$
$\phi^{*\beta}$	$(1, \bar{2}, -\frac{1}{2})$	ϕ_α
Light spin-1/2 ($c_s = -\frac{1}{2}$)		
$\psi_{qj\beta} = \begin{pmatrix} q_{bj\beta} \\ q_{j\beta}^\dagger \end{pmatrix}$	$(3, 2, \frac{1}{6})$	$\bar{\psi}_q^{i\alpha} = (q'^{ai\alpha}, q_a^{\dagger i\alpha})$
$\psi_q^{cj\beta} = \begin{pmatrix} q_b^{j\beta} \\ q^{\dagger bj\beta} \end{pmatrix}$	$(\bar{3}, \bar{2}, -\frac{1}{6})$	$\bar{\psi}_{qi}^c = (q_{i\alpha}^a, q_{\dot{a}i\alpha}^\dagger)$
$\psi_{uj} = \begin{pmatrix} u'_{bj} \\ u_j^\dagger \end{pmatrix}$	$(3, 1, \frac{2}{3})$	$\bar{\psi}_u^i = (u^{ai}, u_a^{\dagger i})$
$\psi_u^{cj} = \begin{pmatrix} u_b^j \\ u^{\dagger bj} \end{pmatrix}$	$(\bar{3}, 1, -\frac{2}{3})$	$\bar{\psi}_{ui}^c = (u_i^{\prime a}, u_{\dot{a}i}^\dagger)$
$\psi_{dj} = \begin{pmatrix} d'_{bj} \\ d_j^\dagger \end{pmatrix}$	$(3, 1, -\frac{1}{3})$	$\bar{\psi}_d^i = (d^{ai}, d_a^{\dagger i})$
$\psi_d^{cj} = \begin{pmatrix} d_b^j \\ d^{\dagger bj} \end{pmatrix}$	$(\bar{3}, 1, \frac{1}{3})$	$\bar{\psi}_{di}^c = (d_i^{\prime a}, d_{\dot{a}i}^\dagger)$
$\psi_{l\beta} = \begin{pmatrix} l_{b\beta} \\ l_\beta^\dagger \end{pmatrix}$	$(1, 2, -\frac{1}{2})$	$\bar{\psi}_l^\alpha = (l'^{a\alpha}, l_a^{\dagger\alpha})$
$\psi_l^{c\beta} = \begin{pmatrix} l_b^\beta \\ l^{\dagger b\beta} \end{pmatrix}$	$(1, \bar{2}, \frac{1}{2})$	$\bar{\psi}_{l\alpha}^c = (l_\alpha^a, l_{\dot{a}\alpha}^\dagger)$
$\psi_e = \begin{pmatrix} e'_b \\ e^{\dagger b} \end{pmatrix}$	$(1, 1, -1)$	$\bar{\psi}_e = (e^a, e_a^{\dagger})$
$\psi_e^c = \begin{pmatrix} e_b \\ e^{\dagger b} \end{pmatrix}$	$(1, 1, 1)$	$\bar{\psi}_e^c = (e^{\prime a}, e_a^\dagger)$
Light spin-1 ($c_s = \frac{1}{2}$)		
G_ν^B	$(8, 1, 0)$	G_μ^A
W_ν^J	$(1, 3, 0)$	W_μ^I
B_ν	$(1, 1, 0)$	B_μ

Table 7.2: (From [132]) Light fields φ_L in the MSSM, their gauge quantum numbers, and conjugate fields (which appear on the left side of \mathcal{Q}_{UV}). Primed Weyl fermion fields are unphysical auxiliary fields, to be set to zero at the end of the calculation.

	Φ	\tilde{q}	\tilde{u}	\tilde{d}	\tilde{l}	\tilde{e}	$\tilde{\chi}$	\tilde{g}	\tilde{W}	\tilde{B}	ϕ	q	u	d	l	e	G	W	B
Φ	φ^2										φ^2							$D\Phi$	$D\Phi$
\tilde{q}	φ^2	φ	φ				u, d	q	q	q		u, d	q						
\tilde{u}	φ	φ^2	$\Phi\phi$				q	u				q							
\tilde{d}	φ	$\Phi\phi$	φ^2				q	d				q							
\tilde{l}				φ^2	φ		e		l	l									
\tilde{e}				φ	φ^2		l			e									
$\tilde{\chi}$	u, d	q	q	q	e	l			φ	φ									
\tilde{g}	q	u	d				φ												
\tilde{W}	q				l														
\tilde{B}	q	u	d	l	l	e	φ												
ϕ	φ^2										φ^2	u, d	q	φ	e	l	$D\phi$	$D\phi$	$D\phi$
q	u, d										u, d	q	φ			q	q		q
u	q										q	φ				u			u
d	q										q	φ				d			d
l	e										e				φ				l
e	l										l			φ					l
G												q	u	d		$G_{\mu\nu}$			
W	$D\Phi$										$D\phi$	q			l		$W_{\mu\nu}, \phi^2, \Phi^2$		
B	$D\Phi$										$D\phi$	q	u	d	l	e			ϕ^2, Φ^2

Table 7.3: (From [132]) Fields contained in the nonzero entries of the MSSM \mathbf{U} matrix, with the heavy fields φ_H to be set to $\varphi_{H,c}$ (which is nonvanishing only for the heavy Higgs Φ). In this table, φ collectively denotes the heavy and light Higgs fields Φ and ϕ , e.g. φ^2 represents $\Phi^2, \Phi\phi, \phi^2$. Also, ψ_f , the Dirac spinors containing SM fermions, are written simply as f for clarity. Detailed expressions of the \mathbf{U} matrix can be found in Appendix C.

fluctuation fields. It turns out that the \mathbf{Z} matrix does not contribute to the operators computed in this chapter (up to Λ^{-1} suppressed corrections), and so will not be considered further.

To write down the \mathbf{U} matrix, we follow the conventions in [242] (Ref. [231] uses an opposite sign for the tree-level Higgsino mass parameter μ), assuming R -parity is conserved. We assume a trivial flavor structure for the soft SUSY breaking parameters for simplicity,

$$\begin{aligned} \mathcal{L}_{\text{MSSM}} \supset & -M_{\tilde{q}}^2 \tilde{q}^* \mathbb{1} \tilde{q} - M_{\tilde{u}}^2 \tilde{u}^* \mathbb{1} \tilde{u} - M_{\tilde{d}}^2 \tilde{d}^* \mathbb{1} \tilde{d} - M_{\tilde{l}}^2 \tilde{l}^* \mathbb{1} \tilde{l} - M_{\tilde{e}}^2 \tilde{e}^* \mathbb{1} \tilde{e} \\ & -A_u \tilde{u}^* \boldsymbol{\lambda}_u \tilde{q} \cdot \epsilon \cdot H_u + A_d \tilde{d}^* \boldsymbol{\lambda}_d \tilde{q} \cdot \epsilon \cdot H_d + A_e \tilde{e}^* \boldsymbol{\lambda}_e \tilde{l} \cdot \epsilon \cdot H_d, \end{aligned} \quad (7.16)$$

where $\boldsymbol{\lambda}_u, \boldsymbol{\lambda}_d, \boldsymbol{\lambda}_e$ are Yukawa matrices in the MSSM. Our results can be easily extended to include flavor mixing, at the cost of making the analytical expressions more complicated. Furthermore, we assume $\mu v, A_f v \ll M_{\tilde{f}}^2$, so that matching in the electroweak-symmetric phase without sfermion mass mixing is justified.

We summarize the fields contained in each nonzero entry of the MSSM \mathbf{U} matrix in Table 7.3, relegating detailed expressions to Appendix C. This \mathbf{U} matrix exhibits a block-diagonal structure because of the assumed R -parity: if i and j have opposite R -parity, U_{ij} would be proportional to a heavy R -parity-odd field, which should be set to $\varphi_{H,c} = 0$ (so that $\frac{\delta \mathcal{L}_{\text{MSSM}}}{\delta \varphi_H} \Big|_{\varphi_H = \varphi_{H,c}} \propto \varphi_{H,c} = 0$). We will demonstrate in Sections 7.2.3 and 7.2.4 how to use Table 7.3 to quickly pick out the U insertions containing the right fields to make up a desired operator in our one-loop matching calculation.

7.2.2 Tree-level matching

The tree-level effective Lagrangian is obtained by solving the equations of motion of the heavy fields. As mentioned in the previous subsection, in the absence of R -parity violation, $\frac{\delta \mathcal{L}_{\text{MSSM}}}{\delta \varphi_H} = 0$ is trivially solved by $\varphi_{H,c} = 0$ for all the heavy fields in the MSSM except the R -parity-even heavy Higgs doublet Φ , for which

$$\begin{aligned} \frac{\delta \mathcal{L}_{\text{MSSM}}}{\delta \Phi^{*\alpha}} &= [(P^2)_\alpha^\beta - M_\Phi^2 \delta_\alpha^\beta] \Phi_\alpha \\ &+ \frac{1}{8} (g^2 + g'^2) s_{4\beta'} |\phi|^2 \phi_\beta + c_{\beta'} \epsilon_{\alpha\beta} \bar{\psi}_q^\beta \boldsymbol{\lambda}_u^\dagger \psi_u + s_{\beta'} \bar{\psi}_d \boldsymbol{\lambda}_d \psi_{q\alpha} + s_{\beta'} \bar{\psi}_e \boldsymbol{\lambda}_e \psi_{l\alpha} \\ &+ \left[\frac{1}{4} (g^2 + g'^2) c_{2\beta'}^2 - \frac{1}{2} g^2 \right] |\phi|^2 \Phi_\alpha - \left[\frac{1}{4} (g^2 + g'^2) s_{2\beta'}^2 - \frac{1}{2} g^2 \right] (\phi^* \Phi) \phi_\alpha \\ &- \frac{1}{4} (g^2 + g'^2) s_{2\beta'}^2 (\Phi^* \phi) \phi_\alpha + \mathcal{O}(\Phi^2 \phi, \Phi^3). \end{aligned} \quad (7.17)$$

in the $\overline{\text{DR}}$ scheme. In the $\overline{\text{MS}}$ scheme, on the other hand, the scalar quartic couplings (and hence the scalar cubic terms in Eq. (7.17)) receive $\mathcal{O}(\frac{g^4}{16\pi^2}, \frac{g^2 g'^2}{16\pi^2}, \frac{g'^4}{16\pi^2})$ corrections [243].

We can solve the equation of motion $\frac{\delta \mathcal{L}_{\text{MSSM}}}{\delta \Phi^*} = 0$ for Φ_c perturbatively, as a power series in M_Φ^{-1} ,

$$\Phi_c = \Phi_c^{(1)} + \Phi_c^{(2)} + \dots \quad \text{where} \quad \Phi_c^{(n)} \sim \mathcal{O}(M_\Phi^{-2n}). \quad (7.18)$$

The first and second order solutions read

$$\Phi_{c\alpha}^{(1)} = \frac{1}{M_\Phi^2} \left[\frac{1}{8} (g^2 + g'^2) s_{4\beta'} |\phi|^2 \phi_\alpha + c_{\beta'} \epsilon_{\alpha\beta} \bar{\psi}_q^\beta \boldsymbol{\lambda}_u^\dagger \psi_u + s_{\beta'} \bar{\psi}_d \boldsymbol{\lambda}_d \psi_{q\alpha} + s_{\beta'} \bar{\psi}_e \boldsymbol{\lambda}_e \psi_{l\alpha} \right], \quad (7.19)$$

$$\begin{aligned} \Phi_{c\alpha}^{(2)} = \frac{1}{M_\Phi^2} \left\{ - (D^2 \Phi_c^{(1)})_\alpha + \left[\frac{1}{4} (g^2 + g'^2) c_{2\beta'}^2 - \frac{1}{2} g^2 \right] |\phi|^2 \Phi_{c\alpha}^{(1)} \right. \\ \left. - \left[\frac{1}{4} (g^2 + g'^2) s_{2\beta'}^2 - \frac{1}{2} g^2 \right] (\phi^* \Phi_c^{(1)}) \phi_\alpha - \frac{1}{4} (g^2 + g'^2) s_{2\beta'}^2 (\Phi_c^{(1)*} \phi) \phi_\alpha \right\}. \quad (7.20) \end{aligned}$$

Only $\Phi_c^{(1)}$ is needed in tree-level matching up to dimension six. We have

$$\begin{aligned} \mathcal{L}_{\text{SMEFT}}^{\text{tree}} &= \mathcal{L}_{\text{MSSM}}|_{\varphi_H \rightarrow \varphi_{H,c}} = \mathcal{L}_{\text{SM}} + M_\Phi^2 |\Phi_c^{(1)}|^2 + \mathcal{O}(\Lambda^{-4}) \\ &= \mathcal{L}_{\text{SM}} + \sum_i C_i^{\text{tree}} \mathcal{O}_i^{(d=6)} + \mathcal{O}(\Lambda^{-4}), \quad (7.21) \end{aligned}$$

where the dimension-six operators $\mathcal{O}_i^{(d=6)}$ generated and their coefficients C_i^{tree} are listed in Table 7.4. We have used the basis of [3], known as the Warsaw basis, for dimension-six operators. Fierz identities have been used to transform some of the four-fermion operators into this basis. Note that with the tree-level matching of Eq. (7.21) alone, each appearance of β in Table 7.4 should really read β' . However, as we will see shortly, part of one-loop matching result can be absorbed into a redefinition of $\beta' \rightarrow \beta$ in the tree-level operator coefficients.

β redefinition

An interesting observation can be made on the tree-level effective Lagrangian computed above. Differentiating $\mathcal{L}_{\text{SMEFT}}^{\text{tree}}$ with respect to β' , we find

$$\begin{aligned} \frac{\partial}{\partial \beta'} \mathcal{L}_{\text{SMEFT}}^{\text{tree}(d=4)} &= \frac{\partial}{\partial \beta'} \left[-\frac{1}{8} (g^2 + g'^2) c_{2\beta'}^2 |\phi|^4 \right. \\ &\quad \left. - (s_{\beta'} \bar{\psi}_u \boldsymbol{\lambda}_u \psi_q \cdot \epsilon \cdot \phi + c_{\beta'} \bar{\psi}_d \boldsymbol{\lambda}_d \psi_q \cdot \phi^* + c_{\beta'} \bar{\psi}_e \boldsymbol{\lambda}_e \psi_l \cdot \phi^* + \text{h.c.}) \right] \\ &= \frac{1}{4} (g^2 + g'^2) s_{4\beta'} |\phi|^4 \end{aligned}$$

Coefficient	Operator
$C_\phi^{\text{tree}} = \frac{1}{64M_\Phi^2} s_{4\beta}^2 (g^2 + g'^2)^2$	$\mathcal{O}_\phi = \phi ^6$
$[C_{u\phi}^{\text{tree}}]_{pr} = -\frac{1}{8M_\Phi^2} s_{4\beta} c_\beta (g^2 + g'^2) [\lambda_u^\dagger]_{pr}$	$[\mathcal{O}_{u\phi}]^{pr} = \phi ^2 (\bar{\psi}_q^p \psi_u^r) \cdot \epsilon \phi^*$
$[C_{d\phi}^{\text{tree}}]_{pr} = \frac{1}{8M_\Phi^2} s_{4\beta} s_\beta (g^2 + g'^2) [\lambda_d^\dagger]_{pr}$	$[\mathcal{O}_{d\phi}]^{pr} = \phi ^2 (\bar{\psi}_q^p \psi_d^r) \cdot \phi$
$[C_{e\phi}^{\text{tree}}]_{pr} = \frac{1}{8M_\Phi^2} s_{4\beta} s_\beta (g^2 + g'^2) [\lambda_e^\dagger]_{pr}$	$[\mathcal{O}_{e\phi}]^{pr} = \phi ^2 (\bar{\psi}_l^p \psi_e^r) \cdot \phi$
$[C_{qu}^{\text{tree}}]_{prst} = -\frac{1}{6M_\Phi^2} c_\beta^2 [\lambda_u^\dagger]_{pt} [\lambda_u]_{sr}$	$[\mathcal{O}_{qu}^{(1)}]^{prst} = (\bar{\psi}_q^p \gamma_\mu \psi_q^r) (\bar{\psi}_u^s \gamma^\mu \psi_u^t)$
$[C_{qu}^{(8)\text{tree}}]_{prst} = -\frac{1}{M_\Phi^2} c_\beta^2 [\lambda_u^\dagger]_{pt} [\lambda_u]_{sr}$	$[\mathcal{O}_{qu}^{(8)}]^{prst} = (\bar{\psi}_q^p \gamma_\mu T^A \psi_q^r) (\bar{\psi}_u^s \gamma^\mu T^A \psi_u^t)$
$[C_{qd}^{(1)\text{tree}}]_{prst} = -\frac{1}{6M_\Phi^2} s_\beta^2 [\lambda_d^\dagger]_{pt} [\lambda_d]_{sr}$	$[\mathcal{O}_{qd}^{(1)}]^{prst} = (\bar{\psi}_q^p \gamma_\mu \psi_q^r) (\bar{\psi}_d^s \gamma^\mu \psi_d^t)$
$[C_{qd}^{(8)\text{tree}}]_{prst} = -\frac{1}{M_\Phi^2} s_\beta^2 [\lambda_d^\dagger]_{pt} [\lambda_d]_{sr}$	$[\mathcal{O}_{qd}^{(8)}]^{prst} = (\bar{\psi}_q^p \gamma_\mu T^A \psi_q^r) (\bar{\psi}_d^s \gamma^\mu T^A \psi_d^t)$
$[C_{le}^{\text{tree}}]_{prst} = -\frac{1}{2M_\Phi^2} s_\beta^2 [\lambda_e^\dagger]_{pt} [\lambda_e]_{sr}$	$[\mathcal{O}_{le}]^{prst} = (\bar{\psi}_l^p \gamma_\mu \psi_l^r) (\bar{\psi}_e^s \gamma^\mu \psi_e^t)$
$[C_{quqd}^{(1)\text{tree}}]_{prst} = -\frac{1}{M_\Phi^2} s_\beta c_\beta [\lambda_u^\dagger]_{pr} [\lambda_d^\dagger]_{st}$	$[\mathcal{O}_{quqd}^{(1)}]^{prst} = (\bar{\psi}_q^p \psi_u^r) \cdot \epsilon \cdot (\bar{\psi}_q^s \psi_d^t)$
$[C_{lequ}^{(1)\text{tree}}]_{prst} = \frac{1}{M_\Phi^2} s_\beta c_\beta [\lambda_e^\dagger]_{pr} [\lambda_u^\dagger]_{st}$	$[\mathcal{O}_{lequ}^{(1)}]^{prst} = (\bar{\psi}_l^p \psi_e^r) \cdot \epsilon \cdot (\bar{\psi}_q^s \psi_u^t)$
$[C_{ledq}^{\text{tree}}]_{prst} = \frac{1}{M_\Phi^2} s_\beta^2 [\lambda_e^\dagger]_{pr} [\lambda_d]_{st}$	$[\mathcal{O}_{ledq}]^{prst} = (\bar{\psi}_l^p \psi_e^r) (\bar{\psi}_d^s \psi_q^t)$

Table 7.4: (From [132]) Dimension-six operators generated at tree level when matching the MSSM onto the SMEFT. p, r, s, t are generation indices. Tree-level matching alone produces the operator coefficients listed here, but with β' in place of β . As explained in Section 7.2.2, adding the one-loop-generated piece $c_{\Phi\phi}(\Phi_c^* \phi + \phi^* \Phi_c)$ to $\mathcal{L}_{\text{SMEFT}}^{\text{tree}}$ amounts to replacing β' by β in all C_i^{tree} .

$$\begin{aligned}
& + \left[\phi^* (c_{\beta'} \epsilon \cdot \bar{\psi}_q \lambda_u^\dagger \psi_u + s_{\beta'} \bar{\psi}_d \lambda_d \psi_q + s_{\beta'} \bar{\psi}_e \lambda_e \psi_l) + \text{h.c.} \right] \\
& = M_\Phi^2 (\Phi_c^{(1)*} \phi + \phi^* \Phi_c^{(1)}), \tag{7.22} \\
\frac{\partial}{\partial \beta'} \mathcal{L}_{\text{SMEFT}}^{\text{tree}(d=6)} & = M_\Phi^2 \left(\Phi_c^{(1)*} \cdot \frac{\partial \Phi_c^{(1)}}{\partial \beta'} + \text{h.c.} \right) \\
& = \Phi_c^{(1)*} \cdot \left[\frac{1}{2} (g^2 + g'^2) c_{4\beta'} |\phi|^2 \phi \right. \\
& \quad \left. - s_{\beta'} \epsilon \cdot \bar{\psi}_q \lambda_u^\dagger \psi_u + c_{\beta'} \bar{\psi}_d \lambda_d \psi_q + c_{\beta'} \bar{\psi}_e \lambda_e \psi_l \right] + \text{h.c.} \\
& \stackrel{\text{EoM}}{=} \Phi_c^{(1)*} \cdot \left[-(D^2 \phi) + \frac{1}{4} (g^2 + g'^2) (c_{2\beta'}^2 - 2s_{2\beta'}^2) |\phi|^2 \phi \right] + \text{h.c.} \\
& \stackrel{\text{IBP}}{=} M_\Phi^2 (\Phi_c^{(2)*} \phi + \phi^* \Phi_c^{(2)}). \tag{7.23}
\end{aligned}$$

In the equations above, we have used the fact that both $m^2 = \mu^2 + m_{H_u}^2 s_{\beta'}^2 + m_{H_d}^2 c_{\beta'}^2 - b s_{2\beta'}$ and $M_\Phi^2 = \mu^2 + m_{H_u}^2 c_{\beta'}^2 + m_{H_d}^2 s_{\beta'}^2 + b s_{2\beta'}$ have vanishing first derivative with respect to β' , when Eq. (7.14) is satisfied. “ $\stackrel{\text{EoM}}{=}$ ” and “ $\stackrel{\text{IBP}}{=}$ ” mean equivalence with the use of the renormalizable

SM equations of motion and integration by parts, respectively — operations that are allowed when we are dealing with dimension-six operators in the SMEFT Lagrangian. We have neglected the m^2 piece and one-loop threshold corrections to the relation $\lambda = \frac{1}{8}(g^2 + g'^2)c_{2\beta'}$ when applying the equation of motion for ϕ , because they lead to $\frac{m^2}{\Lambda^2}$ suppressed and loop-suppressed terms compared to those retained in our results.

Meanwhile, as we will see explicitly in the next subsection, matching the MSSM onto the SMEFT at one-loop level generates

$$\mathcal{L}_{\text{SMEFT}}^{\text{1-loop}} \supset c_{\Phi\phi}(\Phi_c^*\phi + \phi^*\Phi_c), \quad (7.24)$$

with $c_{\Phi\phi} \sim \mathcal{O}(\frac{\Lambda^2}{16\pi^2})$ given in Eq. (7.47). The observation we made above, namely

$$\frac{\partial}{\partial\beta'}\mathcal{L}_{\text{SMEFT}}^{\text{tree}} = M_\Phi^2(\Phi_c^*\phi + \phi^*\Phi_c) \quad (7.25)$$

suggests that we can absorb the part of $\mathcal{L}_{\text{SMEFT}}^{\text{1-loop}}$ shown in Eq. (7.24) into $\mathcal{L}_{\text{SMEFT}}^{\text{tree}}$ via a redefinition of β' ,

$$\mathcal{L}_{\text{SMEFT}}^{\text{tree}}(\beta') + c_{\Phi\phi}(\Phi_c^*\phi + \phi^*\Phi_c) = \mathcal{L}_{\text{SMEFT}}^{\text{tree}}\left(\beta' + \frac{c_{\Phi\phi}}{M_\Phi^2}\right), \quad (7.26)$$

up to two-loop corrections. Comparing $c_{\Phi\phi}$ presented below in Eq. (7.47) and analytical expressions of one-loop tadpoles in [231], we can actually show that

$$c_{\Phi\phi} = s_\beta c_\beta \left(\frac{t_u}{v_u} - \frac{t_d}{v_d}\right) \mathcal{O}\left(\frac{\Lambda^2}{16\pi^2}\right). \quad (7.27)$$

Therefore,

$$\mathcal{L}_{\text{SMEFT}}^{\text{tree}}(\beta') + c_{\Phi\phi}(\Phi_c^*\phi + \phi^*\Phi_c) = \mathcal{L}_{\text{SMEFT}}^{\text{tree}}(\beta), \quad (7.28)$$

with β defined by the minimum of the (loop-corrected) 1PI effective potential, i.e. $\tan\beta = \frac{v_u}{v_d}$ in the tadpole-free scheme; see Eq. (7.15). We see that adding the one-loop-generated piece $c_{\Phi\phi}(\Phi_c^*\phi + \phi^*\Phi_c)$ to $\mathcal{L}_{\text{SMEFT}}^{\text{tree}}$ amounts to simply replacing β' by β in all tree-level operator coefficients.

There is a simple power-counting argument for the relation Eq. (7.28). If instead of Eq. (7.13), we define Φ, ϕ to be related to H_u, H_d by an angle β (as opposed to β') rotation, we would have $\langle\phi\rangle = \frac{v}{\sqrt{2}} \simeq 174 \text{ GeV}$, while $\langle\Phi\rangle = 0$. In this basis (usually referred to as the Higgs basis), integrating out heavy superpartners must not produce $(\Phi_c^*\phi + \phi^*\Phi_c)$ with $\mathcal{O}(\frac{\Lambda^2}{16\pi^2})$ coefficient, because otherwise, the same contribution would be present if we compute the 1PI effective potential of the MSSM — this would lead to an $\mathcal{O}(\frac{v}{16\pi^2})$ contribution to $\langle\Phi\rangle$

which, in fact, is the only possible contribution at this order, thus contradicting $\langle \Phi \rangle = 0$. Technically, what happens is a cancellation of $\mathcal{O}(\frac{\Lambda^2}{16\pi^2}) \cdot (\Phi_c^* \phi + \phi^* \Phi_c)$ pieces between $\mathcal{L}_{\text{SMEFT}}^{\text{tree}}$ and $\mathcal{L}_{\text{SMEFT}}^{1\text{-loop}}$: the same $\mathcal{L}_{\text{SMEFT}}^{1\text{-loop}} \supset c_{\Phi\phi}(\Phi_c^* \phi + \phi^* \Phi_c)$ is generated by one-loop matching, while $\mathcal{L}_{\text{SMEFT}}^{\text{tree}} \supset -c_{\Phi\phi}(\Phi_c^* \phi + \phi^* \Phi_c)$ because the UV theory Lagrangian now contains a mass mixing term,

$$\mathcal{L}_{\text{MSSM}} \supset \left[b c_{2\beta} - \frac{1}{2}(m_{H_u}^2 - m_{H_d}^2) s_{2\beta} \right] (\Phi^* \phi + \phi^* \Phi) = -s_\beta c_\beta \left(\frac{t_u}{v_u} - \frac{t_d}{v_d} \right) \mathcal{O}(\frac{\Lambda^2}{16\pi^2}) (\Phi^* \phi + \phi^* \Phi), \quad (7.29)$$

up to $\frac{m^2}{\Lambda^2}$ suppressed and higher-loop corrections. Note that the presence of mass mixing in this basis does not invalidate our functional matching formalism (which assumes a diagonal mass matrix), if we treat it as a small constant term in the \mathbf{U} matrix. However, the Higgs basis is not a convenient choice for tree-level matching, because Φ_c has to be solved as a double series in Λ^{-1} and $\frac{1}{16\pi^2}$.

7.2.3 One-loop matching: $d \leq 4$ operators and SUSY threshold corrections

Enumerating covariant diagrams

To match the MSSM onto the SMEFT at one-loop level, we draw covariant diagrams contributing to each SMEFT operator of interest, starting from the $d \leq 4$ ones which encode SUSY threshold corrections. Enumerating covariant diagrams is straightforward by looking for desired fields from the MSSM \mathbf{U} matrix. In what follows, we will use a slightly different notation than the previous chapter. Here we prefer to make the distinction between bosonic and fermionic propagators more transparent by using different types of lines (dashed vs. solid). In the previous chapter, on the other hand, more emphasis is put on the treatment of heavy vs. light fields, and solid (dashed) propagators are used for heavy (light) propagators regardless of spin.

Let us demonstrate the procedure with an example operator $\bar{\psi}_d \boldsymbol{\delta y}_d \psi_q \cdot \phi^* + \text{h.c.}$ Obviously we should look for a d , a q and a ϕ in Table 7.3. To begin with, there are several options to get a d , such as from $U_{\tilde{q}\tilde{\chi}}$, or from $U_{\tilde{d}\tilde{g}}$. Let us pick $U_{\tilde{q}\tilde{\chi}}$ first. This $U_{\tilde{q}\tilde{\chi}}$ insertion should be followed by a $\tilde{\chi}$ propagator, and then another U insertion containing either q or ϕ . For this second U insertion, we need to enumerate all viable choices, one of them being $U_{\tilde{\chi}\tilde{u}} \sim q$. With this particular choice, we can then close the loop with a \tilde{u} propagator, followed by a $U_{\tilde{u}\tilde{q}} \sim \phi$ insertion, and then a \tilde{q} propagator connecting back to our starting point $U_{\tilde{q}\tilde{\chi}}$. We

thus end up with the following covariant diagram,

$$\begin{array}{c} \tilde{\chi} \\ \circ \\ \text{---} \\ \circ \\ \tilde{q} \end{array} = -\frac{i}{2}\mu \mathcal{I}_{\tilde{q}\tilde{u}\tilde{\chi}}^{111} \text{tr}(U_{\tilde{q}\tilde{\chi}}U_{\tilde{\chi}\tilde{u}}U_{\tilde{u}\tilde{q}}) \quad (7.30)$$

Plugging in explicit expressions of $U_{\tilde{q}\tilde{\chi}}$, $U_{\tilde{\chi}\tilde{u}}$, $U_{\tilde{u}\tilde{q}}$ from Eqs. (C.15), (C.16), (C.8b), we obtain

$$\begin{aligned} \text{tr}(U_{\tilde{q}\tilde{\chi}}U_{\tilde{\chi}\tilde{u}}U_{\tilde{u}\tilde{q}}) &\supset s_\beta (A_u - \mu \cot \beta) (\bar{\psi}_d \boldsymbol{\lambda}_d \boldsymbol{\lambda}_u^\dagger \boldsymbol{\lambda}_u \psi_q \cdot \phi^* + \bar{\psi}_d^c \boldsymbol{\lambda}_d^* \boldsymbol{\lambda}_u^T \boldsymbol{\lambda}_u^* \psi_q^c \cdot \phi) \\ &= (A_u \tan \beta - \mu) (\bar{\psi}_d \mathbf{y}_d \boldsymbol{\lambda}_u^\dagger \boldsymbol{\lambda}_u \psi_q \cdot \phi^* + \text{h.c.}), \end{aligned} \quad (7.31)$$

where we have dropped similar terms involving Φ which, after setting Φ to Φ_c , contribute to $\bar{\psi}_d \boldsymbol{\delta y}_d \psi_q \cdot \phi^* + \text{h.c.}$ only at higher order in $\frac{1}{\Lambda^2}$. Noting that there is an identical contribution from the mirror reflection of the diagram of Eq. (7.30), we can write the squark-Higgsino loop contribution to $\boldsymbol{\delta y}_d$ as

$$\boldsymbol{\delta y}_d \supset \mathbf{y}_d \bar{\boldsymbol{\delta y}}_d^{(\tilde{q}\tilde{u}\tilde{\chi})}, \quad (7.32)$$

where

$$16\pi^2 \bar{\boldsymbol{\delta y}}_d^{(\tilde{q}\tilde{u}\tilde{\chi})} = \boldsymbol{\lambda}_u^\dagger \boldsymbol{\lambda}_u \mu (A_u \tan \beta - \mu) \tilde{\mathcal{I}}_{\tilde{q}\tilde{u}\tilde{\chi}}^{111}. \quad (7.33)$$

The master integral involved here has the following explicit expression,

$$\tilde{\mathcal{I}}_{ijk}^{111} \equiv \mathcal{I}_{ijk}^{111} / 16\pi^2 = \frac{M_j^2}{(M_i^2 - M_j^2)(M_j^2 - M_k^2)} \log \frac{M_j^2}{M_i^2} + \frac{M_k^2}{(M_j^2 - M_k^2)(M_k^2 - M_i^2)} \log \frac{M_k^2}{M_i^2}, \quad (7.34)$$

see Appendix A.

An alternative route we can take to obtain $\bar{\psi}_d \boldsymbol{\delta y}_d \psi_q \cdot \phi^* + \text{h.c.}$ is to start from $U_{\tilde{d}\tilde{g}}$, and form a \tilde{d} - \tilde{g} - \tilde{q} loop,

$$\begin{array}{c} \tilde{q} \\ \circ \\ \text{---} \\ \circ \\ \tilde{d} \end{array} = -\frac{i}{2} M_3 \mathcal{I}_{\tilde{q}\tilde{d}\tilde{g}}^{111} \text{tr}(U_{\tilde{d}\tilde{g}}U_{\tilde{g}\tilde{q}}U_{\tilde{q}\tilde{d}}). \quad (7.35)$$

Evaluating the trace and adding the mirror diagram, we obtain the squark-gluino loop contribution to $\boldsymbol{\delta y}_d$,

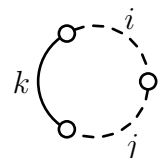
$$\boldsymbol{\delta y}_d \supset \mathbf{y}_d \bar{\boldsymbol{\delta y}}_d^{(\tilde{q}\tilde{d}\tilde{g})}, \quad (7.36)$$

where

$$16\pi^2 \bar{\boldsymbol{\delta y}}_d^{(\tilde{q}\tilde{d}\tilde{g})} = -2 (A_d - \mu \tan \beta) g_3^2 C_2^{SU(3)} M_3 \tilde{\mathcal{I}}_{\tilde{q}\tilde{d}\tilde{g}}^{111}, \quad (7.37)$$

with $C_2^{SU(3)} = \frac{4}{3}$ being the quadratic Casimir of the fundamental representation of $SU(3)_c$. It is worth noting that both the squark-Higgsino loop and the squark-gluino loop computed

above can be viewed as part of a single covariant diagram,



$$= -\frac{i}{2} M_k \mathcal{I}_{ijk}^{111} \text{tr}(U_{ij} U_{jk} U_{ki}), \quad (7.38)$$

with summation over i, j, k understood.

There are several other routes that can take us to the operator $\bar{\psi}_d \delta \mathbf{y}_d \psi_q \cdot \phi^* + \text{h.c.}$, and many others that can take us to other SMEFT operators. Following the procedure demonstrated with the examples above, we enumerate covariant diagrams contributing to each $d \leq 4$ operator in Tables 7.5 and 7.6. In particular, Table 7.5 contains covariant diagrams contributing to the Higgs potential and Yukawa interactions, which involve U insertions only and no P insertions. The kinetic terms (wavefunction renormalization factors δZ), on the other hand, come from covariant diagrams that involve P insertions, as shown in Table 7.6. The $c_{\Phi\phi}(\Phi_c^* \phi + \phi^* \Phi_c)$ piece, which we choose to absorb into $\mathcal{L}_{\text{SMEFT}}^{\text{tree}}$ via a redefinition of β as explained in Section 7.2.2, is computed from the same covariant diagrams contributing to $\delta m^2 |\phi|^2$. In diagrams where permutations of propagator labels produce inequivalent diagrams, such permutations are implicitly assumed to be included. We refrain from elaborating on how to compute each of the tabulated covariant diagrams, as the general procedure should already be clear from the examples given above.

From Tables 7.5 and 7.6, we can see an advantage of our approach is that despite the large number of terms in the final results of one-loop SUSY threshold corrections (which we will present below), *they all derive from just 30 covariant diagrams*. The small number of covariant diagrams can be understood on dimensional grounds. Generally, we have

$$\dim(P_\mu) = 1, \quad \dim(U_{ij}[\varphi]) \geq 1, \quad (7.39)$$

where “dim” means operator dimension. $d \leq 4$ operators can therefore only come from covariant diagrams with at most 4 vertex insertions, as enumerated in the tables for the case of the MSSM⁴.

Results

Now we present the results of one-loop-level coefficients of all $d \leq 4$ SMEFT operators, i.e. $\delta Z_{\phi,f,V}$, δm^2 , $\delta \lambda$, $\delta \mathbf{y}_f$ defined in Eq. (7.4), which are calculated from the 30 covariant

⁴Similarly, dimension-six operators can be obtained from covariant diagrams with at most 6 vertex insertions. This is true regardless of the UV theory, as long as it is Lorentz-invariant and satisfies the general form of Eq. (6.64). This simple observation of finite combinatorics underlies the idea of deriving universal formulas for one-loop effective Lagrangians [56, 58, 61].

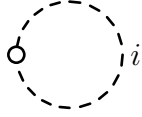
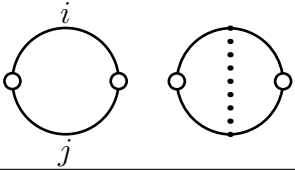
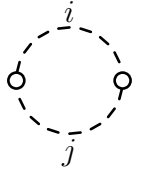
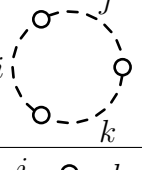
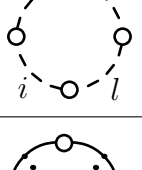
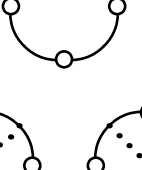
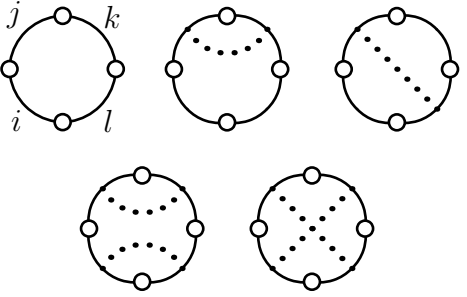
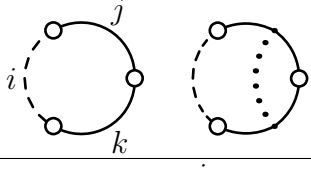
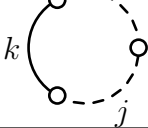
14 U -only covariant diagrams contributing to δm^2 , $\delta\lambda$, $\delta\mathbf{y}_f$		
δm^2		$i = \Phi; \tilde{f}$
		$ij = \tilde{\chi}\tilde{W}, \tilde{\chi}\tilde{B}$
		$ij = \tilde{q}\tilde{u}, \tilde{q}\tilde{d}, \tilde{l}\tilde{e}$
$\delta\lambda$		$ij = \Phi\Phi, \Phi\phi; \tilde{f}\tilde{f}$
		$ijkl = \tilde{q}\tilde{q}\tilde{u}, \tilde{u}\tilde{u}\tilde{q}, \tilde{q}\tilde{q}\tilde{d}, \tilde{d}\tilde{d}\tilde{q}, \tilde{l}\tilde{l}\tilde{e}, \tilde{e}\tilde{e}\tilde{l}$
		$ijkl = \tilde{q}\tilde{u}\tilde{q}\tilde{u}, \tilde{q}\tilde{d}\tilde{q}\tilde{d}, \tilde{l}\tilde{e}\tilde{l}\tilde{e}$
		$ijkl = \tilde{\chi}\tilde{W}\tilde{\chi}\tilde{W}, \tilde{\chi}\tilde{W}\tilde{\chi}\tilde{B}, \tilde{\chi}\tilde{B}\tilde{\chi}\tilde{B}$
$\delta\mathbf{y}_f$		$ijk = \Phi qu, \Phi qd; \tilde{f}\tilde{\chi}\tilde{V}$
		$ijk = \tilde{q}\tilde{u}\tilde{\chi}, \tilde{q}\tilde{d}\tilde{\chi}; \tilde{q}\tilde{u}\tilde{V}, \tilde{q}\tilde{d}\tilde{V}, \tilde{l}\tilde{e}\tilde{V}$

Table 7.5: (From [132]) Covariant diagrams contributing to Higgs potential and Yukawa interactions.

16 P -dependent covariant diagrams contributing to δZ		
		$ij = \tilde{q}\tilde{u}, \tilde{q}\tilde{d}, \tilde{l}\tilde{e}$
δZ_ϕ		$ij = \tilde{\chi}\tilde{W}, \tilde{\chi}\tilde{B}$
δZ_f		$ij = \Phi f; \tilde{f}\tilde{\chi}, \tilde{f}\tilde{V}$
$\delta Z_{G,W,B}$		$i = \Phi, \tilde{f}$
		$i = \tilde{\chi}, \tilde{g}, \tilde{W}$

Table 7.6: (From [132]) Covariant diagrams contributing to kinetic terms.

diagrams in Tables 7.5 and 7.6. These coefficients, together with the tree-level relations,

$$\begin{aligned}
m^2 &\equiv \mu^2 + m_{H_u}^2 s_\beta^2 + m_{H_d}^2 c_\beta^2 - b s_{2\beta}, & \lambda &\equiv \frac{1}{8}(g^2 + g'^2) c_{2\beta}^2, \\
\mathbf{y}_u &= \boldsymbol{\lambda}_u s_\beta, & \mathbf{y}_d &= \boldsymbol{\lambda}_d c_\beta, & \mathbf{y}_e &= \boldsymbol{\lambda}_e c_\beta,
\end{aligned} \tag{7.40}$$

can be readily plugged into Eq. (7.6) to obtain one-loop SUSY threshold corrections (there is a one-loop correction to the equation for λ if we work with the $\overline{\text{MS}}$ scheme [243]). We will use parenthesized subscripts or superscripts to indicate the covariant diagram each term comes from, and mention the reduction formulas used on the master integrals so that all results can be easily reproduced.

We have cross-checked our results against conventional Feynman diagram calculations reported in [231] and found complete agreement; see Appendix D. Note in particular that at one-loop level, MSSM threshold corrections are the same in both $\overline{\text{MS}}$ and $\overline{\text{DR}}$ schemes, as is clear from the absence of ϵ -scalar loops in our matching calculation.

Our notation is the following. $N_c = 3$ is the number of colors. $C_2^{SU(3)} = \frac{4}{3}$ and $C_2^{SU(2)} = \frac{3}{4}$ are quadratic Casimirs of fundamental representations of $SU(3)_c$ and $SU(2)_L$, respectively. The $U(1)_Y$ hypercharges are

$$\{ Y_\phi, Y_q, Y_u, Y_d, Y_l, Y_e \} = \left\{ \frac{1}{2}, \frac{1}{6}, \frac{2}{3}, -\frac{1}{3}, -\frac{1}{2}, -1 \right\}. \tag{7.41}$$

The master integrals $\tilde{\mathcal{I}} \equiv \mathcal{I}/\frac{i}{16\pi^2}$ are functions of tree-level masses of the heavy particles. Their analytical expressions in terms of tree-level heavy particle masses can be found in Appendix A.

Higgs potential. The one-loop coefficient of the $d = 2$ operator $|\phi|^2$ reads

$$\delta m^2 = \delta m_{(\Phi)}^2 + \delta m_{(\tilde{f})}^2 + \delta m_{(\tilde{f}\tilde{f})}^2 + \delta m_{(\tilde{\chi}\tilde{V})}^2, \tag{7.42}$$

where

$$16\pi^2 \delta m_{(\Phi)}^2 = \left[\frac{3}{4} g^2 s_{2\beta}^2 + g'^2 Y_\phi^2 (s_{2\beta}^2 - 2c_{2\beta}^2) \right] \tilde{\mathcal{I}}_\Phi^1, \tag{7.43}$$

$$\begin{aligned}
16\pi^2 \delta m_{(\tilde{f})}^2 &= N_c \text{tr}(\boldsymbol{\lambda}_u^\dagger \boldsymbol{\lambda}_u) s_\beta^2 (\tilde{\mathcal{I}}_{\tilde{q}}^1 + \tilde{\mathcal{I}}_{\tilde{u}}^1) \\
&+ N_c \text{tr}(\boldsymbol{\lambda}_d^\dagger \boldsymbol{\lambda}_d) c_\beta^2 (\tilde{\mathcal{I}}_{\tilde{q}}^1 + \tilde{\mathcal{I}}_{\tilde{d}}^1) + \text{tr}(\boldsymbol{\lambda}_e^\dagger \boldsymbol{\lambda}_e) c_\beta^2 (\tilde{\mathcal{I}}_{\tilde{l}}^1 + \tilde{\mathcal{I}}_{\tilde{e}}^1) \\
&- g'^2 Y_\phi c_{2\beta} (2N_c Y_q \tilde{\mathcal{I}}_{\tilde{q}}^1 - N_c Y_u \tilde{\mathcal{I}}_{\tilde{u}}^1 - N_c Y_d \tilde{\mathcal{I}}_{\tilde{d}}^1 + 2Y_l \tilde{\mathcal{I}}_{\tilde{l}}^1 - Y_e \tilde{\mathcal{I}}_{\tilde{e}}^1), \tag{7.44}
\end{aligned}$$

$$16\pi^2 \delta m_{(\tilde{f}\tilde{f})}^2 = N_c \text{tr}(\boldsymbol{\lambda}_u^\dagger \boldsymbol{\lambda}_u) s_\beta^2 (A_u - \mu \cot \beta)^2 \tilde{\mathcal{I}}_{\tilde{q}\tilde{u}}^{11}$$

$$\begin{aligned}
& + N_c \text{tr}(\boldsymbol{\lambda}_d^\dagger \boldsymbol{\lambda}_d) s_\beta^2 (A_d \cot \beta - \mu)^2 \tilde{\mathcal{I}}_{q\bar{d}}^{11} \\
& + \text{tr}(\boldsymbol{\lambda}_e^\dagger \boldsymbol{\lambda}_e) s_\beta^2 (A_e \cot \beta - \mu)^2 \tilde{\mathcal{I}}_{l\bar{e}}^{11}, \tag{7.45}
\end{aligned}$$

$$\begin{aligned}
16\pi^2 \delta m_{(\tilde{\chi}\tilde{V})}^2 &= -4g^2 C_2^{SU(2)} \left[\frac{M_2(M_2 + s_{2\beta}\mu)}{M_2^2 - \mu^2} \tilde{\mathcal{I}}_{\tilde{W}}^1 - \frac{\mu(s_{2\beta}M_2 + \mu)}{M_2^2 - \mu^2} \tilde{\mathcal{I}}_{\tilde{\chi}}^1 \right] \\
& - 4g'^2 Y_\phi^2 \left[\frac{M_1(M_1 + s_{2\beta}\mu)}{M_1^2 - \mu^2} \tilde{\mathcal{I}}_{\tilde{B}}^1 - \frac{\mu(s_{2\beta}M_1 + \mu)}{M_1^2 - \mu^2} \tilde{\mathcal{I}}_{\tilde{\chi}}^1 \right]. \tag{7.46}
\end{aligned}$$

Note that terms proportional to $\gamma^\mu \gamma_\mu = 4 - \epsilon$ are generally encountered when computing loops involving two fermionic fields. To arrive at Eq. (7.46), we have used Eq. (A.30) to reduce $(4 - \epsilon) \tilde{\mathcal{I}}[q^2]_{\tilde{\chi}\tilde{V}}^{11}$ to $\tilde{\mathcal{I}}_{\tilde{\chi}}^1$, $\tilde{\mathcal{I}}_{\tilde{V}}^1$ and $\tilde{\mathcal{I}}_{\tilde{\chi}\tilde{V}}^{11}$, and further used Eq. (A.5) to reduce $\tilde{\mathcal{I}}_{\tilde{\chi}\tilde{V}}^{11}$ to $\tilde{\mathcal{I}}_{\tilde{\chi}}^1$ and $\tilde{\mathcal{I}}_{\tilde{V}}^1$.

From the expressions of master integrals in Eqs. (A.17) and (A.20), it is clear that each term in the equations above is $\mathcal{O}(\frac{\Lambda^2}{16\pi^2})$. Quite generally, the $|\phi|^2$ operator receives threshold corrections that are quadratically sensitive to the EFT cutoff scale Λ when a high-energy BSM theory is matched onto the SMEFT, as a manifestation of a potential hierarchy problem.

As noted before, the same covariant diagrams contributing to $\delta m^2 |\phi|^2$ can also be used to compute the $c_{\Phi\phi}(\Phi_c^* \phi + \phi^* \Phi_c)$ piece, for which we obtain

$$c_{\Phi\phi} = c_{\Phi\phi}^{(\Phi)} + c_{\Phi\phi}^{(\tilde{f})} + c_{\Phi\phi}^{(\tilde{f}\tilde{f})} + c_{\Phi\phi}^{(\tilde{\chi}\tilde{V})}, \tag{7.47}$$

where

$$16\pi^2 c_{\Phi\phi}^{(\Phi)} = \frac{3}{8}(g^2 + g'^2) s_{4\beta} \tilde{\mathcal{I}}_{\Phi}^1, \tag{7.48}$$

$$\begin{aligned}
16\pi^2 c_{\Phi\phi}^{(\tilde{f})} &= N_c \text{tr}(\boldsymbol{\lambda}_u^\dagger \boldsymbol{\lambda}_u) s_\beta c_\beta (\tilde{\mathcal{I}}_{\tilde{q}}^1 + \tilde{\mathcal{I}}_{\tilde{u}}^1) \\
& - N_c \text{tr}(\boldsymbol{\lambda}_d^\dagger \boldsymbol{\lambda}_d) s_\beta c_\beta (\tilde{\mathcal{I}}_{\tilde{q}}^1 + \tilde{\mathcal{I}}_{\tilde{d}}^1) - \text{tr}(\boldsymbol{\lambda}_e^\dagger \boldsymbol{\lambda}_e) s_\beta c_\beta (\tilde{\mathcal{I}}_{\tilde{l}}^1 + \tilde{\mathcal{I}}_{\tilde{e}}^1) \\
& + 2g'^2 Y_\phi s_\beta c_\beta (2N_c Y_q \tilde{\mathcal{I}}_{\tilde{q}}^1 - N_c Y_u \tilde{\mathcal{I}}_{\tilde{u}}^1 - N_c Y_d \tilde{\mathcal{I}}_{\tilde{d}}^1 + 2Y_l \tilde{\mathcal{I}}_{\tilde{l}}^1 - Y_e \tilde{\mathcal{I}}_{\tilde{e}}^1), \tag{7.49}
\end{aligned}$$

$$\begin{aligned}
16\pi^2 c_{\Phi\phi}^{(\tilde{f}\tilde{f})} &= N_c \text{tr}(\boldsymbol{\lambda}_u^\dagger \boldsymbol{\lambda}_u) s_\beta^2 (A_u - \mu \cot \beta)(A_u \cot \beta + \mu) \tilde{\mathcal{I}}_{\tilde{q}\tilde{u}}^{11} \\
& - N_c \text{tr}(\boldsymbol{\lambda}_d^\dagger \boldsymbol{\lambda}_d) s_\beta^2 (A_d \cot \beta - \mu)(A_d + \mu \cot \beta) \tilde{\mathcal{I}}_{\tilde{q}\tilde{d}}^{11} \\
& - \text{tr}(\boldsymbol{\lambda}_e^\dagger \boldsymbol{\lambda}_e) s_\beta^2 (A_e \cot \beta - \mu)(A_e + \mu \cot \beta) \tilde{\mathcal{I}}_{\tilde{l}\tilde{e}}^{11}, \tag{7.50}
\end{aligned}$$

$$16\pi^2 c_{\Phi\phi}^{(\tilde{\chi}\tilde{V})} = -4g^2 C_2^{SU(2)} c_{2\beta} M_2 \mu \tilde{\mathcal{I}}_{\tilde{\chi}\tilde{W}}^{11} - 4g'^2 Y_\phi^2 c_{2\beta} M_1 \mu \tilde{\mathcal{I}}_{\tilde{\chi}\tilde{B}}^{11}. \tag{7.51}$$

As discussed in Section 7.2.2, we absorb this piece into the tree-level effective Lagrangian via a redefinition of β , and thus do not consider it as contributing to threshold corrections.

The $d = 4$ operator $|\phi|^4$ has the following one-loop coefficient,

$$\delta\lambda = \delta\lambda_{(\Phi\varphi)} + \delta\lambda_{(\tilde{f}\tilde{f})} + \delta\lambda_{(\tilde{f}\tilde{f}\tilde{f})} + \delta\lambda_{(\tilde{f}\tilde{f}\tilde{f}\tilde{f})} + \delta\lambda_{(\tilde{\chi}\tilde{V}\tilde{\chi}\tilde{V})}, \quad (7.52)$$

where

$$16\pi^2 \delta\lambda_{(\Phi\varphi)} = \frac{1}{16} \left[(g^2 + g'^2)^2 (s_{2\beta}^4 - s_{2\beta}^2 c_{2\beta}^2 + c_{2\beta}^4) - 2g^2(g^2 + g'^2)c_{2\beta}^2 + 2g^4 \right] \tilde{\mathcal{I}}_{\Phi}^2 + \frac{3}{8} (g^2 + g'^2)^2 s_{2\beta}^2 c_{2\beta}^2 \tilde{\mathcal{I}}_{\Phi 0}^{11}, \quad (7.53)$$

$$16\pi^2 \delta\lambda_{(\tilde{f}\tilde{f})} = \frac{1}{2} \text{tr} \left\{ N_c \left[\left(\lambda_u^\dagger \lambda_u s_\beta^2 + \frac{1}{4} g^2 c_{2\beta} - g'^2 Y_\phi Y_q c_{2\beta} \right)^2 + \left(\lambda_d^\dagger \lambda_d c_\beta^2 - \frac{1}{4} g^2 c_{2\beta} - g'^2 Y_\phi Y_q c_{2\beta} \right)^2 \right] \tilde{\mathcal{I}}_{\tilde{q}}^2 + N_c (\lambda_u \lambda_u^\dagger s_\beta^2 + g'^2 Y_\phi Y_u c_{2\beta})^2 \tilde{\mathcal{I}}_{\tilde{u}}^2 + N_c (\lambda_d \lambda_d^\dagger c_\beta^2 + g'^2 Y_\phi Y_d c_{2\beta})^2 \tilde{\mathcal{I}}_{\tilde{d}}^2 + \left[\left(\lambda_e^\dagger \lambda_e c_\beta^2 - \frac{1}{4} g^2 c_{2\beta} - g'^2 Y_\phi Y_l c_{2\beta} \right)^2 + \left(\frac{1}{4} g^2 c_{2\beta} - g'^2 Y_\phi Y_l c_{2\beta} \right)^2 \right] \tilde{\mathcal{I}}_{\tilde{l}}^2 + (\lambda_e \lambda_e^\dagger c_\beta^2 + g'^2 Y_\phi Y_e c_{2\beta})^2 \tilde{\mathcal{I}}_{\tilde{e}}^2 \right\}, \quad (7.54)$$

$$16\pi^2 \delta\lambda_{(\tilde{f}\tilde{f}\tilde{f})} = \text{tr} \left\{ N_c (A_u - \mu \cot \beta)^2 \lambda_u^\dagger \lambda_u s_\beta^2 \left[\left(\lambda_u^\dagger \lambda_u s_\beta^2 + \frac{1}{4} g^2 c_{2\beta} - g'^2 Y_\phi Y_q c_{2\beta} \right) \tilde{\mathcal{I}}_{\tilde{q}\tilde{u}}^{21} + (\lambda_u^\dagger \lambda_u s_\beta^2 + g'^2 Y_\phi Y_u c_{2\beta}) \tilde{\mathcal{I}}_{\tilde{q}\tilde{u}}^{12} \right] + N_c (A_d \cot \beta - \mu)^2 \lambda_d^\dagger \lambda_d s_\beta^2 \left[\left(\lambda_d^\dagger \lambda_d c_\beta^2 - \frac{1}{4} g^2 c_{2\beta} - g'^2 Y_\phi Y_q c_{2\beta} \right) \tilde{\mathcal{I}}_{\tilde{q}\tilde{d}}^{21} + (\lambda_d^\dagger \lambda_d c_\beta^2 + g'^2 Y_\phi Y_d c_{2\beta}) \tilde{\mathcal{I}}_{\tilde{q}\tilde{d}}^{12} \right] + (A_e \cot \beta - \mu)^2 \lambda_e^\dagger \lambda_e s_\beta^2 \left[\left(\lambda_e^\dagger \lambda_e c_\beta^2 - \frac{1}{4} g^2 c_{2\beta} - g'^2 Y_\phi Y_l c_{2\beta} \right) \tilde{\mathcal{I}}_{\tilde{l}\tilde{e}}^{21} + (\lambda_e^\dagger \lambda_e c_\beta^2 + g'^2 Y_\phi Y_e c_{2\beta}) \tilde{\mathcal{I}}_{\tilde{l}\tilde{e}}^{12} \right] \right\}, \quad (7.55)$$

$$16\pi^2 \delta\lambda_{(\tilde{f}\tilde{f}\tilde{f}\tilde{f})} = \frac{1}{2} N_c \text{tr} (\lambda_u^\dagger \lambda_u \lambda_u^\dagger \lambda_u) s_\beta^4 (A_u - \mu \cot \beta)^4 \tilde{\mathcal{I}}_{\tilde{q}\tilde{u}}^{22} + \frac{1}{2} N_c \text{tr} (\lambda_d^\dagger \lambda_d \lambda_d^\dagger \lambda_d) s_\beta^4 (A_d \cot \beta - \mu)^4 \tilde{\mathcal{I}}_{\tilde{q}\tilde{d}}^{22} + \frac{1}{2} \text{tr} (\lambda_e^\dagger \lambda_e \lambda_e^\dagger \lambda_e) s_\beta^4 (A_e \cot \beta - \mu)^4 \tilde{\mathcal{I}}_{\tilde{l}\tilde{e}}^{22}, \quad (7.56)$$

$$16\pi^2 \delta\lambda_{(\tilde{\chi}\tilde{V}\tilde{\chi}\tilde{V})} = -\frac{3}{4} g^4 \left\{ \tilde{\mathcal{I}}_{\tilde{\chi}\tilde{W}}^{11} - c_{2\beta}^2 M_2^2 \mu^2 \tilde{\mathcal{I}}_{\tilde{\chi}\tilde{W}}^{22} + 4[2M_2^2 + 4s_{2\beta} M_2 \mu + (1 + s_{2\beta}^2) \mu^2] \tilde{\mathcal{I}}[q^2]_{\tilde{\chi}\tilde{W}}^{22} \right\}$$

$$-\frac{1}{2}g^4c_{2\beta}^2(\tilde{\mathcal{I}}_{\tilde{\chi}\tilde{W}}^{11}-M_2^2\mu^2\tilde{\mathcal{I}}_{\tilde{\chi}\tilde{W}}^{22}+4\mu^2\tilde{\mathcal{I}}[q^2]_{\tilde{\chi}\tilde{W}}^{22}) \quad (7.57)$$

$$\begin{aligned} & -g^2g'^2Y_\phi^2\left\{\tilde{\mathcal{I}}_{\tilde{\chi}\tilde{W}}^{11}+\tilde{\mathcal{I}}_{\tilde{\chi}\tilde{B}}^{11}-(M_2^2+M_1^2-2s_{2\beta}^2M_2M_1)\mu^2\tilde{\mathcal{I}}_{\tilde{\chi}\tilde{W}\tilde{B}}^{211}\right. \\ & \quad \left.+4[(M_2+M_1)^2+4s_{2\beta}(M_2+M_1)\mu+2(1+s_{2\beta}^2)\mu^2]\tilde{\mathcal{I}}[q^2]_{\tilde{\chi}\tilde{W}\tilde{B}}^{211}\right\} \\ & -4g'^4Y_\phi^4\left\{\tilde{\mathcal{I}}_{\tilde{\chi}\tilde{B}}^{11}-c_{2\beta}^2M_1^2\mu^2\tilde{\mathcal{I}}_{\tilde{\chi}\tilde{B}}^{22}\right. \\ & \quad \left.+4[2M_1^2+4s_{2\beta}M_1\mu+(1+s_{2\beta}^2)\mu^2]\tilde{\mathcal{I}}[q^2]_{\tilde{\chi}\tilde{B}}^{22}\right\}. \end{aligned} \quad (7.58)$$

For the $\tilde{\chi}\tilde{V}\tilde{\chi}\tilde{V}$ loops, we have used Eq. (A.33) to eliminate the $\tilde{\mathcal{I}}[q^4]$ master integrals (coming from covariant diagrams with two Lorentz contractions) from Eq. (7.58).

Yukawa interactions. The $d = 4$ Yukawa interaction operators $\bar{\psi}_u \boldsymbol{\delta y}_u \psi_q \cdot \epsilon \cdot \phi + \bar{\psi}_d \boldsymbol{\delta y}_d \psi_q \cdot \phi^* + \bar{\psi}_e \boldsymbol{\delta y}_e \psi_l \cdot \phi^* + \text{h.c.}$ are obtained with the following one-loop coefficients,

$$\boldsymbol{\delta y}_u = \mathbf{y}_u \bar{\boldsymbol{\delta y}}_u = \mathbf{y}_u (\bar{\boldsymbol{\delta y}}_u^{(\Phi q d)} + \bar{\boldsymbol{\delta y}}_u^{(\tilde{q} d \tilde{\chi})} + \bar{\boldsymbol{\delta y}}_u^{(\tilde{q} \tilde{u} \tilde{V})} + \bar{\boldsymbol{\delta y}}_u^{(\tilde{f} \tilde{\chi} \tilde{V})}), \quad (7.59a)$$

$$\boldsymbol{\delta y}_d = \mathbf{y}_d \bar{\boldsymbol{\delta y}}_d = \mathbf{y}_d (\bar{\boldsymbol{\delta y}}_d^{(\Phi q u)} + \bar{\boldsymbol{\delta y}}_d^{(\tilde{q} \tilde{u} \tilde{\chi})} + \bar{\boldsymbol{\delta y}}_d^{(\tilde{q} d \tilde{V})} + \bar{\boldsymbol{\delta y}}_d^{(\tilde{f} \tilde{\chi} \tilde{V})}), \quad (7.59b)$$

$$\boldsymbol{\delta y}_e = \mathbf{y}_e \bar{\boldsymbol{\delta y}}_e = \mathbf{y}_e (\bar{\boldsymbol{\delta y}}_e^{(\tilde{l} \tilde{e} \tilde{V})} + \bar{\boldsymbol{\delta y}}_e^{(\tilde{f} \tilde{\chi} \tilde{V})}), \quad (7.59c)$$

where

$$16\pi^2 \bar{\boldsymbol{\delta y}}_u^{(\Phi q d)} = \boldsymbol{\lambda}_d^\dagger \boldsymbol{\lambda}_d c_\beta^2 \tilde{\mathcal{I}}_{\Phi 0}^{11}, \quad (7.60a)$$

$$16\pi^2 \bar{\boldsymbol{\delta y}}_d^{(\Phi q u)} = \boldsymbol{\lambda}_u^\dagger \boldsymbol{\lambda}_u s_\beta^2 \tilde{\mathcal{I}}_{\Phi 0}^{11}, \quad (7.60b)$$

$$16\pi^2 \bar{\boldsymbol{\delta y}}_u^{(\tilde{q} d \tilde{\chi})} = \boldsymbol{\lambda}_d^\dagger \boldsymbol{\lambda}_d \mu (A_d \cot \beta - \mu) \tilde{\mathcal{I}}_{\tilde{q} d \tilde{\chi}}^{111}, \quad (7.61a)$$

$$16\pi^2 \bar{\boldsymbol{\delta y}}_d^{(\tilde{q} \tilde{u} \tilde{\chi})} = \boldsymbol{\lambda}_u^\dagger \boldsymbol{\lambda}_u \mu (A_u \tan \beta - \mu) \tilde{\mathcal{I}}_{\tilde{q} \tilde{u} \tilde{\chi}}^{111}, \quad (7.61b)$$

$$16\pi^2 \bar{\boldsymbol{\delta y}}_u^{(\tilde{q} \tilde{u} \tilde{V})} = -2(A_u - \mu \cot \beta) (g_3^2 C_2^{SU(3)} M_3 \mathcal{I}_{\tilde{q} \tilde{u} \tilde{g}}^{111} + g'^2 Y_q Y_u M_1 \mathcal{I}_{\tilde{q} \tilde{u} \tilde{B}}^{111}), \quad (7.62a)$$

$$16\pi^2 \bar{\boldsymbol{\delta y}}_d^{(\tilde{q} d \tilde{V})} = -2(A_d - \mu \tan \beta) (g_3^2 C_2^{SU(3)} M_3 \mathcal{I}_{\tilde{q} d \tilde{g}}^{111} + g'^2 Y_q Y_d M_1 \mathcal{I}_{\tilde{q} d \tilde{B}}^{111}), \quad (7.62b)$$

$$16\pi^2 \bar{\boldsymbol{\delta y}}_e^{(\tilde{l} \tilde{e} \tilde{V})} = -2(A_e - \mu \tan \beta) g'^2 Y_l Y_e M_1 \mathcal{I}_{\tilde{l} \tilde{e} \tilde{B}}^{111}, \quad (7.62c)$$

$$\begin{aligned} 16\pi^2 \bar{\boldsymbol{\delta y}}_u^{(\tilde{f} \tilde{\chi} \tilde{V})} &= -2g^2 C_2^{SU(2)} \left[\frac{M_2(M_2 + \mu \cot \beta)}{M_2^2 - \mu^2} \tilde{\mathcal{I}}_{\tilde{q} \tilde{W}}^{11} - \frac{\mu(\mu + M_2 \cot \beta)}{M_2^2 - \mu^2} \tilde{\mathcal{I}}_{\tilde{q} \tilde{\chi}}^{11} \right] \\ &+ 2g'^2 Y_\phi \left[\frac{M_1(M_1 + \mu \cot \beta)}{M_1^2 - \mu^2} (Y_q \tilde{\mathcal{I}}_{\tilde{q} \tilde{B}}^{11} - Y_u \tilde{\mathcal{I}}_{\tilde{u} \tilde{B}}^{11}) \right] \end{aligned}$$

$$-\frac{\mu(\mu + M_1 \cot \beta)}{M_1^2 - \mu^2} (Y_q \tilde{\mathcal{I}}_{q\tilde{\chi}}^{11} - Y_u \tilde{\mathcal{I}}_{u\tilde{\chi}}^{11}) \Big], \quad (7.63a)$$

$$\begin{aligned} 16\pi^2 \bar{\delta} y_d^{(\tilde{f}\tilde{\chi}\tilde{V})} &= -2 g^2 C_2^{SU(2)} \left[\frac{M_2(M_2 + \mu \tan \beta)}{M_2^2 - \mu^2} \tilde{\mathcal{I}}_{q\tilde{W}}^{11} - \frac{\mu(\mu + M_2 \tan \beta)}{M_2^2 - \mu^2} \tilde{\mathcal{I}}_{q\tilde{\chi}}^{11} \right] \\ &\quad - 2 g'^2 Y_\phi \left[\frac{M_1(M_1 + \mu \tan \beta)}{M_1^2 - \mu^2} (Y_q \tilde{\mathcal{I}}_{q\tilde{B}}^{11} - Y_d \tilde{\mathcal{I}}_{d\tilde{B}}^{11}) \right. \\ &\quad \left. - \frac{\mu(\mu + M_1 \tan \beta)}{M_1^2 - \mu^2} (Y_q \tilde{\mathcal{I}}_{q\tilde{\chi}}^{11} - Y_d \tilde{\mathcal{I}}_{d\tilde{\chi}}^{11}) \right], \quad (7.63b) \end{aligned}$$

$$\begin{aligned} 16\pi^2 \bar{\delta} y_e^{(\tilde{f}\tilde{\chi}\tilde{V})} &= -2 g^2 C_2^{SU(2)} \left[\frac{M_2(M_2 + \mu \tan \beta)}{M_2^2 - \mu^2} \tilde{\mathcal{I}}_{l\tilde{W}}^{11} - \frac{\mu(\mu + M_2 \tan \beta)}{M_2^2 - \mu^2} \tilde{\mathcal{I}}_{l\tilde{\chi}}^{11} \right] \\ &\quad - 2 g'^2 Y_\phi \left[\frac{M_1(M_1 + \mu \tan \beta)}{M_1^2 - \mu^2} (Y_l \tilde{\mathcal{I}}_{l\tilde{B}}^{11} - Y_e \tilde{\mathcal{I}}_{e\tilde{B}}^{11}) \right. \\ &\quad \left. - \frac{\mu(\mu + M_1 \tan \beta)}{M_1^2 - \mu^2} (Y_l \tilde{\mathcal{I}}_{l\tilde{\chi}}^{11} - Y_e \tilde{\mathcal{I}}_{e\tilde{\chi}}^{11}) \right]. \quad (7.63c) \end{aligned}$$

We have used Eq. (A.31) to reduce $(4 - \epsilon) \tilde{\mathcal{I}}[q^2]_{\Phi_0}^{12}$ to $\tilde{\mathcal{I}}_{\Phi_0}^{11}$ in Eq. (7.60), and Eqs. (A.5) and (A.30) to reduce $\tilde{\mathcal{I}}_{\tilde{f}\tilde{V}\tilde{\chi}}^{111}$ and $(4 - \epsilon) \tilde{\mathcal{I}}[q^2]_{\tilde{f}\tilde{\chi}\tilde{V}}^{111}$ to $\tilde{\mathcal{I}}_{\tilde{f}\tilde{\chi}}^{11}$ and $\tilde{\mathcal{I}}_{\tilde{f}\tilde{V}}^{11}$ in Eq. (7.63).

In these results, of particular interest is the appearance of terms proportional to $\tan \beta$, originating from $\boldsymbol{\lambda}_{d,e} = \mathbf{y}_{d,e} c_\beta^{-1} = \mathbf{y}_{d,e} s_\beta^{-1} \tan \beta$. Since matching calculations are done with UV theory parameters, it is expected here that $\boldsymbol{\delta} \mathbf{y}_{d,e}$ contain terms of order $\frac{1}{16\pi^2} \boldsymbol{\lambda}_{d,e} \propto \frac{\tan \beta}{16\pi^2} \mathbf{y}_{d,e}$. A large $\tan \beta$ can partially overcome the loop suppression, giving rise to sizable SUSY threshold corrections, which in turn is important for achieving b - τ Yukawa unification. More on this in Section 7.3.

Higgs kinetic term. The one-loop coefficient of the $d = 4$ Higgs kinetic term $|D_\mu \phi|^2$ is

$$\delta Z_\phi = \delta Z_\phi^{(\tilde{f}\tilde{f})} + \delta Z_\phi^{(\tilde{\chi}\tilde{V})}, \quad (7.64)$$

where

$$\begin{aligned} 16\pi^2 \delta Z_\phi^{(\tilde{f}\tilde{f})} &= -2 N_c \text{tr}(\boldsymbol{\lambda}_u^\dagger \boldsymbol{\lambda}_u) s_\beta^2 (A_u - \mu \cot \beta)^2 \tilde{\mathcal{I}}[q^2]_{q\tilde{u}}^{22} \\ &\quad - 2 N_c \text{tr}(\boldsymbol{\lambda}_d^\dagger \boldsymbol{\lambda}_d) s_\beta^2 (A_d \cot \beta - \mu)^2 \tilde{\mathcal{I}}[q^2]_{q\tilde{d}}^{22} \\ &\quad - 2 \text{tr}(\boldsymbol{\lambda}_e^\dagger \boldsymbol{\lambda}_e) s_\beta^2 (A_e \cot \beta - \mu)^2 \tilde{\mathcal{I}}[q^2]_{l\tilde{e}}^{22}, \quad (7.65) \end{aligned}$$

$$\begin{aligned} 16\pi^2 \delta Z_\phi^{(\tilde{\chi}\tilde{V})} &= 2 g^2 C_2^{SU(2)} \left[\tilde{\mathcal{I}}_{\tilde{\chi}\tilde{W}}^{11} + 2(M_2^2 + \mu^2 + 2M_2\mu s_{2\beta}) \tilde{\mathcal{I}}[q^2]_{\tilde{\chi}\tilde{W}}^{22} \right] \\ &\quad + 2 g'^2 Y_\phi^2 \left[\tilde{\mathcal{I}}_{\tilde{\chi}\tilde{B}}^{11} + 2(M_1^2 + \mu^2 + 2M_1\mu s_{2\beta}) \tilde{\mathcal{I}}[q^2]_{\tilde{\chi}\tilde{B}}^{22} \right]. \quad (7.66) \end{aligned}$$

Again, we have used Eq. (A.33) to eliminate $\tilde{\mathcal{I}}[q^4]$ in order to arrive at Eq. (7.66). Note that $D_\mu\phi_\alpha$ is written as $-i[P_\mu, \phi_\alpha]$ in our approach (recall P_μ acts on everything to its right). The covariant diagrams listed in Table 7.6 give us the $\text{tr}(P^\mu\phi^*P_\mu\phi)$ piece of $|D_\mu\phi|^2 = -\text{tr}([P^\mu, \phi^*][P_\mu, \phi]) = \text{tr}(P^2\phi^*\phi) + \text{tr}(P^2\phi\phi^*) - 2\text{tr}(P^\mu\phi^*P_\mu\phi)$, which is sufficient to fix the coefficient of $|D_\mu\phi|^2$.

Note that unlike $\delta\mathbf{y}_{d,e} \sim \frac{1}{16\pi^2}\boldsymbol{\lambda}_{d,e} \sim \frac{\tan\beta}{16\pi^2}\mathbf{y}_{d,e}$, contributions to the threshold corrections $\mathbf{y}_{d,e} - \mathbf{y}_{d,e}^{\text{eff}}$ from δZ_ϕ (and also $\delta\mathbf{Z}_f$ below) are only $\sim \frac{1}{16\pi^2}\mathbf{y}_{d,e}$ (see Eq. (7.6)), and are thus subleading in the large $\tan\beta$ limit.

Fermion kinetic terms. The $d = 4$ fermion kinetic terms $\sum_f \bar{\psi}_f \delta\mathbf{Z}_f i\not{D}\psi_f$ are obtained with the following one-loop coefficients,

$$\delta\mathbf{Z}_q = \delta\mathbf{Z}_q^{(\Phi f)} + \delta\mathbf{Z}_q^{(\tilde{f}\tilde{\chi})} + \delta Z_q^{(\tilde{q}\tilde{V})} \mathbf{1}, \quad (7.67a)$$

$$\delta\mathbf{Z}_u = \delta\mathbf{Z}_u^{(\Phi q)} + \delta\mathbf{Z}_u^{(\tilde{q}\tilde{\chi})} + \delta Z_u^{(\tilde{u}\tilde{V})} \mathbf{1}, \quad (7.67b)$$

$$\delta\mathbf{Z}_d = \delta\mathbf{Z}_d^{(\Phi q)} + \delta\mathbf{Z}_d^{(\tilde{q}\tilde{\chi})} + \delta Z_d^{(\tilde{d}\tilde{V})} \mathbf{1}, \quad (7.67c)$$

$$\delta\mathbf{Z}_l = \delta\mathbf{Z}_l^{(\Phi e)} + \delta\mathbf{Z}_l^{(\tilde{e}\tilde{\chi})} + \delta Z_l^{(\tilde{l}\tilde{V})} \mathbf{1}, \quad (7.67d)$$

$$\delta\mathbf{Z}_e = \delta\mathbf{Z}_e^{(\Phi l)} + \delta\mathbf{Z}_e^{(\tilde{l}\tilde{\chi})} + \delta Z_e^{(\tilde{e}\tilde{V})} \mathbf{1}, \quad (7.67e)$$

where

$$16\pi^2 \delta\mathbf{Z}_q^{(\Phi f)} = 2 (\lambda_u^\dagger \lambda_u c_\beta^2 + \lambda_d^\dagger \lambda_d s_\beta^2) \tilde{\mathcal{I}}[q^2]_{\Phi 0}^{21}, \quad (7.68a)$$

$$16\pi^2 \delta\mathbf{Z}_u^{(\Phi q)} = 4 \lambda_u \lambda_u^\dagger c_\beta^2 \tilde{\mathcal{I}}[q^2]_{\Phi 0}^{21}, \quad (7.68b)$$

$$16\pi^2 \delta\mathbf{Z}_d^{(\Phi q)} = 4 \lambda_d \lambda_d^\dagger s_\beta^2 \tilde{\mathcal{I}}[q^2]_{\Phi 0}^{21}, \quad (7.68c)$$

$$16\pi^2 \delta\mathbf{Z}_l^{(\Phi e)} = 2 \lambda_e^\dagger \lambda_e s_\beta^2 \tilde{\mathcal{I}}[q^2]_{\Phi 0}^{21}, \quad (7.68d)$$

$$16\pi^2 \delta\mathbf{Z}_e^{(\Phi l)} = 4 \lambda_e \lambda_e^\dagger s_\beta^2 \tilde{\mathcal{I}}[q^2]_{\Phi 0}^{21}, \quad (7.68e)$$

$$16\pi^2 \delta\mathbf{Z}_q^{(\tilde{f}\tilde{\chi})} = 2 (\lambda_u^\dagger \lambda_u \tilde{\mathcal{I}}[q^2]_{\tilde{u}\tilde{\chi}}^{21} + \lambda_d^\dagger \lambda_d \tilde{\mathcal{I}}[q^2]_{\tilde{d}\tilde{\chi}}^{21}), \quad (7.69a)$$

$$16\pi^2 \delta\mathbf{Z}_u^{(\tilde{q}\tilde{\chi})} = 4 \lambda_u \lambda_u^\dagger \tilde{\mathcal{I}}[q^2]_{\tilde{q}\tilde{\chi}}^{21}, \quad (7.69b)$$

$$16\pi^2 \delta\mathbf{Z}_d^{(\tilde{q}\tilde{\chi})} = 4 \lambda_d \lambda_d^\dagger \tilde{\mathcal{I}}[q^2]_{\tilde{q}\tilde{\chi}}^{21}, \quad (7.69c)$$

$$16\pi^2 \delta\mathbf{Z}_l^{(\tilde{e}\tilde{\chi})} = 2 \lambda_e^\dagger \lambda_e \tilde{\mathcal{I}}[q^2]_{\tilde{e}\tilde{\chi}}^{21}, \quad (7.69d)$$

$$16\pi^2 \delta\mathbf{Z}_e^{(\tilde{l}\tilde{\chi})} = 4 \lambda_e \lambda_e^\dagger \tilde{\mathcal{I}}[q^2]_{\tilde{l}\tilde{\chi}}^{21}, \quad (7.69e)$$

$$16\pi^2 \delta Z_q^{(\tilde{q}\tilde{V})} = 4 (g_3^2 C_2^{SU(3)} \tilde{\mathcal{I}}[q^2]_{\tilde{q}\tilde{g}}^{21} + g^2 C_2^{SU(2)} \tilde{\mathcal{I}}[q^2]_{\tilde{q}\tilde{W}}^{21} + g'^2 Y_q^2 \tilde{\mathcal{I}}[q^2]_{\tilde{q}\tilde{B}}^{21}), \quad (7.70a)$$

$$16\pi^2 \delta Z_u^{(\tilde{u}\tilde{V})} = 4 (g_3^2 C_2^{SU(3)} \tilde{\mathcal{I}}[q^2]_{\tilde{u}\tilde{g}}^{21} + g'^2 Y_u^2 \tilde{\mathcal{I}}[q^2]_{\tilde{u}\tilde{B}}^{21}), \quad (7.70b)$$

$$16\pi^2 \delta Z_d^{(\tilde{d}\tilde{V})} = 4 (g_3^2 C_2^{SU(3)} \tilde{\mathcal{I}}[q^2]_{\tilde{d}\tilde{g}}^{21} + g'^2 Y_d^2 \tilde{\mathcal{I}}[q^2]_{\tilde{d}\tilde{B}}^{21}), \quad (7.70c)$$

$$16\pi^2 \delta Z_l^{(\tilde{l}\tilde{V})} = 4 (g_2^2 C_2^{SU(2)} \tilde{\mathcal{I}}[q^2]_{\tilde{l}\tilde{W}}^{21} + g'^2 Y_l^2 \tilde{\mathcal{I}}[q^2]_{\tilde{l}\tilde{B}}^{21}), \quad (7.70d)$$

$$16\pi^2 \delta Z_e^{(\tilde{e}\tilde{V})} = 4 g'^2 Y_e^2 \tilde{\mathcal{I}}[q^2]_{\tilde{e}\tilde{B}}^{21}. \quad (7.70e)$$

To arrive at Eqs. (7.69) and (7.70), we have used Eqs. (A.5), (A.12) and (A.30) to simplify

$$\begin{aligned} (2 - \epsilon) \mathcal{I}[q^2]_{ij}^{12} - M_j^2 \mathcal{I}_{ij}^{12} &= (4 - \epsilon) \mathcal{I}[q^2]_{ij}^{12} - M_j^2 \mathcal{I}_{ij}^{12} - 2 \mathcal{I}[q^2]_{ij}^{12} = \mathcal{I}_{ij}^{11} - 2 \mathcal{I}[q^2]_{ij}^{12} \\ &= \frac{1}{M_i^2 - M_j^2} (\mathcal{I}_i^1 - \mathcal{I}_j^1) - 2 \mathcal{I}[q^2]_{ij}^{12} = \frac{2}{M_i^2 - M_j^2} (\mathcal{I}[q^2]_i^2 - \mathcal{I}[q^2]_j^2) - 2 \mathcal{I}[q^2]_{ij}^{12} \\ &= 2(\mathcal{I}[q^2]_{ij}^{21} + \mathcal{I}[q^2]_{ij}^{12}) - 2 \mathcal{I}[q^2]_{ij}^{12} = 2 \mathcal{I}[q^2]_{ij}^{21}. \end{aligned} \quad (7.71)$$

This relation is also valid in the limit $M_j \rightarrow 0$,

$$(2 - \epsilon) \mathcal{I}[q^2]_{i0}^{12} = 2 \mathcal{I}[q^2]_{i0}^{21}, \quad (7.72)$$

which we have used to obtain Eq. (7.68).

Gauge boson kinetic terms. General results of wavefunction renormalization of gauge fields from integrating out heavy matter fields are well-known, see e.g. [55]. The covariant diagrams version of the calculation can be found in [60]. Specializing to the case of integrating out the MSSM heavy fields, we find

$$\delta Z_G = g_3^2 (\bar{\delta} Z_G^{(\tilde{f})} + \bar{\delta} Z_G^{(\tilde{g})}), \quad (7.73a)$$

$$\delta Z_W = g^2 (\bar{\delta} Z_W^{(\Phi)} + \bar{\delta} Z_W^{(\tilde{f})} + \bar{\delta} Z_W^{(\tilde{\chi})} + \bar{\delta} Z_W^{(\tilde{W})}), \quad (7.73b)$$

$$\delta Z_B = g'^2 (\bar{\delta} Z_B^{(\Phi)} + \bar{\delta} Z_B^{(\tilde{f})} + \bar{\delta} Z_B^{(\tilde{\chi})}), \quad (7.73c)$$

where

$$16\pi^2 \bar{\delta} Z_W^{(\Phi)} = \frac{1}{6} \tilde{\mathcal{I}}_\Phi^2, \quad 16\pi^2 \bar{\delta} Z_B^{(\Phi)} = \frac{2}{3} Y_\phi^2 \tilde{\mathcal{I}}_\Phi^2, \quad (7.74)$$

$$\begin{aligned} 16\pi^2 \bar{\delta} Z_G^{(\tilde{f})} &= \frac{1}{6} (2 \tilde{\mathcal{I}}_{\tilde{q}}^2 + \tilde{\mathcal{I}}_{\tilde{u}}^2 + \tilde{\mathcal{I}}_{\tilde{d}}^2), & 16\pi^2 \bar{\delta} Z_W^{(\tilde{f})} &= \frac{1}{6} (N_c \tilde{\mathcal{I}}_{\tilde{q}}^2 + \tilde{\mathcal{I}}_{\tilde{l}}^2), \\ 16\pi^2 \delta Z_B^{(\tilde{f})} &= \frac{1}{3} (2 N_c Y_q^2 \tilde{\mathcal{I}}_{\tilde{q}}^2 + N_c Y_u^2 \tilde{\mathcal{I}}_{\tilde{u}}^2 + N_c Y_d^2 \tilde{\mathcal{I}}_{\tilde{d}}^2 + 2 Y_l^2 \tilde{\mathcal{I}}_{\tilde{l}}^2 + Y_e^2 \tilde{\mathcal{I}}_{\tilde{e}}^2), \end{aligned} \quad (7.75)$$

$$16\pi^2 \bar{\delta} Z_W^{(\tilde{\chi})} = \frac{2}{3} \tilde{\mathcal{I}}_{\tilde{\chi}}^2, \quad 16\pi^2 \bar{\delta} Z_B^{(\tilde{\chi})} = \frac{8}{3} Y_\phi^2 \tilde{\mathcal{I}}_{\tilde{\chi}}^2, \quad (7.76)$$

$$16\pi^2 \bar{\delta} Z_G^{(\tilde{g})} = 2 \tilde{\mathcal{I}}_{\tilde{g}}^2, \quad 16\pi^2 \bar{\delta} Z_W^{(\tilde{W})} = \frac{4}{3} \tilde{\mathcal{I}}_{\tilde{W}}^2. \quad (7.77)$$

We have used Eq. (A.12) to reduce the bosonic loop integral $\mathcal{I}[q^4]_i^4$ to $\frac{1}{24} \mathcal{I}_i^2$. The fermionic loops, on the other hand, are proportional to $-M_i^4 \mathcal{I}_i^4 + 8M_i^2 \mathcal{I}[q^2]_i^4 + (-16 + 10\epsilon) \mathcal{I}[q^4]_i^4$ which, by Eq. (A.32), is equal to $8\mathcal{I}[q^4]_i^4 - \mathcal{I}_i^2 = -\frac{2}{3} \mathcal{I}_i^2$.

7.2.4 One-loop matching: $d = 6$ operators $\mathcal{O}_{d\phi, e\phi}$ in the large $\tan\beta$, low M_Φ limit

We can use the same techniques to obtain one-loop-generated $d = 6$ operators. There is a large number of them, but not all are equally interesting phenomenologically. In fact, given the loop suppression, together with a possibly high superpartner mass scale Λ due to lack of new particle discoveries as well as a SM-like Higgs boson mass of $m_h \simeq 125$ GeV, a generic $d = 6$ operator with $\mathcal{O}(\frac{1}{16\pi^2} \frac{1}{\Lambda^2})$ coefficient is likely to have a negligible effect on observables. In this regard, we would like to identify a region of MSSM parameter space where some $d = 6$ operators have parametrically enhanced observable effects, and can thus point to realistic experimental targets to be pursued.

To do so, we first note that, as in the case of $\bar{\delta}\mathbf{y}_{d,e}$ discussed in the previous subsection, factors of $\tan\beta$ can appear when operator coefficients are written in terms of $\mathbf{y}_{d,e}$ rather than $\boldsymbol{\lambda}_{d,e}$, which can partially overcome the loop suppression if $\tan\beta \gg 1$. We are thus led to consider the large $\tan\beta$ limit. At dimension-six level, $\tan\beta$ enhancement occurs for several operators, among which we focus on $\mathcal{O}_{d\phi}$ and $\mathcal{O}_{e\phi}$, motivated by their relevance to precision Higgs physics as they modify $hb\bar{b}$ and $h\tau^+\tau^-$ couplings; see Eq. (7.11). Note that in contrast, $\mathcal{O}_{u\phi}$, which modifies $ht\bar{t}$ coupling, does not have a $\tan\beta$ enhanced effect.

To further boost observable effects of the operators $\mathcal{O}_{d\phi}$ and $\mathcal{O}_{e\phi}$, we would like to focus on the scenario where M_Φ , the mass of the heavier Higgs doublet, is somewhat lower than Λ . In this case, there are contributions to $C_{d\phi, e\phi}$ that are proportional to $\frac{1}{M_\Phi^2}$, which is parametrically larger compared to $\frac{1}{\Lambda^2}$. There are in principle two sources of such contributions — loops involving Φ propagators, and operators proportional to Φ_c . By carefully enumerating covariant diagrams following the procedure of the previous subsection, we are able to show that loops involving Φ propagators are all free from $\tan\beta$ enhancement, and so will not consider them further.

As for the second option, there are only a few possibilities for writing down $d = 6$ operators that are proportional to Φ_c , since $\Phi_c^{(1)}$ ($\Phi_c^{(2)}$) is already dimension three (five). They are, schematically,

$$(\Phi_c^{(1)})^2, \quad \Phi_c^{(1)}\psi^2, \quad \Phi_c^{(1)}\phi^3, \quad \Phi_c^{(1)}\phi P^2, \quad \Phi_c^{(2)}\phi. \quad (7.78)$$

Among them, $(\Phi_c^{(1)})^2$ and $\Phi_c^{(1)}\psi^2$ do not contain $\mathcal{O}_{d\phi, e\phi}$ with $\tan\beta$ enhanced coefficients, while

$\Phi_c^{(2)}\phi$ has already been absorbed into $\mathcal{L}_{\text{SMEFT}}^{\text{tree}}$ via the redefinition of β discussed before. So we are left with $\Phi_c^{(1)}\phi^3$ and $\Phi_c^{(1)}\phi P^2$. To be explicit, we have

$$\begin{aligned}
\mathcal{L}_{\text{SMEFT}}^{\text{1-loop}} &\supset c_{\Phi\phi^3}|\phi|^2(\Phi_c^{(1)*}\phi + \phi^*\Phi_c^{(1)}) + c_{\Phi\phi P^2}[(D^\mu\Phi_c^{(1)})^*(D_\mu\phi) + (D^\mu\phi)^*(D_\mu\Phi_c^{(1)})] \\
&\stackrel{\text{IBP}}{=} c_{\Phi\phi^3}|\phi|^2(\Phi_c^{(1)*}\phi + \phi^*\Phi_c^{(1)}) - c_{\Phi\phi P^2}[\Phi_c^{(1)*}(D^2\phi) + (D^2\phi)^*\Phi_c^{(1)}] \\
&\stackrel{\text{EoM}}{=} (c_{\Phi\phi^3} + 2\lambda c_{\Phi\phi P^2})|\phi|^2(\Phi_c^{(1)*}\phi + \phi^*\Phi_c^{(1)}) + \dots \\
&\supset \frac{\tan\beta}{M_\Phi^2}(c_{\Phi\phi^3} + 2\lambda c_{\Phi\phi P^2})\left([\mathbf{y}_d^\dagger]_{pr}[\mathcal{O}_{d\phi}]^{pr} + [\mathbf{y}_e^\dagger]_{pr}[\mathcal{O}_{e\phi}]^{pr}\right). \tag{7.79}
\end{aligned}$$

Note that there is also a tree-level matching contribution to $\Phi_c^{(1)}\phi^3$, which we already computed in Section 7.2.2. Though $\overline{\text{DR}}$ scheme was assumed there, the one-loop difference between $\overline{\text{MS}}$ and $\overline{\text{DR}}$ is not $\tan\beta$ enhanced and negligible.

The operator coefficients $c_{\Phi\phi^3}$ and $c_{\Phi\phi P^2}$ can be computed from the same covariant diagrams that give rise to $\delta\lambda$ and δZ_ϕ , respectively. In fact, we just need to retrieve $\mathcal{O}(\Phi\phi^3)$ and $\mathcal{O}(\Phi\phi)$ pieces from products of \mathbf{U} matrix elements, instead of $\mathcal{O}(\phi^4)$ and $\mathcal{O}(\phi^2)$ pieces. From Appendix C we see that, with the exception of diagrams involving $U_{\varphi\varphi}$, this amounts to starting from the latter, and replacing $s_\beta\phi \rightarrow c_\beta\Phi$, $c_\beta\phi \rightarrow -s_\beta\Phi$ in all possible ways. In other words, from the form of the \mathbf{U} matrix we can infer that

$$\begin{aligned}
\mathcal{L}_{\text{SMEFT}} &\supset \delta\lambda|\phi|^4 + \frac{1}{2}\left(\frac{\partial}{\partial\beta}\delta\lambda\right)|\phi|^2(\Phi_c^*\phi + \phi^*\Phi_c) \\
&\quad + \delta Z_\phi|D_\mu\phi|^2 + \frac{1}{2}\left(\frac{\partial}{\partial\beta}\delta Z_\phi\right)(D^\mu\Phi_c^*D_\mu\phi + D^\mu\phi^*D_\mu\Phi_c), \tag{7.80}
\end{aligned}$$

up to loops involving Φ propagators. We have verified Eq. (7.80) by explicit calculation.

The simple replacement rule observed above, which connects different operators involving ϕ and Φ_c , can be understood by considering a variation of the EFT matching problem we are dealing with now. Suppose, instead of integrating out all BSM fields of the MSSM, we integrate out only the R -parity-odd fields, while keeping both Higgs doublets in the low-energy EFT. The calculation in this case would be more conveniently done in the (H_u, H_d) basis, and the angle β does not appear in the effective Lagrangian in the electroweak symmetric phase. Afterward, we can substitute

$$H_u \rightarrow s_\beta\phi + c_\beta\Phi, \quad H_d \rightarrow \epsilon \cdot (c_\beta\phi - s_\beta\Phi)^*, \tag{7.81}$$

so as to write the effective Lagrangian in terms of ϕ and Φ . From Eq. (7.81) it is clear that for each term involving $s_\beta\phi$ ($c_\beta\phi$), if we replace $s_\beta\phi \rightarrow c_\beta\Phi$ ($c_\beta\phi \rightarrow -s_\beta\Phi$), the result would also be a term in the effective Lagrangian. Further integrating out Φ to arrive at the SMEFT

does not change the conclusion for the terms that already existed, namely those generated by integrating out R -parity-odd fields. Meanwhile, additional terms, such as $\delta\lambda_{(\Phi\varphi)}|\phi|^4$ (see Eq. (7.53)), are generated by loops involving Φ , for which the simple replacement rule above does not apply. However, none of these terms is $\tan\beta$ enhanced, and we will thus neglect them in the $d = 6$ part of the EFT Lagrangian.

To sum up, in the limit $\tan\beta \gg 1$, $M_\Phi \lesssim \Lambda$, we have

$$\mathbf{C}_{d\phi}^{1\text{-loop}} \simeq \frac{\tan\beta}{M_\Phi^2} (c_{\Phi\phi^3} + 2\lambda c_{\Phi\phi P^2}) \mathbf{y}_d^\dagger, \quad \mathbf{C}_{e\phi}^{1\text{-loop}} \simeq \frac{\tan\beta}{M_\Phi^2} (c_{\Phi\phi^3} + 2\lambda c_{\Phi\phi P^2}) \mathbf{y}_e^\dagger, \quad (7.82)$$

where

$$\begin{aligned} c_{\Phi\phi^3} &\simeq c_{\Phi\phi^3}^{(\tilde{f}\tilde{f})} + c_{\Phi\phi^3}^{(\tilde{f}\tilde{f}\tilde{f})} + c_{\Phi\phi^3}^{(\tilde{f}\tilde{f}\tilde{f}\tilde{f})} + c_{\Phi\phi^3}^{(\tilde{\chi}\tilde{V}\tilde{\chi}\tilde{V})} \\ &= \frac{1}{2} \frac{\partial}{\partial\beta} (\delta\lambda^{(\tilde{f}\tilde{f})} + \delta\lambda^{(\tilde{f}\tilde{f}\tilde{f})} + \delta\lambda^{(\tilde{f}\tilde{f}\tilde{f}\tilde{f})} + \delta\lambda^{(\tilde{\chi}\tilde{V}\tilde{\chi}\tilde{V})}), \end{aligned} \quad (7.83)$$

$$c_{\Phi\phi P^2} \simeq c_{\Phi\phi P^2}^{(\tilde{f}\tilde{f})} + c_{\Phi\phi P^2}^{(\tilde{\chi}\tilde{V})} = \frac{1}{2} \frac{\partial}{\partial\beta} \delta Z_\phi, \quad (7.84)$$

with various contributions to $\delta\lambda$ and δZ_ϕ computed in the previous subsection.

7.3 Bottom-tau Yukawa unification

In this section, we study implications of b - τ Yukawa unification on the SUSY spectrum in the EFT framework. To simplify the analyses, we neglect Yukawa couplings of the first two generation fermions, and impose the following relations among MSSM parameters,

$$M_{\tilde{q}} = M_{\tilde{u}} = M_{\tilde{d}} = M_{\tilde{l}} = M_{\tilde{\tau}} \equiv M_s, \quad (7.85)$$

$$A_u = A_d = A_e \equiv A_t, \quad (7.86)$$

$$M_{\tilde{g}} = 3M_{\tilde{W}} = 6M_{\tilde{B}} \equiv M_3. \quad (7.87)$$

As a result, above the SUSY threshold Λ , we have a theory of 13 parameters:

$$g', g, g_3, \lambda_t, \lambda_b, \lambda_\tau, m^2, A_t, \quad (7.88a)$$

$$M_\Phi, M_s, \mu, M_3, \tan\beta. \quad (7.88b)$$

Below the SUSY threshold Λ , they are mapped onto parameters in the SMEFT, as we have worked out in detail in Section 7.2. We shall keep only the renormalizable operators and dimension-six ones that are generated at tree level. The EFT is therefore a theory

characterized by 20 parameters:

$$g'^{\text{eff}}, g^{\text{eff}}, g_3^{\text{eff}}, y_t^{\text{eff}}, y_b^{\text{eff}}, y_\tau^{\text{eff}}, \lambda_{\text{eff}}, m_{\text{eff}}^2, \quad (7.89\text{a})$$

$$C_\phi, C_{t\phi}, C_{b\phi}, C_{\tau\phi}, C_{qu}^{(1)}, C_{qu}^{(8)}, C_{qd}^{(1)}, C_{qu}^{(8)}, C_{le}, C_{quqd}^{(1)}, C_{lequ}^{(1)}, C_{ledq}. \quad (7.89\text{b})$$

It is implicit here that all generation indices are set to 3 in the four-fermion operator coefficients.

We numerically evolve the 13 parameters in Eq. (7.88) in the regime $Q > \Lambda$ according to two-loop RG equations of the MSSM [244], and the 20 parameters in Eq. (7.89) in the regime $Q < \Lambda$ according to two-loop RG equations of the renormalizable SM [245] and one-loop RG equations of the dimension-six SMEFT [76, 77, 80]. At $Q = \Lambda$, the two sets of parameters are connected by the matching calculation presented in Section 7.2, together with one-loop scheme conversion between $\overline{\text{MS}}$ (used for RG evolution in the SMEFT) and $\overline{\text{DR}}$ (used for RG evolution in the MSSM) [243].

As boundary conditions for the entire set of RG equations, we set

$$\begin{aligned} g'^{\text{eff}} &= 0.35827, & g^{\text{eff}} &= 0.64779, & g_3^{\text{eff}} &= 1.1671, \\ y_t^{\text{eff}} - \frac{v^2}{2}C_{t\phi} &= 0.93612, & y_b^{\text{eff}} - \frac{v^2}{2}C_{b\phi} &= 0.01539, & y_\tau^{\text{eff}} - \frac{v^2}{2}C_{\tau\phi} &= 0.00988, \\ \lambda_{\text{eff}} - \frac{3v^2}{2}C_\phi &= 0.12592, & m_{\text{eff}}^2 + \frac{3v^4}{4}C_\phi &= -(92.964 \text{ GeV})^2, \end{aligned} \quad (7.90)$$

at $Q = m_t = 173.21 \text{ GeV}$, where $v^2 = -m_{\text{eff}}^2/\lambda_{\text{eff}}$. These linear combinations of SMEFT parameters are what would be actually extracted when mapping the SM Lagrangian to low-energy observables, including $m_W = 80.385 \text{ GeV}$, $m_h = 125.09 \text{ GeV}$, $\alpha_s(m_Z) = 0.1185$, etc. The numbers in Eq. (7.90) are taken from [245], except for $y_b^{\text{eff}} - \frac{v^2}{2}C_{b\phi}$, which is taken from [246], and $y_\tau^{\text{eff}} - \frac{v^2}{2}C_{\tau\phi}$, which is fixed by requiring $m_\tau^{\text{pole}} = 1.77686 \text{ GeV}$ is reproduced when the SM is matched onto five-flavor QCD \times QED and RG evolved down to the low scale according to [247].

The 8 boundary conditions in Eq. (7.90) reduce the number of free parameters from 13 to 5. We choose them to be those in Eq. (7.88b). Thus, for any specific values of M_Φ , M_s , μ , M_3 , $\tan\beta$, we can ask whether the entire set of equations admits a solution with all couplings in the perturbative regime, and if it does, whether λ_b and λ_τ unify at the grand unification scale Q_{GUT} .

To be precise, we shall set the matching scale $\Lambda = M_s$, and determine Q_{GUT} by

$$(5/3)^{1/2}g'(Q_{\text{GUT}}) = g(Q_{\text{GUT}}). \quad (7.91)$$

We define “ b - τ Yukawa unification” by $|\lambda_b(Q_{\text{GUT}})/\lambda_\tau(Q_{\text{GUT}})-1| < 0.02$ here, as it is generally difficult to have a larger GUT threshold correction [233].

We further set $M_\Phi = M_s$ in this section for simplicity, since M_Φ does not play a significant role in b - τ Yukawa unification. For several choices of $\tan \beta = 50, 10, 4, 2$, we scan M_s between 10^3 GeV and 10^{10} GeV, and scan μ and $|M_3| = -M_3$ within a factor of 50 from M_s , to search for solutions with b - τ Yukawa unification (no solution exists when $\mu M_3 > 0$, see below)⁵. We refrain from going beyond $M_s = 10^{10}$ GeV for the present analysis, because additional GUT-scale input, namely gauge coupling threshold corrections, would be needed to precisely define Q_{GUT} . Also, larger mass ratios are disallowed so as not to compromise the validity of our matching calculation, where all BSM fields are assumed to have similar masses and thus integrated out together.

Figures 7.1 and 7.2 show points in the MSSM parameter space that allow consistent matching of the MSSM onto the SMEFT and meanwhile realize b - τ Yukawa unification, projected onto $(\log M_s, \mu/M_s)$ and $(\log M_s, |M_3|/M_s)$ planes, respectively. Different colors (blue, yellow, green, red) are used for solutions with $x_t \equiv (A_t - \mu \cot \beta)/M_s$ in different ranges ($-4 < x_t < -\sqrt{6}$, $-\sqrt{6} < x_t < 0$, $0 < x_t < \sqrt{6}$, $\sqrt{6} < x_t < 4$, respectively). We have quite conservatively considered a large interval $(-4, 4)$ for x_t , keeping in mind the caveat that x_t values past maximal mixing $\pm\sqrt{6}$ (blue and red dots) may run afoul of charge and color breaking vacuum constraints [248, 249]. In addition, points with $|M_3| < 2$ TeV, potentially already in tension with gluino searches at the LHC (depending on decay kinematics, see e.g. [250]), are represented by empty circles in all plots.

An immediate observation from these figures is that b - τ Yukawa unification is achievable for SUSY scales from TeV all the way up to (at least) 10^{10} GeV, with suitable choices of mass ratios and $\tan \beta$. It is worth noting, though, that a large Higgsino mass $\mu > M_s$ is always required for $\tan \beta \lesssim 10$, which may be less preferable from the point of view of fine-tuned electroweak symmetry breaking.

There are two issues that are key to understanding these results in more detail, which we now discuss in turn.

7.3.1 Matching of the Higgs quartic

First of all, it should be noted that it is not always possible to match the MSSM onto the SMEFT while satisfying the boundary conditions of Eq. (7.90), for arbitrary choices of SUSY parameters. This is largely due to the fact that the Higgs quartic coupling λ is a derived quantity in the MSSM, given by $\frac{1}{8}(g^2 + g'^2)c_{2\beta}^2$ at tree level. A threshold correction of just

⁵We can fix the signs of μ and M_3 , keeping their relative sign, without loss of generality here, because the MSSM Lagrangian is invariant under simultaneous sign change of μ , $M_{3,2,1}$ and $A_{u,d,e}$.

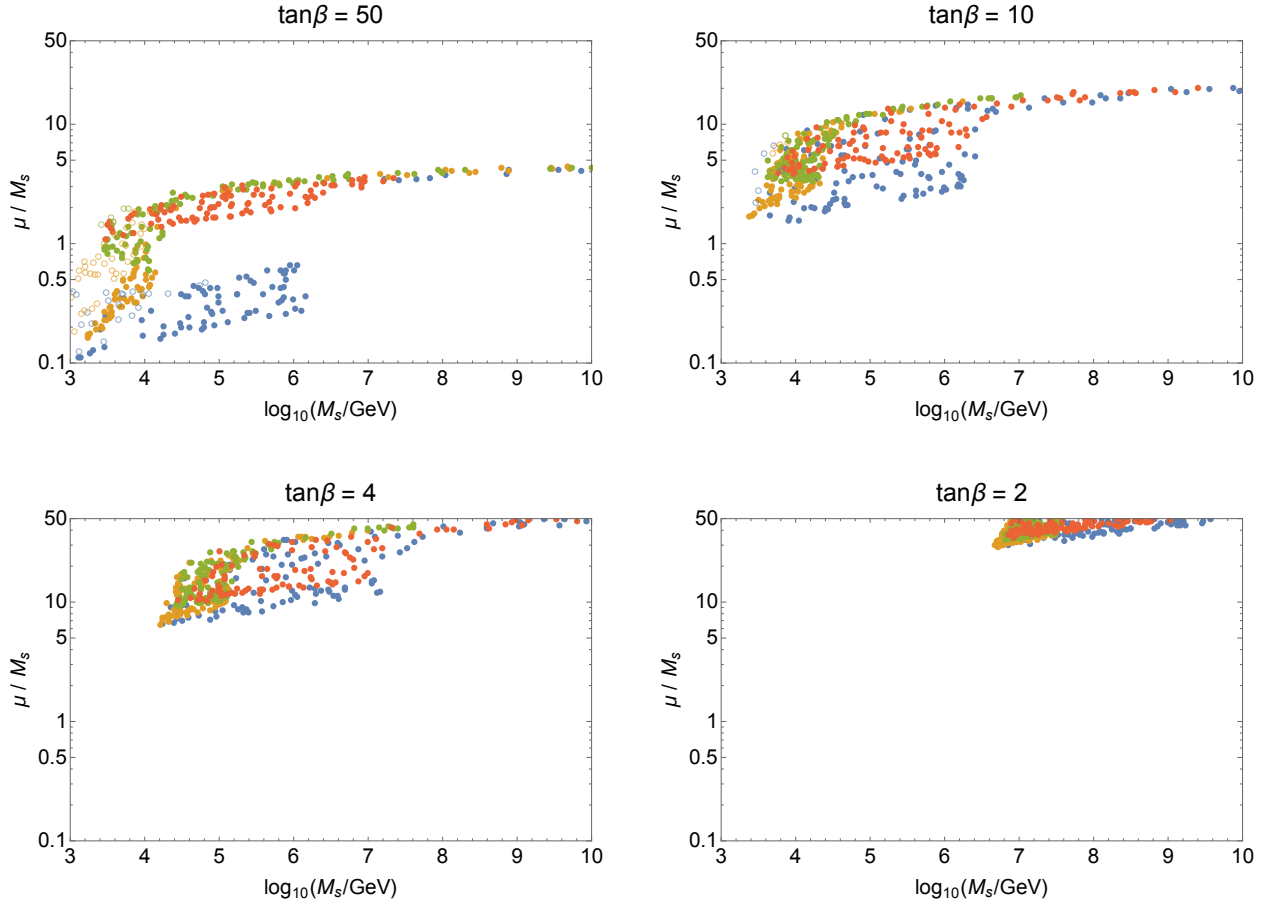


Figure 7.1: (From [132]) Points in the MSSM parameter space that allow consistent matching onto the SMEFT and meanwhile realize b - τ Yukawa unification, projected onto $(\log M_s, \mu/M_s)$ plane, for several choices of $\tan\beta$. Blue, yellow, green, red points have $x_t \equiv (A_t - \mu \cot\beta)/M_s \in (-4, -\sqrt{6}), (-\sqrt{6}, 0), (0, \sqrt{6}), (\sqrt{6}, 4)$, respectively. Empty circles represent solutions with a gluino lighter than 2 TeV, potentially already in tension with direct LHC searches, depending on decay kinematics.

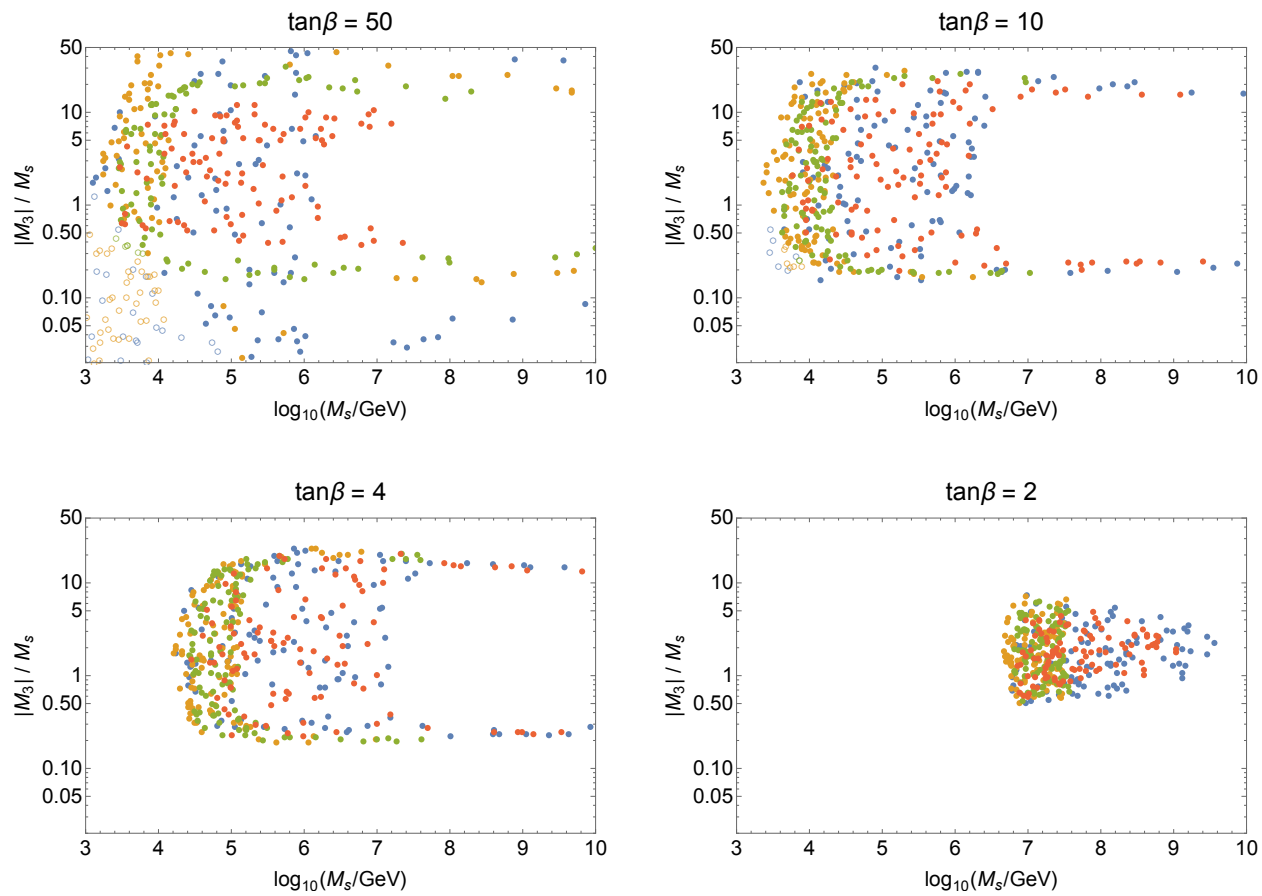


Figure 7.2: (From [132]) Same as Figure 7.1, now projected onto $(\log M_s, |M_3|/M_s)$ plane.

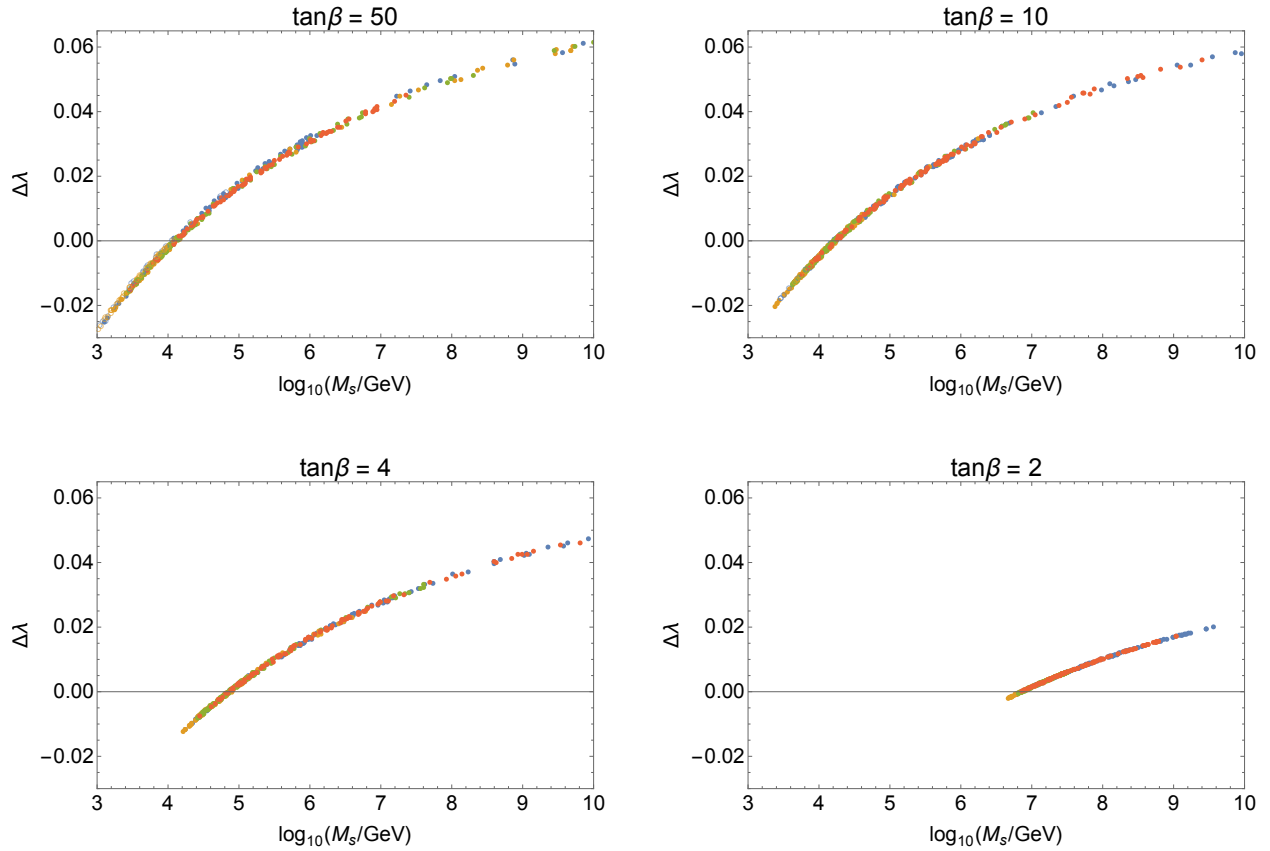


Figure 7.3: (From [132]) Same as Figure 7.1, now showing SUSY threshold correction for the Higgs quartic coupling, defined as $\Delta\lambda \equiv \lambda - \lambda_{\text{eff}}$ at the matching scale $\Lambda = M_s$.

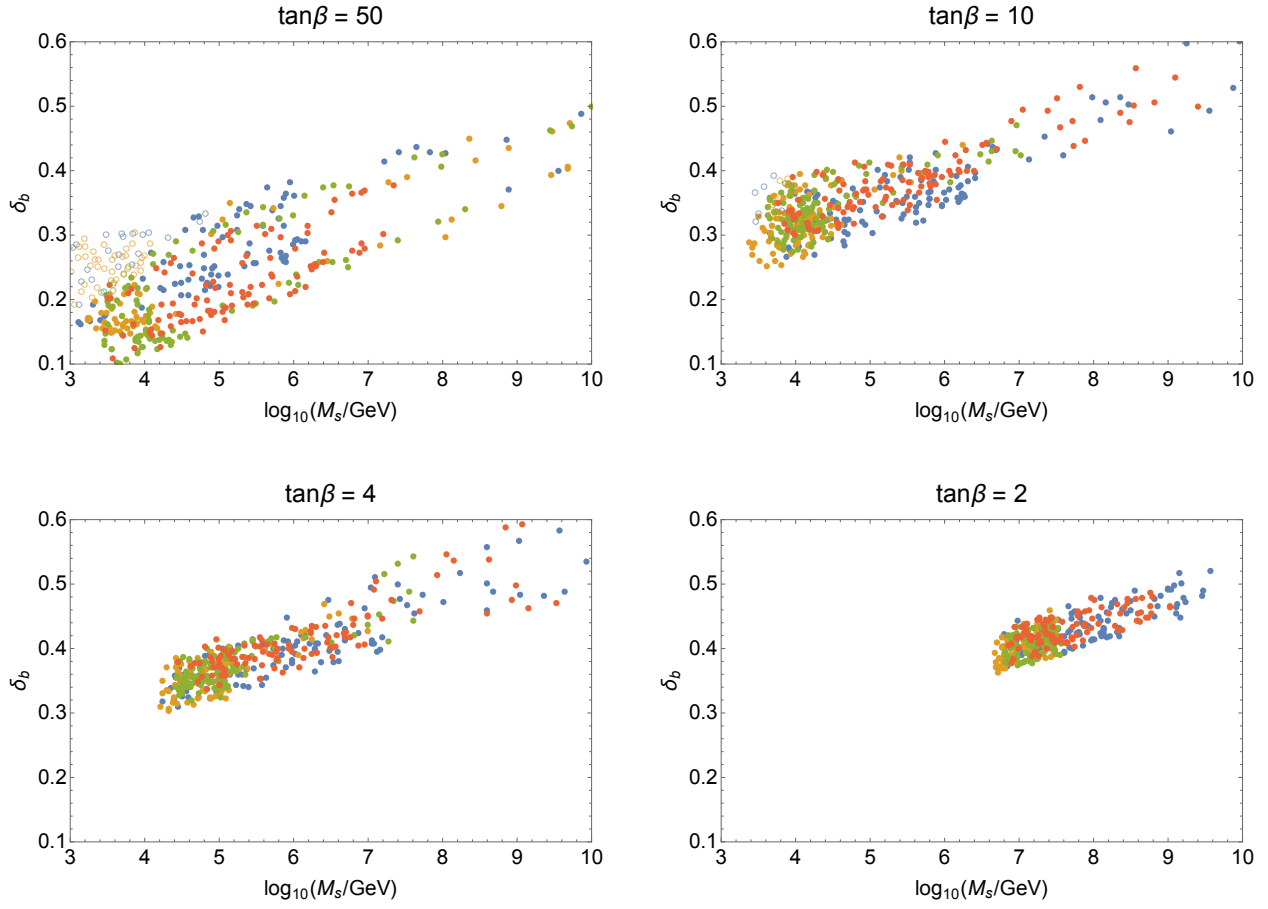


Figure 7.4: (From [132]) Same as Figure 7.1, now showing SUSY threshold correction for the bottom Yukawa coupling, defined as $\delta_b \equiv (y_b - y_b^{\text{eff}})/y_b^{\text{eff}}$ at the matching scale $\Lambda = M_s$.

the right size is needed for λ_{eff} to match the low-energy determination, most importantly from $m_h = 125 \text{ GeV}$.

To see this explicitly, we plot in Figure 7.3 the value of

$$\Delta\lambda \equiv \lambda - \lambda_{\text{eff}}, \quad (7.92)$$

for each point in our sample of b - τ Yukawa unification solutions, evaluated at the matching scale $\Lambda = M_s$. For the most part of parameter space, this threshold correction can be approximated by

$$\begin{aligned} \Delta\lambda &\simeq \delta\lambda_{(\tilde{f}\tilde{f}\tilde{f})} + \delta\lambda_{(\tilde{f}\tilde{f}\tilde{f}\tilde{f})} \\ &\simeq \frac{N_c}{16\pi^2} \left\{ 2 y_t^4 (A_t - \mu \cot \beta)^2 \tilde{\mathcal{I}}_{\tilde{f}}^3 \right. \\ &\quad \left. + \frac{1}{2} [y_t^4 (A_t - \mu \cot \beta)^4 + (y_b \tan \beta)^4 (\mu - A_t \cot \beta)^4] \mathcal{I}_{\tilde{f}}^4 \right\} \\ &\simeq \frac{N_c}{16\pi^2} \frac{1}{12} \left[\left(y_b \tan \beta \frac{\mu}{M_s} \right)^4 + y_t^4 ((x_t^2 - 6)^2 - 36) \right], \end{aligned} \quad (7.93)$$

see Eqs. (7.55) and (7.56). The dependence on x_t in Eq. (7.93) explains the existence of up to four branches of solutions, separated by $x_t = -\sqrt{6}$, 0 and $\sqrt{6}$.

Matching of the Higgs quartic essentially selects a range of μ/M_s for any given M_s , for which Eq. (7.93) can possibly be of the right size with suitable choice of x_t . Since the required threshold correction increases logarithmically with the SUSY threshold scale, and is meanwhile insensitive to $\tan \beta$ when $c_{2\beta}^2 \simeq 1$, the range of μ/M_s being selected roughly scales as $\cot \beta (\log M_s)^{1/4}$ for $\tan \beta \gg 1$. Of course, on each branch of x_t , part of this range can be excluded by either lack of b - τ Yukawa unification, or a mass ratio μ/M_s or $|M_3|/M_s$ outside of the interval (1/50, 50). Nevertheless, the general trend of $\mu/M_s \sim \cot \beta (\log M_s)^{1/4}$ is still visible in Figure 7.1.

Another feature of the figures is that the available parameter space is cut off at low M_s . Here the $\Delta\lambda$ needed becomes too small to be achievable by Eq. (7.93), which is bounded from below, while maintaining a large enough threshold correction for the bottom Yukawa (which is roughly proportional to $(\mu/M_s) \tan \beta$, see below). The issue is more severe at smaller $\tan \beta$ because of a smaller $\lambda \simeq \frac{1}{8}(g^2 + g'^2) c_{2\beta}^2$ at any given $\Lambda = M_s$. These conclusions are perhaps more familiar when phrased as “raising the SM Higgs mass to 125 GeV requires large one-loop corrections from heavy stops.” Here, instead of computing m_h from the full theory (the MSSM), we have taken an EFT approach, where m_h is computed from the SM to fix λ_{eff} , and the problem becomes matching λ_{eff} with λ with the right amount of threshold correction. See also [251] for related discussion.

7.3.2 Bottom Yukawa threshold correction

Next, let us take a closer look at the SUSY threshold correction for the bottom Yukawa coupling, which is a key ingredient for b - τ Yukawa unification. Our discussion in what follows in this subsection is consistent with previous studies [252–255].

In Figure 7.4 we plot

$$\delta_b \equiv \frac{y_b - y_b^{\text{eff}}}{y_b^{\text{eff}}}, \quad (7.94)$$

evaluated at the matching scale $\Lambda = M_s$, for our sample of b - τ Yukawa unification solutions. We see that they correspond to a specific range of δ_b for any given M_s , with numbers ranging from 10% to 60%.

At this point, it is worth emphasizing again that threshold corrections, which originate from renormalizable operators generated in EFT matching, do not decouple as the EFT cutoff is raised. In fact, as we see from Figures 7.3 and 7.4, for both the Higgs quartic and the bottom Yukawa, a higher M_s calls for a larger SUSY threshold correction, in order to compensate for a longer period of running in the SMEFT.

Returning to the issue of bottom Yukawa threshold correction, we note that for the most part of parameter space, δ_b is dominated by contribution from the squark-gluino loop,

$$\delta_b \simeq \delta_b^{(\tilde{q}\tilde{d}\tilde{g})} \simeq \frac{g_3^2}{16\pi^2} \frac{y_b}{y_b^{\text{eff}}} \cdot 2 C_2^{SU(3)} \left(\frac{\mu}{M_s} \tan \beta \right) \left(M_3 M_s \tilde{\mathcal{I}}_{\tilde{f}\tilde{g}}^{21} \right), \quad (7.95)$$

see Eq. (7.62b). Since $\tilde{\mathcal{I}}_{\tilde{f}\tilde{g}}^{21}$ is negative-definite, a positive δ_b is only possible when $\mu M_3 < 0$, which explains our sign choice. We have checked explicitly that no solutions can be found when the sign of either μ or M_3 is reversed.

The factor $(M_3 M_s \tilde{\mathcal{I}}_{\tilde{f}\tilde{g}}^{21})$ in Eq. (7.95) only depends on the mass ratio. It is approximately $-\frac{M_3}{M_s}$ when $|M_3|/M_s \ll 1$, and $-\frac{M_s}{M_3} (\log \frac{M_3^2}{M_s^2} - 1)$ when $|M_3|/M_s \gg 1$, with a maximum absolute value of about 0.566 at $|M_3|/M_s \simeq 2.12$. Thus, for any given value of $(\mu/M_s) \tan \beta$ that is sufficiently large, we expect to have two solutions for $|M_3|/M_s$ – one on each side of 2.12 – which lead to the same desired δ_b (up to higher-order corrections from e.g. gluino loop contribution to g_3 threshold correction). This degeneracy is clearly visible in Figure 7.2, especially in the high M_s regime of the first three plots, where the range of μ/M_s , as determined by the Higgs quartic matching condition, is narrow due to the x_t -dependent terms in Eq. (7.93) becoming subdominant. For the $\tan \beta = 2$ plot, on the other hand, only a region near $|M_3|/M_s \simeq 2.12$ survives because of a much smaller $(\mu/M_s) \tan \beta$ (~ 100 as opposed to ~ 200 for the first three plots, as can be inferred from Figure 7.1).

In addition to Eq. (7.95), there is a subdominant contribution to δ_b from squark-Higgsino

loop, which is responsible for some finer details of the plots. From Eq. (7.61b) we have

$$\delta_b^{(\tilde{q}\tilde{u}\tilde{\chi})} = \frac{\lambda_t^2}{16\pi^2} \frac{y_b}{y_b^{\text{eff}}} \cdot x_t \left(\frac{\mu}{M_s} \tan \beta \right) \left(M_s^2 \tilde{\mathcal{I}}_{f\tilde{\chi}}^{21} \right). \quad (7.96)$$

Comparing Eqs. (7.95) and (7.96), we see that $\delta_b^{(\tilde{q}\tilde{d}\tilde{g})}$ and $\delta_b^{(\tilde{q}\tilde{u}\tilde{\chi})}$ have opposite (same) signs when $x_t > 0$ ($x_t < 0$). Thus, higher values of μ/M_s are required for the $x_t > 0$ branches (green and red) to compensate for the cancellation between $\delta_b^{(\tilde{q}\tilde{d}\tilde{g})}$ and $\delta_b^{(\tilde{q}\tilde{u}\tilde{\chi})}$, as we can see from Figure 7.1.

7.4 Higgs couplings in TeV-scale SUSY

In the previous section, we have seen that b - τ Yukawa unification alone does not point to a unique scale for the masses of superpartners in the MSSM. However, if in addition, we would like the MSSM to provide a dark matter candidate in the form of the lightest neutralino, that would be further motivation for TeV-scale SUSY. For example, two classic thermal dark matter benchmarks are a ~ 1 TeV Higgsino LSP and a ~ 2.7 TeV wino LSP [256]. A wider range of masses is allowed if the LSP is a mixture of bino, wino and Higgsino states or if the sfermions do not decouple [257, 258], or if non-thermal production mechanisms are at work. Therefore, we will broadly consider the 1-10 TeV regime for superpartner masses, while remaining agnostic about the detailed cosmology of dark matter. We will focus on precision Higgs coupling measurements as an indirect probe of TeV-scale SUSY, and discuss how they can be complementary to direct superpartner searches at the LHC.

To compute Higgs coupling modifications, we follow the same numerical procedure as outlined at the beginning of Section 7.3. Now the 20 SMEFT parameters in Eq. (7.89) should be evolved down to $Q = m_h = 125.09$ GeV, in order to compute $\delta\kappa_b$ and $\delta\kappa_\tau$ according to Eq. (7.11). As discussed in Section 7.2.4, we shall focus on the scenario where M_Φ , the mass of the second Higgs doublet, is relatively low. To be precise, let us first fix $M_\Phi = 1$ TeV, and allow M_s and $|M_3|$ to vary between 1 TeV and 10 TeV. The Higgsino mass μ is determined by requiring exact b - τ Yukawa unification, i.e. $\lambda_b(Q_{\text{GUT}}) = \lambda_\tau(Q_{\text{GUT}})$. Solutions may exist on multiple branches of x_t , in which case we find all of them.

Our results are displayed in Figures 7.5, 7.6 and 7.7, for $\tan \beta = 50, 20, 8$, respectively. For each of the four x_t branches, we show variation of $\delta\kappa_b$ in the region of the $|M_3|$ - M_s plane where a solution exists. Also shown in the plots are contours of μ/M_s (black) and x_t (red dashed) which, as we will see shortly, are the key quantities that determine the value of $\delta\kappa_b$. In addition, light green contours represent $\mu = 1$ TeV, corresponding to the Higgsino thermal dark matter benchmark. Plots of $\delta\kappa_\tau$ (not shown here) exhibit the same patterns

of variation in the $|M_3|$ - M_s plane, but with smaller overall sizes than $\delta\kappa_b$ as a consequence of $C_{\tau\phi} \propto y_\tau/y_\tau^{\text{eff}} < y_b/y_b^{\text{eff}}$.

From these plots, it is first of all interesting to see how large one-loop effects can be. Indeed, as we have fixed $M_\Phi = 1$ TeV, a tree-level calculation would yield constant $C_{b\phi}$ (and hence $\delta\kappa_b$) for given $\tan\beta$; see Table 7.4. The pattern of $\delta\kappa_b$ observed in the figures is a result of interplay between tree- and one-loop-level contributions. For the most part of parameter space (with large $\tan\beta$ and low M_Φ), we can approximate

$$\begin{aligned} C_{b\phi} &\simeq C_{b\phi}^{\text{tree}} + \frac{y_b}{M_\Phi^2} \tan\beta \left(c_{\Phi\phi^3}^{(\tilde{f}\tilde{f}\tilde{f})} + c_{\Phi\phi^3}^{(\tilde{f}\tilde{f}\tilde{f}\tilde{f})} \right) \\ &\simeq -\frac{y_b}{2M_\Phi^2} \left[(g^2 + g'^2) - \frac{\tan\beta}{16\pi^2} y_t^4 \left(\frac{\mu}{M_s} \right) x_t (x_t^2 - 6) \right]. \end{aligned} \quad (7.97)$$

at the matching scale $\Lambda = M_s$. We see that tree-level matching always gives a negative contribution to $C_{b\phi}$, and thus a positive contribution to $\delta\kappa_b$. On the other hand, the one-loop piece can have either sign, depending on the value of x_t . On two of the four branches, $x_t < -\sqrt{6}$ and $0 < x_t < \sqrt{6}$, its contribution to $C_{b\phi}$ is negative, resulting in an enhanced (positive) $\delta\kappa_b$. More specifically, for $x_t < -\sqrt{6}$ (upper-left plot in each figure), $\delta\kappa_b$ is seen to increase monotonically with both μ/M_s and $|x_t|$, while for $0 < x_t < \sqrt{6}$ (lower-left plot in each figure), $\delta\kappa_b$ also increases with μ/M_s , but now exhibits a plateau around $x_t = \sqrt{2}$ where $-x_t(x_t^2 - 6)$ is maximized, in agreement with Eq. (7.97). In contrast, the other two branches feature a negative one-loop contribution to $\delta\kappa_b$: for $-\sqrt{6} < x_t < 0$ (upper-right plot in each figure), we have a suppressed but still positive $\delta\kappa_b$, with the suppression being more severe in regions with large μ/M_s and x_t close to $-\sqrt{2}$; for $x_t > \sqrt{6}$ (lower-right plot in each figure), one-loop correction becomes large enough in part of the parameter space so as to make $\delta\kappa_b$ negative, and, as expected, $\delta\kappa_b$ tends to be smaller (more negative) in regions with larger μ/M_s and x_t .

Precision Higgs measurements – $h \rightarrow b\bar{b}$ in particular – are most sensitive to regions of parameter space with the largest $|\delta\kappa_b|$, which in most cases (all $x_t < -\sqrt{6}$ and $0 < x_t < \sqrt{6}$ plots, and $x_t > \sqrt{6}$ plots for $\tan\beta = 50, 20$ as well) are those with heavy sfermions and light to intermediate-mass gluino, once b - τ Yukawa unification is stipulated. In these regions, as we have discussed in Section 7.3, b - τ Yukawa unification calls for relatively large μ/M_s to boost SUSY threshold correction for y_b (recall $\delta_b \propto |M_3|/M_s$ for $|M_3|/M_s \lesssim 2.12$, and larger δ_b is needed for heavier sfermions), which in turn enhances one-loop contributions to $\delta\kappa_b$ according to Eq. (7.97); meanwhile, there is a visible suppression of $|\delta\kappa_b|$ for the largest μ/M_s (hence smallest $|M_3|/M_s$) due to $|x_t|$ approaching $\sqrt{6}$ in order to match the Higgs quartic (see Eq. (7.93)).

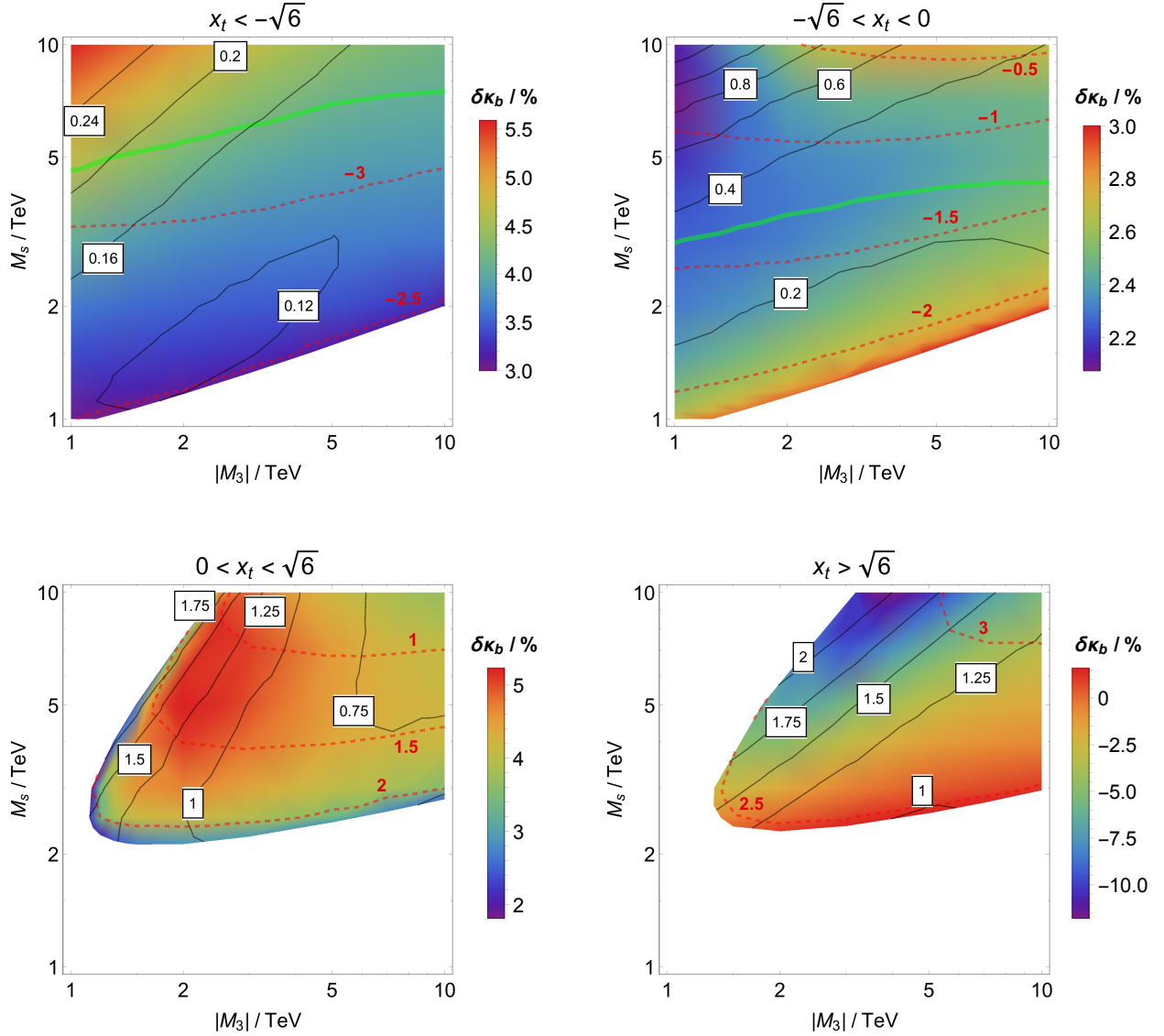


Figure 7.5: (From [132]) Variation of $\delta\kappa_b$ in the region of the $|M_3|$ - M_s plane where a solution exists for exact b - τ Yukawa unification, on each x_t branch, with $M_\Phi = 1$ TeV and $\tan\beta = 50$. Superimposed are contours of μ/M_s (black) and x_t (red dashed). Light green curves in the $x_t < 0$ plots correspond to the 1 TeV Higgsino dark matter benchmark. Direct superpartner searches probe lower mass regions of the parameter space (with $|M_3| \lesssim 2$ TeV potentially already excluded at the LHC depending on decay kinematics), while precision Higgs measurements can be more sensitive to higher mass regions where $\delta\kappa_b$ is enhanced by one-loop corrections.

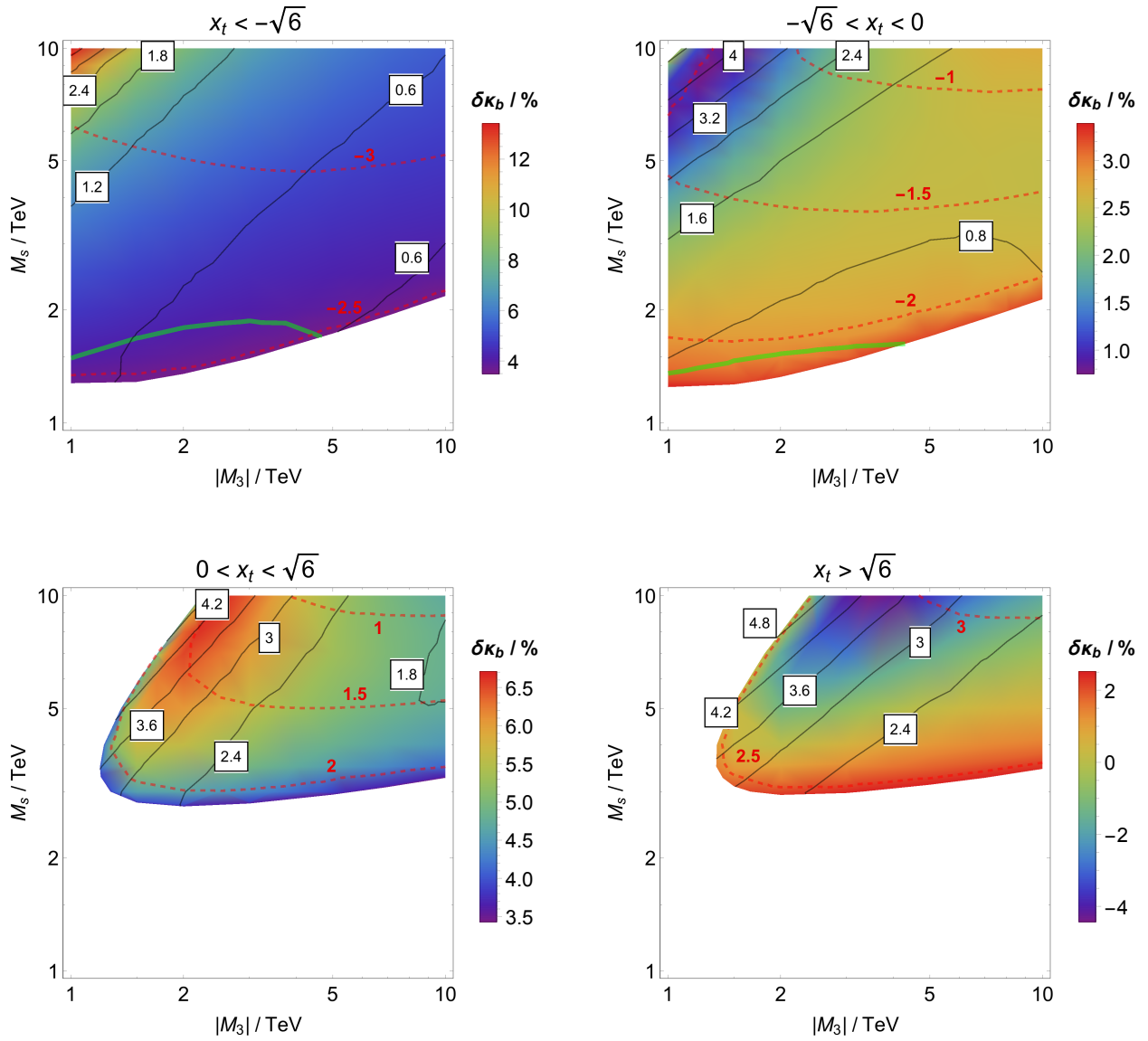


Figure 7.6: (From [132]) Same as Figure 7.5, now with $\tan\beta = 20$.

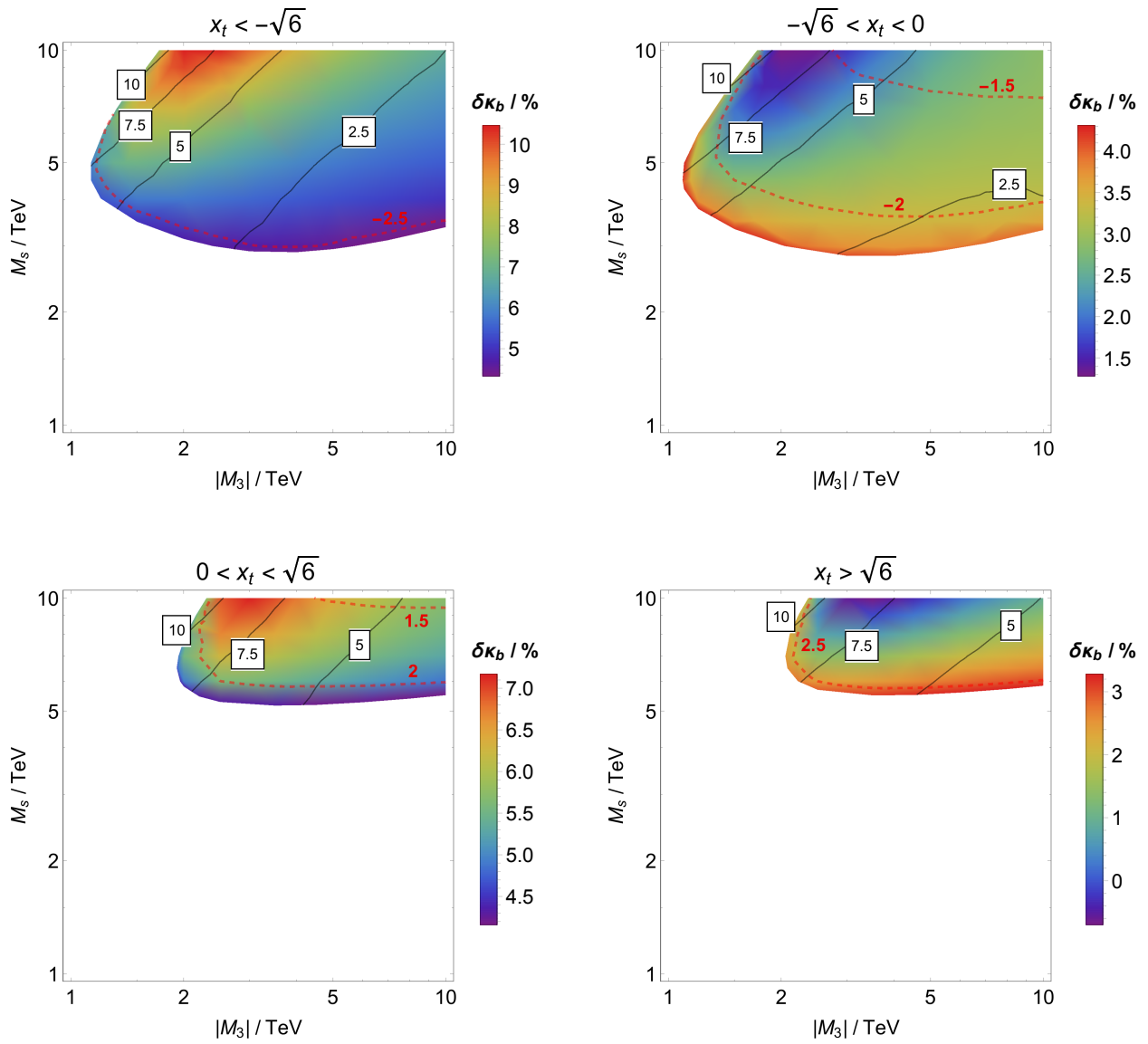


Figure 7.7: (From [132]) Same as Figure 7.5, now with $\tan\beta = 8$.

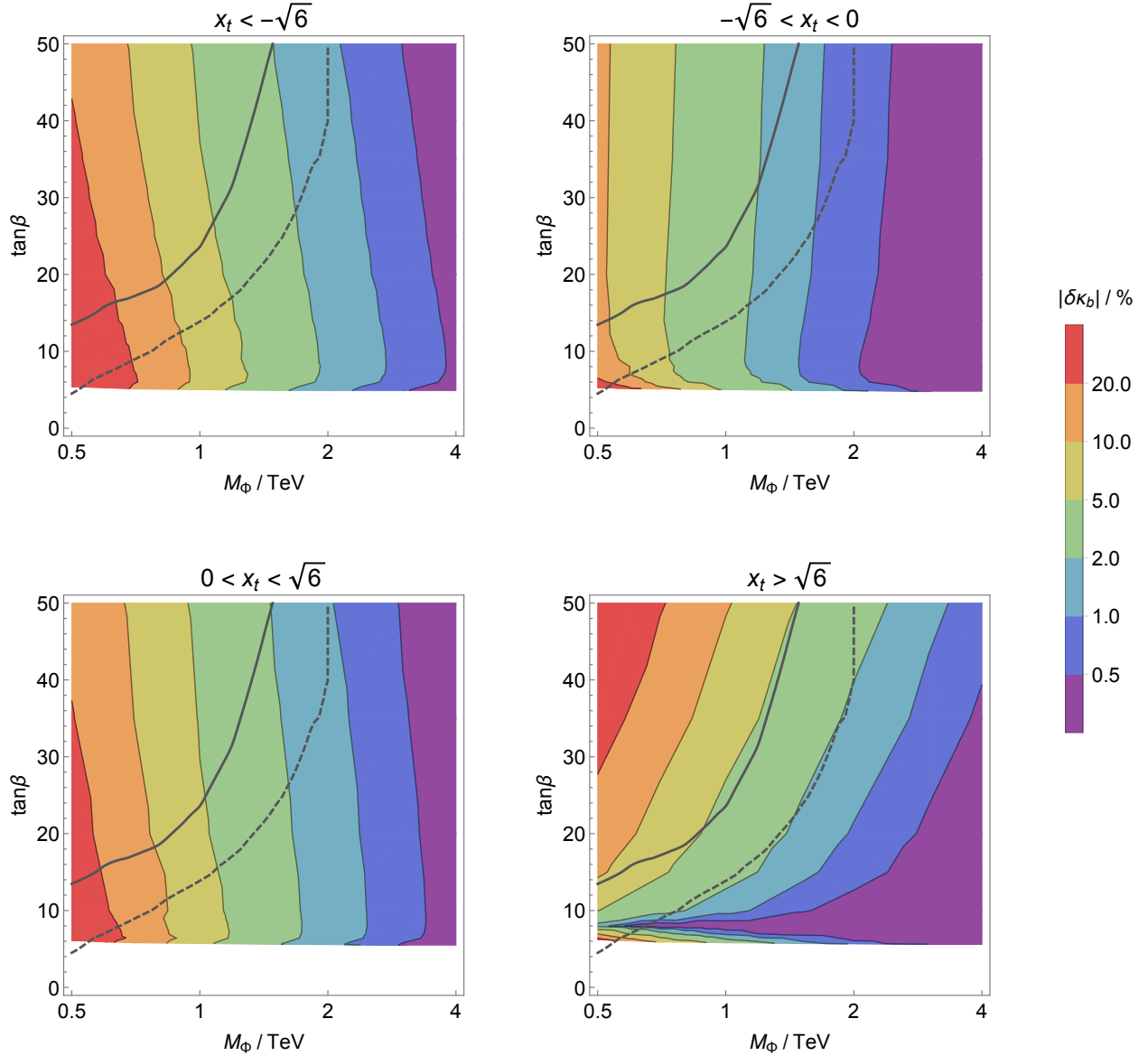


Figure 7.8: (From [132]) Contours of $|\delta\kappa_b|$ in the M_Φ - $\tan\beta$ plane, for our benchmark scenario $|M_3| = 5$ TeV, $M_s = 10$ TeV, which will evade gluino and stop searches at the LHC. The Higgsino mass is determined by exact b - τ Yukawa unification, for which solutions exist for $\tan\beta \gtrsim 5$. Dark solid and dashed curves represent current exclusion limit (95% CL) and projected high-luminosity reach (95% CL with 3 ab^{-1} at 14 TeV) from heavy Higgs searches in the di-tau channel at the LHC, reported assuming the $m_h^{\text{mod}+}$ benchmark scenario. Future Higgs factories, with 0.5-1% projected precision for the $hb\bar{b}$ coupling, will be able to probe much of the parameter space displayed.

In comparison, direct searches can most easily access the region of parameter space with light squarks and gluino. Our results show a nice complementarity between direct superpartner searches and precision Higgs measurements, as they probe the SUSY parameter space from different directions.

To further demonstrate this complementarity, let us consider a scenario where the gluino and sfermions are beyond direct LHC reach, even after the high luminosity phase [259, 260]. We choose $|M_3| = 5 \text{ TeV}$, $M_s = 10 \text{ TeV}$ as a benchmark, and allow M_Φ and $\tan\beta$ to vary. The Higgsino mass μ is still determined by exact b - τ Yukawa unification, and is not a free parameter in this analysis.

Figure 7.8 shows plots of $|\delta\kappa_b|$ in the M_Φ - $\tan\beta$ plane for this benchmark scenario, on all four x_t branches. The LHC will be able to probe $|\delta\kappa_b| \sim 10\%$ [261, 262], corresponding to part of the sub-TeV regime for M_Φ (red and orange regions). Meanwhile, direct heavy Higgs searches can put stronger constraints in the high $\tan\beta$ regime. For illustration, we show in Figure 7.8 current exclusion limit from the ATLAS search in the di-tau channel [263] (the CMS limit [264] is slightly weaker) and projected high luminosity LHC reach (up to $M_\Phi = 2 \text{ TeV}$) in the same channel from the CMS analysis [265] (dark solid and dashed curves, respectively), both of which are reported assuming the “ $m_h^{\text{mod+}}$ benchmark scenario” (see [266]).

On the other hand, a 0.5-1% level determination of the $hb\bar{b}$ coupling, as envisioned at possible future Higgs factories (ILC, CLIC, CEPC and FCC-ee — see e.g. [267–269] for recent studies), would extend the sensitivity to M_Φ potentially up to $\sim(2\text{-}4) \text{ TeV}$, even for lower $\tan\beta$, and beyond direct and indirect LHC reach. The existence of well-motivated scenarios, like trans-TeV SUSY with b - τ Yukawa unification studied here, which escape LHC search but nevertheless can manifest themselves as modified Higgs couplings, highlights the opportunity of BSM discoveries through precision Higgs measurements.

To close this section, we finally comment on the availability of a 1 TeV Higgsino thermal dark matter candidate. From the figures we see that $\mu = 1 \text{ TeV}$ (light green curves) can only be achieved on the $x_t < 0$ branches for $\tan\beta \gtrsim 20$.⁶ The $x_t > 0$ branches cannot support such a small Higgsino mass because of cancellation between the squark-gluino and squark-Higgsino loops contributing to δ_b , as discussed below Eq. (7.96). Meanwhile, when $\tan\beta$ is reduced, a larger μ/M_s is generally needed to obtain sufficient threshold corrections for both λ and y_b . The disappearance of the $\mu = 1 \text{ TeV}$ curve is further accelerated by a shrinking parameter space where matching of the Higgs quartic is simultaneously possible.

⁶The quantitative discrepancy between our conclusion and that of [233] is due to differences in the matching calculation for the Higgs quartic. Our results are in good agreement with the more recent calculation in [49].

7.5 Conclusions

As traditional naturalness and weak-scale new physics are under siege, it is worth considering more attentively trans-TeV regimes. Here, effective field theory becomes the tool of choice to accurately connect a vast range of BSM ideas to low-energy observation. In this chapter, we have focused on the specific case of the MSSM, and performed a matching calculation onto the SMEFT. In particular, we computed the full set of renormalizable operators of the SMEFT by integrating out heavy superpartners from the path integral up to one-loop level, which allowed us to extract SUSY threshold corrections with ease.

Our calculation highlights the simplicity of recently-developed functional matching and covariant diagrams techniques. In fact, we were able to reproduce one-loop SUSY threshold corrections for all SM parameters from just 30 covariant diagrams (shown in Tables 7.5 and 7.6), each of which is straightforward to compute. Essentially, we have taken a more economic route than traditional Feynman diagram calculations, where just the information needed for deriving the low-energy limit of the theory has been extracted from the path integral. In the long run, it is hoped that these novel EFT techniques will aid the program of (automated) precision calculation in trans-TeV supersymmetry, and other BSM scenarios as well.

Taking unification as a key motivation for SUSY, we investigated implications of b - τ Yukawa unification on the MSSM parameter space, while remaining agnostic about further details of the grand unified theory. The EFT approach we have taken allowed us to take advantage of existing precision calculations within the SM, to ensure consistency with low-energy observations, in particular $m_h = 125$ GeV. We found solutions that realize b - τ Yukawa unification for SUSY scales from TeV up to 10^{10} GeV, with suitable choices of superpartner mass ratios and $\tan\beta$ (see Figures 7.1 and 7.2). In this analysis, a key role is played by SUSY threshold corrections to the Higgs quartic and bottom Yukawa couplings, which, when forced to have the correct (finite) sizes (see Figures 7.3 and 7.4), dramatically constrain the predicted SUSY parameter space.

The lower edge of this broad trans-TeV window is further motivated by the possibility of having a dark matter candidate. For superpartners in the (1-10) TeV regime, we showed that one-loop matching contributions can drastically modify tree-level predictions for the $hb\bar{b}$ (and also $h\tau^+\tau^-$) coupling, rendering some regions of the MSSM parameter space with heavier squarks more accessible to precision Higgs measurements (see Figures 7.5, 7.6 and 7.7).

It is interesting to see that, even for superpartner masses out of LHC reach, precision Higgs measurements can offer a powerful indirect probe of TeV-scale SUSY. For example, in a benchmark scenario with a 5 TeV gluino and 10 TeV degenerate sfermions that realizes

b - τ Yukawa unification, we showed that a 0.5-1% level determination of the $hb\bar{b}$ coupling will be able to probe the heavy Higgs mass up to $\sim(2-4)$ TeV for a wide range of $\tan\beta$ (see Figure 7.8). This constitutes an unambiguous example of a motivated BSM scenario that may only reveal itself through precision Higgs measurements of the future.

Chapter 8

Summary and Outlook

We are living in an exciting time for particle physics research. Steady experimental progress, at the LHC in particular, is met with continual theoretical developments. The full establishment of the Standard Model (SM), including the Higgs boson as the last building block, together with lack of new physics discoveries so far, has consolidated our view of elementary particle interactions as described by layers of effective field theories (EFTs). Precision tests of the SM in all sectors and critical examination of the EFT framework have become more important than ever.

In this context, we have studied in this dissertation various aspects of precision analyses and EFT. In particular, we have covered topics in precision tests of the electroweak and Higgs sectors of the SM, and discussed how EFT techniques can shed light on both bottom-up and top-down studies of new physics.

Continued exploration of the high energy frontier – the LHC at present, and possibly next-generation colliders in the future – will put the SM to more stringent tests. The tremendous experimental effort needed must be supported by improved understanding on the theory side to give meaning to our data. We have reassessed the current status of state-of-the-art precision electroweak calculations in Chapter 2, and pointed out new challenges in precision Higgs calculations in Chapter 3. Especially, given the plethora of well-motivated new physics scenarios that may show up in future precision Higgs measurements only at the percent level, it is an urgent issue to understand and reduce theory uncertainties, especially from our inadequate knowledge of the bottom and charm quark masses, so that they do not become a limiting factor in our hunt for new physics.

Bottom-up EFT approaches have been widely used recently, in an effort to interpret experimental measurements of SM processes, and extract broad features of new physics consistent with data. In this process, various consistency issues arise, especially when one attempts to embed historically influential simplified parameterizations of new physics effects

into a more general EFT framework. We have critically examined the issues associated with oblique parameters and triple gauge couplings in Chapters 4 and 5, respectively, and argued for the necessity to go beyond these historical parameterizations to learn more general lessons about new physics within the bottom-up EFT approach. Ongoing and future experimental programs promise to deliver more and more data, which will likely reshape our conventional view of the SMEFT parameter space. Our analysis frameworks should be updated in time to serve the need of extracting most useful information from future data.

Meanwhile, top-down EFT approaches are also receiving more interest, as hypothesized new particles are excluded up to higher masses. In this case, EFT provides the appropriate framework to perform precision calculations of lower energy observables from a higher energy theory of new physics. We have developed a diagrammatic framework for systematic functional matching calculations in Chapter 6, and applied it in a top-down EFT study of trans-TeV supersymmetry in Chapter 7. As new model-building ideas continue to emerge, it will be a fruitful exercise to study them in such top-down EFT approaches, in order to form more accurate pictures of their low energy behaviors to guide experimental searches. At the same time, we hope progress will continue to be made on functional matching and related ideas, which will further expand our theoretical toolbox beyond conventional Feynman diagram-based techniques, and perhaps also teach us new knowledge about quantum field theory.

It is not an exaggeration to say that the EFT mindset has played a major role in shaping our modern view of fundamental physics. It has guided us all the way through the establishment of the Standard Model, and we are now hoping it will help us reach the next deeper level of particle interactions. It is not certain how much further the EFT paradigm can take us in our quest of Nature, or whether and when a paradigm change would be needed to move forward. We should always keep our mind open to new ideas. However, there is no denying that EFT research will continue to be fruitful in teaching us about the SM and new physics, and quantum field theory as well. We should try our best to understand the subtleties and limitations of EFT approaches, while making progress in both theory and experiment toward uncovering a deeper structure of Nature.

Appendix A

Master Integrals in One-Loop Matching

In this appendix, we discuss calculations of the master integrals encountered in one-loop matching calculations of Chapters 6 and 7. Recall from Eq. (6.67) that the master integrals $\mathcal{I}[q^{2n_c}]_{ij\dots 0}^{n_i n_j \dots n_L}$ are defined by

$$\int \frac{d^d q}{(2\pi)^d} \frac{q^{\mu_1} \dots q^{\mu_{2n_c}}}{(q^2 - M_i^2)^{n_i} (q^2 - M_j^2)^{n_j} \dots (q^2)^{n_L}} \equiv g^{\mu_1 \dots \mu_{2n_c}} \mathcal{I}[q^{2n_c}]_{ij\dots 0}^{n_i n_j \dots n_L}, \quad (\text{A.1})$$

where $g^{\mu_1 \dots \mu_{2n_c}}$ is the completely symmetric tensor, e.g. $g^{\mu\nu\rho\sigma} = g^{\mu\nu}g^{\rho\sigma} + g^{\mu\rho}g^{\nu\sigma} + g^{\mu\sigma}g^{\nu\rho}$. We have also defined the rescaled version,

$$\tilde{\mathcal{I}}[q^{2n_c}]_{ij\dots 0}^{n_i n_j \dots n_L} \equiv \mathcal{I}[q^{2n_c}]_{ij\dots 0}^{n_i n_j \dots n_L} / \frac{i}{16\pi^2}. \quad (\text{A.2})$$

These master integrals can in general be evaluated via the following decomposition formula,

$$\begin{aligned} \tilde{\mathcal{I}}[q^{2n_c}]_{ij\dots 0}^{n_i n_j \dots n_L} &= \sum_{p_i=0}^{n_i-1} \left[\frac{1}{p_i!} \left(\frac{\partial}{\partial M_i^2} \right)^{p_i} \frac{1}{(M_i^2)^{n_L} \prod_{a \neq i} (\Delta_{ia}^2)^{n_a}} \right] \mathcal{I}[q^{2n_c}]_i^{n_i - p_i} \\ &+ \sum_{p_j=0}^{n_j-1} \left[\frac{1}{p_j!} \left(\frac{\partial}{\partial M_j^2} \right)^{p_j} \frac{1}{(M_j^2)^{n_L} \prod_{a \neq j} (\Delta_{ja}^2)^{n_a}} \right] \mathcal{I}[q^{2n_c}]_j^{n_j - p_j} + \dots \end{aligned} \quad (\text{A.3})$$

where $\Delta_{ij}^2 \equiv M_i^2 - M_j^2$. To derive Eq. (A.3), we first recall the definition,

$$\int \frac{d^d q}{(2\pi)^d} \frac{q^{\mu_1} \dots q^{\mu_{2n_c}}}{(q^2 - M_i^2)^{n_i} (q^2 - M_j^2)^{n_j} \dots (q^2)^{n_L}} \equiv g^{\mu_1 \dots \mu_{2n_c}} \mathcal{I}[q^{2n_c}]_{ij\dots 0}^{n_i n_j \dots n_L}, \quad (\text{A.4})$$

where $g^{\mu_1 \dots \mu_{2n_c}}$ is the completely symmetric tensor, e.g. $g^{\mu\nu\rho\sigma} = g^{\mu\nu}g^{\rho\sigma} + g^{\mu\rho}g^{\nu\sigma} + g^{\mu\sigma}g^{\nu\rho}$. It is easy to see that

$$\mathcal{I}[q^{2n_c}]_{ij\dots 0}^{n_i n_j \dots n_L} = \frac{1}{\Delta_{ij}^2} (\mathcal{I}[q^{2n_c}]_{ij\dots 0}^{n_i, n_j-1, \dots, n_L} - \mathcal{I}[q^{2n_c}]_{ij\dots 0}^{n_i-1, n_j, \dots, n_L}), \quad (\text{A.5})$$

$$\mathcal{I}[q^{2n_c}]_{ij\dots 0}^{n_i n_j \dots n_L} = \frac{1}{M_i^2} (\mathcal{I}[q^{2n_c}]_{ij\dots 0}^{n_i n_j, \dots, n_L-1} - \mathcal{I}[q^{2n_c}]_{ij\dots 0}^{n_i-1, n_j, \dots, n_L}), \quad (\text{A.6})$$

$$\frac{\partial}{\partial M_i^2} \mathcal{I}[q^{2n_c}]_{ij\dots 0}^{n_i n_j \dots n_L} = n_i \mathcal{I}[q^{2n_c}]_{ij\dots 0}^{n_i+1, n_j, \dots, n_L}, \quad (\text{A.7})$$

Note that in principle, we can just start from $\mathcal{I}[q^{2n_c}]_{ij\dots 0}^{n_i n_j \dots n_L}$ and use Eqs. (A.5) and (A.6) repeatedly to reduce the number of propagators, until arriving at a sum of heavy-only degenerate master integrals of the form $\mathcal{I}[q^{2n_c}]_i^{n_i}$ (recall $\mathcal{I}[q^{2n_c}]_0^{n_L} = 0$), which cannot be further reduced. However, the same result can be obtained via a more systematic and often easier path, starting from applying Eq. (A.7),

$$\mathcal{I}[q^{2n_c}]_{ij\dots 0}^{n_i n_j \dots n_L} = \frac{1}{(n_i - 1)!} \left(\frac{\partial}{\partial M_i^2} \right)^{n_i-1} \frac{1}{(n_j - 1)!} \left(\frac{\partial}{\partial M_j^2} \right)^{n_j-1} \dots \mathcal{I}[q^{2n_c}]_{ij\dots 0}^{11 \dots n_L}. \quad (\text{A.8})$$

The master integrals $\mathcal{I}[q^{2n_c}]_{ij\dots 0}^{11 \dots n_L}$, where each heavy propagator appears only once, are much easier to reduce via Eqs. (A.5) and (A.6) compared to the original master integral. In fact, we can show that

$$\begin{aligned} \mathcal{I}[q^{2n_c}]_{ij\dots 0}^{11 \dots n_L} &= \frac{1}{\Delta_{ij}^2 \Delta_{ik}^2 \Delta_{il}^2 \dots} \mathcal{I}[q^{2n_c}]_{i0}^{1n_L} + \frac{1}{\Delta_{ji}^2 \Delta_{jk}^2 \Delta_{jl}^2 \dots} \mathcal{I}[q^{2n_c}]_{j0}^{1n_L} + \dots \\ &= \frac{1}{(M_i^2)^{n_L} \Delta_{ij}^2 \Delta_{ik}^2 \Delta_{il}^2 \dots} \mathcal{I}[q^{2n_c}]_i^1 + \frac{1}{(M_j^2)^{n_L} \Delta_{ji}^2 \Delta_{jk}^2 \Delta_{jl}^2 \dots} \mathcal{I}[q^{2n_c}]_j^1 + \dots \\ &= \frac{1}{(M_i^2)^{n_L} \prod_{a \neq i} \Delta_{ia}^2} \mathcal{I}[q^{2n_c}]_i^1 + \frac{1}{(M_j^2)^{n_L} \prod_{a \neq j} \Delta_{ja}^2} \mathcal{I}[q^{2n_c}]_j^1 + \dots \end{aligned} \quad (\text{A.9})$$

Plugging Eq. (A.9) into Eq. (A.8) and taking derivatives according to Eq. (A.7), we obtain

$$\begin{aligned} \mathcal{I}[q^{2n_c}]_{ij\dots 0}^{n_i n_j \dots n_L} &= \frac{1}{(n_i - 1)!} \left(\frac{\partial}{\partial M_i^2} \right)^{n_i-1} \frac{1}{(M_i^2)^{n_L} (\Delta_{ij}^2)^{n_j} (\Delta_{ik}^2)^{n_k} (\Delta_{il}^2)^{n_l} \dots} \mathcal{I}[q^{2n_c}]_i^1 \\ &\quad + \frac{1}{(n_j - 1)!} \left(\frac{\partial}{\partial M_j^2} \right)^{n_j-1} \frac{1}{(M_j^2)^{n_L} (\Delta_{ji}^2)^{n_i} (\Delta_{jk}^2)^{n_k} (\Delta_{jl}^2)^{n_l} \dots} \mathcal{I}[q^{2n_c}]_j^1 \\ &\quad + \dots, \end{aligned} \quad (\text{A.10})$$

which can be easily seen to lead to Eq. (A.3).

Eq. (A.3) allows us to decompose an arbitrary master integral $\mathcal{I}[q^{2n_c}]_{ij\dots 0}^{n_i n_j \dots n_L}$ into a sum

of *degenerate* master integrals of the form $\mathcal{I}[q^{2n_c}]_i^{n_i}$. For example,

$$\mathcal{I}[q^2]_{ij0}^{211} = \frac{1}{M_i^2 \Delta_{ij}^2} \mathcal{I}[q^2]_i^2 + \frac{\partial}{\partial M_i^2} \left(\frac{1}{M_i^2 \Delta_{ij}^2} \right) \mathcal{I}[q^2]_i^1 + \frac{1}{M_j^2 (\Delta_{ji}^2)^2} \mathcal{I}[q^2]_j^1. \quad (\text{A.11})$$

The degenerate master integrals $\mathcal{I}[q^{2n_c}]_i^{n_i}$ cannot be decomposed further in this way, but can be worked out explicitly and tabulated; see Table 7 of [60]. Here, we note that if $n_i \geq 2$ and $n_c \geq 1$, $\mathcal{I}[q^{2n_c}]_i^{n_i}$ can in fact be further reduced using

$$\mathcal{I}[q^{2n_c}]_i^{n_i} = \frac{1}{2(n_i - 1)} \mathcal{I}[q^{2(n_c-1)}]_i^{n_i-1}, \quad (\text{A.12})$$

which follows from the explicit expression

$$\mathcal{I}[q^{2n_c}]_i^{n_i} = \frac{i}{16\pi^2} (-M_i^2)^{2+n_c-n_i} \frac{1}{2^{n_c}(n_i-1)!} \frac{\Gamma(\frac{\epsilon}{2} - 2 - n_c + n_i)}{\Gamma(\frac{\epsilon}{2})} \left(\frac{2}{\bar{\epsilon}} - \log \frac{M_i^2}{\mu^2} \right), \quad (\text{A.13})$$

where $\frac{2}{\bar{\epsilon}} \equiv \frac{2}{\epsilon} - \gamma + \log 4\pi$ with $\epsilon = 4 - d$, and Q is the renormalization scale. For example, Eq. (A.11) can be further reduced to

$$\mathcal{I}[q^2]_{ij0}^{211} = \frac{1}{2M_i^2 \Delta_{ij}^2} \mathcal{I}_i^1 + \frac{\partial}{\partial M_i^2} \left(\frac{1}{M_i^2 \Delta_{ij}^2} \right) \mathcal{I}[q^2]_i^1 + \frac{1}{M_j^2 (\Delta_{ji}^2)^2} \mathcal{I}[q^2]_j^1. \quad (\text{A.14})$$

We therefore only list irreducible master integrals here. For $n_i = \{1, 2, 3, 4, 5, 6\}$,

$$\tilde{\mathcal{I}}_i^{n_i} = \left\{ M_i^2 (1 - \log M_i^2), -\log M_i^2, -\frac{1}{2M_i^2}, \frac{1}{6M_i^4}, -\frac{1}{12M_i^6}, \frac{1}{20M_i^8} \right\}, \quad (\text{A.15})$$

while for $n_c = \{1, 2, 3\}$,

$$\tilde{\mathcal{I}}[q^{2n_c}]_i^1 = \left\{ \frac{M_i^4}{4} \left(\frac{3}{2} - \log M_i^2 \right), \frac{M_i^6}{24} \left(\frac{11}{6} - \log M_i^2 \right), \frac{M_i^8}{192} \left(\frac{25}{12} - \log M_i^2 \right) \right\}, \quad (\text{A.16})$$

where we have dropped the $\frac{1}{\bar{\epsilon}}$ poles (as in $\overline{\text{MS}}$ and $\overline{\text{DR}}$ schemes), and abbreviated $\log \frac{M_i^2}{Q^2}$ to $\log M_i^2$. In cases where $\mathcal{O}(\epsilon)$ terms are produced from e.g. gamma matrix algebra, the $\frac{1}{\bar{\epsilon}}$ pieces in the master integrals that have been subtracted off can be recovered by simply replacing $-\log M_i^2 \rightarrow \frac{2}{\bar{\epsilon}} - \log M_i^2$.

Using the formulas above, we can compute explicit expressions for the master integrals appearing in our one-loop matching results in Chapters 6 and 7. As a convenient reference, we list some frequently used master integrals in the following,

$$\tilde{\mathcal{I}}_i^1 = M_i^2 (1 - \log M_i^2), \quad \tilde{\mathcal{I}}_i^2 = -\log M_i^2, \quad (\text{A.17})$$

$$\tilde{\mathcal{I}}_i^3 = -\frac{1}{2M_i^2}, \quad \tilde{\mathcal{I}}_i^4 = \frac{1}{6M_i^4}, \quad \tilde{\mathcal{I}}_{i0}^{11} = 1 - \log M_i^2, \quad (\text{A.18})$$

$$\tilde{\mathcal{I}}[q^2]_i^3 = -\frac{1}{4} \log M_i^2, \quad \tilde{\mathcal{I}}[q^2]_i^4 = -\frac{1}{12M_i^2}, \quad \tilde{\mathcal{I}}[q^2]_{i0}^{21} = \frac{1}{8} - \frac{1}{4} \log M_i^2, \quad (\text{A.19})$$

$$\tilde{\mathcal{I}}_{ij}^{11} = 1 - \frac{1}{\Delta_{ij}^2} (M_i^2 \log M_i^2 - M_j^2 \log M_j^2), \quad (\text{A.20})$$

$$\tilde{\mathcal{I}}_{ij}^{21} = -\frac{1}{\Delta_{ij}^2} - \frac{M_j^2}{(\Delta_{ij}^2)^2} \log \frac{M_j^2}{M_i^2}, \quad (\text{A.21})$$

$$\tilde{\mathcal{I}}_{ij}^{22} = -\frac{2}{(\Delta_{ij}^2)^2} - \frac{M_i^2 + M_j^2}{(\Delta_{ij}^2)^3} \log \frac{M_j^2}{M_i^2}, \quad (\text{A.22})$$

$$\tilde{\mathcal{I}}_{ij}^{31} = \frac{M_i^2 + M_j^2}{2M_i^2 (\Delta_{ij}^2)^2} + \frac{M_j^2}{(\Delta_{ij}^2)^3} \log \frac{M_j^2}{M_i^2}, \quad (\text{A.23})$$

$$\tilde{\mathcal{I}}[q^2]_{ij}^{21} = \frac{M_i^2 - 3M_j^2}{8\Delta_{ij}^2} - \frac{1}{4(\Delta_{ij}^2)^2} \left[M_i^2 (M_i^2 - 2M_j^2) \log M_i^2 + M_j^4 \log M_j^2 \right], \quad (\text{A.24})$$

$$\tilde{\mathcal{I}}[q^2]_{ij}^{22} = -\frac{M_i^2 + M_j^2}{4(\Delta_{ij}^2)^2} - \frac{M_i^2 M_j^2}{2(\Delta_{ij}^2)^3} \log \frac{M_j^2}{M_i^2}, \quad (\text{A.25})$$

$$\tilde{\mathcal{I}}[q^2]_{ij}^{31} = -\frac{M_i^2 - 3M_j^2}{8(\Delta_{ij}^2)^2} + \frac{M_j^4}{4(\Delta_{ij}^2)^3} \log \frac{M_j^2}{M_i^2}, \quad (\text{A.26})$$

$$\tilde{\mathcal{I}}_{ijk}^{111} = \frac{M_j^2}{\Delta_{ij}^2 \Delta_{jk}^2} \log \frac{M_j^2}{M_i^2} + \frac{M_k^2}{\Delta_{jk}^2 \Delta_{ki}^2} \log \frac{M_k^2}{M_i^2}, \quad (\text{A.27})$$

$$\tilde{\mathcal{I}}_{ijk}^{211} = -\frac{1}{\Delta_{ij}^2 \Delta_{ik}^2} - \frac{1}{\Delta_{jk}^2} \left[\frac{M_j^2}{(\Delta_{ij}^2)^2} \log \frac{M_j^2}{M_i^2} - \frac{M_k^2}{(\Delta_{ik}^2)^2} \log \frac{M_k^2}{M_i^2} \right], \quad (\text{A.28})$$

$$\tilde{\mathcal{I}}[q^2]_{ijk}^{211} = -\frac{M_i^2}{4\Delta_{ij}^2 \Delta_{ik}^2} - \frac{1}{4\Delta_{jk}^2} \left[\frac{M_j^4}{(\Delta_{ij}^2)^2} \log \frac{M_j^2}{M_i^2} - \frac{M_k^4}{(\Delta_{ik}^2)^2} \log \frac{M_k^2}{M_i^2} \right]. \quad (\text{A.29})$$

In the equations above, we have used the notation $\Delta_{ij}^2 \equiv M_i^2 - M_j^2$.

Finally, let us also present some formulas that can be used to decrease n_c , because they are often useful for simplifying loops involving fermions. When $n_c = 1$, we can contract both sides of Eq. (A.4) with $g_{\mu_1 \mu_2}$ to obtain

$$(4 - \epsilon) \mathcal{I}[q^2]_{ij\dots 0}^{n_i n_j \dots n_L} = \mathcal{I}_{ij\dots 0}^{n_i-1, n_j \dots n_L} + M_i^2 \mathcal{I}_{ij\dots 0}^{n_i n_j \dots n_L} \quad (\text{A.30})$$

$$(4 - \epsilon) \mathcal{I}[q^2]_{ij\dots 0}^{n_i n_j \dots n_L} = \mathcal{I}_{ij\dots 0}^{n_i n_j \dots, n_L-1} \quad (n_L \geq 1) \quad (\text{A.31})$$

Similarly, when $n_c = 2$, we can contract both sides of Eq. (A.4) with $g_{\mu_1 \mu_2} g_{\mu_3 \mu_4}$ to obtain

$$(24 - 10\epsilon) \mathcal{I}[q^4]_{ij\dots 0}^{n_i n_j \dots n_L} = \int \frac{d^d q}{(2\pi)^d} \frac{(q^2 - M_i^2)^2 + 2M_i^2 q^2 - M_i^4}{(q^2 - M_i^2)^{n_i} (q^2 - M_j^2)^{n_j} \dots (q^2)^{n_L}}$$

$$= \mathcal{I}_{ij\dots 0}^{n_i-2, n_j\dots n_L} + 2(4 - \epsilon)M_i^2 \mathcal{I}[q^2]_{ij\dots 0}^{n_i n_j\dots n_L} - M_i^4 \mathcal{I}_{ij\dots 0}^{n_i n_j\dots n_L} \quad (n_i \geq 2). \quad (\text{A.32})$$

Alternatively,

$$\begin{aligned} (24 - 10\epsilon) \mathcal{I}[q^4]_{ij\dots 0}^{n_i n_j\dots n_L} &= \int \frac{d^d q}{(2\pi)^d} \frac{(q^2 - M_i^2)(q^2 - M_j^2) + (M_i^2 + M_j^2)q^2 - M_i^2 M_j^2}{(q^2 - M_i^2)^{n_i} (q^2 - M_j^2)^{n_j} \dots (q^2)^{n_L}} \\ &= \mathcal{I}_{ij\dots 0}^{n_i-1, n_j-1, \dots, n_L} + (4 - \epsilon)(M_i^2 + M_j^2) \mathcal{I}[q^2]_{ij\dots 0}^{n_i n_j\dots n_L} - M_i^2 M_j^2 \mathcal{I}_{ij\dots 0}^{n_i n_j\dots n_L} \quad (n_i, n_j \geq 1). \end{aligned} \quad (\text{A.33})$$

These formulas have been used in our calculation in Chapter 7.

Appendix B

Explicit Expressions of Universal Coefficients

Here we give explicit expressions of the universal coefficients, namely coefficients of operator traces in the UOLEA master formula Eq. (6.68) rederived in Section 6.4.1 (see Table 6.5), in terms of heavy particle masses M_i , M_j , etc. In many cases, our expressions simplify those originally derived in [56]. We define $f_N = \frac{i}{16\pi^2} \tilde{f}_N$ as in [56], and list \tilde{f}_N in the following:

$$\tilde{f}_2^i = M_i^2 \left(1 - \log \frac{M_i^2}{\mu^2} \right), \quad (\text{B.1})$$

$$\tilde{f}_3^i = -\frac{1}{12} \log \frac{M_i^2}{\mu^2}, \quad (\text{B.2})$$

$$\tilde{f}_4^{ij} = \frac{1}{2} \left(1 - \frac{M_i^2 \log \frac{M_i^2}{\mu^2}}{\Delta_{ij}^2} - \frac{M_j^2 \log \frac{M_j^2}{\mu^2}}{\Delta_{ji}^2} \right), \quad (\text{B.3})$$

$$\tilde{f}_5^i = -\frac{1}{60M_i^2}, \quad (\text{B.4})$$

$$\tilde{f}_6^i = -\frac{1}{90M_i^2}, \quad (\text{B.5})$$

$$\tilde{f}_7^{ij} = -\frac{M_i^2 + M_j^2}{4(\Delta_{ij}^2)^2} + \frac{M_i^2 M_j^2 \log \frac{M_i^2}{M_j^2}}{2(\Delta_{ij}^2)^3}, \quad (\text{B.6})$$

$$\tilde{f}_8^{ijk} = -\frac{1}{3} \left(\frac{M_i^2 \log M_i^2}{\Delta_{ij}^2 \Delta_{ik}^2} + \frac{M_j^2 \log M_j^2}{\Delta_{ji}^2 \Delta_{jk}^2} + \frac{M_k^2 \log M_k^2}{\Delta_{ki}^2 \Delta_{kj}^2} \right), \quad (\text{B.7})$$

$$\tilde{f}_9^i = -\frac{1}{12M_i^2}, \quad (\text{B.8})$$

$$\tilde{f}_{10}^{ijkl} = -\frac{1}{4} \left(\frac{M_i^2 \log M_i^2}{\Delta_{ij}^2 \Delta_{ik}^2 \Delta_{il}^2} + \frac{M_j^2 \log M_j^2}{\Delta_{ji}^2 \Delta_{jk}^2 \Delta_{jl}^2} + \frac{M_k^2 \log M_k^2}{\Delta_{ki}^2 \Delta_{kj}^2 \Delta_{kl}^2} + \frac{M_l^2 \log M_l^2}{\Delta_{li}^2 \Delta_{lj}^2 \Delta_{lk}^2} \right), \quad (\text{B.9})$$

$$\begin{aligned} \tilde{f}_{11}^{ijk} = & \frac{M_i^2 M_j^2 + M_i^2 M_k^2 + M_j^2 M_k^2 - 3M_k^4}{2(\Delta_{ik}^2)^2 (\Delta_{jk}^2)^2} + \frac{M_i^2 M_k^2 \log M_i^2}{\Delta_{ij}^2 (\Delta_{ik}^2)^3} + \frac{M_j^2 M_k^2 \log M_j^2}{\Delta_{ji}^2 (\Delta_{jk}^2)^3} \\ & + \frac{[M_i^2 M_j^2 (M_i^2 + M_j^2 - 3M_k^2) + M_k^6] M_k^2 \log M_k^2}{(\Delta_{ki}^2)^3 (\Delta_{kj}^2)^3}, \end{aligned} \quad (\text{B.10})$$

$$\tilde{f}_{12}^{ij} = \frac{M_i^4 + 10M_i^2 M_j^2 + M_j^4}{12(\Delta_{ij}^2)^4} - \frac{M_i^2 M_j^2 (M_i^2 + M_j^2) \log \frac{M_i^2}{M_j^2}}{2(\Delta_{ij}^2)^5}, \quad (\text{B.11})$$

$$\tilde{f}_{13}^{ij} = \frac{2M_i^4 + 5M_i^2 M_j^2 - M_j^4}{12M_i^2 (\Delta_{ij}^2)^3} - \frac{M_i^2 M_j^2 \log \frac{M_i^2}{M_j^2}}{2(\Delta_{ij}^2)^4} \quad (\text{B.12})$$

$$\tilde{f}_{14}^{ij} = -\frac{M_i^4 + 10M_i^2 M_j^2 + M_j^4}{6(\Delta_{ij}^2)^4} + \frac{M_i^2 M_j^2 (M_i^2 + M_j^2) \log \frac{M_i^2}{M_j^2}}{(\Delta_{ij}^2)^5}, \quad (\text{B.13})$$

$$\tilde{f}_{15}^{ij} = \frac{2M_i^4 + 11M_i^2 M_j^2 - 7M_j^4}{18(\Delta_{ij}^2)^4} - \frac{M_j^2 (3M_i^4 - M_j^4) \log \frac{M_i^2}{M_j^2}}{6(\Delta_{ij}^2)^5} \quad (\text{B.14})$$

$$\begin{aligned} \tilde{f}_{16}^{ijklm} = & -\frac{1}{5} \left(\frac{M_i^2 \log M_i^2}{\Delta_{ij}^2 \Delta_{ik}^2 \Delta_{il}^2 \Delta_{im}^2} + \frac{M_j^2 \log M_j^2}{\Delta_{ji}^2 \Delta_{jk}^2 \Delta_{jl}^2 \Delta_{jm}^2} + \frac{M_k^2 \log M_k^2}{\Delta_{ki}^2 \Delta_{kj}^2 \Delta_{kl}^2 \Delta_{km}^2} \right. \\ & \left. + \frac{M_l^2 \log M_l^2}{\Delta_{li}^2 \Delta_{lj}^2 \Delta_{lk}^2 \Delta_{lm}^2} + \frac{M_m^2 \log M_m^2}{\Delta_{mi}^2 \Delta_{mj}^2 \Delta_{mk}^2 \Delta_{ml}^2} \right), \end{aligned} \quad (\text{B.15})$$

$$\begin{aligned} \tilde{f}_{17}^{ijkl} = & -\frac{M_i^2 M_j^2 M_k^2 + (M_i^2 M_j^2 + M_i^2 M_k^2 + M_j^2 M_k^2) M_l^2 - 3(M_i^2 + M_j^2 + M_k^2) M_l^4 + 5M_l^6}{2(\Delta_{il}^2)^2 (\Delta_{jl}^2)^2 (\Delta_{kl}^2)^2} \\ & + \frac{M_i^2 M_l^2 \log M_i^2}{\Delta_{ij}^2 \Delta_{ik}^2 (\Delta_{il}^2)^3} + \frac{M_j^2 M_l^2 \log M_j^2}{\Delta_{ji}^2 \Delta_{jk}^2 (\Delta_{jl}^2)^3} + \frac{M_k^2 M_l^2 \log M_k^2}{\Delta_{ki}^2 \Delta_{kj}^2 (\Delta_{kl}^2)^3} + \frac{M_l^2 \log M_l^2}{(\Delta_{li}^2)^3 (\Delta_{lj}^2)^3 (\Delta_{lk}^2)^3} \\ & \left[(M_i^2 M_j^2 M_k^2 + M_l^6) (M_i^2 M_j^2 + M_i^2 M_k^2 + M_j^2 M_k^2 - 3(M_i^2 + M_j^2 + M_k^2) M_l^2 + 6M_l^4) \right. \\ & \left. + M_l^6 (M_i^4 + M_j^4 + M_k^4 - 3M_l^4) \right], \end{aligned} \quad (\text{B.16})$$

$$\begin{aligned} \tilde{f}_{18}^{ijkl} = & \frac{1}{4(\Delta_{ik}^2)^2 (\Delta_{jk}^2)^2 (\Delta_{il}^2)^2 (\Delta_{jl}^2)^2} \\ & [-M_i^2 M_j^2 M_k^2 (M_i^4 + M_j^4 + M_k^4) - M_i^2 M_j^2 M_l^2 (M_i^4 + M_j^4 + M_l^4) \\ & - M_i^2 M_k^2 M_l^2 (M_i^4 + M_k^4 + M_l^4) - M_j^2 M_k^2 M_l^2 (M_j^4 + M_k^4 + M_l^4) \\ & + 2M_i^2 M_j^2 (M_i^2 + M_j^2) (M_k^4 + M_l^4) + 2M_k^2 M_l^2 (M_i^4 + M_j^4) (M_k^2 + M_l^2) \\ & + 3M_i^4 M_j^4 (M_i^2 + M_j^2) + 3M_k^4 M_l^4 (M_k^2 + M_l^2) \\ & + 3M_i^2 M_j^2 M_k^2 M_l^2 (M_i^2 + M_j^2 + M_k^2 + M_l^2) \\ & - 7M_i^4 M_j^4 (M_k^2 + M_l^2) - 7M_k^4 M_l^4 (M_i^2 + M_j^2)] \\ & + \frac{[M_i^6 + M_k^2 M_l^2 (M_k^2 + M_l^2 - 3M_i^2)] M_i^2 \log M_i^2}{2\Delta_{ij}^2 (\Delta_{ik}^2)^3 (\Delta_{il}^2)^3} \end{aligned}$$

$$\begin{aligned}
& + \frac{[M_j^6 + M_k^2 M_l^2 (M_k^2 + M_l^2 - 3M_j^2)] M_j^2 \log M_j^2}{2\Delta_{ji}^2 (\Delta_{jk}^2)^3 (\Delta_{jl}^2)^3} \\
& + \frac{[M_k^6 + M_i^2 M_j^2 (M_i^2 + M_j^2 - 3M_k^2)] M_k^2 \log M_k^2}{2\Delta_{kl}^2 (\Delta_{ki}^2)^3 (\Delta_{kj}^2)^3} \\
& + \frac{[M_l^6 + M_i^2 M_j^2 (M_i^2 + M_j^2 - 3M_l^2)] M_l^2 \log M_l^2}{2\Delta_{lk}^2 (\Delta_{li}^2)^3 (\Delta_{lj}^2)^3},
\end{aligned} \tag{B.17}$$

$$\begin{aligned}
\tilde{f}_{19}^{ijklmn} = & -\frac{1}{6} \left(\frac{M_i^2 \log M_i^2}{\Delta_{ij}^2 \Delta_{ik}^2 \Delta_{il}^2 \Delta_{im}^2 \Delta_{in}^2} + \frac{M_j^2 \log M_j^2}{\Delta_{ji}^2 \Delta_{jk}^2 \Delta_{jl}^2 \Delta_{jm}^2 \Delta_{jn}^2} + \frac{M_k^2 \log M_k^2}{\Delta_{ki}^2 \Delta_{kj}^2 \Delta_{kl}^2 \Delta_{km}^2 \Delta_{kn}^2} \right. \\
& \left. + \frac{M_l^2 \log M_l^2}{\Delta_{li}^2 \Delta_{lj}^2 \Delta_{lk}^2 \Delta_{lm}^2 \Delta_{ln}^2} + \frac{M_m^2 \log M_m^2}{\Delta_{mi}^2 \Delta_{mj}^2 \Delta_{mk}^2 \Delta_{ml}^2 \Delta_{mn}^2} + \frac{M_n^2 \log M_n^2}{\Delta_{ni}^2 \Delta_{nj}^2 \Delta_{nk}^2 \Delta_{nl}^2 \Delta_{nm}^2} \right).
\end{aligned} \tag{B.18}$$

As in the previous appendix, we have used the shorthand notation $\Delta_{ij}^2 \equiv M_i^2 - M_j^2$, etc.

Appendix C

The MSSM \mathbf{U} Matrix

In this appendix, we present detailed expressions for the entries of the MSSM \mathbf{U} matrix needed in our one-loop matching calculation in Chapter 7. They are obtained from the MSSM Lagrangian by the background field method explained in Chapter 6. Keeping in mind that the \mathbf{U} matrix is to be used at one-loop level, we do not distinguish between β and β' , and write β throughout. Also, tree-level SUSY relations between couplings can be used regardless of scheme choice, e.g. gaugino-sfermion-fermion couplings are identified with gauge couplings (which is true beyond tree level in $\overline{\text{DR}}$ but not $\overline{\text{MS}}$ scheme).

In what follows, the heavy Higgs field Φ is understood as Φ_c obtained in Section 7.2.2. The other heavy fields do not appear because they are set to zero by the classical equations of motion. We carefully keep all color and weak indices explicit for clarity, using i (A) and α (I) for $SU(3)_c$ and $SU(2)_L$ fundamental (adjoint) indices on the conjugate fields to appear on the left side of the \mathbf{U} matrix, and j , B , β , J for those on the fields on the right side. We will not explicitly show the entries involving leptons, because they can always be obtained from those involving quarks by the obvious substitutions $q \rightarrow l$, $d \rightarrow e$, $\lambda_u \rightarrow 0$, $\lambda_d \rightarrow \lambda_e$, $g_3 \rightarrow 0$.

C.1 R -parity-even block

Higgs-Higgs entries. From the MSSM Higgs potential, we obtain

$$\begin{aligned}
 U_{\Phi\Phi} = & \frac{1}{4}(g^2 + g'^2) \begin{pmatrix} -\delta_\alpha^\beta c_{2\beta}^2 |\phi|^2 + s_{2\beta}^2 \phi_\alpha \phi^{*\beta} & s_{2\beta}^2 \phi_\alpha \phi_\beta \\ s_{2\beta}^2 \phi^{*\alpha} \phi^{*\beta} & -\delta_\beta^\alpha c_{2\beta}^2 |\phi|^2 + s_{2\beta}^2 \phi^{*\alpha} \phi_\beta \end{pmatrix} \\
 & + \frac{1}{2}g^2 \begin{pmatrix} \delta_\alpha^\beta |\phi|^2 - \phi_\alpha \phi^{*\beta} & 0 \\ 0 & \delta_\beta^\alpha |\phi|^2 - \phi^{*\alpha} \phi_\beta \end{pmatrix}
 \end{aligned}$$

$$\begin{aligned}
& +\frac{1}{8}(g^2 + g'^2) s_{4\beta} \begin{pmatrix} \delta_\alpha^\beta & 0 \\ 0 & \delta_\beta^\alpha \end{pmatrix} (\phi^* \Phi + \Phi^* \phi) \\
& +\frac{1}{8}(g^2 + g'^2) s_{4\beta} \begin{pmatrix} \phi_\alpha \Phi^{*\beta} + \Phi_\alpha \phi^{*\beta} & \phi_\alpha \Phi_\beta + \Phi_\alpha \phi_\beta \\ \phi^{*\alpha} \Phi^{*\beta} + \Phi^{*\alpha} \phi^{*\beta} & \phi^{*\alpha} \Phi_\beta + \Phi^{*\alpha} \phi_\beta \end{pmatrix} \\
& +\frac{1}{4}(g^2 + g'^2) c_{2\beta}^2 \begin{pmatrix} \delta_\alpha^\beta |\Phi|^2 + \Phi_\alpha \Phi^{*\beta} & \Phi_\alpha \Phi_\beta \\ \Phi^{*\alpha} \Phi^{*\beta} & \delta_\beta^\alpha |\Phi|^2 + \Phi^{*\alpha} \Phi_\beta \end{pmatrix}, \tag{C.1}
\end{aligned}$$

$$\begin{aligned}
U_{\Phi\phi} = & -\frac{1}{8}(g^2 + g'^2) s_{4\beta} \begin{pmatrix} \delta_\alpha^\beta |\phi|^2 + \phi_\alpha \phi^{*\beta} & \phi_\alpha \phi_\beta \\ \phi^{*\alpha} \phi^{*\beta} & \delta_\beta^\alpha |\phi|^2 + \phi^{*\alpha} \phi_\beta \end{pmatrix} \\
& +\frac{1}{4}(g^2 + g'^2) s_{2\beta}^2 \begin{pmatrix} \delta_\alpha^\beta (\phi^* \Phi + \Phi^* \phi) + \phi_\alpha \Phi^{*\beta} & \phi_\alpha \Phi_\beta \\ \phi^{*\alpha} \Phi^{*\beta} & \delta_\beta^\alpha (\phi^* \Phi + \Phi^* \phi) + \phi^{*\alpha} \Phi_\beta \end{pmatrix} \\
& -\frac{1}{4}(g^2 + g'^2) c_{2\beta}^2 \begin{pmatrix} \Phi_\alpha \phi^{*\beta} & \Phi_\alpha \phi_\beta \\ \Phi^{*\alpha} \phi^{*\beta} & \Phi^{*\alpha} \phi_\beta \end{pmatrix} \\
& +\frac{1}{2}g^2 \begin{pmatrix} -\delta_\alpha^\beta (\phi^* \Phi) + \Phi_\alpha \phi^{*\beta} & -\phi_\alpha \Phi_\beta + \Phi_\alpha \phi_\beta \\ -\phi^{*\alpha} \Phi^{*\beta} + \Phi^{*\alpha} \phi^{*\beta} & -\delta_\beta^\alpha (\Phi^* \phi) + \Phi^{*\alpha} \phi_\beta \end{pmatrix} \\
& +\frac{1}{8}(g^2 + g'^2) s_{4\beta} \begin{pmatrix} \delta_\alpha^\beta |\Phi|^2 + \Phi_\alpha \Phi^{*\beta} & \Phi_\alpha \Phi_\beta \\ \Phi^{*\alpha} \Phi^{*\beta} & \delta_\beta^\alpha |\Phi|^2 + \Phi^{*\alpha} \Phi_\beta \end{pmatrix}. \tag{C.2}
\end{aligned}$$

The other two entries $U_{\phi\phi}$ and $U_{\phi\Phi}$ can be obtained from $U_{\Phi\Phi}$ and $U_{\Phi\phi}$ by simply exchanging $\Phi \leftrightarrow \phi$, $s_\beta \leftrightarrow c_\beta$.

Higgs-fermion entries. From the MSSM Yukawa interactions, we obtain

$$U_{\Phi q} = \begin{pmatrix} -s_\beta \delta_\alpha^\beta \bar{\psi}_d^j \boldsymbol{\lambda}_d & -c_\beta \epsilon_{\alpha\beta} \bar{\psi}_{uj}^c \boldsymbol{\lambda}_u^* \\ -c_\beta \epsilon^{\alpha\beta} \bar{\psi}_u^j \boldsymbol{\lambda}_u & -s_\beta \delta_\beta^\alpha \bar{\psi}_{dj}^c \boldsymbol{\lambda}_d^* \end{pmatrix}, \tag{C.3a}$$

$$U_{q\Phi} = \begin{pmatrix} -s_\beta \delta_\alpha^\beta \boldsymbol{\lambda}_d^\dagger \psi_{di} & -c_\beta \epsilon_{\beta\alpha} \boldsymbol{\lambda}_u^\dagger \psi_{ui} \\ -c_\beta \epsilon^{\beta\alpha} \boldsymbol{\lambda}_u^T \psi_u^{ci} & -s_\beta \delta_\beta^\alpha \boldsymbol{\lambda}_d^T \psi_d^{ci} \end{pmatrix}, \tag{C.3b}$$

$$U_{\Phi u} = c_\beta \begin{pmatrix} (\bar{\psi}_q \epsilon)_\alpha^j \lambda_u^\dagger & 0 \\ 0 & (\bar{\psi}_q^c \epsilon)_j^\alpha \lambda_u^T \end{pmatrix}, \quad U_{u\Phi} = c_\beta \begin{pmatrix} \lambda_u (\psi_q \epsilon)_i^\beta & 0 \\ 0 & \lambda_u^* (\psi_q^c \epsilon)_\beta^i \end{pmatrix}, \quad (\text{C.4})$$

$$U_{\Phi d} = -s_\beta \begin{pmatrix} 0 & \bar{\psi}_{qj\alpha}^c \lambda_d^T \\ \bar{\psi}_q^{j\alpha} \lambda_d^\dagger & 0 \end{pmatrix}, \quad U_{d\Phi} = -s_\beta \begin{pmatrix} 0 & \lambda_d \psi_{qi\beta} \\ \lambda_d^* \psi_q^{ci\beta} & 0 \end{pmatrix}. \quad (\text{C.5})$$

The ϕf , $f\phi$ entries (not needed in our calculation) can be obtained from the equations above by simple substitutions $\lambda_u c_\beta \rightarrow \lambda_u s_\beta$, $\lambda_d s_\beta \rightarrow -\lambda_d c_\beta$.

Fermion-fermion entries. The Yukawa interactions also give rise to

$$U_{qu} = s_\beta \begin{pmatrix} \delta_i^j \lambda_u^\dagger (\epsilon \phi^*)_\alpha & 0 \\ 0 & \delta_j^i \lambda_u^T (\epsilon \phi)^\alpha \end{pmatrix} + c_\beta \begin{pmatrix} \delta_i^j \lambda_u^\dagger (\epsilon \Phi^*)_\alpha & 0 \\ 0 & \delta_j^i \lambda_u^T (\epsilon \Phi)^\alpha \end{pmatrix}, \quad (\text{C.6a})$$

$$U_{uq} = s_\beta \begin{pmatrix} \delta_i^j \lambda_u (\epsilon \phi)^\beta & 0 \\ 0 & \delta_j^i \lambda_u^* (\epsilon \phi^*)_\beta \end{pmatrix} + c_\beta \begin{pmatrix} \delta_i^j \lambda_u (\epsilon \Phi)^\beta & 0 \\ 0 & \delta_j^i \lambda_u^* (\epsilon \Phi^*)_\beta \end{pmatrix}, \quad (\text{C.6b})$$

$$U_{qd} = c_\beta \begin{pmatrix} \delta_i^j \lambda_d^\dagger \phi_\alpha & 0 \\ 0 & \delta_j^i \lambda_d^T \phi^{*\alpha} \end{pmatrix} - s_\beta \begin{pmatrix} \delta_i^j \lambda_d^\dagger \Phi_\alpha & 0 \\ 0 & \delta_j^i \lambda_d^T \Phi^{*\alpha} \end{pmatrix}, \quad (\text{C.7a})$$

$$U_{dq} = c_\beta \begin{pmatrix} \delta_i^j \lambda_d \phi^{*\beta} & 0 \\ 0 & \delta_j^i \lambda_d^* \phi_\beta \end{pmatrix} - s_\beta \begin{pmatrix} \delta_i^j \lambda_d \Phi^{*\beta} & 0 \\ 0 & \delta_j^i \lambda_d^* \Phi_\beta \end{pmatrix}. \quad (\text{C.7b})$$

In addition, there are nonzero entries involving the SM gauge bosons, which are however not needed in our calculation.

C.2 R -parity-odd block

Sfermion-sfermion entries. From the sfermion-sfermion-Higgs interactions, we obtain

$$U_{\tilde{q}\tilde{u}} = (A_u s_\beta - \mu c_\beta) \begin{pmatrix} \delta_i^j \lambda_u^\dagger (\epsilon \phi^*)_\alpha & 0 \\ 0 & \delta_j^i \lambda_u^T (\epsilon \phi)^\alpha \end{pmatrix} + (A_u c_\beta + \mu s_\beta) \begin{pmatrix} \delta_i^j \lambda_u^\dagger (\epsilon \Phi^*)_\alpha & 0 \\ 0 & \delta_j^i \lambda_u^T (\epsilon \Phi)^\alpha \end{pmatrix}, \quad (\text{C.8a})$$

$$\begin{aligned}
U_{\tilde{u}\tilde{q}} = & (A_u s_\beta - \mu c_\beta) \begin{pmatrix} \delta_i^j \lambda_u (\epsilon\phi)^\beta & 0 \\ 0 & \delta_j^i \lambda_u^* (\epsilon\phi^*)_\beta \end{pmatrix} \\
& + (A_u c_\beta + \mu s_\beta) \begin{pmatrix} \delta_i^j \lambda_u (\epsilon\Phi)^\beta & 0 \\ 0 & \delta_j^i \lambda_u^* (\epsilon\Phi^*)_\beta \end{pmatrix}, \tag{C.8b}
\end{aligned}$$

$$U_{\tilde{q}\tilde{d}} = (A_d c_\beta - \mu s_\beta) \begin{pmatrix} \delta_i^j \lambda_d^\dagger \phi_\alpha & 0 \\ 0 & \delta_j^i \lambda_d^T \phi^{*\alpha} \end{pmatrix} - (A_d s_\beta + \mu c_\beta) \begin{pmatrix} \delta_i^j \lambda_d^\dagger \Phi_\alpha & 0 \\ 0 & \delta_j^i \lambda_d^T \Phi^{*\alpha} \end{pmatrix}, \tag{C.9a}$$

$$U_{\tilde{d}\tilde{q}} = (A_d c_\beta - \mu s_\beta) \begin{pmatrix} \delta_i^j \lambda_d \phi^{*\beta} & 0 \\ 0 & \delta_j^i \lambda_d^* \phi_\beta \end{pmatrix} - (A_d s_\beta + \mu c_\beta) \begin{pmatrix} \delta_i^j \lambda_d \Phi^{*\beta} & 0 \\ 0 & \delta_j^i \lambda_d^* \Phi_\beta \end{pmatrix}. \tag{C.9b}$$

Meanwhile, the scalar quartic interactions give rise to

$$U_{\tilde{q}\tilde{q}} = \begin{pmatrix} \delta_i^j \mathbf{U}_{\tilde{q}\alpha}^\beta & 0 \\ 0 & \delta_j^i \mathbf{U}_{\tilde{q}\beta}^T \alpha \end{pmatrix}, \quad U_{\tilde{u}\tilde{u}} = \begin{pmatrix} \delta_i^j \mathbf{U}_{\tilde{u}} & 0 \\ 0 & \delta_j^i \mathbf{U}_{\tilde{u}}^T \end{pmatrix}, \quad U_{\tilde{d}\tilde{d}} = \begin{pmatrix} \delta_i^j \mathbf{U}_{\tilde{d}} & 0 \\ 0 & \delta_j^i \mathbf{U}_{\tilde{d}}^T \end{pmatrix}, \tag{C.10}$$

where

$$\begin{aligned}
\mathbf{U}_{\tilde{q}\alpha}^\beta = & \lambda_u^\dagger \lambda_u \left[s_\beta^2 (\delta_\alpha^\beta |\phi|^2 - \phi_\alpha \phi^{*\beta}) \right. \\
& \left. + s_\beta c_\beta (\delta_\alpha^\beta (\phi^* \Phi + \Phi^* \phi) - \phi_\alpha \Phi^{*\beta} - \Phi_\alpha \phi^{*\beta}) + c_\beta^2 (\delta_\alpha^\beta |\Phi|^2 - \Phi_\alpha \Phi^{*\beta}) \right] \\
& + \lambda_d^\dagger \lambda_d \left[c_\beta^2 \phi_\alpha \phi^{*\beta} - s_\beta c_\beta (\phi_\alpha \Phi^{*\beta} + \Phi_\alpha \phi^{*\beta}) + s_\beta^2 \Phi_\alpha \Phi^{*\beta} \right] \\
& + g^2 \frac{1}{4} \sigma_\alpha^{I\beta} \left[(s_\beta^2 - c_\beta^2) (\phi^* \sigma^I \phi - \Phi^* \sigma^I \Phi) + 2s_\beta c_\beta (\phi^* \sigma^I \Phi + \Phi^* \sigma^I \phi) \right] \\
& + g'^2 Y_\phi Y_q \delta_\alpha^\beta \left[(s_\beta^2 - c_\beta^2) (|\phi|^2 - |\Phi|^2) + 2s_\beta c_\beta (\phi^* \Phi + \Phi^* \phi) \right] \tag{C.11}
\end{aligned}$$

$$\begin{aligned}
\mathbf{U}_{\tilde{u}} = & \lambda_u \lambda_u^\dagger \left[s_\beta^2 |\phi|^2 + s_\beta c_\beta (\phi^* \Phi + \Phi^* \phi) + c_\beta^2 |\Phi|^2 \right] \\
& - g'^2 Y_\phi Y_u \left[(s_\beta^2 - c_\beta^2) (|\phi|^2 - |\Phi|^2) + 2s_\beta c_\beta (\phi^* \Phi + \Phi^* \phi) \right], \tag{C.12}
\end{aligned}$$

$$\begin{aligned}
\mathbf{U}_{\tilde{d}} = & \lambda_d \lambda_d^\dagger \left[c_\beta^2 |\phi|^2 - s_\beta c_\beta (\phi^* \Phi + \Phi^* \phi) + s_\beta^2 |\Phi|^2 \right] \\
& - g'^2 Y_\phi Y_d \left[(s_\beta^2 - c_\beta^2) (|\phi|^2 - |\Phi|^2) + 2s_\beta c_\beta (\phi^* \Phi + \Phi^* \phi) \right]. \tag{C.13}
\end{aligned}$$

There are also off-diagonal entries between \tilde{u} and \tilde{d} ,

$$U_{\tilde{u}\tilde{d}} = \begin{pmatrix} \delta_i^j \lambda_u \lambda_d^\dagger (\phi \epsilon \Phi) & 0 \\ 0 & \delta_j^i (\lambda_d \lambda_u^\dagger)^T (\phi^* \epsilon \Phi^*) \end{pmatrix}, \quad (\text{C.14a})$$

$$U_{\tilde{d}\tilde{u}} = \begin{pmatrix} \delta_i^j \lambda_d \lambda_u^\dagger (\phi^* \epsilon \Phi^*) & 0 \\ 0 & \delta_j^i (\lambda_u \lambda_d^\dagger)^T (\phi \epsilon \Phi) \end{pmatrix}. \quad (\text{C.14b})$$

Sfermion-Higgsino entries. From the sfermion-fermion-Higgsino interactions, we obtain

$$U_{\tilde{q}\tilde{\chi}} = \begin{pmatrix} -\delta_\alpha^\beta \bar{\psi}_{di}^c \lambda_d^* & \epsilon_{\alpha\beta} \bar{\psi}_{ui}^c \lambda_u^* \\ \epsilon^{\alpha\beta} \bar{\psi}_u^i \lambda_u & -\delta_\beta^\alpha \bar{\psi}_d^i \lambda_d \end{pmatrix}, \quad U_{\tilde{\chi}\tilde{q}} = \begin{pmatrix} -\delta_\alpha^\beta \lambda_d^T \psi_d^{cj} & -\epsilon_{\alpha\beta} \lambda_u^\dagger \psi_{uj} \\ -\epsilon^{\alpha\beta} \lambda_u^T \psi_u^{cj} & -\delta_\beta^\alpha \lambda_d^\dagger \psi_{dj} \end{pmatrix} \quad (\text{C.15})$$

$$U_{\tilde{u}\tilde{\chi}} = \begin{pmatrix} (\bar{\psi}_q^c \epsilon)_i^\beta \lambda_u^T & 0 \\ 0 & (\bar{\psi}_q \epsilon)_\beta^i \lambda_u^\dagger \end{pmatrix}, \quad U_{\tilde{\chi}\tilde{u}} = \begin{pmatrix} \lambda_u^* (\psi_q^c \epsilon)_\alpha^j & 0 \\ 0 & \lambda_u (\psi_q \epsilon)_j^\alpha \end{pmatrix}, \quad (\text{C.16})$$

$$U_{\tilde{d}\tilde{\chi}} = \begin{pmatrix} 0 & -\bar{\psi}_{qi}^c \lambda_d^T \\ -\bar{\psi}_q^{i\beta} \lambda_d^\dagger & 0 \end{pmatrix}, \quad U_{\tilde{\chi}\tilde{d}} = \begin{pmatrix} 0 & -\lambda_d \psi_{qj\alpha} \\ -\lambda_d^* \psi_q^{cj\alpha} & 0 \end{pmatrix}. \quad (\text{C.17})$$

Sfermion-gaugino entries. From the sfermion-fermion-gaugino interactions, we obtain

$$U_{\tilde{q}\tilde{g}} = \sqrt{2} g_3 \begin{pmatrix} (T^B \bar{\psi}_q^c)_{i\alpha} \\ (\bar{\psi}_q T^B)_{i\alpha} \end{pmatrix}, \quad U_{\tilde{g}\tilde{q}} = \sqrt{2} g_3 \begin{pmatrix} (\psi_q^c T^A)^{j\beta} & (T^A \psi_q)_{j\beta} \end{pmatrix}, \quad (\text{C.18})$$

$$U_{\tilde{q}\tilde{W}} = \sqrt{2} g \frac{1}{2} \begin{pmatrix} (\sigma^J \bar{\psi}_q^c)_{i\alpha} \\ (\bar{\psi}_q \sigma^J)_{i\alpha} \end{pmatrix}, \quad U_{\tilde{W}\tilde{q}} = \sqrt{2} g \frac{1}{2} \begin{pmatrix} (\psi_q^c \sigma^I)^{j\beta} & (\sigma^I \psi_q)_{j\beta} \end{pmatrix}, \quad (\text{C.19})$$

$$U_{\tilde{q}\tilde{B}} = \sqrt{2} g' Y_q \begin{pmatrix} \bar{\psi}_{qi}^c \\ \bar{\psi}_q^{i\alpha} \end{pmatrix}, \quad U_{\tilde{B}\tilde{q}} = \sqrt{2} g' Y_q \begin{pmatrix} \psi_q^{cj\beta} & \psi_{qj\beta} \end{pmatrix}, \quad (\text{C.20})$$

$$U_{\tilde{u}\tilde{g}} = -\sqrt{2} g_3 \begin{pmatrix} (T^B \bar{\psi}_u^c)_i \\ (\bar{\psi}_u T^B)_i \end{pmatrix}, \quad U_{\tilde{g}\tilde{u}} = -\sqrt{2} g_3 \begin{pmatrix} (\psi_u^c T^A)^j & (T^A \psi_u)_j \end{pmatrix}, \quad (\text{C.21})$$

$$U_{\tilde{u}\tilde{B}} = -\sqrt{2} g' Y_u \begin{pmatrix} \bar{\psi}_{ui}^c \\ \bar{\psi}_u^i \end{pmatrix}, \quad U_{\tilde{B}\tilde{u}} = -\sqrt{2} g' Y_u \begin{pmatrix} \psi_u^{cj} & \psi_{uj} \end{pmatrix}, \quad (\text{C.22})$$

$$U_{\tilde{d}\tilde{V},\tilde{V}\tilde{d}} = U_{\tilde{u}\tilde{V},\tilde{V}\tilde{u}} \Big|_{u \rightarrow d}. \quad (\text{C.23})$$

Higgsino-gaugino entries. Finally, from the Higgs-Higgsino-gaugino interactions, we obtain

$$U_{\tilde{\chi}\tilde{V}} = U_{\tilde{\chi}\tilde{V}}^{(S)} + U_{\tilde{\chi}\tilde{V}}^{(P)} \gamma^5, \quad U_{\tilde{V}\tilde{\chi}} = U_{\tilde{V}\tilde{\chi}}^{(S)} + U_{\tilde{V}\tilde{\chi}}^{(P)} \gamma^5, \quad (\text{C.24})$$

with

$$U_{\tilde{\chi}\tilde{W}}^{(S)} = \frac{g}{\sqrt{2}} \frac{1}{2} (s_\beta + c_\beta) \begin{pmatrix} (\sigma^J \phi)_\alpha \\ (\phi^* \sigma^J)^\alpha \end{pmatrix} - \frac{g}{\sqrt{2}} \frac{1}{2} (s_\beta - c_\beta) \begin{pmatrix} (\sigma^J \Phi)_\alpha \\ (\Phi^* \sigma^J)^\alpha \end{pmatrix}, \quad (\text{C.25a})$$

$$U_{\tilde{W}\tilde{\chi}}^{(S)} = \frac{g}{\sqrt{2}} \frac{1}{2} (s_\beta + c_\beta) \begin{pmatrix} (\phi^* \sigma^I)^\beta & (\sigma^I \phi)_\beta \end{pmatrix} - \frac{g}{\sqrt{2}} \frac{1}{2} (s_\beta - c_\beta) \begin{pmatrix} (\Phi^* \sigma^I)^\beta & (\sigma^I \Phi)_\beta \end{pmatrix}, \quad (\text{C.25b})$$

$$U_{\tilde{\chi}\tilde{W}}^{(P)} = \frac{g}{\sqrt{2}} \frac{1}{2} (s_\beta - c_\beta) \begin{pmatrix} (\sigma^J \phi)_\alpha \\ -(\phi^* \sigma^J)^\alpha \end{pmatrix} + \frac{g}{\sqrt{2}} \frac{1}{2} (s_\beta + c_\beta) \begin{pmatrix} (\sigma^J \Phi)_\alpha \\ -(\Phi^* \sigma^J)^\alpha \end{pmatrix}, \quad (\text{C.25c})$$

$$U_{\tilde{W}\tilde{\chi}}^{(P)} = -\frac{g}{\sqrt{2}} \frac{1}{2} (s_\beta - c_\beta) \begin{pmatrix} (\phi^* \sigma^I)^\beta & -(\sigma^I \phi)_\beta \end{pmatrix} - \frac{g}{\sqrt{2}} \frac{1}{2} (s_\beta + c_\beta) \begin{pmatrix} (\Phi^* \sigma^I)^\beta & -(\sigma^I \Phi)_\beta \end{pmatrix}, \quad (\text{C.25d})$$

$$U_{\tilde{\chi}\tilde{B}}^{(S)} = \frac{g'}{\sqrt{2}} Y_\phi (s_\beta + c_\beta) \begin{pmatrix} \phi_\alpha \\ \phi^{*\alpha} \end{pmatrix} - \frac{g'}{\sqrt{2}} Y_\phi (s_\beta - c_\beta) \begin{pmatrix} \Phi_\alpha \\ \Phi^{*\alpha} \end{pmatrix}, \quad (\text{C.26a})$$

$$U_{\tilde{B}\tilde{\chi}}^{(S)} = \frac{g'}{\sqrt{2}} Y_\phi (s_\beta + c_\beta) \begin{pmatrix} \phi^{*\beta} & \phi_\beta \end{pmatrix} - \frac{g'}{\sqrt{2}} Y_\phi (s_\beta - c_\beta) \begin{pmatrix} \Phi^{*\beta} & \Phi_\beta \end{pmatrix}, \quad (\text{C.26b})$$

$$U_{\tilde{\chi}\tilde{B}}^{(P)} = \frac{g'}{\sqrt{2}} Y_\phi (s_\beta - c_\beta) \begin{pmatrix} \phi_\alpha \\ -\phi^{*\alpha} \end{pmatrix} + \frac{g'}{\sqrt{2}} Y_\phi (s_\beta + c_\beta) \begin{pmatrix} \Phi_\alpha \\ -\Phi^{*\alpha} \end{pmatrix}, \quad (\text{C.26c})$$

$$U_{\tilde{B}\tilde{\chi}}^{(P)} = -\frac{g'}{\sqrt{2}} Y_\phi (s_\beta - c_\beta) \begin{pmatrix} \phi^{*\beta} & -\phi_\beta \end{pmatrix} - \frac{g'}{\sqrt{2}} Y_\phi (s_\beta + c_\beta) \begin{pmatrix} \Phi^{*\beta} & -\Phi_\beta \end{pmatrix}. \quad (\text{C.26d})$$

Appendix D

Cross-Check of SUSY Threshold Corrections Against Feynman Diagram Calculation

Our results for one-loop SUSY threshold corrections presented in Section 7.2.3, which are obtained from computing just 30 covariant diagrams, have been cross-checked against conventional Feynman diagram calculations reported in [231], with full agreement found. In this final appendix, we explain how this comparison is made.

The general procedure is as follows. From [231], we obtain analytical relations between the full theory parameters g_3, g, g', y_f, m^2 and λ (related to MSSM Lagrangian parameters via Eq. (7.40)) and the standard set of SM input observables (denoted with hats) $\hat{\alpha}_s(m_Z), \hat{m}_Z, \hat{G}_F, \hat{\alpha}_{\text{em}}, \hat{m}_f$ and \hat{m}_h , computed via Feynman diagrams up to one-loop accuracy (we consistently drop higher loop order corrections, some of which are also reported in [231]). The same relations, with BSM contributions removed, define the corresponding effective parameters $g_3^{\text{eff}}, g^{\text{eff}}, g'^{\text{eff}}, y_f^{\text{eff}}, m_{\text{eff}}^2$ and λ_{eff} in the SMEFT, up to power-suppressed corrections from $d \geq 4$ operators. One-loop threshold corrections are then obtained by comparing the two, which should agree with what we have found via the more elegant covariant diagrams approach. Note that the tadpole-free scheme for Higgs vevs is adopted in [231], so their results should be compared to ours when $\mathcal{L}_{\text{SMEFT}}$ is written in terms of β (as opposed to β'), i.e. when the one-loop-generated piece $c_{\Phi\phi}(\Phi_c^*\phi + \phi^*\Phi_c)$ has been absorbed into $\mathcal{L}_{\text{SMEFT}}^{\text{tree}}$.

Let us start with the strong coupling g_3 , which is simply extracted from $\hat{\alpha}_s(m_Z)$ via

$$g_3^2 = \frac{4\pi \hat{\alpha}_s(m_Z)}{1 - \Delta\alpha_s}. \quad (\text{D.1})$$

Therefore,

$$g_3^{\text{eff}} = g_3 \left[1 - \frac{1}{2} (\Delta\alpha_s)_{\mathcal{O}(1)}^{\text{SUSY}} \right], \quad (\text{D.2})$$

where, according to [231],

$$\begin{aligned} (\Delta\alpha_s)^{\text{SUSY}} &= -\frac{g_3^2}{16\pi^2} \left(\frac{1}{6} \sum_{f=u,d} \sum_{i=1}^2 \log m_{f_i}^2 + 2 \log M_3^2 \right) \\ &= \frac{g_3^2}{16\pi^2} \left[\frac{1}{6} (2\tilde{\mathcal{I}}_{\tilde{q}}^2 + \mathcal{I}_{\tilde{u}}^1 + \mathcal{I}_{\tilde{d}}^2) + 2\mathcal{I}_{\tilde{g}}^2 + \mathcal{O}\left(\frac{v^2}{\Lambda^2}\right) \right], \end{aligned} \quad (\text{D.3})$$

with summation over three generations implicit. The $\frac{v^2}{\Lambda^2}$ power-suppressed terms come from electroweak symmetry breaking contributions to squark masses, and are not relevant here. For simplicity, throughout this appendix, we denote non-power-suppressed terms as $\mathcal{O}(1)$ (as in Eq. (D.2)) although they are formally $\mathcal{O}(\frac{1}{16\pi^2})$ when loop counting is also taken into account. It is readily seen that Eq. (D.3) is in agreement with our δZ_G in Eq. (7.73a).

Next, to extract electroweak gauge couplings g and g' , we recall the relations

$$\alpha = \frac{\hat{\alpha}_{\text{em}}}{1 - \Delta\alpha}, \quad c_\theta^2 s_\theta^2 = \frac{\pi \alpha}{\sqrt{2} \hat{m}_Z^2 \hat{G}_F (1 - \Delta r)}, \quad (\text{D.4})$$

where

$$\Delta r = \frac{\Pi_{WW}^T(0)}{m_W^2} - \text{Re} \frac{\Pi_{ZZ}^T(m_Z^2)}{m_Z^2} + \delta_{\text{VB}}. \quad (\text{D.5})$$

Here, $\Pi_{WW}^T(p^2)$ and $\Pi_{ZZ}^T(p^2)$ are transverse parts of the W and Z self-energies, which represent “universal” contributions to $\mu^- \rightarrow e^- \bar{\nu}_e \nu_\mu$ which determines \hat{G}_F . On the other hand, δ_{VB} contains non-universal contributions from vertex corrections, box diagrams, and wave-function renormalizations. Only the universal part of Δr , i.e.

$$\Delta r_u \equiv \frac{\Pi_{WW}^T(0)}{m_W^2} - \text{Re} \frac{\Pi_{ZZ}^T(m_Z^2)}{m_Z^2} \quad (\text{D.6})$$

is relevant for g, g' threshold corrections, because δ_{VB} has an EFT counterpart in terms of local effective operator contributions to muon decay. Thus, from Eq. (D.4),

$$\alpha^{\text{eff}} = \alpha \left[1 - (\Delta\alpha)_{\mathcal{O}(1)}^{\text{SUSY}} \right], \quad (c_\theta^2 s_\theta^2)^{\text{eff}} = c_\theta^2 s_\theta^2 \left[1 - (\Delta\alpha)_{\mathcal{O}(1)}^{\text{SUSY}} - (\Delta r_u)_{\mathcal{O}(1)}^{\text{SUSY}} \right]. \quad (\text{D.7})$$

The QED coupling and weak mixing angle can be directly translated into $SU(2)_L \times U(1)_Y$ gauge couplings via $4\pi\alpha = gs_\theta = g'c_\theta$. We therefore obtain

$$g^{\text{eff}} = g \left\{ 1 + \frac{1}{2} \frac{1}{c_\theta^2 - s_\theta^2} \left[s_\theta^2 (\Delta\alpha)_{\mathcal{O}(1)}^{\text{SUSY}} + c_\theta^2 (\Delta r_u)_{\mathcal{O}(1)}^{\text{SUSY}} \right] \right\}$$

$$= g \left\{ 1 + \frac{1}{2} \frac{1}{c_\theta^2 - s_\theta^2} \left[s_\theta^2 (\Delta\alpha)_{\mathcal{O}(1)}^{\text{SUSY}} + c_\theta^2 \frac{4}{v^2} \left(\frac{1}{g^2} \Pi_{WW}^T(0) - \frac{c_\theta^2}{g^2} \Pi_{ZZ}^T(m_Z^2) \right)_{\mathcal{O}(v^2)}^{\text{SUSY}} \right] \right\}, \quad (\text{D.8})$$

$$\begin{aligned} g'^{\text{eff}} &= g' \left\{ 1 - \frac{1}{2} \frac{1}{c_\theta^2 - s_\theta^2} \left[c_\theta^2 (\Delta\alpha)_{\mathcal{O}(1)}^{\text{SUSY}} + s_\theta^2 (\Delta r_u)_{\mathcal{O}(1)}^{\text{SUSY}} \right] \right\} \\ &= g' \left\{ 1 - \frac{1}{2} \frac{1}{c_\theta^2 - s_\theta^2} \left[c_\theta^2 (\Delta\alpha)_{\mathcal{O}(1)}^{\text{SUSY}} + s_\theta^2 \frac{4}{v^2} \left(\frac{1}{g^2} \Pi_{WW}^T(0) - \frac{c_\theta^2}{g^2} \Pi_{ZZ}^T(m_Z^2) \right)_{\mathcal{O}(v^2)}^{\text{SUSY}} \right] \right\}. \quad (\text{D.9}) \end{aligned}$$

The SUSY part of the self-energies Π_{WW}^T and Π_{ZZ}^T are to be expanded in powers of $\frac{v^2}{\Lambda^2}$. Analytical expressions of these and other self-energies to appear below can be found in [231]. They are rather tedious and will not be displayed here.

Then, moving on to Yukawa couplings y_f , we note that

$$\hat{m}_f = \frac{1}{\sqrt{2}} y_f v \left(1 - \text{Re} \frac{\Sigma_f(m_f)}{m_f} \right), \quad (\text{D.10})$$

where $\Sigma_f(\not{p})$ is the fermion self-energy, and the light Higgs vev v is extracted via

$$v^2 = 4 \frac{\hat{m}_Z^2 + \text{Re} \Pi_{ZZ}^T(m_Z^2)}{g^2 + g'^2}. \quad (\text{D.11})$$

In the SMEFT, it is \hat{v} , the vev of the canonically normalized light Higgs field $\hat{\phi}$, that is extracted via this procedure,

$$\hat{v}^2 = 4 \frac{\hat{m}_Z^2 + \text{Re} (\Pi_{ZZ}^T(m_Z^2))^{\text{SM}}}{(g^{\text{eff}})^2 + (g'^{\text{eff}})^2}. \quad (\text{D.12})$$

With Eqs. (D.8) and (D.9), it is easily seen that

$$\hat{v}^2 = v^2 \left[1 - \left(\frac{\Pi_{WW}^T(0)}{m_W^2} \right)_{\mathcal{O}(1)}^{\text{SUSY}} \right]. \quad (\text{D.13})$$

Therefore,

$$y_f^{\text{eff}} = y_f \frac{v}{\hat{v}} \left[1 - \left(\frac{\Sigma_f(m_f)}{m_f} \right)_{\mathcal{O}(1)}^{\text{SUSY}} \right] = y_f \left[1 - \left(\frac{\Sigma_f(m_f)}{m_f} \right)_{\mathcal{O}(1)}^{\text{SUSY}} + \frac{1}{2} \left(\frac{\Pi_{WW}^T(0)}{m_W^2} \right)_{\mathcal{O}(1)}^{\text{SUSY}} \right]. \quad (\text{D.14})$$

When cross-checking with our results, it is worth noting the following correspondence between the terms in Eq. (D.14) and those in Eq. (7.6) (using $f = t$ as an example),

$$\left(\frac{\Sigma_t(m_t)}{m_t} \right)_{\mathcal{O}(1), B_0 \text{ part}}^{\text{SUSY}} = \frac{\delta y_t}{y_t}, \quad \left(\frac{\Sigma_t(m_t)}{m_t} \right)_{\mathcal{O}(1), B_1 \text{ part}}^{\text{SUSY}} = \frac{1}{2} (\delta Z_q + \delta Z_u),$$

$$\left(\frac{\Pi_{WW}^T(0)}{m_W^2}\right)_{\mathcal{O}(1)}^{\text{SUSY}} = -\delta Z_\phi, \quad (\text{D.15})$$

where B_0 and B_1 are different loop integrals that appear in Σ_f .

Finally, we discuss the Higgs potential parameters m^2 and λ . The minimization condition of the 1PI effective potential,

$$\begin{aligned} 0 &= \mu^2 + m_{H_u}^2 - b \cot \beta - \frac{1}{8}(g^2 + g'^2)c_{2\beta} v^2 - \frac{t_u}{v_u} \\ &= \mu^2 + m_{H_d}^2 - b \tan \beta + \frac{1}{8}(g^2 + g'^2)c_{2\beta} v^2 - \frac{t_d}{v_d} \end{aligned} \quad (\text{D.16})$$

allows us to eliminate $\mu^2 + m_{H_u}^2$ and $\mu^2 + m_{H_d}^2$ in favor of v and β . From Eq. (7.40) we see that m^2 and λ are related by

$$m^2 = \mu^2 + m_{H_u}^2 s_\beta^2 + m_{H_d}^2 c_\beta^2 - b s_{2\beta} = -\frac{1}{8}(g^2 + g'^2)c_{2\beta}^2 v^2 + \frac{t_h}{v} = -\lambda v^2 + \frac{t_h}{v}, \quad (\text{D.17})$$

where

$$\frac{t_h}{v} \equiv \frac{s_\beta t_u + c_\beta t_d}{v} = s_\beta^2 \frac{t_u}{v_u} + c_\beta^2 \frac{t_d}{v_d}. \quad (\text{D.18})$$

To extract them from \hat{m}_h , we write the tree-level mass matrix squared in the (H_u, H_d) basis,

$$\mathbf{M}_H^2 = \begin{pmatrix} b \cot \beta + 2\lambda v^2 c_{2\beta}^{-2} s_\beta^2 + \frac{t_u}{v_u} & -b - 2\lambda v^2 c_{2\beta}^{-2} s_\beta c_\beta \\ -b - 2\lambda v^2 c_{2\beta}^{-2} s_\beta c_\beta & b \tan \beta + 2\lambda v^2 c_{2\beta}^{-2} c_\beta^2 + \frac{t_d}{v_d} \end{pmatrix}. \quad (\text{D.19})$$

Therefore,

$$\hat{m}_h^2 = \text{smaller eigenvalue of } \mathbf{M}_H^2 - \begin{pmatrix} \Pi_{uu} & \Pi_{ud} \\ \Pi_{ud} & \Pi_{dd} \end{pmatrix} = 2\lambda v^2 + \frac{t_h}{v} - \Pi_{hh}, \quad (\text{D.20})$$

where $\Pi_{uu,ud,dd}$ are one-loop self-energies of the Higgs doublets H_u, H_d , and

$$\Pi_{hh} \equiv s_\beta^2 \Pi_{uu} + c_\beta^2 \Pi_{dd} + 2s_\beta c_\beta \Pi_{ud}. \quad (\text{D.21})$$

From Eq. (D.20) we obtain

$$\lambda_{\text{eff}} = \lambda \frac{v^2}{\hat{v}^2} + \frac{1}{2v^2} \left(\frac{t_h}{v} - \Pi_{hh} \right)_{\mathcal{O}(v^2)}^{\text{SUSY}} = \lambda \left[1 + \left(\frac{\Pi_{WW}^T(0)}{m_W^2} \right)_{\mathcal{O}(1)}^{\text{SUSY}} \right] + \frac{1}{2v^2} \left(\frac{t_h}{v} - \Pi_{hh} \right)_{\mathcal{O}(v^2)}^{\text{SUSY}}, \quad (\text{D.22})$$

and then from Eq. (D.17),

$$m_{\text{eff}}^2 = -\lambda_{\text{eff}} \hat{v}^2 + \left(\frac{t_h}{v} - \Pi_{hh} \right)^{\text{SM}} = m^2 - \frac{1}{2} \left(3 \frac{t_h}{v} - \Pi_{hh} \right)_{\mathcal{O}(\Lambda^2)}^{\text{SUSY}}. \quad (\text{D.23})$$

Note that while both $\frac{t_h}{v}$ and Π_{hh} contain $\mathcal{O}(\Lambda^2)$ terms, they cancel in the combination $\frac{t_h}{v} - \Pi_{hh}$ appearing in Eq. (D.22). The subleading $\mathcal{O}(v^2)$ terms needed here come from both expanding the loop integrals involved up to next-to-leading order, and electroweak symmetry breaking contributions to superpartner masses. Also, note the different notation adopted in [231]: $t_{1,2} = t_{d,u}$, $\Pi_{s_1 s_1, s_1 s_2, s_2 s_2} = \Pi_{dd, ud, uu}$.

Bibliography

- [1] G. Aad *et al.* [ATLAS Collaboration], “Observation of a new particle in the search for the Standard Model Higgs boson with the ATLAS detector at the LHC,” *Phys. Lett. B* **716**, 1 (2012) [arXiv:1207.7214 [hep-ex]].
- [2] S. Chatrchyan *et al.* [CMS Collaboration], “Observation of a new boson at a mass of 125 GeV with the CMS experiment at the LHC,” *Phys. Lett. B* **716**, 30 (2012) [arXiv:1207.7235 [hep-ex]].
- [3] B. Grzadkowski, M. Iskrzynski, M. Misiak and J. Rosiek, “Dimension-Six Terms in the Standard Model Lagrangian,” *JHEP* **1010**, 085 (2010) [arXiv:1008.4884 [hep-ph]].
- [4] B. Henning, X. Lu, T. Melia and H. Murayama, “2, 84, 30, 993, 560, 15456, 11962, 261485, ...: Higher dimension operators in the SM EFT,” *JHEP* **1708**, 016 (2017) [arXiv:1512.03433 [hep-ph]].
- [5] S. Willenbrock and C. Zhang, “Effective Field Theory Beyond the Standard Model,” *Ann. Rev. Nucl. Part. Sci.* **64**, 83 (2014) [arXiv:1401.0470 [hep-ph]].
- [6] A. Falkowski, “Effective field theory approach to LHC Higgs data,” *Pramana* **87**, no. 3, 39 (2016) [arXiv:1505.00046 [hep-ph]].
- [7] D. de Florian *et al.* [LHC Higgs Cross Section Working Group], “Handbook of LHC Higgs Cross Sections: 4. Deciphering the Nature of the Higgs Sector,” arXiv:1610.07922 [hep-ph].
- [8] A. de Gouvea *et al.* [Intensity Frontier Neutrino Working Group], “Working Group Report: Neutrinos,” arXiv:1310.4340 [hep-ex].
- [9] J. L. Hewett *et al.*, “Fundamental Physics at the Intensity Frontier,” arXiv:1205.2671 [hep-ex].
- [10] J. D. Wells, “Lectures on Higgs Boson Physics in the Standard Model and Beyond,” arXiv:0909.4541 [hep-ph].
- [11] G. F. Giudice, “Naturally Speaking: The Naturalness Criterion and Physics at the LHC,” In *Kane, Gordon (ed.), Pierce, Aaron (ed.): Perspectives on LHC physics* 155-178 [arXiv:0801.2562 [hep-ph]].
- [12] Y. Grossman, “Introduction to flavor physics,” arXiv:1006.3534 [hep-ph].

- [13] G. D’Ambrosio, G. F. Giudice, G. Isidori and A. Strumia, “Minimal flavor violation: An Effective field theory approach,” Nucl. Phys. B **645**, 155 (2002) [hep-ph/0207036].
- [14] C. Csaki and P. Tanedo, “Beyond the Standard Model,” arXiv:1602.04228 [hep-ph].
- [15] B. C. Allanach, “Beyond the Standard Model Lectures for the 2016 European School of High-Energy Physics,” arXiv:1609.02015 [hep-ph].
- [16] The ATLAS collaboration [ATLAS Collaboration], “Search for the Supersymmetric Partner of the Top Quark in the Jets+Emiss Final State at $\sqrt{s} = 13$ TeV,” ATLAS-CONF-2016-077.
- [17] CMS Collaboration [CMS Collaboration], “Search for direct top squark pair production in the fully hadronic final state in proton-proton collisions at $\sqrt{s} = 13$ TeV corresponding to an integrated luminosity of 12.9/fb,” CMS-PAS-SUS-16-029.
- [18] The ATLAS collaboration [ATLAS Collaboration], “Search for top squarks in final states with one isolated lepton, jets, and missing transverse momentum in $\sqrt{s} = 13$ TeV pp collisions with the ATLAS detector,” ATLAS-CONF-2016-050.
- [19] CMS Collaboration [CMS Collaboration], “Search for direct top squark pair production in the single lepton final state at $\sqrt{s} = 13$ TeV,” CMS-PAS-SUS-16-028.
- [20] The ATLAS collaboration [ATLAS Collaboration], “Search for direct top squark pair production and dark matter production in final states with two leptons in $\sqrt{s} = 13$ TeV pp collisions using 13.3 fb⁻¹ of ATLAS data,” ATLAS-CONF-2016-076.
- [21] CMS Collaboration [CMS Collaboration], “Search for direct top squark pair production in the dilepton final state at $\sqrt{s} = 13$ TeV,” CMS-PAS-SUS-16-027.
- [22] The ATLAS collaboration [ATLAS Collaboration], “Search for pair production of vector-like top partners in events with exactly one lepton and large missing transverse momentum in $\sqrt{s} = 13$ TeV pp collisions with the ATLAS detector,” ATLAS-CONF-2016-101.
- [23] The ATLAS collaboration, “Search for production of vector-like top quark pairs and of four top quarks in the lepton-plus-jets final state in pp collisions at $\sqrt{s} = 13$ TeV with the ATLAS detector,” ATLAS-CONF-2016-013.
- [24] O. Eberhardt, G. Herbert, H. Lacker, A. Lenz, A. Menzel, U. Nierste and M. Wiebusch, “Impact of a Higgs boson at a mass of 126 GeV on the standard model with three and four fermion generations,” Phys. Rev. Lett. **109**, 241802 (2012) [arXiv:1209.1101 [hep-ph]].
- [25] M. Ciuchini, E. Franco, S. Mishima and L. Silvestrini, “Electroweak Precision Observables, New Physics and the Nature of a 126 GeV Higgs Boson,” JHEP **1308**, 106 (2013) [arXiv:1306.4644 [hep-ph]].

- [26] M. Baak *et al.* [Gfitter Group Collaboration], “The global electroweak fit at NNLO and prospects for the LHC and ILC,” *Eur. Phys. J. C* **74**, 3046 (2014) [arXiv:1407.3792 [hep-ph]].
- [27] M. Ciuchini, E. Franco, S. Mishima, M. Pierini, L. Reina and L. Silvestrini, “Update of the electroweak precision fit, interplay with Higgs-boson signal strengths and model-independent constraints on new physics,” *Nucl. Part. Phys. Proc.* **273-275**, 2219 (2016) [arXiv:1410.6940 [hep-ph]].
- [28] J. Charles *et al.*, “Current status of the Standard Model CKM fit and constraints on $\Delta F = 2$ New Physics,” *Phys. Rev. D* **91**, no. 7, 073007 (2015) [arXiv:1501.05013 [hep-ph]].
- [29] A. Pomarol and F. Riva, “Towards the Ultimate SM Fit to Close in on Higgs Physics,” *JHEP* **1401**, 151 (2014) [arXiv:1308.2803 [hep-ph]].
- [30] A. A. Petrov, S. Pokorski, J. D. Wells and Z. Zhang, “Role of low-energy observables in precision Higgs boson analyses,” *Phys. Rev. D* **91**, no. 7, 073001 (2015) [arXiv:1501.02803 [hep-ph]].
- [31] J. Erler, P. Langacker, S. Munir and E. Rojas, “Improved Constraints on Z-prime Bosons from Electroweak Precision Data,” *JHEP* **0908**, 017 (2009) [arXiv:0906.2435 [hep-ph]].
- [32] S. Heinemeyer, W. Hollik and G. Weiglein, “Electroweak precision observables in the minimal supersymmetric standard model,” *Phys. Rept.* **425**, 265 (2006) [hep-ph/0412214].
- [33] J. R. Ellis, S. Heinemeyer, K. A. Olive, A. M. Weber and G. Weiglein, “The Supersymmetric Parameter Space in Light of B^- physics Observables and Electroweak Precision Data,” *JHEP* **0708**, 083 (2007) [arXiv:0706.0652 [hep-ph]].
- [34] J. Hubisz, P. Meade, A. Noble and M. Perelstein, “Electroweak precision constraints on the lightest Higgs model with T parity,” *JHEP* **0601**, 135 (2006) [hep-ph/0506042].
- [35] K. Agashe and R. Contino, “The Minimal composite Higgs model and electroweak precision tests,” *Nucl. Phys. B* **742**, 59 (2006) [hep-ph/0510164].
- [36] R. Barbieri, D. Buttazzo, F. Sala, D. M. Straub and A. Tesi, “A 125 GeV composite Higgs boson versus flavour and electroweak precision tests,” *JHEP* **1305**, 069 (2013) [arXiv:1211.5085 [hep-ph]].
- [37] J. Elias-Miro, C. Grojean, R. S. Gupta and D. Marzocca, “Scaling and tuning of EW and Higgs observables,” *JHEP* **1405**, 019 (2014) [arXiv:1312.2928 [hep-ph]].
- [38] J. Elias-Miro, J. R. Espinosa, E. Masso and A. Pomarol, “Higgs windows to new physics through d=6 operators: constraints and one-loop anomalous dimensions,” *JHEP* **1311**, 066 (2013) [arXiv:1308.1879 [hep-ph]].

- [39] G. Buchalla and O. Cata, “Effective Theory of a Dynamically Broken Electroweak Standard Model at NLO,” *JHEP* **1207**, 101 (2012) [arXiv:1203.6510 [hep-ph]].
- [40] G. Buchalla, O. Cat and C. Krause, “Complete Electroweak Chiral Lagrangian with a Light Higgs at NLO,” *Nucl. Phys. B* **880**, 552 (2014) Erratum: [*Nucl. Phys. B* **913**, 475 (2016)] [arXiv:1307.5017 [hep-ph]].
- [41] G. Buchalla, O. Cat and C. Krause, “On the Power Counting in Effective Field Theories,” *Phys. Lett. B* **731**, 80 (2014) [arXiv:1312.5624 [hep-ph]].
- [42] G. Buchalla, O. Cata, A. Celis and C. Krause, “Fitting Higgs Data with Nonlinear Effective Theory,” *Eur. Phys. J. C* **76**, no. 5, 233 (2016) [arXiv:1511.00988 [hep-ph]].
- [43] G. Buchalla, O. Cata, A. Celis, M. Knecht and C. Krause, “Complete One-Loop Renormalization of the Higgs-Electroweak Chiral Lagrangian,” *Nucl. Phys. B* **928**, 93 (2018) [arXiv:1710.06412 [hep-ph]].
- [44] J. de Blas, O. Eberhardt and C. Krause, “Current and future constraints on Higgs couplings in the nonlinear Effective Theory,” arXiv:1803.00939 [hep-ph].
- [45] A. Falkowski and F. Riva, “Model-independent precision constraints on dimension-6 operators,” *JHEP* **1502**, 039 (2015) [arXiv:1411.0669 [hep-ph]].
- [46] J. Ellis, V. Sanz and T. You, “The Effective Standard Model after LHC Run I,” *JHEP* **1503**, 157 (2015) [arXiv:1410.7703 [hep-ph]].
- [47] P. Draper, G. Lee and C. E. M. Wagner, “Precise estimates of the Higgs mass in heavy supersymmetry,” *Phys. Rev. D* **89**, no. 5, 055023 (2014) [arXiv:1312.5743 [hep-ph]].
- [48] E. Bagnaschi, G. F. Giudice, P. Slavich and A. Strumia, “Higgs Mass and Unnatural Supersymmetry,” *JHEP* **1409**, 092 (2014) [arXiv:1407.4081 [hep-ph]].
- [49] J. Pardo Vega and G. Villadoro, “SusyHD: Higgs mass Determination in Supersymmetry,” *JHEP* **1507**, 159 (2015) [arXiv:1504.05200 [hep-ph]].
- [50] G. Lee and C. E. M. Wagner, “Higgs bosons in heavy supersymmetry with an intermediate m_A ,” *Phys. Rev. D* **92**, no. 7, 075032 (2015) [arXiv:1508.00576 [hep-ph]].
- [51] P. Athron, J. h. Park, T. Steudtner, D. Stckinger and A. Voigt, “Precise Higgs mass calculations in (non-)minimal supersymmetry at both high and low scales,” *JHEP* **1701**, 079 (2017) [arXiv:1609.00371 [hep-ph]].
- [52] F. Staub and W. Porod, “Improved predictions for intermediate and heavy Supersymmetry in the MSSM and beyond,” *Eur. Phys. J. C* **77**, no. 5, 338 (2017) [arXiv:1703.03267 [hep-ph]].
- [53] E. Bagnaschi, J. Pardo Vega and P. Slavich, “Improved determination of the Higgs mass in the MSSM with heavy superpartners,” *Eur. Phys. J. C* **77**, no. 5, 334 (2017) [arXiv:1703.08166 [hep-ph]].

- [54] W. Skiba, “Effective Field Theory and Precision Electroweak Measurements,” arXiv:1006.2142 [hep-ph].
- [55] B. Henning, X. Lu and H. Murayama, “How to use the Standard Model effective field theory,” JHEP **1601**, 023 (2016) [arXiv:1412.1837 [hep-ph]].
- [56] A. Drozd, J. Ellis, J. Quevillon and T. You, “The Universal One-Loop Effective Action,” JHEP **1603**, 180 (2016) [arXiv:1512.03003 [hep-ph]].
- [57] B. Henning, X. Lu and H. Murayama, “One-loop Matching and Running with Covariant Derivative Expansion,” JHEP **1801**, 123 (2018) [arXiv:1604.01019 [hep-ph]].
- [58] S. A. R. Ellis, J. Quevillon, T. You and Z. Zhang, “Mixed heavy-light matching in the Universal One-Loop Effective Action,” Phys. Lett. B **762**, 166 (2016) [arXiv:1604.02445 [hep-ph]].
- [59] J. Fuentes-Martin, J. Portoles and P. Ruiz-Femenia, “Integrating out heavy particles with functional methods: a simplified framework,” JHEP **1609**, 156 (2016) [arXiv:1607.02142 [hep-ph]].
- [60] Z. Zhang, “Covariant diagrams for one-loop matching,” JHEP **1705**, 152 (2017) [arXiv:1610.00710 [hep-ph]].
- [61] S. A. R. Ellis, J. Quevillon, T. You and Z. Zhang, “Extending the Universal One-Loop Effective Action: Heavy-Light Coefficients,” JHEP **1708**, 054 (2017) [arXiv:1706.07765 [hep-ph]].
- [62] C. Degrande, N. Greiner, W. Kilian, O. Mattelaer, H. Mebane, T. Stelzer, S. Willenbrock and C. Zhang, “Effective Field Theory: A Modern Approach to Anomalous Couplings,” Annals Phys. **335**, 21 (2013) [arXiv:1205.4231 [hep-ph]].
- [63] G. Passarino, “NLO Inspired Effective Lagrangians for Higgs Physics,” Nucl. Phys. B **868**, 416 (2013) [arXiv:1209.5538 [hep-ph]].
- [64] E. Mass and V. Sanz, “Limits on anomalous couplings of the Higgs boson to electroweak gauge bosons from LEP and the LHC,” Phys. Rev. D **87**, no. 3, 033001 (2013) [arXiv:1211.1320 [hep-ph]].
- [65] T. Corbett, O. J. P. Eboli, J. Gonzalez-Fraile and M. C. Gonzalez-Garcia, “Robust Determination of the Higgs Couplings: Power to the Data,” Phys. Rev. D **87**, 015022 (2013) [arXiv:1211.4580 [hep-ph]].
- [66] C. Grojean, E. E. Jenkins, A. V. Manohar and M. Trott, “Renormalization Group Scaling of Higgs Operators and $\Gamma(h \rightarrow \gamma\gamma)$,” JHEP **1304**, 016 (2013) [arXiv:1301.2588 [hep-ph]].
- [67] J. Elias-Miro, J. R. Espinosa, E. Masso and A. Pomarol, “Renormalization of dimension-six operators relevant for the Higgs decays $h \rightarrow \gamma\gamma, \gamma Z$,” JHEP **1308**, 033 (2013) [arXiv:1302.5661 [hep-ph]].

- [68] G. Buchalla, O. Cata, R. Rahn and M. Schlaffer, “Effective Field Theory Analysis of New Physics in $e^+e^- \rightarrow W^+W^-$ at a Linear Collider,” *Eur. Phys. J. C* **73**, no. 10, 2589 (2013) [arXiv:1302.6481 [hep-ph]].
- [69] A. Falkowski, F. Riva and A. Urbano, “Higgs at last,” *JHEP* **1311**, 111 (2013) [arXiv:1303.1812 [hep-ph]].
- [70] R. Contino, M. Ghezzi, C. Grojean, M. Muhlleitner and M. Spira, “Effective Lagrangian for a light Higgs-like scalar,” *JHEP* **1307**, 035 (2013) [arXiv:1303.3876 [hep-ph]].
- [71] T. Corbett, O. J. P. boli, J. Gonzalez-Fraile and M. C. Gonzalez-Garcia, “Determining Triple Gauge Boson Couplings from Higgs Data,” *Phys. Rev. Lett.* **111**, 011801 (2013) [arXiv:1304.1151 [hep-ph]].
- [72] E. E. Jenkins, A. V. Manohar and M. Trott, “On Gauge Invariance and Minimal Coupling,” *JHEP* **1309**, 063 (2013) [arXiv:1305.0017 [hep-ph]].
- [73] H. Mebane, N. Greiner, C. Zhang and S. Willenbrock, “Constraints on Electroweak Effective Operators at One Loop,” *Phys. Rev. D* **88**, no. 1, 015028 (2013) [arXiv:1306.3380 [hep-ph]].
- [74] M. B. Einhorn and J. Wudka, “The Bases of Effective Field Theories,” *Nucl. Phys. B* **876**, 556 (2013) [arXiv:1307.0478 [hep-ph]].
- [75] M. B. Einhorn and J. Wudka, “Higgs-Boson Couplings Beyond the Standard Model,” *Nucl. Phys. B* **877**, 792 (2013) [arXiv:1308.2255 [hep-ph]].
- [76] E. E. Jenkins, A. V. Manohar and M. Trott, “Renormalization Group Evolution of the Standard Model Dimension Six Operators I: Formalism and lambda Dependence,” *JHEP* **1310**, 087 (2013) [arXiv:1308.2627 [hep-ph]].
- [77] E. E. Jenkins, A. V. Manohar and M. Trott, “Renormalization Group Evolution of the Standard Model Dimension Six Operators II: Yukawa Dependence,” *JHEP* **1401**, 035 (2014) [arXiv:1310.4838 [hep-ph]].
- [78] I. Brivio, T. Corbett, O. J. P. boli, M. B. Gavela, J. Gonzalez-Fraile, M. C. Gonzalez-Garcia, L. Merlo and S. Rigolin, “Disentangling a dynamical Higgs,” *JHEP* **1403**, 024 (2014) [arXiv:1311.1823 [hep-ph]].
- [79] C. Y. Chen, S. Dawson and C. Zhang, “Electroweak Effective Operators and Higgs Physics,” *Phys. Rev. D* **89**, no. 1, 015016 (2014) [arXiv:1311.3107 [hep-ph]].
- [80] R. Alonso, E. E. Jenkins, A. V. Manohar and M. Trott, “Renormalization Group Evolution of the Standard Model Dimension Six Operators III: Gauge Coupling Dependence and Phenomenology,” *JHEP* **1404**, 159 (2014) [arXiv:1312.2014 [hep-ph]].
- [81] J. Ellis, V. Sanz and T. You, “Complete Higgs Sector Constraints on Dimension-6 Operators,” *JHEP* **1407**, 036 (2014) [arXiv:1404.3667 [hep-ph]].

- [82] H. Belusca-Maito, “Effective Higgs Lagrangian and Constraints on Higgs Couplings,” arXiv:1404.5343 [hep-ph].
- [83] R. Alonso, H. M. Chang, E. E. Jenkins, A. V. Manohar and B. Shotwell, “Renormalization group evolution of dimension-six baryon number violating operators,” Phys. Lett. B **734**, 302 (2014) [arXiv:1405.0486 [hep-ph]].
- [84] E. Masso, “An Effective Guide to Beyond the Standard Model Physics,” JHEP **1410**, 128 (2014) [arXiv:1406.6376 [hep-ph]].
- [85] A. Biekötter, A. Knochel, M. Krmer, D. Liu and F. Riva, “Vices and virtues of Higgs effective field theories at large energy,” Phys. Rev. D **91**, 055029 (2015) [arXiv:1406.7320 [hep-ph]].
- [86] C. Englert and M. Spannowsky, “Effective Theories and Measurements at Colliders,” Phys. Lett. B **740**, 8 (2015) [arXiv:1408.5147 [hep-ph]].
- [87] M. Trott, “On the consistent use of Constructed Observables,” JHEP **1502**, 046 (2015) [arXiv:1409.7605 [hep-ph]].
- [88] L. Lehman, “Extending the Standard Model Effective Field Theory with the Complete Set of Dimension-7 Operators,” Phys. Rev. D **90**, no. 12, 125023 (2014) [arXiv:1410.4193 [hep-ph]].
- [89] M. Gonzalez-Alonso, A. Greljo, G. Isidori and D. Marzocca, “Pseudo-observables in Higgs decays,” Eur. Phys. J. C **75**, no. 3, 128 (2015) [arXiv:1412.6038 [hep-ph]].
- [90] G. Buchalla, O. Cata and C. Krause, “A Systematic Approach to the SILH Lagrangian,” Nucl. Phys. B **894**, 602 (2015) [arXiv:1412.6356 [hep-ph]].
- [91] L. Berthier and M. Trott, “Towards consistent Electroweak Precision Data constraints in the SMEFT,” JHEP **1505**, 024 (2015) [arXiv:1502.02570 [hep-ph]].
- [92] A. Efrati, A. Falkowski and Y. Soreq, “Electroweak constraints on flavorful effective theories,” JHEP **1507**, 018 (2015) [arXiv:1503.07872 [hep-ph]].
- [93] G. Buchalla, O. Cata, A. Celis and C. Krause, “Note on Anomalous Higgs-Boson Couplings in Effective Field Theory,” Phys. Lett. B **750**, 298 (2015) [arXiv:1504.01707 [hep-ph]].
- [94] M. Gonzalez-Alonso, A. Greljo, G. Isidori and D. Marzocca, “Electroweak bounds on Higgs pseudo-observables and $h \rightarrow 4\ell$ decays,” Eur. Phys. J. C **75**, no. 7, 341 (2015) [arXiv:1504.04018 [hep-ph]].
- [95] C. Hartmann and M. Trott, “On one-loop corrections in the standard model effective field theory; the $\Gamma(h \rightarrow \gamma\gamma)$ case,” JHEP **1507**, 151 (2015) [arXiv:1505.02646 [hep-ph]].
- [96] M. Ghezzi, R. Gomez-Ambrosio, G. Passarino and S. Uccirati, “NLO Higgs effective field theory and κ -framework,” JHEP **1507**, 175 (2015) [arXiv:1505.03706 [hep-ph]].

- [97] T. Corbett, O. J. P. Eboli, D. Goncalves, J. Gonzalez-Fraile, T. Plehn and M. Rauch, “The Higgs Legacy of the LHC Run I,” *JHEP* **1508**, 156 (2015) [arXiv:1505.05516 [hep-ph]].
- [98] A. Buckley, C. Englert, J. Ferrando, D. J. Miller, L. Moore, M. Russell and C. D. White, “Global fit of top quark effective theory to data,” *Phys. Rev. D* **92**, no. 9, 091501 (2015) [arXiv:1506.08845 [hep-ph]].
- [99] J. de Blas, M. Chala and J. Santiago, “Renormalization Group Constraints on New Top Interactions from Electroweak Precision Data,” *JHEP* **1509**, 189 (2015) [arXiv:1507.00757 [hep-ph]].
- [100] J. D. Wells and Z. Zhang, “Status and prospects of precision analyses with $e^+e^- \rightarrow W^+W^-$,” *Phys. Rev. D* **93**, no. 3, 034001 (2016) [*Phys. Rev. D* **93**, 034001 (2016)] [arXiv:1507.01594 [hep-ph]].
- [101] M. Bordone, A. Greljo, G. Isidori, D. Marzocca and A. Pattori, “Higgs Pseudo Observables and Radiative Corrections,” *Eur. Phys. J. C* **75**, no. 8, 385 (2015) [arXiv:1507.02555 [hep-ph]].
- [102] C. Hartmann and M. Trott, “Higgs Decay to Two Photons at One Loop in the Standard Model Effective Field Theory,” *Phys. Rev. Lett.* **115**, no. 19, 191801 (2015) [arXiv:1507.03568 [hep-ph]].
- [103] A. Falkowski, M. Gonzalez-Alonso, A. Greljo and D. Marzocca, “Global constraints on anomalous triple gauge couplings in effective field theory approach,” *Phys. Rev. Lett.* **116**, no. 1, 011801 (2016) [arXiv:1508.00581 [hep-ph]].
- [104] L. Berthier and M. Trott, “Consistent constraints on the Standard Model Effective Field Theory,” *JHEP* **1602**, 069 (2016) [arXiv:1508.05060 [hep-ph]].
- [105] A. Falkowski, B. Fuks, K. Mawatari, K. Mimasu, F. Riva and V. Sanz, “Rosetta: an operator basis translator for Standard Model effective field theory,” *Eur. Phys. J. C* **75**, no. 12, 583 (2015) [arXiv:1508.05895 [hep-ph]].
- [106] A. David and G. Passarino, “Through precision straits to next standard model heights,” *Rev. Phys.* **1**, 13 (2016) [arXiv:1510.00414 [hep-ph]].
- [107] J. Brehmer, A. Freitas, D. Lopez-Val and T. Plehn, “Pushing Higgs Effective Theory to its Limits,” *Phys. Rev. D* **93**, no. 7, 075014 (2016) [arXiv:1510.03443 [hep-ph]].
- [108] J. Ellis and T. You, “Sensitivities of Prospective Future e^+e^- Colliders to Decoupled New Physics,” *JHEP* **1603**, 089 (2016) [arXiv:1510.04561 [hep-ph]].
- [109] J. D. Wells and Z. Zhang, “Effective theories of universal theories,” *JHEP* **1601**, 123 (2016) [arXiv:1510.08462 [hep-ph]].
- [110] A. Falkowski and K. Mimouni, “Model independent constraints on four-lepton operators,” *JHEP* **1602**, 086 (2016) [arXiv:1511.07434 [hep-ph]].

- [111] J. D. Wells and Z. Zhang, “Renormalization group evolution of the universal theories EFT,” JHEP **1606**, 122 (2016) [arXiv:1512.03056 [hep-ph]].
- [112] A. Butter, O. J. P. Boli, J. Gonzalez-Fraile, M. C. Gonzalez-Garcia, T. Plehn and M. Rauch, “The Gauge-Higgs Legacy of the LHC Run I,” JHEP **1607**, 152 (2016) [arXiv:1604.03105 [hep-ph]].
- [113] R. Contino, A. Falkowski, F. Goertz, C. Grojean and F. Riva, “On the Validity of the Effective Field Theory Approach to SM Precision Tests,” JHEP **1607**, 144 (2016) [arXiv:1604.06444 [hep-ph]].
- [114] L. Berthier, M. Bjr and M. Trott, “Incorporating doubly resonant W^\pm data in a global fit of SMEFT parameters to lift flat directions,” JHEP **1609**, 157 (2016) [arXiv:1606.06693 [hep-ph]].
- [115] A. Falkowski, M. Gonzalez-Alonso, A. Greljo, D. Marzocca and M. Son, “Anomalous Triple Gauge Couplings in the Effective Field Theory Approach at the LHC,” JHEP **1702**, 115 (2017) [arXiv:1609.06312 [hep-ph]].
- [116] M. Farina, G. Panico, D. Pappadopulo, J. T. Ruderman, R. Torre and A. Wulzer, “Energy helps accuracy: electroweak precision tests at hadron colliders,” Phys. Lett. B **772**, 210 (2017) [arXiv:1609.08157 [hep-ph]].
- [117] Z. Zhang, “Time to Go Beyond Triple-Gauge-Boson-Coupling Interpretation of W Pair Production,” Phys. Rev. Lett. **118**, no. 1, 011803 (2017) [arXiv:1610.01618 [hep-ph]].
- [118] J. Ellis, P. Roloff, V. Sanz and T. You, “Dimension-6 Operator Analysis of the CLIC Sensitivity to New Physics,” JHEP **1705**, 096 (2017) [arXiv:1701.04804 [hep-ph]].
- [119] R. Franceschini, G. Panico, A. Pomarol, F. Riva and A. Wulzer, “Electroweak Precision Tests in High-Energy Diboson Processes,” JHEP **1802**, 111 (2018) [arXiv:1712.01310 [hep-ph]].
- [120] J. Ellis, C. W. Murphy, V. Sanz and T. You, “Updated Global SMEFT Fit to Higgs, Diboson and Electroweak Data,” arXiv:1803.03252 [hep-ph].
- [121] L. G. Almeida, S. J. Lee, S. Pokorski and J. D. Wells, “Study of the 125 GeV Standard Model Higgs Boson Partial Widths and Branching Fractions,” Phys. Rev. D **89**, 033006 (2014) [arXiv:1311.6721 [hep-ph]].
- [122] R. Alonso, E. E. Jenkins and A. V. Manohar, “Holomorphy without Supersymmetry in the Standard Model Effective Field Theory,” Phys. Lett. B **739**, 95 (2014) [arXiv:1409.0868 [hep-ph]].
- [123] J. Elias-Miro, J. R. Espinosa and A. Pomarol, “One-loop non-renormalization results in EFTs,” Phys. Lett. B **747**, 272 (2015) [arXiv:1412.7151 [hep-ph]].
- [124] C. Cheung and C. H. Shen, “Nonrenormalization Theorems without Supersymmetry,” Phys. Rev. Lett. **115**, no. 7, 071601 (2015) [arXiv:1505.01844 [hep-ph]].

- [125] L. Lehman and A. Martin, “Hilbert Series for Constructing Lagrangians: expanding the phenomenologist’s toolbox,” *Phys. Rev. D* **91**, 105014 (2015) [arXiv:1503.07537 [hep-ph]].
- [126] L. Lehman and A. Martin, “Low-derivative operators of the Standard Model effective field theory via Hilbert series methods,” *JHEP* **1602**, 081 (2016) [arXiv:1510.00372 [hep-ph]].
- [127] B. Henning, X. Lu, T. Melia and H. Murayama, “Hilbert series and operator bases with derivatives in effective field theories,” *Commun. Math. Phys.* **347**, no. 2, 363 (2016) [arXiv:1507.07240 [hep-th]].
- [128] A. Azatov, R. Contino, C. S. Machado and F. Riva, “Helicity selection rules and noninterference for BSM amplitudes,” *Phys. Rev. D* **95**, no. 6, 065014 (2017) [arXiv:1607.05236 [hep-ph]].
- [129] A. Azatov, J. Elias-Miro, Y. Reymiujaji and E. Venturini, “Novel measurements of anomalous triple gauge couplings for the LHC,” *JHEP* **1710**, 027 (2017) [arXiv:1707.08060 [hep-ph]].
- [130] G. Panico, F. Riva and A. Wulzer, “Diboson Interference Resurrection,” *Phys. Lett. B* **776**, 473 (2018) [arXiv:1708.07823 [hep-ph]].
- [131] J. D. Wells and Z. Zhang, “Precision Electroweak Analysis after the Higgs Boson Discovery,” *Phys. Rev. D* **90**, no. 3, 033006 (2014) [arXiv:1406.6070 [hep-ph]].
- [132] J. D. Wells and Z. Zhang, “Effective field theory approach to trans-TeV supersymmetry: covariant matching, Yukawa unification and Higgs couplings,” arXiv:1711.04774 [hep-ph].
- [133] S. Chatrchyan *et al.* [CMS Collaboration], “Study of the Mass and Spin-Parity of the Higgs Boson Candidate Via Its Decays to Z Boson Pairs,” *Phys. Rev. Lett.* **110**, 081803 (2013) [arXiv:1212.6639 [hep-ex]].
- [134] D. Y. Bardin, P. Christova, M. Jack, L. Kalinovskaya, A. Olchevski, S. Riemann and T. Riemann, “ZFITTER v.6.21: A Semianalytical program for fermion pair production in e^+e^- annihilation,” *Comput. Phys. Commun.* **133**, 229 (2001) [hep-ph/9908433].
- [135] A. B. Arbuzov, M. Awramik, M. Czakon, A. Freitas, M. W. Grunewald, K. Monig, S. Riemann and T. Riemann, “ZFITTER: A Semi-analytical program for fermion pair production in e^+e^- annihilation, from version 6.21 to version 6.42,” *Comput. Phys. Commun.* **174**, 728 (2006) [hep-ph/0507146].
- [136] J. Beringer *et al.* [Particle Data Group Collaboration], “Review of Particle Physics (RPP),” *Phys. Rev. D* **86**, 010001 (2012). And 2013 partial update for the 2014 edition.
- [137] See <http://physics.nist.gov/cuu/Constants/>.

- [138] K. G. Chetyrkin, J. H. Kuhn and A. Kwiatkowski, “QCD corrections to the e^+e^- cross-section and the Z boson decay rate: Concepts and results,” *Phys. Rept.* **277**, 189 (1996).
- [139] S. Schael *et al.* [ALEPH and DELPHI and L3 and OPAL and SLD and LEP Electroweak Working Group and SLD Electroweak Group and SLD Heavy Flavour Group Collaborations], “Precision electroweak measurements on the Z resonance,” *Phys. Rept.* **427**, 257 (2006) [hep-ex/0509008].
- [140] V. M. Abazov *et al.* [D0 Collaboration], “Measurement of $\sin^2 \theta_{\text{eff}}^\ell$ and Z -light quark couplings using the forward-backward charge asymmetry in $p\bar{p} \rightarrow Z/\gamma^* \rightarrow e^+e^-$ events with $\mathcal{L} = 5.0 \text{ fb}^{-1}$ at $\sqrt{s} = 1.96 \text{ TeV}$,” *Phys. Rev. D* **84**, 012007 (2011) [arXiv:1104.4590 [hep-ex]].
- [141] J. Han [CDF Collaboration], “The Angular Coefficients and A_{fb} of Drell-Yan e^+e^- Pairs in the Z Mass Region from $p\bar{p}$ Collision at $\sqrt{s} = 1.96 \text{ TeV}$,” arXiv:1110.0153 [hep-ex].
- [142] Electroweak Working Group [CDF and D0 Collaborations], “2012 Update of the Combination of CDF and D0 Results for the Mass of the W Boson,” arXiv:1204.0042 [hep-ex].
- [143] J. Alcaraz *et al.* [ALEPH and DELPHI and L3 and OPAL and LEP Electroweak Working Group Collaborations], “A Combination of preliminary electroweak measurements and constraints on the standard model,” hep-ex/0612034.
- [144] M. Muether *et al.* [Tevatron Electroweak Working Group and CDF and D0 Collaborations], “Combination of CDF and DO results on the mass of the top quark using up to 8.7 fb^{-1} at the Tevatron,” arXiv:1305.3929 [hep-ex].
- [145] See, e.g., P. Bamert, C. P. Burgess, J. M. Cline, D. London and E. Nardi, “ R_b and new physics: A Comprehensive analysis,” *Phys. Rev. D* **54**, 4275 (1996) [hep-ph/9602438].
- [146] M. E. Peskin and T. Takeuchi, “Estimation of oblique electroweak corrections,” *Phys. Rev. D* **46**, 381 (1992).
- [147] J. D. Wells, “TASI lecture notes: Introduction to precision electroweak analysis,” hep-ph/0512342.
- [148] S. Heinemeyer and G. Weiglein, “Top, GigaZ, MegaW,” arXiv:1007.5232 [hep-ph].
- [149] M. Bicer *et al.* [TLEP Design Study Working Group Collaboration], “First Look at the Physics Case of TLEP,” *JHEP* **1401**, 164 (2014) [arXiv:1308.6176 [hep-ex]].
- [150] G. Aad *et al.* [ATLAS Collaboration], “Measurements of Higgs boson production and couplings in diboson final states with the ATLAS detector at the LHC,” *Phys. Lett. B* **726**, 88 (2013) [arXiv:1307.1427 [hep-ex]].

- [151] The ATLAS collaboration, “Updated coupling measurements of the Higgs boson with the ATLAS detector using up to 25 fb^{-1} of proton-proton collision data,” ATLAS-CONF-2014-009, ATLAS-COM-CONF-2014-013 (March 20, 2014).
- [152] C. Englert, A. Freitas, M. M. Mhleitner, T. Plehn, M. Rauch, M. Spira and K. Walz, “Precision Measurements of Higgs Couplings: Implications for New Physics Scales,” J. Phys. G **41**, 113001 (2014) [arXiv:1403.7191 [hep-ph]].
- [153] A. Djouadi, “Implications of the Higgs discovery for the MSSM,” Eur. Phys. J. C **74**, 2704 (2014) [arXiv:1311.0720 [hep-ph]].
- [154] K. A. Olive *et al.* [Particle Data Group Collaboration], “Review of Particle Physics,” Chin. Phys. C **38**, 090001 (2014).
- [155] S. Heinemeyer *et al.* [LHC Higgs Cross Section Working Group Collaboration], “Handbook of LHC Higgs Cross Sections: 3. Higgs Properties,” arXiv:1307.1347 [hep-ph].
- [156] The PDG averaging procedure usually involve inflation of errors to combine statistically incompatible measurements. The same procedure is also applied to the results of theoretical calculations in [154] (page 729, or page 13 of “Quark masses” review in the online version) to account for possibly missing systematic uncertainties.
- [157] B. Dehnadi, A. H. Hoang, V. Mateu and S. M. Zebarjad, “Charm Mass Determination from QCD Charmonium Sum Rules at Order α_s^3 ,” JHEP **1309**, 103 (2013) [arXiv:1102.2264 [hep-ph]].
- [158] D. M. Asner, T. Barklow, C. Calancha, K. Fujii, N. Graf, H. E. Haber, A. Ishikawa and S. Kanemura *et al.*, “ILC Higgs White Paper,” arXiv:1310.0763 [hep-ph].
- [159] M. E. Peskin, “Estimation of LHC and ILC Capabilities for Precision Higgs Boson Coupling Measurements,” arXiv:1312.4974 [hep-ph].
- [160] J. Fan, M. Reece and L. T. Wang, “Possible Futures of Electroweak Precision: ILC, FCC-ee, and CEPC,” JHEP **1509**, 196 (2015) [arXiv:1411.1054 [hep-ph]].
- [161] M. Ruan, “Higgs Measurement at e^+e^- Circular Colliders,” Nucl. Part. Phys. Proc. **273-275**, 857 (2016) [arXiv:1411.5606 [hep-ex]].
- [162] J. H. Kuhn, M. Steinhauser and C. Sturm, “Heavy Quark Masses from Sum Rules in Four-Loop Approximation,” Nucl. Phys. B **778**, 192 (2007) [hep-ph/0702103 [HEP-PH]].
- [163] J. H. Kuhn and M. Steinhauser, “Determination of $\alpha(s)$ and heavy quark masses from recent measurements of $R(s)$,” Nucl. Phys. B **619**, 588 (2001) [Erratum-ibid. B **640**, 415 (2002)] [hep-ph/0109084].
- [164] K. G. Chetyrkin, J. H. Kuhn, A. Maier, P. Maierhofer, P. Marquard, M. Steinhauser and C. Sturm, “Charm and Bottom Quark Masses: An Update,” Phys. Rev. D **80**, 074010 (2009) [arXiv:0907.2110 [hep-ph]].

- [165] A. Signer, “The Charm quark mass from non-relativistic sum rules,” *Phys. Lett. B* **672**, 333 (2009) [arXiv:0810.1152 [hep-ph]].
- [166] A. Hoang, P. Ruiz-Femenia and M. Stahlhofen, “Renormalization Group Improved Bottom Mass from Upsilon Sum Rules at NNLL Order,” *JHEP* **1210**, 188 (2012) [arXiv:1209.0450 [hep-ph]].
- [167] A. A. Penin and N. Zerf, “Bottom Quark Mass from Υ Sum Rules to $\mathcal{O}(\alpha_s^3)$,” *JHEP* **1404**, 120 (2014) [arXiv:1401.7035 [hep-ph]].
- [168] M. Beneke, A. Maier, J. Piclum and T. Rauh, “The bottom-quark mass from non-relativistic sum rules at NNNLO,” *Nucl. Phys. B* **891**, 42 (2015) [arXiv:1411.3132 [hep-ph]].
- [169] S. Bodenstein, J. Bordes, C. A. Dominguez, J. Penarrocha and K. Schilcher, “QCD sum rule determination of the charm-quark mass,” *Phys. Rev. D* **83**, 074014 (2011) [arXiv:1102.3835 [hep-ph]].
- [170] S. Bodenstein, J. Bordes, C. A. Dominguez, J. Penarrocha and K. Schilcher, “Bottom-quark mass from finite energy QCD sum rules,” *Phys. Rev. D* **85**, 034003 (2012) [arXiv:1111.5742 [hep-ph]].
- [171] P. Gambino and C. Schwanda, “Inclusive semileptonic fits, heavy quark masses, and V_{cb} ,” *Phys. Rev. D* **89**, 014022 (2014) [arXiv:1307.4551 [hep-ph]].
- [172] O. L. Buchmuller and H. U. Flacher, “Fit to moment from $B \rightarrow_c X(c) l \text{ anti-}\nu$ and $B \rightarrow_c X(s) \gamma$ decays using heavy quark expansions in the kinetic scheme,” *Phys. Rev. D* **73**, 073008 (2006) [hep-ph/0507253].
- [173] C. W. Bauer, Z. Ligeti, M. Luke, A. V. Manohar and M. Trott, “Global analysis of inclusive B decays,” *Phys. Rev. D* **70**, 094017 (2004) [hep-ph/0408002].
- [174] A. David (for the CMS Collaboration), “Precise determination of the mass of the Higgs boson and studies of the compatibility of its couplings with the standard model,” Talk at ICHEP14 (Valencia). CMS PAS HIG-14-009 (03 July 2014).
- [175] C. McNeile, C. T. H. Davies, E. Follana, K. Hornbostel and G. P. Lepage, “High-Precision c and b Masses, and QCD Coupling from Current-Current Correlators in Lattice and Continuum QCD,” *Phys. Rev. D* **82**, 034512 (2010) [arXiv:1004.4285 [hep-lat]].
- [176] B. Colquhoun, R. J. Dowdall, C. T. H. Davies, K. Hornbostel and G. P. Lepage, “The Υ and Υ' Leptonic Widths, a_μ^b and m_b from full lattice QCD,” arXiv:1408.5768 [hep-lat].
- [177] B. Chakraborty, C. T. H. Davies, G. C. Donald, R. J. Dowdall, B. Galloway, P. Knecht, J. Koponen and G. P. Lepage *et al.*, “High-precision quark masses and QCD coupling from $n_f = 4$ lattice QCD,” arXiv:1408.4169 [hep-lat].

- [178] G. P. Lepage, P. B. Mackenzie and M. E. Peskin, “Expected Precision of Higgs Boson Partial Widths within the Standard Model,” arXiv:1404.0319 [hep-ph].
- [179] V. A. Novikov, L. B. Okun, M. A. Shifman, A. I. Vainshtein, M. B. Voloshin and V. I. Zakharov, “Charmonium and Gluons: Basic Experimental Facts and Theoretical Introduction,” Phys. Rept. **41**, 1 (1978).
- [180] M. A. Shifman, “Snapshots of hadrons or the story of how the vacuum medium determines the properties of the classical mesons which are produced, live and die in the QCD vacuum,” Prog. Theor. Phys. Suppl. **131**, 1 (1998) [hep-ph/9802214].
- [181] P. Colangelo and A. Khodjamirian, “QCD sum rules, a modern perspective,” In *Shifman, M. (ed.): At the frontier of particle physics, vol. 3* 1495-1576 [hep-ph/0010175].
- [182] A. Maier, P. Maierhofer, P. Marquard and A. V. Smirnov, “Low energy moments of heavy quark current correlators at four loops,” Nucl. Phys. B **824**, 1 (2010) [arXiv:0907.2117 [hep-ph]].
- [183] D. J. Broadhurst, P. A. Baikov, V. A. Ilyin, J. Fleischer, O. V. Tarasov and V. A. Smirnov, “Two loop gluon condensate contributions to heavy quark current correlators: Exact results and approximations,” Phys. Lett. B **329**, 103 (1994) [hep-ph/9403274].
- [184] K. Chetyrkin, J. H. Kuhn, A. Maier, P. Maierhofer, P. Marquard, M. Steinhauser and C. Sturm, “Precise Charm- and Bottom-Quark Masses: Theoretical and Experimental Uncertainties,” Theor. Math. Phys. **170**, 217 (2012) [arXiv:1010.6157 [hep-ph]].
- [185] B. L. Ioffe, “QCD at low energies,” Prog. Part. Nucl. Phys. **56**, 232 (2006) [hep-ph/0502148].
- [186] K. G. Chetyrkin, J. H. Kuhn and M. Steinhauser, “RunDec: A Mathematica package for running and decoupling of the strong coupling and quark masses,” Comput. Phys. Commun. **133**, 43 (2000) [hep-ph/0004189].
- [187] B. Dehnadi, A. H. Hoang and V. Mateu, “Charm and Bottom Masses from Sum Rules with a Convergence Test,” arXiv:1411.5597 [hep-ph].
- [188] S. J. Brodsky, G. P. Lepage and P. B. Mackenzie, “On the Elimination of Scale Ambiguities in Perturbative Quantum Chromodynamics,” Phys. Rev. D **28**, 228 (1983).
- [189] S. J. Brodsky, M. Mojaza and X. G. Wu, “Systematic Scale-Setting to All Orders: The Principle of Maximum Conformality and Commensurate Scale Relations,” Phys. Rev. D **89**, 014027 (2014) [arXiv:1304.4631 [hep-ph]].
- [190] X. G. Wu, S. J. Brodsky and M. Mojaza, “The Renormalization Scale-Setting Problem in QCD,” Prog. Part. Nucl. Phys. **72**, 44 (2013) [arXiv:1302.0599 [hep-ph]].
- [191] A. L. Kataev and S. V. Mikhailov, “Generalization of the Brodsky-Lepage-Mackenzie optimization within the $\{\beta\}$ -expansion and the principle of maximal conformality,” Phys. Rev. D **91**, no. 1, 014007 (2015) [arXiv:1408.0122 [hep-ph]]

- [192] D. C. Kennedy and B. W. Lynn, “Electroweak Radiative Corrections with an Effective Lagrangian: Four Fermion Processes,” Nucl. Phys. B **322**, 1 (1989).
- [193] I. Maksymyk, C. P. Burgess and D. London, “Beyond S, T and U,” Phys. Rev. D **50**, 529 (1994) [hep-ph/9306267].
- [194] R. Barbieri, A. Pomarol, R. Rattazzi and A. Strumia, “Electroweak symmetry breaking after LEP-1 and LEP-2,” Nucl. Phys. B **703**, 127 (2004) [hep-ph/0405040].
- [195] A. Drozd, J. Ellis, J. Quevillon and T. You, “Comparing EFT and Exact One-Loop Analyses of Non-Degenerate Stops,” JHEP **1506**, 028 (2015) [arXiv:1504.02409 [hep-ph]].
- [196] C. W. Chiang and R. Huo, “Standard Model Effective Field Theory: Integrating out a Generic Scalar,” JHEP **1509**, 152 (2015) [arXiv:1505.06334 [hep-ph]].
- [197] R. Huo, “Standard Model Effective Field Theory: Integrating out Vector-Like Fermions,” JHEP **1509**, 037 (2015) [arXiv:1506.00840 [hep-ph]].
- [198] R. Huo, “Effective Field Theory of Integrating out Sfermions in the MSSM: Complete One-Loop Analysis,” arXiv:1509.05942 [hep-ph].
- [199] R. Gauld, B. D. Pecjak and D. J. Scott, “One-loop corrections to $h \rightarrow b\bar{b}$ and $h \rightarrow \tau\bar{\tau}$ decays in the Standard Model Dimension-6 EFT: four-fermion operators and the large- m_t limit,” JHEP **1605** (2016) 080 [arXiv:1512.02508 [hep-ph]].
- [200] R. Gauld, B. D. Pecjak and D. J. Scott, “QCD radiative corrections for $h \rightarrow b\bar{b}$ in the Standard Model Dimension-6 EFT,” Phys. Rev. D **94**, no. 7, 074045 (2016) [arXiv:1607.06354 [hep-ph]].
- [201] M. B. Gavela, K. Kanshin, P. A. N. Machado and S. Saa, “On the renormalization of the electroweak chiral Lagrangian with a Higgs,” JHEP **1503**, 043 (2015) [arXiv:1409.1571 [hep-ph]].
- [202] G. Altarelli and R. Barbieri, “Vacuum polarization effects of new physics on electroweak processes,” Phys. Lett. B **253**, 161 (1991).
- [203] G. Altarelli, R. Barbieri and S. Jadach, “Toward a model independent analysis of electroweak data,” Nucl. Phys. B **369**, 3 (1992) [Nucl. Phys. B **376**, 444 (1992)].
- [204] O. Domenech, A. Pomarol and J. Serra, “Probing the SM with Dijets at the LHC,” Phys. Rev. D **85**, 074030 (2012) [arXiv:1201.6510 [hep-ph]].
- [205] S. Schael *et al.* [ALEPH and DELPHI and L3 and OPAL and LEP Electroweak Collaborations], “Electroweak Measurements in Electron-Positron Collisions at W-Boson-Pair Energies at LEP,” Phys. Rept. **532**, 119 (2013) [arXiv:1302.3415 [hep-ex]].
- [206] K. Hagiwara, R. D. Peccei, D. Zeppenfeld and K. Hikasa, “Probing the Weak Boson Sector in $e^+ e^- \rightarrow j W^+ W^-$,” Nucl. Phys. B **282**, 253 (1987).

- [207] G. Aad *et al.* [ATLAS Collaboration], “Measurement of total and differential W^+W^- production cross sections in proton-proton collisions at $\sqrt{s} = 8$ TeV with the ATLAS detector and limits on anomalous triple-gauge-boson couplings,” JHEP **1609**, 029 (2016) [arXiv:1603.01702 [hep-ex]].
- [208] V. Khachatryan *et al.* [CMS Collaboration], “Measurement of the W^+W^- cross section in pp collisions at $\sqrt{s} = 8$ TeV and limits on anomalous gauge couplings,” Eur. Phys. J. C **76**, no. 7, 401 (2016) [arXiv:1507.03268 [hep-ex]].
- [209] G. Aad *et al.* [ATLAS Collaboration], “Measurements of $W^\pm Z$ production cross sections in pp collisions at $\sqrt{s} = 8$ TeV with the ATLAS detector and limits on anomalous gauge boson self-couplings,” Phys. Rev. D **93**, no. 9, 092004 (2016) [arXiv:1603.02151 [hep-ex]].
- [210] CMS Collaboration [CMS Collaboration], “Measurement of WZ production rate,” CMS-PAS-SMP-12-006.
- [211] H. Baer *et al.*, “The International Linear Collider Technical Design Report - Volume 2: Physics,” arXiv:1306.6352 [hep-ph].
- [212] L. Bian, J. Shu and Y. Zhang, “Prospects for Triple Gauge Coupling Measurements at Future Lepton Colliders and the 14 TeV LHC,” JHEP **1509**, 206 (2015) [arXiv:1507.02238 [hep-ph]].
- [213] R. S. Gupta, A. Pomarol and F. Riva, “BSM Primary Effects,” Phys. Rev. D **91**, no. 3, 035001 (2015) [arXiv:1405.0181 [hep-ph]].
- [214] A Combination of Preliminary Results on Gauge Boson Couplings Measured by the LEP Experiments - 2002. ALEPH, DELPHI, L3, OPAL, and the LEP TGC Working Group. LEPEWWG-TGC-2002-02.
- [215] T. Barklow, J. Brau, K. Fujii, J. Gao, J. List, N. Walker and K. Yokoya, “ILC Operating Scenarios,” arXiv:1506.07830 [hep-ex].
- [216] M. K. Gaillard, “The Effective One Loop Lagrangian With Derivative Couplings,” Nucl. Phys. B **268**, 669 (1986). doi:10.1016/0550-3213(86)90264-6
- [217] L. H. Chan, “Derivative Expansion for the One Loop Effective Actions With Internal Symmetry,” Phys. Rev. Lett. **57**, 1199 (1986). doi:10.1103/PhysRevLett.57.1199
- [218] O. Cheyette, “Effective Action for the Standard Model With Large Higgs Mass,” Nucl. Phys. B **297**, 183 (1988). doi:10.1016/0550-3213(88)90205-2
- [219] F. del Aguila, Z. Kunszt and J. Santiago, “One-loop effective Lagrangians after matching,” Eur. Phys. J. C **76**, no. 5, 244 (2016) doi:10.1140/epjc/s10052-016-4081-1 [arXiv:1602.00126 [hep-ph]].
- [220] M. Boggia, R. Gomez-Ambrosio and G. Passarino, “Low energy behaviour of standard model extensions,” JHEP **1605**, 162 (2016) doi:10.1007/JHEP05(2016)162 [arXiv:1603.03660 [hep-ph]].

- [221] S. Dittmaier and C. Grosse-Knetter, “Deriving nondecoupling effects of heavy fields from the path integral: A Heavy Higgs field in an SU(2) gauge theory,” *Phys. Rev. D* **52**, 7276 (1995) doi:10.1103/PhysRevD.52.7276 [hep-ph/9501285].
- [222] S. Dittmaier and C. Grosse-Knetter, “Integrating out the standard Higgs field in the path integral,” *Nucl. Phys. B* **459**, 497 (1996) doi:10.1016/0550-3213(95)00551-X [hep-ph/9505266].
- [223] M. Beneke and V. A. Smirnov, “Asymptotic expansion of Feynman integrals near threshold,” *Nucl. Phys. B* **522**, 321 (1998) doi:10.1016/S0550-3213(98)00138-2 [hep-ph/9711391].
- [224] V. A. Smirnov, “Applied asymptotic expansions in momenta and masses,” *Springer Tracts Mod. Phys.* **177**, 1 (2002).
- [225] B. Jantzen, “Foundation and generalization of the expansion by regions,” *JHEP* **1112**, 076 (2011) doi:10.1007/JHEP12(2011)076 [arXiv:1111.2589 [hep-ph]].
- [226] J. Santiago, “One-loop effective Lagrangians after matching,” talk at Planck 2016, 23-27 May 2016, Valencia, Spain.
- [227] M. E. Peskin and D. V. Schroeder, “An Introduction to quantum field theory,” Reading, USA: Addison-Wesley (1995) 842 p
- [228] L. F. Abbott, “Introduction to the Background Field Method,” *Acta Phys. Polon. B* **13**, 33 (1982).
- [229] A. Pich, “Effective field theory: Course,” hep-ph/9806303.
- [230] M. S. Bilenky and A. Santamaria, “One loop effective Lagrangian for a standard model with a heavy charged scalar singlet,” *Nucl. Phys. B* **420**, 47 (1994) doi:10.1016/0550-3213(94)90375-1 [hep-ph/9310302].
- [231] D. M. Pierce, J. A. Bagger, K. T. Matchev and R. j. Zhang, “Precision corrections in the minimal supersymmetric standard model,” *Nucl. Phys. B* **491**, 3 (1997) [hep-ph/9606211].
- [232] K. Tobe and J. D. Wells, “Revisiting top bottom tau Yukawa unification in supersymmetric grand unified theories,” *Nucl. Phys. B* **663**, 123 (2003) [hep-ph/0301015].
- [233] G. Elor, L. J. Hall, D. Pinner and J. T. Ruderman, “Yukawa Unification and the Superpartner Mass Scale,” *JHEP* **1210**, 111 (2012) [arXiv:1206.5301 [hep-ph]].
- [234] P. A. Baikov, K. G. Chetyrkin and J. H. Kuhn, “Scalar correlator at $\mathcal{O}(\alpha_s^4)$, Higgs decay into b-quarks and bounds on the light quark masses,” *Phys. Rev. Lett.* **96**, 012003 (2006) [hep-ph/0511063].
- [235] M. Butenschoen, F. Fugel and B. A. Kniehl, “ $\mathcal{O}(G_F^2 m_t^4)$ two-loop electroweak correction to Higgs-boson decay to bottom quarks,” *Nucl. Phys. B* **772**, 25 (2007) [hep-ph/0702215 [hep-ph]].

- [236] J. Davies, M. Steinhauser and D. Wellmann, “Completing the hadronic Higgs boson decay at order α_s^4 ,” Nucl. Phys. B **920**, 20 (2017) [arXiv:1703.02988 [hep-ph]].
- [237] D. Noth and M. Spira, “Supersymmetric Higgs Yukawa Couplings to Bottom Quarks at next-to-next-to-leading Order,” JHEP **1106**, 084 (2011) [arXiv:1001.1935 [hep-ph]].
- [238] L. Mihaila and C. Reisser, “ $\mathcal{O}(\alpha_s^2)$ corrections to fermionic Higgs decays in the MSSM,” JHEP **1008**, 021 (2010) [arXiv:1007.0693 [hep-ph]].
- [239] A. Crivellin and C. Greub, “Two-loop supersymmetric QCD corrections to Higgs-quark-quark couplings in the generic MSSM,” Phys. Rev. D **87**, 015013 (2013) Erratum: [Phys. Rev. D **87**, 079901 (2013)] [arXiv:1210.7453 [hep-ph]].
- [240] B. M. Gavela, E. E. Jenkins, A. V. Manohar and L. Merlo, “Analysis of General Power Counting Rules in Effective Field Theory,” Eur. Phys. J. C **76**, no. 9, 485 (2016) [arXiv:1601.07551 [hep-ph]].
- [241] G. Buchalla, O. Cata, A. Celis and C. Krause, “Comment on ‘Analysis of General Power Counting Rules in Effective Field Theory’,” arXiv:1603.03062 [hep-ph].
- [242] S. P. Martin, “A Supersymmetry primer,” Adv. Ser. Direct. High Energy Phys. **21** (2010) 1 [Adv. Ser. Direct. High Energy Phys. **18** (1998) 1] [hep-ph/9709356].
- [243] S. P. Martin and M. T. Vaughn, “Regularization dependence of running couplings in softly broken supersymmetry,” Phys. Lett. B **318**, 331 (1993) [hep-ph/9308222].
- [244] S. P. Martin and M. T. Vaughn, “Two loop renormalization group equations for soft supersymmetry breaking couplings,” Phys. Rev. D **50**, 2282 (1994) Erratum: [Phys. Rev. D **78**, 039903 (2008)] [hep-ph/9311340].
- [245] D. Buttazzo, G. Degrassi, P. P. Giardino, G. F. Giudice, F. Sala, A. Salvio and A. Strumia, “Investigating the near-criticality of the Higgs boson,” JHEP **1312**, 089 (2013) [arXiv:1307.3536 [hep-ph]].
- [246] A. V. Bednyakov, B. A. Kniehl, A. F. Pikelner and O. L. Veretin, “On the b -quark running mass in QCD and the SM,” Nucl. Phys. B **916**, 463 (2017) [arXiv:1612.00660 [hep-ph]].
- [247] H. Arason, D. J. Castano, B. Keszthelyi, S. Mikaelian, E. J. Piard, P. Ramond and B. D. Wright, “Renormalization group study of the standard model and its extensions. 1. The Standard model,” Phys. Rev. D **46**, 3945 (1992).
- [248] J. A. Casas, A. Lleyda and C. Munoz, “Strong constraints on the parameter space of the MSSM from charge and color breaking minima,” Nucl. Phys. B **471**, 3 (1996) [hep-ph/9507294].
- [249] W. G. Hollik, “A new view on vacuum stability in the MSSM,” JHEP **1608**, 126 (2016) [arXiv:1606.08356 [hep-ph]].

- [250] A. Ventura [ATLAS and CMS Collaborations], “Searches for supersymmetry,” arXiv:1711.00152 [hep-ex].
- [251] S. A. R. Ellis and J. D. Wells, “High-scale supersymmetry, the Higgs boson mass, and gauge unification,” Phys. Rev. D **96**, no. 5, 055024 (2017) [arXiv:1706.00013 [hep-ph]].
- [252] L. J. Hall, R. Rattazzi and U. Sarid, “The Top quark mass in supersymmetric SO(10) unification,” Phys. Rev. D **50**, 7048 (1994) [hep-ph/9306309].
- [253] R. Hempfling, “Yukawa coupling unification with supersymmetric threshold corrections,” Phys. Rev. D **49**, 6168 (1994).
- [254] M. Carena, M. Olechowski, S. Pokorski and C. E. M. Wagner, “Electroweak symmetry breaking and bottom - top Yukawa unification,” Nucl. Phys. B **426**, 269 (1994) [hep-ph/9402253].
- [255] C. F. Kolda, L. Roszkowski, J. D. Wells and G. L. Kane, “Predictions for constrained minimal supersymmetry with bottom tau mass unification,” Phys. Rev. D **50**, 3498 (1994) [hep-ph/9404253].
- [256] M. Cirelli, A. Strumia and M. Tamburini, “Cosmology and Astrophysics of Minimal Dark Matter,” Nucl. Phys. B **787**, 152 (2007) [arXiv:0706.4071 [hep-ph]].
- [257] M. Beneke, C. Hellmann and P. Ruiz-Femenia, “Heavy neutralino relic abundance with Sommerfeld enhancements - a study of pMSSM scenarios,” JHEP **1503**, 162 (2015) [arXiv:1411.6930 [hep-ph]].
- [258] M. Beneke, A. Bharucha, F. Dighera, C. Hellmann, A. Hryczuk, S. Recksiegel and P. Ruiz-Femenia, “Relic density of wino-like dark matter in the MSSM,” JHEP **1603**, 119 (2016) [arXiv:1601.04718 [hep-ph]].
- [259] ATLAS Collaboration, “Search for Supersymmetry at the high luminosity LHC with the ATLAS experiment,” ATL-PHYS-PUB-2014-010.
- [260] CMS Collaboration, “Supersymmetry discovery potential in future LHC and HL-LHC running with the CMS detector,” CMS-PAS-SUS-14-012.
- [261] ATLAS Collaboration, “Projections for measurements of Higgs boson signal strengths and coupling parameters with the ATLAS detector at a HL-LHC,” ATL-PHYS-PUB-2014-016.
- [262] CMS Collaboration, “Projected Performance of an Upgraded CMS Detector at the LHC and HL-LHC: Contribution to the Snowmass Process,” arXiv:1307.7135 [hep-ex].
- [263] M. Aaboud *et al.* [ATLAS Collaboration], “Search for additional heavy neutral Higgs and gauge bosons in the ditau final state produced in 36 fb^{-1} of pp collisions at $\sqrt{s} = 13 \text{ TeV}$ with the ATLAS detector,” arXiv:1709.07242 [hep-ex].
- [264] CMS Collaboration [CMS Collaboration], “Search for a neutral MSSM Higgs boson decaying into $\tau\tau$ with 12.9 fb^{-1} of data at $\sqrt{s} = 13 \text{ TeV}$,” CMS-PAS-HIG-16-037.

- [265] CMS Collaboration [CMS Collaboration], “Projected performance of Higgs analyses at the HL-LHC for ECFA 2016,” CMS-PAS-FTR-16-002.
- [266] M. Carena, S. Heinemeyer, O. Stl, C. E. M. Wagner and G. Weiglein, “MSSM Higgs Boson Searches at the LHC: Benchmark Scenarios after the Discovery of a Higgs-like Particle,” *Eur. Phys. J. C* **73**, no. 9, 2552 (2013) [arXiv:1302.7033 [hep-ph]].
- [267] G. Durieux, C. Grojean, J. Gu and K. Wang, “The leptonic future of the Higgs,” *JHEP* **1709**, 014 (2017) [arXiv:1704.02333 [hep-ph]].
- [268] T. Barklow, K. Fujii, S. Jung, R. Karl, J. List, T. Ogawa, M. E. Peskin and J. Tian, “Improved Formalism for Precision Higgs Coupling Fits,” arXiv:1708.08912 [hep-ph].
- [269] K. Fujii *et al.*, “Physics Case for the 250 GeV Stage of the International Linear Collider,” arXiv:1710.07621 [hep-ex].